Elevated-Temperature Properties of ASTM A992 Steel for Structural-Fire Engineering Analysis

by

Jinwoo Lee, B.S.; M.S.

Dissertation

Presented to the Faculty of the Graduate School of

The University of Texas at Austin

in Partial Fulfillment

of the Requirements

for the Degree of

Doctor of Philosophy

The University of Texas at Austin

December 2012

OFFICE OF THE VICE PROVOST AND DEAN OF GRADUATE STUDIES

THE UNIVERSITY OF TEXAS AT AUSTIN

1 University Station G0400 • Main Building 101 • Austin, Texas 78712-0531
(512) 471-4511 • FAX (512) 471-7620 • www.utexas.edu/ogs/
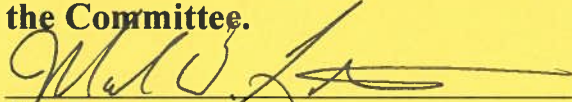
REPORT OF DISSERTATION DEFENSE

The Doctoral Dissertation Committee for   JINWOO LEE
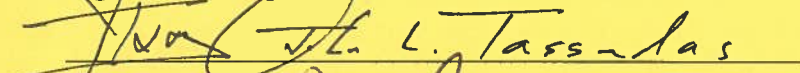
jl33357

Has conducted a final examination on: AUGUST 17, 2012

On the dissertation submitted in partial fulfillment of the requirements for the degree of Doctor of Philosophy. The student has passed the final oral; completed a dissertation which is an independent investigation and which constitutes an original contribution to knowledge and meets the approval of the Committee.

Signature of Supervisor

The Graduate Studies Committee has determined this student has completed all assigned work and passed all examinations required by the graduate program, and recommends that the degree of Doctor of Philosophy be granted.

Signature of GSC Chair:

Date: 8/17/12

Return this form to: Doctoral Degree Evaluator, Office of Graduate Studies, G0400
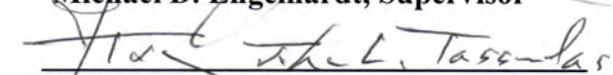
Rev. 0412

The Dissertation Committee for Jinwoo Lee certifies that
this is the approved version of the following dissertation:

Elevated-Temperature Properties of ASTM A992 Steel
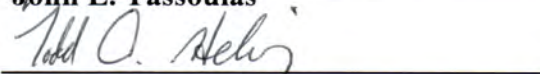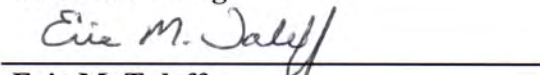
for Structural-Fire Engineering Analysis

Committee:

_____
Michael D. Engelhardt, Supervisor

_____
John L. Tassoulas

_____
Todd A. Helwig

_____
Eric M. Taleff

_____
Ofodike A. Ezekoye

Elevated-Temperature Properties of ASTM A992 Steel for Structural-Fire Engineering Analysis

by

Jinwoo Lee, B.S.; M.S.

Dissertation

Presented to the Faculty of the Graduate School of

The University of Texas at Austin

in Partial Fulfillment

of the Requirements

for the Degree of

Doctor of Philosophy

The University of Texas at Austin

December 2012

Dedication

To my wife and best friend, Jeongim,

for her undying love

and to my three lovely children,

Jisoo, Haesoo and Keunsoo,

for the eternal delights

they give my life.

Acknowledgements

First of all, I would like to thank my dissertation committee for their support of my research study. Dr. Engelhardt's leadership provided the vision for the research conducted during my graduate program. Dr. Taleff's insights into experimental creep testing and analysis lent my research success beyond my means. Dr. Tassoulas's experience with nonlinear analysis served as a bridge between the analytical models and experimental testing results. Dr. Ezekoye's experience in the area of fire science improved my background knowledge. Dr. Helwig's feel for experimentation was essential, especially as it related to concerns of stability at elevated temperatures.

The staff of the Ferguson Structural Engineering Laboratories at The University of Texas at Austin was absolutely critical in conducting the large number of coupon tests I did at elevated temperatures. Eric Schell, Dennis Fillip, Blake Stasney, Andrew Valentine and Mike Wason introduced me to lab techniques, helped me when I needed it and encouraged me through hard times. The long and sometimes boring journey of experimental research could not have been completed without their assistance.

Nor could it have been completed without the help of other students also working on elevated-temperature studies. Thanks are in order for Guanyu Hu and Mohammed Ali Morovat. Their contributions were tremendously helpful to the timely completion of my research.

Finally, I would like to thank the administrative staff: Barbara Howard for keeping life nice at the Ferguson Laboratory and Kathleen Rose for keeping me up to date with all the miscellaneous requirements of graduate school.

August 17, 2012

Elevated-Temperature Properties of ASTM A992 Steel
for Structural-Fire Engineering Analysis

Jinwoo Lee, Ph.D.

The University of Texas at Austin, 2012

Supervisor: Michael D. Engelhardt

Recently in the United States, there has been increasing interest in developing engineered approaches to structural fire safety of buildings as an alternative to conventional code-based prescriptive approaches. With an engineered approach, the response of a structure to fire is computed and appropriate design measures are taken to assure acceptable response. In the case of steel buildings, one of the key elements of this engineered approach is the ability to predict the elevated-temperature properties of structural steel. Although several past research studies have examined elevated-temperature properties of structural steel, there are still major gaps in the experimental database and in the available constitutive models, particularly for ASTM A992 structural steel, a commonly used grade. Accordingly, the overall objective of this dissertation is to significantly enlarge the experimental database of the elevated-temperature properties for ASTM A992 structural steel and developing improved constitutive models for application in structural-fire engineering analysis.

Specific issues examined in this dissertation include the following: tensile properties at elevated temperatures; room-temperature mechanical properties after heating and cooling; and creep and relaxation properties at elevated temperatures. For the

elevated-temperature studies of tension, creep and relaxation, constitutive models were developed to describe the measured experimental data. These models were compared to existing theoretical and empirical models from the literature.

Table of Contents

x

xiv

List of Tables

List of Figures

xxi

xxii

CHAPTER 1
Introduction

1.1 OVERVIEW

Recently in the United States, there has been increasing interest in developing engineered approaches to structural fire safety of buildings as an alternative to conventional code-based prescriptive approaches. With an engineered approach, the response of a structure to fire is computed and appropriate design measures are taken to assure acceptable response. In the case of steel buildings, one of the key elements of this engineered approach is the ability to predict the elevated-temperature properties of structural steel. Not only necessary in design and analysis, knowledge of the mechanical properties of structural steel subjected to elevated temperature is also useful for evaluating structural integrity after a fire.

1.2 OBJECTIVE OF RESEARCH

The objective of this research is to develop experimental data on the mechanical properties of ASTM A992 steel at elevated temperatures for use in structural-fire engineering analysis. Although several past research studies have examined elevated-temperature properties of structural steel, there are still major gaps in the experimental database and in the available constitutive models. Accordingly, the overall goal of this dissertation is to enhance understanding of the topic, through significantly enlarging the experimental database of the elevated-temperature properties for structural steel and developing improved constitutive models for application in structural-fire engineering analysis. The models developed—for tension, creep and relaxation behaviors—were validated against the experimental data collected in this research as well as data reported in the literature.

In addition to the extensive experimental investigations, this research will also examine different approaches to defining material design parameters, such as yield stress, based on the experimentally measured stress-strain data. Finally, the experimental data collected in this research will be combined with data reported in the literature to suggest improved constitutive models for structural steel at elevated temperatures with uniaxial tension response as well as with creep and relaxation response.

1.3 OUTLINE OF DISSERTATION

This dissertation is organized with the results from different series of testing presented in separate chapters. A brief literature review is first provided in Chapter 2. Chapter 3 presents a discussion of the experimental techniques used in this research and their effect on the test results. Testing for basic mechanical properties like yield stress is less standardized at elevated temperature than at room temperature. It was therefore important to thoroughly document the testing methods used. At some points during testing, pilot testing was required before accurate results could be obtained consistently. Pilot testing was conducted to obtain uniform temperature throughout the test furnace, and accurate measurement of both coupon temperature and strain. For measurement of coupon temperature, studies of the effect of thermocouple type and methods of shielding and contact were undertaken. For strain measurement, different extensometers were tested and compared to one another for measurements of both small and large strains. Also related to strain measurement was the challenge of generating full stress-strain curves from strain data that was discontinuously measured due to the need to periodically reset the extensometers during testing as they would approach their measurement range.

Chapter 4 discusses tension testing conducted at elevated temperatures. Test temperatures ranged from room temperature to 1000°C, in 100°C increments. All testing was thermal steady state, that is, the furnace was heated to the target temperature and held at that temperature throughout testing. Loading of the specimen to failure was performed under displacement control. For each temperature, the tensile test was repeated

at least three times: the test with the best, most representative stress-strain curve was selected for analysis. Curve fits of the stress-strain data were performed, and two constitutive models for the tensile behavior of A992 steel were developed. One of these models was a detailed model, aimed primarily for use in advanced analysis; the other was a simplified model for simplified analysis and design.

Chapter 5 covers a series of tests performed at room temperature on coupons that had previously been heated and cooled. This testing was performed to provide data to help evaluate the post-fire properties of steel. Coupons were heated to a target temperature, held there for an hour; then removed and allowed to cool to room temperature. Three methods of cooling were investigated: Cooling-in-Air, Cooling-in-Blanket and Cooling-in-Water; with their corresponding cooling rates being normal, slow and very rapid. Tension testing was then performed on the heated-and-cooled coupons. In addition, toughness and hardness testing was performed. Toughness testing was performed using the Charpy V-Notch (CVN) test. For this test, smaller, pre-notched specimens were fabricated from the ends of heated coupons. Hardness testing was then performed on these CVN specimens. All test results for coupons subject to heating and cooling were compared to the test results of a virgin unheated coupon.

Tensile creep at elevated temperature is discussed in Chapter 6. Coupons were subjected to constant load, and the variation of strain with time was then measured. Analysis of the obtained creep curves was performed in terms of the observed behavior—primary, secondary or tertiary creep. Four loading levels were used for each temperature to provide creep data over a range of stress values. A constitutive model was developed based on curve fits of the creep curves for each temperature.

The final test series is presented in Chapter 7 on stress relaxation at elevated temperature. Coupons were subject to a constant displacement, and the variation of load with time was then measured. A constitutive model was developed from the curve fits of the relaxation behavior.

Finally, Chapter 8 provides summary and conclusions from this research program.

CHAPTER 2
Literature Review

2.1 OVERVIEW

The primary objective of this research program is to develop an experimental database on the elevated temperature properties of ASTM A992 steel for use in structural-fire engineering analysis. Typical building fires can achieve temperatures up to about 1000°C (Buchanan 2002), and if unprotected, structural steel members can reach these same temperatures. Thus, in this research, properties of ASTM A992 steel will be measured at temperatures varying from room temperature up to 1000°C.

While the literature on the elevated-temperature mechanical properties of ASTM A992 steel specifically is sparse, a number of tests have been conducted throughout the years on other grades of steel. While some of these previous tests focused on structure-fire applications, many focused on industrial applications of steel where the temperatures of interest are considerably less than in structure-fire problems.

This chapter will provide a brief literature review of subjects pertinent to the experimental determination of elevated temperature properties of steel for structure-fire problems. The literature review will be organized according to the chapter topics in this dissertation, as follows:

a. Experimental considerations for testing of structural steel at elevated temperatures (Chapter 3)
b. Tension testing at elevated temperatures (Chapter 4)
c. Mechanical properties after heating and cooling (Chapter 5)
d. Creep testing at elevated temperatures (Chapter 6)
e. Relaxation testing at elevated temperatures (Chapter 7)

Each of the subsequent chapters in this dissertation will provide additional background from the literature, as pertinent to specific topics within those chapters.

2.2   EXPERIMENTAL CONSIDERATIONS FOR TESTING AT ELEVATED TEMPERATURES

In terms of general approaches for testing steel at elevated temperatures, two basic options are reported in the literature: thermal transient state and thermal steady state testing. With thermal transient-state methods, a constant load is applied to a steel coupon while the temperature is increased with time. Strains in the coupon are then measured as a function of temperature and time. Thermal transient state testing can be used to develop elevated temperature stress-strain curves as well as elevated temperature creep strain curves. To obtain a stress-strain curve from transient-state testing, the temperature-strain curves must be converted into stress strain curves. (Kirby and Preston 1988; Chen 2006), (Schneider and Lange 2010).

For thermal steady-state methods, static load is monotonically increased while temperature is held constant. Thermal steady-state testing can be used to generate elevated temperature stress strain curves, creep strain curves, and stress relaxation curves. Most previous research of steel properties at elevated temperatures has been conducted by steady-state methods due to their simplicity, accuracy and practicality (Outinen 2001; Lee, Mahendran et al. 2003). Some researchers have suggested that thermal transient state testing is more realistic for structural-fire engineering applications, since temperatures vary with time during an actual fire (Kirby and Preston 1988). However, a review of the literature found no specific data to support this point of view, or to suggest that either transient state or steady state testing are fundamentally more correct or useful.

Measurement of strain in elevated temperature testing poses special difficulties since specialized equipment is needed. Ranawka and Mahendran (2009) discussed these difficulties, and for their testing, used a contact-free laser extensometer. The laser extensometer was validated against other extensometers of known quality, at both room and elevated temperature.

5

Latella and Humphries (2004) developed another contact-free method, but for modulus rather than stress-strain data. Their impulse excitation technique was successfully used to find the elastic and shear modulus of 2.25Cr-1Mo steel at room and elevated temperature. When more conventional contact type extensometers are used, special techniques are generally needed to collect accurate strain data at elevated temperatures. Measuring strain becomes particularly difficult when accuracy is needed at small strain values, to compute elastic modulus for example, while at the same time capturing the full stress-strain curve up to fracture, which may occur at strains greater than 100%. A special technique that involves resetting of a high accuracy extensometer was developed in this research to accomplish this goal, and is described in detail in Chapter 3.

Additional items that are critical in elevated temperature testing of steel is temperature measurement and control. A review of the literature revealed little useful guidance on these issues. Consequently, a major portion of this research program was focused on development of techniques to accurately measure and controls the temperature of steel coupons during testing. These techniques are also described in Chapter 3.

2.3   TENSION TESTING AT ELEVATED TEMPERATURES

Although many researchers have investigated the elevated-temperature properties of carbon steel, there is insufficient fundamental experimental data on the high-strength, low-carbon ASTM A992 steel, despite the prevalence of this steel in U.S. building construction practice. In fact, a review of the literature uncovered no previous experimental studies on the elevated temperature mechanical properties of ASTM A992 steel.

Despite the lack of data on A992 steel, there have been several past studies that have measured elevated temperature properties of steel for structural-fire engineering analysis. Harmathy (1970) performed fundamental research on the tensile and creep

properties of A36 mild steel. In the U.K., Kirby and Preston (1988) investigated the mechanical properties of hot-rolled BS4360 structural steel. Outinen et al. (2001) and Schneider and Lange (2010) contributed to the understanding of S350, S355 and S460 steel properties in Europe. In China, Li et al. (2003) and Chen et al. (2006) performed elevated-temperature tests on 16Mn wrought steel and Bisplate 80 high-strength steel. Lastly, in Australia, a number of researchers have investigated the mechanical properties of light-gage, cold-formed steel and stainless steel. These include Lee et al. (2003), Ranawaka and Mahendran (2009), Gardner et al. (2010) and Kankanamge and Mahendran (2011).

While there have been several past studies on the elevated temperature properties of various steels, the overall number of studies are actually quite limited. Consequently, the experimental database on elevated temperature properties of steel for temperatures of interest in structure-fire problems is actually quite small. Further, as noted earlier, there appear to be no previous studies on ASTM A992 steel.

2.4   MECHANICAL PROPERTIES AFTER HEATING AND COOLING

When a structure has been exposed to fire, an issue of concern following the fire is evaluating the safety of the structure and the need for repairs (Gosain et al., 2008; Tide, 1998). In the case of a steel structure, questions arise on the effect that the exposure to heating and cooling may have had on the mechanical properties of the structural steel. Limited past studies have addressed the post-fire mechanical properties of structural steel (Smith, Kirby et al. 1981; Outinen and Makelainen 2004) whereas other studies have examined the effects of various cooling rates from a more fundamental metallurgical and microstructure point of view (Davis and King 1993; Dhua, Mukerjee et al. 2003; Pyshmintsev, Boryakova et al. 2008).

However, the available experimental data pertinent to post-fire evaluation of structural steel is very limited. Furthermore, there is no data available on the effects of heating and cooling on the mechanical properties of ASTM A992 steel.

7

2.5   CREEP TESTING AT ELEVATED TEMPERATURES

At room temperature, creep of steel is not normally a design consideration. However, at elevated temperatures, creep of steel can become very significant. A significant amount of past research has been conducted to collect experimental data and to develop mathematical models to predict creep strain as a function for steel at elevated temperature (Andrade 1910; Bailey 1929; Norton 1929; McVetty 1943; Dorn 1955; Walles and Graham 1955; Harmathy 1967; Sherby and Burke 1968; Ahmadieh and Mukherjee 1975; Fields 1989; Poh 1998; Mukherjee 2002; NIST 2005). The majority of this past research has evaluated creep of steel for industrial applications, such as in boilers. As such, the temperatures and times considered in this research were significantly different than those found in structure-fire problems. For example, in industrial applications, temperatures of interest are typically below 400°C and durations of exposure are on the order of years. For structure-fire problems, temperatures of interest are as high as 1000°C and durations of exposure are typically less than one hour. Thus despite the significant amount of past research on creep of steel at elevated temperatures, the amount of research pertinent to structure-fire problems is very limited.

A review of the literature identified only a limited number of studies of creep on interest in structural-fire engineering applications. Harmathy (1967), studied creep of ASTM A36 steel, and was one of the first researchers to develop formulas for predicting the strains associated with primary and secondary creep of structural steels at elevated temperatures for specific application to structure-fire analysis. Harmathy's creep equation was based on the concept of temperature compensated time from Dorn's creep theory (Dorn 1955). Fields and Fields (1989) adapted the Norton-Bailey power-law creep model for Australian steel AS A149 and Japanese steel SS41 at elevated temperatures, and provided guidance for adjusting the model to accommodate for an-isothermal temperature conditions found in actual fires. Finally, during the investigation of the collapse of the World Reade Center Towers, the National Institute of Standards and Technology (NIST

2005) collected experimental creep data on steels recovered from the collapsed towers and suggested some modifications to the creep model previously developed by Fields and Fields.

The review of literature indicates that little creep testing has been conducted on structural steel of any type for temperatures, times and stress levels of interest in structure fire problems. Further, there appears to be no creep test data available for ASTM A992 steel.

2.6   RELAXATION TESTING AT ELEVATED TEMPERATURES

The behavior of steel at elevated temperature can show a significant dependence on time. One manifestation of the time-dependent response of steel is creep, as discussed in the previous section. In creep testing, steel samples are subjected to a constant stress, and strain is measured as a function of time. Stress relaxation is another manifestation of time dependent response of steel at elevated temperature. In relaxation testing, steel samples are subjected to constant strain and stress is measured as a function of time. In creep testing, strain increases with time under constant stress, whereas in relaxation test, stress decreases with time under constant strain. Stress relaxation may be particularly significant in structure-fire problems when evaluation structural response to thermally induced strains.

Several past researchers have studied stress relaxation experimentally and have developed mathematical models to predict stress relaxation as a function of temperature, time, and strain (Getsov and Borzdyka 1988, Aoto et al 1986, Batsoulas 2003, Ellis and Tordonato 2000, Jia 2004, Woodford and Swindemann 2005, Beddoes and Mohammadi 2010). As creep and stress relaxation of both representations of time-dependent material response, some researchers have developed more comprehensive models that consider both creep and stress relaxation (Aoto 1986, Batsoulas 2003). However, as is the case with creep, very little past research on stress relaxation has considered temperatures and exposure times that are pertinent to structure-fire problems. In fact, the review of

literature revealed no past experimental studies on elevated temperature stress relaxation of steel with temperature levels (up to 1000°C) and times (minutes up to several hours) of interest in structural-fire engineering analysis.

2.7 SUMMARY

This chapter has provided a brief review of previous research on elevated temperature testing of steel. This review indicates there has been substantial work in this area, but that the majority of this work has been aimed at elevated temperature properties of steel for use in industrial applications. The temperatures, exposure times, and stress levels considered in industrial applications are significantly different than found in typical structure-fire problems. The amount of experimental data on the elevated temperature properties of steel that is pertinent to structure-fire problems is, in fact, highly limited. Further, there appears to be no data whatsoever on ASTM A992 steel, which is widely used for building construction in the U.S. The available literature also indicates that time dependent effects can be highly significant in the response of steel materials at elevated temperature, which is very different form typical room temperature design. Time dependent response can be studied experimentally a number of ways; most commonly by creep testing and by stress relaxation testing. Again, there appears to be little data available in the literature on the creep and stress relaxation characteristics of steel for structure-fire applications. Another issue of interest in structural-fire engineering is the post-fire properties of steel. These are of interest when evaluating the condition and safety of a steel structure after a fire. Little data is available in the literature on the post-fire properties of structural steel, and no data on the post-fire properties of ASTM A992 steel. Finally, the literature review indicates that highly specialized techniques are needed to collect high quality experimental data on steel at elevated temperatures. Issues of interest include the need for specialized equipment, temperature control and temperature measurement of steel samples, and measurement of strain. Elevated temperature testing techniques are not as well developed and standardized as they are at room temperature,

thereby posing additional challenges in collecting experimental data on the elevated temperature properties of steel.

The lack of experimental data on the elevated temperature properties of structural steel represents an important gap in the structural-fire engineering literature, and also serves as an impediment to progress in advancing structural-fire engineering practice. The research summarized in this dissertation is intended to help fill this gap, by substantially expanding the experimental database on the elevated temperature properties of structural steel for use in structural-fire engineering analysis. All of the testing reported herein will be on samples of ASTM A992 steel, as this steel is widely used in U.S. building construction practice, and there appears to be no data whatsoever on the elevated temperature properties of this steel. Finally, the research conducted for this dissertation is also intended to make a contribution to the development of testing techniques for steel at elevated temperatures.

CHAPTER 3
Experimental Considerations

3.1   OVERVIEW

This chapter provides a description of the experimental techniques used in this research project, with an emphasis on the techniques used for tension testing of steel coupons at elevated temperatures. Subsequent chapters will provide further information on experimental techniques specific to other types of tests. Considerable detail is provided in this chapter on experimental techniques, since elevated-temperature testing of steel is not common and the techniques are not as well recognized or standardized as they are for testing at normal temperature. Also, as it was found that the test results can be quite sensitive to the testing techniques, it was considered important to carefully document the experimental techniques used in this research.

This chapter begins with a discussion of the basic approach used in this research for testing at elevated temperatures, that is, thermal steady state testing. A description is provided of the testing equipment used followed by descriptions of the steel materials used in this research and of the methods used to prepare the test coupons. Next, the methods used to measure and control the temperature of the coupons are described, followed by a description of the techniques used to measure strain.

3.2   GENERAL TESTING APPROACH

The elevated temperature testing conducted for this research was thermal steady state, that is, the temperature was held constant while load was applied. Another testing approach sometimes seen in the literature for elevated temperature testing is thermal transient state testing. The differences between these two approaches are outlined in Table 3.1.

Table 3.1 Differences between steady- and transient-state testing

Test Method	Constant	Variable	Measurement
Steady-State	Temperature	Loading and Displacement	Load and Strain
Transient-State	Loading	Temperature	Temperature and Total Strain

3.2.1 Steady-State Testing

In steady-state testing, the specimen is heated to a target temperature while free to elongate. The temperature is then maintained as load is applied to the specimen until failure is reached. Tests may be run under load or displacement control. The direct result of this testing is a temperature-specific stress-strain curve, from which a variety of mechanical properties can be calculated.

In the literature (Outinen and Makelainen 2004), thermal steady-state testing is widely used because of its simplicity. With a simpler procedure, results may be more reproducible. A disadvantage of the method is that it does not represent a real fire event, in which the temperature is varying with time.

3.2.2 Transient-State Testing

In transient-state testing, the specimen is held under constant load while the temperature is raised until failure is achieved. Temperature and total strain are measured during the test; typically, results are reported in terms of a strain-temperature curve like that of Figure 3.1.
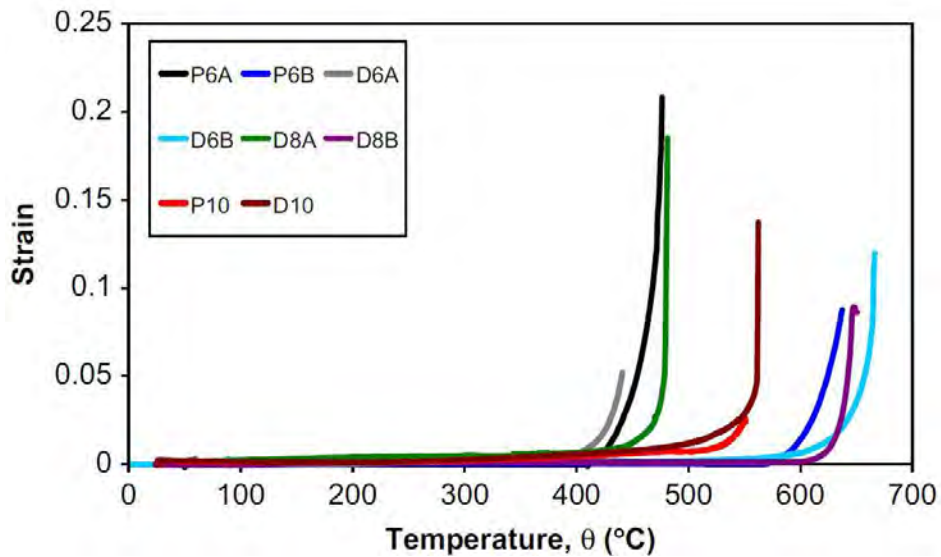
***Figure 3.1 Sample strain-temperature plot from transient-state testing
(2009, Elghazouli)***

Transient-state testing may be a more realistic simulation of conditions in an actual fire (Elghazouli, Cashell et al. 2009). As tests may be many hours long, some creep effects not seen in thermal steady-state tests may be present. However, creep effects are also included in steady-state tests, depending on the loading rate and duration of test. There are significant disadvantages to the transient-state testing approach, however. While it is possible to convert a strain-temperature curve into the more conventional stress-strain curve, doing so requires estimates to be made for the mechanical properties at elevated temperature (Lee, Mahendran et al. 2003). In addition, controlling temperature of the test coupon is more difficult in a transient-state test, as there may not be sufficient time for the entire coupon to reach a uniform temperature. This introduces a potentially significant source of experimental error.

3.2.3 Choice of Steady State

All tests conducted for this research were thermal steady-states. That is, steel coupons were heated to the target temperature under zero load, and held at that

temperature a sufficient time to allow uniform heating of the coupon. Then, while holding the temperature constant, load was applied to the coupon and was increased up to fracture of the coupon. As noted above, both transient-state and steady-state test results will include effects of creep to some extent, depending on the heating rate used in transient-state tests and on the loading rate used in steady-state tests. Thus, it is unclear if one test method provides more representative stress-strain curves than the other. Ultimately, steady-state testing was chosen for this research for two reasons. First, the equipment available for these tests did not allow sufficiently accurate control of heating rate to allow transient-state testing. Secondly, it was felt that steady-state testing was simpler and less prone to experimental error due to non-uniform heating of the test coupons.

3.3 TEST EQUIPMENT

The section describes the equipment used to load and heat the test specimens. A brief description of the test specimen is provided first, followed by a description of the test equipment.

3.3.1 Test Specimen

Most materials testing conducted in this research used standard steel test coupons 18 inches in length and a ½ inch in width. The thickness of the coupon corresponded to the thickness of the material from which the coupon was cut, which will be described later.

Figure 3.2 shows the dimensions of the tension coupons. The dimensions were taken in accordance with ASTM A370 (2010). Details on the techniques used to fabricate the coupon can be found in Section 3.4.
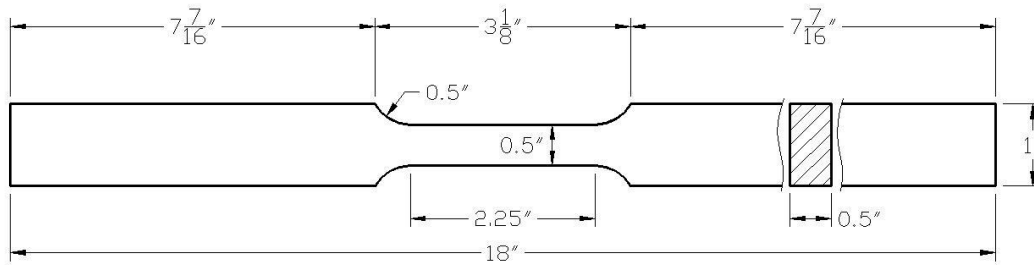
Figure 3.2 18-inch coupon dimensions

3.3.2 Test Machine and Furnace

Central to the testing of steel at elevated temperatures are the MTS test machine and furnace, shown with other required equipment in Figure 3.3.

The test machine used was an MTS 810, a servo-controlled, hydraulic model. This test machine is characterized by low capacity (22 kip) and high accuracy. Loading can be specified by crosshead displacement rate (used for tension and creep tests) or loading rate (used for relaxation tests). The test machine was equipped with water-cooled hydraulic grips for gripping the ends of the coupon.

For testing at elevated temperature, the MTS 810 was fitted with an MTS 653.04 furnace. This furnace is capable of achieving temperatures of 1400°C. For the purposes of this research, it was used for elevated temperatures in the range of 200 to 1000°C.

The MTS 653 furnace consists of two halves, each 10 in. long, which were positioned to surround the middle portion of the specimen being tested. Three heating elements, spaced along the height of furnace, could be controlled individually through use of the MTS 409.83 temperature controller (also shown in Figure 3.3).

Free thermal expansion during heating was allowed for all tests. That is, the bottom crosshead was allowed to move freely while the specimen was heated to its target temperature. The specimen typically reached the steady-state target temperature after about 20 minutes heating. At that time, loading of the coupon was begun.

16
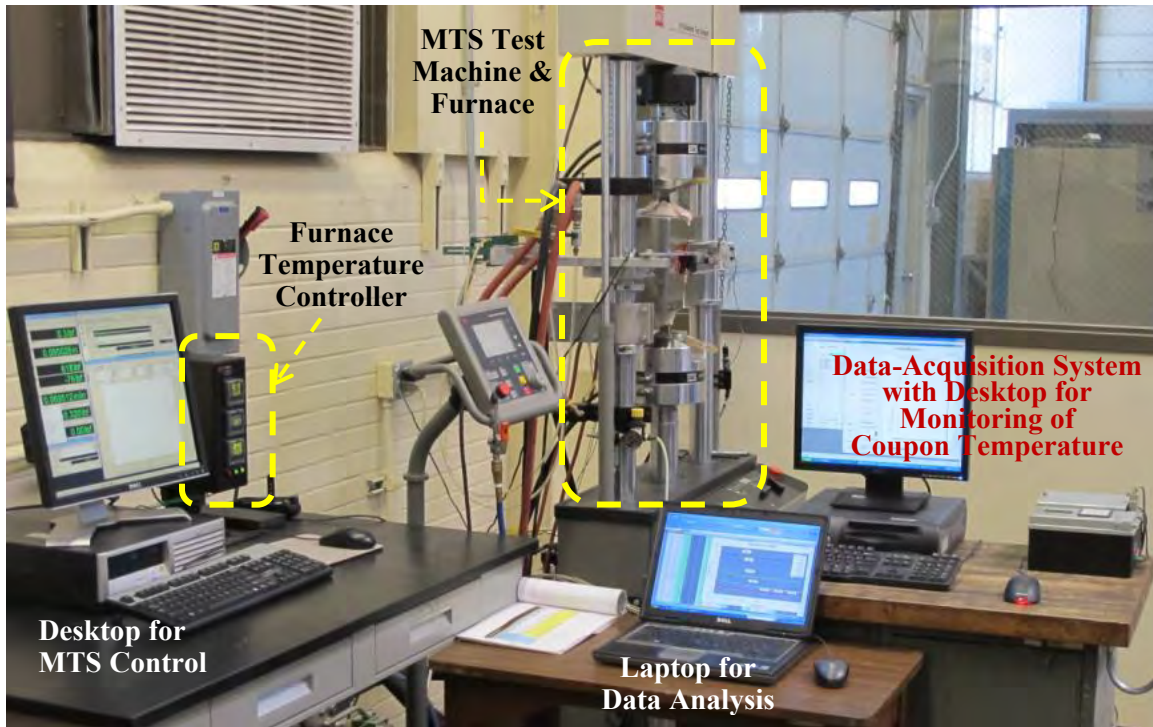
Figure 3.3 MTS test machine with temperature controller and data-acquisition system

Also shown in the Figure 3.3 is the temperature-monitoring system, consisting of a CR5000 data logger and a computer with Campbell Scientific PC9000 software. Monitoring of the specimen temperature was conducted separately from the monitoring (and control) of the furnace temperature.

3.3.3 Furnace Temperature Control

As noted in the previous section, a dedicated temperature controller (MTS 409.83) was used to specify the temperatures of the upper, middle and lower zones of the furnace. Heating elements at each of these locations were turned on or off independently based on the reading of an adjacent thermocouple.

The temperature control system for the furnace is shown on the left side of Figure 3.4. Attempts to connect specimen thermocouples directly to the temperature controller

17

proved unsuccessful, so a separate system (right side of figure) was used to monitor the temperature of the test specimen.
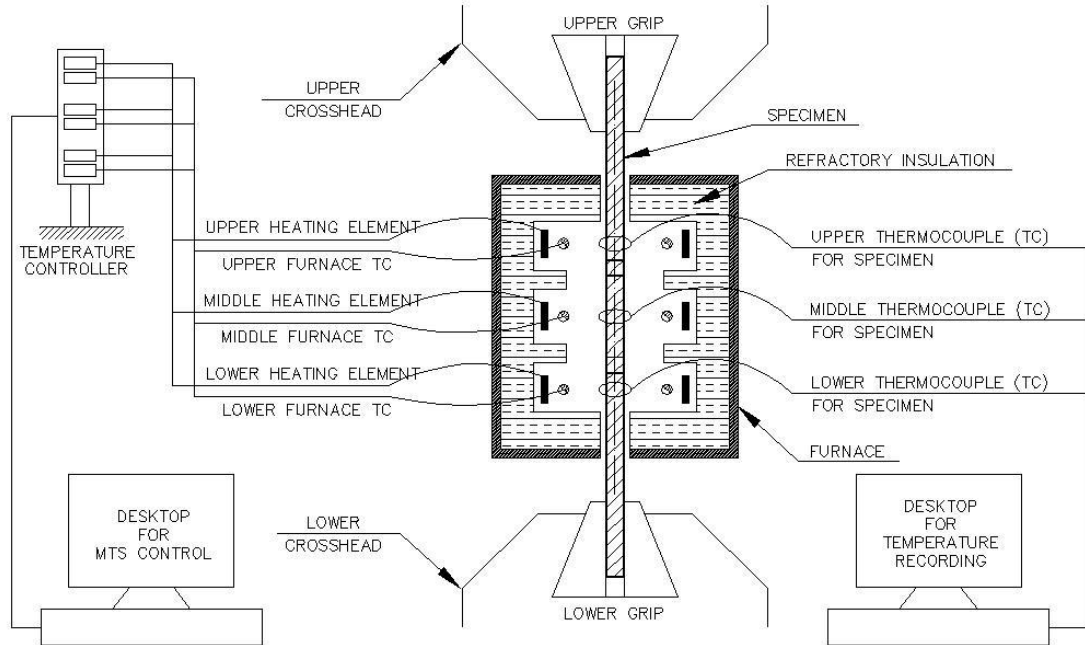
Figure 3.4 Components of temperature control and monitoring systems

The ability to control specimen temperature within a tight tolerance is a challenge in thermal steady-state testing. Existing ASTM standards, summarized in Table 3.2, give tolerances of 2 to 5°C for mechanical testing of steel at elevated temperatures. Tolerances are tighter in tests for the time-dependent effects of creep and relaxation.

Table 3.2 ASTM temperature tolerances for elevated-temperature testing

Standard		Tolerance	
		Temps < 1000°C	Temps ≥ 1000°C
ASTM E21-09	Tension	± 3°C	± 5°C
ASTM E139-11	Creep and Relaxation	± 2°C	± 3°C

Changes in furnace temperature that exceeded the above tolerances can lead inaccurate test results. An example of this phenomenon is shown in Figure 3.5 for a relaxation test conducted at 400°C for an imposed strain equal to 75% of the yield strain. As shown in Figure 3.5, approximately 30 minutes into the test, a sudden increase in the measured rate of relaxation was observed. This unexpected behavior can be explained in light of the specimen temperature profile. The lower specimen thermocouple (red) showed a sudden increase in temperature of 5°C, approximately double the acceptable tolerance. Within a few minutes, the increase in relaxation occurred.
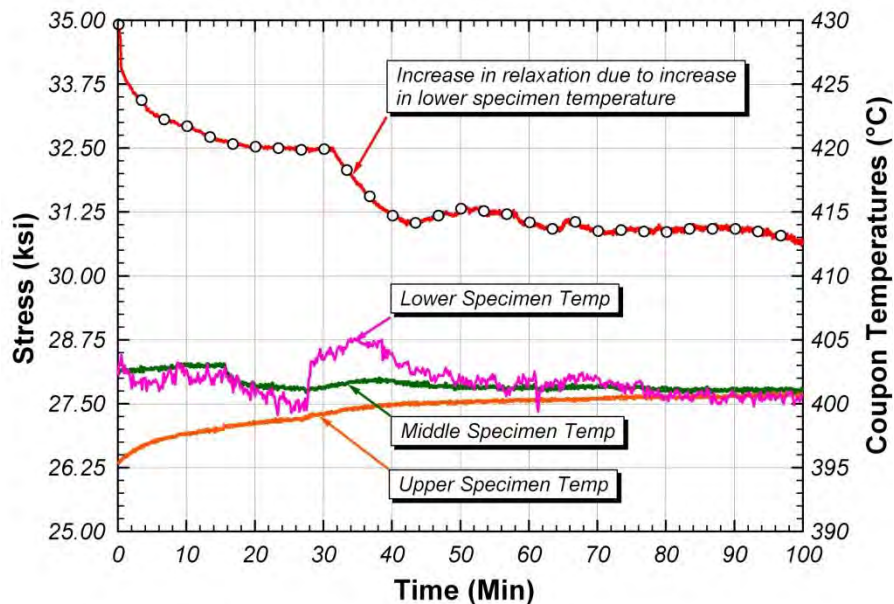
Figure 3.5 Effect of temperature change on relaxation test (400°C, 0.75εy)

3.3.4 Balancing the Furnace

Heat was lost from the furnace through both convection and conduction: convection through gaps at the top and bottom of the furnace, less than 1 in. on all sides surrounding the test specimen; and conduction through the test specimen itself.

This uneven heat loss could be compensated for by setting the upper, middle and lower heating elements of the furnace to difference temperatures. If all three were set to

19

the specimen target temperature, the middle portion of the specimen would be too hot and the upper and lower portions too cold. The furnace could be balanced, however, to achieve a uniform target temperature along the test length of the specimen. If uniform temperature were not achieved, test results would be influenced. For example, necking of the section could occur at the hottest spot.

A pilot test was conducted to determine appropriate setpoints for the three heating elements of the furnace; results are shown in Table 3.3 and Figure 3.6.

Table 3.3 Setpoints for furnace heating elements to reach specimen target temperatures

Target Temp for Specimen (°C)	Setpoints (°C) for Furnace Heating Elements			Deviation from Specimen Target Temperature (°C)		
	Upper	Middle	Lower	Upper	Middle	Lower
400	481.5	393.3	490.0	+81.5	-6.8	+90.0
500	555.0	487.5	567.5	+55.0	-12.5	+67.5
600	638.8	587.5	660.0	+38.8	-12.5	+60.0
700	735.0	700.5	776.3	+35.0	+0.5	+76.3
800	831.3	782.5	873.8	+31.3	-17.5	+73.8
900	927.5	893.8	948.8	+27.5	-6.3	+48.8
1000	1010.0	990.0	1055.0	+10.0	-10.0	+55.0
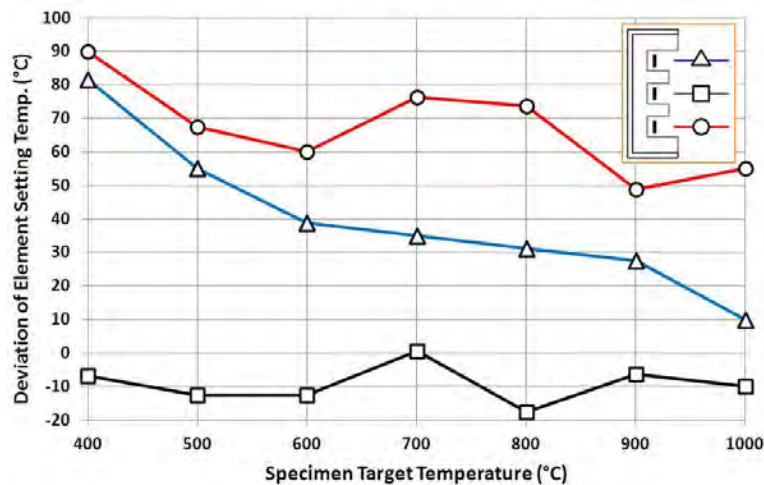
Figure 3.6 Deviation of setpoints for heating elements from target temperature

20

To achieve uniform specimen temperature, the lower heating element of the furnace had to be set hottest, then the upper heating element, and lastly, the middle. For most target temperatures, the middle element was set at a temperature lower than the target. The deviation of the appropriate setpoint for the upper heating element from the target temperature was highly dependent on the target temperature: for 400°C, the upper element should be set 80°C hot; for 1000°C, only 10°C. The deviation of the lower setpoint also decreased with increasing target temperature, but less dramatically.

While the setpoints found in the pilot test (Table 3.3) were good starting points, additional care was needed. It was found that the most effective technique to achieve uniform temperature over the specimen test length was to modify the furnace setpoints slightly several times during heating. New setpoints were determined based on the measured temperatures at the upper, middle and lower portions of the specimen. Typically, the furnace was reset three times during heating as shown in Figure 3.7.
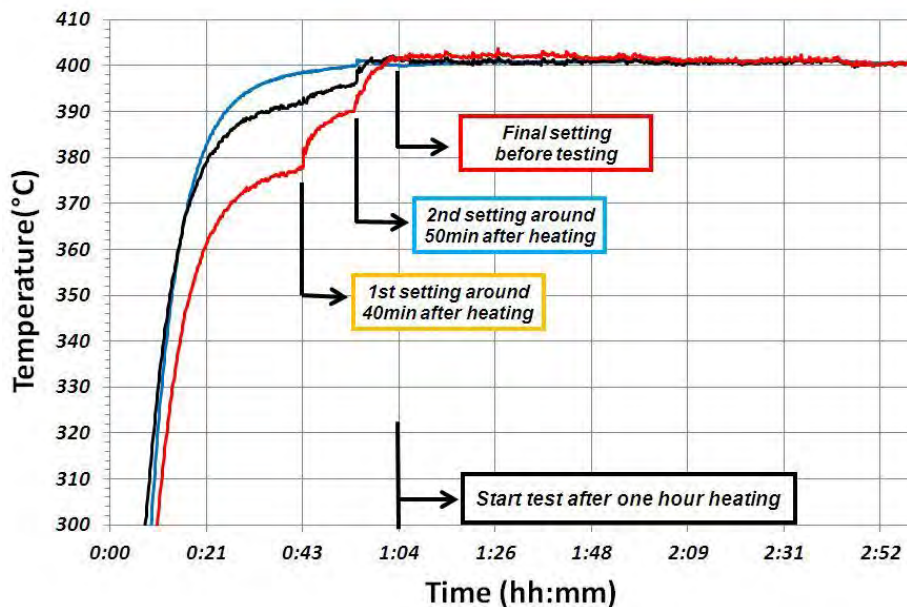
Figure 3.7 Heating using multiple furnace settings over time

21

3.4   STEEL MATERIAL PROPERTIES AND TEST SPECIMENS

3.4.1   Material Classification

All of the testing conducted in this research was on samples of ASTM A992 steel (A992 2011). Steel samples were cut from three different wide-flange members for various phases of the testing program. The three material types are referred to as "MA," "MB," and "MC." (Table 3.4) The MA and MB materials were cut from the web of two different sections of W30x99, coming from two different heats of steel. The MC material was cut from the flange of a W4x13 section.

Table 3.4 lists the measured room temperature values of yield stress and tensile strength for each of the three types of steel. These values are based on tests conducted in this research, rather than the values listed on the Certified Mill Test Reports (CMTRs). Also shown in the table is the specified values of yield stress (F_y) and tensile strength (F_u) for ASTM A992 steel. Table 3.5 lists the chemical composition for the three types of steel, along with the ASTM A992 chemical requirements. The chemical composition for the MC steel was taken from the CMTR. CMTRs were not available for the MA and MB steels, so the chemical composition was determined by sending samples of the steel to a commercial testing laboratory. Note that in terms of yield stress, tensile strength and chemical composition, all three materials used in this research complied with ASTM A992 requirements.

22

Table 3.4 Room-temperature properties of A992 samples used in research

Type	Source	F_y (ksi)	F_u (ksi)	Tests	
MA	W30x99	63.5	76.1	Ch 4	*ET* Tension
MB	W30x99	51.3	66.2	Ch 5	*RT* Tension, Toughness & Hardness after Heating/Cooling
MC	W4x13	51.0	68.3	Ch 6	*ET* Creep
				Ch 7	*ET* Relaxation
ASTM	-	50 to 65	min 65 or $F_y / 0.85$	-	-

Note: ET = Elevated Temperature, RT = Room Temperature

Table 3.5 Chemical composition of ASTM A992 samples used in research (%)

Type	C	Cr	Mo	V	Ni	Mn	Si	P	S	Cu
MA	0.081	0.09	0.034	0.065	0.11	1.41	0.21	0.019	0.022	0.39
MB	0.079	0.09	0.026	0.027	0.13	0.97	0.20	0.014	0.024	0.38
MC	0.080	0.10	0.026	0.002	0.09	0.91	0.23	0.011	0.025	0.24
ASTM	0.23 max	0.35 max	0.15 max	0.15 max	0.45 max	0.50 to 1.60	0.40 max	0.035 max	0.045 max	0.60 max

3.4.2 General Considerations for Coupon Preparation

This section describes the methods used to prepare the tension coupons for this research. Included are descriptions of how material samples were cut from the wide flange sections, machined into coupons and subsequently prepared for testing.

3.4.2.1 Cutting Plate from Wide Flange Section

Materials MA and MB were cut from the web of two different W30x99 sections of A992 steel. As a first stage in coupon preparation, sections of plate were cut from the webs, as shown in Figure 3.8. When cutting the plates from the web, the plate orientation with respect to the rolling direction was noted. All coupons cut from the plate were

oriented along the rolling direction. The web plates were removed from the wide flange section by torch cutting. However, the strips cut from the plates for making coupons were away from the torch cut edges, to avoid any potential influence of the torch-cutting process on the mechanical properties of the coupons.
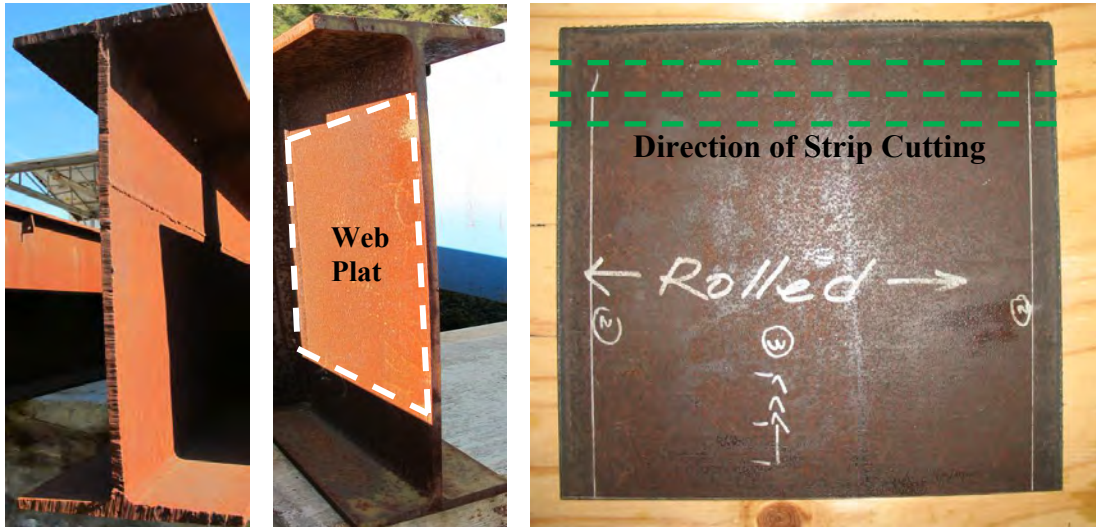
a) W30x99 section used for coupons   *b) Plate cut from W30x99web*
Figure 3.8 W30x99 section and plate cut from web

Material type MC was taken from the flange of a W4x13 section, as shown in Figure 3.9. The orientation of the coupons was again along the rolling direction.

a) Flange cutting using horizontal saw   *b) Strip from flange*
Figure 3.9 W4x13 section and strips cut from flange

24

The dimensions of the tension coupons were in accordance with ASTM A370 (A370 2008). Figure 3. shows the dimensions of the coupons.
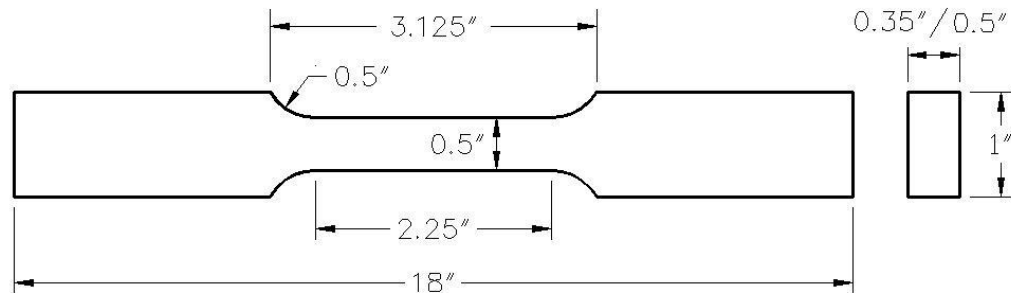
Figure 3.10 Rectangular tension specimen (ASTM E8/E8M, 2010)

3.4.2.2 Strip Milling

As a next step in coupon preparation, the strips of steel cut from the W30x99 web plates and from the W4x13 flanges were milled to provide a 1-inch width. Figure 3.11 shows photos of the milling. After milling, the edges of the coupons were very sharp, so they were smoothed for safe handling using a de-burring tool or fine sandpaper.

a) Strip side-milling   *b) Completed strip side-milling*
Figure 3.11 Strip side-milling work

3.4.2.3 Coupon Shaping

A computer numerical controlled (CNC) milling machine was used to cut the reduced sections of the coupons. The CNC milling machine was programmed to provide

the desired dimensions of the reduced section considering the strip plate width. To minimize thermal damage by cutting friction and for good performance of the milling machine, two passes were made on each side. The cutting depth per pass used on each side was one half of the final cut depth. Details of the cutting process are shown in Figure 3.12 and Figure 3.13.
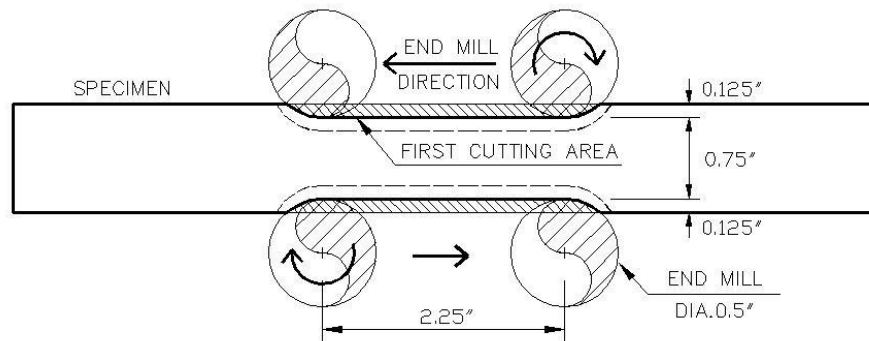
a) First-pass cutting
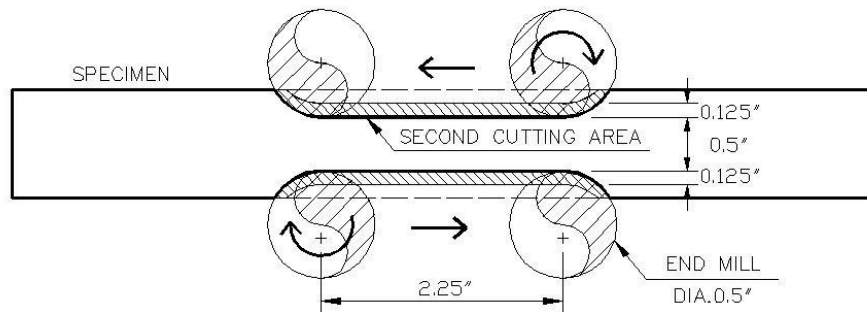
b) Second-pass cutting
Figure 3.12 Specimen cutting processes (plan view)

| a) Cutting of specimen | b) Specimens after cutting |
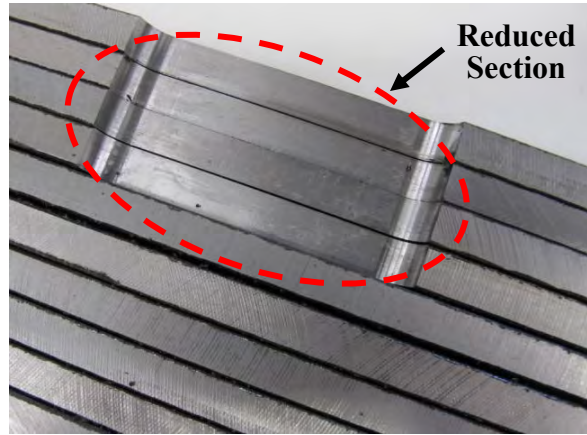
Figure 3.13 Making reduced section from strip plate

3.4.2.4   Coupon Grinding

The surface of the wide-flange members used to make the coupons had mill scale and rust, as shown in Figure 3.14. The coupon surfaces were therefore cleaned by grinding. The reduced sections of the coupons were cleaned with a steel wire brush grinder (Figure 3.15) in manner to avoid any striations on the finished surface. The final surface was suitable for making accurate measurements of cross-section dimensions (to provide accurate cross-sectional area) and to allow proper attachment of the thermocouples and the extensometer. The coupons' ends were finished with a bench grinder in a manner that left a series of striations in transverse direction, as shown in Figure 3.16. During tension testing, the roughened surface at the coupon ends helped prevent slip of the coupons within the machine grips.

27

a) W30x99 rust surface   *b) W4x13 rust surface*

Figure 3.14 Rust and mill scale on W30x99 and W4x13 surfaces

Surface before grinding

Surface after grinding
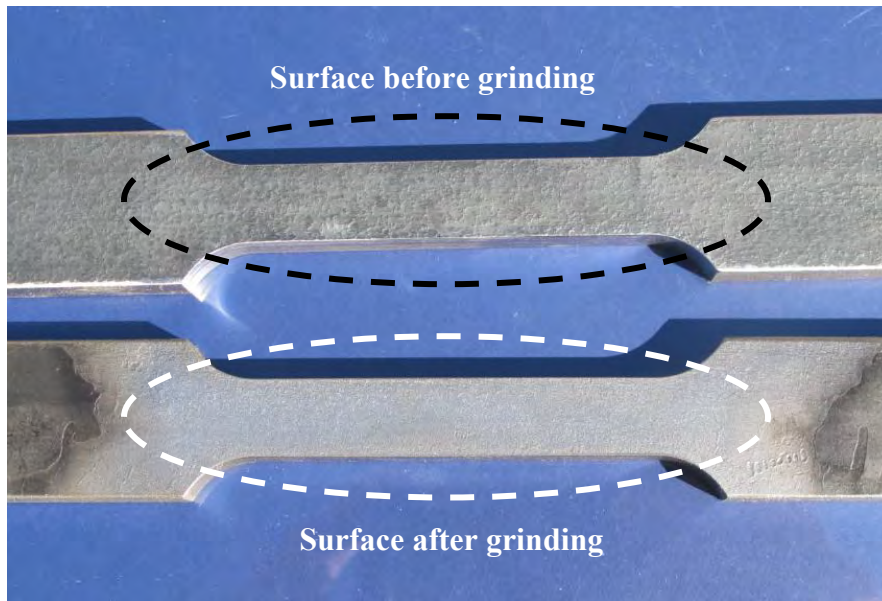
Figure 3.15 Before and after grinding reduced section of coupon

Direction of striations
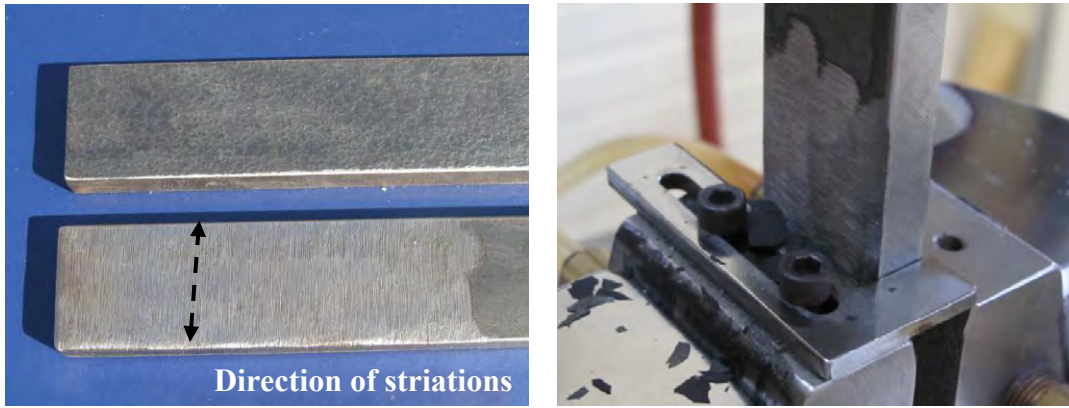
| *a) Grinding of coupon ends* | *b) Coupon end in test-machine grip.* |

Figure 3.16 Grinding of coupon ends

3.4.2.5   Coupon Punching

For each coupon, a series of punch marks were made along the reduced section. The distance between punch marks was measured before and after testing of the coupons. These measurements were used as part of the extensometer resetting process, which will be described in detail later. As part of the process of capturing the full stress-strain curve for the coupons, it was necessary to capture the strain within the necked portion of the coupon. Consequently, the punch marks were located to allow measurement of the total elongation of a gauge length that included the necked region, for various locations of necking, as shown in Figure 3.17. To accommodate various possible locations of necking, two punch marks were placed on one side of the coupon, and three punch marks were made on the opposite side, as shown in Figure 3.18 and Figure 3.19. The punch marks made were shallow, less than 1/32 inch deep, to avoid initiation of fracture at a punch mark. During the actual testing of the coupons, it was found that fracture rarely initiated at a punch mark, so it is believed that the punch marks themselves had little effect on the measures stress-strain response.
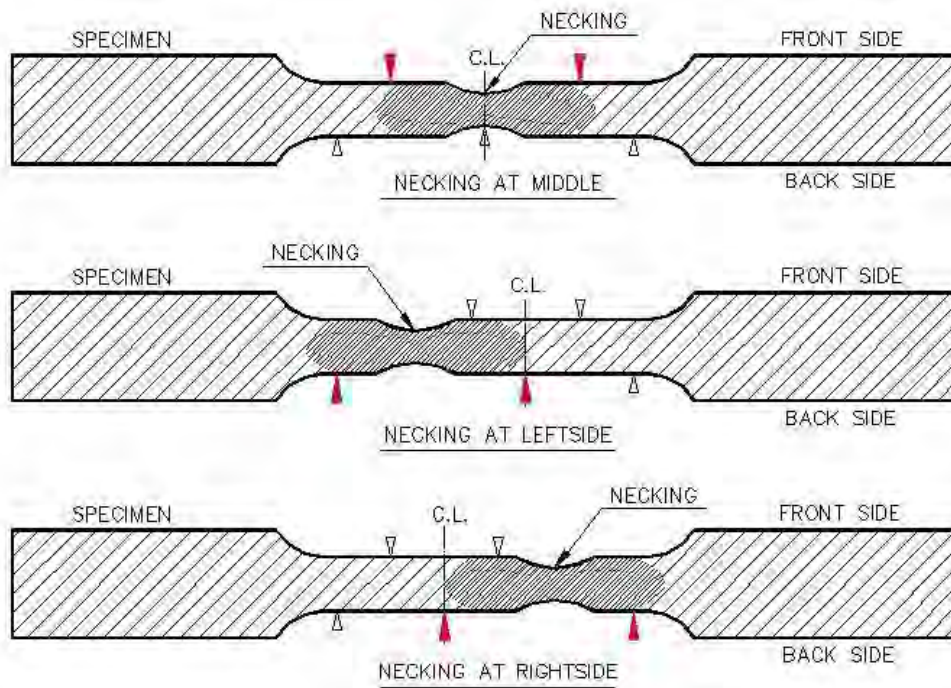
Figure 3.17 Possible locations for necking
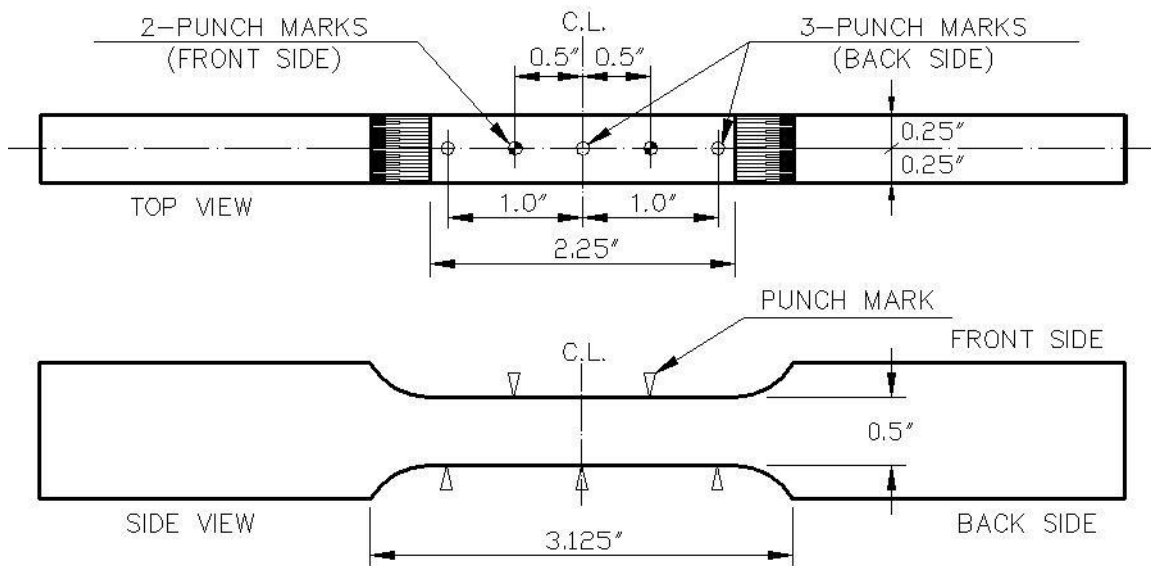
Figure 3.18 Location of punch marks

30
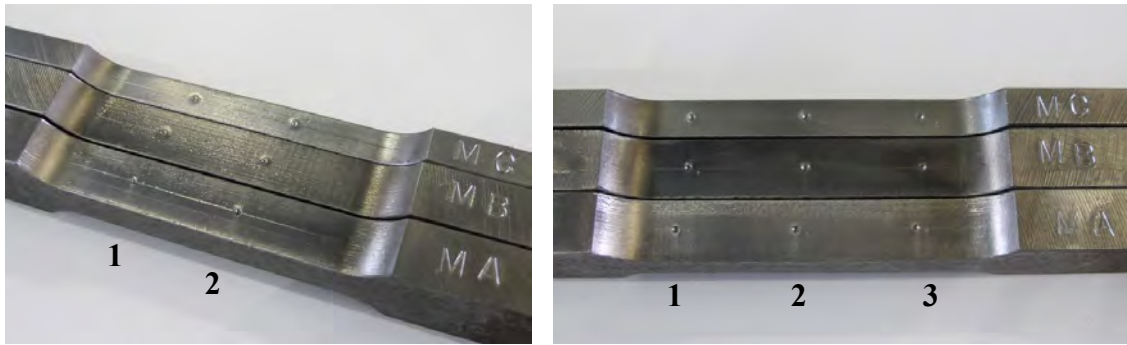
| *a) Front side* | *b) Back side* |

Figure 3.19 Punch marks on coupons

3.4.2.6 Coupon Marking

During the course of this research, a very large number of tension coupons were tested. Consequently, a system was needed to place identifying marks on the coupons that would survive the heating and cooling process, and would still be visible following the test. It was found that punched marks in the end region of the coupons provided the most reliable method for marking the coupons, as shown in Figure 3.20.

Figure 3.20 Coupon identification method

3.5   TEMPERATURE MEASUREMENT

Measurement of temperature in this research was done using thermocouples. The properties of the thermocouples and installation techniques chosen are presented in this section, along with data from pilot testing supporting these techniques.

3.5.1   Thermocouples

Type K wire thermocouples consisting of Chromel (90%/Ni + 10%/Cr) and Alumel (95%/Ni + 2%/Mn + 2%/Al + 1%/Si) were used to measure and control the temperature of the coupons during testing. This type of thermocouple was selected for three reasons:

- the measurement range of the thermocouple (-270 to 1370°C) was appropriate for both testing at temperatures ranging from room temperature to 1000°C;
- the type of thermocouple is mentioned in two relevant ASTM standards (E220 and E235) and as such, recognized as adequate for elevated-temperature materials testing; and
- the price of the thermocouple, compared to other elevated-temperature-measurement options, was economical.

Furnace temperature measurements were made with type R thermocouples provided with the furnace. The thermocouples connect to an MTS model 409.83 temperature controller which uses three Eurotherm 2216 temperature control modules. The temperature control system and thermocouples were calibrated by the manufacturer.

Specimen temperature measurements were taken using type K thermocouple as noted above. The thermocouples were connected to three Omega model DRF-TC signal conditioners located in an environmental cabinet. An Omega CL3512A digital temperature calibrator was used to calibrate the signal conditioners and analog input channels.

As shown in Figure 3.21, the TC setup for elevated-temperature tensile testing consisted of TCs attached at three locations along the length of each coupon. One TC was placed near the middle of the reduced section, with the other two TCs placed just outside the reduced section: one above and one below.

Figure 3.21 Thermocouples placement on coupon

Several methods of attaching thermocouples to the steel coupons were evaluated through the trial-and-error process discussed in the next section. The method ultimately adopted is shown in Figure 3.22. It consists of thermocouple wire wrapped around the coupon, twisted several times to prevent slip, and covered in foil. The foil was bound to the coupon using spare thermocouple wire (not used for temperature measurement).

The method for twisting the thermocouple wire proved important for measurement accuracy. Multiple twists were required to prevent the thermocouple from slipping along the surface of the coupon during testing. Since the first twist would be the point at which temperature was measured, care was taken to ensure that this point was held in contact with the steel.
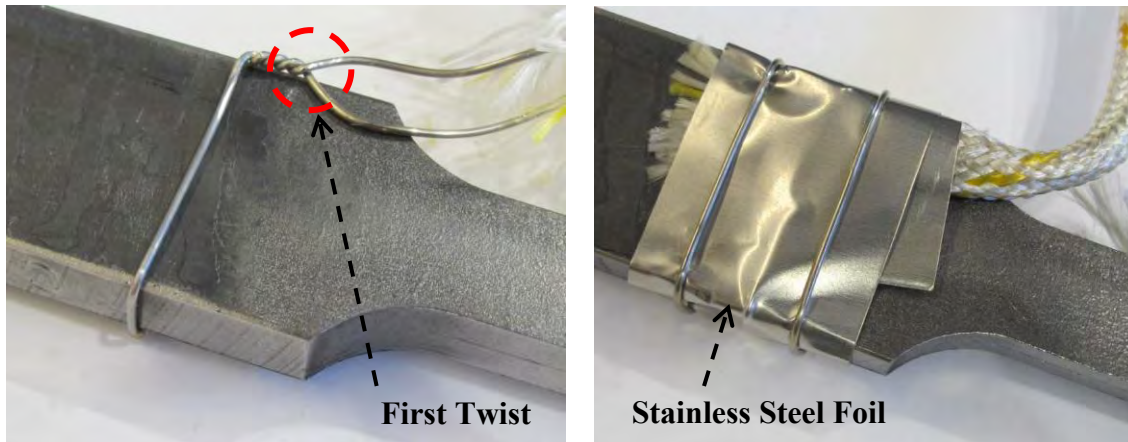
a) Before wrapping with SS foil   *b) After wrapping with SS foil*

Figure 3.22 Attachment of thermocouples to steel coupons

Providing shielding for the thermocouples also proved important. It was found that, covered in foil, the thermocouple could do a better job recording the coupon temperature independent of the effects of thermal radiation emanating from the furnace heating coils. As described in Section 3.2, the testing was steady state with respect to temperature. The heating coils would turn on and off during testing to maintain the target temperature, and as such, the amount of thermal radiation was controlled but not constant. The type of foil used was Type 321 stainless steel.

The width of the foil shielding used was approximately 1 inch for the outer thermocouples and ½ inch for the middle thermocouple. Less shielding foil was used for the middle thermocouple out of concern for interference with the strain measurement equipment during testing. The extensometer was placed to best capture necking, which might mean that the extension rods were placed nearby the foil shielding, as shown in Figure 3.23. Since the foil was not under load, if the rods were coming into contact with it, poor strain readings would result.

3.5.2 Goals of Temperature-Verification Testing

Pilot testing was conducted in order to verify that the techniques used to measure temperature were appropriate. This testing had two purposes:

34

- To verify the uniformity of specimen temperature, and

- To investigate the reliability of different thermocouple installation techniques.

| a) Shielding for middle thermocouple | b) Coupon at elevated temperature with extensometer shown |
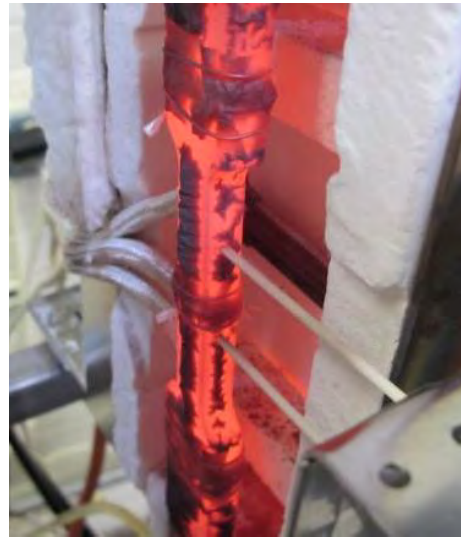
Figure 3.23 Potential interference of middle-thermocouple shielding and extensometer

3.5.2.1 Verification of Temperature Uniformity

There were two aspects to this investigation of temperature uniformity: the variation of surface temperature within the coupon reduced section and the variation of temperature between the surface and inside of coupon.

The variation of surface temperature within the reduced section was expected to be minimal. Through the furnace-balancing process described in Section 3.3.4, appropriate setpoints had been found for the three heating elements of the furnace such that the coupon temperature would be relatively uniform. This assumption was confirmed by placing thermocouples on the surface of the coupon, up and down the reduced section, and comparing the observed variation to the tolerance (2 to 5°C, Table 3.2).

Additionally, an attempt was made to investigate a potential temperature difference between the surface and the interior of the coupon. To this end, a hole was drilled into the coupon (Figure 3.24) so that a thermocouple could be placed inside the specimen. As the removal of one-sixth of the cross section would clearly affect the coupon properties, this sort of thermocouple installation could only be used during this pilot-testing stage.
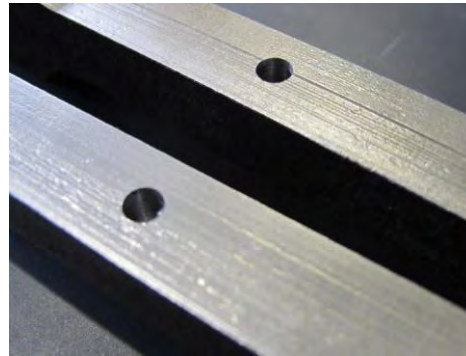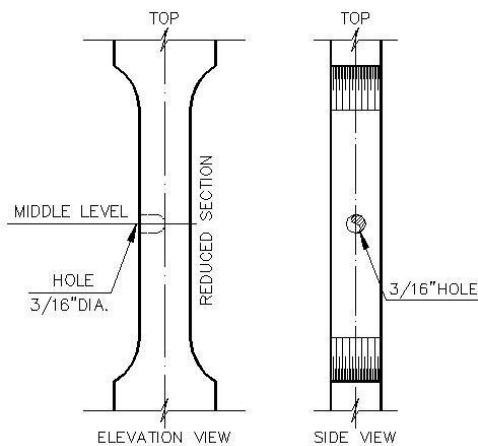
a) Hole location   b) Hole drilled into specimen
Figure 3.24 Drilled hole to measure interior temperature of coupon

3.5.2.2 Investigation of Different Thermocouple Installations

The process of determining which method of installing thermocouples yielded the most reliable and accurate measurements were trial and error. Experimentation was conducted on two different forms of the Type K thermocouple as well as different methods of shielding and attachment.

The two forms of thermocouple—wire and rod—used for this pilot testing are shown in Figure 3.25. The wire thermocouple consisted of two 20-gage conductors, protected by a braided fiberglass sheath. The thermocouple itself required some assembly at each installation: the two conductors needed to be twisted together to create measurement point. Quicker to install could be the preassembled, plug-in rod thermocouple. For this form of thermocouples, the tip only needed to be placed in contact

36

with the specimen: the electrical connection between the two conductors had already been made inside the probe. Protection of the conductors was provided, in this case, by an 1/8-inch stainless steel sheath.

a) Wire   b) Rod
Figure 3.25 Forms of Type K thermocouples

Two other variables were investigated: shielding and method of attachment. Shielding of the thermocouple by two methods was tried, using stainless steel foil and ceramic paste. Some thermocouples were deployed with no shielding to test its effect. In terms of methods of attachment, direct contact and welding were investigated.

3.5.3 Temperature Verification
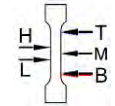
For temperature verification, multiple pilot tests were conducted. In these, the forms of and methods of shielding and attachment for the installed thermocouples were varied, as well as the location of the thermocouples. One thermocouple installation was kept consistent for all cases to serve as a point of reference. It should be noted that all thermocouples used in this research, even in preliminary testing stages, were Type K.

Testing was performed by heating an instrumented coupon up to a series of target temperatures. The coupon was held at each target temperature 40 minutes or longer, to ensure that steady state was reached.

For the purposes of this dissertation, a total of five case studies will be discussed. The thermocouple design for these case studies is presented in brief in Table 3.6. The

rows of this table shaded in blue correspond to the reference thermocouple: a foil-shielded wire thermocouple located just about midpoint.

Table 3.6 Summary of temperature-verification case studies

Case		TC Style		Shielding / Surroundings			Attachment	
		Wire	Rod	Foil	Ceramic	Hole	Contact	Weld
1	H	X		X			X	
	M		X	X			X	
			X			X	X	
	L	X					X	
2	H	X		X			X	
	M		X	X			X	
			X			X	X	
	L	X					X	
			X				X	
3	T	X		X			X	
	H	X		X			X	
	M		X			X	X	
	L	X		X			X	
	B	X		X			X	
4	T	X		X			X	
	H	X		X			X	
	M	X			X	X	X	
	L	X		X			X	
	B	X		X			X	
5	H	X		X				X
	H	X		X			X	
	M	X			X		X	
	L	X		X			X	

Shaded rows correspond to the reference thermocouple, the same for all cases.

38

A case-by-case analysis of the temperature verification studies outlined in the previous table will follow. Case 1 data is shown in Figure 3.26.
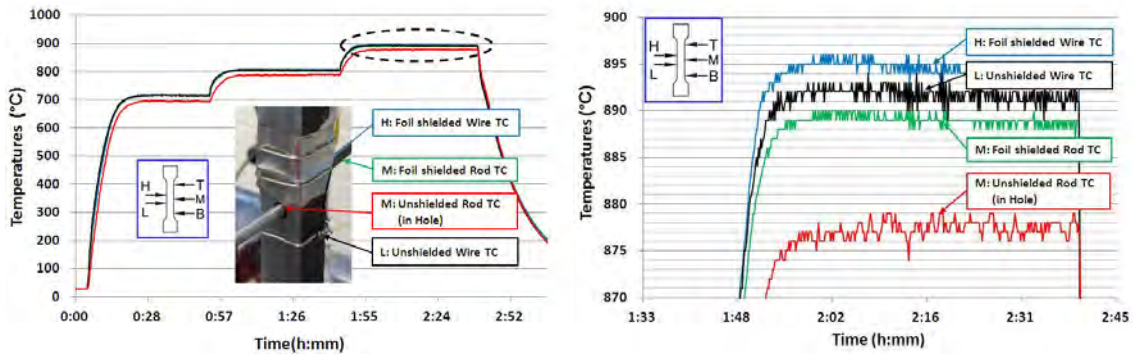
a) Test view and results   *b) Temperature profile at 900°C*

Figure 3.26 Temperature profile for Case 1

For Case 1, four thermocouples—two wire and two rod thermocouples—were installed within an inch of the coupon midpoint. Two of the thermocouples were shielded using foil, one was unshielded and the last was placed inside the drilled hole. Such is shown in Figure 3.26a, along with the temperature profile of the four thermocouples.

There were three temperatures at which the furnace was allowed to reach steady state: approximately 700, 800 and 900°C. Results shown in Figure 3.26b for ~900°C are typical for the other two temperatures. The two wire thermocouples and the rod thermocouple on the coupon surface all returned similar readings: within 2°C of the average of the three. The rod thermocouple placed in the hole gave a reading 15°C lower.
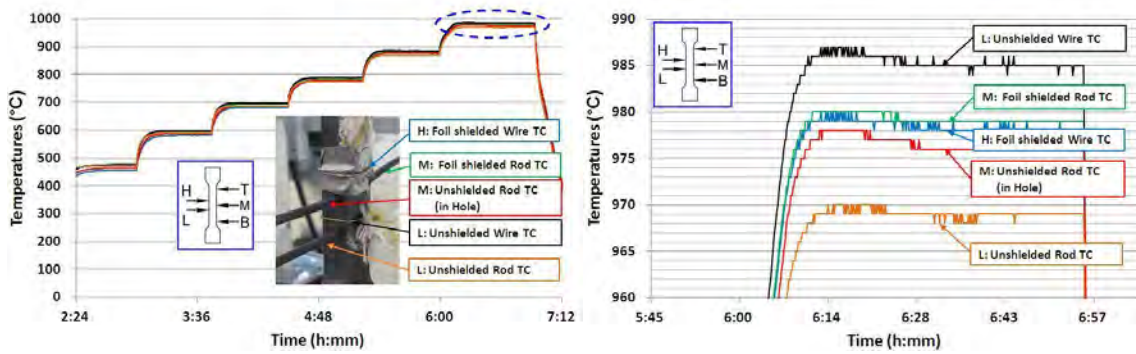
a) Test view and results   *b) Temperature profile at 1000°C*

Figure 3.27 Temperature profile for Case 2

Case 2 was designed to investigate the effect of foil shielding on rod thermocouple readings. For Case 1, a foil-shielded rod thermocouple (green) returned a surface reading effectively the same as the wire thermocouple readings. For Case 2, then, an additional, unshielded, rod thermocouple was used; all other thermocouples were kept the same and shown in Figure 3.27.

The results for Case 2 were very different from Case 1, but not illogically so. Again, three thermocouples returned very similar results, but in this case it was the two foil-shielded thermocouples (one wire and one rod) and the rod thermocouple in the drilled hole. The two unshielded, surface thermocouples produced results that were deviated 7–10°C from the others. This data supported the hypothesis that foil shielding could be used to minimize the difference in readings between thermocouples. The foil would protect the thermocouple from direct exposure to the thermal radiation from the heating coils, which would fluctuate as the coils were cycled on and off.

The rod thermocouple placed in the hole, kept the same between these two cases, returned markedly different results. Rather than being 15°C low, it was essentially the same as the reference thermocouple for Case 2. The effort to match a temperature measurement from inside the specimen to one made on the surface was proving difficult to execute.

40

a) Test view and results   *b) Temperature profile at 600°C*
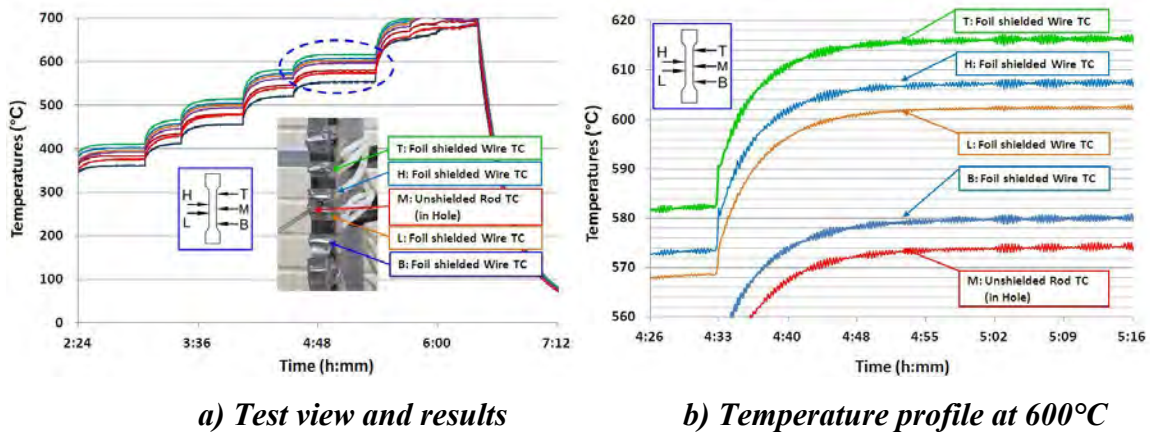
Figure 3.28 Temperature profile for Case 3

Given the demonstrated importance of foil shielding in Case 2, foil-shielded wire thermocouples were chosen for Case 3 shown in Figure 3.28. Placed top to bottom covering the reduced section, the thermocouples were used to investigate temperature uniformity.

Compared to previous testing, the deviation between thermocouples was unsatisfactory: readings differed by 45°C between the most extreme. However, some observations can still be made. The lowest reading, like in Case 1, was for the unshielded rod thermocouple placed in the drilled hole. Alternatively, this reading being the lowest could be used as further support of the argument presented on the necessity of shielding, or as further demonstration that the effort to compare inside and surface temperatures was ineffectual.

Though the 2-3°C tolerance at 600°C was exceeded, the readings for the wire thermocouples at the top (*T*) and middle (*H* and *L*) positions were more tightly grouped than the others. Examining only the surface thermocouples, there seems to have been a significant temperature gradient present, with the bottom of the specimen being the coolest and the top the hottest. Since heat rises, this observation suggests the setpoints for the furnace heating elements required slight adjustment. Such was done before the next case, with success.

41

a) Test view and results   *b) Temperature profile at 1000°C*
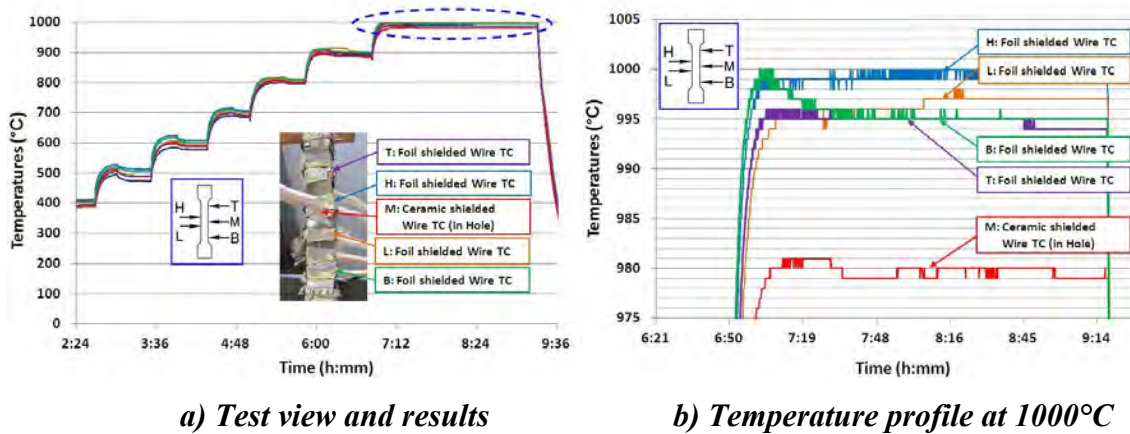
Figure 3.29 Temperature profile for Case 4

The intent of Case 4 shown in Figure 3.29 was similar to the previous case, but was better executed. At 1000°C, all surface thermocouples read within tolerance for tension testing (5°C). The foil-shielded wire thermocouple was thus shown satisfactory, though another test would be conducted to verify that the temperature-uniformity problems experienced in Case 3 had truly been resolved.

A different sort of thermocouple was used for the drilled hole in Case 4. Rather than a rod thermocouple, which may have had issues consistently contacting the interior surface of the hole, a wire thermocouple was used. Thermally conductive ceramic paste was used to fill the hole, both serving as shielding and allowing the much smaller wire thermocouple to be placed in a hole drilled for the larger rod. Despite the change in thermocouple installation, the results were similar to Case 1 and 3: the thermocouple in the hole registered a low temperature compared to the surface thermocouples.

42

a) Test view and results   *b) Temperature profile at 1000°C*
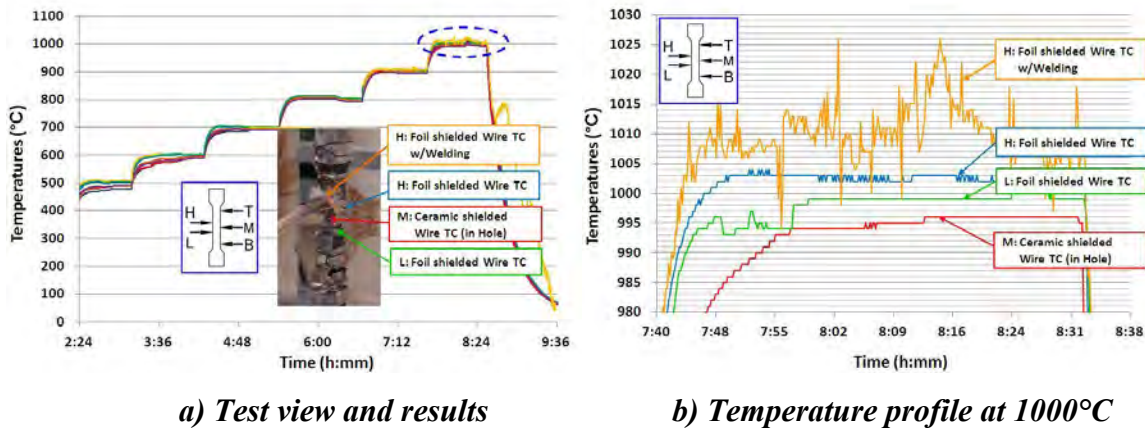
Figure 3.30 Temperature profile for Case 5

For Case 5, an additional option was investigated, and subsequently abandoned: welded thermocouples were shown in Figure 3.30. The data from the welded thermocouple was erratic, indicating a probable incompatibility between the weld material and the thermocouple metals.

The two foil-shielded wire thermocouples again were demonstrated to read the same result within tolerance. Given the success of this installation, it was chosen for deployment throughout all subsequent testing.

Based on the review of temperature profile analysis, wire and rod thermocouples with foil shielding provided the most consistent temperature readings. Therefore, wire thermocouples with foil shielding were used throughout the remainder of the test program.

3.6   STRAIN MEASUREMENT

For this research, strain was measured using extensometers mounted on or placed in contact with the steel coupons. At elevated temperatures, the performance requirements for these extensometers are demanding. As such, a pilot program was undertaken to better evaluate the ability of each extensometer to deliver an accurate and precise strain measurement in real time without data loss. Data from the extensometers

were compared with elongation at failure, measured directly from punch marks using calipers.

3.6.1 Description of Strain-Measurement Devices

Figure 3.31 are shown the three extensometers used. Each was used for a different application, and the properties of each will be described in turn.
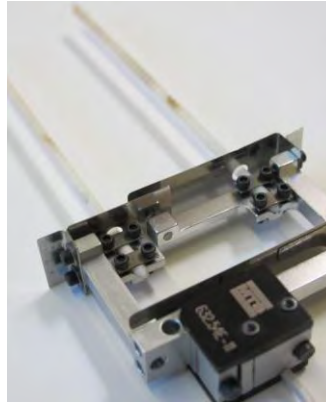
a) 2-inch extensometer   *b) 1-inch extensometer*   *c) 2-inch extensometer*
for room temperature   *for elevated temperature*   *for elevated temperature*
(Section 3.6.1.1)   *(Section 3.6.1.2)*
Figure 3.31 Three extensometers used in research

3.6.1.1 Extensometer for Room-Temperature Testing (2SS)

For tension testing conducted at room temperature, a MTS 634.25E-24 extensometer (Table 3.7 and Figure 3.32 2SS extensometer (room temperature)) was used. This extensometer was of a fairly common design: it had a 2-inch gauge length and would mount to a specimen using spring-loaded clips. The extensometer, when mounted on a coupon, could be said to be "self-standing." The designation chosen for the device was 2SS. Specifications for the 2SS extensometer are listed below. Especially important here is the 50% tensile strain limit, which can be compared to the room-temperature elongation at failure for A992 steel of ~40%. No resetting of the extensometer was therefore required during testing to capture the entire stress-strain curve.

44

Table 3.7 Specifications for 2SS extensometer

Model	Gauge Length (in)	Maximum Travel (in)	Maximum Strain (%)	Temperature Range (°C)	Activation Force (g)
634.25E-24	2.00	-0.20 – 1.00	-10 – 50	-85 – 120	30

Figure 3.32 2SS extensometer (room temperature)

3.6.1.2 Extensometers for Elevated Temperatures (1PS and 2PS)

Two extensometers with different gauge lengths by different manufacturers were used to measure strain at elevated temperatures. These extensometers differed in style from the self-standing extensometer used for room-temperature testing in several ways. First, rather than mounting to the specimen at the extensometer contact points, they were supported externally. Strain was measured over the gauge length defined by two stiff, ceramic rods extending from the instrument body. These extension rods were held in contact with the specimen with a spring-loaded hold-down system (part of the fixture). Because this spring-loaded system applied positive pressure against the specimen, these extensometers were designated "PS" extensometers: the initials for "pressure-standing."

Particular to their design for elevated-temperature usage were two aspects: the heat shield on the specimen-side of the extensometer and the compressed-air cooling system. Both elevated-temperature extensometers were rated for use up to 1200°C.

The primary extensometer used at elevated temperatures was an MTS 632.54E-11 with a 1 inch gauge length (Table 3.8 and Figure 3.33). By design, this extensometer sacrificed some degree of usability for accuracy: it was only capable of measuring tensile strains up to 10%. The failure strain from every tensile test, regardless of temperature, was larger than this strain limit. As such, it was necessary to reset the 1PS extensometer multiple times during the testing, and connect the strain data after the test to produce a complete stress-strain curve. The resetting and reconnection process is described later in Section 3.7.

The contact force between the ceramic rods and the specimen was provided by the spring-loaded hold-down system mentioned previously. It was possible to adjust the spring in this system to vary the contact force. Because there was no load cell as part of the system, achieving the specified contact force was a matter of trial and error. With too little contact force, the extension rods would slide relative to the specimen; too much force and the strain data would come out jittery.

Table 3.8 Specifications for 1PS extensometer

Model	Gauge Length (in)	Maximum Travel (in)	Maximum Strain (%)	Temperature Range (°C)	Contact Force/rod (g)
632.54E-11	1.00	-0.05 – 0.10	-5 – 10	up to 1200	100
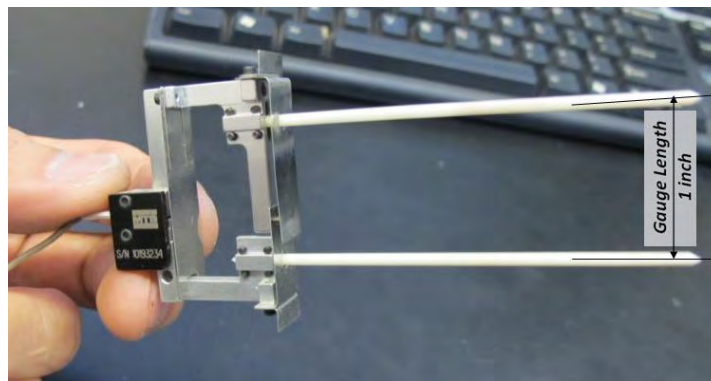
Figure 3.33 1PS extensometer (elevated temperature)

A 2-inch extensometer (2PS) was used as a supplemental extensometer for tension testing at elevated temperatures. Less accurate than the 1PS extensometer, it had a much wider measurement range: up to 50% tensile strain. At most temperatures, the steel failed before the 2PS extensometer had to be reset. As such, the 2PS extensometer provided continuous strain data for the periods of time during which the 1PS was being reset.

Table 3.9 Specification of Epsilon E3548-0200-050-ST

Model	Gauge Length (in)	Maximum Travel (in)	Maximum Strain (%)	Temperature Range (°C)	Contact Force/rod (g)
E3548	2.00	-0.4 – 0.40	-25 – 50	20 – 1200	500
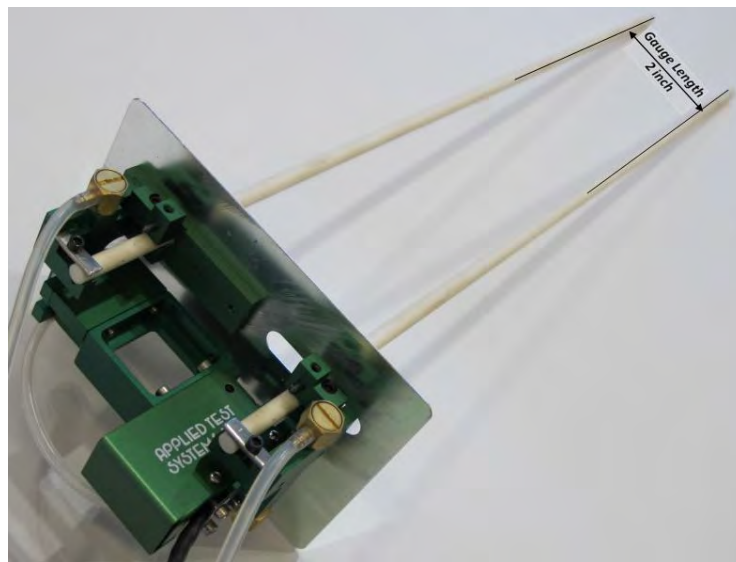
Figure 3.34 2PS extensometer (elevated temperature)

By design, the pressure-standing extensometers were supported by the spring-induced pressure, the reaction of which was provided by the test specimen. At the time the specimen failed, however, the reaction would be suddenly removed. To provide additional security against the extensometers falling or being otherwise damaged by the sudden movement that might be transmitted via the extensometer rods, a string was used

to provide backup vertical support, as shown in Figure 3.35. The spring-loaded system providing horizontal support is also shown in this figure.
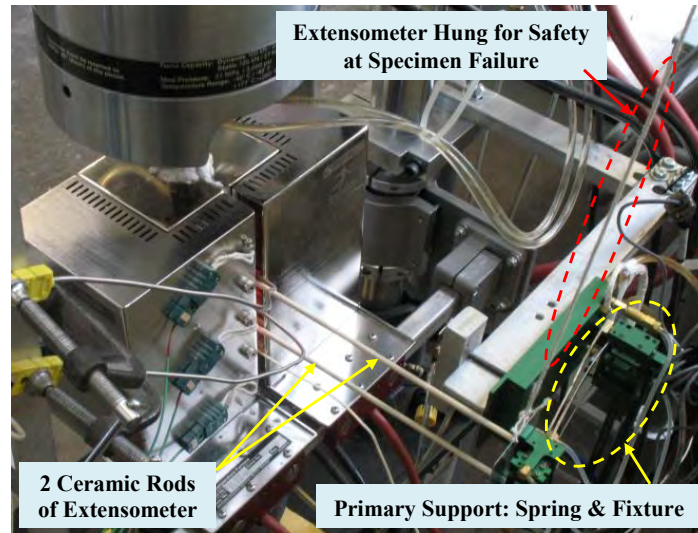
Figure 3.35 Extensometer support system

3.6.1.3 Calipers for Elongation at Failure

As discussed in Section 3.4.2.5, punch marks were made on each coupon for a post-test validation of the failure strain measured by the extensometers. The distances between the various punch marks were measured both before (Figure 3.36) and after (Figure 3.37) the test. The caliper strain measured between the two punch marks that best encompassed the necking zone was compared to the extensometer readings.
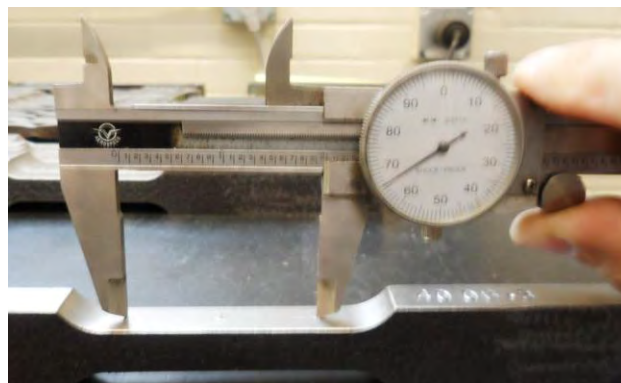
Figure 3.36 Measuring distance between punch marks, before testing

Figure 3.37 Coupons after failure requiring measurement of failure elongation

3.6.2 Operational Considerations for Extensometers

Testing at elevated temperatures is less forgiving than at room temperatures. A number of factors were found to matter considerably in terms of the quality of the strain data that would be produced. This was especially true for the 1PS extensometer, whose light weight left it very sensitive to vibration coming from various sources. Unless controlled, this vibration would lead to oscillations in the strain data that were quite noticeable.

Among the considerations required for good operation are the following, which will be discussed in turn:

1. Frequent calibration
2. Proper positioning of extensometer
3. Good contact with the specimen
4. Modifications to cooling system
5. Quick reset of the extensometer

3.6.2.1 Frequent calibration

Prior to each test series (e.g. tension at elevated temperature), calibration was performed on each extensometer to be used for those tests. While the manufacturers of the extensometers did provide calibration data, those values represented the instruments

when they had left the factory. It was possible—with time, use and different environmental conditions—for the value for output sensitivity to shift slightly.

The method adopted for calibration was through comparison with strain-gauge data. A total of four strain gauges were mounted on a coupon: one on each side to compensate for unintentional loading eccentricity. The calibration coupon loaded at room temperature, strain data would be recorded for both the strain gauges and the extensometer being calibrated.

Given the specifications of the cyanoacrylate adhesive used to bond the strain gauges to the calibration coupon, testing could only be carried out to 5% strain before de-bonding was expected to occur. It was thus impossible to calibrate the extensometers for their full strain range. However, it should be noted that the calibration range was large enough to encompass the regions of the stress-strain curve in which most of the mechanical properties of interest are defined, e.g. elastic modulus, proportional limit, yield strength.

3.6.2.2 *Proper Positioning of Extensometer*

To achieve good axial strain readings, it was necessary to properly align the extensometer with the centerline of the specimen. If the extensometer were to be skewed, it would measure less strain than truly occurred, by a factor of the cosine of the angle of misalignment as shown in Figure 3.38.
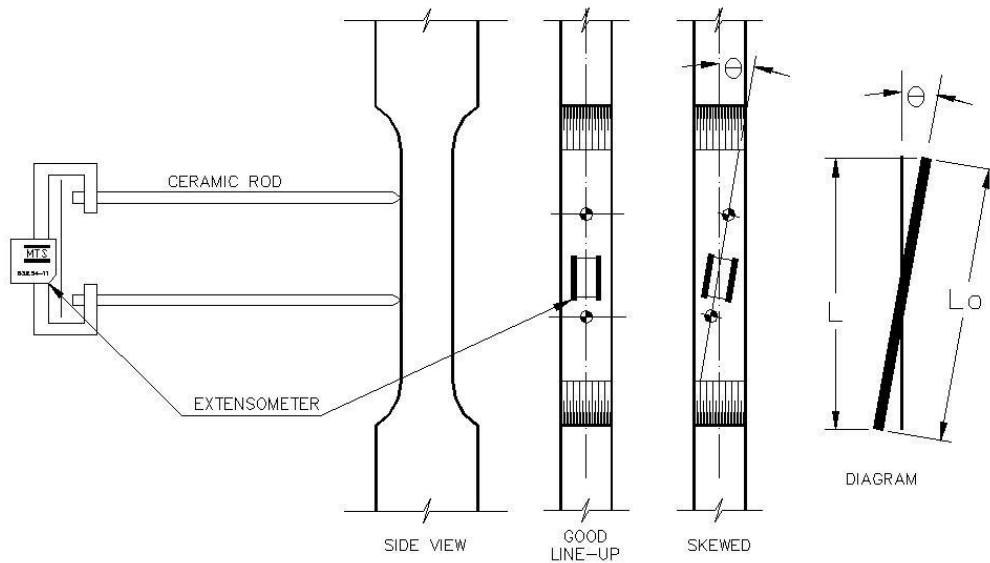
Figure 3.38 Furnace launched with Epsilon 2 inches extensometer

In addition to angular alignment, the vertical position of the extensometer would matter after initiation of necking. Before necking, strain was uniform over the length of the coupon's reduced section; after, concentrated in the necking zone. Necking could occur anywhere within the length of the reduction section. It was very possible to position the 1PS extensometer gauge length such that, at 40% of the reduced section length, the extensometer missed necking.

If the extensometer missed the necking zone during part of the test, it was often evident in the character of the stress-strain curve, e.g. Figure 3.39. When the necking zone was missed, after reaching the peak stress, the stress-strain curve would curl downward (red). If, then, the extensometer were reset and this time placed properly to capture necking, the apparent strain rate would increase again (blue).
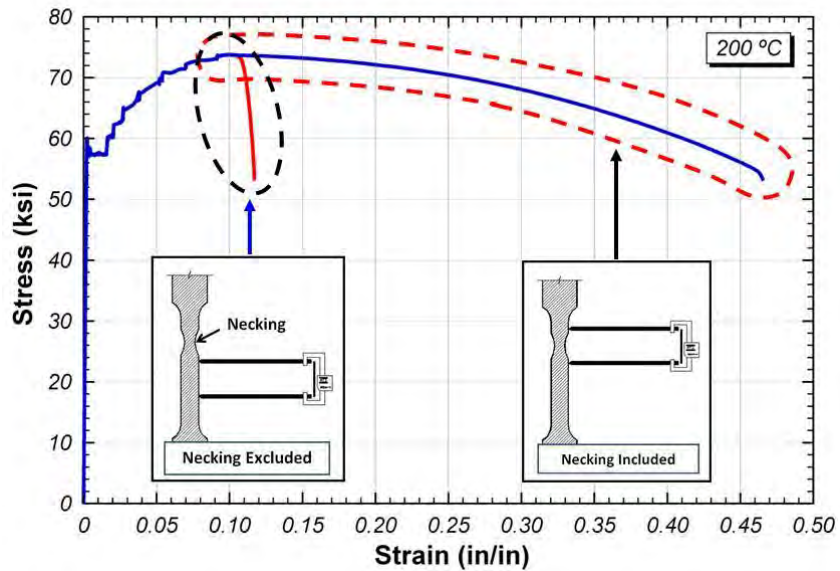
Figure 3.39 Effect of extensometer placement on tension test results (200°C)

While generally the 1PS extensometer was reset when it was approaching its strain limit of 10%, it occasionally was necessary to reset it solely to relocate it so that necking would be captured properly. To locate the necking zone, continuous visual observation was necessary. Visual observation was performed through the small gap between the two furnace halves left open for extensometer access. Most of the gap was filled with an insulating material to limit heat loss, but a small window was kept open, as shown in Figure 3.40. If necking was found to be occurring outside the range of the extensometer, the instrument was promptly relocated.

52
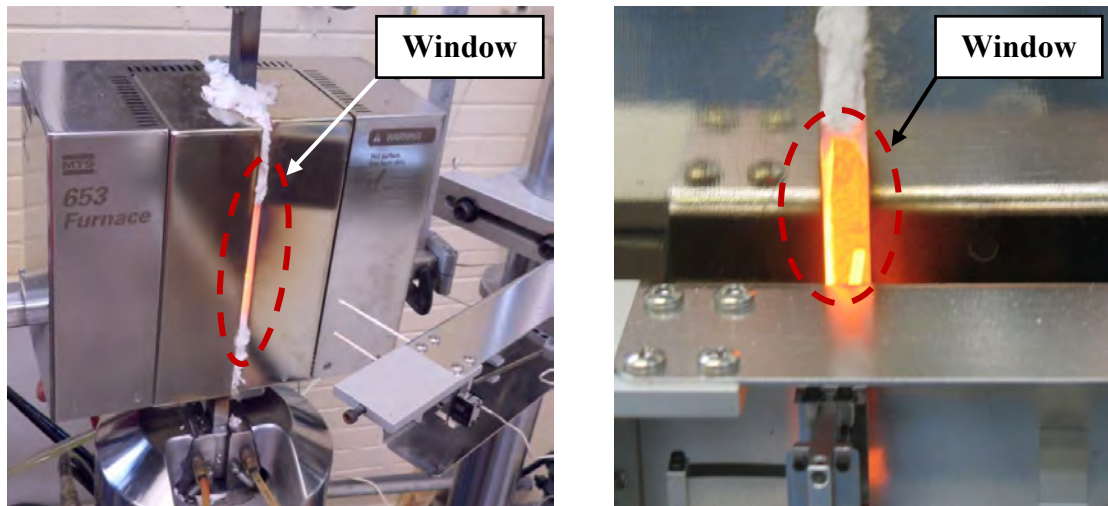
a) Gap left between furnace halves *b) Specimen through window*

Figure 3.40 Window between furnace halves through which necking was observed

It should be noted that locating the necking zone visually was difficult, especially at its beginning, before substantial necking had occurred. The window between the furnace halves was kept small to minimize heat loss and improve furnace control.

Additionally the process of relocating the extensometer to the necking location was challenging due to time pressure. A quicker reset of the extensometer is decreased strain data loss. While lost data was corrected for after the test—assuming that, considering the time immediately before and immediately after the extensometer reset, the average strain rate prevailed during the resetting process—the less time the extensometer was not recording data, the more accurate the test.

Knowing the location of necking prior to the test was impossible, but it was found that review of the coupon dimensions could be helpful. Precise measurements of as-built coupon dimensions were made at the top, middle and bottom of the reduced section. A location with a marginally smaller cross-sectional area would experience marginally higher stresses; necking would be more likely to occur there. While coupons were made through precision machining, this process still had tolerances.

3.6.2.3 Good contact with the specimen

Achieving good contact between the pressure-standing extensometers and the specimen throughout testing depended on three factors:

- selection of chisel shape for extension-rod tip
- maintenance of chisel tips through removal of scale
- provision of sufficient contact force

The last of these was accomplished through trial-and-error adjustment of the horizontal spring support system, and was discussed in detail in Section 3.6.1.2.

As for chisel shape, the three alternatives available from the manufacturers are shown in Figure 3.41. Both the straight chisel and the conical chisel may be appropriate for flat-surfaced specimens, but the straight chisel was selected due to its increased contact area with the specimen. The greater contact area, the less likely the slip.
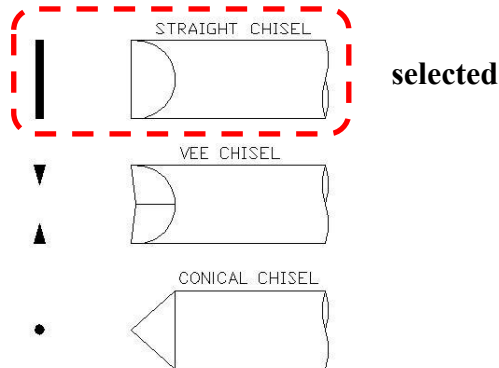
Figure 3.41 Options for chisel shape with corresponding contact area

It was found that the chisel tips needed to be maintained between tests done at high temperatures. At temperatures in excess of 500°C, the surface of A992 steel would start to scale. The scale particles would grow in size and thickness with increasing temperature, starting to delaminate at 900°C. At the point of delamination, the scale would stick to the extension rods (Figure 3.42). If, after coupon failure, an attempt were made to remove the extensometer immediately, the extension rods could break, being so

54

firmly stuck to the specimen. Through allowing the coupon to cool fully and then pulling the extensometer off slowly, fewer rods were broken.
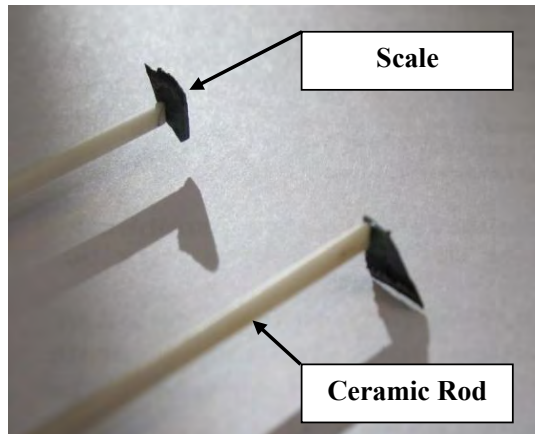
Figure 3.42 Scale on rod tip after testing at elevated temperatures

If scale was attached to the chisel tips at the end of one test, it would be removed before the next test using a blunt object (flathead screwdriver). The straight chisel shape would be restored to the rod using a diamond grinder and a fine metal file.

3.6.2.4 *Modifications to Cooling System*

As mentioned previously, the two pressure-standing extensometers were outfitted with cooling systems. These consisted of an intake for compressed air, the expansion of which was to cool the instrument.

It was found that, while satisfactorily protecting the instrument from damage, this cooling system adversely affected the strain data in the initial portion of the stress-strain curve. As shown in Figure 3.43, shaking was seen in the strain data. Condensation was observed on the surface of the extensometer, so it was hypothesized that this shaking was due to the presence of moisture in the available compressed-air lines. As the air expanded, water droplets would form and subsequently hit the extensometer at high velocity. With the low weight of the 1PS extensometer, the water droplets could be enough to impact the data in this way. This hypothesis was confirmed in part by the observation that shaking worsened in the summer months, in which the humidity was typically higher.

A solution to this problem was found by changing cooling methods to the fan shown in Figure 3.44. The fan proved satisfactory in terms of heat abatement, and as shown in Figure 3.43b, eliminated the problem with shaking. It should be mentioned that experimentation was required to set the distance of the fan from the extensometer. When the fan was placed very close to the extensometer body, a similar shaking behavior was observed, though it was lesser in extent that that shown for the compressed-air system.
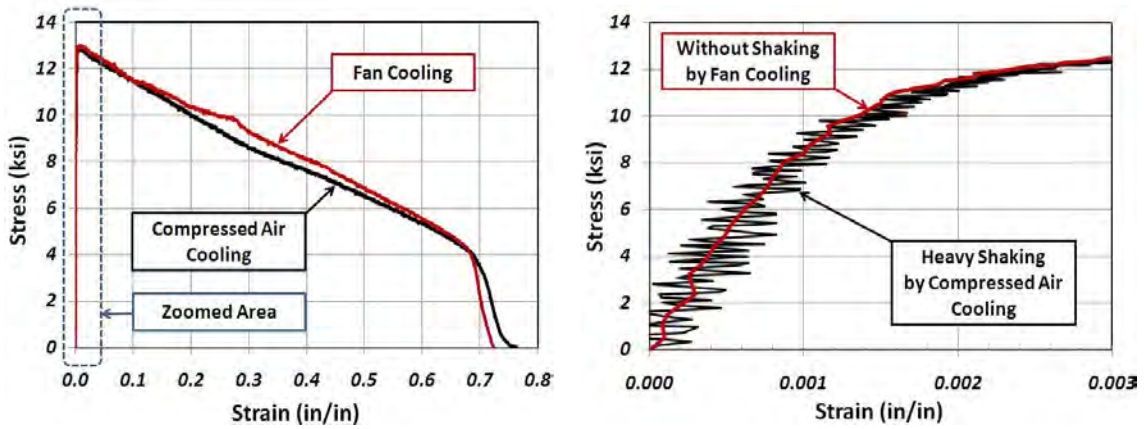
a) Full stress-strain curve   *b) Curve at elastic region*
Figure 3.43 Shaking phenomenon due to cooling system (tension test, 700°C)
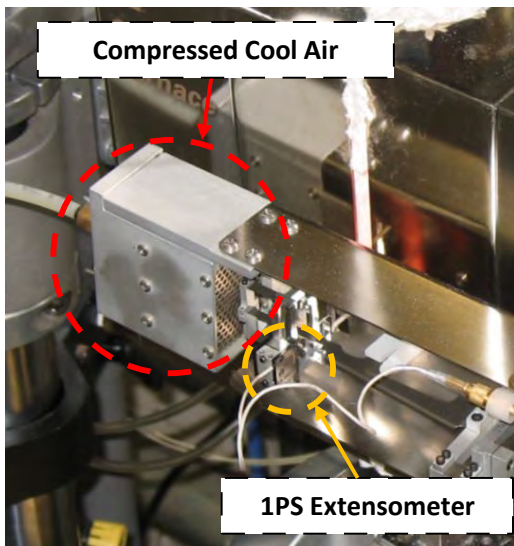
a) Expansion of compressed air   *b) Fan-cooling*
Figure 3.44 Before and after change to cooling system
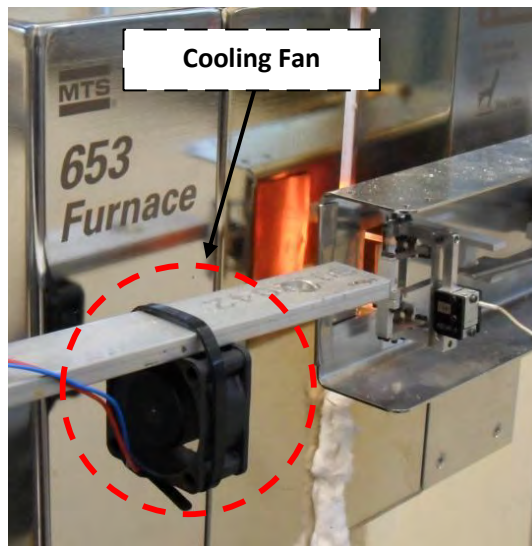
3.6.2.5 Quick Reset of the Extensometer

As mentioned in the description of the 1PS extensometer, its limited strain range of 10% meant that it had to be reset several times during each tension test. With practice, the extensometer was able to be reset as fast as 10 seconds, although closer to 60 seconds was more typical. The strain "lost" during the resetting time was compensated for after the test, with the assumption of a consistent strain rate before and after reset.

After being reset, the resulting raw stress-strain curve would look like that shown in Figure 3.45. Detailed information on the process to generate a smooth stress-strain curve from this discontinuous data is given in Section 3.7.
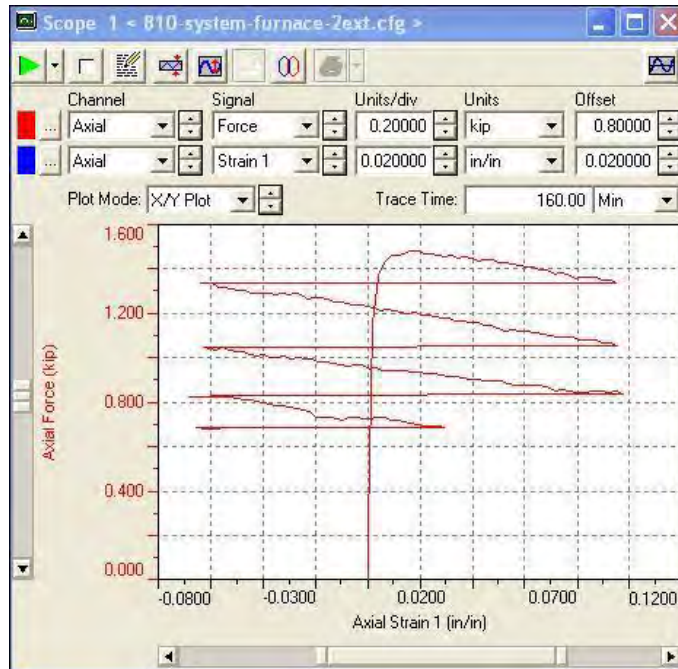
Figure 3.45 Captured screen of tensile test at 700°C with several extensometer resets

3.6.3 Extensometer Verification

The validation and verification of the extensometers for room- and elevated-temperature use were performed by comparison of axial strain data from different devices. The extensometers were compared to each other, and also tested against foil strain gauges

(SGs). The following Table 3.10 outlines the different verification tests performed; the results of each will be discussed in the upcoming sections.

Table 3.10 Test plan for extensometer verification

Case	Case 1	Case 2	Case 3	Case 4
Extensometer Type	1PS-2SS	2PS-2SS	1PS-2SS-SG	1PS-2PS
Temperatures	20°C	20°C	20°C	20°C / 700°C

3.6.3.1 Case 1: 2SS and 1PS at room temperature

The first extensometer-verification test was performed with the 1PS and 2SS extensometers at room temperature. As shown in Figure 3.46, these extensometers were mounted to a test coupon, which was subsequently loaded up to 10% strain while strain data for each extensometer was recorded. While the test could have been taken to failure, that would require multiple resets of the 1PS extensometer. The strain data for the 1PS could be corrected for resetting, but testing to its strain limit seemed more appropriate for validation testing: differences in readings would be definitively due to differences in the extensometers rather than assumptions of the extensometer reset–compensation process.

2" Self-Standing (2SS)   **1" Pressure-Standing (1PS)**
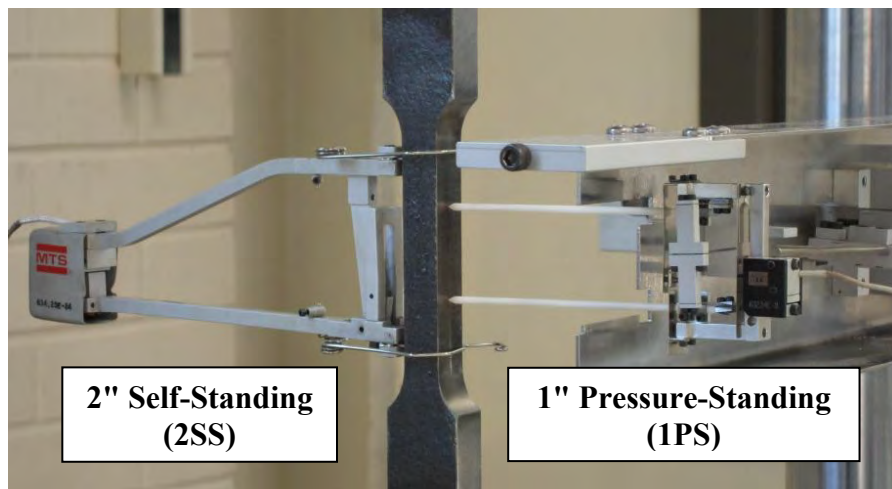
Figure 3.46 Case 1: 2SS and 1PS at room temperature

The results of the testing are shown in Figure 3.47. It was desired that a data comparison be completed for both elastic and inelastic behavior.
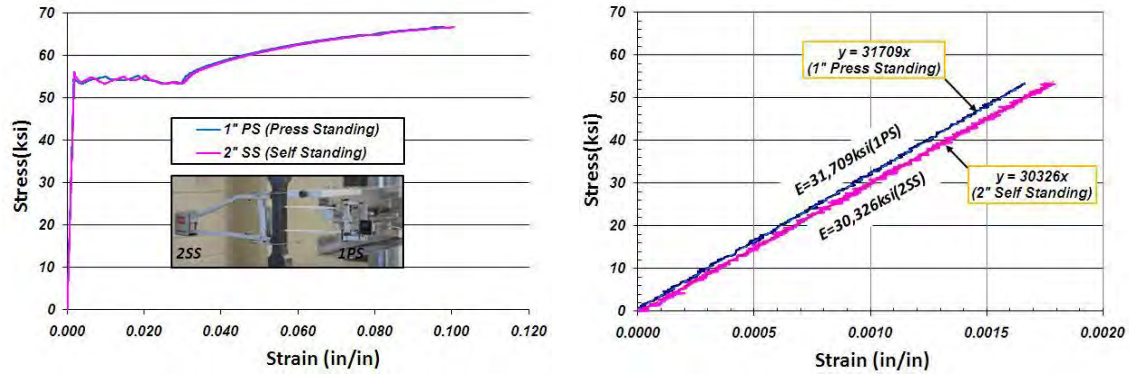
a) Stress-strain curve to 10% strain   *b) Elastic Response*
Figure 3.47 Stress strain of 2SS and 1PS at room temperature

In terms of the inelastic behavior, Figure 3.47a shows that very close correspondence between the two extensometers. A slight difference in elastic modulus is shown in Figure 3.47b, however. In both cases, the measured elastic modulus was similar to common values measured for A992 steel: 29,000 to 30,000 ksi. A slight angular misalignment of the extensometers could account for the fact that both measured values exceed 30,000. In Table 3.11, the elastic-zone accuracy of the two extensometers is given as a ratio of the measured elastic modulus to the reference value of 29,000 ksi.

Table 3.11 Elastic modulus of Case 1 at room temperature

Measurement	1PS	2SS
Elastic Modulus (ksi)	31,379	30,326
Modulus Ratio to 29,000 ksi	1.093	1.046

3.6.3.2 Case 2: 2SS and 2PS at room temperature

For Case 2, the 2SS extensometer was used again, compared this time to the results of the other elevated-temperature extensometer, the 2PS. The test setup is shown in Figure 3.48. In this case, since resetting of the extensometers was not an issue, testing was carried out to failure.

59
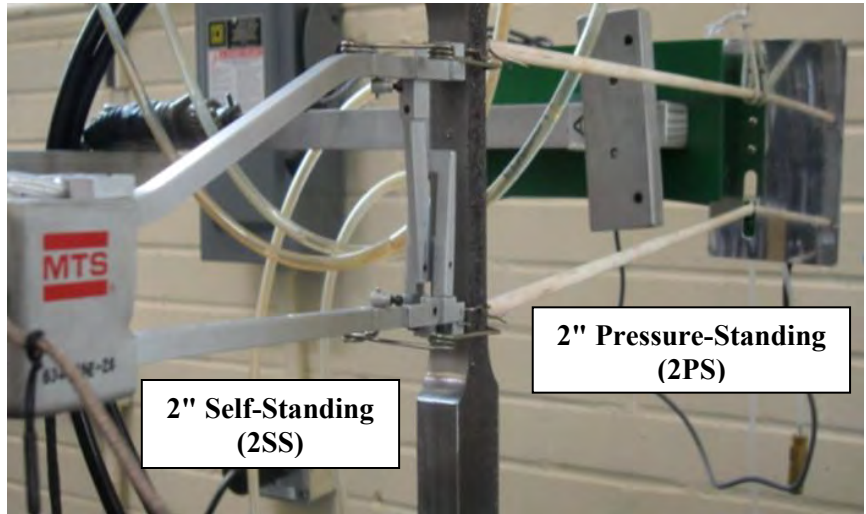
Figure 3.48 Case 1: 2SS and 2PS at room temperature

The pattern of the overall stress-strain data is the same as that found in Case 1: the two extensometers have good correspondence in the inelastic range. The failure strain for the 2SS (0.424 inch) was almost exactly that measured by calipers (0.427 inch, using the method described in Section 3.6.1.3), but the failure strain measured by the 2SS was within 5% of this value.

A marked difference can be seen between the two extensometer readings in the elastic zone. The 2SS again gave a reasonable value for the elastic modulus, but the 2PS data suggested an elastic modulus roughly half the standard value.
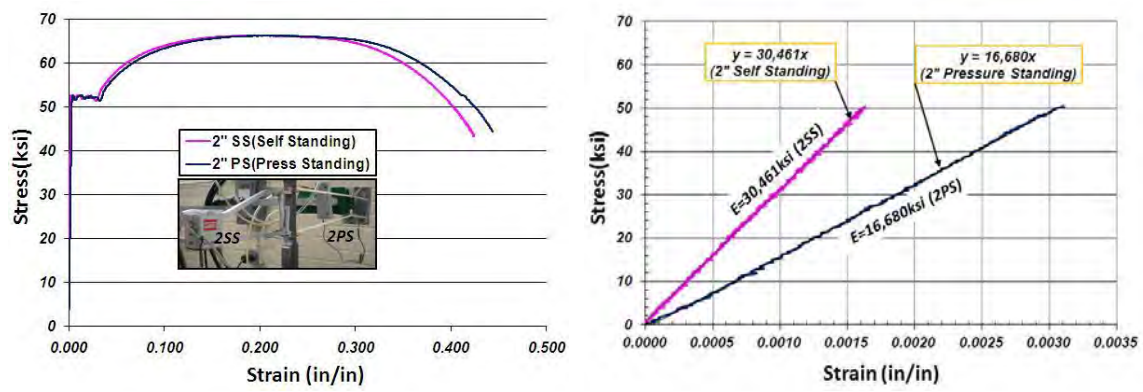
a) Overall stress-strain curve   *b) Elastic modulus*

Figure 3.49 Stress strain of 2SS and 2PS at room temperature

60

At first, it appeared like the instrument gauge factor was improperly entered for the 2PS, off by a factor of two. Though it was verified to be correct, the reader should be reminded that any parameter affecting the elastic behavior would also influence the inelastic behavior. Halving the failure strain shown in Figure 3.49a would cause a greater error in the full stress-strain curve. A better explanation was that, with its large measurement range and high contact force, the 2PS extensometer was ill-equipped to measure such small strains.

Case 2, summed up in Table 3.12, further substantiated the accuracy of the 2SS extensometer, while returning mixed results for the 2PS. It appeared to be accurate in the inelastic range, but inaccurate for measurements of elastic behavior.

Table 3.12 Elastic modulus and failure strains for Case 2 at room temperature

Measurement	2PS	2SS
Elastic Modulus (ksi)	16,680	30,461
Modulus Ratio to 29,000 ksi	0.575	1.050
Failure Strain (in/in)	0.443754	0.423840
Strain Ratio to 0.42740 in. (caliper measurement)	1.038	0.992

3.6.3.3 Case 3: 1PS, 2SS and SG at room temperature

As further verification that the 2PS extensometer in Case 2 truly did greatly overestimate the elastic-zone strains, a repeat of Case 1 was performed. This time, however, foil strain gauges were deployed to independently evaluate the accuracy of the 2SS and 1PS extensometers (Figure 3.50).

Foil strain gauges were installed according to the manufacturer's specifications, which consisted of preparing the surface mechanically and chemically before adhering the gauges to the surface. Gauges were installed on all four sides of the reduced section to correct for accidental eccentricity.
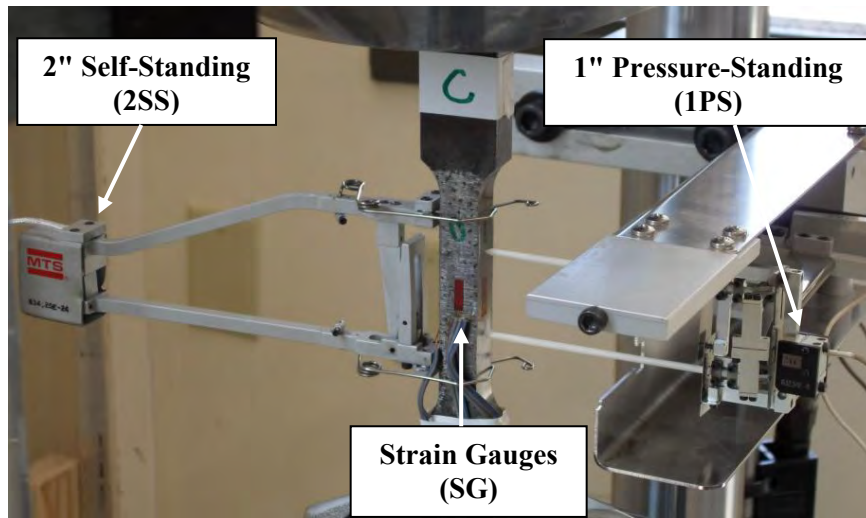
Figure 3.50 Case 3: 1PS and 2SS extensometer, with strain gauges

Due to the strain limits on the strain-gauge adhesive used, the extent of testing for Case 3 was 5% strain. To better study the elastic response, the coupon was loaded to 1%, unloaded and then reloaded to the final strain value. Results from this testing are shown in Figure 3.51.
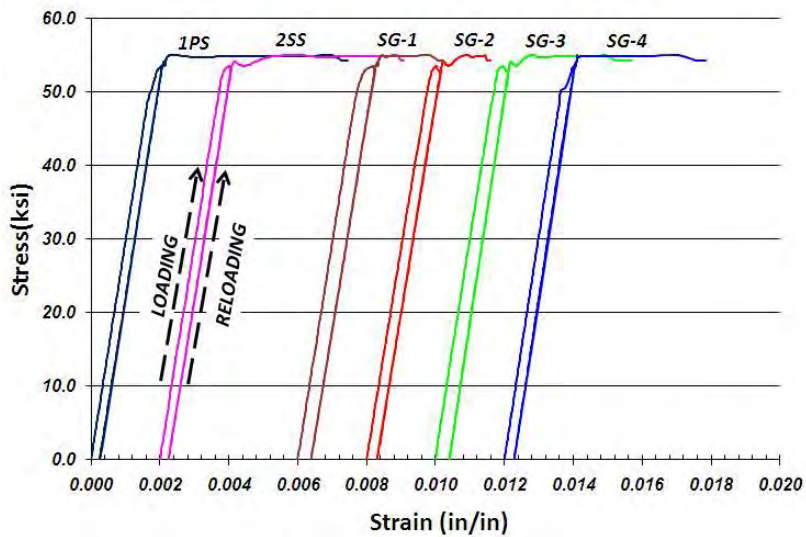
a) Stress-strain curves when loading and reloading

b) Elastic modulus during loading   *c) Elastic modulus during reloading*
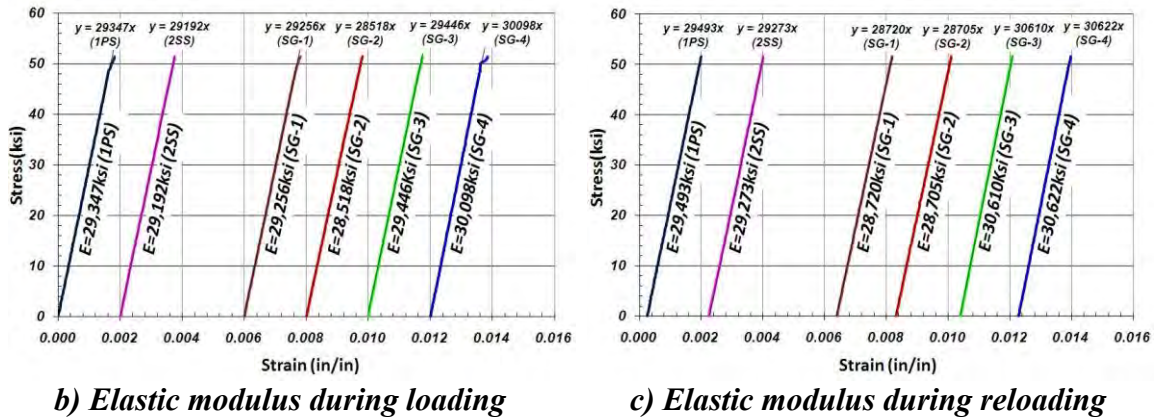
Figure 3.51 2SS, 1PS and SG at room temperature

The findings for the elastic moduli measured during loading and reloading are shown in Table 3.13. During loading, the results from the extensometers and the strain gauges were remarkably similar: 1PS, 2SS and the average of the strain gauges returned values 0.5% of each other. The difference was a little greater for the reloading condition, but still all were within 1.5%.

Table 3.13 Elastic modulus of Case 3 at room temperature

Measure-ment	Condition	Extensometers		Strain Gauges				
		1PS	2SS	1	2	3	4	avg
Elastic Modulus (ksi)	Loading	29,347	29,192	29,256	28,518	29,446	30,098	29,330
	Reloading	29,493	29,273	28,720	28,705	30,610	30,622	29,664
Modulus Ratio to 29,000ksi	Loading	1.012	1.007	1.009	0.983	1.015	1.038	1.011
	Reloading	1.017	1.009	0.990	0.990	1.056	1.056	1.023

As shown in Figure 3.52, for both the loading and unloading conditions, the elastic moduli for the 1PS and 2SS extensometers were within the standard range of values. (While individual strain gauges were outside this range, the average of the four was within it.) Case 3 thus served as validation of the elastic-zone strain data produced by both the 1PS and 2SS at room temperature.
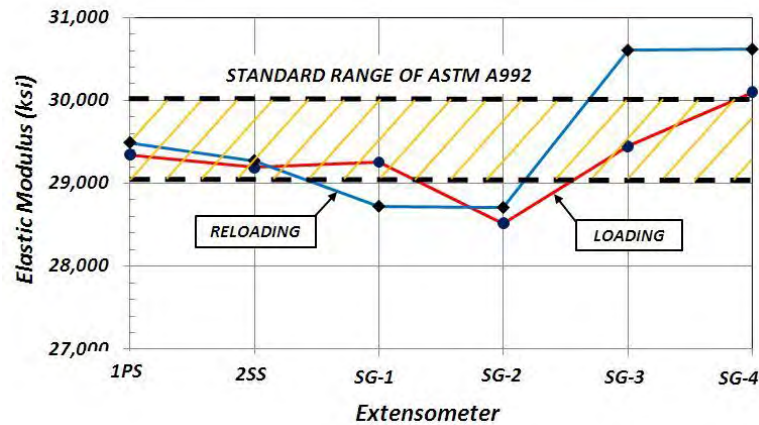
Figure 3.52 Elastic modulus summary graph of 1PS, 2SS and SG

3.6.3.4   Case 4: 1PS and 2PS at elevated temperature

While the 2SS extensometer was demonstrated accurate through the results of the previous three cases, its design prevented it from being used at elevated temperatures. Since validation at elevated temperature was desired, for Case 4, the 1PS and 2PS extensometers were used (Figure 3.53).

While Case 2 results threw into question the accuracy of the 2PS extensometer for measuring the small strains necessary to find elastic properties, they also supported the idea that it was suitable to measure inelastic strains, e.g. to failure. The use of 2PS concurrently with the 1PS extensometer during testing would, then, serve the purpose of independently verifying the failure strains, and more generally, all strains significantly beyond the elastic zone.

Two tests were performed: the first at room temperature, and the second at the elevated temperature of 700°C. For the elevated-temperature testing, the coupon was heated for an hour to allow it to achieve thermal equilibrium. During this time, it was allowed to expand freely.

64
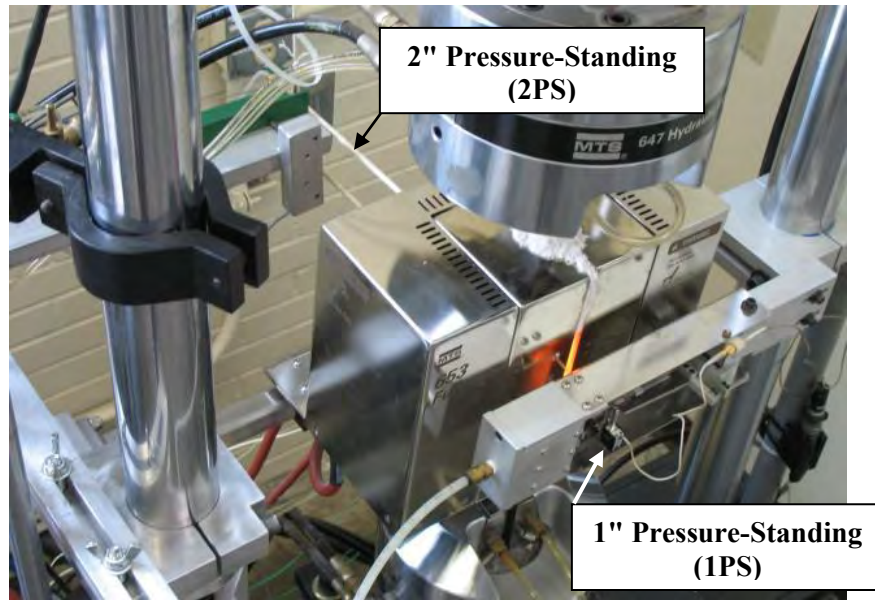
Figure 3.53 Case 4: 1PS and 2PS extensometer with furnace

The results of Case 4 testing are shown in Figure 3.54. The overall stress-strain behavior at both room- and elevated temperature are similar in that the strain data from the two extensometers are essentially identical up to the point necking occurred. Beyond that point, strain is no longer uniform along the specimen and the difference in gauge length between the two extensometers matters. If all of the strain after necking were concentrated at a single necking point, the post-necking strain for the 2PS would be 50% that of the 1PS. As it turned out, for both 20 and 700°C, the measured strain after necking for the 2PS was 55 to 60% that of the 1PS. This indicates that the assumption that all the post-necking elongation would occur in the necking zone, while not exactly true, was fairly descriptive of the behavior observed.

In terms of elastic-zone performance at room temperature, the findings were similar to the previous cases. The elastic modulus measured by the 2PS extensometer was a little under 60% of the reference value at room temperature; the 1PS returned a highly accurate value. At the elevated temperature, the two readings were closer together, but the 2PS modulus was still only 70% of the 1PS. This data is summarized in Table 3.14.

65
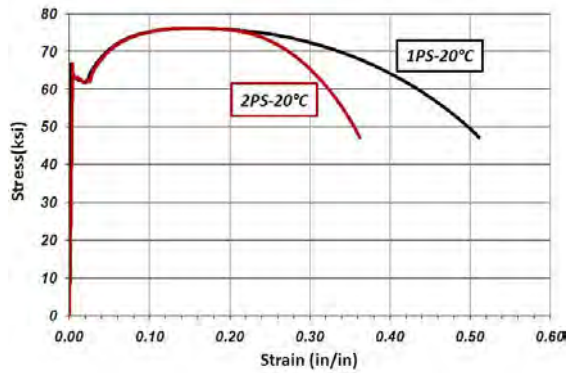
a) Overall stress-strain at 20°C
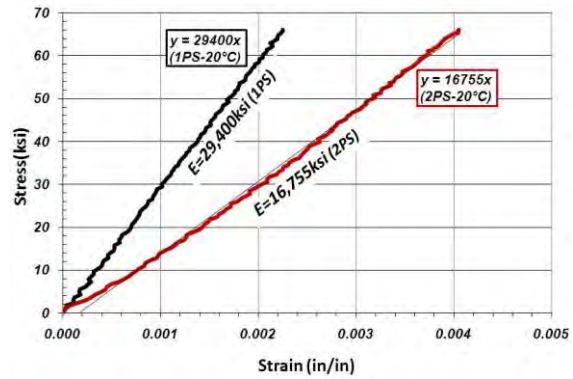
b) Elastic modulus
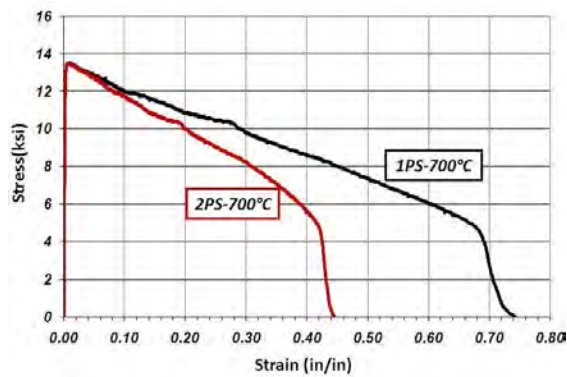
c) Overall stress-strain at 700°C
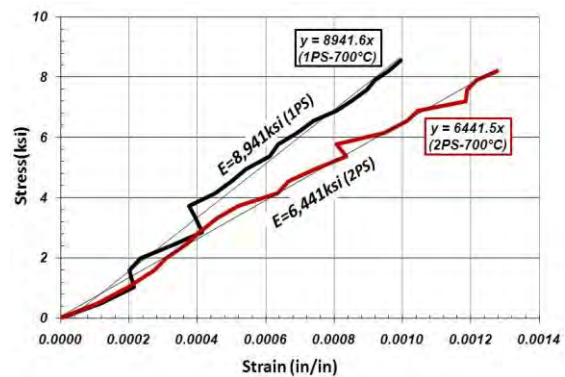
d) Elastic modulus

Figure 3.54 1PS and 2PS at elevated temperature

Table 3.14 Elastic modulus of Case 4 at room and elevated temperatures

Extensometer	Condition	1PS	2PS
Elastic Modulus (ksi)	20°C	29,400	16,755
	700°C	8,941	6,441
Modulus Ratio to 29,000 ksi at 20°C and 8,941 ksi at 700°C	20°C	1.014	0.578
	700°C	1.000	0.720

3.6.3.5 Summary of extensometer verification test

In terms of measurements of elastic behavior, both the 1PS and 2SS extensometers performed very well. The measured elastic moduli for these two

66

extensometers corresponded well with the expected value for A992 steel, that is, in the range of 29,000 to 30,000 ksi.

The 2PS extensometer proved incapable of measuring elastic strains accurately. Its measured elastic modulus was typically 40% low at room temperature. The large measurement range of this instrument—up to 50% tensile strain—may have inhibited its ability to perform measurements of elastic strains —less than 2%—accurately.

The elastic component of the strain-verification testing is shown in Table 3.15.

Table 3.15 Elastic modulus ratio to 29,000ksi for extensometer verification

Case	Condition	1PS	2PS	2SS	SG avg
1	20°C	1.093	-	1.046	-
2	20°C	-	0.575	1.050	-
3	Loading	1.012	-	1.007	1.011
	Reloading	1.017	-	1.009	1.023
4	20°C	1.014	0.578	-	-
	700°C	0.308	0.222	-	-

All three extensometers returned relatively similar inelastic strain readings prior to the onset of necking: the maximum observed variation was on the order of 5%. After necking, at both room and elevated temperature, the 1PS measured higher strains than the 2PS, but this behavior was due to the shorter gauge length.

In terms of potential usage during testing, the 1PS extensometer was shown adequate at both room and elevated temperatures. The 2SS was shown adequate for room temperature. Elastic-zone measurements from the 2PS should be considered inaccurate, but measurements of large inelastic strains proved accurate. As such, the 2PS extensometer could be used, but only in conjunction with another extensometer if any elastic properties were desired.

3.7 CORRECTION FOR EXTENSOMETER RESET DURING TESTING

For the temperature range tested, the steel coupons experienced up to 130% elongation before rupturing in tension. In comparison, the measurement range of the primary extensometer—1PS—was 10% strain. As such, during a given tension test, it was necessary to physically reset the extensometer up to thirteen times. This process produced discontinuous strain data, which was converted to a complete stress-strain curve through a process of connection and adjustment (Figure 3.55). This section provides information on how this process was completed. A more detailed, step-by-step presentation can be found in Appendix A.
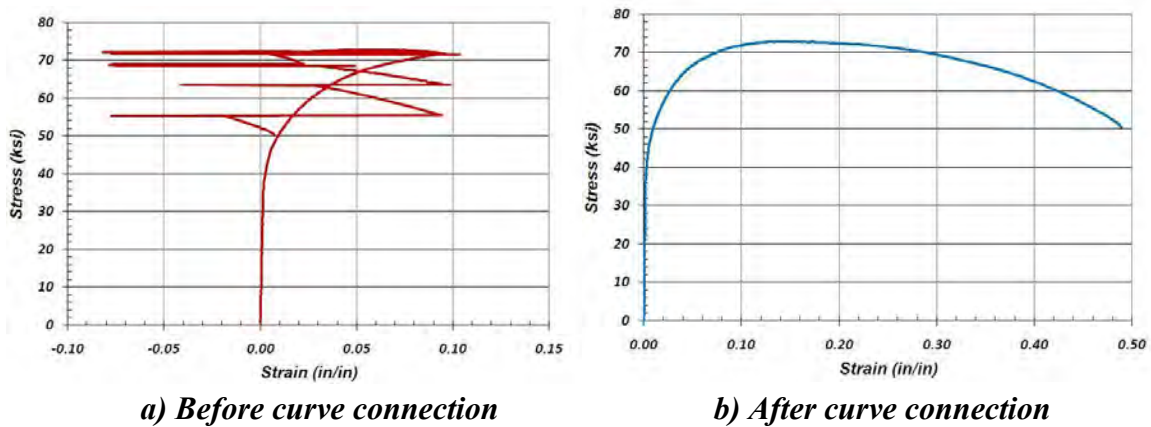
a) Before curve connection   *b) After curve connection*
Figure 3.55 Before and after curve connection of tensile test at 400°C

3.7.1 Process Followed to Correct Strain Data

The process of generating a stress-strain curve can be described by the six steps shown in Figure 3.56. From the output data, the random strains recorded during the resetting process were deleted. The remaining curve segments were shifted and, with recovered data, connected. (More discussion will be provided on data recovery in the Section 3.7.1.1.) The now-connected "raw" stress-strain curve was adjusted to the fracture strain directly measured using the punch marks on the coupon and calipers.
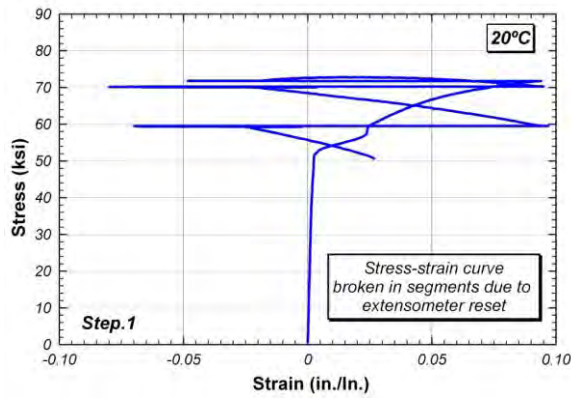
a) Step.1
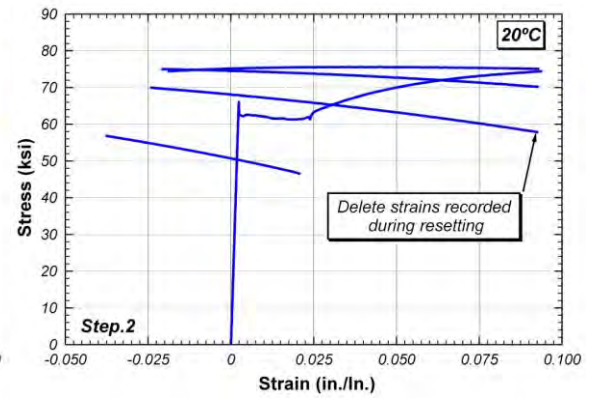
b) Step.2
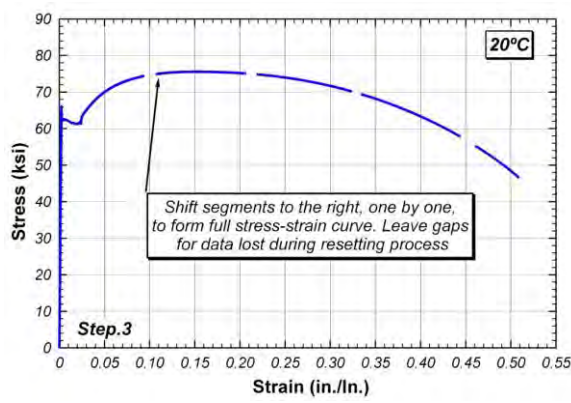
c) Step.3
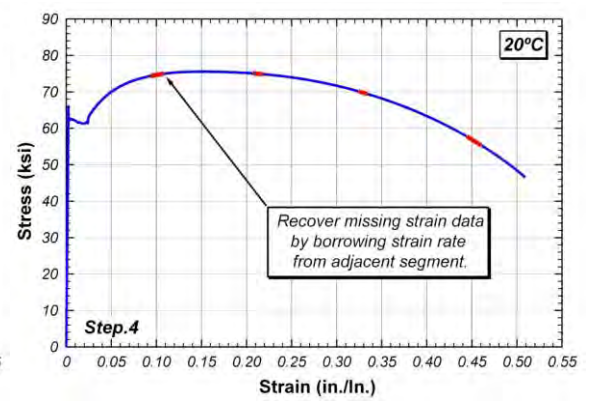
d) Step.4
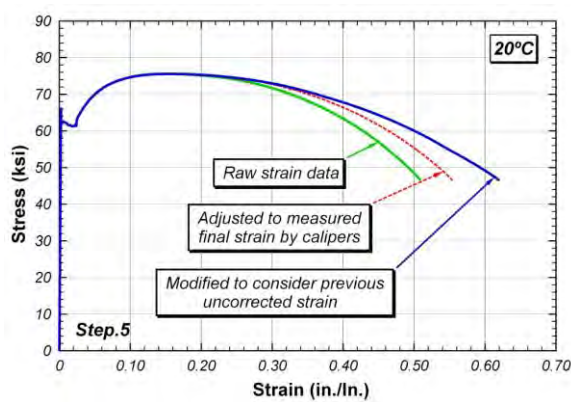
e) Step.5
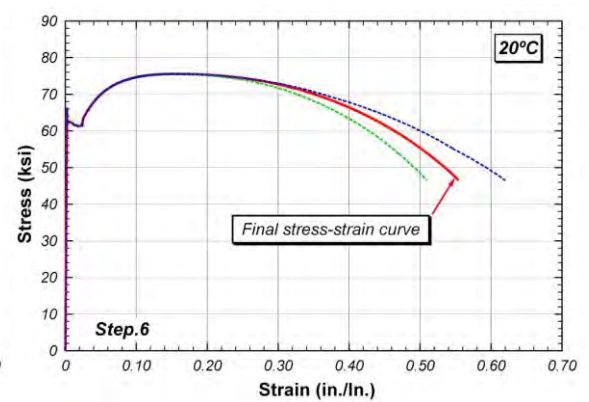
f) Step.6

Figure 3.56 Sample of curve connection showing process step by step

69

3.7.1.1 Recovery of Data Lost During Resetting Using Adjacent Data

During the time the extensometer was in the process of being reset, typically 15-30 seconds, no strain data was recorded. However, it is reasonable to assume that the strain rate during this period is likely to be similar to the rates observed immediately before and after resetting. The time interval between strain readings was constant. So, once a strain rate for the resetting period was assumed, the strain lost due to resetting could be calculated. At times, it took several attempts to properly seat the extensometer on the specimen. When strain data was only collected for a short time before another reset (only for a few seconds, covering less than 1% strain), this data was judged to be of questionable quality, and was typically deleted and then recovered. The segments of the stress-strain curve that would be connected were typically greater than 8% strain in length (compared to the 10% strain limit of the extensometer).

3.7.1.2 Adjustment so Final Strain Matches Caliper Measurement

After the stress-strain curve was connected, it was adjusted such that the final strain would match that measured directly after the test using the punch marks and calipers. In all cases, this meant an increase from the raw extensometer strain values.

There were several reasons to adjust the final strain. Since most are related to the fact that the extensometer was reset, it was decided to adjust the strains starting only beyond the nominal strain at which the extensometer was reset the first time: 10%. A strain for the final stress-strain curve could be then calculated as given in Equation (3.1.

$$\varepsilon = 0.10 + (\varepsilon_i - 0.10)\left(\frac{\varepsilon_f - 1}{\varepsilon_l - 1}\right) \tag{3.1}$$

where

ε_i = Arbitrary strain greater than 0.10 in/in (that is, 10%)

ε_f = Final strain measured after failure with calipers

ε_l = Last strain from raw data, after completing reconnection

70

As will be presented in detail in the next section, an extensometer, if reset during testing, is not capable of measuring all the strain experienced by a specimen. Each time the extensometer is reset, it is made to cover a smaller and smaller portion of the initial length that was instrumented. This is shown in Figure 3.57. The strain should be considered relative to the initial length, however. The portion of the strain corresponding to the stretching of the previously-but-now-uninstrumented zone is not included in the extensometer data.
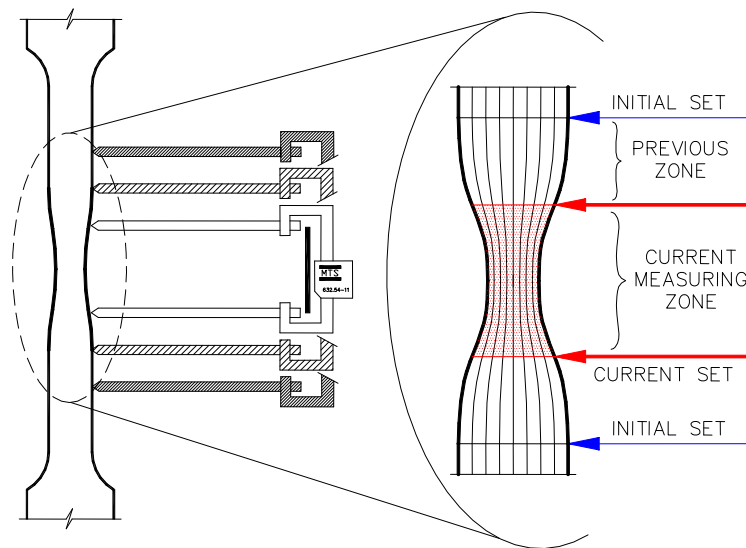
Figure 3.57 Zone for which strain is no longer measured after reset of extensometer

A theoretical compensation factor could be generated for this phenomenon—this topic is presented in Section 3.7.2—but it was found that the amount of adjustment that could be applied this way was not always sufficient to match the directly measured failure strain. This observation is likely due primarily to assumptions made during curve reconnection. The choice to use the measured value rather than a theoretical estimate as a basis for final-strain adjustment also provides compensation for other sources of error related to the extensometer measurement and curve connection process.

71

3.7.2 Theoretical Adjustment of Strain due to Stretching of Previously Instrumented Length of Specimen

As discussed in the previous section, an addition to the raw strain values is required for the stretching of portions of the specimen instrumented initially but no longer instrumented after multiple extensometer resets. This section presents a theoretical approach on this topic. It should be noted that while stress-strain curves compensating for this effect were generated, a different method of adjustment—using the caliper-measured final strain—was ultimately implemented. The use of a directly measured final strain does empirically compensate for the phenomenon here described.

Discussion will proceed by following the strains—those recorded by the extensometer and those that actually occur—over a period that covers multiple extensometer resets. Before the first reset, the coupon has elongated an amount α_0 and the strain situation is as illustrated in Figure 3.58 and Equation (3.2. The parameters β_0 and γ_0, defined by strain from previous steps, are zero here: this is the first step.
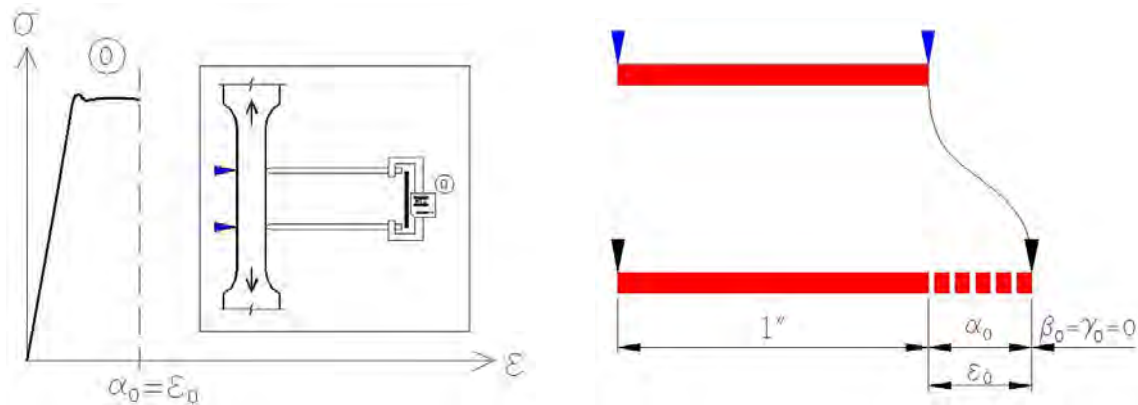
a) Stress-strain curve   *b) Strain during this period*

Figure 3.58 Strain-correction schematic diagram before first reset

$$\varepsilon_0 = \alpha_0 \tag{3.2}$$

where

ε_0 = Total measured strain

α_0 = Strain recorded during this step (since last extensometer reset)

β_0, γ_0 = Defined by strains from previous steps

During the next step, the strain recorded by the extensometer is again α_1. Strain carried over from the previous step, β_1, is elongated an additional amount due to the stretching of the coupon during this step. If assumed that the extensometer is reset to its nominal gauge length (1 inch) each time, the correction to the strain, γ_1, can be expressed as $a\alpha_1\beta_1$, where a is the ratio of strain for the previously instrumented as compared to the current gauge length spanning necking zone. Before necking, strain is uniform over the test length of the specimen, so $a = 1$. After necking, the strain rate in the necking zone is greater than over the other length, so $0 < a < 1$.

As shown in Equation (3.3, the equation for total measured strain at this step, ε_1, can be reduced to be dependent only on the strain from the previous step, ε_0, and the partial-stretch reduction factor, a.
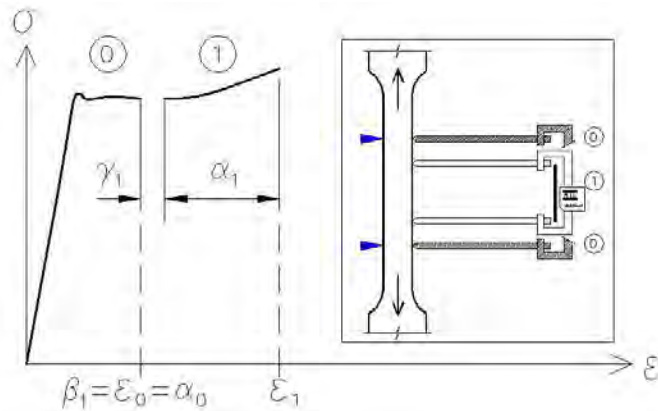
a) Stress-strain curve

Figure 3.59 Strain-correction schematic diagram after first reset

(continued on next page)
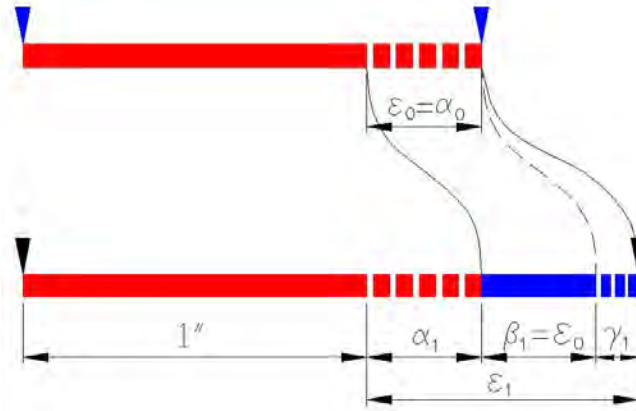
b) Components of strain during this period

Figure 3.59 Strain-correction schematic diagram after first reset (continued)

$$\begin{aligned} \varepsilon_1 &= \alpha_1 + \beta_1 + \gamma_1 \\ &= \alpha_1 + \beta_1 + a\alpha_1\beta_1 \\ &= \beta_1 + \alpha_1(1 + a\beta_1) \\ &= \varepsilon_0 + \alpha_1(1 + a\varepsilon_0) \end{aligned} \quad (3.3)$$

where

ε_1 = Total measured strain

α_1 = Strain recorded during this step

β_1 = Uncorrected strain from previous step = ε_0

γ_1 = Strain increment due to previous uncorrected strain = $a\alpha_1\beta_1$

a = Reduction factor accounting for partial stretching of previously instrumented length vs. current gauge length spanning necking zone

During the last step as shown in Equation (3.4, after the final extensometer and before failure, total measured strain is calculated similar to the strain recorded after the first reset, dependent only on the strain from the previous step and the partial-stretch reduction factor.
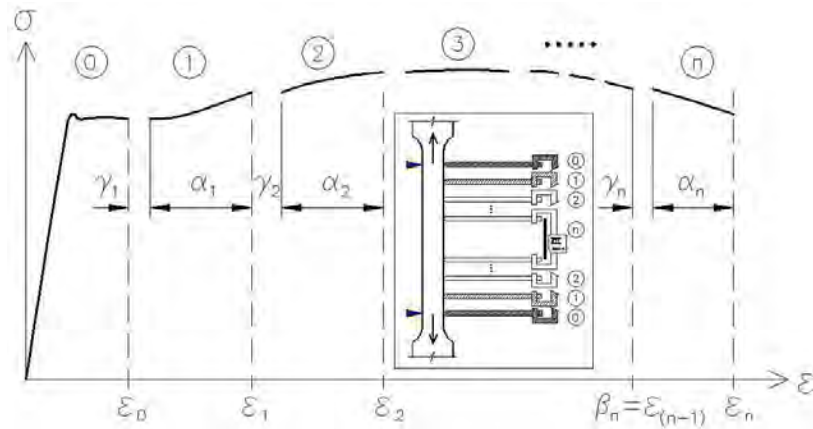
a) Stress-strain curve
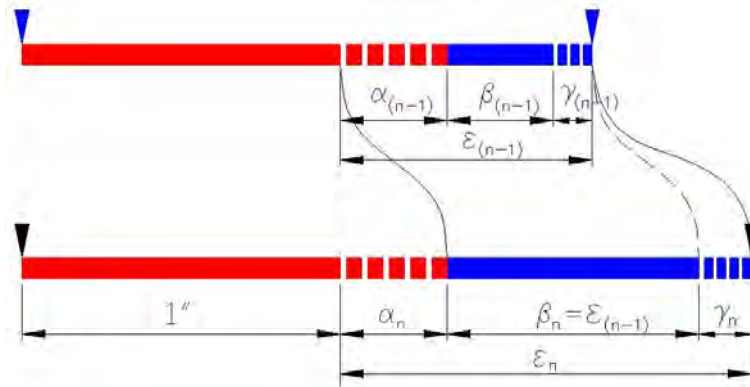
b) Components of strain during this period

Figure 3.60 Strain-correction schematic diagram when coupon failure

$$\varepsilon_n = \alpha_n + \beta_n + \gamma_n$$
$$= \beta_n + \alpha_n(1 + a\beta_n) \qquad (3.4)$$
$$= \varepsilon_{(n-1)} + \alpha_n[1 + a\varepsilon_{(n-1)}]$$

where

ε_n = Total measured strain

α_n = Strain recorded during this step

β_n = Uncorrected strain from previous step

γ_n = Strain increment due to previous uncorrected strain

a = Reduction factor for partial stretching of previously instrumented length

Combining the strain schematic diagrams from the steps considered above, Figure 3.61 is generated. Again, it can be noted that with an assumption for the ratio of strains between the previously instrumented zone and the current zone, the final strain is dependent only on the strain calculated for the penultimate step.
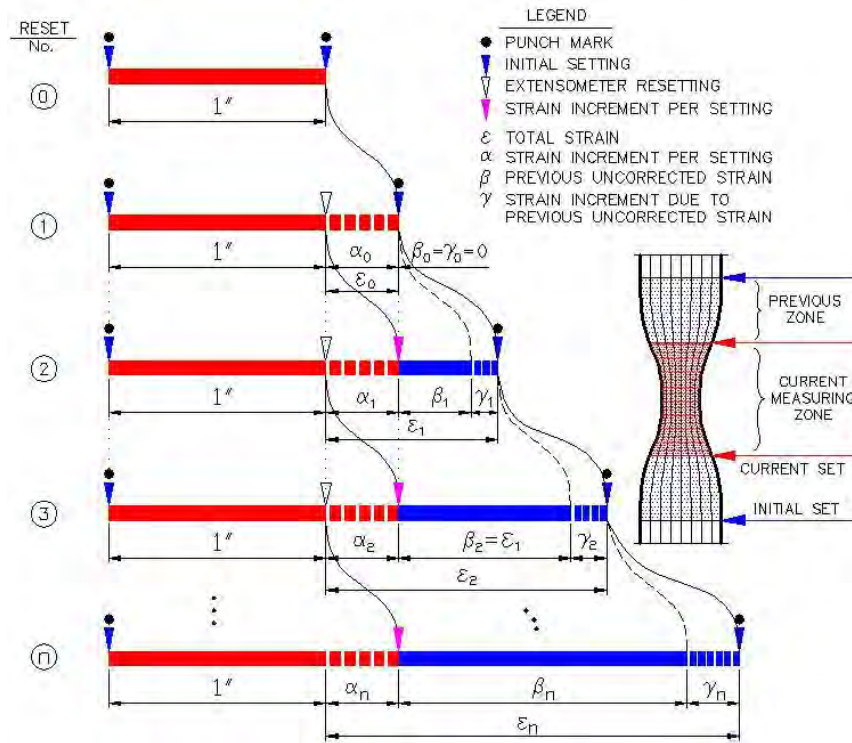
Figure 3.61 Schematic diagram of total strain from initial step to failure

In all cases, the raw strain from curve connection was less than the measured strain by calipers. Compensating for the stretching of no-longer-instrumented segments of the coupon improved the correlation to measured strain. Figure 3.62 and Table 3.16 show the ratio of γ-compensated strain, that is, strains corrected using the method described in this section, to measured strain. For this figure, it is assumed that $a = 1$: that all portions of the coupon stretch equally throughout the test. The ratios of the two strains range from 0.84 to 1.12, with most γ-compensated strains falling within 10% of measured.

76
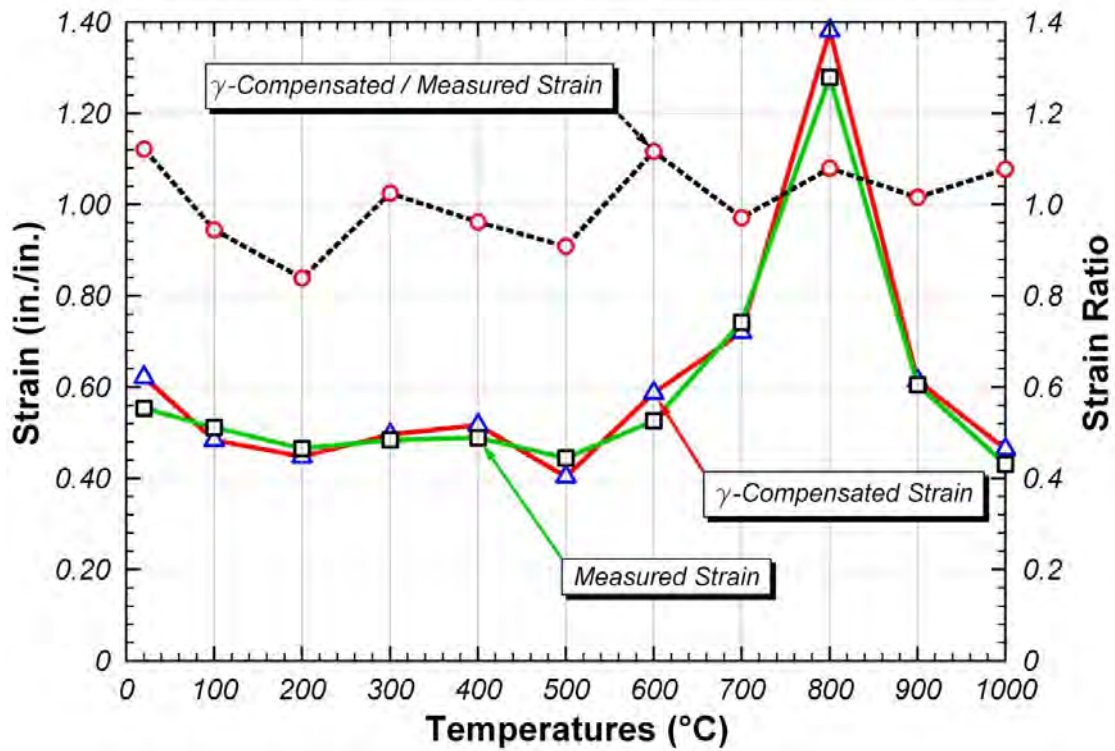
Figure 3.62 Strain after correction and failure

Table 3.16 Strain ratios by correction method and by caliper measurement

| Temp (°C) | Strain | | Ratio |
	y-Compensated	Caliper-Measured	
20	0.6213	0.5540	1.12
100	0.4837	0.5118	0.95
200	0.3907	0.4657	0.84
300	0.4960	0.4841	1.03
400	0.4707	0.4892	0.96
500	0.4038	0.4444	0.91
600	0.5875	0.5259	1.12
700	0.7204	0.7423	0.97
800	1.3813	1.2793	1.08
900	0.6144	0.6049	1.02
1000	0.4644	0.4308	1.08

77

Some investigation was made into finding a fitting value for *a*, the partial-stretch reduction factor, considering the areas at failure of the necking zone and other portions of the coupon reduced section. However, these efforts were unsuccessful for two reasons. First, the value of *a* is not constant throughout the test. Before necking, it approaches unity; afterwards, it is less than one. Second, adjustments need to be made for errors inherent in the curve connection process. In some cases, the value of the strain measured by calipers suggested an experimental value of *a* greater than one. This finding does not invalidate the above theory, just suggests that correction by final measured strain is a more robust technique than a theoretical compensation for the strains out of range for the reset extensometer.

CHAPTER 4

Tension Testing at Elevated Temperatures

4.1 OVERVIEW

This chapter describes the procedures for and results from tension testing of ASTM A992 steel at elevated temperatures. Tests were conducted for temperatures ranging from room temperature to 1000°C to determine mechanical properties including yield stress, tensile strength, and elastic modulus. Two constitutive models were developed based on the experimental data to predict elevated temperature stress-strain response. One is a detailed model that captures many of the features of the measured stress-strain curves; this model is appropriate for advanced analysis of steel structures subjected to fire. The second is a simplified trilinear model that may be more useful in design calculations. Results from these models are compared with an existing, widely used model, from Eurocode 3 (Eurocode 1993).

4.2 TEST COMPONENTS AND PROCEDURES

The general testing procedures used for most elevated temperature tests conducted for this dissertation were discussed in Chapter 3. This section provides some additional details specific to tension testing at elevated temperature.

4.2.1 Test Specimens

In order to better assess the behavior of ASTM A992 steel at high temperatures considering the possible variability in steel material, specimens were cut from different wide-flange sections from different heats of ASTM A992 steel. Tests were conducted on two different samples of ASTM A992 material. These materials are designated as MA, MB and MC, as described in Chapter 3. Specimens designated as MA and MB were cut from the web of a W30×99 section with different heat number, and those designated as

MC were cut from the flanges of a W4×13 section. To provide further evaluation of the effects of material variability, the results of tests conducted herein will be compared with the results of elevated temperature tests on ASTM A992 steel. MA coupon of steel cut from the web of a W30×99 section, but this section was from a different heat of ASTM A992 steel than the W30×99 used for the MB specimens. Thus, test results reported in this chapter are from three different samples of ASTM A992 steel designated as MA, MB, and MC (Figure 4.1a). Room-temperature mechanical properties and results of chemical analysis for all three materials are provided in Section 3.4.1.

Details of the dimensions of the specimens, in accordance with ASTM Standard A370 (A370 2012), are shown in Figure 4.1b. The coupons were prepared so that their longitudinal dimension (18 inch) was along the rolling direction of the wide flange sections. Moreover, though not specified by ASTM A370, the 18-inch length of the coupon was selected to create enough clearance between the furnace and the grips of the testing machine. Coupon fabrication followed the procedures described in Section 3.4.2.
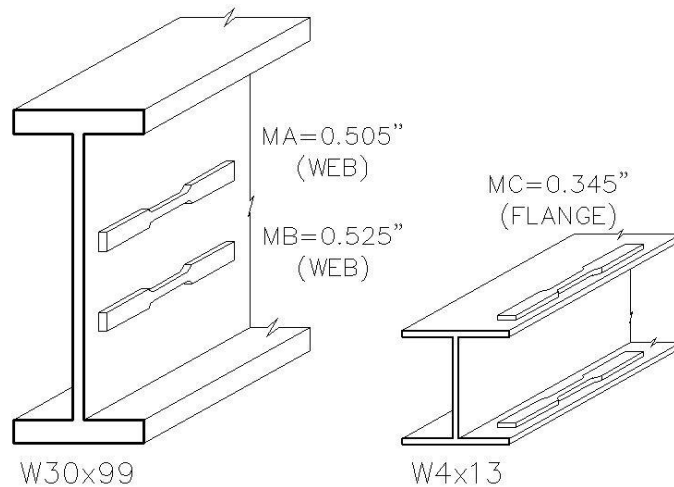
a) Coupon sources beam and location
Figure 4.1 Experimental coupon details used in testing (continued on next page)
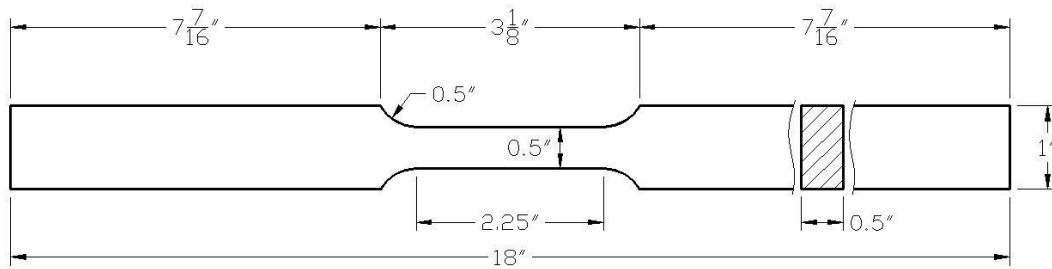
b) Coupon dimensions
Figure 4.1 Experimental coupon details used in testing (continued)

4.2.2 Strain Measurement

Coupon strain was measured during elevated-temperature testing through simultaneous use of two extensometers, designated as "1PS" and "2PS", shown in Figure 4.2. As discussed in Section 3.6, these extensometers were both of the same design (pressure-standing extensometers, with ceramic arms and an air-cooling system for high-temperature use), but had different gauge lengths (1 and 2 inch) and different measurement ranges (10 and 50% strain, respectively).

Most notably, however, the two extensometers had different uses. The 2PS, due to its large strain capacity, was less accurate for measuring response at very small strains. On the other hand, the 2PS allowed the measurement of very large strains with a minimum number of resets. The 1PS extensometer allowed more accurate measurement at small strain levels, but required a larger number of resets to capture the full stress-strain curve. The difference in measurement range meant that the 1PS needed to be reset at least ten times for 800°C. While the 1PS was reset, the 2PS was still in contact with the specimen, collecting strain data. More information on the effects of resetting and controlling the extensometers during the test and corrections made for reset can be found in Section 3.7.
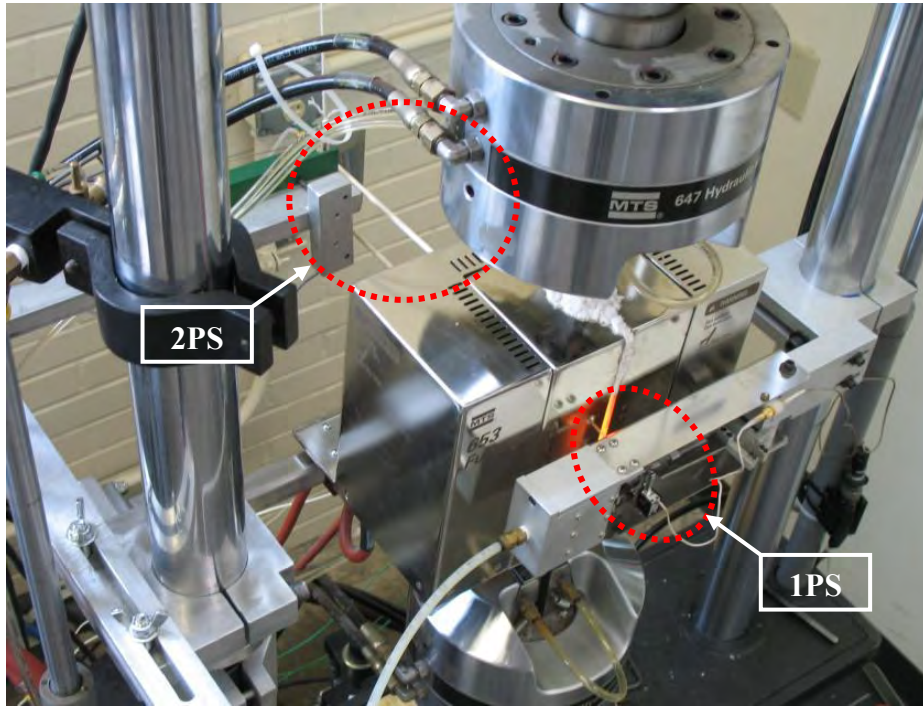
Figure 4.2 Use of 1PS and 2PS extensometers

4.2.3 Temperature Measurement

Temperature measurement is a critical factor in elevated-temperature testing. Having a uniform temperature distribution over the gauge length of the steel coupon is crucial in order to accurately evaluate mechanical properties of steel at a specific temperature.

Type K thermocouple wires were used to measure the temperature at different locations along the gauge length of the coupon. Due to the fact that the thermocouple extension wire measures the temperature at the first contact point of its two dissimilar metals, this first contact point has to touch the surface of the steel coupon and maintain the initial position without moving during the test. Therefore, to have a reliable temperature measurement, thermocouple extension wires should be firmly attached to the surface of specimens. In addition, to be protected from radiation from the furnace heating elements, the thermocouple wires were wrapped by Type 321 stainless steel tool wrap or

82

foil, which is commonly used in heat treatment of tool steels. Figure 4.3 shows, for representative steel coupons, the attachment of the thermocouple wires covered by the stainless steel tool wraps at their contact points with the specimens. Three Type K thermocouples were attached to each coupon, and protected with stainless steel foil. This system for attaching thermocouples to the steel coupons was developed after extensive study of various temperature measurement approaches. Methods for attaching the thermocouple to the steel coupons were described in greater detail in Section 3.5.

Figure 4.3 Coupon with Type K wire thermocouples

4.2.4 Furnace and Test Machine

Specifics of the MTS 653.04 furnace and MTS 810 test machine can be found in Section 3.3. All tests were conducted by displacement control, using a constant crosshead displacement rate to load the steel coupons. All tests conducted on materials MA, MB and MC were at a crosshead displacement rate of 0.01 inches per minute. Thus, all tension test results reported in this chapter were conducted at a constant crosshead rate of 0.01 inches per minute. For laboratory convenience, it was desirable to heat the coupons to their target temperature in a similar time, regardless of the magnitude of the

temperature. As such, rates of heating were varied (Table 4.1), and the furnace reached its target temperature in approximately 30–40 minutes (Figure 4.4).

The furnace was held at the target temperature until at least 60 minutes had passed after the start of heating to allow the coupon to achieve greater uniformity of temperature. During the heating process, the coupons were allowed to freely expand under zero load. Consequently, all strains reported in the stress-strain curves in this chapter are mechanical strain only, and do not include thermal strain.

Table 4.1 Heating Rate (°C/min)

Time(min)	Temperature (°C)								
	200	**300**	**400**	**500**	**600**	**700**	**800**	**900**	**1000**
1	77.0	124.9	141.7	150.0	200.4	210.2	177.8	256.3	365.3
2	2.4	31.3	43.8	78.0	93.0	79.9	97.7	107.3	101.5
3	5.4	13.9	26.7	47.9	53.4	54.3	73.3	68.7	50.2
4	5.7	13.1	22.5	26.8	44.9	48.5	50.6	52.5	42.8
5	6.0	12.1	13.2	22.6	40.0	44.2	45.5	36.6	31.9
6	5.7	10.1	12.2	17.9	22.0	40.0	38.5	35.6	30.3
7	6.6	8.6	14.1	17.6	19.0	31.3	34.6	30.4	25.8
8	6.4	9.3	11.9	14.7	15.1	27.0	32.6	25.6	24.8
9	5.3	8.0	12.6	11.6	10.5	21.7	31.0	24.4	25.3
10	5.2	5.7	8.3	12.5	10.0	18.2	28.9	24.3	25.0
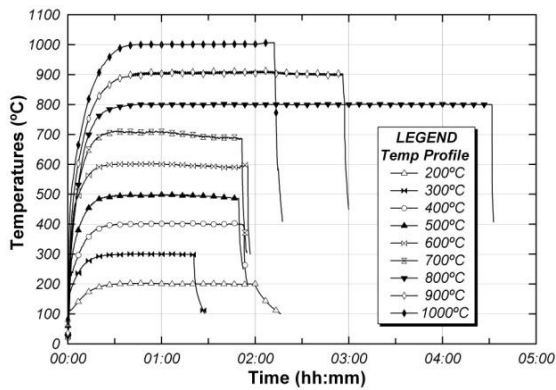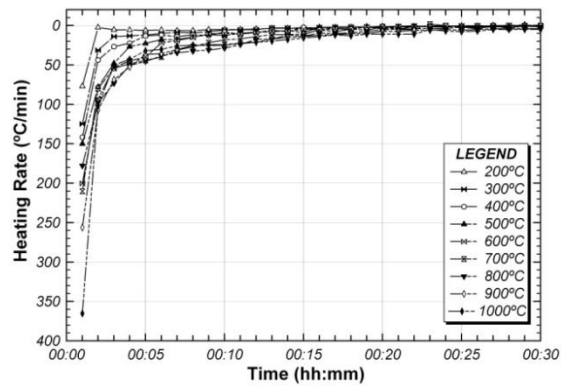
a) Temperature profile   *b) Heating rate*

Figure 4.4 Temperature profile and heating rate

84

4.2.5 Test Repetitions

To help ensure accurate results, three to seven tensile tests were performed at each temperature, depending on the consistency in and quality of the stress-strain curves obtained in each test. It should be noted that virtually all tests showed good repeatability with respect to three parameters typically extracted from tension testing: yield stress, tensile strength and elastic modulus. Issues with repeatability, when they did arise, were related to the descending branch of the stress-strain curve (the post-peak behavior), which was difficult to capture consistently.

Inconsistencies in the stress-strain data occurred for several reasons, but most notably due to extensometer resetting. At times, when the extensometer was reset, the necking point ended up outside the range of the extensometer. In that case, the large deformations that occur at the necking point were not reflected by the readings of the extensometer. It proved difficult to find the necking point through the small window of the furnace (Figure 4.5) when the material was red hot.
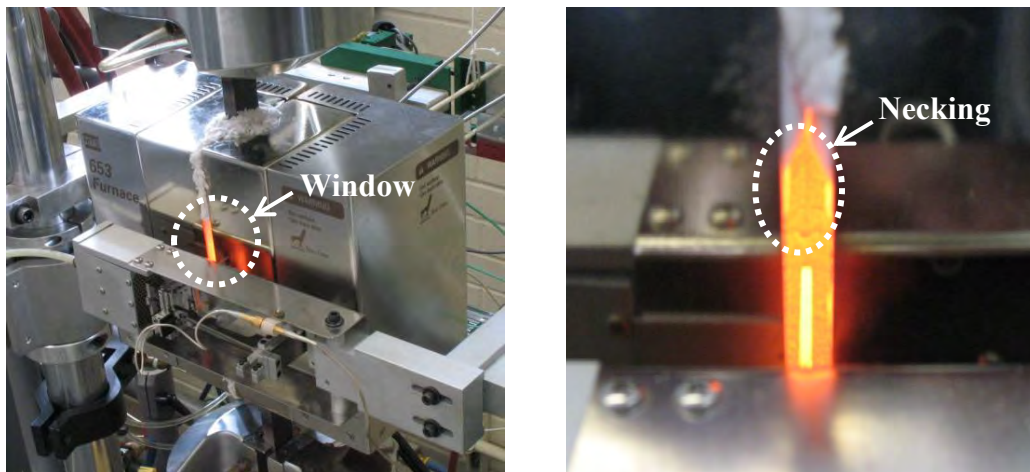
a) Window in furnace   *b) View through furnace window*
Figure 4.5 Necking behavior as viewed through furnace window

An example of inconsistent stress-strain data resulting from improper placement of the extensometer after resetting is given for three tests conducted at 300°C in Figure 4.6. For Test 1 and 2, the extensometer was reset three times. It was reset four times in

the Test 3. Test 3 was taken as the most representative result, as the final elongation most closely matched the elongation measured from punch marks on the coupon. The lower strain values measured for the first two tests indicate that the extensometer did not capture necking optimally. At ultimate, 5 to 8% smaller strains were measured (in absolute terms). The sharp decrease in stress at constant strain seen in the Test 2 (highlighted in Figure 4.6b) indicates that the extensometer was set to a location where it entirely missed necking, whereas the shortened plateau at maximum stress seen in Test 1 is indicative of partially missed necking.
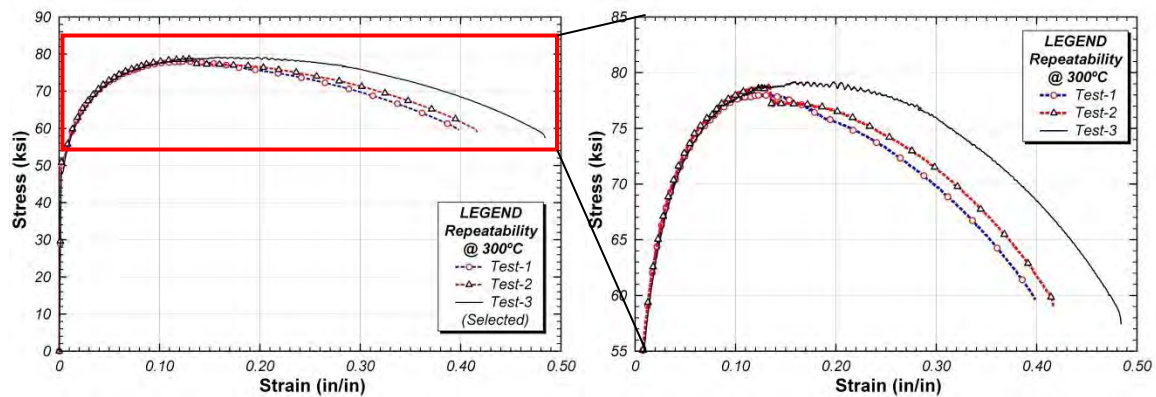
a) Full stress-strain curves   *b) Curve for upper range of stress*
Figure 4.6 Effect of necking in repeated tension tests at 300°C

Another source of inaccurate stress-strain data, shown for five tests performed at 600°C (Figure 4.7), was non-uniform temperature during the testing period. While for most tests, the target temperature was maintained within a tolerance of 3°C, during one test temperatures fluctuated by up to 20°C. This increase in temperature leads to considerable error in the stress-strain curve, as illustrated in Figure 4.7.
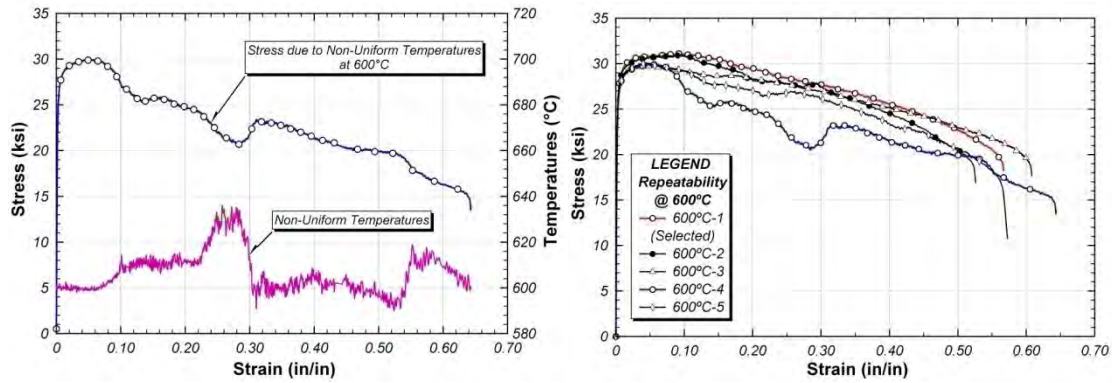
a) Stress- and temperature-strain curves   *b) Results from repeated testing*
Figure 4.7 Effect of temperature variation in repeated tension tests at 600°C

Different sources of error—those identified in the previous two figures and otherwise—affected each tension test in a unique way. As such, averaging the results of all tests conducted at a given temperature was not considered to provide a representative stress-strain curve at elevated temperature. Rather, for repeated tests at a given temperature, the data was evaluated carefully to choose the curve that was least affected by errors.

4.3   TEST RESULTS

This section presents the results of the elevated temperature tension tests. As described earlier, tests on materials MA, MB and MC were conducted as part of this current research. Test results are provided are provided in this section in several different formats. First, stress-strain curves are provided according to the material type (MA, MB and MC), and are then given according to temperature. Finally, stress-strain curves given by extensometer type are presented.

All stress-strain curves presented in this section are from tests conducted at a constant crosshead rate of 0.01 inches per minute. Further, unless noted otherwise, strains were measured using the 1PS extensometer using the resetting technique described in Chapter 3.

4.3.1   Stress-Strain Curves by Material

To illustrate the effect of different heats of ASTM A992 steel materials at elevated temperatures, stress-strain curves are presented for materials MA, MB and MC in Figure 4.8 to Figure 4.10, respectively. In these figures, stress-strain curves are plotted up to 80% strain, which includes strains from the start of loading to the fracture of the coupons at different temperatures, except for materials MA and MB at 800°C, for which the strains at fracture are 110% and 130%, respectively. As can be seen in Figures 4.8a, 4.9a and 4.10a for each material, the tensile strength increases compared to the corresponding one at room temperature, at temperatures of 200°C and 300°C. At higher temperatures, progressive loss in the tensile strength can be clearly observed. Another important property, ductility, as measured by the final elongation of the coupons, exhibits a small reduction up to 500°C, then increases in the range of 600 to 800°C, and then reduces again at 900°C. On the other hand, ductility, as measured by the strain at which the tensile strength is developed, shows a dramatic decrease with increasing temperature from 400 to 700°C.

Figures 4.8b, 4.9b and 4.10b plot the initial parts of the stress-strain curves up to 0.5% strain for each material. These figures clearly show that the yield stress and modulus of elasticity decrease with temperatures.
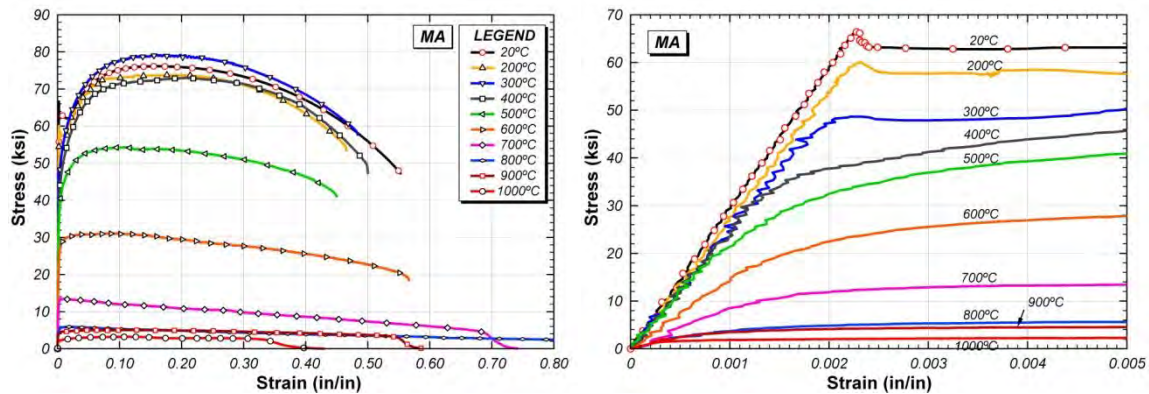
a) Full-range stress-strain curves   *b) Initial portion of stress-strain curves*

Figure 4.8 Stress-strain curves for MA at elevated temperatures

88
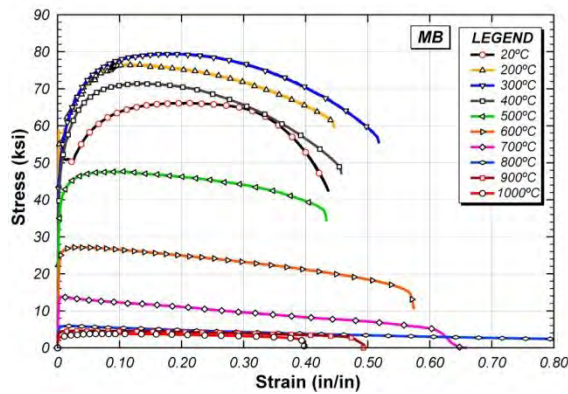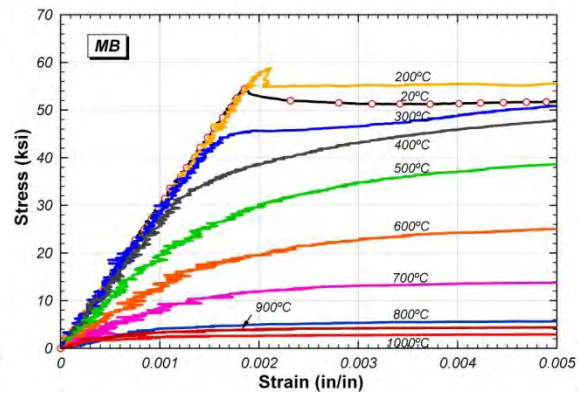
a) Full-range stress-strain curves   *b) Initial portion of stress-strain curves*

Figure 4.9 Stress-strain curves for MB at elevated temperatures
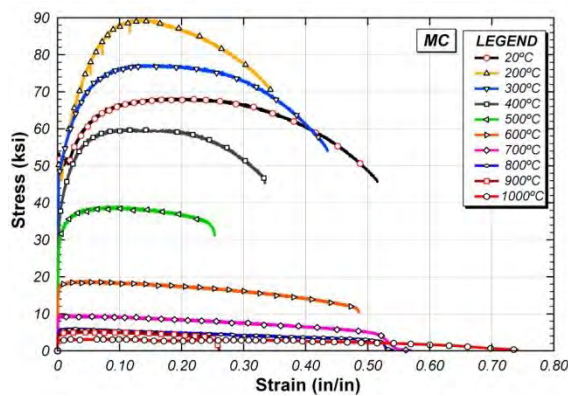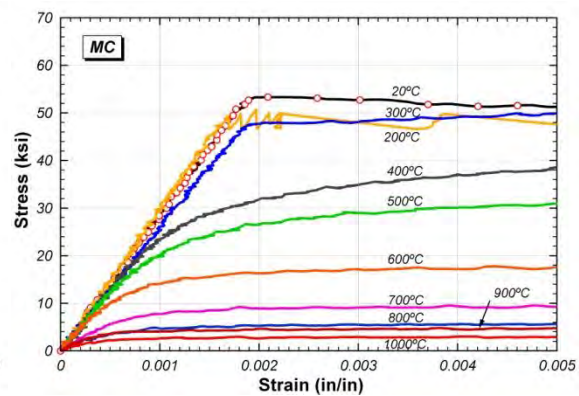
a) Full-range stress-strain curves   *b) Initial portion of stress-strain curves*

Figure 4.10 Stress-strain curves for MC at elevated temperatures

As observed in previous tension tests reported in the literature, this data shows that the fundamental shape of the stress-strain curve changes as temperature increases. At 400°C and above, the steel no longer exhibits a well-defined yield plateau, and shows significant nonlinearity at low levels of stress and strain. Likewise, as described above, the strain corresponding to the maximum engineering stress (tensile strength) decreases rapidly as temperature increases, and the stress-strain curve subsequently shows a long, gradual decline.

At ambient temperature, the initial portion of the stress-strain curve is often modeled using a simple elastic-perfectly plastic approximation in which the response is

linear-elastic up to yield, and then follows a plateau. Simple elastic-perfectly plastic stress-strain models may be less appropriate at elevated temperatures due to early nonlinearity in stress-strain curves, as seen in Figure 4.8 to Figure 4.10. This early nonlinearity may be particularly significant when considering stability phenomena, wherein tangent stiffness is a critical material property.

4.3.2 Stress-Strain Curves by Elevated Temperatures

Figure 4.11 illustrates the effect of material variability by presenting stress-strain curves at specific temperatures for materials designated as MA, MB and MC. As is clear from this figure, there is appreciable difference in material stress-strain response among these three materials that are all classified ASTM A992 steel. More specifically, it can be observed from this figure that materials MA and MB, both of which are from the web of W30×99 sections of different heats, show similar stress-strain behaviors, especially at temperatures lower than 500°C. It can also be observed that the stress-strain curves of material MC, which is from the flange of a W4×13 section, are very different from those of materials MA and MB at elevated temperatures. Of particular interest is the comparison amongst these three materials at 200°C, where very large strain hardening and a very large increase in tensile strength are seen in the stress-strain behavior of material MC. At first, this behavior was suspected to be experimental error. However, several coupons of MC material were retested at 200°C, and this same behavior was consistently observed. These observations suggest that there may be considerable variability in stress-strain response for a particular grade of steel.

90
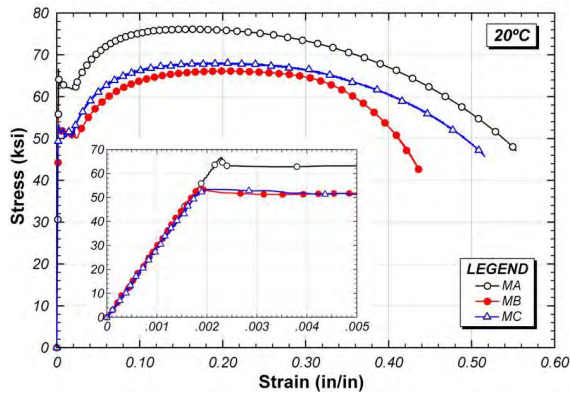
a) 20°C
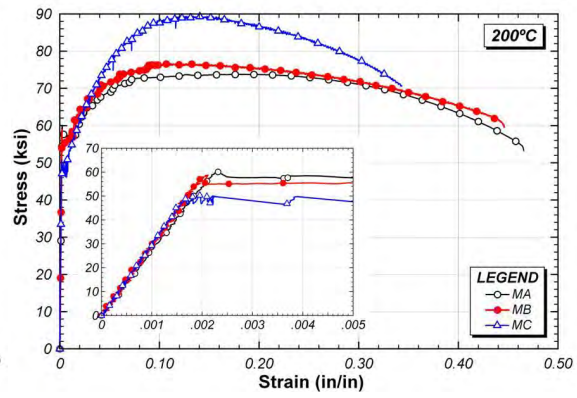
b) 200°C
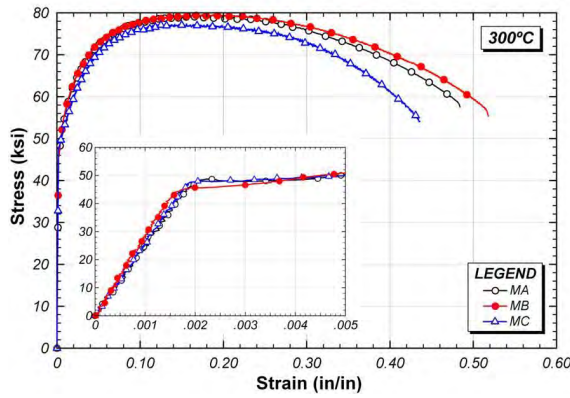
c) 300°C
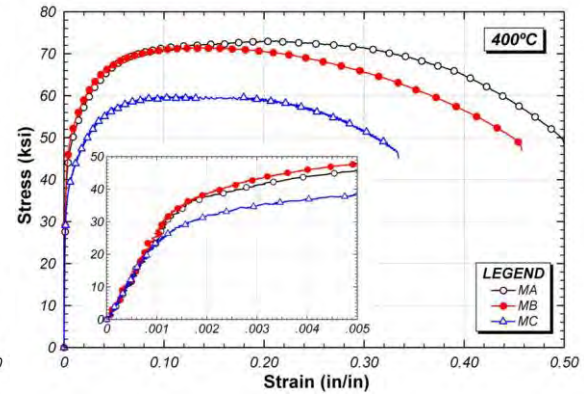
d) 400°C
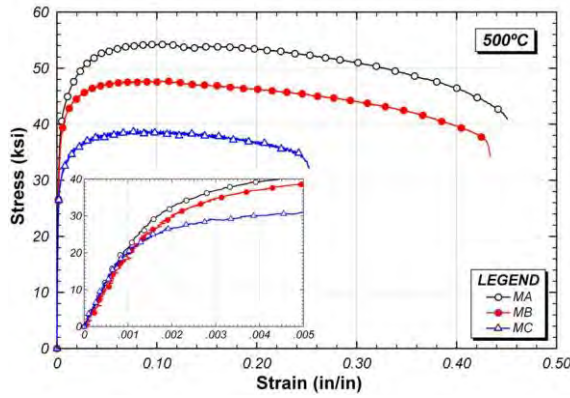
e) 500°C
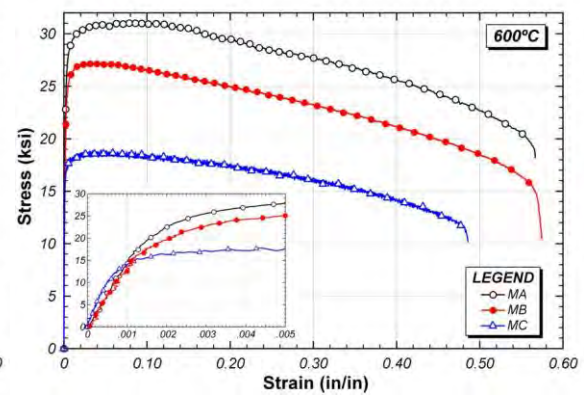
f) 600°C

Figure 4.11 Stress-strain curves for MA, MB, and MC at elevated temperatures

91
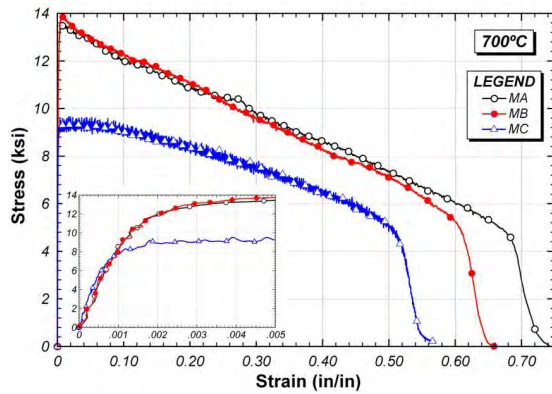
g) 700°C
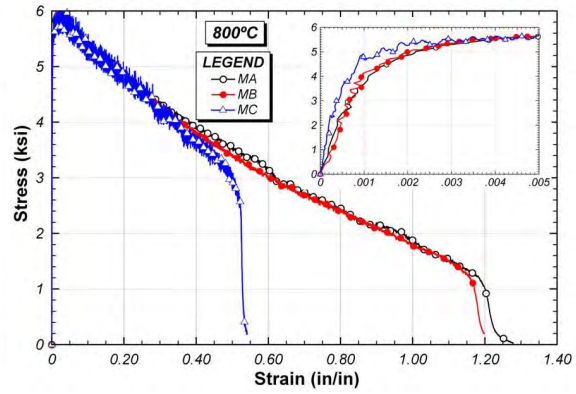
h) 800°C
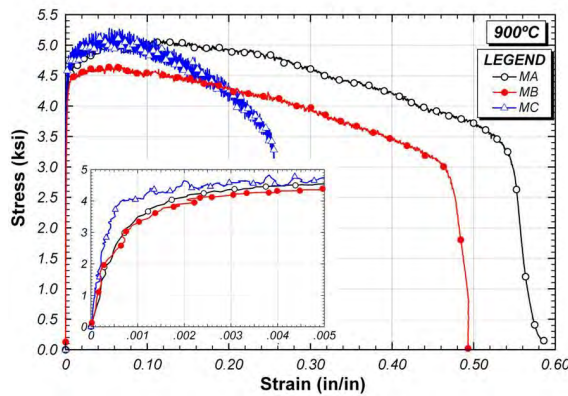
i) 900°C
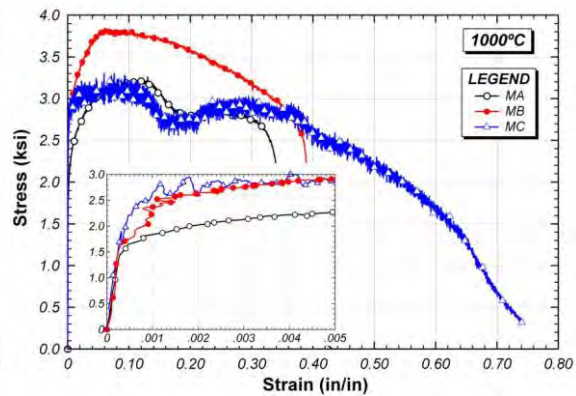
j) 1000°C

Figure 4.11 Stress-strain curves for MA, MB and MC at elevated temperatures
(continued)

4.3.3 Stress-Strain Curves by Extensometer

Test results plotted according to extensometer type are shown in Figure 4.14 for material MA. Stress-strain curves are shown for two cases. One is for strains measured by the 1PS extensometer (1-inch gauge length; 10% strain limit), and the second is for strains measured using the 2PS extensometer (2-inch gauge length; 50% strain limit). Note that each pair of curves is for the same coupon. That is, as a coupon was being loaded, strains were measured on the coupon using the two different extensometers simultaneously.

In comparing stress-strain curves for the two different extensometers, it can be observed that the curves are essentially the same up through the development of the highest engineering stress, that is, until the development of the tensile strength of the material. Once the tensile strength is achieved, necking initiates in the coupon, and the stress-strain curves for the two different extensometers begin to deviate. The differences in the curves after necking is likely related to the different gauge lengths of the extensometers; 1 inch for the 1PS and 2 inches for the 2PS. Once necking initiates, strain is no longer uniform over the gauge length of the coupon, but rather is concentrated within the necked region. The 2PS extensometer, because of its longer gauge length, averages the strain over a larger length than the 1PS extensometer. As a result of this larger averaging length, the 2PS extensometer is expected to record a smaller average strain over its gauge length than the 1PS extensometer. This is clearly reflected in the stress-strain curves in Figure 4.14, where the strains for the 2PS extensometer are consistently smaller than for the 1PS extensometer once necking begins. The effect of extensometer gauge length on the post-necking portion of the stress-strain curve was also discussed in Chapter 3.

Mechanical properties of interest in design include the modulus of elasticity, proportional limit, yield stress, and tensile strength. These properties are all derived from the portion of the stress strain curve that occurs prior to necking. Thus, these properties are largely independent of extensometer gauge length. An additional property of interest is the elongation of the coupon, which is the strain at fracture. The apparent strain at fracture is dependent on extensometer gauge length, as is clear from Figure 4.12. The dependence of measured elongation on extensometer gauge length is well recognized in material specifications. For example, the required minimum elongation of ASTM A992 steel is 18% for an 8-inch gauge length and is 21% for a 2-inch gauge length.
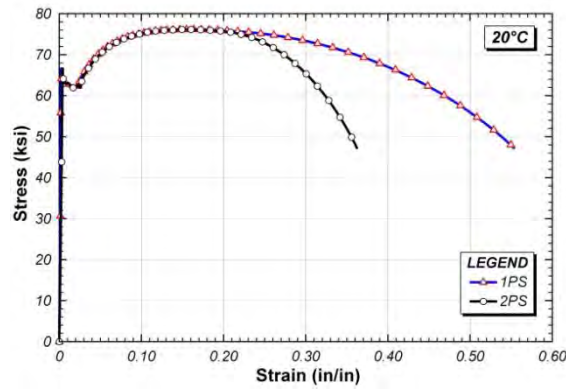
a) 20°C
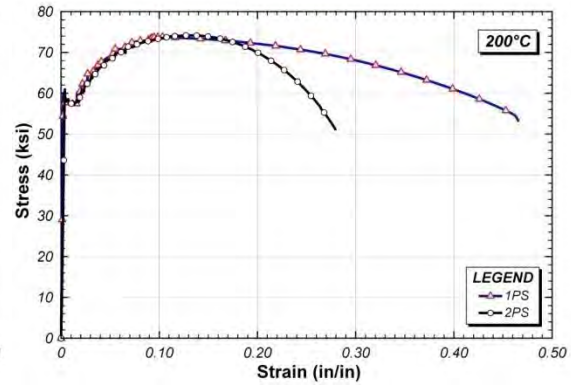
b) 200°C
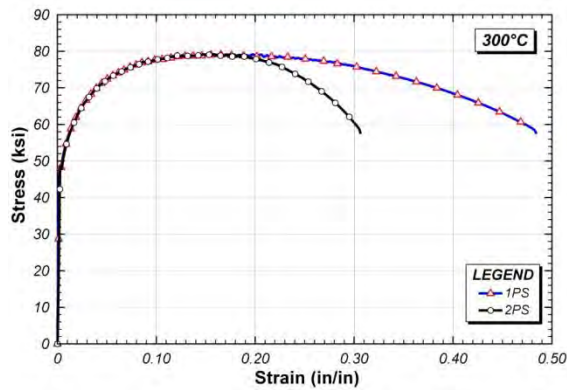
c) 300°C
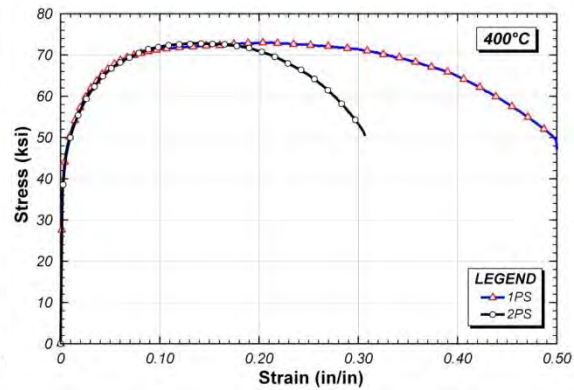
d) 400°C
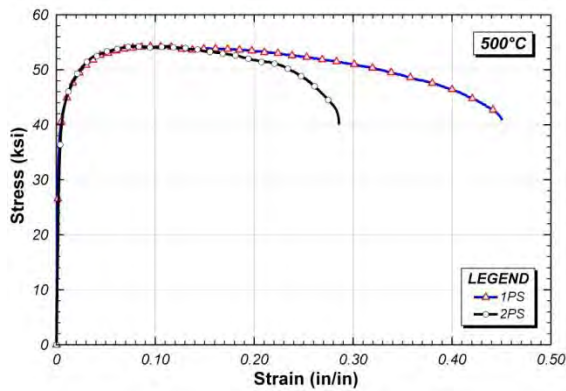
e) 500°C
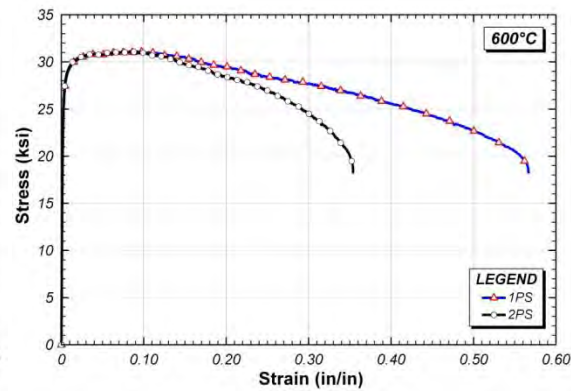
f) 600°C

Figure 4.12 Full stress-strain curves by 1PS and 2PS extensometers
(continued on next page)

f) 700°C

g) 800°C

h) 900°C

i) 1000°C
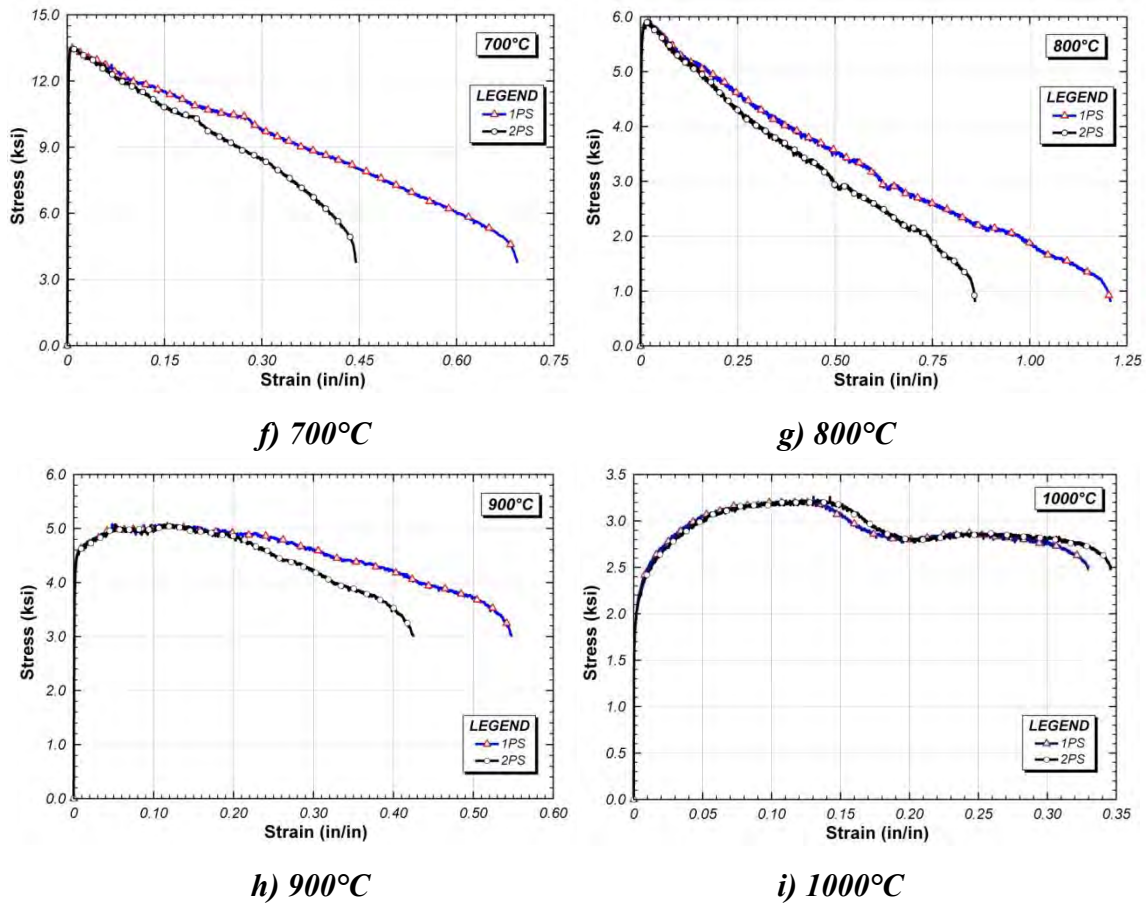
Figure 4.12 Full stress-strain curves by 1PS and 2PS extensometers (continued)

4.4 MECHANICAL PROPERTIES AT ELEVATED TEMPERATURE

The mechanical properties of steel derived from tension testing include elastic modulus, yield stress, proportional limit, tensile strength and total elongation. The last two properties are maximum values, so are easy to define: tensile strength is the highest stress observed during testing and total elongation the highest strain. The other properties describe behavior at low values of strain; in the elastic zone and just beyond. Figure 4.13 qualitatively shows the initial portion of an elevated temperature stress-strain curve, and graphically illustrates the elastic modulus, proportional limit, and yield stress. Since elevated temperature stress-strain curves typically do not exhibit a well-defined yield

95

plateau, various definitions of yield stress are possible. The definition of yield stress will be discussed in greater detail later.
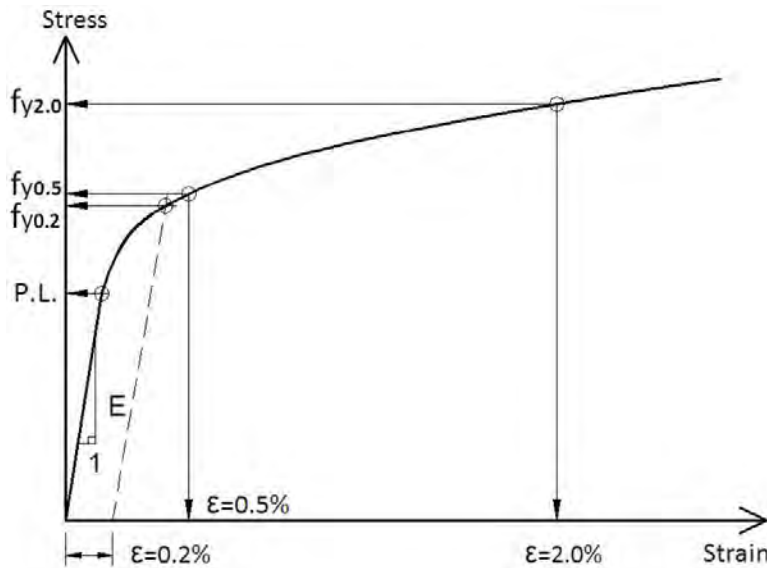
Figure 4.13 Definitions for elastic modulus, yield stress and proportional limit

The elastic modulus (E) is the initial slope of the stress-strain curve. The proportional limit defines the stress at which linear behavior ceases. For the elevated-temperature yield stress (f_y), three definitions are provided in the figure: the 0.2% offset method, 0.5% total strain and 2.0% total strain. The first of these definitions, the 0.2% offset method, is widely adopted for testing at room temperature. The last of these, 2% strain, is used in Eurocode 3 (Eurocode 1993). The intermediate value of 0.5% total strain is sometimes seen in the literature (Kirby and Preston, 1988).

4.4.1 Yield Stress

The yield stress was determined by the three methods discussed in Section 4.4: the 0.2% offset method, 0.5% total strain and 2.0% total strain. At temperatures above approximately 300 to 400°C, the measured stress-strain curves do not exhibit a well-defined yield plateau. Consequently, defining yield stress becomes more subjective at elevated temperatures than at ambient temperature. For metals that do not exhibit a yield

plateau, the 0.2% offset yield stress definition is widely used and is specified by ASTM E21 (ASTM, 2009) for defining the yield stress at elevated temperatures. With this method, yield stress is defined as the stress at the intersection of the stress-strain curve and the proportional line offset by 0.2% strain. Within the literature on elevated-temperature properties of structural steel, various definitions of yield stress have been used. In addition to the conventional 0.2% offset definition, the yield stress has also been defined as the stress corresponding to 0.5% total strain, the stress corresponding to 2% total strain, as well as other definitions. Both Eurocode 3 (Eurocode 1993) and AISC Specification (AISC 2005) have adopted the 2% total strain definition for the yield stress of structural steel at elevated temperatures.

Figure 4.14 shows the initial portion of a stress-strain curve from this test program for 400°C and a crosshead displacement rate of 0.01 in/min. The values of yield stress are shown for the three definitions of yield stress: 43.8 ksi for 0.2% offset strain, 45.8 ksi for 0.5% total strain, and 57.5 ksi for 2% total strain definition. It is clear that the choice of the definition of yield stress can have a very large impact on the resulting value of yield stress.
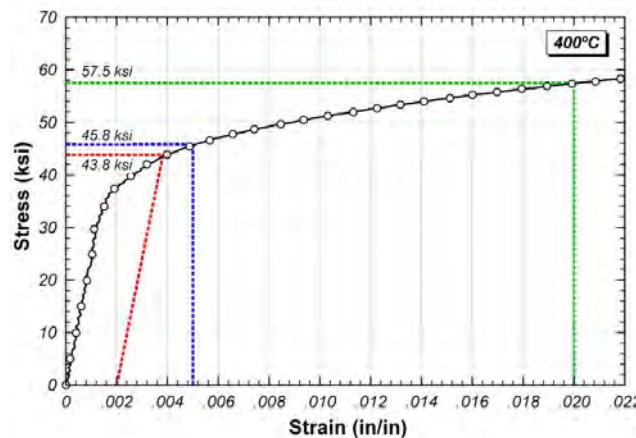
Figure 4.14 Example of yield stress definitions at 400°C

Yield stress–retention factors based on the data collected in this research are plotted in Figure 4.15. The yield stress–retention factor is defined as the yield stress at a

97

specific temperature (using stress-strain curves at 0.01 in/min crosshead displacement rate) divided by the yield stress at ambient temperature. The retention factors for yield stress based on the 0.2% offset, 0.5% total strain and 2% total strain definitions are compared with retention factors from the Eurocode 3 and from the AISC Specification in Figure 4.15. Note that Eurocode 3 and the AISC Specification use the same retention factors for yield stress, and are therefore plotted as a single line. As can clearly be seen on MA and MC from Figure 4.15a and Figure 4.15b, for temperatures in the range of 100 to 500°C, the yield stress–retention factors from tests, based on the 0.2% offset and 0.5% total strain definitions, are significantly lower than the corresponding values specified by Eurocode 3 and the AISC Specification except for MB material. To the contrary, Figure 4.15c shows a good agreement between retention factors from test data of MA material and those predicted by the codes, when the retention factors for the test data are based on the 2% total strain definition of yield stress. However, MB has high conservative from room temperature to 500°C while MC has it around 400°C. Similar observations can be made from Figure 4.15d, Figure 4.15e and Figure 4.15f, where yield stress–retention factors are presented and compared with code predictions for materials MA, MB, and MC, respectively. From these figures, it can be seen that the values of yield stress from the test data are fairly close to one another for the 0.2% offset and 0.5% total strain definitions. Further, above about 600°C, all three definitions of yield stress give similar values. However, below 600°C, the yield stress based on the 2% total strain definition is significantly higher than the yield stress values based on the other two definitions.

As is clear from Figure 4.15, the yield stress of steel at elevated temperatures up to about 600°C is highly dependent on the manner in which it is defined. Based on Twilt and Both (1991), it appears that the yield stress–retention factors for structural steel at elevated temperatures used in Eurocode 3 were adopted from British Steel Corporation data (Kirby and Preston, 1988). However, little was found in the literature to support this definition of yield stress for structural-fire engineering design of steel structures. It seems that the most appropriate definition for yield stress of steel at elevated temperatures

98

ultimately lies in how these values are used in design formulas, and further investigation and discussion of this issue appears justified.

a) 0.2% offset definition   *d) MA: Different yield stress definitions*

b) 0.5% offset definition   *e) MB: Different yield stress definitions*

c) 2.0% offset definition   *f) MC: Different yield stress definitions*
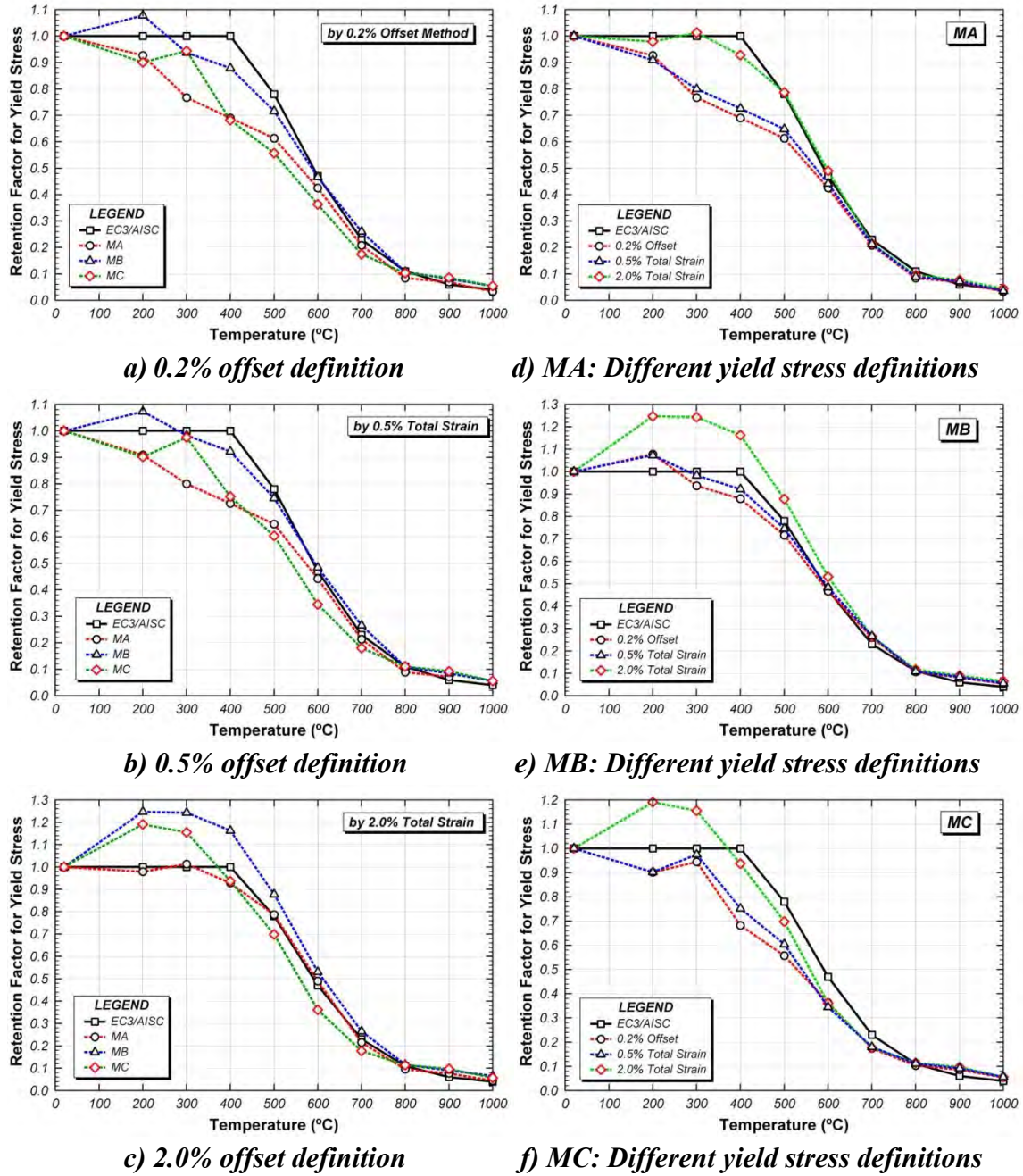
Figure 4.15 Yield stress–retention factors

99

The yield stresses and associated retention factors obtained by representative material MA are summarized in Table 4.2 for the different definitions of yield stress. Table 4.3 shows how the room-temperature value of yield stress was retained at higher temperatures. For comparison, the yield stress–retention factors from Eurocode 3 (Eurocode 1993), and Outinen (Outinen and Makelainen 2004) are provided.

Table 4.2 Yield stress for Material MA (ksi)

Method	Temperature (°C)									
	20	200	300	400	500	600	700	800	900	1000
0.2% offset	63.1	58.5	48.4	43.5	38.7	26.8	13.1	5.3	4.4	2.1
0.5% strain	63.2	57.4	50.5	45.8	41.0	27.9	13.5	5.6	4.6	2.3
2.0% strain	61.9	60.6	62.8	57.5	48.7	30.3	13.3	5.9	4.7	2.7

Table 4.3 Yield stress–retention factor for Material MA

Method or Source	Temperature (°C)									
	20	200	300	400	500	600	700	800	900	1000
0.2% offset	1.00	0.93	0.77	0.69	0.61	0.43	0.21	0.08	0.07	0.03
0.5% strain	1.00	0.91	0.80	0.73	0.65	0.44	0.21	0.09	0.07	0.04
2.0% strain	1.00	0.98	1.01	0.93	0.78	0.49	0.22	0.09	0.08	0.04
Eurocode 3	1.00	1.00	1.00	1.00	0.78	0.47	0.23	0.11	0.06	0.04
Outinen	1.00	0.93	0.89	0.86	0.62	0.38	0.14	0.11	0.07	0.03

4.4.2 Tensile Strength

The tensile strength was defined as the maximum measured engineering stress. The retention factors for tensile strength, obtained for all steel materials tested in this program, are compared with the corresponding values in Eurocode 3 and AISC Specification in Figure 4.16. In Figure 4.16a, the tensile strength–retention factor is defined as the tensile strength measured at a specific temperature divided by the yield stress measured at ambient temperature. The data is presented in this manner as this is how the tensile strength–retention factor is defined in both Eurocode 3 and the AISC

Specification. For temperatures at and above 400°C, both Eurocode 3 and the AISC Specification take the elevated-temperature tensile strength equal to the elevated-temperature yield stress.

Figure 4.16b shows the tensile strength–retention factors from the tests, where the retention factor is defined as tensile strength measured at a specific temperature divided by the tensile strength measured at ambient. This seems to be a more conventional definition of tensile strength–retention factor. For reference, the tensile strength values obtained for each steel material at elevated temperatures are shown in Table 4.4. Comparing the elevated-temperature tensile strength values listed in Table 4.4 with the elevated-temperature yield stress values based on the 2% total strain definition, it can be seen that the tensile strength generally exceeds the yield strength for temperatures up through and including 500°C. For 600°C and above, the measured tensile strength and yield strength values are essentially the same. The experimentally determined tensile strengths are summarized on Table 4.4 and plotted in Figure 4.16.

a) By ($f_{u,T}/f_{y,20°C}$) definition   *b) By ($f_{u,T}/f_{u,20°C}$) definition*
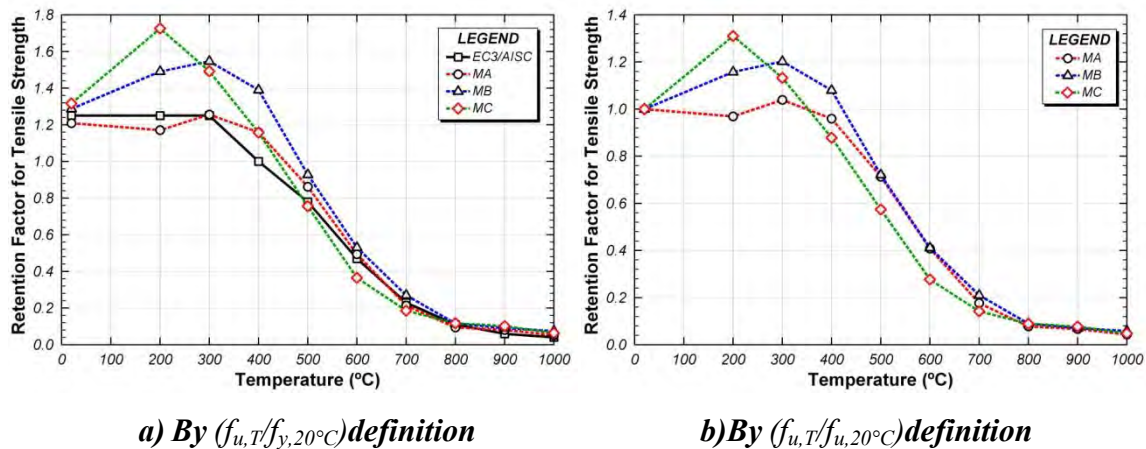
Figure 4.16 Tensile strength–retention factors

Table 4.4 Tensile strength (ksi)

Material Type	Temperature (°C)									
	20	**200**	**300**	**400**	**500**	**600**	**700**	**800**	**900**	**1000**
MA	76.2	73.8	79.2	73.1	54.3	31.1	13.5	5.9	5.1	3.3
MB	66.2	76.6	79.5	71.5	47.7	27.2	13.9	5.9	4.7	3.9
MC	68.3	89.4	77.4	60.0	39.2	18.9	9.7	6.1	5.3	3.3

4.4.3   Elastic Modulus

The elastic modulus at elevated temperature is defined as the slope of the stress-strain curve in the linear-elastic range just as at room temperature, as shown in Figure 4.17 and Table 4.5. The elastic modulus was determined by measuring the slope of the initial linear portion of the stress-strain curves for tests conducted at a crosshead displacement rate of 0.01 in/min. Strains were measured in the tension coupon tests using a non-averaging type extensometer, i.e. strains were measured on only one side of the coupon. Consequently, errors at small strain levels can occur due to bending of the coupon resulting in errors in the measured strain. As such, the elastic modulus values derived from the stress-strain curves may be subject to some error. Nonetheless, the elastic modulus data were still examined for general trends.
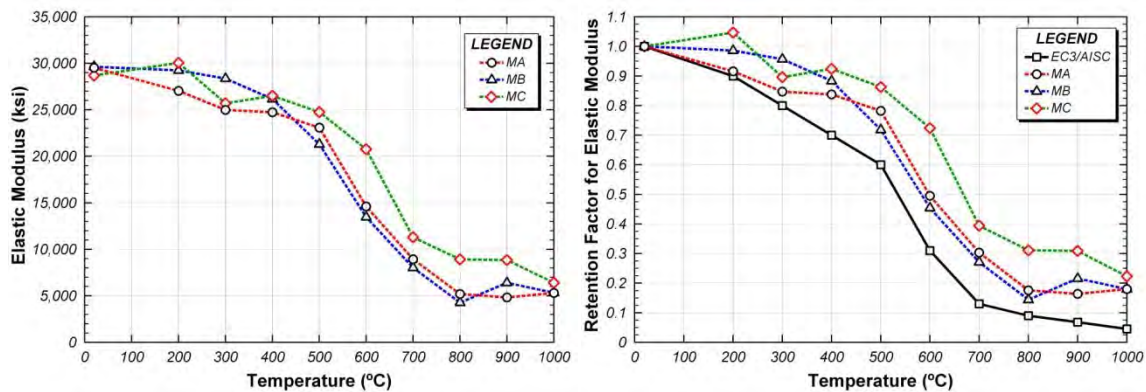
a) Elastic modulus   *b) Retention factors*

Figure 4.17 Elastic modulus and retention factor

102

Table 4.5 Elastic modulus (ksi)

Matl. Type	Temperature (°C)									
	20	200	300	400	500	600	700	800	900	1000
MA	29500	27000	25000	24700	23100	14600	8900	5190	4830	5320
MB	29600	29200	28600	26200	21300	14000	8350	4260	6400	5320
MC	28700	30000	25700	26500	24800	20800	11300	8900	8900	6400

Another way to look at this data is in terms of the ratio of elastic modulus at a given elevated temperature to the room-temperature elastic modulus. This elastic modulus–retention factor is presented in Table 4.6 and plotted in Figure 4.17. Also included, for sake of comparison, are results from the Eurocode 3 (Eurocode 1993).

Table 4.6 Elastic modulus–retention factor

Material or Source	Temperature (°C)									
	20	200	300	400	500	600	700	800	900	1000
MA	1.00	0.91	0.84	0.83	0.77	0.49	0.27	0.18	0.16	0.18
MB	1.00	0.99	0.97	0.88	0.72	0.47	0.28	0.14	0.22	0.18
MC	1.00	1.05	0.90	0.92	0.86	0.72	0.39	0.31	0.31	0.22
Eurocode 3	1.00	0.90	0.80	0.70	0.60	0.30	0.10	0.00	0.07	0.05

4.4.4 Proportional Limit

The proportional limit is defined as the stress at which the linear portion of the stress-strain curve ends. The value of the proportional limit is used in Eurocode 3 to compute buckling capacities of steel members (column buckling, lateral torsional buckling, etc.). Some judgment was needed in interpreting the stress strain curve to establish the end of the linear portion, so the proportional limit values reported here should be considered approximate. The experimentally determined proportional limits are summarized in Table 4.7. The retention factor for proportional limit from the tests are

compared to the predictions of Eurocode 3 (Eurocode 1993) in Table 4.8 and plotted in Figure 4.18b. In general, reasonable agreement can be found between experimental retention factors for proportional limit and those predicted by Eurocode 3 and by AISC Specification.

a) Proportional limit strength   b) Retention factor
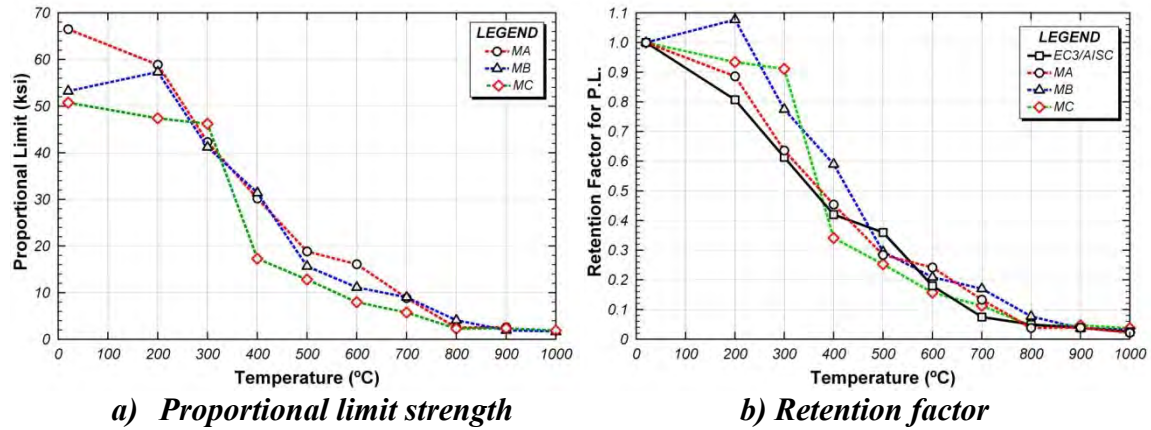
Figure 4.18 Proportional limit and associated retention factor

Table 4.7 Proportional limit (ksi)

Material Type	Temperature (°C)									
	20	200	300	400	500	600	700	800	900	1000
MA	66.5	58.9	42.3	30.2	18.9	16.1	8.9	2.5	2.6	1.4
MB	53.2	57.3	41.7	31.4	15.7	11.1	9.0	4.1	2.0	1.7
MC	50.7	47.4	46.2	17.3	12.9	8.0	5.7	2.3	2.4	1.9

Table 4.8 Proportional limit–retention factor

Material or Source	Temperature (°C)									
	20	200	300	400	500	600	700	800	900	1000
MA	1.00	0.89	0.64	0.45	0.28	0.24	0.13	0.04	0.04	0.02
MB	1.00	1.08	0.78	0.59	0.29	0.21	0.17	0.08	0.04	0.03
MC	1.00	0.93	0.91	0.34	0.25	0.16	0.11	0.05	0.05	0.04
Eurocode 3	1.00	0.81	0.61	0.42	0.36	0.18	0.08	0.05	0.04	0.03

4.4.5 Elongation

To evaluate differences in the measured elongation based on extensometer gauge length, elongations were measured simultaneously using the 1PS and 2PS extensometers for material MA coupons. The elongation at failure and the associated retention factor for the 1PS (1-inch gauge length) and 2PS (2-inch gauge length) extensometers are summarized in Table 4.9, Table 4.10, and plotted in Figure 4.19. The elongation at failure measured by 2PS was approximately two-thirds that measured by 1PS due to the different gauge lengths, as discussed earlier. Although the two extensometers give significantly different values of elongation, the elongation retention factors are quite similar, as seen in Figure 4.19b.
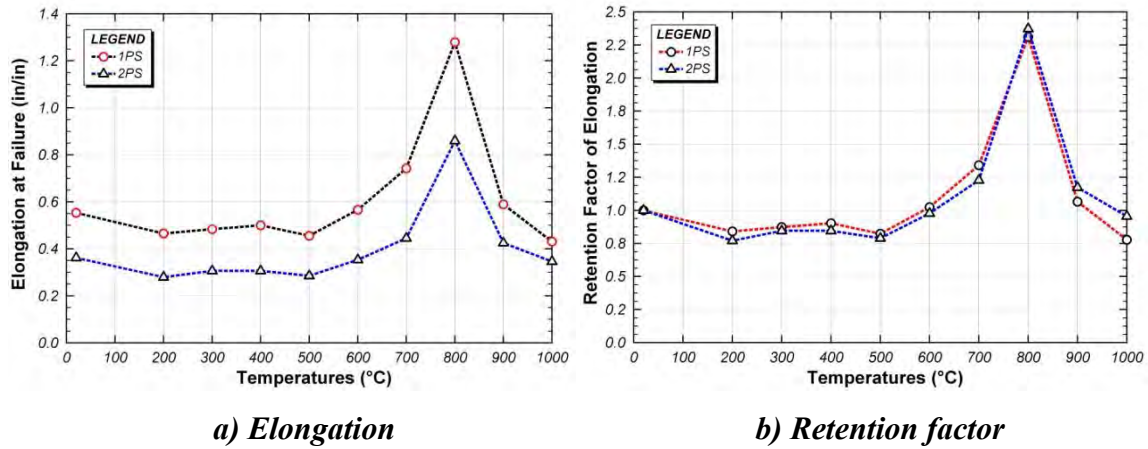
| a) Elongation | b) Retention factor |

Figure 4.19 Elongation and associated retention factor

Table 4.9 Elongation at failure (in/in) for Material MA

Source	Temperature (°C)									
	20	**200**	**300**	**400**	**500**	**600**	**700**	**800**	**900**	**1000**
1PS	0.55	0.47	0.48	0.50	0.46	0.57	0.74	1.28	0.59	0.43
2PS	0.36	0.28	0.31	0.31	0.29	0.35	0.45	0.86	0.43	0.35

Table 4.10 Elongation retention factor for Material MA

Source	Temperature (°C)									
	20	200	300	400	500	600	700	800	900	1000
1PS	1.00	0.84	0.87	0.90	0.82	1.02	1.34	2.31	1.07	0.78
2PS	1.00	0.77	0.85	0.85	0.79	0.98	1.23	2.37	1.17	0.96

The elongation at failure for steel coupons for materials MA, MB and MC are shown in Figure 4.20 and Table 4.11. For this comparison, all values of elongation are for the 1PS extensometer. That is, all values of elongation are for a 1-inch gauge length. As seen in this figure, the elongation for materials MA and MB is relatively constant for temperatures up to 500°C and then shows a sharp increase up to 800°C, and finally a sharp decrease at 900°C, almost to its corresponding value except for room temperature. The elongation at failure was fairly constant with a sharp maximum value at 800°C. Here the elongation was more than double that at room temperature. This occurs due to a phase change in the steel: the austenite (γ-Fe), which forms above the eutectoid point can withstand more elongation (Callister 2007).

In case of material MC, the same trend can be observed although with less variation than seen for materials MA and MB. The primary difference in the trend of elongations can be seen in the temperature range of 900 to 1000°C, where material MA and MB see a drop in elongation while material MC experiences a rise in elongation.
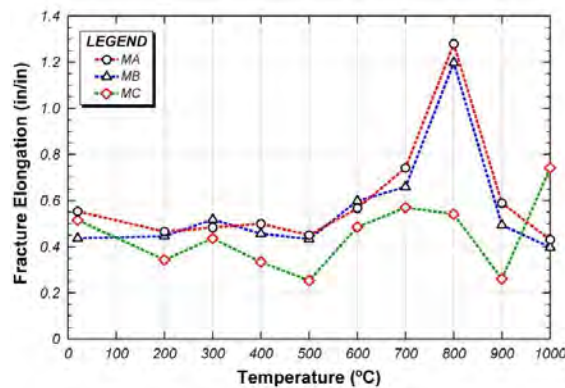
Figure 4.20 Elongations for Material MA, MB and MC

Table 4.11 Elongations for Materials MA, MB and MC (in/in)

Material Type	Temperature (°C)									
	20	**200**	**300**	**400**	**500**	**600**	**700**	**800**	**900**	**1000**
MA	0.55	0.47	0.48	0.50	0.45	0.57	0.74	1.28	0.59	0.43
MB	0.44	0.45	0.52	0.46	0.43	0.60	0.66	1.20	0.49	0.40
MC	0.52	0.34	0.44	0.33	0.25	0.49	0.57	0.54	0.26	0.74

4.5   CURVE FITTING AND ANALYSIS

In order to develop a constitutive model for elevated temperature stress-strain curves for ASTM A992 steel, curve fitting was performed on the stress-strain data at each temperature as a first step. The different types of curves fit for the test results at room and elevated temperatures are explained in the following sections. Based on this curve fitting, a detailed stress-strain model will subsequently be developed.

4.5.1   Curve Type

Two different types of stress-strain curves were seen in testing as shown in Figure 4.21. Curve Type I is the same shape as tension test results at room temperature. It has an elastic zone, a plastic zone, and a strain-hardening zone before strain softening and failure. Curve Type II was seen at high temperatures. There is no plastic plateau, and strain softening makes up a more significant portion of the response. Curve fitting was conducted according to the type of the curve.
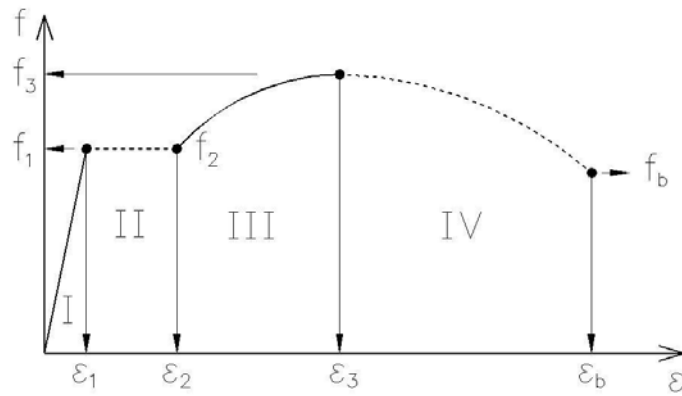
a) Curve Type I
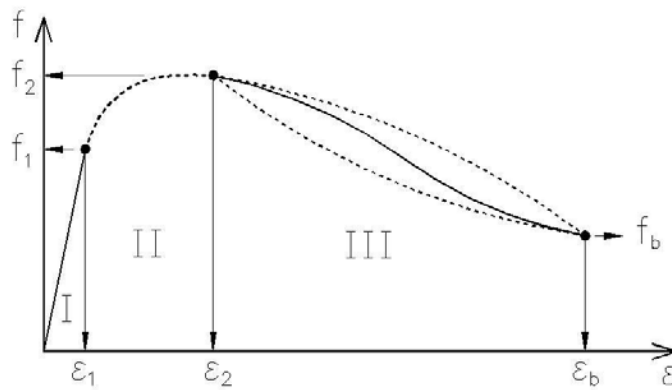
b) Curve Type II

Figure 4.**21 Curve types used for fitting**

Curve fitting was conducted based on the shape of the stress-strain curve for each temperature. Type I curves were used up to 300°C. Beyond that temperature, the Type II curve was more descriptive (Table 4.12).

Table 4.12 Curve types selected by temperature

Temp(°C)	20	200	300	400	500	600	700	800	900	1000
Type	I	I	I	II	II	II	II	II	II	II

4.5.2 Curve Fitting Equations

The following sections explain the six kinds of equations used for Type I and Type II curve fitting.

108

4.5.2.1 Lognormal Equation

The lognormal shown on Equation 4.1 was well suited for the strain-hardening zones of both Type I and Type II curve fits, as well as for the strain softening for the temperatures of 400 and 500°C.

$$y = y_0 + A \, Exp\left[-\left(\frac{LN\left(\frac{x}{x_0}\right)}{w}\right)^2\right] \tag{4.1}$$

where y = stress, y_0= initial stress, A = amplitude,
x_0 = peak position, w = peak width

4.5.2.2 Hill Equation

The Hill equation shown on Equation 4.2 was used for the strain hardening region of the Type II stress-strain curves at 600°C to 800°C.

$$y = y_0 + \frac{(A - y_0)}{1 + \left(\frac{x_{1/2}}{x}\right)^r} \tag{4.2}$$

where x = strain, y = stress, y_0= base: stress at small strain,
A = max: stress at large strain, r = rise rate,
$x_{1/2}$ = strain at which stress is $(y_0 + A)/2$

4.5.2.3 Power Law

A power law equation shown on Equation 4.3 was used for strain softening for most temperatures.

$$y = y_0 + A \, X^p \tag{4.3}$$

where x = strain, y = stress, y_0 = initial stress, A = amplitude,
p = power >1 or close to zero.

4.5.2.4 Exponential Equation

A decaying exponential equation shown on Equation 4.4 was used in the strain softening region at 800°C with a Type II curve fit.

109

$$y = y_0 + A\,Exp\left(\frac{x_0 - x}{\tau}\right)$$

(4.4)

where x = strain, y = stress, x_0 = initial strain value, y_0 = initial stress, A = amplitude, τ = fit coefficient

4.5.2.5 Polynomial Equation

A polynomial equation shown on Equation 4.5 was adopted for strain softening at 1000°C. The behavior at this temperature was different from others because of the re-crystallization phenomena, which manifests itself as a second phase of strain hardening after the onset of strain softening.

$$y = y_0 + k_1 x + k_2\,x^2 + ...$$

(4.5)

where x = strain, y = stress, y_0 = initial stress; k_1, k_2... = parameters.

4.5.2.6 Linear Equation

A linear equation shown on Equation 4.6 was used in plastic plateau region at low temperatures.

$$y = y_0 + A\,x$$

(4.6)

where x = strain, y = stress, y_0 = initial stress, A = slope

4.5.3 Curve Fitting by Temperatures

The following sections present the curve fits of the stress-strain data. For each temperature, the equations selected and parameters determined for each region of the response are shown. The strain data used here is that measured by the 1PS extensometer. After the curve fits for each temperature are individually presented, a summary of the stresses and strains at the transition points between the different zones of response is given for all temperatures (Table 4.23). These transition points are the proportional limit, the 0.2% offset yield point, the point of ultimate tensile stress, and the fracture point.

110

4.5.3.1 Curve fitting at 20°C

The curve Type I model was adopted at this temperature and the detailed curve fitting results are shown in Figure 4.22 and Table 4.13.

a) Zone I

b) Zone II

c) Zone III

d) Zone IV
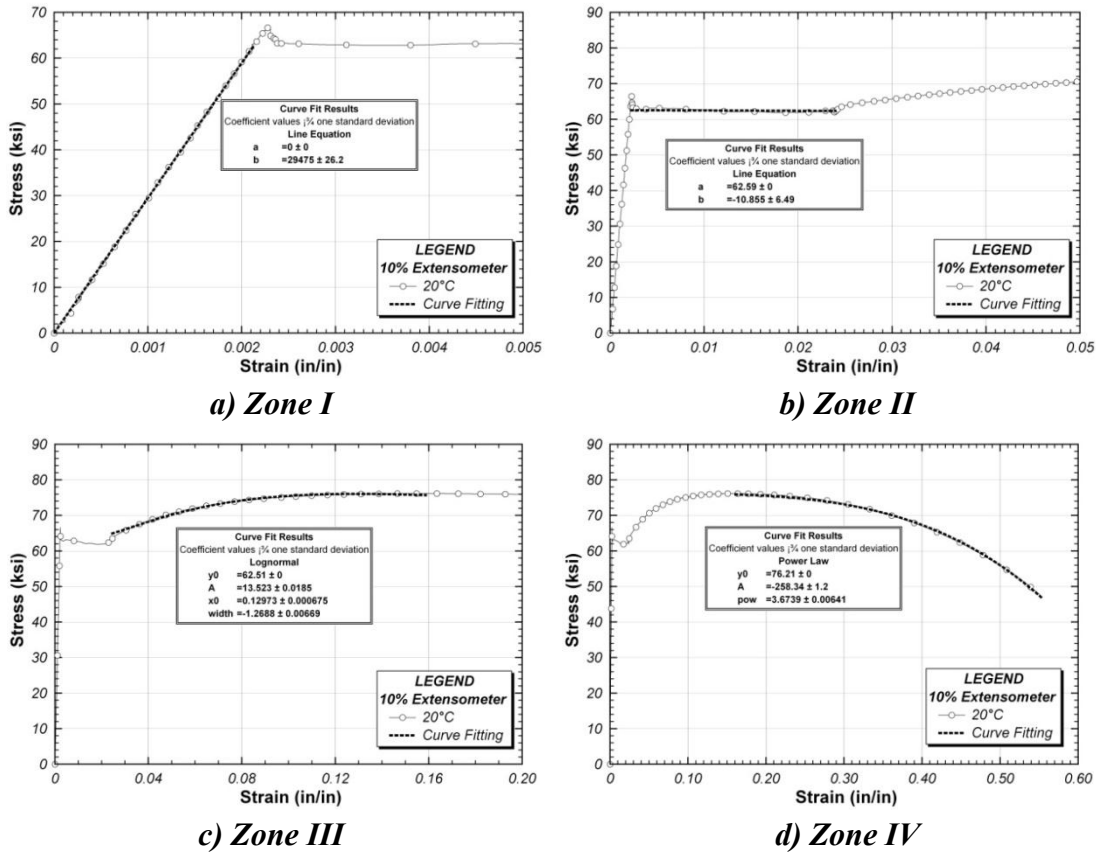
Figure 4.22 Fitted equations at 20°C stress-strain curve

Table 4.13 Parameters after curve fitting at 20°C

Zone	Equation	Parameters for Type I model			
I	Line	$a = 0$	$b = 29,475$	-	-
II	Line	$a = 62.59$	$b = -10.855$	-	-
III	Lognormal	$y_0 = 62.51$	$A = 13.523$	$x_0 = 0.12973$	$w = -1.2688$
IV	Power Law	$y_0 = 76.21$	$A = -258.34$	$p = 3.6739$	-

111

4.5.3.2 Curve fitting at 200°C

The curve Type I model was adopted at this temperature and the detailed curve fitting results are shown in Figure 4.23 and Table 4.14.

a) Zone I

b) Zone II

c) Zone III

d) Zone IV
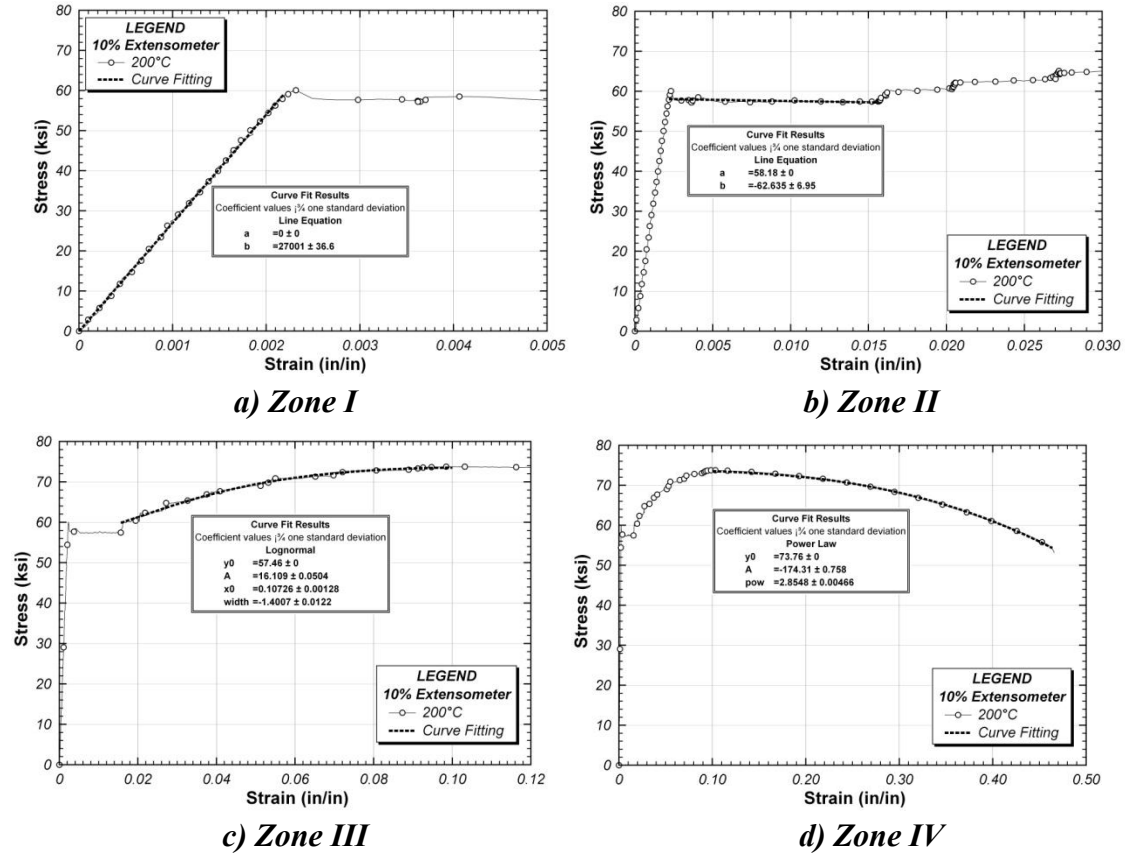
Figure 4.23 Fitted equation at 200°C stress-strain curve

Table 4.14 Parameters after curve fitting at 200°C

Zone	Equation	Parameters for Type I model			
I	Line	$a = 0$	$b = 27{,}001$	-	-
II	Line	$a = 58.18$	$b = -62.635$	-	-
III	Lognormal	$y_0 = 57.46$	$A = 16.109$	$x_0 = 0.10726$	$w = -1.4007$
IV	Power Law	$y_0 = 73.76$	$A = -174.31$	$p = 2.8548$	-

112

4.5.3.3 Curve fitting at 300°C

The curve Type I model was adopted at this temperature and the detailed curve fitting results are shown in Figure 4.24 and Table 4.15.

a) Zone I

b) Zone II

c) Zone III

d) Zone IV
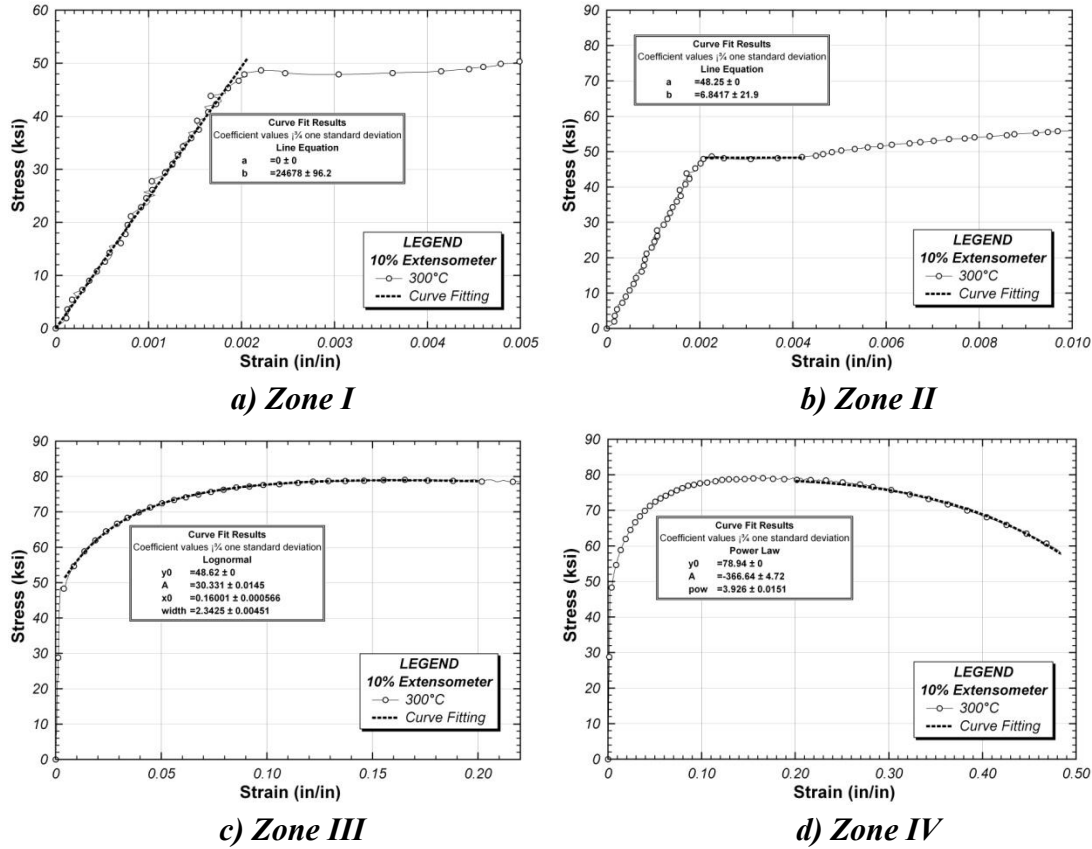
Figure 4.24 Fitted equations at 300°C stress-strain curve

Table 4.15 Parameters after curve fitting at 300°C

Zone	Equation	Parameters for Type I model			
I	Line	$a = 0$	$b = 24{,}678$	-	-
II	Line	$a = 48.25$	$b = 6.842$	-	-
III	Lognormal	$y_0 = 48.62$	$A = 30.331$	$x_0 = 0.16001$	$w = 2.3425$
IV	Power Law	$y_0 = 78.94$	$A = -366.64$	$p = 3.926$	-

4.5.3.4 Curve fitting at 400°C

The curve Type II model was adopted at this temperature and the detailed curve fitting results are shown in Figure 4.25 and Table 4.16.

a) Zone I

b) Zone II

c) Zone III
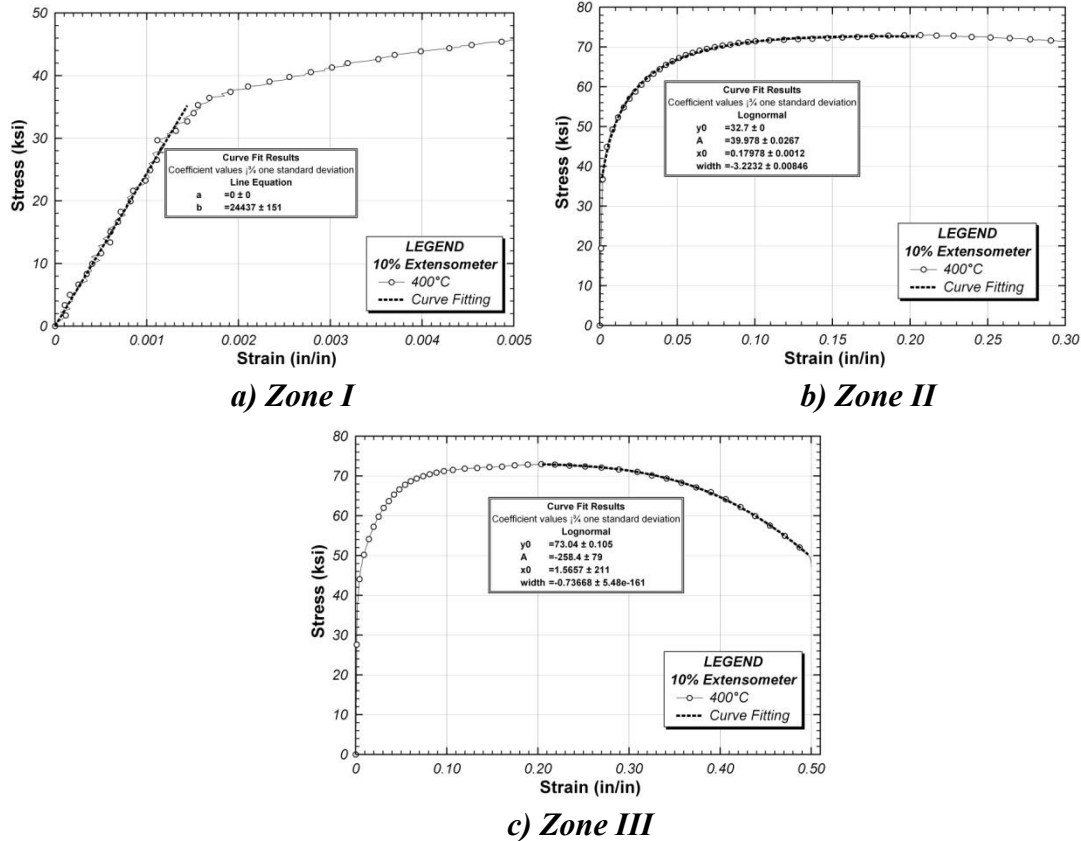
Figure 4.25 Fitted equations at 400°C stress-strain curve

Table 4.16 Parameters after curve fitting at 400°C

Zone	Equation	Parameters for Type II model			
I	Line	$a = 0$	$b = 24{,}437$	-	-
II	Lognormal	$y_0 = 73.04$	$A = -258.4$	$x_0 = 1.5657$	$w = -0.73668$
III	Lognormal	$y_0 = 32.70$	$A = 39.978$	$x_0 = 0.17978$	$w = -3.2232$

114

4.5.3.5 Curve fitting at 500°C

The curve Type II model was adopted at this temperature and the detailed curve fitting results are shown in Figure 4.26 and Table 4.17.

a) Zone I

b) Zone II

c) Zone III
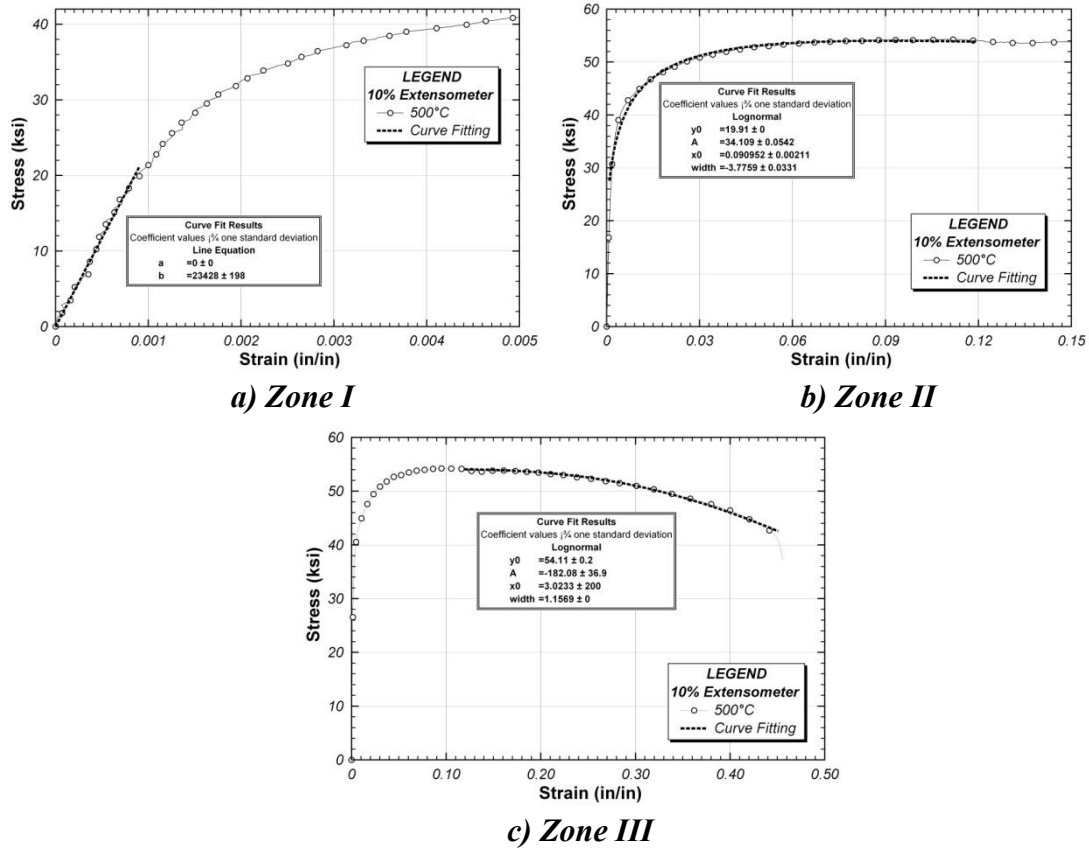
Figure 4.26 Fitted equations at 500°C stress-strain curve

Table 4.17 Parameters after curve fitting at 500°C

Zone	Equation	Parameters for Type II model			
I	Line	$a = 0$	$b = 23{,}428$	-	-
II	Lognormal	$y_0 = 19.91$	$A = 34.109$	$x_0 = 0.090952$	$w = -3.7759$
III	Lognormal	$y_0 = 54.11$	$A = -182.08$	$x_0 = 3.0233$	$w = 1.1569$

4.5.3.6 Curve fitting at 600°C

The curve Type II model was adopted at this temperature and the detailed curve fitting results are shown in Figure 4.27 and Table 4.18.

a) Zone I

b) Zone II

c) Zone III
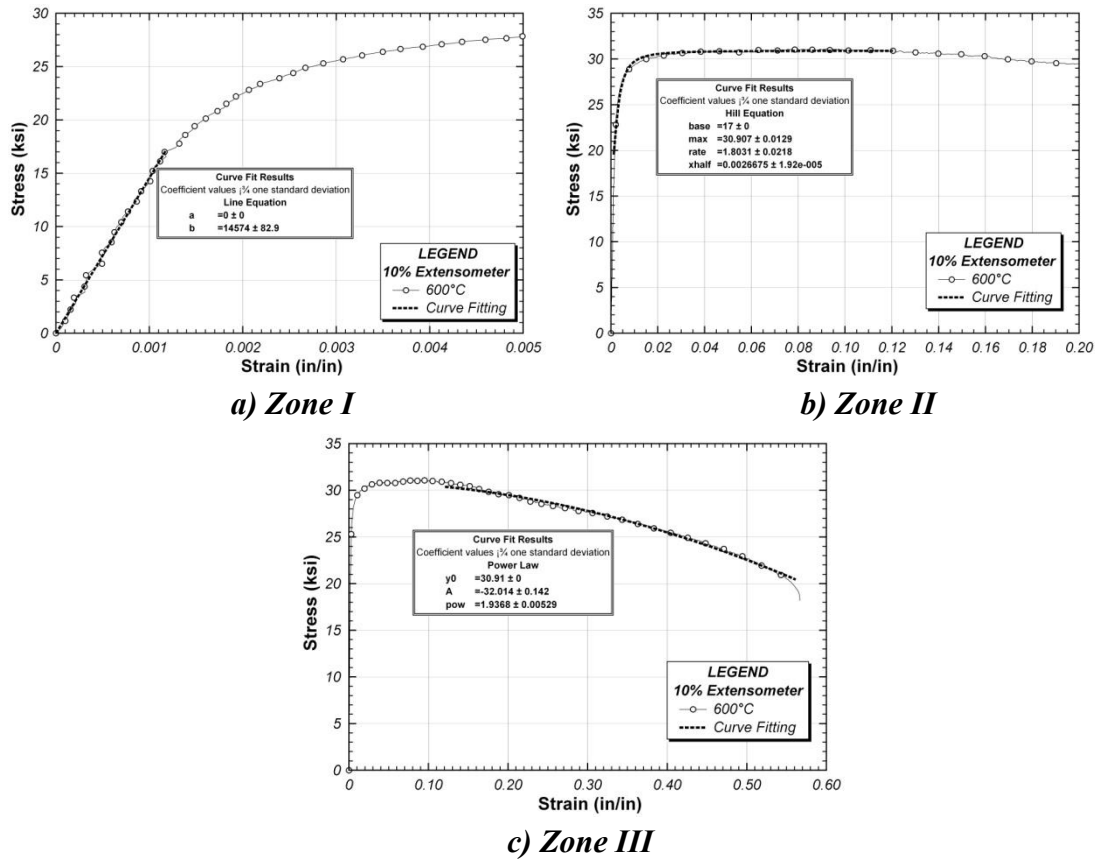
Figure 4.27 Fitted equations at 600°C stress-strain curve

Table 4.18 Parameters after curve fitting at 600°C

Zone	Equation	Parameters for Type II model			
I	Line	$a = 0$	$b = 14,574$	-	-
II	Hill Equation	$y_0 = 17.00$	$A = 30.907$	$r = 1.8031$	$x_{1/2} = 0.0026675$
III	Power Law	$y_0 = 30.91$	$A = -32.014$	$p = 1.9368$	-

4.5.3.7 Curve fitting at 700°C

The curve Type II model was adopted at this temperature and the detailed curve fitting results are shown in Figure 4.28 and Table 4.19.

a) Zone I

b) Zone II

c) Zone III
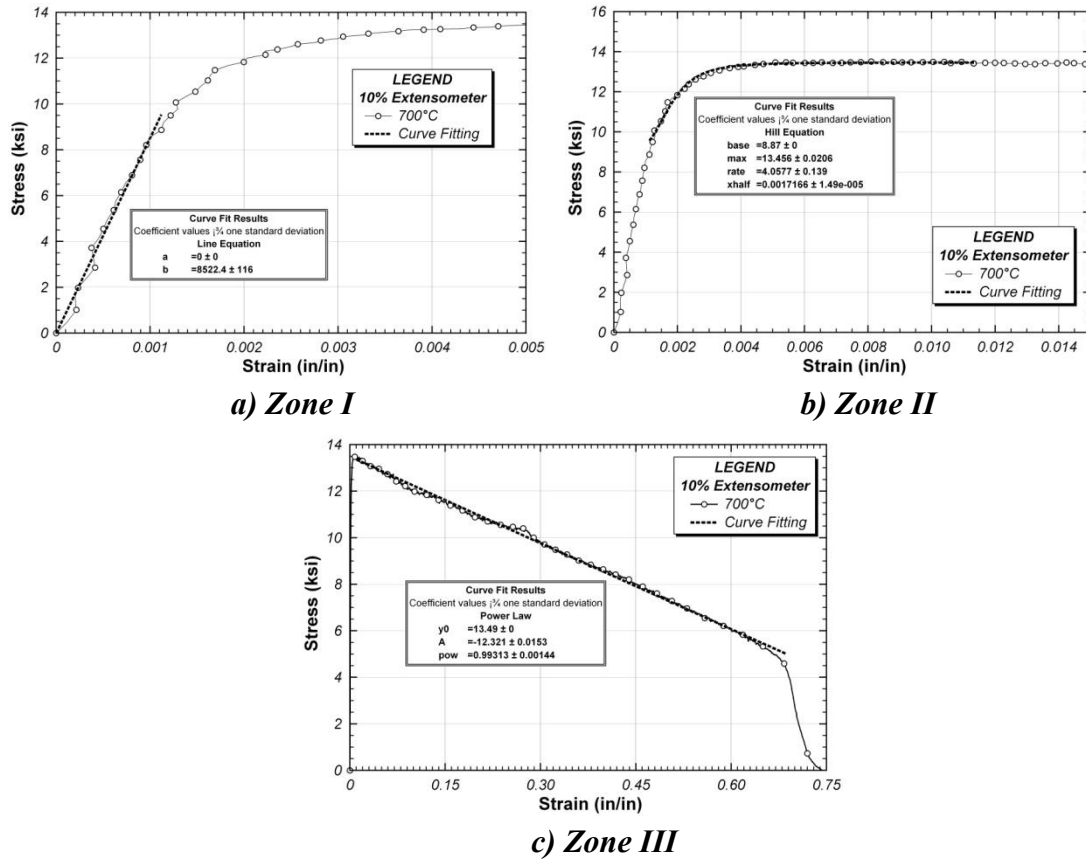
Figure 4.28 Fitted equations at 700°C stress-strain curve

Table 4.19 Parameters after curve fitting at 700°C

Zone	Equation	Parameters for Type II model			
I	Line	$a = 0$	$b = 8,522$	-	-
II	Hill Equation	$y_0 = 8.87$	$A = 13.456$	$r = 4.0577$	$x_{1/2} = 0.0017166$
III	Power Law	$y_0 = 13.49$	$A = -12.321$	$p = 0.99313$	-

4.5.3.8 Curve fitting at 800°C

The curve Type II model was adopted at this temperature and the detailed curve fitting results are shown in Figure 4.29 and Table 4.20.

a) Zone I   *b) Zone II*

c) Zone III
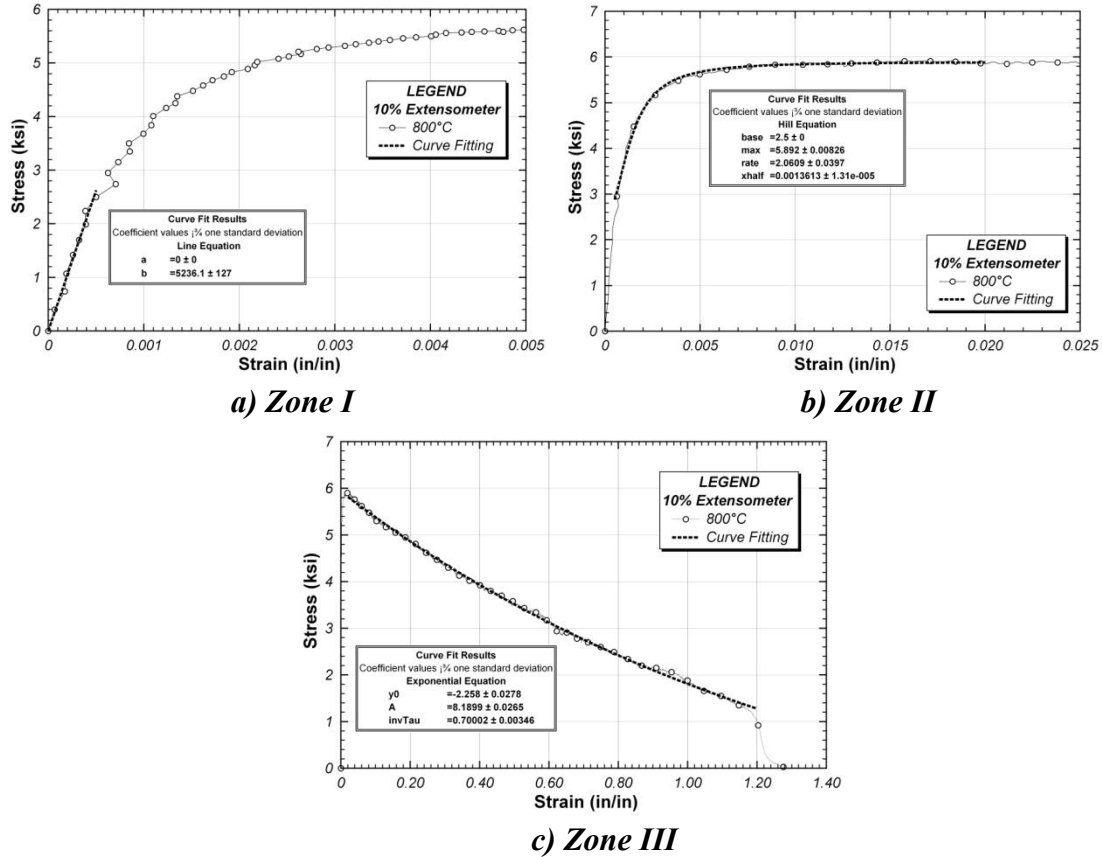
Figure 4.29 Fitted equations at 800°C stress-strain curve

Table 4.20 Parameters after curve fitting at 800°C

Zone	Equation	Parameters for Type II model			
I	Line	$a = 0$	$b = 5,236$	-	-
II	Hill Equation	$y_0 = 2.50$	$A = 5.892$	$r = 2.0609$	$x_{1/2} = 0.0013613$
III	Exponential	$y_0 = -2.26$	$A = 8.1899$	$p = 0.70002$	-

4.5.3.9 Curve fitting at 900°C

The curve Type II model was adopted at this temperature and the detailed curve fitting results are shown in Figure 4.30 and Table 4.21.

a) Zone I

b) Zone II

c) Zone III
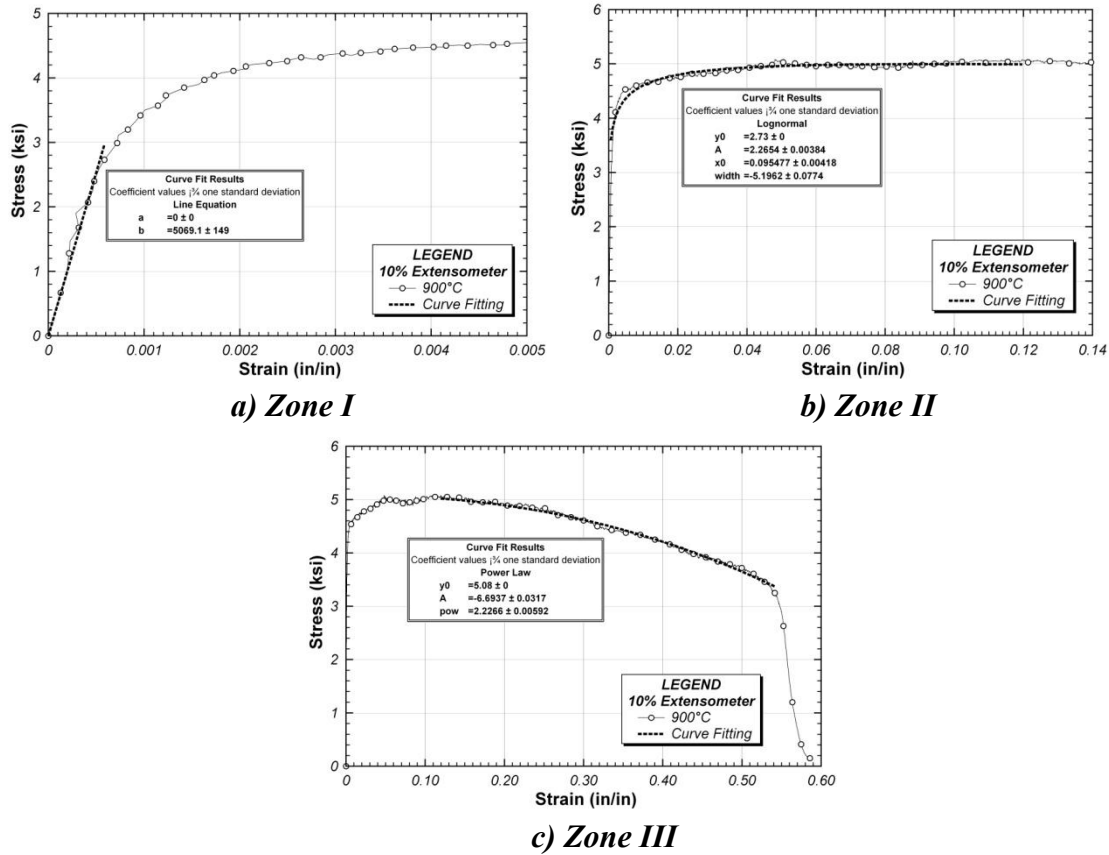
Figure 4.30 Fitted equations at 900°C stress-strain curve

Table 4.21 Parameters after curve fitting at 900°C

Zone	Equation	Parameters for Type II model			
I	Line	$a = 0$	$b = 5{,}069$	-	-
II	Lognormal	$y_0 = 2.73$	$A = 2.2654$	$x_0 = 0.095477$	$w = -5.1962$
III	Power Law	$y_0 = 5.08$	$A = -6.6937$	$p = 2.2266$	-

4.5.3.10 Curve fitting at 1000°C

The curve Type II model was adopted at this temperature and the detailed curve fitting results are shown in Figure 4.31 and Table 4.22.

a) Zone I

b) Zone II

c) Zone III
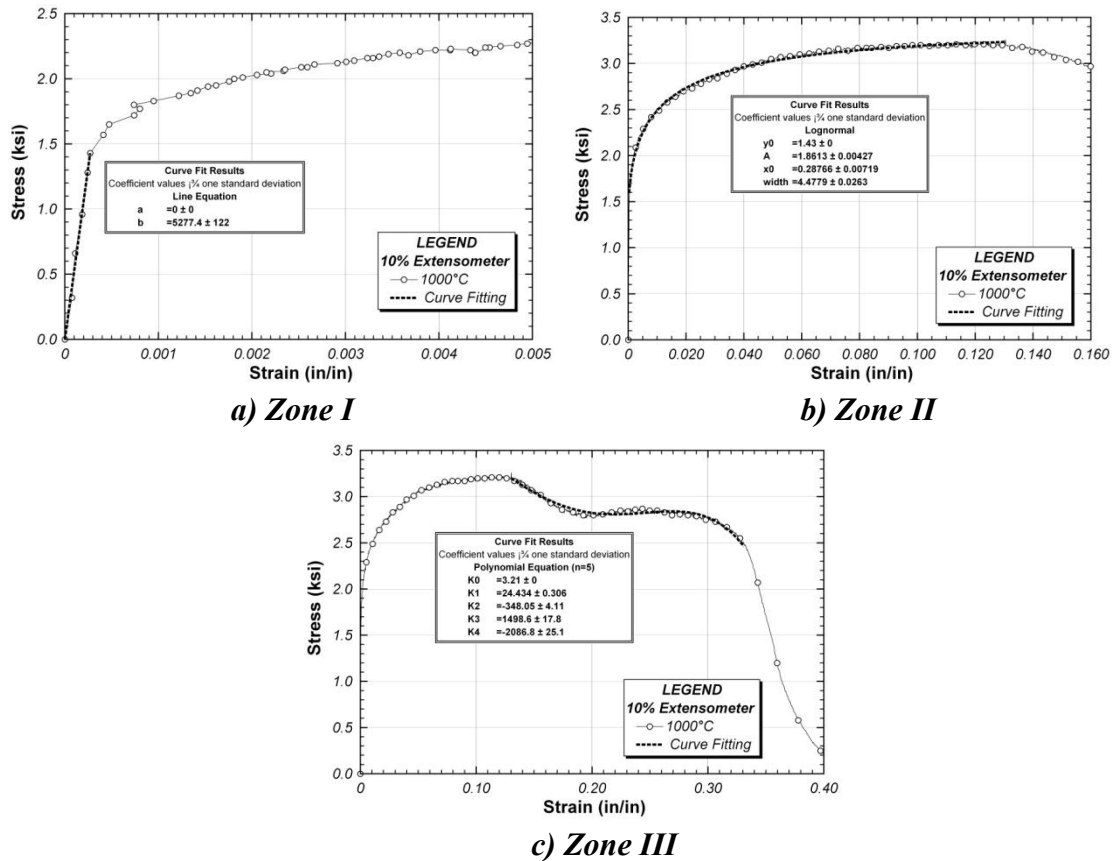
Figure 4.31 Fitted equations at 1000°C stress-strain curve

Table 4.22 Parameters after curve fitting at 1000°C

Zone	Equation	Parameters for Type II model			
I	Line	$a = 0$	$b = 5,277$	-	-
II	Lognormal	$y_0 = 1.43$	$A = 1.8613$	$x_0 = 0.28766$	$w = 4.4799$
III	Polynomial	$y_0 = 3.21$	$k_1 = 24.434$	$k_2 = -348.05$	$k_3 = 1498.6$ $k_4 = -2086.8$

Table 4.23 Curve connection points between fitted curves

Temp(°C)	20	200	300	400	500	600	700	800	900	1000
f_p	62.59	58.18	48.25	32.7	19.91	17.00	8.87	2.50	2.73	1.43
f_y	62.51	57.46	48.62	43.30	38.48	26.86	13.23	5.30	4.32	2.08
f_u	76.21	73.76	78.94	73.04	54.11	30.91	13.49	5.87	5.08	3.21
f_b	47.02	54.03	58.07	50.06	40.83	19.57	4.45	1.01	3.2	2.5
ε_p	.0119	.0022	.0020	.0013	.0008	.0012	.0010	.0005	.0005	.0003
ε_y	.0042	.0042	.0040	.0038	.0036	.0038	.0038	.0050	.0028	.0024
ε_u	.1593	.1001	.2000	.2045	.1194	.1204	.0100	.0200	.1197	.1301
ε_b	.5536	.4638	4832	.4968	.4508	.5614	.6856	1.200	.5427	.3310

4.6   CONSTITUTIVE EQUATION S AND DISCUSSION

Two models were developed to predict the stress-strain behavior of ASTM A992 steel at elevated temperature, based on the test data developed in this test program. These two models will be referred to as the "Detailed Model' and the "Simple Model." The Detailed Model is intended for use in advanced analysis of steel structures subjected to fire, using finite element programs such as Abaqus or ANSYS. The Simple Model is intended where a simplified stress-strain law gives sufficiently accurate results, as may be the case in many design applications.

4.6.1   Detailed Model for Stress-Strain Behavior

The objective of the Detailed Model was to closely simulate the measured stress-strain results of ASTM A992 at each temperature while using a consistent set of equations. This last point is a point of difference with the curve fits developed in the previous sections, which consisted of a unique combination of the six equation types. The equations used in this model and their applicable strain and temperature ranges are shown in Figure 4.32 and Table 4.24. The parameters for each equation are provided in Table 4.25.

121
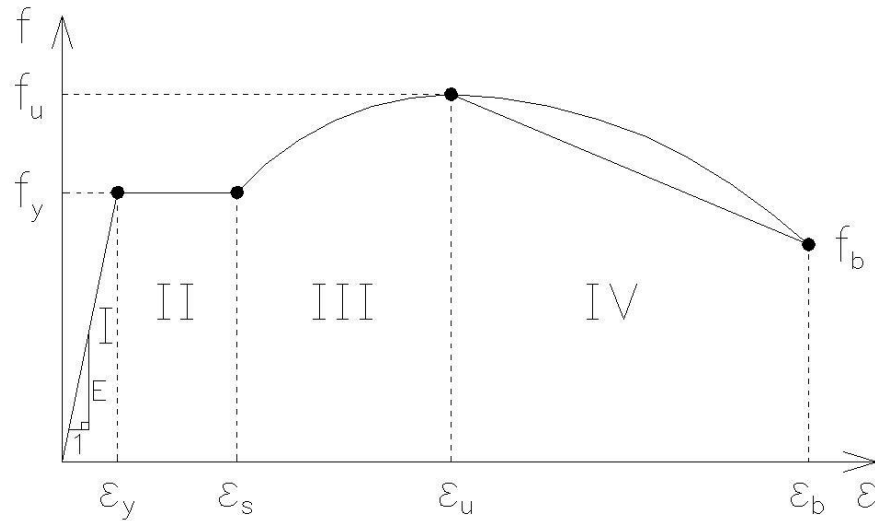
Figure 4.32 Assumed behavior for Detailed Model

Table 4.24 Detailed Model for Stress-Strain Behavior

Zone	Strain Range	Stress	Temp Range
I	$\varepsilon \leq \varepsilon_y$	$E\,\varepsilon$	20 – 1000°C
II	$\varepsilon_y \leq \varepsilon \leq \varepsilon_s$	f_y	20–300°C (for ≥400°C, $\varepsilon_s = \varepsilon_y$, there is no Zone II)
III	$\varepsilon_s \leq \varepsilon \leq \varepsilon_u$	$f_y + c\left[1 - \left(\dfrac{\varepsilon - \varepsilon_s - a}{a}\right)^2\right]^{1/2}$	20–1000°C
IV	$\varepsilon_u \leq \varepsilon \leq \varepsilon_b$	$f_b + d\left[1 - \left(\dfrac{\varepsilon - \varepsilon_u}{c}\right)^2\right]^{1/2}$	20–1000°C (except for 700 and800°C)
		$f_u + \dfrac{d}{b}(\varepsilon - \varepsilon_u)$	700–800°C only
Parameters		$a = \varepsilon_u - \varepsilon_s,\ b = \varepsilon_b - \varepsilon_u,\ c = f_u - f_y,\ d = f_u - f_b$	

Table 4.25 Detailed Model parameters

Parameter	Temperature (°C)									
	20	200	300	400	500	600	700	800	900	1000
E_θ / E	1.000	0.909	0.843	0.830	0.771	0.492	0.274	0.176	0.163	0.180
$f_{y\theta} / f_y$	1.000	0.928	0.769	0.688	0.611	0.427	0.210	0.084	0.069	0.033
f_u / f_y	1.20	1.25	1.65	1.70	1.40	1.15	1.00	1.10	1.15	1.53
f_b / f_y	0.60	0.80	1.00	1.00	1.00	0.60	0.30	0.05	0.60	1.15
ε_s	0.024	0.02	0.004	ε_y	ε_y	ε_y	ε_y	ε_y	ε_y	ε_y
ε_u	0.150	0.100	0.150	0.150	0.100	0.050	0.005	0.010	0.100	0.100
ε_b	0.554	0.466	0.484	0.500	0.450	0.567	0.694	1.208	0.548	0.330

where

E_θ = Elastic modulus at elevated temperatures

$f_{y\theta}$ = Yield stress by 0.2% offset methods at elevated temperatures

f_u = Tensile strength

f_b = Breaking strength at failure

ε_y = Yield strain

ε_s = Beginning strain at strain hardening

ε_u = Tensile strength at ultimate point

ε_b = Breaking strain at failure

4.6.2 Simple Model for Stress-Strain Behavior

Given the complexities of the first constitutive model, a much simpler model was developed for use in design. The cost of simplicity is less accuracy. The normalized stress-strain curves (Figure 4.33) proved to be a good starting point when developing the simplified model. Viewed on this basis, it was apparent that for many temperatures, the stress at failure was higher than that at yield.
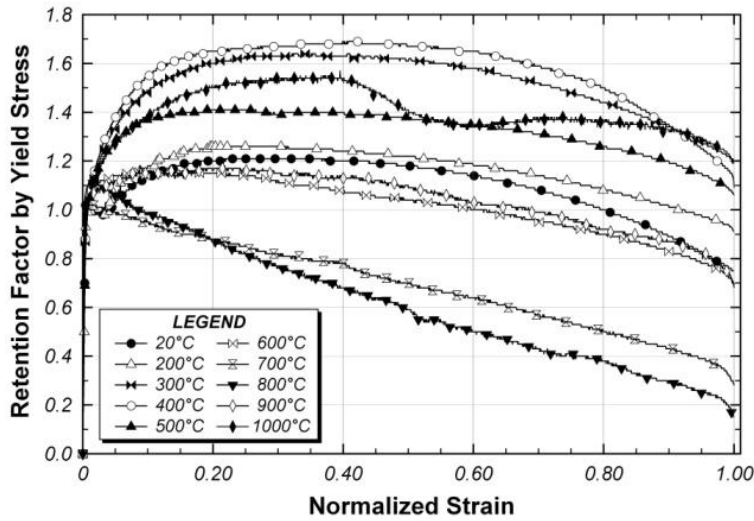
Figure 4.33 Normalized stress-strain curves for all temperatures

A bi- and tri-linear stress-strain model was developed by using the 0.2% proof stress and strain, 5% total strain and initial tangent slope up to 10–15% strain as illustrated in Figure 4.34. The first step to construct the Simple Model is to find the yield stress using the 0.2% offset method (Point "A") and then to find the stress at 5% total strain and stress by using the given stress ratio relation (Point "B"). The strain limit of the Simple model is defined as the last strain (Point "C") and is provided in Table 4.26. The strain limit is set around 10 to 15% because necking was occurred near these strain values
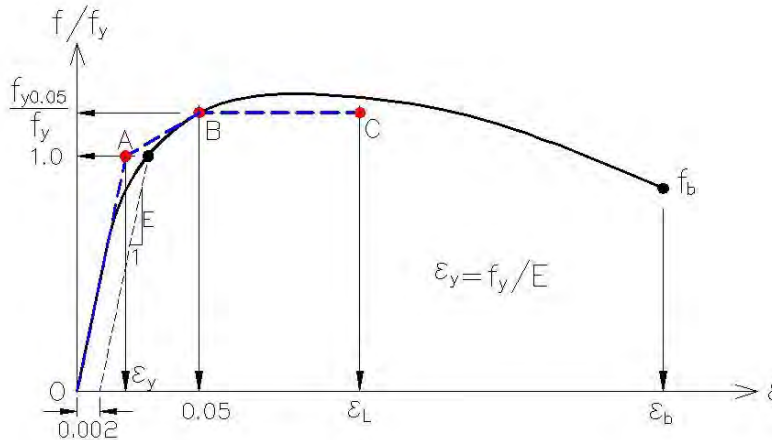
Figure 4.34 Schematic diagram of Simple Model

124

There are two ways for generating the Simple model. The first way is to generate the Simple model by using the parameters summarized in Table 4.26.

Table 4.26 Simple Model parameters

Parameter	Temperature (°C)									
	20	**200**	**300**	**400**	**500**	**600**	**700**	**800**	**900**	**1000**
E (ksi)	29,600	26,900	24,900	24,500	22,800	14,500	8,100	5,200	4,800	5,300
f_y (ksi)	62.9	58.4	48.4	43.3	38.5	26.9	12.0	5.3	4.3	2.1
$f_{y0.05}$ (ksi)	70.6	69.2	72.3	67.1	53.0	30.8	12.0	5.3	4.8	3.0
ε_L	0.15	0.15	0.15	0.15	0.15	0.15	0.10	0.10	0.15	0.15

The second way is able to generate the Simple Model by using generalized equations. The generalized equation was constructed with polynomial equations and correction factors as a function of temperature. The equation, constants and parameters are provided in Equation 4.7, Table 4.27 and Table 4.28 respectively.

$$F_y = \alpha\,(a\,x^3 + b\,x^2 + c\,x + d)$$
$$E = \beta\,(a\,x^3 + b\,x^2 + c\,x + d) \tag{4.7}$$
$$\varepsilon_y = \frac{F_y}{E}$$

where

F_y, ε_y, E = yield stress, yield strain and elastic modulus at elevated temperatures

a, b, c, d = constants, α, β = correction factors, x = applied temperature (°C)

Table 4.27 Constants for Simple Model equation

Constants	a	b	c	d
F_y (ksi)	1.442E-07	-2.261E-04	2.139E-02	6.193E+01
E (ksi)	8.797E-05	-1.425E-01	3.118E+01	2.788E+04

Table 4.28 Parameters for generalized Simple Model

Parameter	Temperature (°C)									
	20	**200**	**300**	**400**	**500**	**600**	**700**	**800**	**900**	**1000**
α	1.011	1.001	0.932	0.995	1.128	1.096	0.770	0.649	1.366	1.465
β	1.040	0.923	0.931	1.059	1.209	1.018	0.805	0.779	1.040	1.174
$f_{y0.05}/f_y$	1.122	1.185	1.496	1.549	1.377	1.147	1.000	1.000	1.111	1.466
ε_L	0.15	0.15	0.15	0.15	0.15	0.15	0.10	0.10	0.15	0.15

4.6.3 Model Verification

The Detailed and Simple models are evaluated by comparing the stress-strain curves at every specific elevated temperature. Also included, for sake of comparison, are results derived from the Eurocode 3 model, the only existing codified model that provides steel stress-strain equations for steel at elevated at elevated temperatures. The comparison of constitutive model was performed with Eurocode 3, experimental results, Detailed and Simple models. These comparisons are provided in Figure 4.35 to a) Initial portion of stress-strain curve   b) Full stress-strain curve

.

In examining these comparisons, several observations can be made. First, the Detailed model matches the experimental data quite closely. This is no surprise, since the model is based on curve fitting to the experimental data. The Simplified model provides a reasonable representation of the initial potion of the experimental data, although the model somewhat underestimates strain hardening at lower temperatures. The Eurocode 3 model, also underestimates strain hardening at lower temperatures but somewhat overestimates hardening at higher temperatures.
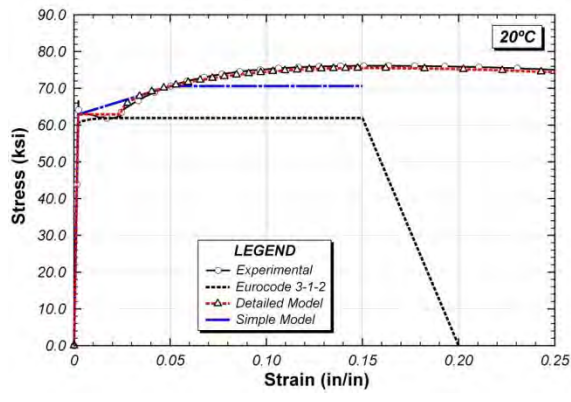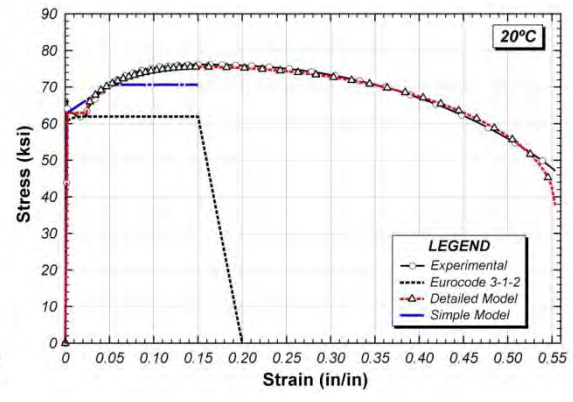
a) Initial portion of stress-strain curve   *b) Full stress-strain curve*
Figure 4.35 Constitutive models at 20°C
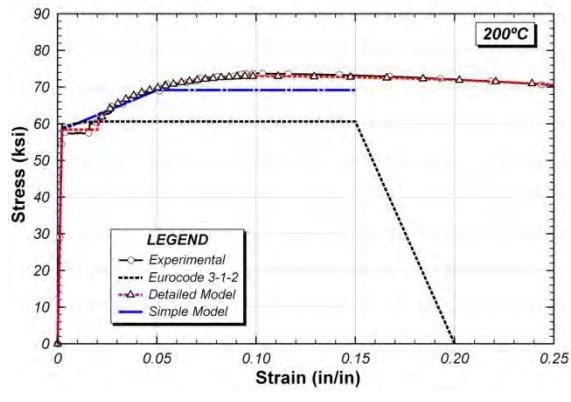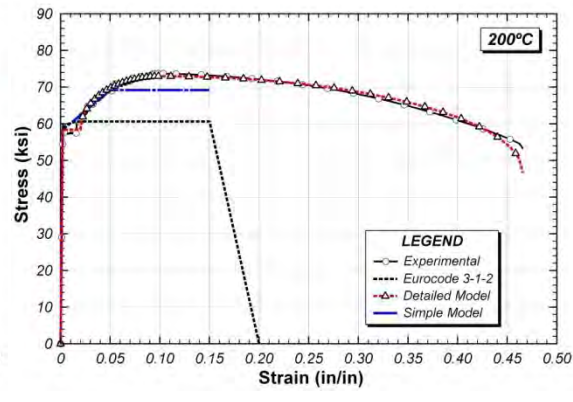
a) Initial portion of stress-strain curve   *b) Full stress-strain curve*
Figure 4.36 Constitutive models at 200°C
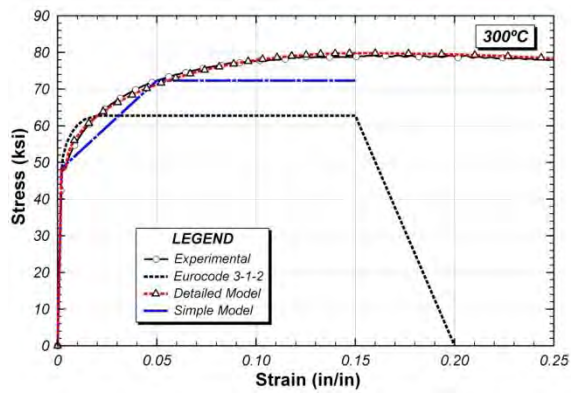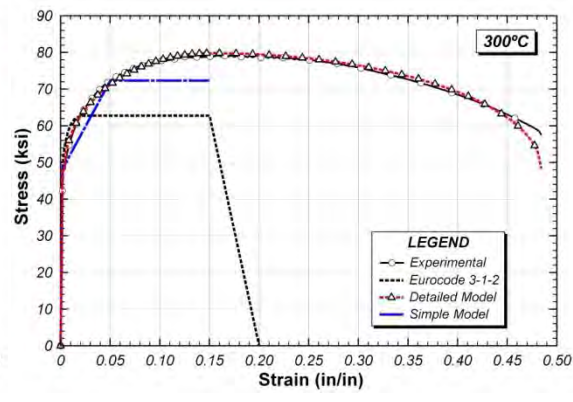
a) Initial portion of stress-strain curve   *b) Full stress-strain curve*
Figure 4.37 Constitutive models at 300°C

127
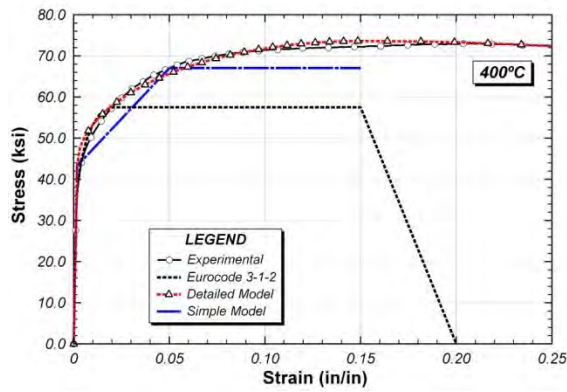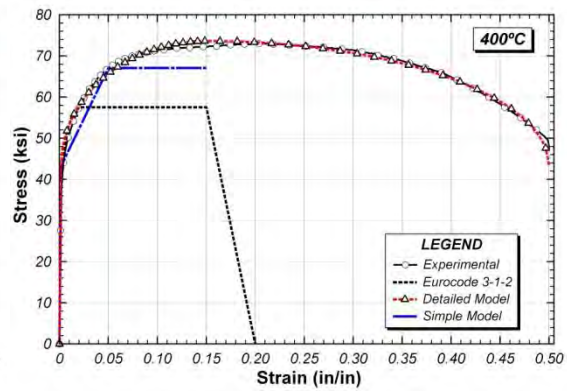
a) Initial portion of stress-strain curve   *b) Full stress-strain curve*

Figure 4.38 Constitutive model at 400 ℃
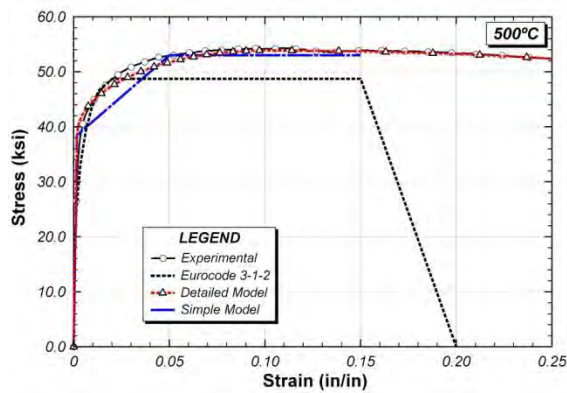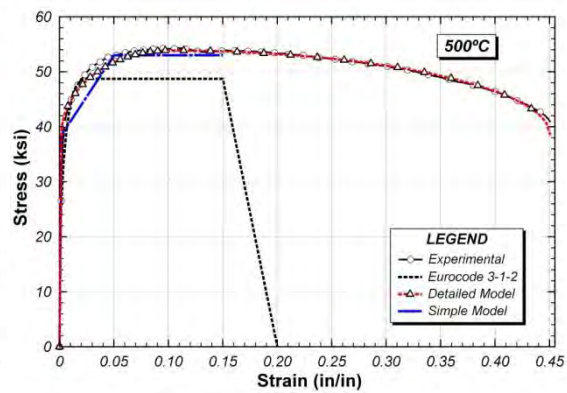
a) Initial portion of stress-strain curve   *b) Full stress-strain curve*

Figure 4.39 Constitutive models at 500℃
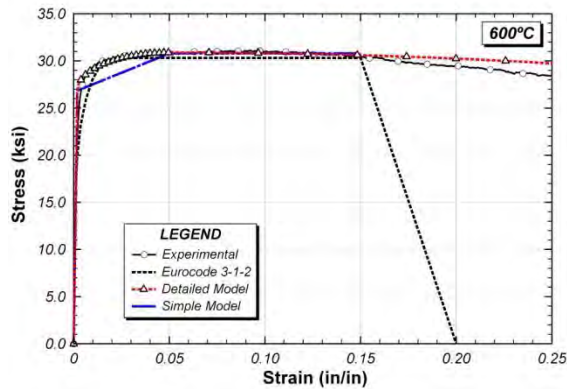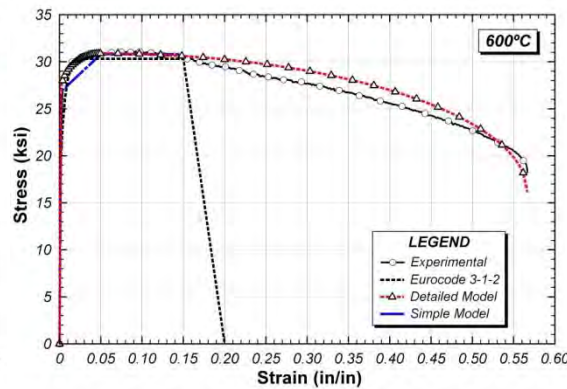
a) Initial portion of stress-strain curve   *b) Full stress-strain curve*

Figure 4.40 Constitutive models at 600℃

128
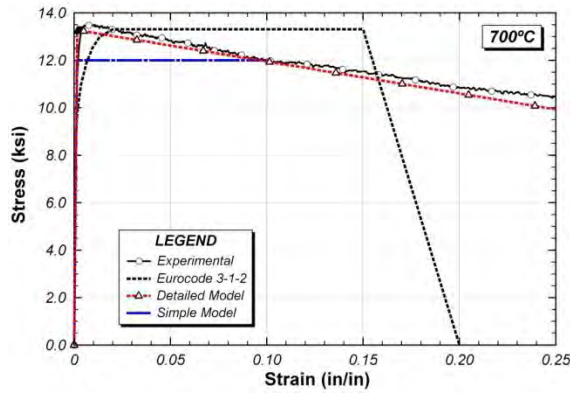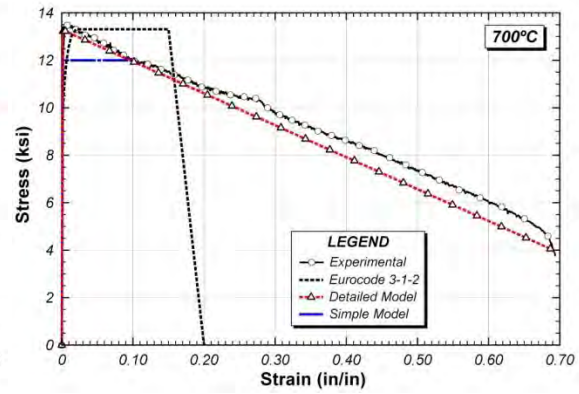
a) Initial portion of stress-strain curve *b) Full stress-strain curve*

Figure 4.41 Constitutive models at 700°C
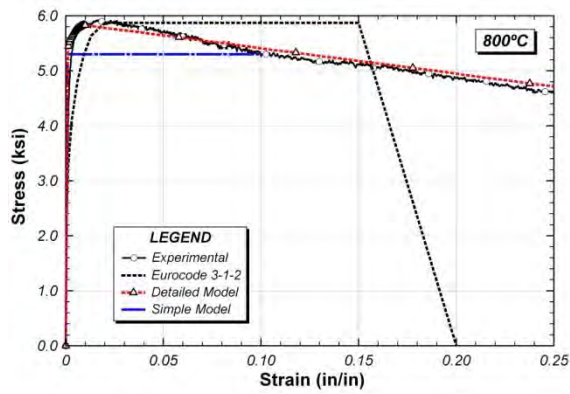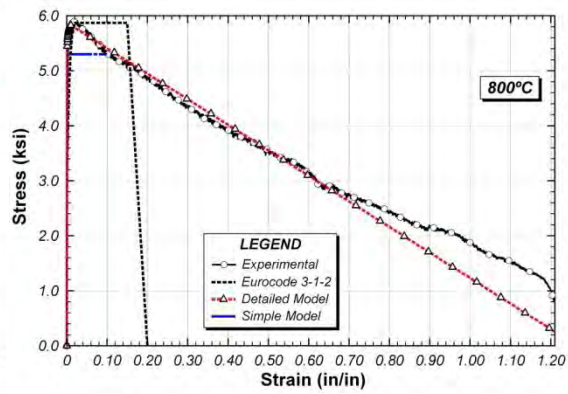
a) Initial portion of stress-strain curve *b) Full stress-strain curve*

Figure 4.42 Constitutive models at 800°C
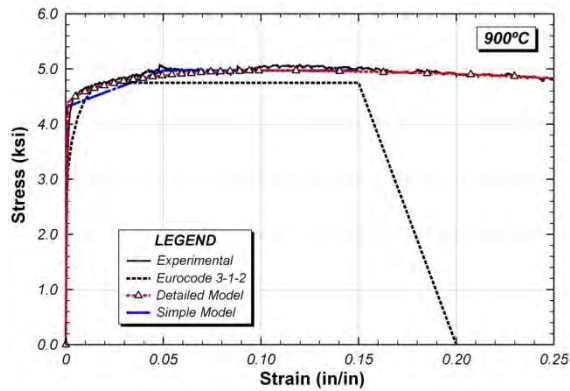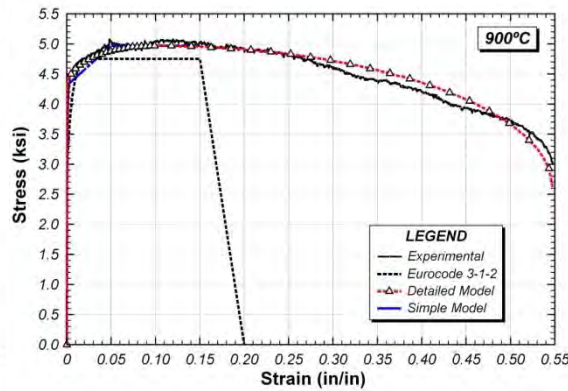
a) Initial portion of stress-strain curve *b) Full stress-strain curve*

Figure 4.43 Constitutive models at 900°C

129
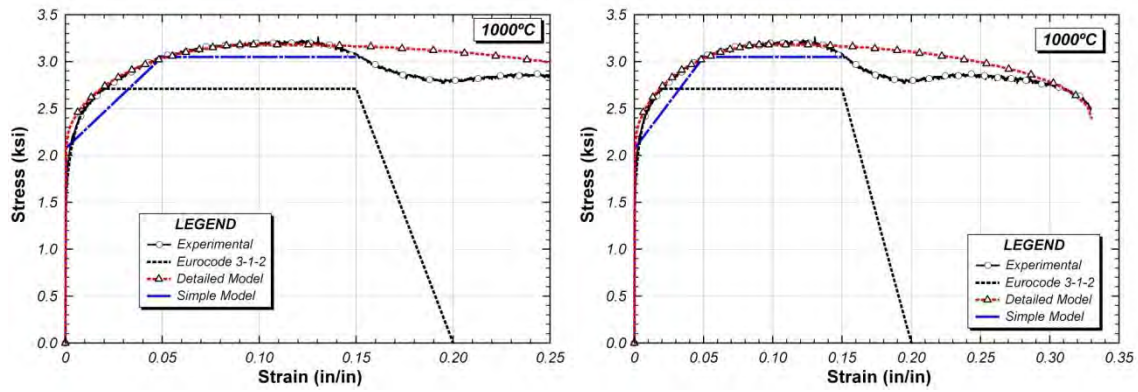
a) Initial portion of stress-strain curve   *b) Full stress-strain curve*

Figure 4.44 Constitutive models at 1000°C

4.7 SUMMARY AND CONCLUSIONS

This chapter presented results of tension tests of A992 steel at elevated temperatures. From this test data, curve fits for stress-strain behavior at each individual temperature were developed, as well as two temperature-dependent models for stress-strain behavior.

Testing indicated that most mechanical properties of steel (elastic modulus, yield stress, proportional limit, and tensile strength) decrease dramatically with increasing temperatures up to the highest temperature tested, 1000°C. The elongation was fairly constant at lower temperatures, with a slight rise at 700°C and then a sharp maximum at 800°C before returning to lower values up to 1000°C. This phenomenon, for low carbon steel such as A992, is directly related to the phase change to ferrite (α-Fe) and austenite (γ-Fe) above the eutectoid temperature of the phase diagram. The tensile strength dropped to two-thirds of its room temperature value by 500°C, to one-third by 600°C, and to a fifth by 700°C. Above 800°C, the tensile strength was less than 5% of its room temperature value.

Though two extensometers were used for the testing, the results obtained from the 2PS extensometer were not accurate in the elastic region, as they resulted in unreliable elastic modulus measurements. However, the full stress-strain results from the 2PS

130

extensometer were helpful because less resetting of the extensometer was required during testing. It should be noted that the failure strain measured by the 1PS and 2PS extensometers was not same because of the different gauge lengths for these two extensometers

Curve fitting was carried out using best-fit equations on defined zones of the experimental stress-strain curves: elastic, plastic plateau, strain-hardening and strain-softening regions. The curve-fitting results were helpful to derive the constitutive models of the stress-strain curves at room and elevated temperatures. Two different stress-strain models were developed, referred to as the Detailed Model and the Simple Model.

CHAPTER 5

Mechanical Properties after Heating and Cooling

5.1 OVERVIEW

In this chapter, the results of a different kind of testing are described. Rather than performing tests at the elevated temperatures as in Chapter 4, the tests in this chapter were performed after heating and cooling: that is, heating specimens to the target elevated temperature, then allowing them to cool down, back to room temperature. This test procedure was developed to investigate the post-fire mechanical properties of ASTM A992 steel.

Most structures affected by fire do not collapse as a result of the fire event. Afterwards, an evaluation of the structural steel elements may be needed to establish the safety of the structure and to assess the need for repair or replacement of damaged members. Such a post-fire evaluation should be conducted on the basis of the structural integrity of the steel considering the continued service of the structure. As such, a detailed investigation of the room-temperature material properties of structural steel after exposure to high temperatures is justified.

One factor known to affect heat-treated steel is the rate of cooling the metal experiences. In a real-world fire-affected structure, a variety of cooling rates would be expected. Some members might cool gradually, left exposed to the atmosphere. Others might cool even more slowly, being insulated either by the fireproofing or other nonstructural materials. Yet others might be quenched, cooling rapidly after being sprayed by water used by emergency personnel to extinguish the fire. These three cases were simulated in this test program by the Cooled-in-Air (CIA), Cooled-in-Blanket (CIB) and Cooled-in-Water (CIW) conditions.

5.2 EXPERIMENTAL INVESTIGATION

Extensive discussion of the experimental techniques used for the tension testing at elevated temperatures was provided in Chapter 3. Many of those techniques are the same as those used for testing at room temperature after heating and cooling; these description will not be repeated. This section, rather, will highlight the differences between methods used for this testing and the methods previously described.

In addition to tension testing, testing for two additional properties, toughness and hardness, was performed. Standard testing for these properties requires use of special test machine. Toughness testing was conducted using the Charpy V-Notch (CVN) test. The additional steps taken to make the CVN specimens will be described. Following that, brief descriptions of the toughness and hardness test methods will be provided.

5.2.1 Test Specimen

The heating and cooling treatments described in this section were performed on coupons of two different lengths: 14 inch and 18 inch. The dimensions of the two coupons differed only in overall specimen length: the reduced sections of both specimens were identically sized at 2.25 inch long and 0.5 inch square (Figure 5.1). The chemical composition of steel coupon was shown in Table 5.1.

The 14-inch coupons were used for the tension testing described in this chapter. This shorter coupon length, based on the minimum practical grip length, was chosen for easier handling during the cooling process. The 18-inch coupons were cut down to produce Charpy V-Notch specimens after heating and cooling, and subsequently tested for toughness.

133
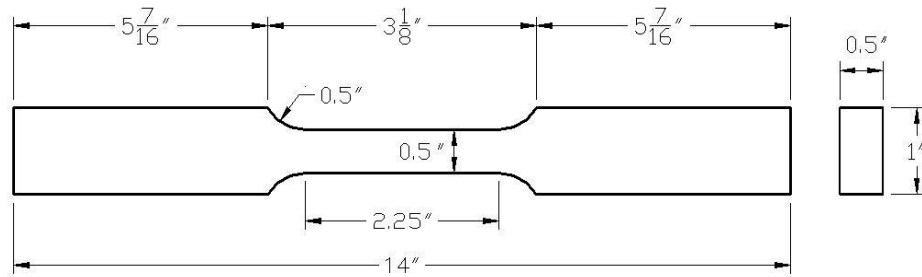
a) 14-inch coupon, used for tension testing
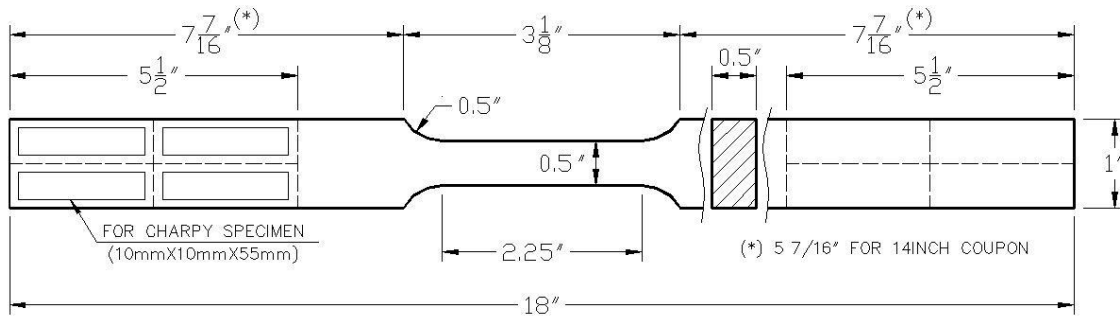
b) 18-inch coupon, used for toughness testing

Figure 5.1 Coupon dimensions

Table 5.1 Chemical composition for Material MB

Matl. Type	C	Cr	Mo	V	Ni	Mn	Si	P	S	Cu
MB	0.079	0.09	0.026	0.027	0.13	0.97	0.20	0.014	0.024	0.38

In both cases, coupons were fabricated of material type MB, which conformed to ASTM A992 as is shown in Table 3.4 and Table 5.2. Further description of this and the other steel material types used in this research can be found in Section 3.4.1.

Table 5.2 Room-temperature properties for Material MB

Material Type	Source	F_y (ksi)	F_u (ksi)
MB	Web of W30x99	51.3	66.2

134

5.2.2 Heating

An enclosed, stand-alone furnace was used to heat eight coupons at a time—four each of the 14 and 18 inch lengths—to specified target temperatures ranging from 200 to 1000°C. The coupons were heated and cooled side-by-side, so that their temperature profiles were the same, and as such, direct comparisons of the data from tension and toughness testing could be made.

5.2.2.1 Furnace

The furnace used for heat treatment was a 12,000-Watt Applied Test Systems (ATS) model with a rated temperature capacity of 1000°C. Similar to the MTS furnace used for elevated-temperature tension testing, this furnace had three heating elements, each of which could be controlled individually. Specifications of the furnace are given in the Table 5.3; it is depicted in Figure 5.2.

Table 5.3 Furnace specifications

Furnace	Wattage	Current per Zone	Voltage	Max Temp	Dimensions (D x W x H)
Applied Test Systems 3160	12,000 W	19.2 A	208 V	1000°C	24 x 24 x 28 inch
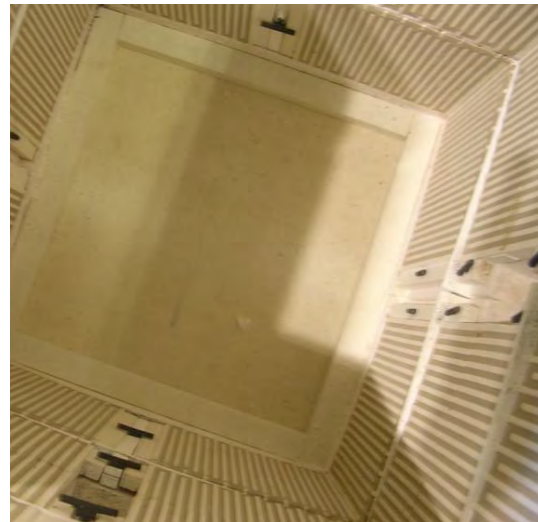
a) Exterior view   b) Interior view, with three heating zones visible
Figure 5.2 Furnace used for coupon heating

Inside the furnace, the coupons were suspended by nickel wire to allow for free thermal expansion and even exposure to heating on all surfaces. This type of wire was chosen as the material to minimize creep (and subsequent wire sagging) at elevated temperatures. The coupon mounting setup is shown in Figure 5.3. The refractory board on top was used both to close the furnace and for handling of the coupon.
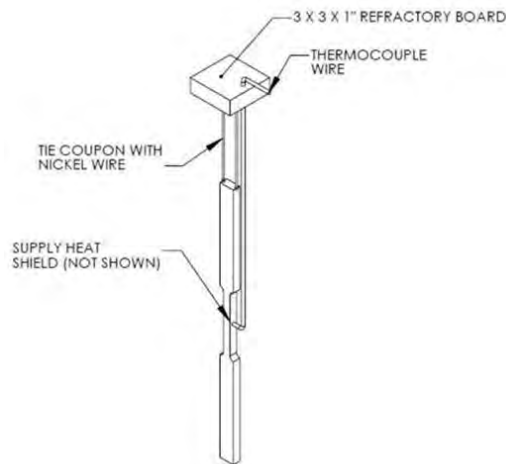
a) Coupon suspended by nickel wire   b) Handled using refractory board
Figure 5.3 Coupon suspension and handling scheme

Since free expansion was allowed, there was no need to monitor strain during heating, or to leave open small gaps in the furnace for this purpose. The heat-treatment furnace could then be fully enclosed. This setup allowed a more uniform temperature distribution over the coupon length as compared to the MTS setup discussed in Chapter 3. The use of one thermocouple, installed at the middle of the reduced section, was found to be adequate to track the coupon temperature throughout heating and cooling. The thermocouple installation consisted of one Type K wire thermocouple with stainless steel foil shielding; more information is available in Section 3.5.1. The coupon setup in the furnace can be seen in Figure 5.4.

a) Topside view of furnace   *b) Elevation view, with coupons*
                                      (duplicate specimens not shown)
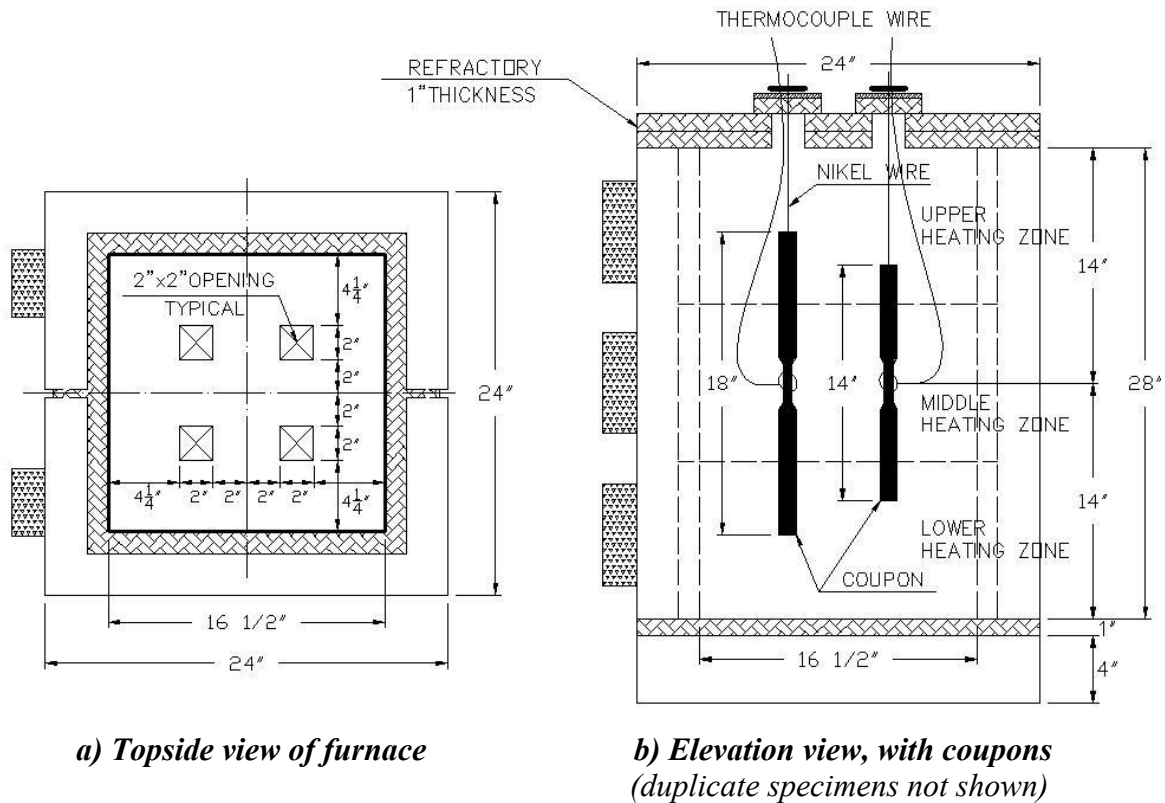
Figure 5.4 Coupon placement in furnace

To keep the temperature profiles of the side-by-side coupons as similar as possible, it was desirable to hang them as shown in Figure 5.4b: so that the centers of the

specimens—and accordingly, of their reduced sections—lined up and were contained within the same heating zone.

5.2.2.2 Heating Procedure

The procedure chosen for heating to the various target temperatures (200 to 1000°C) was adapted from ASTM E119. The E119 standard provides for a simulated fire event in which, initially, the temperature is ramped up rapidly, reaching 840°C in 30 minutes. After the initial period of heating, temperature increase is more gradual. Temperature reaches 1200°C after 8 hours of testing.

Since the target temperatures varied for this research, it would have been impossible to follow E119. The plan instead was to heat the specimen to temperature in less than 30 minutes and then maintain the specimen at the target temperature for 1 hour. After this step, the coupon was removed from the furnace and the cooling stage began. Figure 5.5 shows typical time-temperature curves for the three heating/cooling scenarios for the 1000°C target temperature, along with that prescribed by the ASTM standard. At this temperature, the heating rate adopted was higher than E119; however it should be noted that for lesser temperatures, this was not always true.
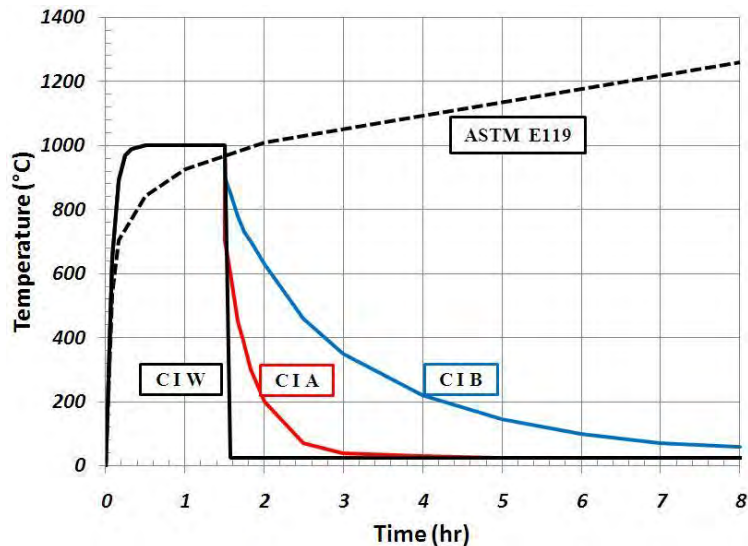
Figure 5.5 Typical time-temperature curves for heating and cooling stages (1000°C)

138

Prior to heat-treatment of coupons for tension testing, pilot testing was done on the furnace. One finding from this pilot testing was that, early in the heating cycle, the temperature of heated coupons would exceed the temperature set for the furnace. With enough time (several hours), the coupon temperature would settle down to the target temperature. It was determined that this behavior resulted from the disparity in conductivity between the highly conductive steel coupons and the insulating material that made up the walls of the furnace. Once the furnace walls got hot enough, using furnace setpoints equal to the target temperature was appropriate.

For this research, it was desirable that the coupon temperature never exceed its target value, within a reasonable tolerance. An appropriate sequence of setpoints for the furnace temperature was developed through a trial-and-error process, and is reported in Table 5.4.

Table 5.4 Furnace setpoint temperatures to achieve given coupon target temperature

Coupon Temp (°C)	Furnace Setpoints (°C) for Time Period (min)			
	0–40	40–55	55–70	70–100
200	120	160	170	180
300	220	220	250	250
400	310	350	355	355
500	420	420	440	440
600	520	530	545	550
700	630	630	650	650
800	720	720	750	800
900	820	820	850	850
1000	930	950	950	950

The temperature values above were programmed into the furnace controller as shown in Figure 5.6. The same setpoints were used for all three heating zones: upper, middle and lower. At times, due to convection, the upper zone would be slightly hotter than the lower zones, but this effect was minimal.
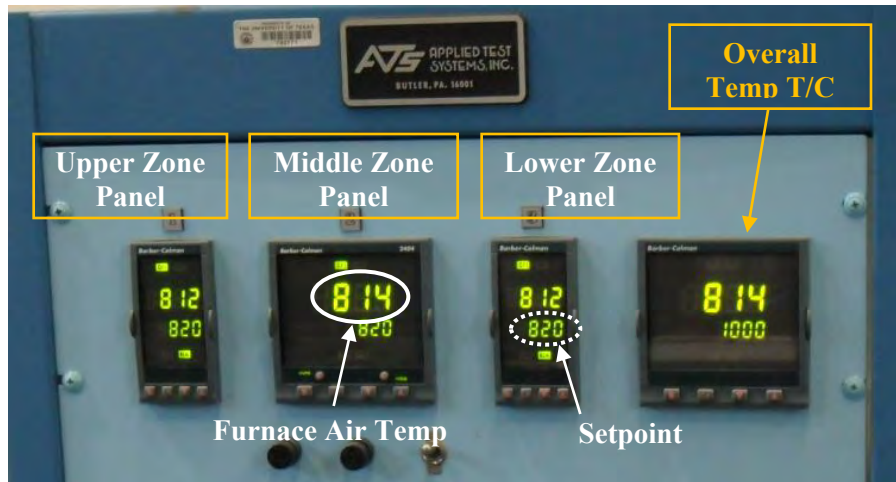
Figure 5.6 Furnace controller set for 900°C coupon target temperature

The heating rates for each target temperature are given in Table 5.5.

Table 5.5 Heating rates for specific target temperature

Temp (°C)	200	300	400	500	600	700	800	900	1000
Heating Rate (°C/sec)	0.20	0.30	0.40	0.51	0.91	1.06	0.81	1.36	1.52

5.2.2.3 Temperature Monitoring and Recording System

As previously mentioned, coupon temperatures were monitored using thermocouples installed at the middle of the specimen. During heating and cooling, a real-time readout of temperature values was possible using Campbell Scientific PC9000 software. Temperature values were logged independently, using a CR5000 data logger (also by Campbell Scientific). Temperatures were recorded at 10-second intervals.

5.2.3 Cooling

The actual cooling rates for structural steel after a fire can depend on a number of factors, including the cooling rate of the fire itself, whether or not the steel is insulated, whether or not the steel is exposed to water from fire-fighting operations or sprinklers, and others. Three different cooling methods were used for the test coupons in an attempt

140

to provide a range of cooling rates that might reasonably bracket realistic conditions. The three cooling methods are referred to as Cooled-In-Air (CIA), Cooled-In-Blanket (CIB), and Cooled-In-Water (CIW).

The approximate amount of time required for the coupons to fully cool from 1000°C to room temperature was 4 hours, 14 hours and 1 minute for the CIA, CIB and CIW cases, respectively, as was shown in Figure 5.5.

5.2.3.1 Cooled-in-Air Specimens

For the CIA case, a heated coupon was taken from the furnace and allowed to cool sitting on a non-flammable concrete or stone block as shown in Figure 5.7. While the room in which the coupons were set to cool was not temperature-controlled, coupons were protected from large temperature changes during cooling. Temperature was monitored for a total of 12 hours.

a) 14 inch coupon air-cooling   *b) 18 inch coupon air cooling*
Figure 5.7 Cooled-in-air (CIA) coupons

Regardless of the temperature to which the coupon was heated, the CIA time-temperature curves were similar in shape. As shown in Figure 5.8, all CIA specimens approached room temperature after 30 to 90 minutes of cooling. That said, the cooling process continued, at a very slow rate, for up to 4 hours.

141
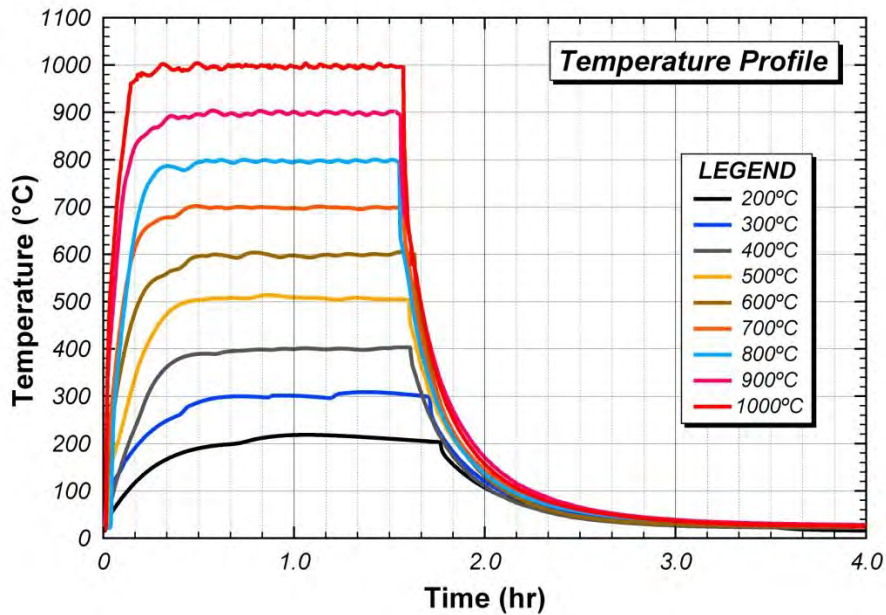
Figure 5.8 CIA temperature profile

The cooling rates measured by time period are reported in Table 5.6. By 60 minutes, it is clear that most of the cooling has occurred: for all temperatures, the cooling rate is less than 1°C/min.

Table 5.6 Cooling rate of CIA

Temp (°C)	Cooling Rate (°C/min) over Time Period (min)						
	0−30	30−60	60−90	60−120	120−180	180−240	240−720
200	4.48	0.97	0.32	0.13	0.04	0.02	0.01
300	7.26	1.46	0.36	0.14	0.05	0.02	0.01
400	10.49	1.61	0.39	0.09	0.01	0.01	0.0
500	13.32	1.88	0.55	0.19	0.05	0.0	0.0
600	16.87	1.83	0.37	0.1	0.02	0.01	0.01
700	19.28	2.27	0.64	0.23	0.07	0.02	0.01
800	22.62	2.27	0.62	0.18	0.04	0.03	0.01
900	25.05	2.95	0.75	0.23	0.06	0.02	0.01
1000	28.97	2.52	0.70	0.24	0.06	0.01	0.0

5.2.3.2 Cooled-in-Blanket Specimens

For the CIB case, a heated coupon was wrapped in a ceramic-fiber refractory blanket and placed inside a box constructed of ceramic fiberboard. The CIB setup is shown in Figure 5.9, and the thermal properties of the blanket and fiberboard given in Table 5.7.

a) Exterior view   *b) Interior view, with blanket and coupons*
Figure 5.9 Ceramic-fiber blanket and box used for CIB testing

Table 5.7 Properties of blanket and ceramic fiberboard

Properties	Blanket (Inswool)	Fiberboard (Nutec)
Thermal Conductivity (W/m·°C)	0.26	0.17
Thickness (in)	1	1
Density (lb/ft^3)	6	21−25

Temperature loss was very gradual, given the excellent insulating properties of the blanket-and-box setup. It was necessary to double the amount of temperature-monitoring time compared to CIA, from 12 to 24 hours. The CIB temperature profiles are as given in Figure 5.10. The shapes of the curves are slightly more differentiated than the CIA time-temperature curves.

It should be noted that there was some degree of temperature loss due to handling. Though care was taken to move the heated coupons from the furnace to the insulated box as quickly as possible, a rapid temperature loss of 10 to 50°C can be observed in every curve.
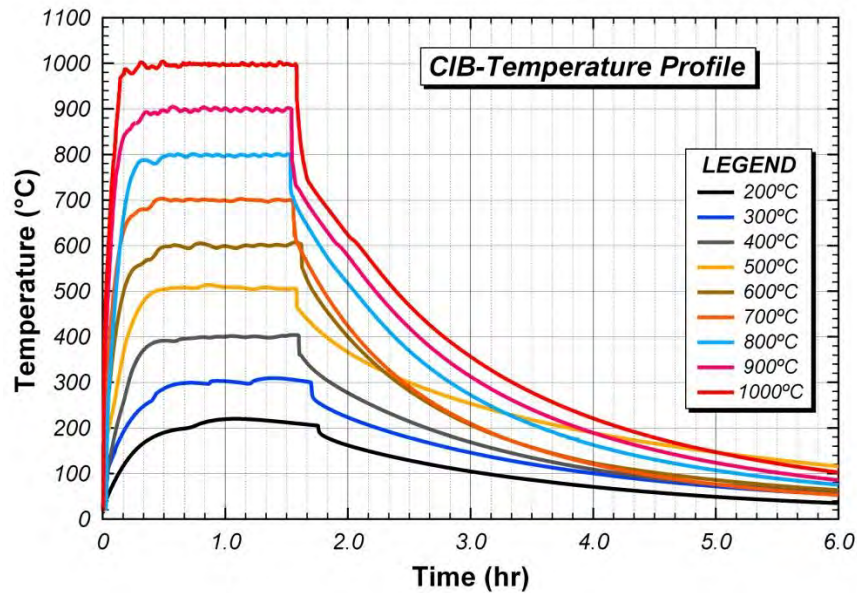
Figure 5.10 CIB temperature profile

Over the first 30 minutes, the cooling rates for the CIB specimens were slightly less than half of their corresponding CIA values. The drop-off in the cooling rate happened much more slowly, however: the CIB rates did not reach the one-hour values of the CIA rates until 3 hours of cooling passed. The cooling rate of CIB is shown in Table 5.8.

Table 5.8 Cooling rate of CIB

Temp (°C)	Cooling Rate (°C/min) over Time Period (min)						
	0−30	30−60	60−90	60−120	120−180	180−240	240−720
200	1.89	0.93	0.70	0.56	0.41	0.26	0.04
300	3.21	1.30	0.99	0.77	0.55	0.35	0.08
400	4.57	1.95	1.43	1.07	0.71	0.38	0.09
500	6.08	2.44	1.77	1.30	0.87	0.51	0.10
600	7.79	3.51	2.25	1.50	0.84	0.45	0.10
700	9.77	4.21	2.58	1.69	1.00	0.52	0.09
800	9.73	4.85	3.15	2.09	1.27	0.68	0.14
900	11.21	5.14	3.45	2.34	1.44	0.82	0.16
1000	13.22	5.17	3.52	2.49	1.57	0.91	0.19

5.2.3.3   Cooled-in-Water Specimens

For the CIW case, a heated coupon was removed from the furnace and immediately dunked in a 5-gallon bucket containing room-temperature water (Figure 5.11). While this procedure likely resulted in more rapid cooling than might be experienced by a steel member sprayed by water in a fire situation, the procedure was simple, repeatable and considered a limiting case of cooling rate for steel sprayed with water by fire fighters.

Figure 5.11 Coupons cooled in water (CIW)

145

As shown in Figure 5.12, cooling for the CIW specimens happened very rapidly. Within the course of one minute, the temperature was decreased to that of the room-temperature water. Though the accuracy of the calculated cooling rates was impaired by the slow rate of data collection (every 10 seconds), the rates shown in Table 5.9 do increase with temperature with the exception of the 1000°C data point. It should be noted that CIW testing was performed only for the temperatures of 500°C and up.
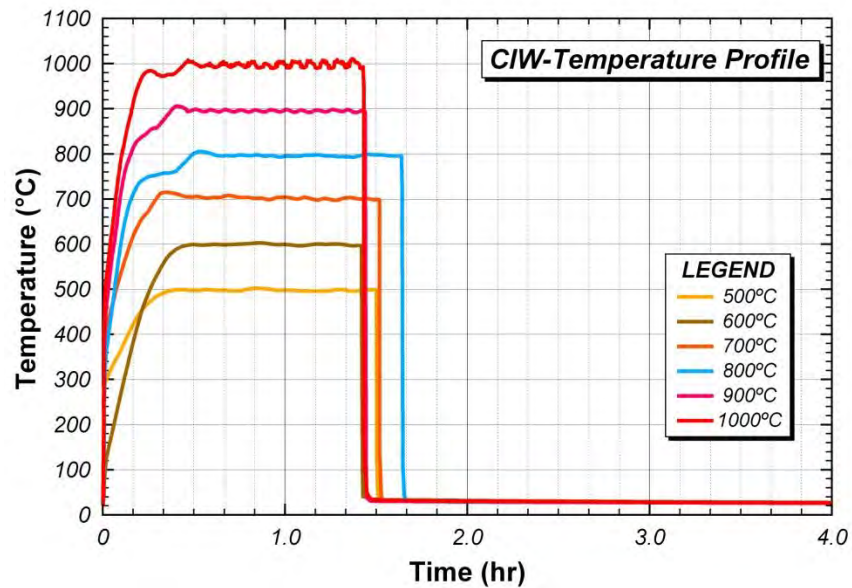
Figure 5.12 CIW temperature profile

Table 5.9 Cooling rate of CIW

Temp (°C)	Temperature (°C)		Cooling Time (sec)	Cooling Rate	
	Before Cooling	After Cooling		°C/Sec	°C/Min
500	498.1	39.2	50	9.2	550.7
600	596.0	42.6	60	9.2	553.3
700	698.6	41.8	40	16.4	985.2
800	794.9	42.4	50	15.1	903.0
900	894.0	38.1	40	21.4	1283.9
1000	993.0	41.3	110	8.7	519.1

5.2.4   Tension Testing at Room Temperature

Aside from the absence of the furnace during testing, most components of the procedure for room-temperature tension testing for the heated and cooled specimens were identical to their elevated-temperature counterparts. For example, testing was performed under displacement control, at a rate of 0.01 inch/min. The cleaning process required after heating and cooling were complete, and the strain measurement techniques, however, were unique and deserve further explanation.

5.2.4.1   *Specimen Preparation after Heating and Cooling*

After heating and cooling, coupons were cleaned and punch-marked for final strain measurement. Punch-marking was performed in a similar manner to that described in Chapter 3.4.2.6, only the timing was different: after heating and cooling rather than during initial fabrication.

With regards to cleaning, very little was need for coupons heated below 500°C. The heating process had changed their color (200°C to gold, 300°C to light blue, 400°C to silver) but had not otherwise affected the surface properties. For coupons heated to 500°C and up, however, the surface began to scale. The thickness and degree of delamination of the scale increased with temperature. For the highest temperatures tested, the thickness of the scale was measured at 1/32 inch. Surface color change and scaling are shown for each temperature in Figure 5.13.
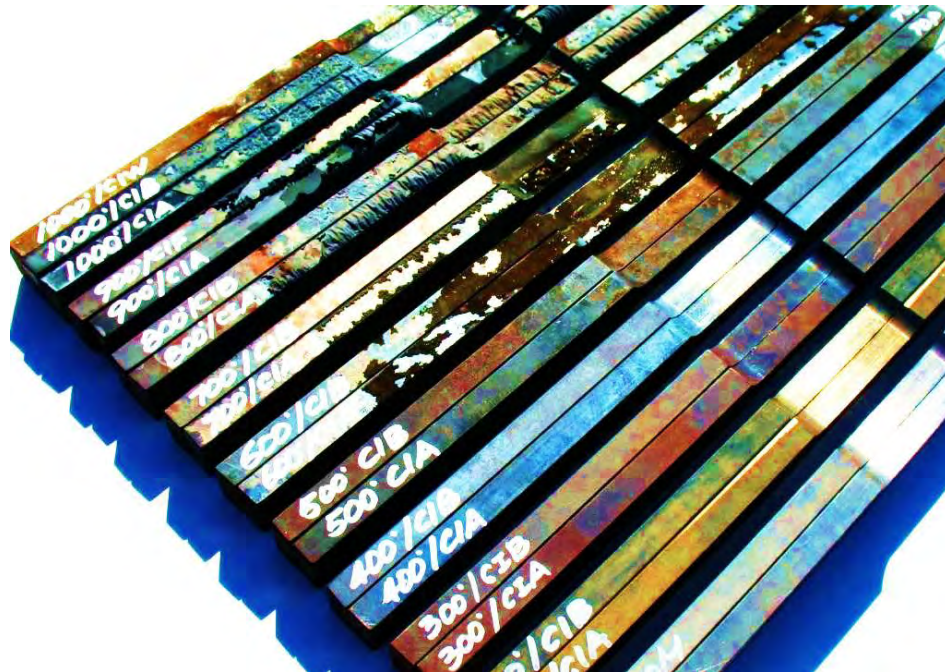
Figure 5.13 Coupons after heating and cooling to various temperatures

It was necessary to remove the scale on the surface for two reasons: to minimize slipping of the coupon in the MTS test machine grips, and to maximize accuracy of coupon section-area measurements. The scale was removed using a rotary wire-brush grinder. Special care was taken not to damage the reduced section. The effect of the wire brush can be seen with the before-and-after comparison of Figure 5.14. It should be noted that some scale was impossible to remove with the wire brush, having melted to the surface (Figure 5.14b). These surface deformations were highly discontinuous, and did not affect either section-area measurement or structural performance.

a) Coupon surface scaling, after cooling stage, for all three cases
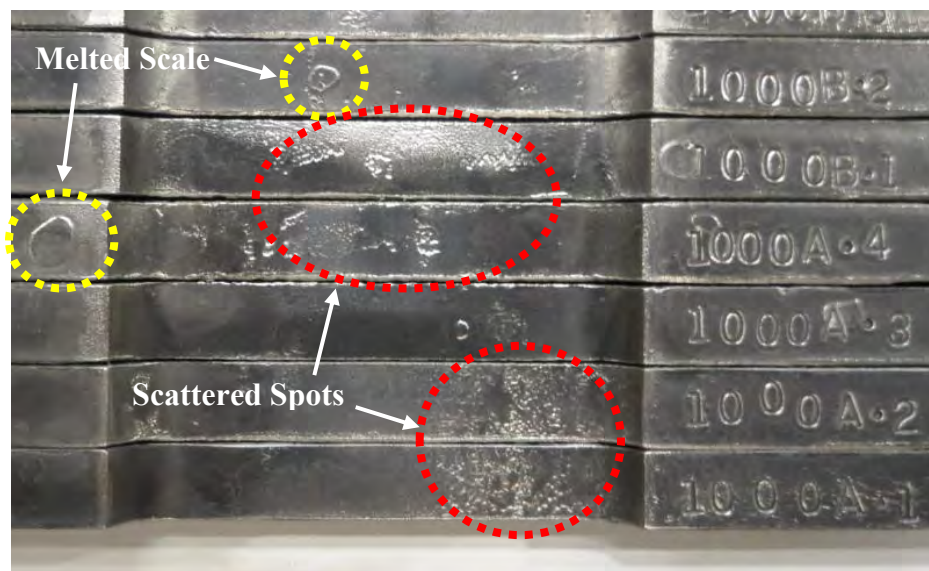
b) Deformations on surface after cleaning by rotary wire brush
Figure 5.14 State of coupon surface (1000°C)

5.2.4.2 Strain Measurement for Tension Testing

Strain measurement was performed using the 2SS extensometer: the 2-inch, self-standing model shown in Figure 5.15. More details on the extensometer are available in Section 3.6. It should be noted that the 2SS was verified as accurate for both small and large strains and returned similar results to the primary extensometer used for elevated-temperature testing, the 1SS. The strain capacities of these two extensometers differed greatly—50% for the 2SS, 10% for the 1SS—meaning that testing with the 2SS was much simpler, requiring fewer resets of the extensometer before failure. In most cases, no resets were required.

a) Before necking   *b) After necking*   *c) After failure*
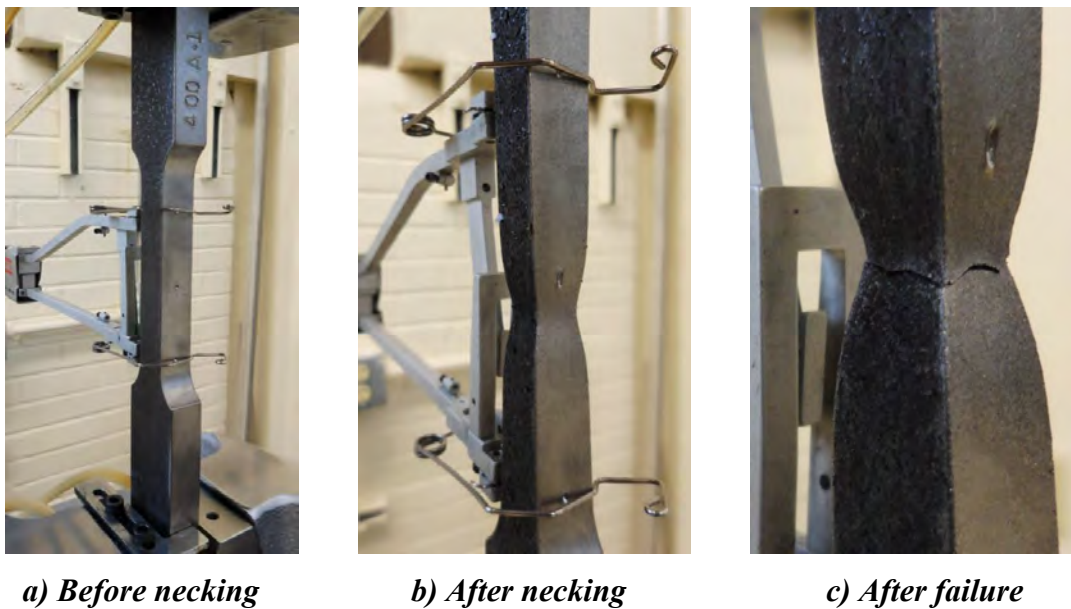
Figure 5.15 2SS extensometer throughout course of room-temperature test

5.2.5   Toughness Testing (Charpy V-Notch)

The toughness of steel, a measurement of how much energy the material can absorb before fracture, is an essential parameter for both impact and fatigue loading scenarios. In current design specifications for bridges a minimum toughness required to avoid fracture is typically specified.

Toughness testing was performed essentially in accordance with ASTM E23 (2007), the Charpy V-Notch (CVN) impact test. In this test, a small piece of steel is fractured by a pendulum axe. The energy absorbed during fracture is measured by the difference in the height of the hammer before and after fracturing the specimen. A V-shaped notch is cut into the specimen before testing. For this research, CVN specimens were cut from the ends of heat-treated coupons, as shown in Figure 5.16.
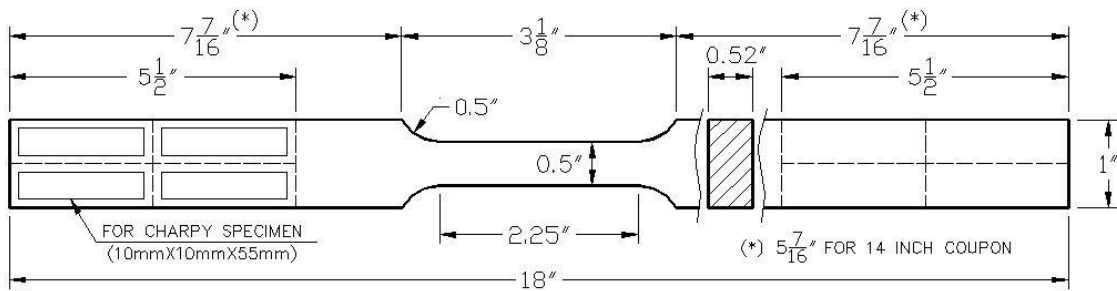
a) 18-inch coupon, before being cut down into CVN specimens
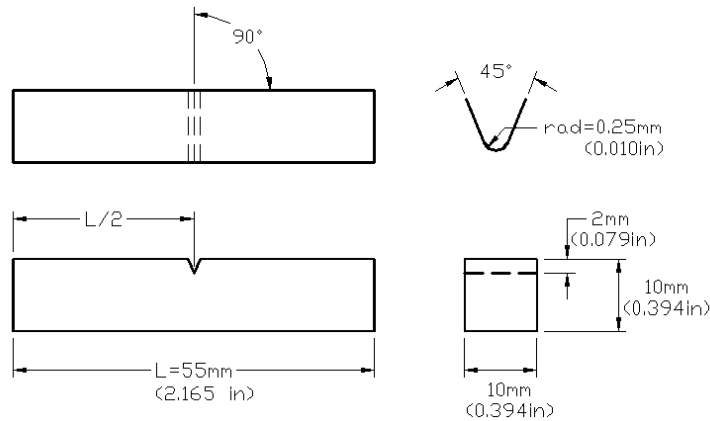
b) CVN specimen
Figure 5.16 Charpy V-Notch specimen made from heated coupon

151

5.2.5.1 *Charpy V-Notch Specimen Fabrication*

The techniques required to fabricate the CVN specimens were similar to those previously discussed in Section 3.4.2 for coupon fabrication. It should be noted, however, the tolerances allowed for the dimensions of the CVN specimen (Table 5.10) are tighter than those allowable for tension coupons.

Table 5.10 Permissible variation of CVN specimen dimensions (ASTM A370)

Specimen Size	Dimension (mm)	Dimension Tolerance		
		Notch Centering	Length	Cross Section
Standard	10×10×55	±1 mm (±0.039 in)	+0, -2.5 mm (+0, -0.100 in)	±0.075mm (±0.003 in)

After heating and cooling, the ends of the 18-inch coupon were cut off and ground down to the specified thickness using a sand-disk grinder with 1 mil precision, as shown in Figure 5.17. The ends were then cut into four. The length and width of the CVN specimen were end-milled, ground and de-burred.
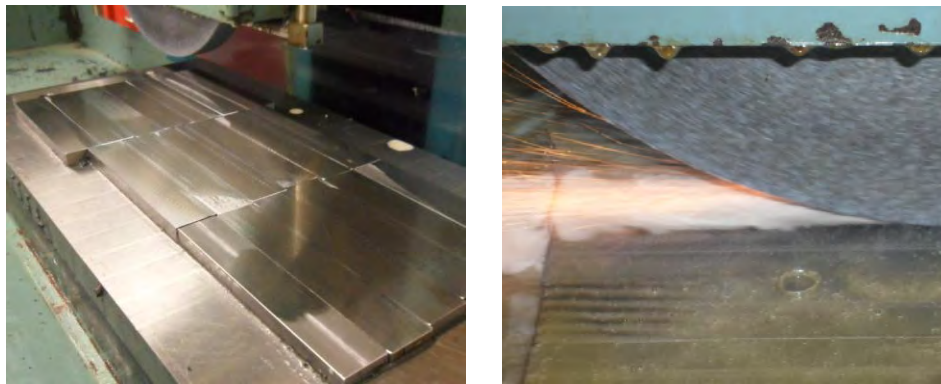
a) Coupon ends on grinding table   *b) Ground to a precise thickness*
Figure 5.17 Sand-disk grinding of coupon ends

The CVN specimen was notched perpendicular to the rolling surface using a Mini-Broach machine (Figure 5.18a). After notching, the angle, depth and other dimensions of the notch were measured using a Starrett HE400 optical comparator (Figure 5.18c) to ensure conformity to ASTM A370 within tolerance (Table 5.11).

152
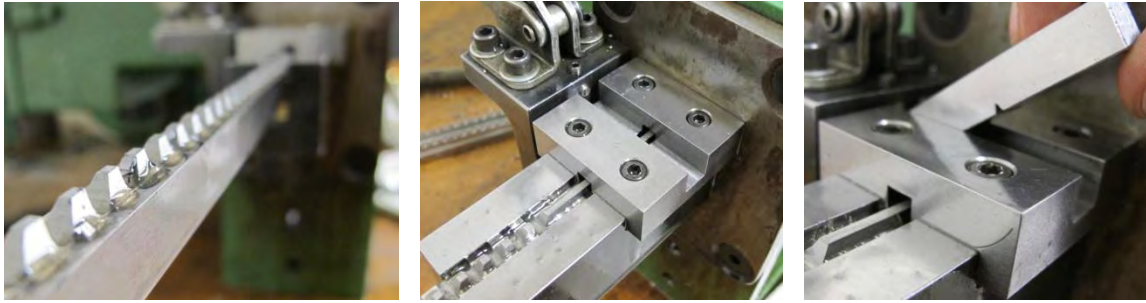
a) Mini-Broach V-Notching Machine

b) After notching
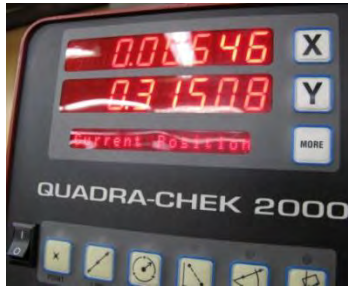
c) Examination of V-Notch dimensions

d) Completed CVN specimen

Figure 5.18 V-Notching process

Table 5.11 Permissible variables of V-Notch by ASTM A370

Angle of Notch	Angle to Adj. Sides	Depth of Notch	Radius at Base of Notch	Finish
45° ± 1°	90° ± 10 min	2 ± 0.025 mm (0.079±0.001 in)	0.25 ± 0.025 mm (0.010±0.001 in)	+2 μm (63 μin)

5.2.5.2 Charpy V-Notch Testing

Charpy V-Notch testing was performed with the Tinius Olsen machine shown in Figure 5.19a. The test machine consists of a pendulum axe swung to fracture the notched specimen described in the previous section. The energy transferred to the steel by the pendulum can be inferred by comparing the difference in height of the hammer before and after striking the specimen (Figure 5.19b). The test machine was calibrated such that, after the test, the amount of absorbed energy could be read directly off a dial gauge (Figure 5.19c).
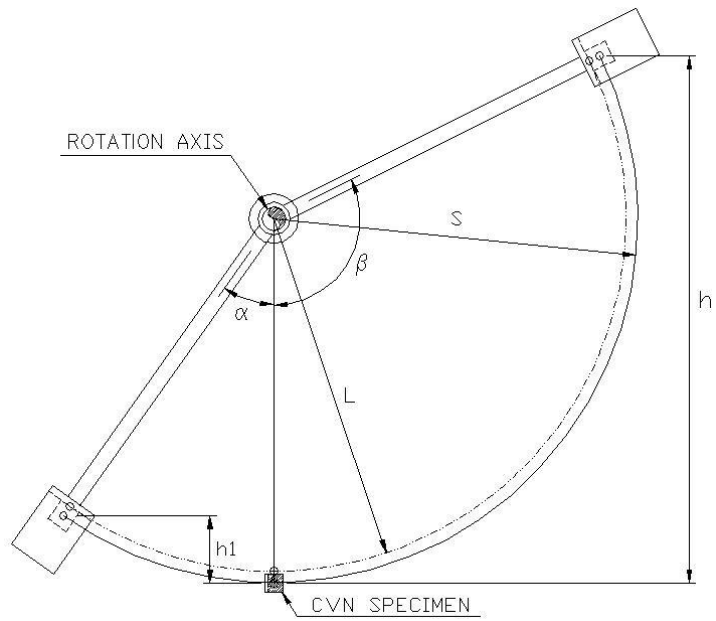
a) Test machine   *b) Height of hammer before and after swing*

c) Reading test result off dial gauge

Figure 5.19 Tinius Olsen CVN test machine

5.2.6 Hardness Testing

The hardness of the A992 steel was measured using ASTM E18, the Rockwell hardness test. In the test, an indenter is pressed into the test sample with specific force values. The measured depth of indentation is inversely proportional to the Rockwell hardness number.

The standard provides several scales by which hardness may be measured: for each, the indenter, initial load and final load are specified. The scales are arbitrary, but within one scale, values may be compared. For this research, the B and C scales as specified in Table 5.12 were used.

Table 5.12 Prescribed indenter and test force for Rockwell hardness scales

Scale	Indenter		Test Force (kgf)	
	Material	Tip Shape	Initial	Final
B	Tungsten Carbide	1/16 inch Ball	10	100
C	Diamond	Spheroconical	10	150

One reason to perform hardness testing on steel is its correlation to tensile strength: hardness testing can be considered a non-destructive strength-estimation technique. It should be noted, however, that strength values obtained through this procedure are "at best, an approximation" (E18).

Hardness testing was performed on the previously tested CVN specimens using the Wilson Rockwell Series 2000 test machine, as depicted in Figure 5.20.

***Figure 5.20 Hardness testing of previously tested CVN specimen
using Wilson Rockwell machine***

5.3   TEST RESULTS

Stress-strain curves are presented both for a particular method of cooling—CIA, CIB or CIW—and for each target temperature. Figure 5.21 to Figure 5.35 were illustrated the variety of stress-strain curves after heating and cooling.

5.3.1 Stress-Strain Curve by Method of Cooling
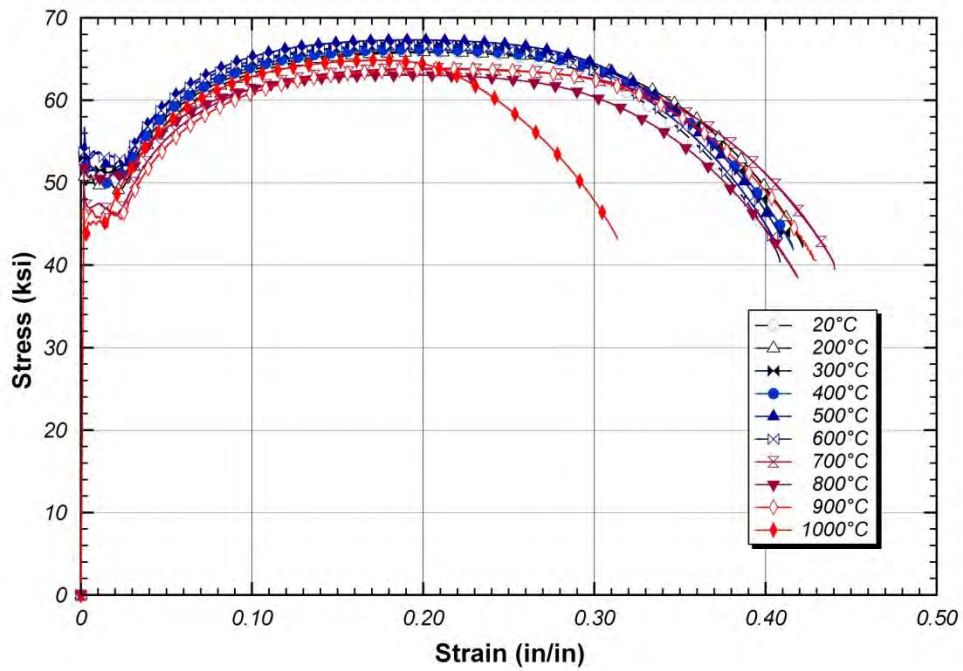
Figure 5.21 Full stress-strain curve for CIA
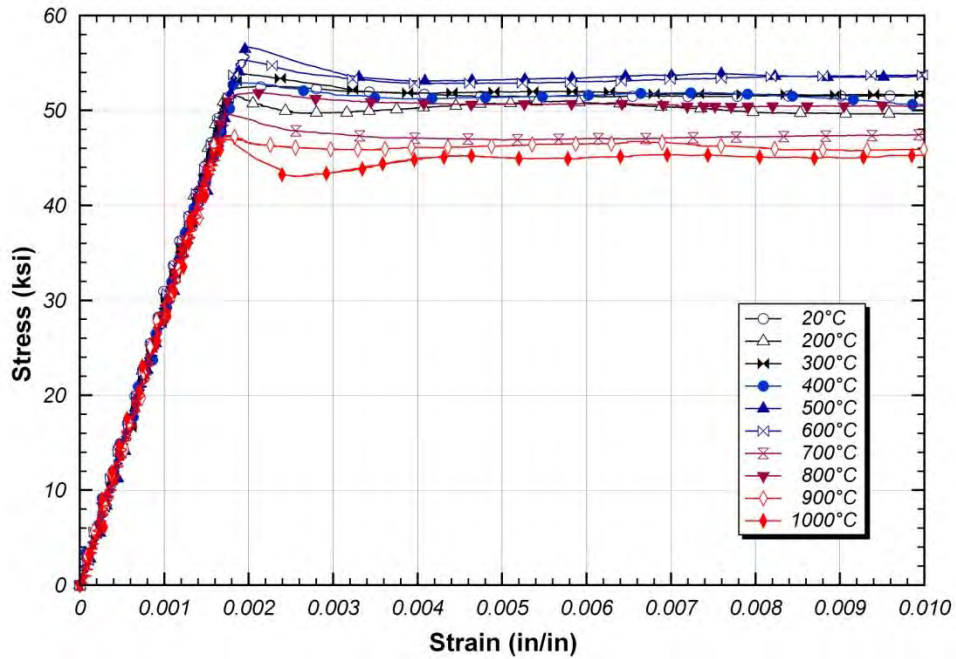
Figure 5.22 CIA – Initial portion of stress-strain curve

157
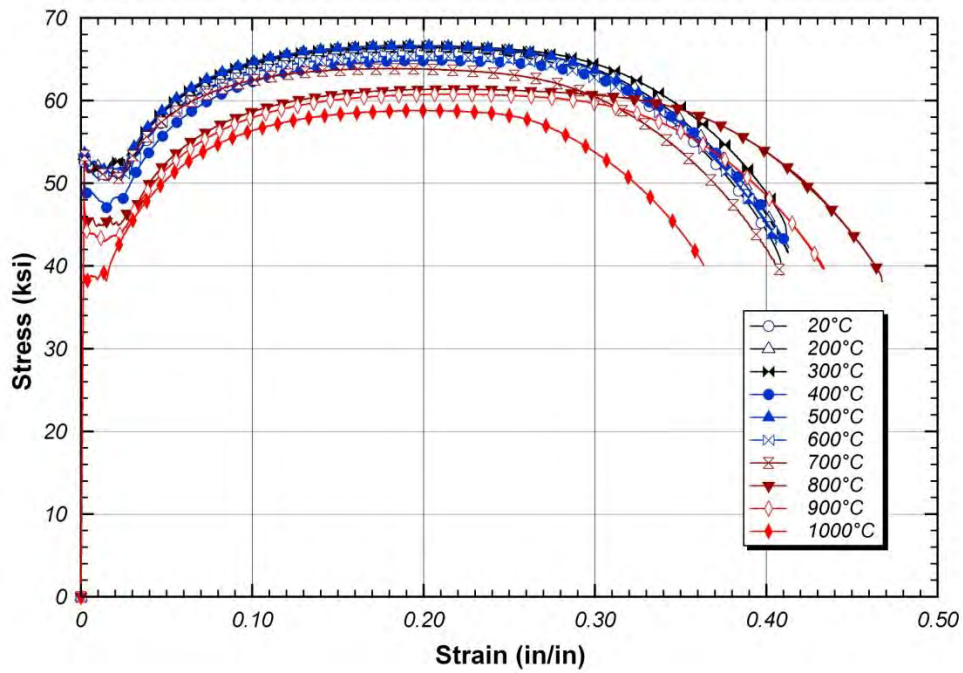
Figure 5.23 Full stress-strain curve for CIB
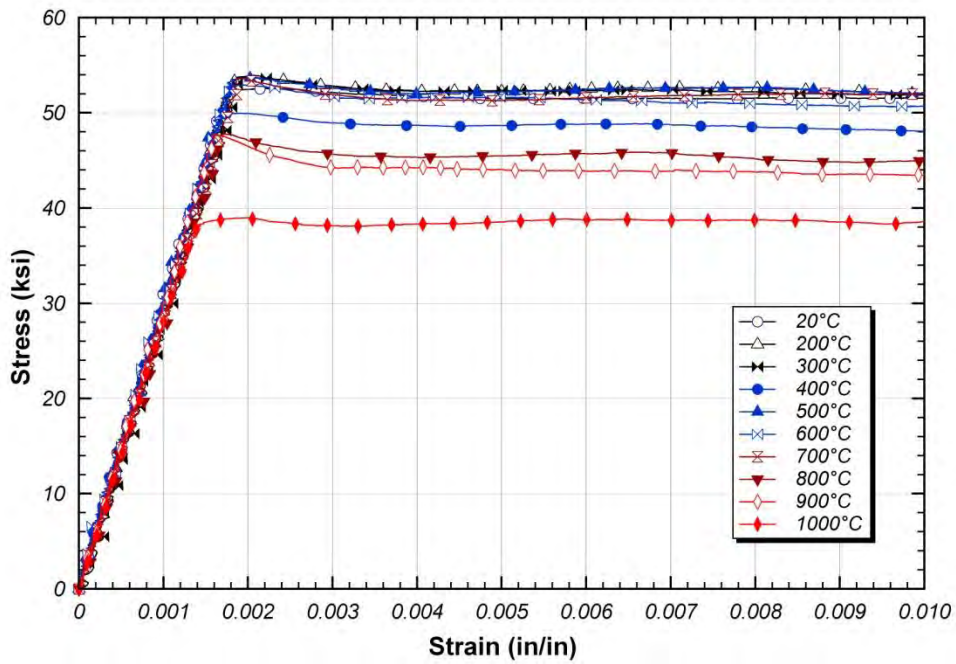
Figure 5.24 CIB – Initial portion of stress-strain curve

158
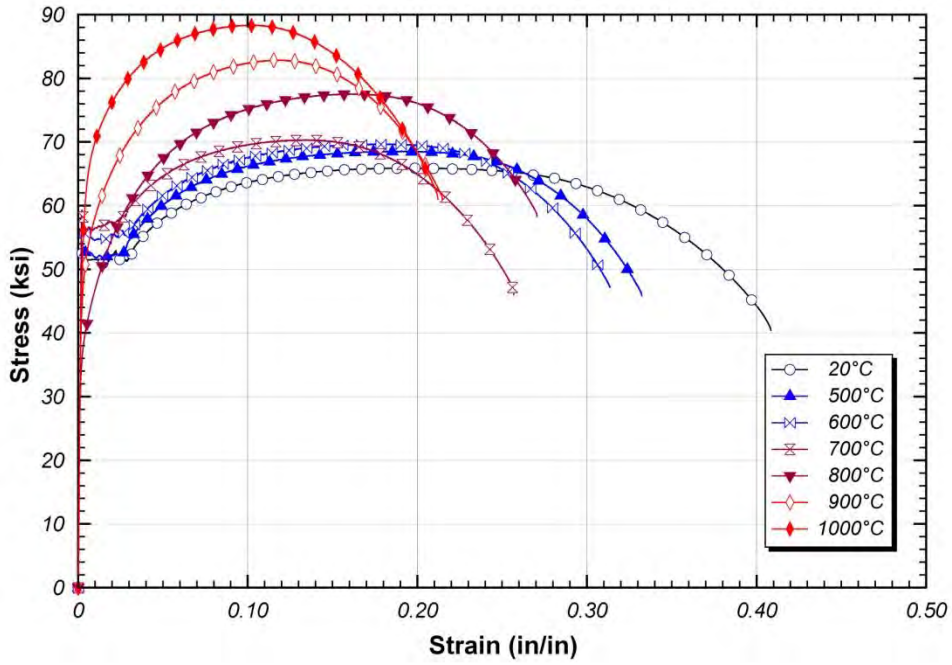
Figure 5.25 Full stress-strain curve for CIW
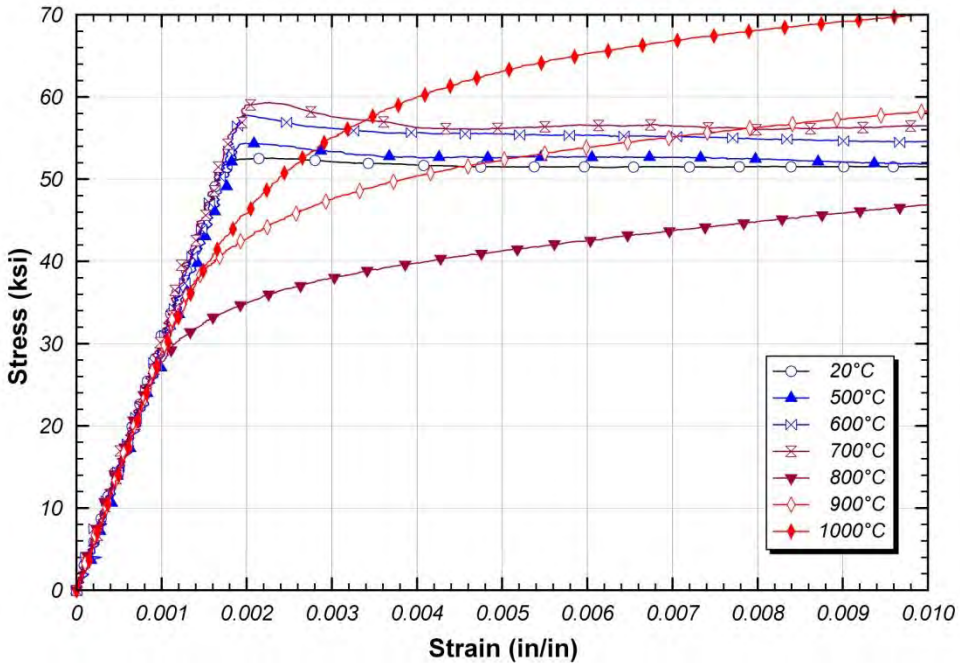
Figure 5.26 CIW – Initial portion of stress-strain curve

159

5.3.2   Stress-Strain Curve by Temperatures
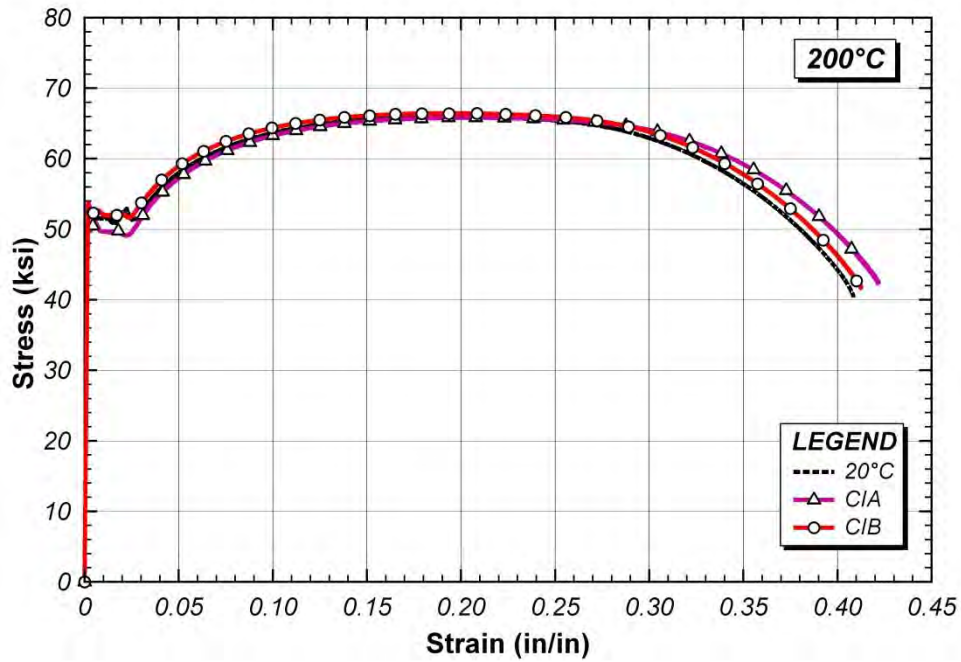
Figure 5.27 Combined stress-strain curves for steel heated up to 200°C
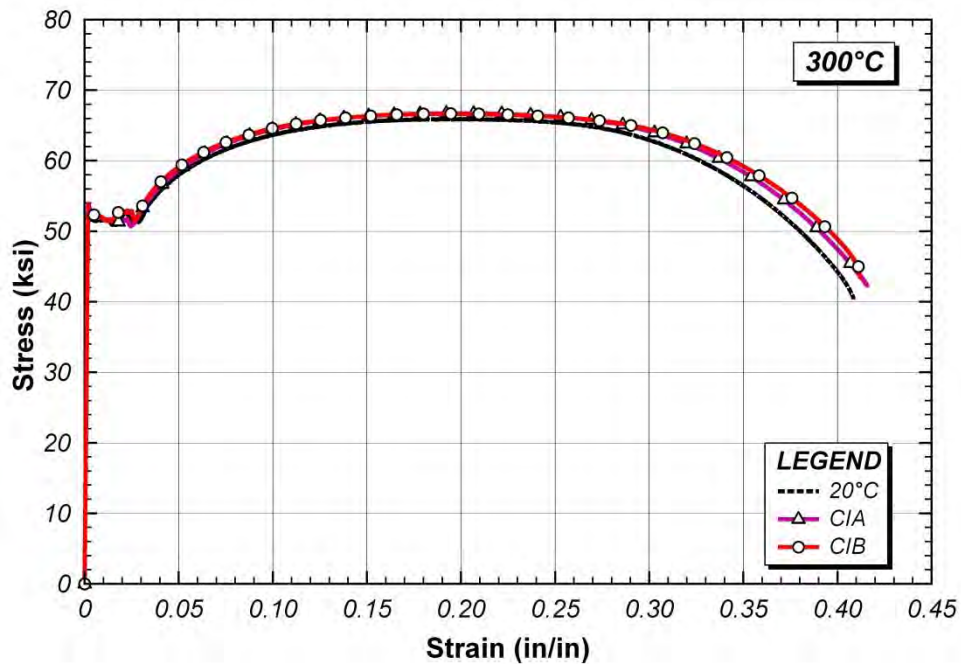
Figure 5.28 Combined stress-strain curves for steel heated up to 300°C

160
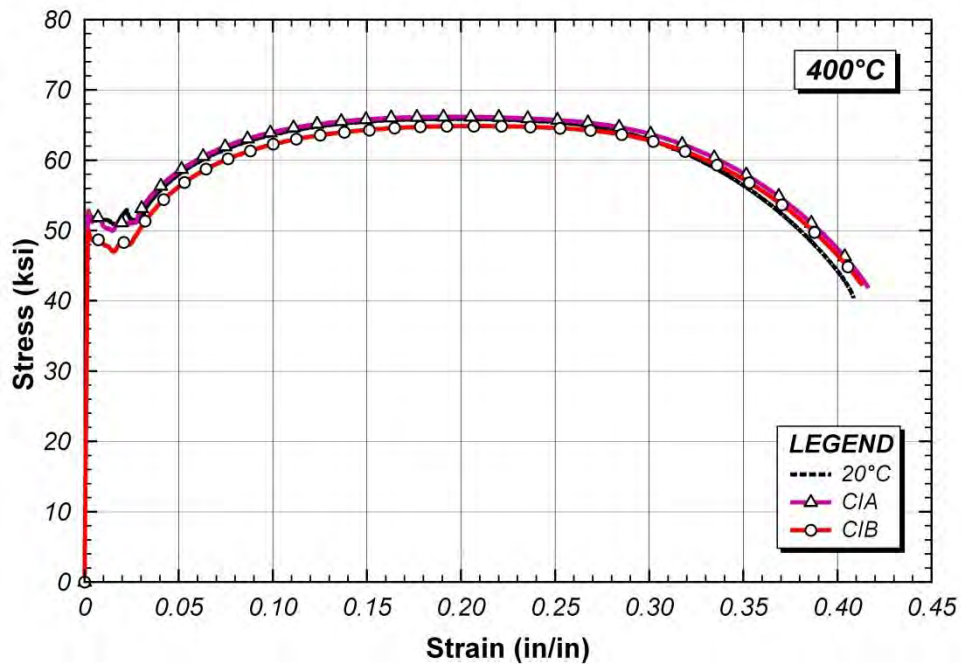
Figure 5.29 Combined stress-strain curves for steel heated up to 400°C
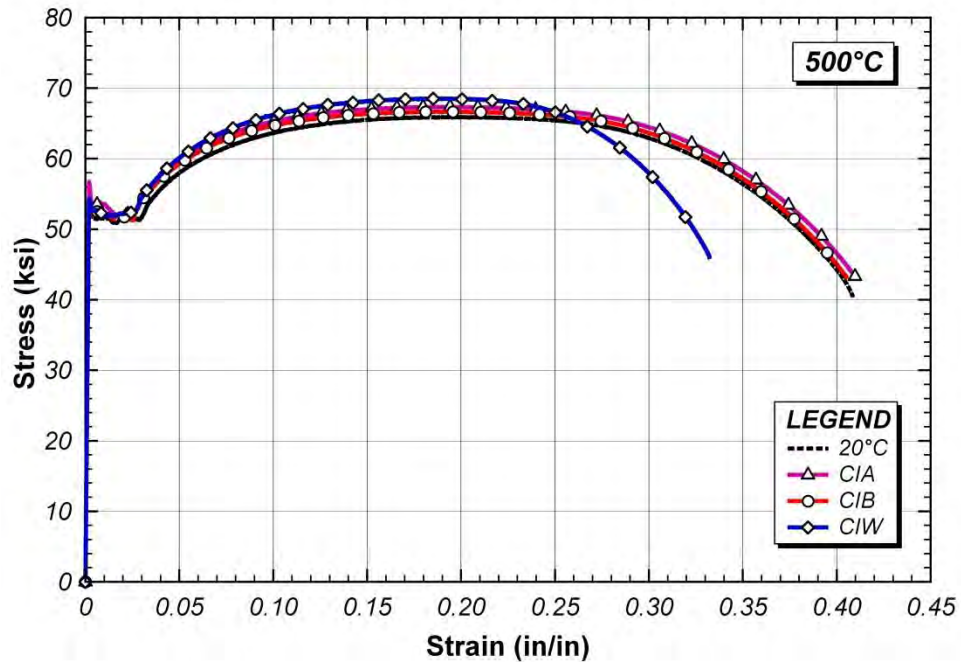
Figure 5.30 Combined stress-strain curves for steel heated up to 500°C

161
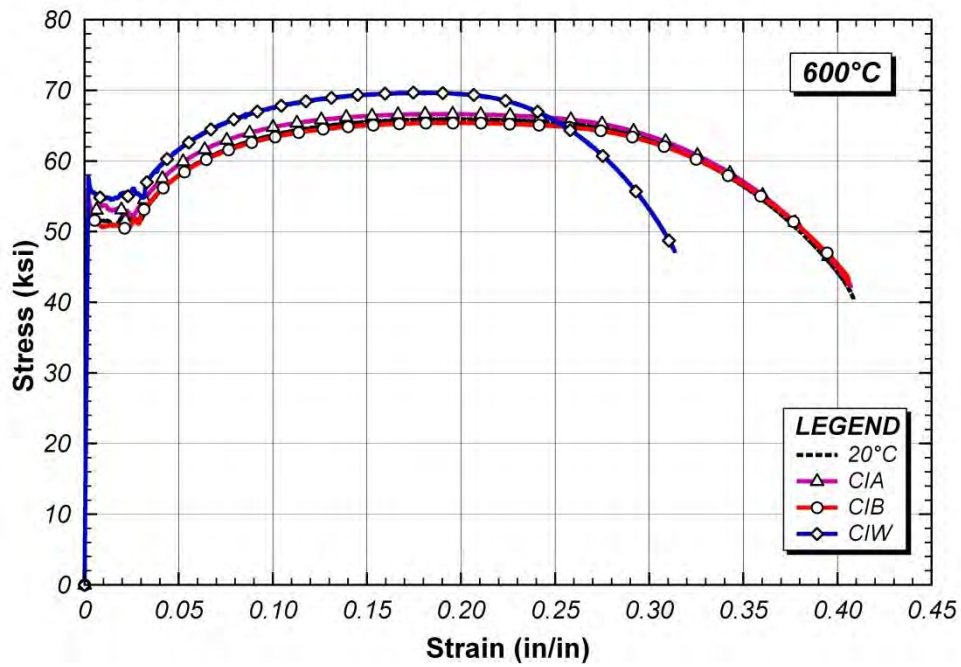
Figure 5.31 Combined stress-strain curves for steel heated up to 600°C
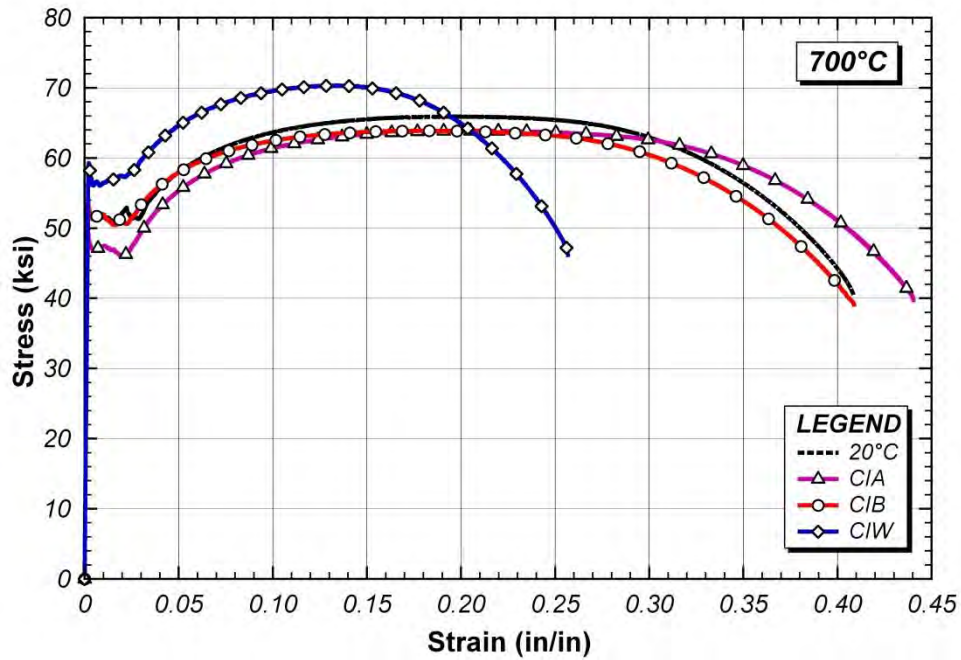
Figure 5.32 Combined stress-strain curves for steel heated up to 700°C

162
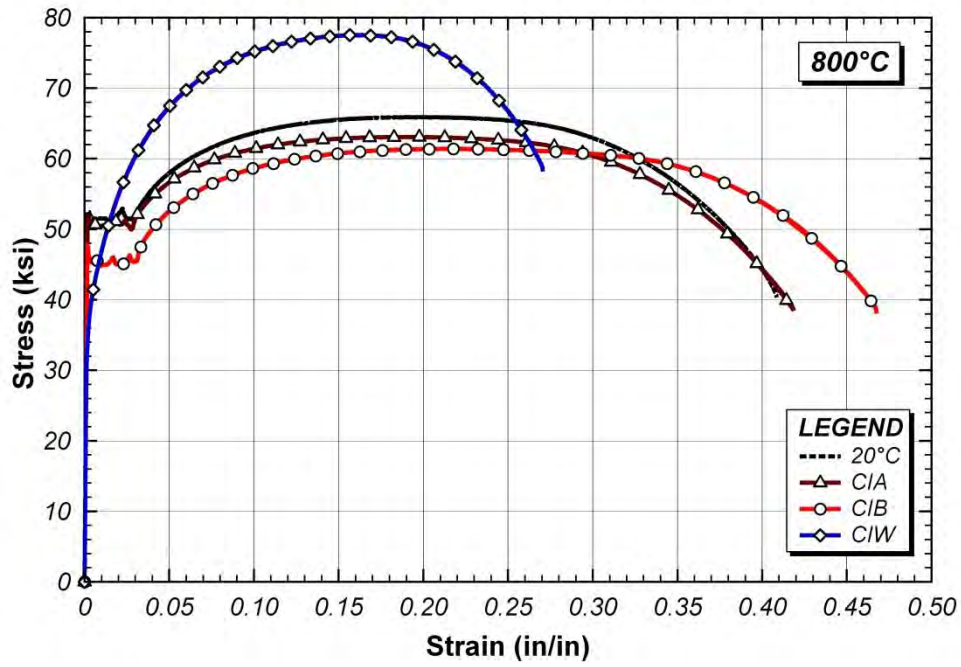
Figure 5.33 Combined stress-strain curves for steel heated up to 800°C
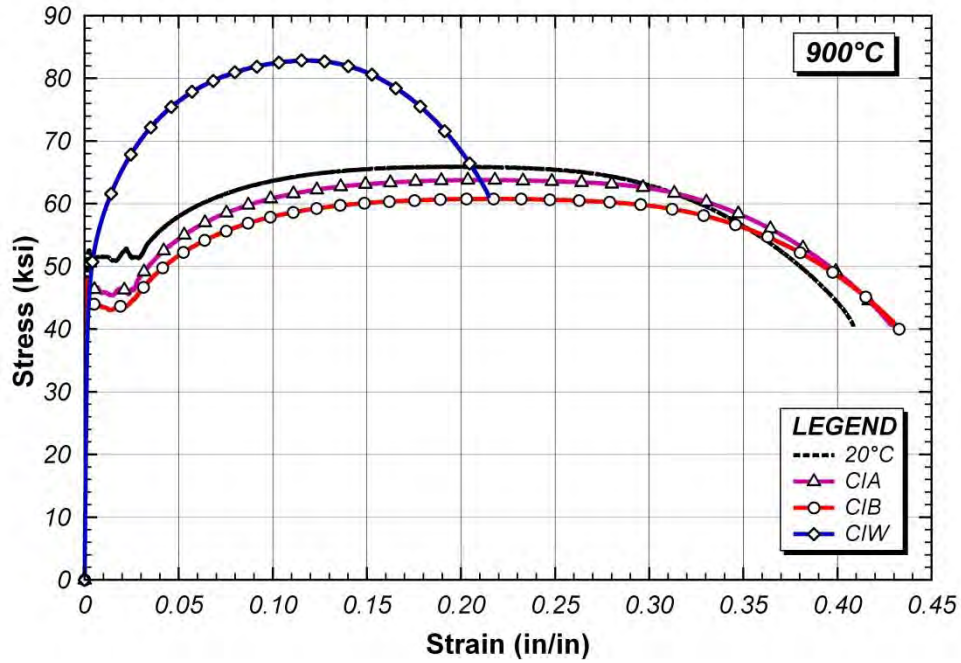
Figure 5.34 Combined stress-strain curves for steel heated up to 900°C

163
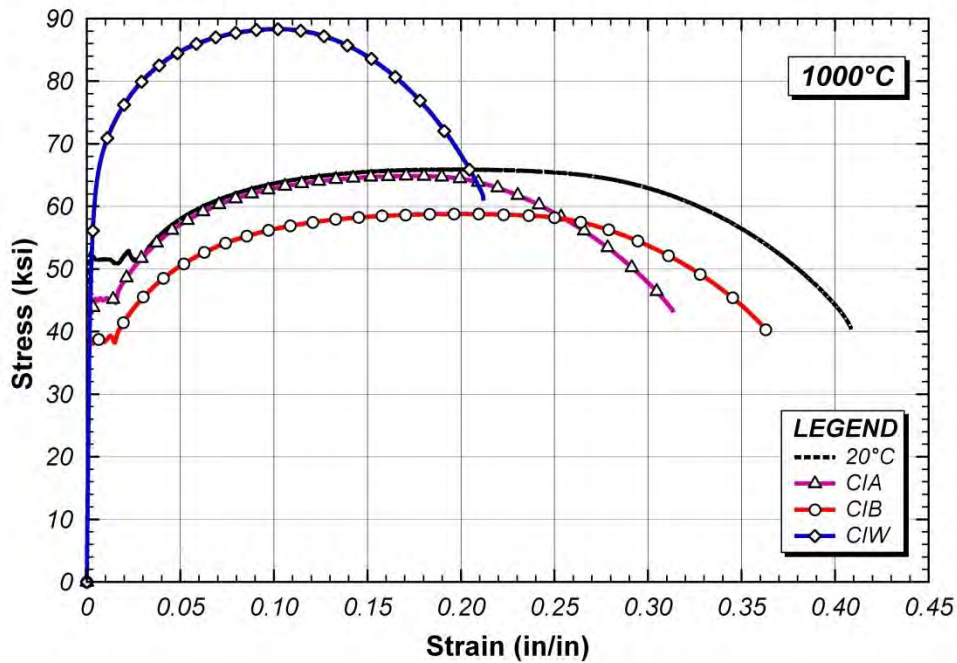
Figure 5.35 Combined stress-strain curves for steel heated up to 1000°C

5.4 MECHANICAL PROPERTIES

In this section, mechanical properties derived from the results of tension, toughness and hardness testing are presented. Additional information on the definitions for the tension-test mechanical properties can be found in Section 4.4. Yield stress, for this room-temperature testing, was calculated by the 0.2% offset method. Data for a particular test value will be presented along with its associated retention factor: that is, the ratio of the test value to the corresponding value from testing performed on a virgin unheated coupon.

5.4.1 Elastic Modulus

The elastic modulus of the coupons after heating and cooling was estimated from the initial linear portion of the stress-strain curves. Results for the CIA, CIB and CIW cases are given in Table 5.13 and Figure 5.36.

164

Table 5.13 Elastic modulus (ksi) and associated retention factor

Test	Temperature (°C)									
	20	**200**	**300**	**400**	**500**	**600**	**700**	**800**	**900**	**1000**
CIA	29910 *1.00*	29900 *1.00*	29420 *0.99*	28780 *0.96*	28930 *0.97*	29510 *0.99*	29040 *0.97*	28830 *0.96*	29010 *0.97*	28200 *0.94*
CIB		28720 *0.96*	29270 *0.98*	29360 *0.98*	29590 *0.99*	28800 *0.96*	28060 *0.94*	28080 *0.94*	29680 *0.99*	27610 *0.92*
CIW		-	-	-	29090 *0.97*	29690 *0.99*	30380 *1.02*	29380 *0.98*	29520 *0.99*	28650 *0.96*

a) Elastic modulus   *b) Retention factor*
Figure 5.36 Elastic modulus and associated retention factor

Minor variations in the elastic modulus can be observed over the tested temperature range. Since strains were measured on one side of the coupon only, error at small strain levels can occur due to bending of the coupon. As such, the elastic modulus values derived from the stress-strain curves is subject to some error. The data are inconclusive as to whether the observed variations in elastic modulus resulted from structural changes to the coupons from heating and cooling, strain-measurement errors or some combination thereof. Even considering possible strain measurement errors,

165

however, the data shows no dramatic changes in elastic modulus after heating and cooling.

5.4.2   Yield Stress

The yield stress of the coupons after heating and cooling was determined by the 0.2% offset method. Results for the three cooling conditions are given in Table 5.14 and Figure 5.37. The ratio of the test data to that of a virgin unheated coupon, the retention factor, is also given.

Table 5.14 Yield stress (ksi) and associated retention factor

Test	Temperature (°C)									
	20	**200**	**300**	**400**	**500**	**600**	**700**	**800**	**900**	**1000**
CIA	51.9	50.1	52.1	51.3	53.1	52.9	50.8	47.1	46.0	44.6
		0.97	*1.01*	*0.99*	*1.02*	*1.02*	*0.98*	*0.91*	*0.89*	*0.86*
CIB		52.4	52.3	48.7	52.2	51.6	51.4	45.4	44.3	38.1
	1.00	*1.01*	*1.01*	*0.94*	*1.01*	*1.00*	*0.99*	*0.88*	*0.85*	*0.74*
CIW		-	-	-	52.7	55.6	56.6	38.7	49.4	60.1
					1.02	*1.07*	*1.09*	*0.75*	*1.26*	*1.16*
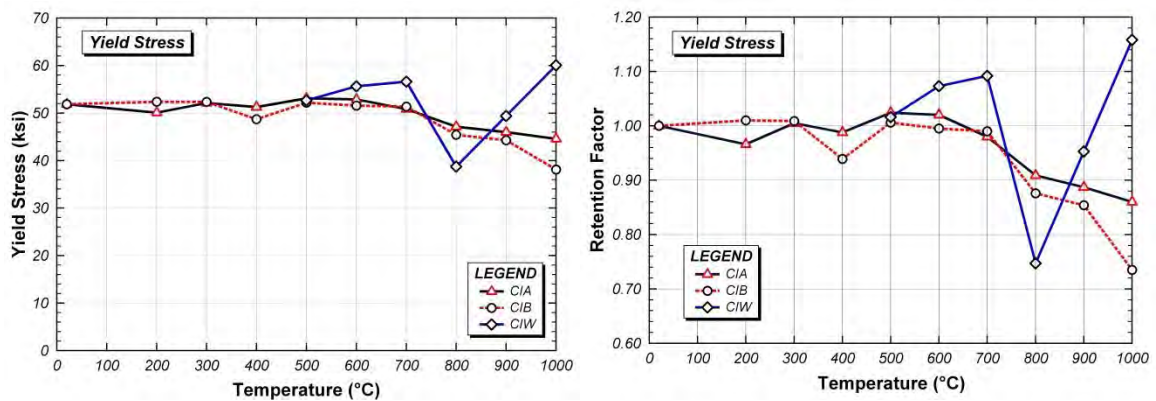
a) Yield stress   b) Retention factor
Figure 5.37 Yield stress and associated retention factor

166

Reasonably significant reductions in yield stress, up to about 25 %, for CIA and CIB cooling are seen for coupons heated to temperatures of 800 to 1000°C. The CIW coupons also show significant changes in yield stress in the range of 800 to 1000°C, with the yield stress first dropping and then increasing within this temperature range.

Specimens heated to temperatures higher than 727°C at least partially transform to austenite (γ-Fe), and subsequent cooling can produce microstructures different from the original material (Callister 2007). This is one reason that yield stress does not change significantly in specimens heated to 700°C and lower temperatures. The decrease in yield stress with increase in temperature at 800°C and higher in the CIB and CIA specimens results from increasing volume fractions transformed to austenite during heating. Upon subsequent cooling, the ferrite (α-Fe) produced may be coarser than that of the original material, leading to decreased yield stress. A992 steel has sufficient carbon to potentially form some pearlite following cooling from these temperatures. Pearlite consists of ferrite (α-Fe) and cememtite (Fe_3C) in a lamellar configuration. The amount of pearlite possible increases with the amount of austenite transformed during heating, which should increase from 727°C up to a maximum near 900°C. The microstructures expected after cooling from 800°C or higher are a normalized microstructure with some coarse pearlite for slow cooling rates (e.g., CIB) and some slightly finer pearlite for moderate cooling rates (e.g., CIA). This may explain the slightly greater yield stress reduction observed for the CIB specimens compared to the CIA specimens. An increase in cooling rate (e.g., CIW) will reduce the pearlite interlamellar spacing, and in accordance with the continuous cooling transformation curve, will lead to an increase in yield stress, such as that observed for the CIW specimen heated at 1,000°C. Thus, the variations of yield stress with heating temperature and cooling rate, as seen in Figure 5.37, are consistent with the expected microstructural transformations.

167

5.4.3 Tensile Strength

The tensile strength of the coupons after heating and cooling was taken directly from the stress-strain curves. In Table 5.15 and Figure 5.38, tensile strength data is presented for the various test conditions. The retention factor is also given: the ratio of the test data to the tensile strength of a virgin unheated coupon.

Table 5.15 Tensile strength (ksi) and associated retention factor

Test	Temperature (°C)									
	20	200	300	400	500	600	700	800	900	1000
CIA	65.9	65.9	66.8	66.2	67.4	66.7	63.1	63.91	63.8	64.9
		1.00	*1.01*	*1.01*	*1.02*	*1.01*	*0.96*	*0.97*	*0.97*	*0.98*
CIB	*1.000*	66.5	66.7	64.9	66.7	65.4	63.9	61.47	60.8	58.8
		1.01	*1.01*	*0.99*	*1.01*	*0.99*	*0.97*	*0.93*	*0.92*	*0.90*
CIW		-	-	-	68.6	69.7	70.4	77.6	82.9	88.4
					1.04	*1.06*	*1.07*	*1.18*	*1.26*	*1.34*
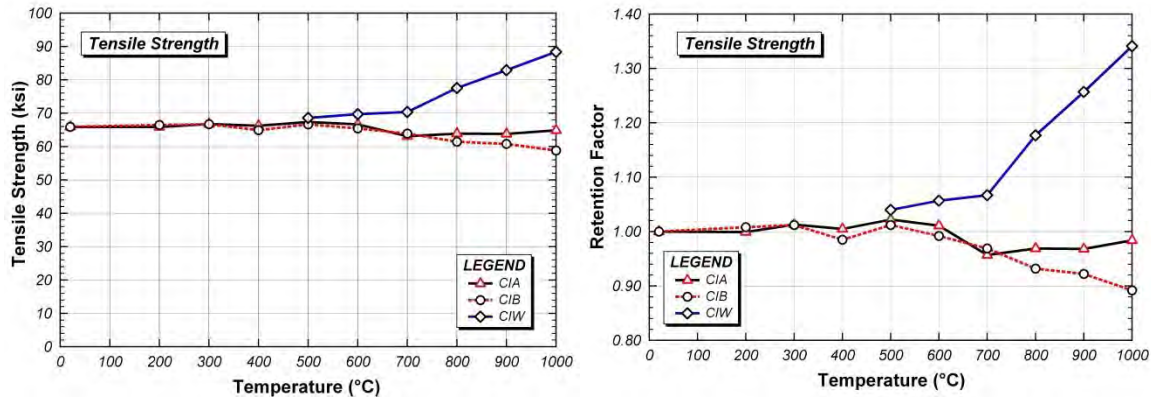
a) Tensile strength   *b) Retention factor*
Figure 5.38 Tensile strength and reduction factor

For the CIA and CIB cooling methods, there is a modest reduction in tensile strength for coupons heated above about 600°C. On the other hand, for the CIW cooling method, there is a large increase in tensile strength for coupons heated above about 600°C due to the quenching effect which induced a martensite microstructure of metal with quick cooling process. A transformed martensite generally results in increased

168

strength and decreased ductility because of trapped austenite microstructures produced by rapid cooling (Callister 2007).

5.4.4 Elongation

The elongation of the coupons after heating and cooling was taken as the strain at fracture of the coupon. Elongation data is summarized in Table 5.16 and Figure 5.39. The retention factor given is the ratio of the elongation at failure under the test conditions to that of an unheated coupon.

Table 5.16 Elongation at failure (in/in) and associated retention factor

Test	Temperature (°C)									
	20	**200**	**300**	**400**	**500**	**600**	**700**	**800**	**900**	**1000**
CIA	0.41	0.42	0.42	0.42	0.41	0.41	0.44	0.42	0.43	0.31
		1.03	*1.02*	*1.02*	*1.00*	*1.00*	*1.08*	*1.03*	*1.05*	*0.77*
CIB		0.41	0.41	0.41	0.41	0.41	0.41	0.47	0.43	0.36
	1.00	*1.01*	*1.01*	*1.01*	*0.99*	*0.99*	*1.00*	*1.15*	*1.06*	*0.89*
CIW		-	-	-	0.33	0.31	0.26	0.27	0.22	0.21
					0.81	*0.77*	*0.63*	*0.66*	*0.53*	*0.52*
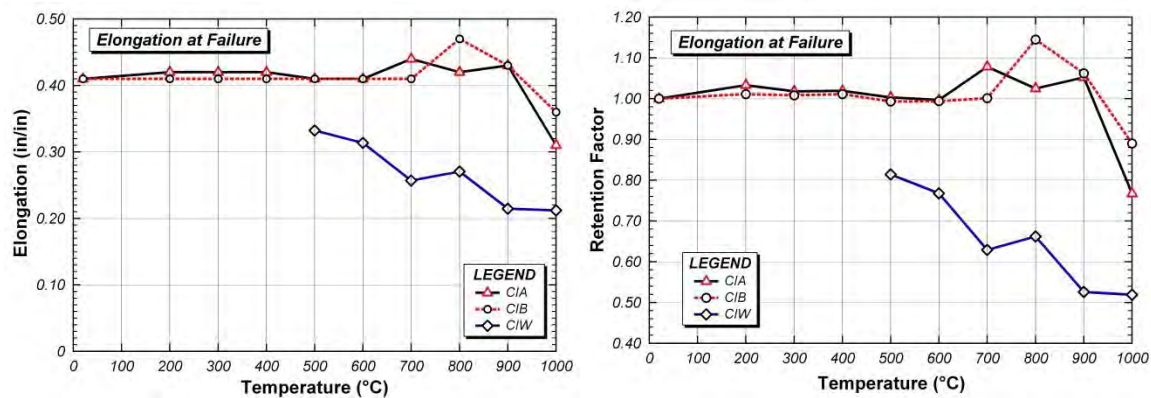
a) Elongation   *b) Retention factor*

Figure 5.39 Elongation and associated retention factor

For the CIA and CIB cooling methods, there is no significant change in elongation for temperatures up to 900°C. There is a reduction in the measured elongation for the

169

coupons heated to 1000°C. Even for this case, however, the elongation was still above 30%. The CIW coupons, on the other hand, show a rather significant reduction in elongation over the 500 to 100° range of temperatures tested.

5.4.5 Charpy V-Notch (CVN) Impact Test

Charpy V-Notch impact test data is summarized in Table 5.17 and Figure 5.40. The values given are typically the average of four test values. The retention factor given is the ratio of the CVN data to that measured for a virgin unheated specimen.

Table 5.17 CVN energy (ft-lbs) and associated retention factor

Test	Temperature (°C)									
	20	200	300	400	500	600	700	800	900	1000
CIA	171	220 *1.28*	244 *1.42*	244 *1.43*	240 *1.40*	206 *1.20*	247 *1.44*	245 *1.43*	252 *1.47*	188 *1.09*
CIB		233 *1.36*	238 *1.39*	226 *1.32*	219 *1.28*	250 *1.46*	247 *1.44*	259 *1.51*	251 *1.47*	239 *1.40*
CIW	*1.00*	-	-	-	95 *0.55*	93 *0.54*	76 *0.44*	79 *0.46*	86 *0.50*	38 *0.22*

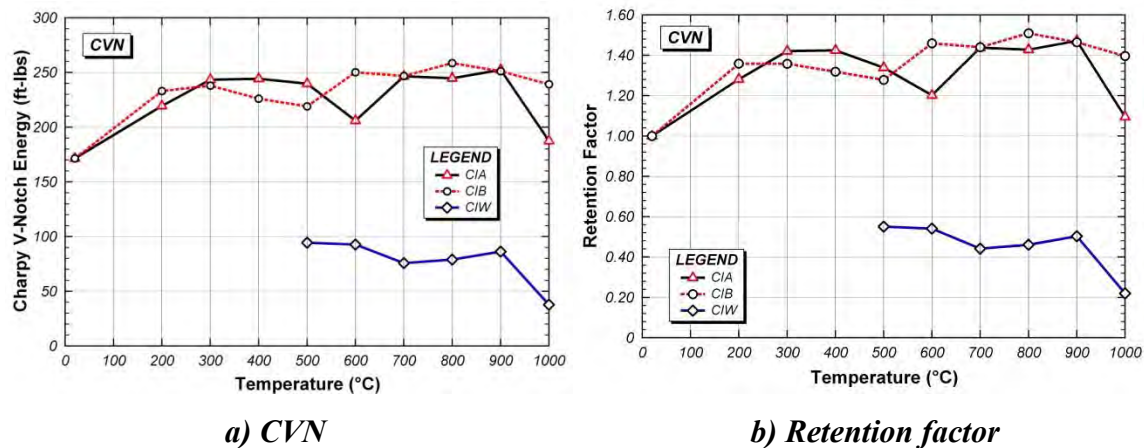*a) CVN*   *b) Retention factor*
Figure 5.40 CVN energy and associated retention factor

The results for the CIA and CIB specimens show an increase in CVN values over the full temperature range tested. The CIW specimens, on the other hand, show a large

170

reduction in CVN values for the temperature range tested, which was 500 to 1000°C. Note that specimens heated to 1000°C and then cooled in water showed a CVN value that was only 20% of the original virgin specimen.

5.4.6 Hardness Test

The hardness test results are summarized in Table 5.18 and Figure 5.41.

Table 5.18 Rockwell hardness numbers (HRB or equivalent) and retention factor

Test	Temperature (°C)									
	20	200	300	400	500	600	700	800	900	1000
CIA	89.0	90.7	87.2	83.5	84.3	86.3	83.3	84.0	81.6	88.5
		1.02	0.98	0.94	0.95	0.97	0.94	0.94	0.92	0.99
CIB		87.8	88.0	89.3	89.4	88.6	86.2	83.5	80.7	83.7
		0.99	0.99	1.00	1.00	1.00	0.97	0.94	0.91	0.94
CIW	1.00	-	-	-	83.9	85.4	88.4	92.6	96.6	104*
					0.94	0.96	0.99	1.04	1.09	1.16

*Converted from HRC measurement

a) Hardness   b) Retention factor

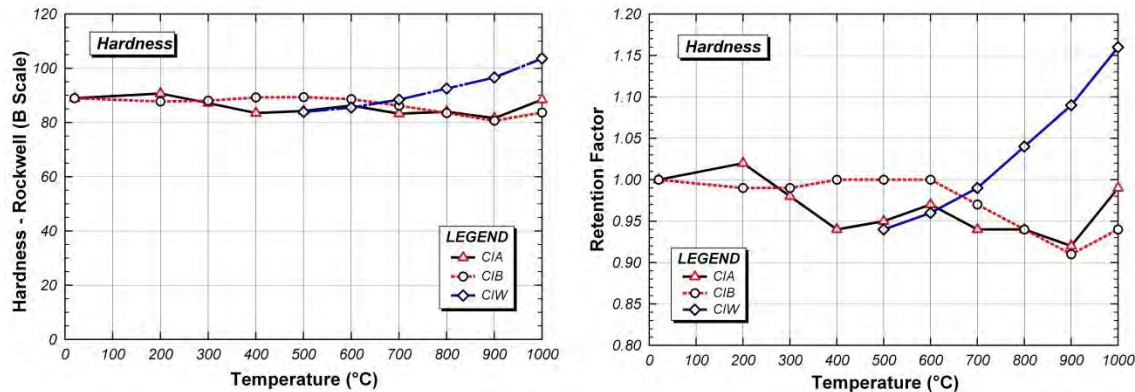**Figure 5.41 Rockwell hardness and associated retention factor**

All values measured were within the B-scale range except for the 1000°C CIW coupon, which was too hard (HRB > 100). For this specimen, the Rockwell C scale was used. The measured C-scale value of 25.9 was converted to an equivalent B-scale value through consideration of the estimated tensile strength per ASTM A370 for each scale as

shown in Figure 5.42. While this converted strength data was for A36 steel, no similarly authoritative data is available for A992. The resulting value for 1000°C, 104, matched the trend otherwise observed for the CIW coupons.
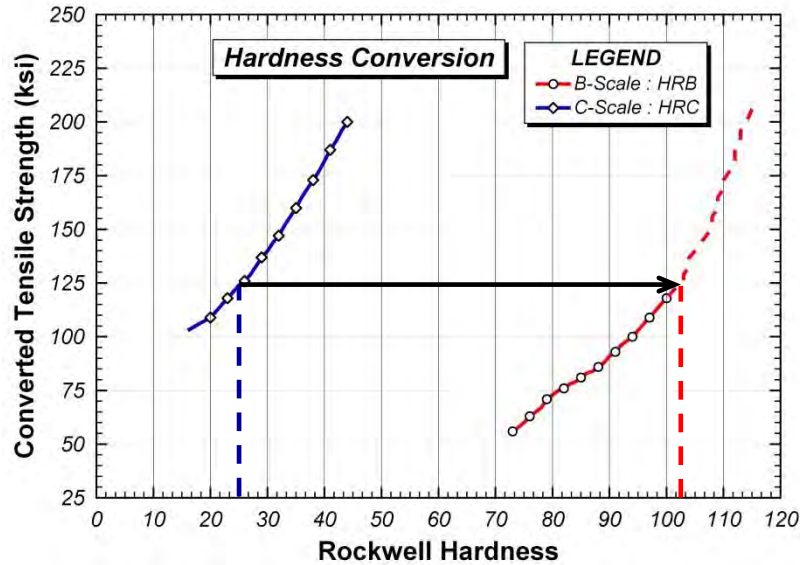
Figure 5.42 Approximate hardness – tensile strength relationship for A36 steel

The trends in Rockwell hardness with heating temperature and cooling method are very similar to the corresponding trends in tensile strength. This is expected since there is typically a strong correlation between hardness and tensile strength (Figure 5.38). On the other hand, the correlation between hardness and yield stress (Figure 5.37) is rather poor. Consequently, when evaluating steel after a fire, hardness testing may not be effective in diagnosing loss of yield stress. Hardness testing, on the other hand, may be useful for diagnosing steel that has been exposed to high temperatures, and then rapidly cooled by water.

5.5 SUMMARY

This chapter has presented results of tension, toughness and hardness tests on samples of A992 steel subjected to heating and cooling. Three different test conditions were investigated: Cooled-in-Air (CIA), Cooled-in-Blanket (CIB) and Cooled-in-Water

(CIW). The CIA condition is intended to be representative of normal cooling after a fire; CIB representative of slower cooling due to the presence of insulating material; and CIW representative of very rapid cooling of steel by water from a fire hose or sprinkler.

These tests were intended to provide insights into the post-fire mechanical properties of A992 steel. The trends in the data can be summarized as follows. In terms of yield stress, there was no significant reduction until the temperature exceeded 700°C. However, even up to 1000°C, the reduction in yield stress is only about 20%. For tensile strength, there is essentially no change, even for coupons heated to 1000°C. It is noted that the CIW case actually increased the tensile strength.

The most significant effect of water cooling appears to be in fracture toughness, as represented by CVN values. Steel samples that were heated above 600°C and then cooled rapidly in water showed a large drop in CVN values. CVN values are indicative of fracture toughness, and the loss of fracture toughness due to heating and then rapid cooling in water may be of concern in some applications, for example in a steel bridge girder subjected to fire and then cooled rapidly by water from fire-fighting operations. It may be possible to detect hardening of steel in a structure that was subjected to fire and then cooled rapidly by the use of field hardness measurements.

The data presented in this chapter can assist in assessing the post-fire condition of a steel structure. However, this data presumes that the maximum temperature achieved in the steel during the fire is known. This, of course, is rarely the case. A review of the literature suggests there are no simple and reliable approaches for estimating the maximum temperature achieved in a steel element during a fire. Some approaches for addressing this question are discussed in Banovic and Foecke (Banovic 2005). Nonetheless, the tests reported herein examined temperature exposures up to 1000°C, which would represent quite an extreme exposure. Even when exposed to such an extreme temperature, there was little degradation in mechanical properties after cooling, with the possible exception of steel cooled rapidly in water. It is important to note, however, that tests on high strength bolts have shown significant loss of strength after

173

heating and cooling (Yu and Frank 2009). Thus, when assessing the condition of a steel structure following a fire, the effect of the fire on the strength of bolts is likely to be a greater concern than the effect of the fire on the structural steel members.

CHAPTER 6

Creep Testing at Elevated Temperatures

6.1 OVERVIEW

Experimental testing investigating the tensile creep behavior of ASTM A992 steel at elevated temperatures is described in this chapter. Creep of steel can be potentially significant in predicting the response of steel structures to fire (NIST 2005). The literature review revealed no previous investigations providing experimental data on the creep properties of A992 steel, however. As such, an extensive testing program was completed to develop elevated-temperature creep data for A992 steel. Tested temperatures (up to 1000°C) and time durations (up to 2 hours) were aimed at structural fire-engineering applications.

In the first portion of this chapter, the experimental procedure followed for creep testing is discussed. The testing results are presented as creep curves, both of strain versus time and creep strain rate versus time, followed by analysis of these curves. Using these results as a basis, a creep model for A992 steel was developed: its parameters are described at the close of the chapter.

6.2 EXPERIMENTAL INVESTIGATION

Many techniques for creep testing at elevated temperatures were similar to those for elevated-temperature tension testing, described in detail in Chapter 3. Emphasis is placed in this section on ways in which the test procedures were different.

6.2.1 Test Specimen

The test specimen used for creep testing was a coupon taken from the flange of an ASTM A992 W4x13 section, and is shown in Figure 6.1. The coupons were cut and

machined as described in Section 3.4.2. It should be noted that the thickness of the coupon was ~0.35 inch, 30% less than tension coupons.
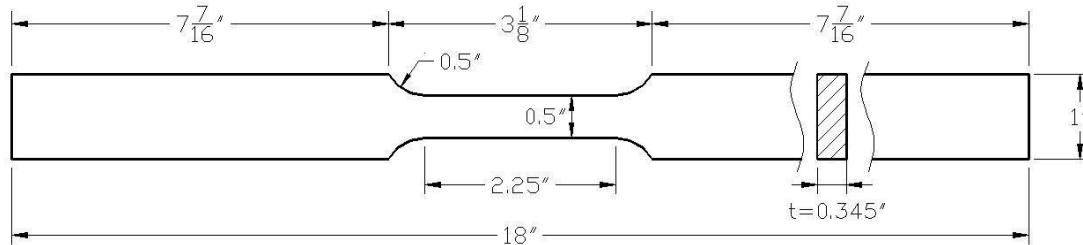

Figure 6.1 Dimensions of coupon used in creep testing

The chemical composition of the W4x13 material, as reported on the Certified Mill Test Report, is shown in Table 6.1. For testing purposes, this was designated material type MC. Tension-test results for the material, presented in Chapter 4, are summarized in Table 6.2. Yield stress was determined by the 0.2% offset method.

Table 6.1 Chemical composition of test specimen

Material Type	C	Cr	Mo	V	Ni	Mn	Si	P	S	Cu
MC	0.08	0.10	0.026	0.002	0.09	0.91	0.23	0.011	0.025	0.24

Table 6.2 Elevated-temperature tensile properties for Material MC

Property	Temperature (°C)									
	20	200	300	400	500	600	700	800	900	1000
F_y (ksi)	51.8	46.7	48.9	35.4	28.9	16.8	9.0	5.3	4.5	2.8
F_u (ksi)	68.3	89.4	77.4	60.0	39.2	18.9	9.7	6.1	5.3	3.3

6.2.2 Determining Stress Levels for Creep Testing

To characterize creep behavior at elevated temperatures, four stress levels were used for testing. Three of these ($0.50F_y$, $0.75F_y$ and $0.90F_y$) were selected to investigate elastic creep behavior, with the last stress level ($0.90F_u$) selected to investigate inelastic

creep behavior. The terms *elastic* and *inelastic* creep behavior, as used herein, are intended to describe whether the stress level is in the elastic or inelastic range of the material's stress-strain curve at the temperature of interest. These terms are not intended to suggest that the creep strain should be treated an elastic recoverable strain or an inelastic non-recoverable strain.

The applied stress levels chosen for creep testing are given in Figure 6.2 and Table 6.3. It should be noted that while tension tests were run at elevated temperatures as low as 200°C, creep testing was performed only for temperatures in excess of 400°C. At temperatures below 40% of its melting point, steel does not show significant creep deformation under tensile loadings (Sherby and Burke 1967; Callister 2007).
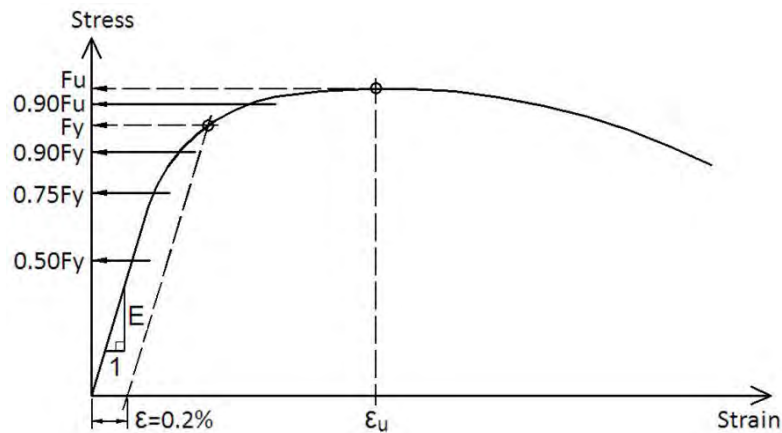

Figure 6.2 Scheme of selected stress levels for creep test

Table 6.3 Stress levels used in creep test (ksi)

Stress Level	Temperature (°C)						
	400	500	600	700	800	900	1000
$0.50F_y$	17.7	14.4	9.4	4.5	2.7	2.2	1.4
$0.75F_y$	26.5	21.6	14.1	6.8	4.0	3.4	2.1
$0.90F_y$	31.8	26.0	16.9	8.1	4.8	4.0	2.5
$0.90F_u$	54.0	35.3	17.0	8.7	5.5	4.8	3.0

6.2.3   Strain and Temperature Measurement

During creep testing, strains were recorded every 0.5 seconds from measurements made using a one-inch pressure-standing (1PS) extensometer, shown in Figure 6.3. This extensometer, used for all tests performed at elevated temperatures, is discussed in greater detail in Section 3.6.
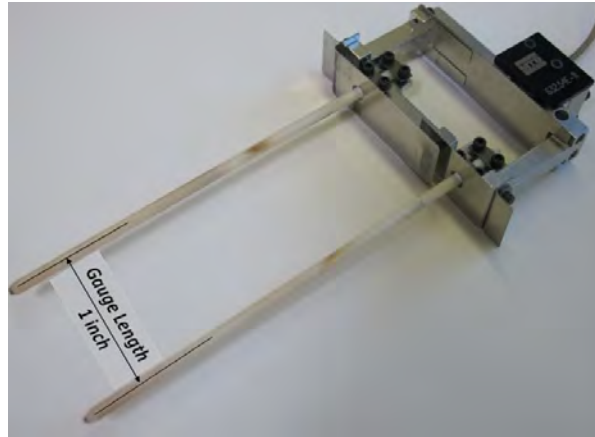

Figure 6.3 1PS extensometer used for creep testing

For measurement of coupon temperatures, three Type K wire thermocouples were installed over the reduced section of the coupon. Foil covering provided shielding for the thermocouples from radiation emanating from the heating elements of the furnace (Figure 6.4). Again, this setup was similar to that performed for elevated-temperature tension testing; a detailed description was provided in Section 3.5.

Figure 6.4 Thermocouples installed on coupons

6.2.4 Furnace and Test Machine

Like tensile testing, creep testing at elevated temperatures was performed using an MTS 810 test machine fitted with an MTS 653 furnace. More information on the testing equipment, shown in Figure 6.5, can be found in Chapter 3.
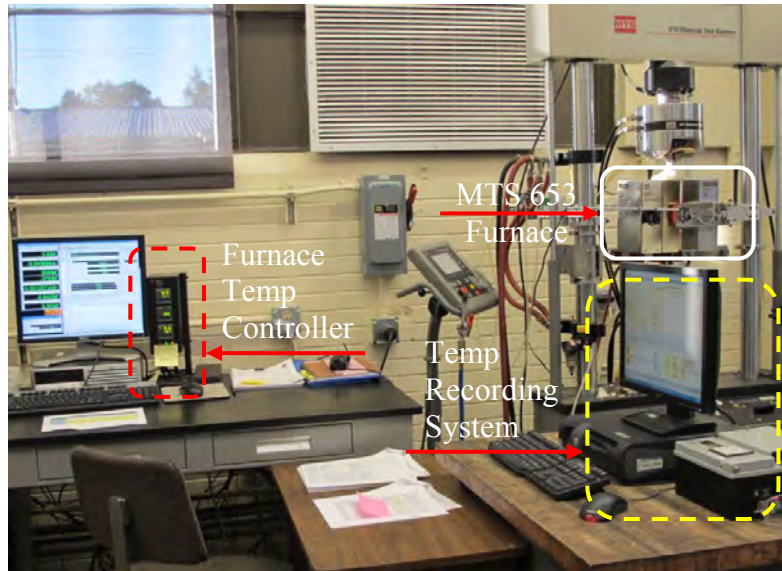

Figure 6.5 Tensile and creep test facility

After allowing an hour of heating for the coupon to reach thermal steady state at the target temperature, the coupon was loaded. Unlike for tensile testing, conducted by crosshead displacement control at a rate of 0.01 inch/minute, creep testing was performed using force control. The initially applied loads were maintained throughout the entire test. For most of the test conditions, the target loads for creep tests were reached within 5 seconds, as shown in Figure 6.6.
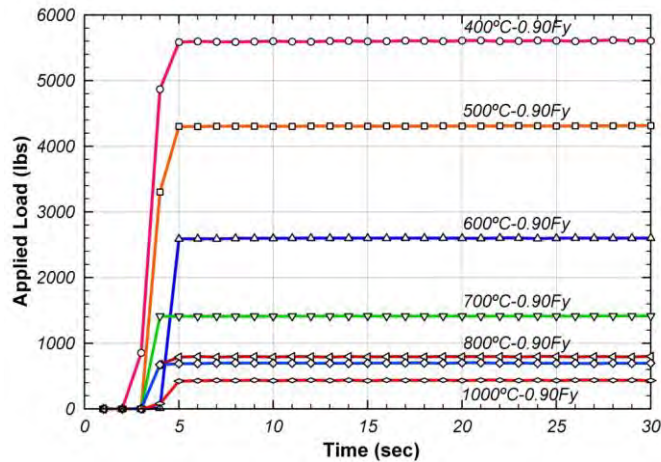
Figure 6.6 Time and loading curve at initial stage

### 6.2.5 Repetitions of Creep Test and Repeatability

Testing for a given temperature and stress level was repeated at least three times to obtain a representative result. Based on the experience of this testing, it was found that at elevated temperatures, creep test results can be very sensitive to a number of parameters, including the following:

- success with which the control system and furnace maintained a target temperature within a given tolerance;
- cycling (on/off) of the hydraulic pump in the MTS machine throughout the test;
- vibration in test machine elements, especially apparent when the applied load was much less than machine capacity; and
- eccentric loading induced despite efforts to center the coupon in the machine grips.

The first three sources of error listed above could result in the measurement of strain values which would oscillate about the values obtained in a more reliable test, as shown in Figure 6.7a. Eccentric loading could lead to the result shown in Figure 6.7b, where repeated testing led to higher measured strains.

180
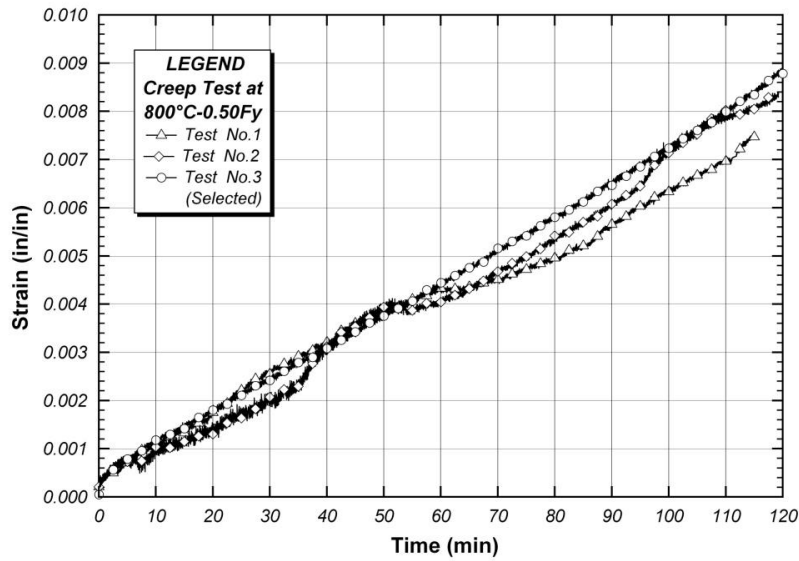
a) Oscillations in measured creep strains
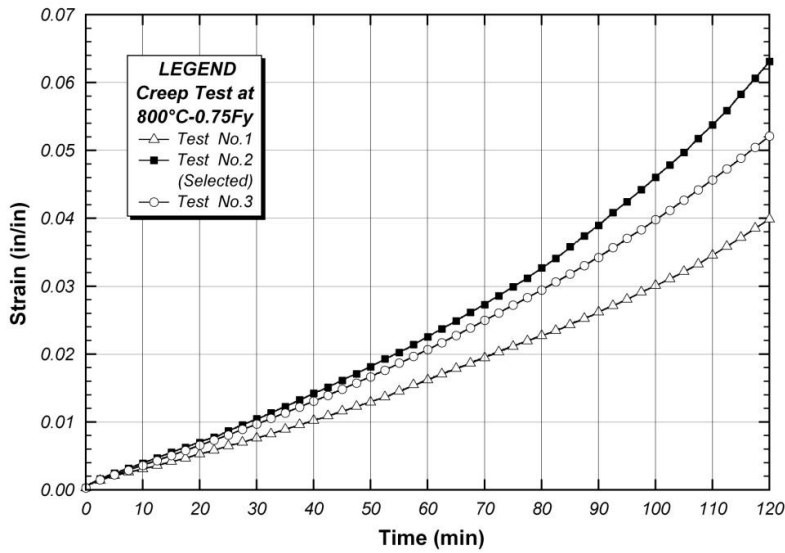
b) Higher values of creep strain determined through repeated testing

Figure 6.7 Repeatability study for creep test results at 800°C

Given the sources of error outlined above, creep testing was repeated until a reliable and representative result was obtained. What was considered reliable and representative was based on judgment guided by careful examination of variations in the test data. Furthermore, given that some test results seemed clearly affected by testing

errors, the final creep curve presented for a given stress level and temperature was the result of what was judged as a single e good test rather than data averaged from multiple tests. Despite these challenges, it should be noted that testing at most temperatures and stress levels showed good repeatability, e.g. Figure 6.8.
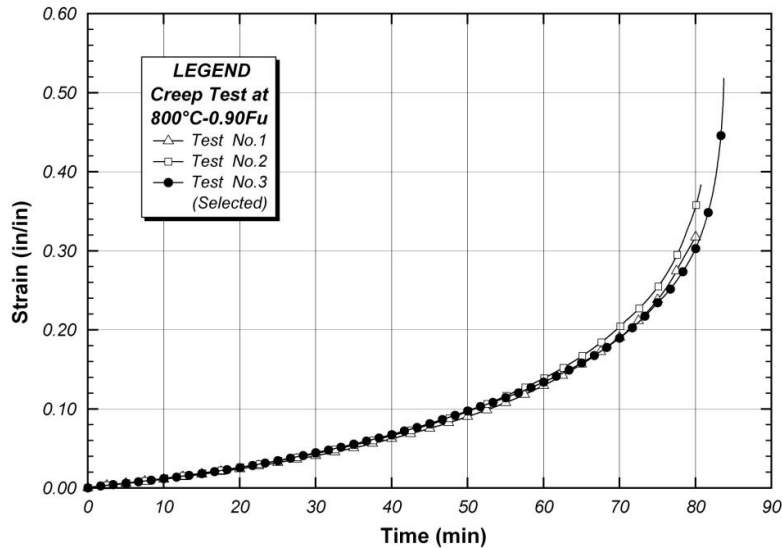

Figure 6.8 Repeatable results for creep testing at 800°C-0.90Fu

Two factors proved crucial in producing repeatable tests. First, the coupon temperatures needed to be controlled at its target temperature within close tolerance during the entire testing period. Second, the extensometer needed to be placed such to capture the necking of the reduced section. Tests that did not satisfy these two criteria definitely required repeating.

6.3   TEST RESULTS

Before discussing specific results from this research, a description of typical creep behavior is provided. After this discussion, test results are broken down by temperature and stress level.

6.3.1   Typical Creep Behavior

A typical creep curve under steady state conditions (constant load and temperature) is shown in Figure 6.9. After the initial application of load and the associated instantaneous strain, three stages of creep may be present. The creep stages are characterized by their strain rate: primary creep occurs while the strain rate is decreasing; secondary creep while it is constant, and tertiary creep while it is increasing. Tertiary creep may lead to creep rupture with sufficient time.
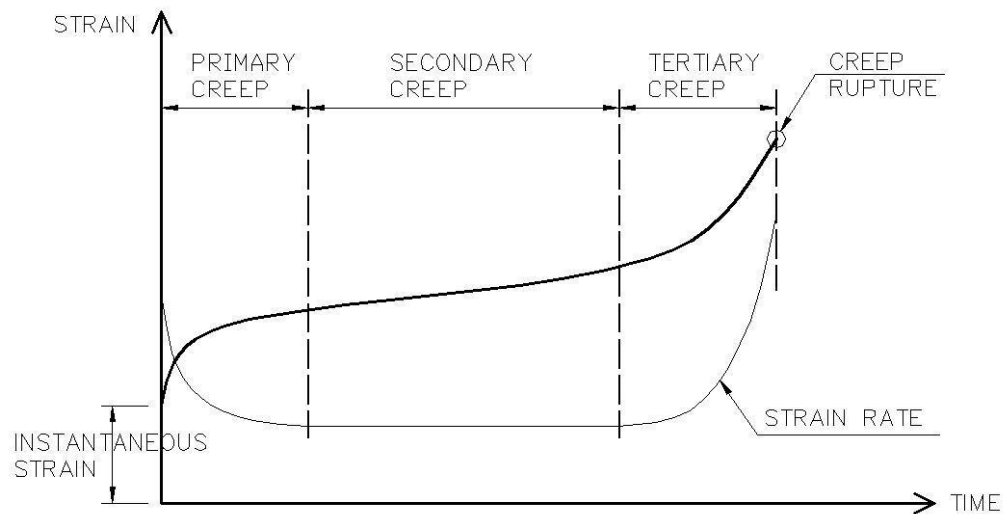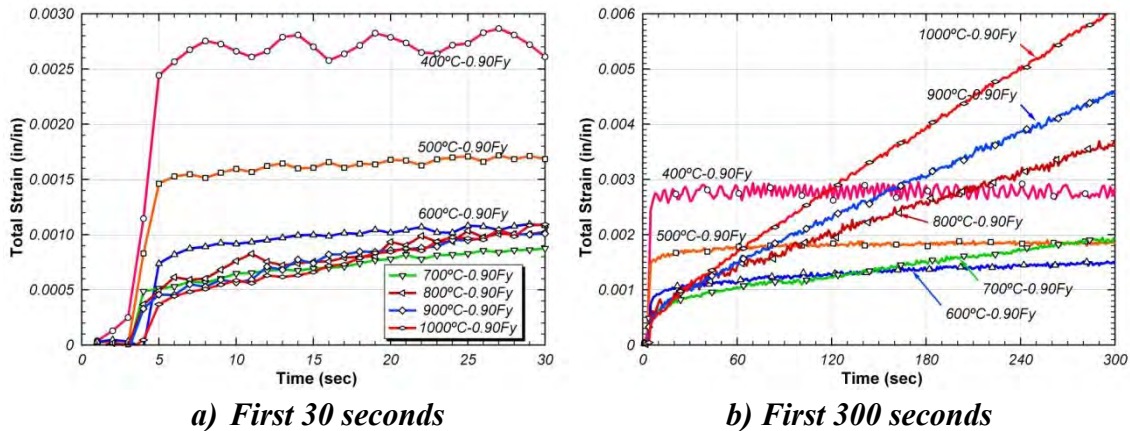

Figure 6.9 Typical steady-state creep curve (constant load and temperature)

The term *instantaneous strain*, as used in this chapter, refers to the strain developed as the load value was increased from zero to achieve the target stress value. The time taken to perform the initial loading was generally less than 5 seconds, as is shown in Figure 6.10.

a) First 30 seconds   *b) First 300 seconds*

Figure 6.10 Initial stages of time-strain curve (0.90Fy stress level)

The instantaneous strain is differentiated from the *creep strain*, where the creep strain is taken to be all strain that is developed by the coupon once the target load (stress) level is reached. Generally, the amount of instantaneous strain depends on the value of applied loads relative to specimen properties. As illustrated in Equation (6.1), when the applied stress is less than the yield stress, the instantaneous strain is equal to the elastic strain; when the applied stress is greater than the yield stress, the instantaneous strain also includes an inelastic strain component. For testing conducted at room temperature, creep is minimal and the majority of the strain response is instantaneous.

$$\varepsilon_i = \varepsilon_e \text{ when P} \leq \text{A} f_y$$
$$\varepsilon_i = \varepsilon_e + \varepsilon_p \text{ when A} f_y \leq \text{P} \leq \text{A} f_u$$

(6.1)

where

$\varepsilon_i, \varepsilon_e, \varepsilon_p$ = Instantaneous, elastic and inelastic strains, respectively; P = Load;

A = Section area of coupon; f_y= Yield stress; f_u= Tensile strength

6.3.2 Creep Curves by Temperatures

The creep curves at elevated temperatures from 400 to 1000°C are illustrated in Figure 6.11 to Figure 6.14. Note that the strain versus time curves presented here includes

184

both the instantaneous strain as well as the creep strain. Thus, the plots show total strain (instantaneous plus creep) versus time. Time equal to zero corresponds to the start of loading, so the load on the coupon is zero when the time is zero. For most cases, the test was continued for duration of 2 hours, which is the time duration of interest for typical structure fire problems.

Each plot shows the total strain and creep strain versus time for the four stress levels considered in these tests: $0.50F_y$, $0.75F_y$, $0.90F_y$, and $0.90F_u$, where F_y and F_u are the yield stress and tensile strength at the temperature of interest. The legend in each plot also lists the actual engineering stress values used for the tests. The total strain includes both the instantaneous strain and creep strain whereas the plot of creep strain does not include the instantaneous strain.
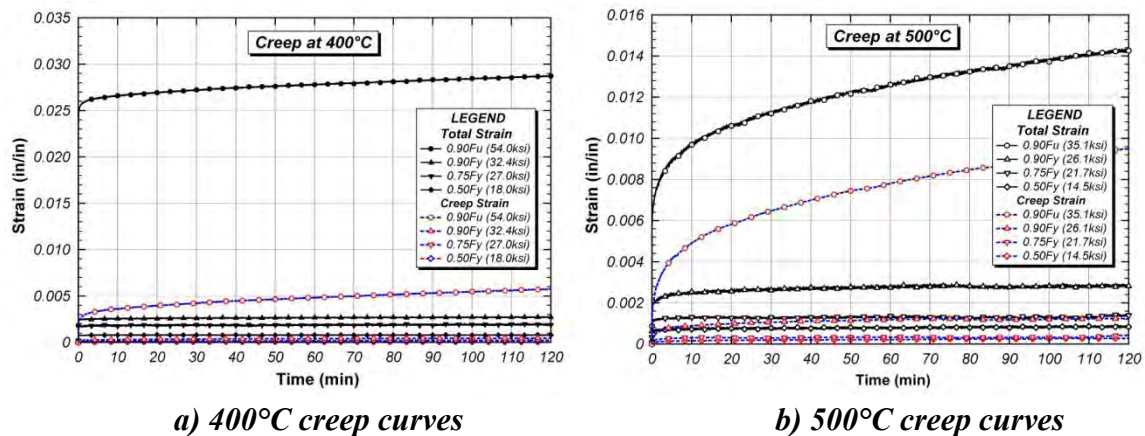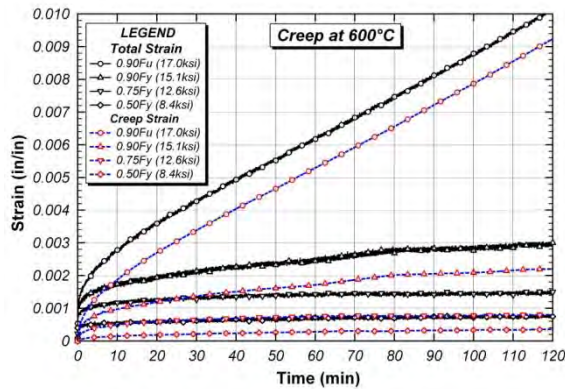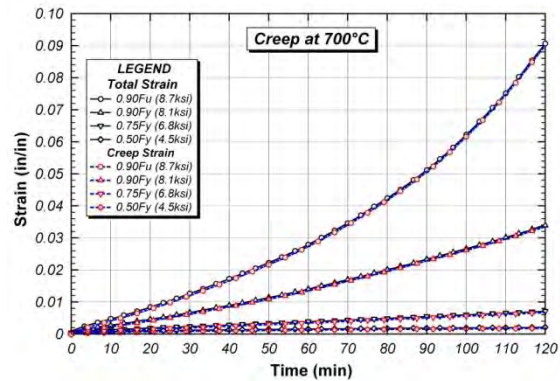

a) 400°C creep curves   b) 500°C creep curves

Figure 6.11 Creep curves at 400 and 500°C

At 400°C, a large instantaneous strain was generated for $0.90Fu$. Primary creep was also present, but at a value 20% that of the instantaneous strain. The creep strain was obtained from total strain by removing the elastic strain due to instantaneously applied loading. The large portion of elastic strain was involved at this stage. For $0.90Fu$ at 500°C, the same two stages, instantaneous strain and primary creep, were similarly dominant, but the amount of instantaneous strain was decreased significantly for total strain and creep strain both.

185

a) 600°C creep curves   *b) 700°C creep curves*

Figure 6.12 Creep curves at 600 and 700°C

At 600°C, most of the creep measured was primary, except for the $0.90F_u$ loading. The instantaneous strain for $0.90F_u$ was much less as well as the gap between creep strain and total strain was less than that for 400°C. At 700°C, the secondary and tertiary creep stage governed the creep behavior without any significant instantaneous strain or primary creep strain. There is similar the total strain and creep strain at 700°C.
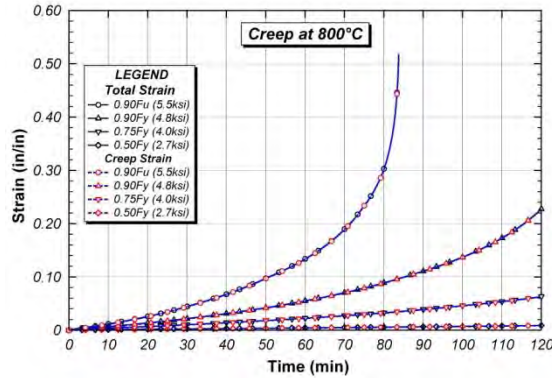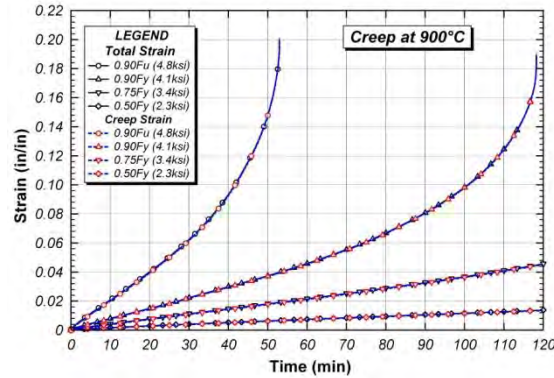
a) 800°C creep curves   *b) 900°C creep curves*

Figure 6.13 Creep curves at 800 and 900°C

Creep rupture first occurred at 800°C and at the $0.90F_u$ stress level. The coupon fracture occurred 80 minutes into the test. For all stress levels, secondary and tertiary creep were dominant at this temperature. Two coupons experienced creep rupture at

186

900°C for the highest two stress levels. The behavior for the other two loading cases was governed by the secondary creep stage. There is specific difference between creep strain and total strain for 800 and 900°C.
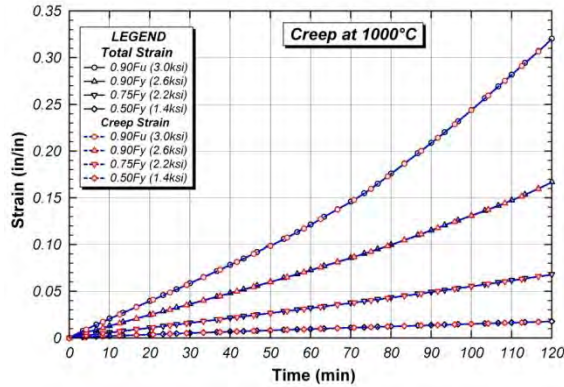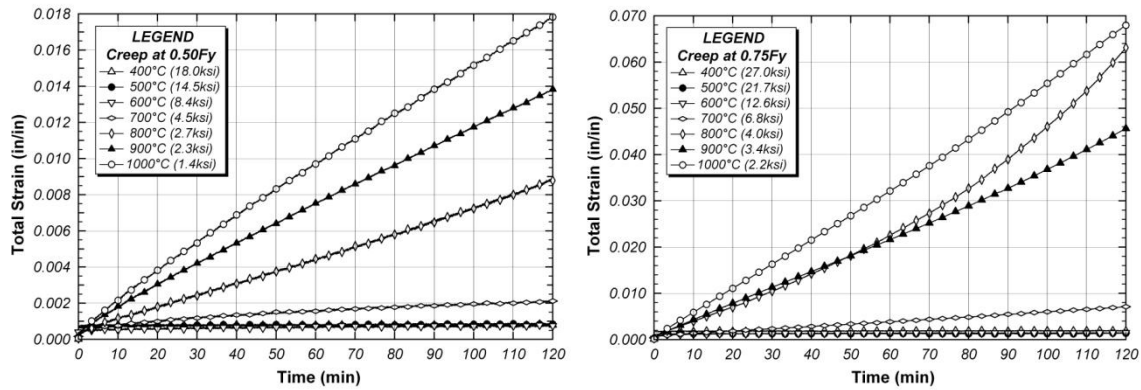

Figure 6.14 Creep curves at 1000°C

Unlike the previous two temperature levels, no creep ruptures occurred at 1000°C. Secondary and tertiary creep still dominated. The creep strain and total strain at 1000°C were nearly the same.

6.3.3 Creep Curves by Stress Level

Creep curves with total strain for the varying stress levels are illustrated for the tests at 400 to 1000°C in Figure 6.15 to Figure 6.16.
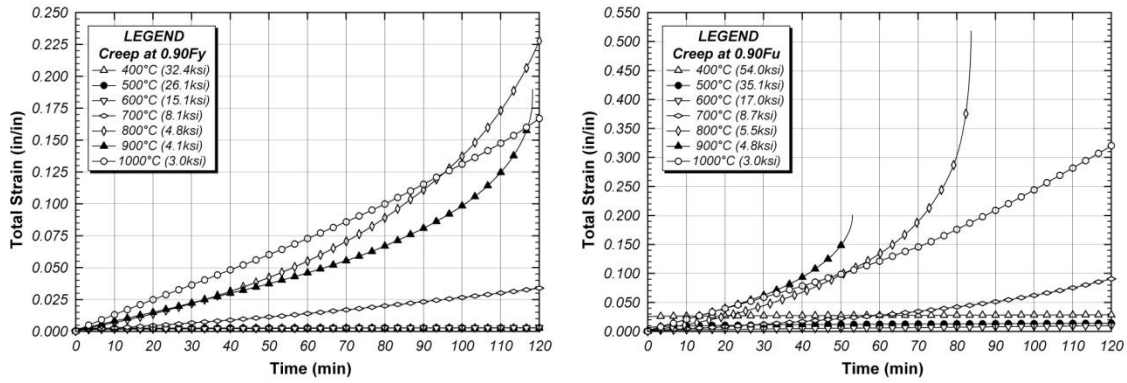

a) 0.50F$_y$ creep curves   *b) 0.75F$_y$ creep curves*

Figure 6.15 Creep curves at 0.50F$_y$ and 0.75F$_y$

187

Most of creep at the 0.50F_y stress level was primary except for 800°C, for which the majority was secondary. Secondary and tertiary creep was both observed to varying degrees at the 0.75F_y stress level.


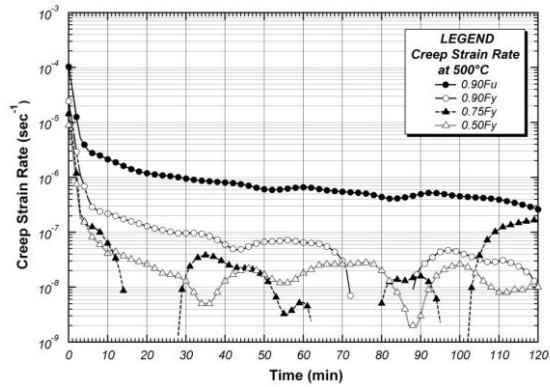| a) 0.90F_y creep curves | b) 0.90F_u creep curves |

Figure 6.16 Creep curves at 0.90F_y and 0.90F_u

Except at temperatures below 600°C, tertiary creep governed the behavior at 0.90F_y and 0.90F_u, sometimes resulting in creep rupture. The creep ruptures observed within the 2-hour duration of the test occurred at 800°C and 900°C of 0.90F_u.

6.3.4 Creep Strain Rates by Temperatures

Figure 6.17 to Figure 6.20 show the creep strain rate for the test temperatures. Creep strain rate is the slope of the strain versus time curve, and was obtained by dividing the incremental displacement by the incremental time. This type of curve is helpful in differentiating between the three creep stages of primary (decreasing strain rate), secondary (constant strain rate) and tertiary (increasing strain rate after secondary creep stage) creep.
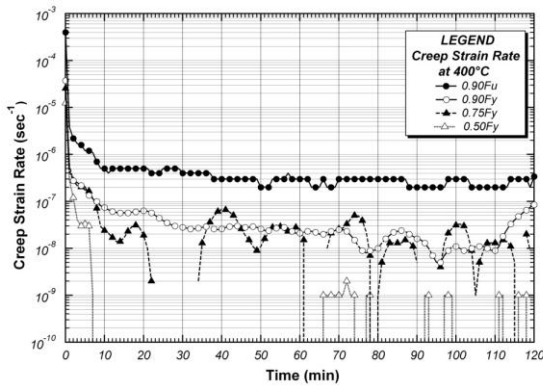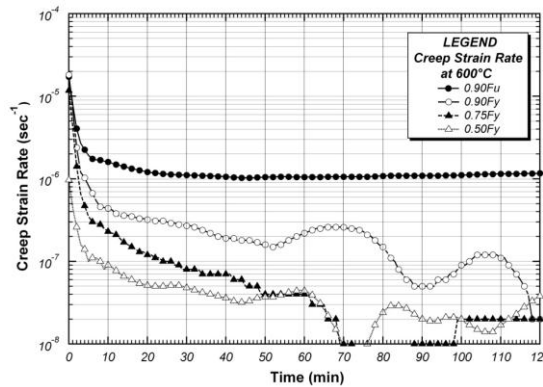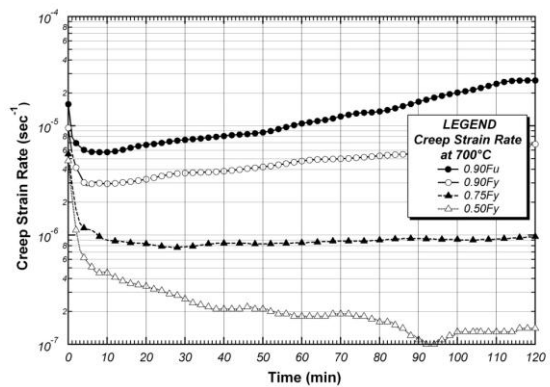
a) 400°C creep strain rate   *b) 500°C creep strain rate*

Figure 6.17 Creep strain rate at 400°C and 500°C

Secondary and tertiary creep were not encountered for either 400 or 500°C with one exception: 0.90Fu at 400°C. In all cases, the majority of the creep was primary. The discontinuities shown in the curves for 0.50Fy and 0.75Fy are an artifact of the accuracy of the extensometer, as the creep growth was especially slow for these cases.
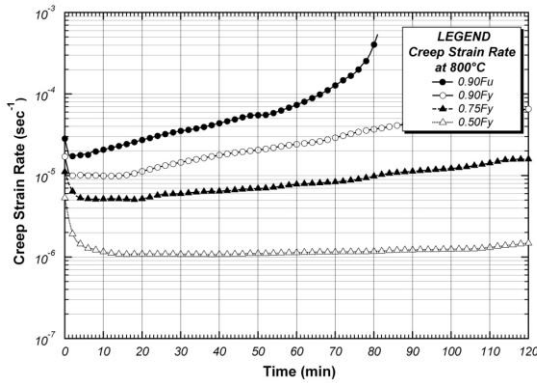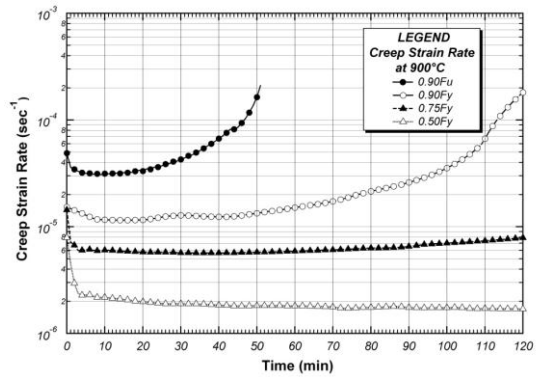

a) 600°C creep strain rate   *b) 700°C creep strain rate*

Figure 6.18 Creep strain rate at 600°C and 700°C

Secondary creep was generated at $0.90Fu$ whereas all other stress levels exhibited only primary creep at 600°C. At 700°C, all three creep stages were seen at $0.75Fy$, $0.90Fy$ and $0.90Fu$, but not for the $0.50Fy$ stress level.

189

a) 800°C creep strain rate   *b) 900°C creep strain rate*

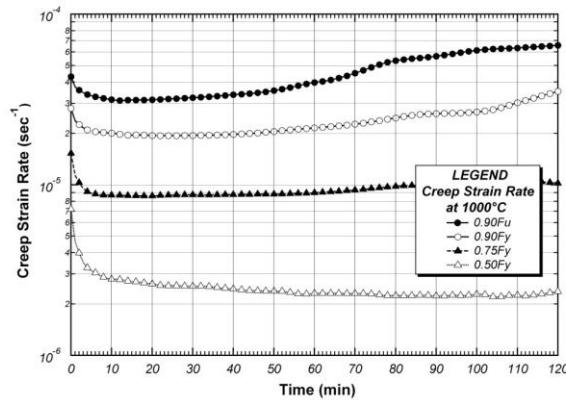*Figure 6.19 Creep strain rate at 800°C and 900°C*

Figure 6.20 Creep strain rate curves at 1000°C

All three stages of creep behavior can be seen in the creep strain rate curves for 800 to 1000°C for all stress levels.

6.4 ANALYSIS OF CREEP CURVES

Based on the results presented above, the creep behavior of A992 steel at elevated temperatures can be examined in terms of the four categories described in Table 6.4.

Table 6.4 Classification of creep curve descriptions

Stress	Temperature (°C)						
Level	400	500	600	700	800	900	1000
$0.50F_y$	Elastic loading at lower temperatures (Section 6.4.1)			Elastic loading at higher temperatures (Section 6.4.2)			
$0.75F_y$							
$0.90F_y$							
$0.90F_u$	Inelastic loading at lower temperature (Section 6.4.3)			Inelastic loading at higher temperature (Section 6.4.4)			

6.4.1 Elastic Creep at Temperatures ≤ 600°C

For elastic loading at temperatures of 600°C or less, only primary creep was observed. The amount of primary creep was typically less than the amount of instantaneous strain. The data for $0.75F_y$ is shown in Figure 6.21. The test data at $0.50F_y$ and $0.90F_y$ exhibited similar behavior except for the portion of instantaneous strain at initial time.
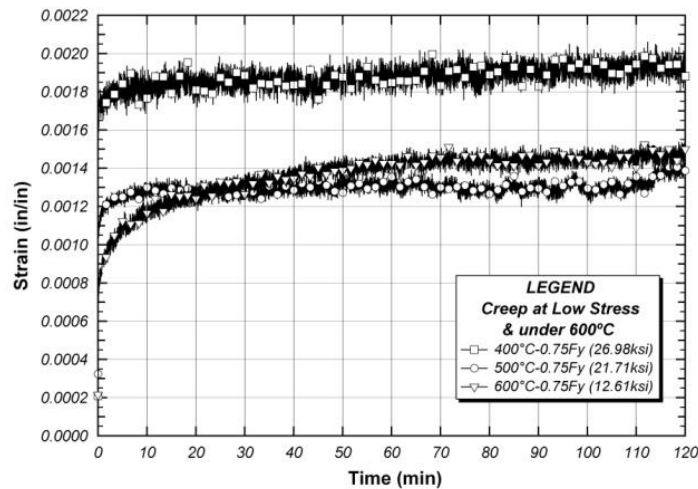

Figure 6.21 Creep curves for elastic loading at lower elevated temperatures

191

6.4.2   Inelastic Creep at Temperatures ≤ 600°C

For the inelastic loading condition $(0.90F_u)$ at lower elevated temperatures, primary and secondary creep was observed. Most notable in the test data (Figure 6.22a), however, is a large temperature-dependent variation in recorded instantaneous strain. Instantaneous strain is highest for 400°C and decreases with increasing temperature to 600°C.
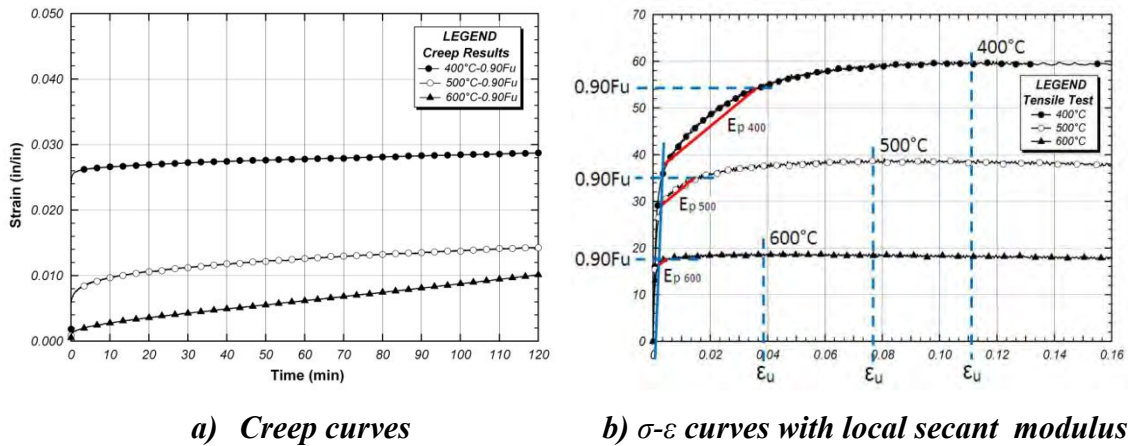

a) Creep curves   *b) σ-ε curves with local secant modulus*

Figure 6.22 Creep curves for inelastic loading at lower elevated temperatures

Though the elastic strain at the yield stress does decrease with temperature, the main source of the difference in instantaneous strain is the inelastic strain. This difference in inelastic strain comes from two sources: less stress applied after yield, and a stiffer response in the initial inelastic range. As Figure 6.22b shows, as the test temperature increases, the difference in stress (that is, $0.9F_u - F_y$) decreases. As such, given a constant local secant modulus, the inelastic strain would decrease. However, the local secant modulus is affected by temperature (Table 6.5). As shown in Figure 6.23b, the response is stiffer at lower temperatures. The combination of these two effects is responsible for the instantaneous strain with temperature for the tests in this category.

192

Table 6.5 Local secant modulus under 600°C

Parameter		Temperature (°C)		
		400	**500**	**600**
Yield Stress	F_y (ksi)	36.0	29.0	16.8
90% Ultimate Strength	$0.90F_u$ (ksi)	54.0	35.1	17.0
Yield Strain	ε_y (in/in)	0.00138	0.00121	0.00084
90% Ultimate Strain	$\varepsilon_{0.90Fu}$ (in/in)	0.03591	0.01605	0.00288
Elastic Modulus	E (ksi)	26,063	23,972	19,923
Tangent Modulus	E_t (ksi)	523	414	107
Modulus Ratio	$n=E\,/\,E_t$	50	58	186

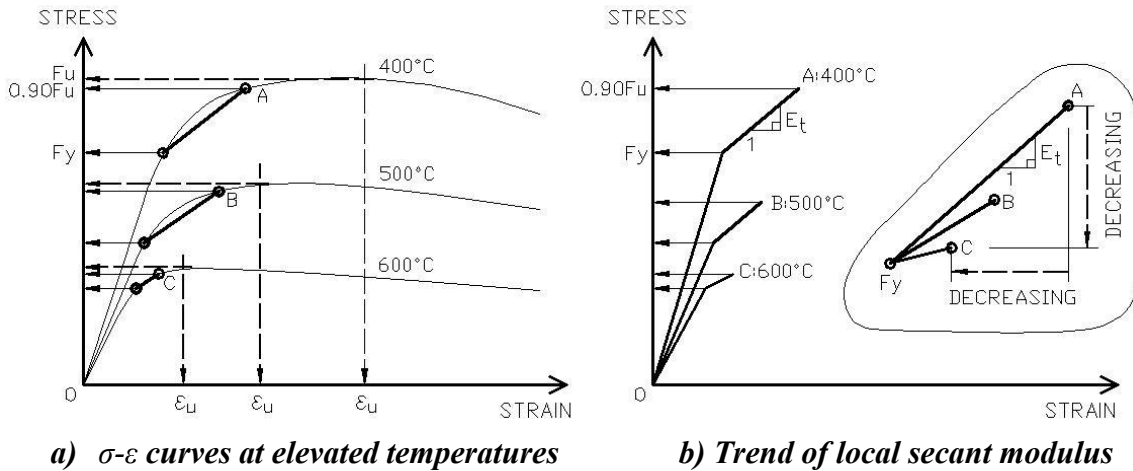*a) σ-ε curves at elevated temperatures*   *b) Trend of local secant modulus*

Figure 6.23 Local secant modulus and effect on instantaneous strain

6.4.3 Elastic Creep at Temperature > 600°C

The creep response for elastic loading at the highest elevated temperatures was characterized by secondary creep for most tests. In all cases, primary creep was negligible compared to the other stages. Three tests also showed significant tertiary creep:

0.75F_y and 0.90F_y at 800°C and 0.90F_y at 900°C, with the last of these ending in creep rupture. Tertiary creep was observed a minimal for tests conducted at 1000°C.
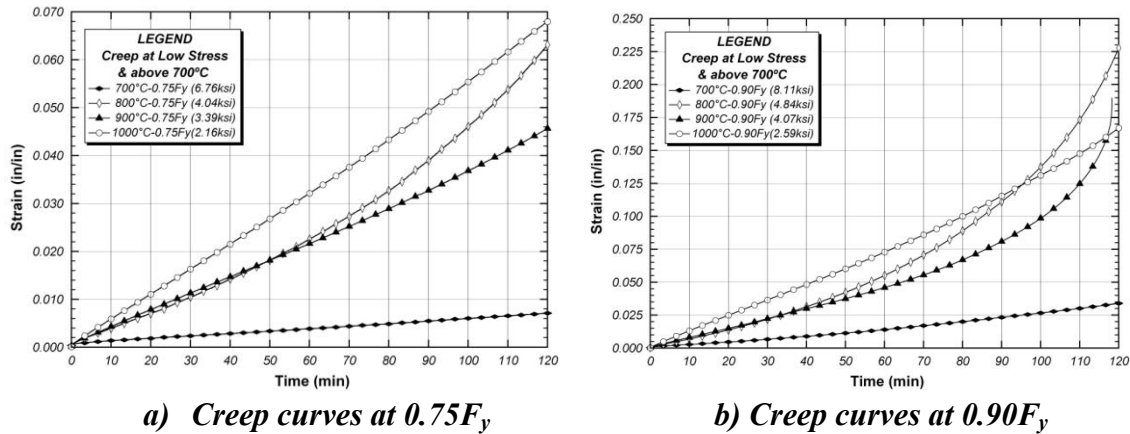

a) *Creep curves at 0.75F_y*   b) *Creep curves at 0.90F_y*

Figure 6.24 Creep curves for elastic loading at higher elevated temperatures

6.4.4   Inelastic Creep at Temperature > 600°C

As seen in Figure 6.25, secondary and tertiary creep were the dominant phases of the creep response for testing conducted at high stress and high temperature. Creep rupture was observed during testing at 800 and 900°C but not 1000°C.
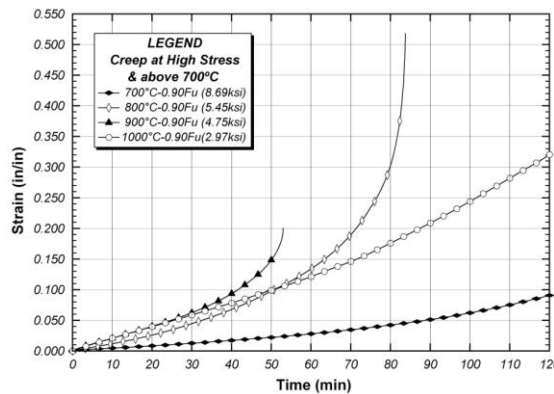

Figure 6.25 Creep curves for inelastic loading at higher elevated temperatures

As tertiary creep was observed for the inelastic loading at 1000°C, given enough time (testing was limited to 2 hours), creep rupture would likely have occurred. The time

to creep rupture was reduced slightly by the increase in temperature from 800 to 900°C, but then decreased significantly for the next temperature increase.

6.4.5   Overview of Patterns in Creep Behavior

The preceding sections have described the observed creep behaviors based on stress and temperature conditions. A summary is presented in Table 6.6. For each testing condition, the observed stages of creep are noted. It can be seen that creep behavior becomes more significant with increasing applied stress and temperature until 1000°C is reached. It should be noted, that while this behavior is expected to be similar to coupons taken from different steel sections, testing was limited to samples taken from a lightweight section (W4x13).

Table 6.6 Stages of creep observed for each test condition

Stress Level	Temperature (°C)						
	400	**500**	**600**	**700**	**800**	**900**	**1000**
$0.50F_y$	P	P	P	P	p, S, T	p, S	p, S
$0.75F_y$	P	P	P	p, S	p, S, T	p, S, T	p, S, T
$0.90F_y$	P	P	P	p, S, T	p, S, T	p, S, T, R	p, S, T
$0.90F_u$	P	P	P, S	p, S, T	p, S, T, R	p, S, T, R	p, S, T

Legend: P=Primary creep, p=Negligible primary creep, S=Secondary creep, T=Tertiary creep, R=Creep rupture

6.5   ANALYSIS OF CREEP PROPERTIES

In this section, two properties of creep behavior are discussed: steady-state creep rate and activation energy. The activation energy is a parameter included in some creep models from the literature; it is computed based, in part, on the steady-state creep rate.

6.5.1   Steady-State Creep Rates

The steady-state and minimum steady-state creep rates were examined for providing purpose of A992 steel at elevated temperatures by observation of creep test

results. For the specimens that showed secondary creep (creep at constant strain rate), two distinct steady-state behaviors were noted. Coupons tested under lower applied stress tended to have longer periods of secondary creep; at higher applied stress, the time period for steady-state creep behavior was reduced. This pattern for steady-state creep is tabulated in Table 6.7. Here $\dot{\varepsilon}_{ss}$ denotes a long period of steady-state creep (Figure 6.26a) and $\dot{\varepsilon}_{min}$ is a minimal period of steady-state creep (Figure 6.26b), for the purposes of this discussion, defined as less than 10 minutes.

a) **Steady-state strain rate**   b) **Min. steady-state strain rate**
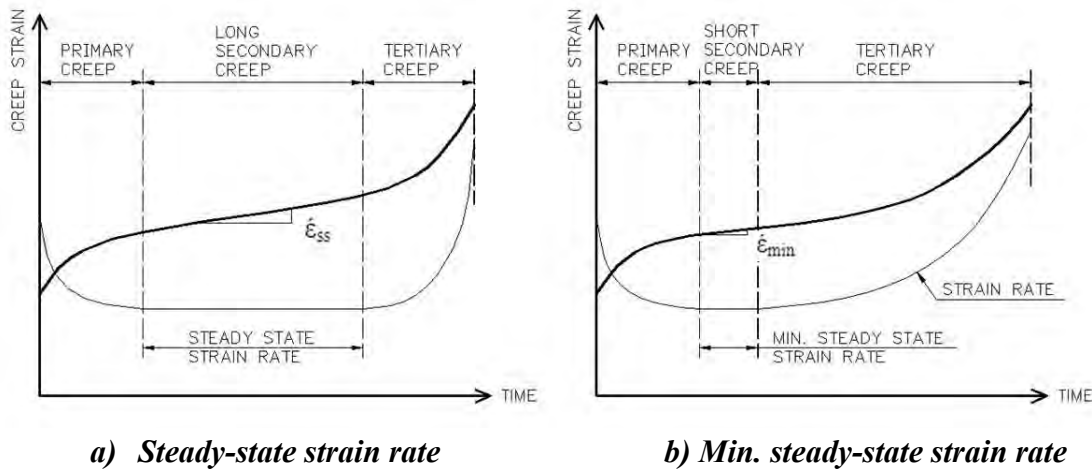
Figure 6.26 Two steady-state creep behaviors observed

Table 6.7 Classification of steady-state creep

Stress Level	Temperature (°C)						
	400	**500**	**600**	**700**	**800**	**900**	**1000**
$0.50F_y$	N/A	N/A	N/A	N/A	$\dot{\varepsilon}_{ss}$	$\dot{\varepsilon}_{ss}$	$\dot{\varepsilon}_{ss}$
$0.75F_y$	N/A	N/A	N/A	$\dot{\varepsilon}_{ss}$	$\dot{\varepsilon}_{ss}$	$\dot{\varepsilon}_{ss}$	$\dot{\varepsilon}_{ss}$
$0.90F_y$	N/A	N/A	N/A	$\dot{\varepsilon}_{min}$	$\dot{\varepsilon}_{ss}$	$\dot{\varepsilon}_{ss}$	$\dot{\varepsilon}_{min}$
$0.90F_u$	N/A	N/A	$\dot{\varepsilon}_{ss}$	$\dot{\varepsilon}_{min}$	$\dot{\varepsilon}_{min}$	$\dot{\varepsilon}_{min}$	$\dot{\varepsilon}_{min}$

The minimum creep strain rate which is generally defined as less than 10 minutes steady state strain observed during the steady state phase, which in all cases was also the minimum observed throughout the test, is tabulated in Table 6.8. These minimum creep

strain rates are plotted against applied stress on a log-log scale in Figure 6.27. Linear behavior is this plot indicates a power-law relationship between the variables. The parameters for this model are tabulated in Table 6.9.

Table 6.8 Creep strain rates (sec $^{-1}$)

Stress Level	Temperature (°C)				
	600	**700**	**800**	**900**	**1000**
0.50F_y	*N/A*	*N/A*	1.08E-06	1.66E-06	2.26E-06
0.75F_y	*N/A*	8.19E-07	5.15E-06	5.55E-06	8.57E-06
0.90F_y	*N/A*	2.85E-06	1.03E-05	1.14E-05	1.92E-05
0.90F_u	9.63E-07	5.76E-06	1.70E-05	3.11E-05	3.12E-05
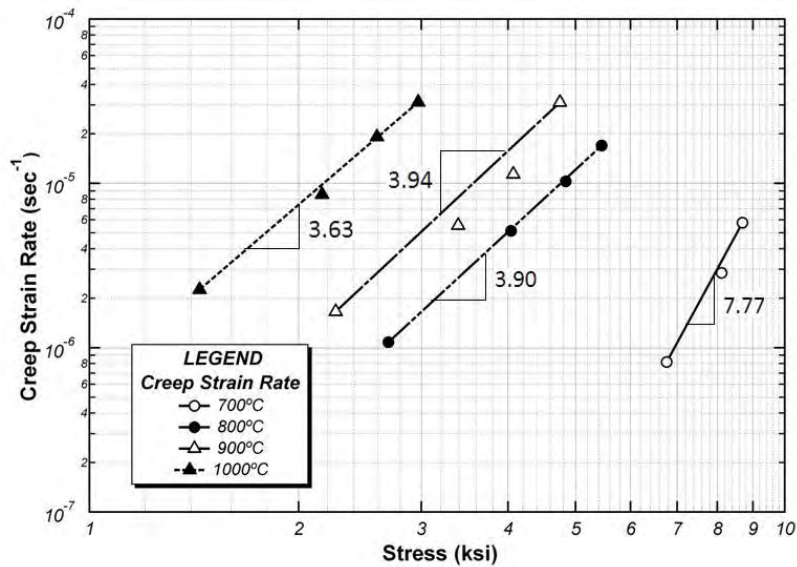
Figure 6.27 Steady-state creep strain rates

Table 6.9 Creep strain rates based on curve fitting

Curve-Fit Equation	Temperature (°C)			
	700	**800**	**900**	**1000**
Power Law	3E-13$\sigma^{7.77}$	2E-08$\sigma^{3.90}$	7E-08$\sigma^{3.95}$	6E-07$\sigma^{3.63}$

6.5.2 Activation Energy

Creep is a thermally-activated process, that is, an increased testing temperature leads to increasing rate of creep. In this section, activation energy is calculated from the test data for reference only. Creep rate can be described with an Arrhenius equation (Sherby and Burke 1967) shown in Equation (6.2), as follows:

$$\dot{\varepsilon} = K \exp\left(-\frac{Q_c}{R\,T}\right)$$

(6.2)

where

$\dot{\varepsilon}$ = Steady-state creep rate (sec^{-1})

Q_c = Activation energy for creep (J / mol)

R = Gas constant, 8.3145 J / mol-K

K = Constant between creep rate and temperatures

T = Absolute temperature (K)

The activation energy for creep is a fundamental material property which can be calculated per Equation (6.3) if the creep rate is known at two arbitrary temperatures (Sherby and Burke 1967).

$$Q_c|_{\sigma,\varepsilon} = \left.R \, \mathrm{Ln}\left(\frac{\dot{\varepsilon}_1}{\dot{\varepsilon}_2}\right)\middle/ (1/T_2 - 1/T_1)\right.$$

(6.3)

where

$\dot{\varepsilon}_1$, $\dot{\varepsilon}_2$ = Creep rate at arbitrary temperatures 1 and 2 (sec^{-1})

T_1, T_2 = Absolute temperature at arbitrary temperatures 1 and 2 (K)

The activation energy was calculated (Table 6.10) using the steady-state creep rates associated with the temperatures of 800 to 1000°C. As seen in Figure 6.27, the creep strain rate – stress curves at these temperature levels overlap. A stress within this overlap region, 2.8 ksi, was chosen for calculation, and its associated creep strain rate

198

was calculated using the best-fit power law from Table 6.9. The activation energy was then calculated using the above equation. The calculated activation energy for A992 steel was 135.6 kJ/mol for 800 to 900°C and 226.0 kJ/mol for 900 to 1000°C shown in Table 9.8. This is smaller than the A36 activation energy which is 323.3 kJ/mol (Harmathy 1967).

Table 6.10 Activation energy determined by experiment

Temp (°C)	T (K)	Stress (ksi)	Creep Strain Rate $\dot{\varepsilon}$ (sec^{-1})		Q_c (kJ/mol)
800	1073	2.80	$2E\text{-}08\sigma^{3.90}$	1.113E-06	**135.6**
900	1173	2.80	$7E\text{-}08\sigma^{3.9}$	4.066E-06	
1000	1273	2.80	$6E\text{-}07\sigma^{3.63}$	2.509E-05	**226.0**

6.6 DEVELOPMENT OF CREEP MODEL

A creep model for the ASTM A992 steel tested in this research was developed based on the test results The model is a best fit for the creep strain found under the four stress levels (0.50F_y, 0.75F_y, 0.90F_y, and 0.90F_u) for a given temperature examined during testing (400 to 1000°C, at 100C° intervals). As such, it can be used directly to estimate the creep strain that would occur for any stress imposed at one of these temperatures. For a temperature within the test range, but not explicitly tested for, creep curves can be generated for the adjacent test temperatures, and interpolation conducted between two creep strain values.

The model includes the consideration of instantaneous strain and the time-dependent behaviors of primary creep, secondary creep, tertiary creep, and creep rupture (if any occurred), as shown in Figure 6.28. It is noted that the applicability of the suggested creep model may be limited by the particulars of the testing performed: two hours of testing performed on a coupon from an ASTM A992 W4x13 flange at elevated temperatures of 400 to 1000°C.

199
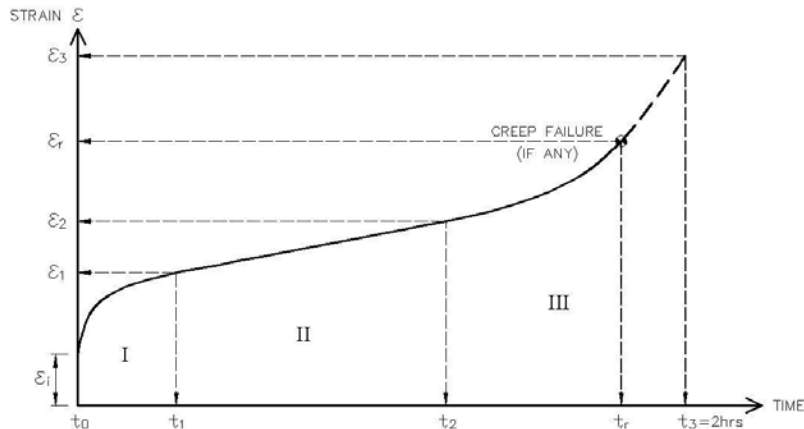
Figure 6.28 General form of creep curve

6.6.1 Patterns in Creep Data

After the occurrence of instantaneous strain, the typical creep curve provided in the previous figures shows two zones of exponential behavior (primary and tertiary creep) and one zone of linear behavior (secondary creep). It was determined that modeling the creep behavior as a linear combination of two exponential functions was appropriate. The first of these exponentials was parameterized for primary creep, and the second for the other creep phases. A generic strain power-law equation provided as shown in Equation (6.4).

$$\varepsilon = A\,t^n$$

(6.4)

where A = Constant depending on applied stress, n = Exponent

Most creep curves, shown in Section 6.3, were either dominated by primary creep or secondary creep. The first of these two cases is shown by example as Figure 6.29. Only one power-law function, parameterized for primary creep, was required. To account for the behavior of decreasing strain rate with time, the exponent n was less than one.

200
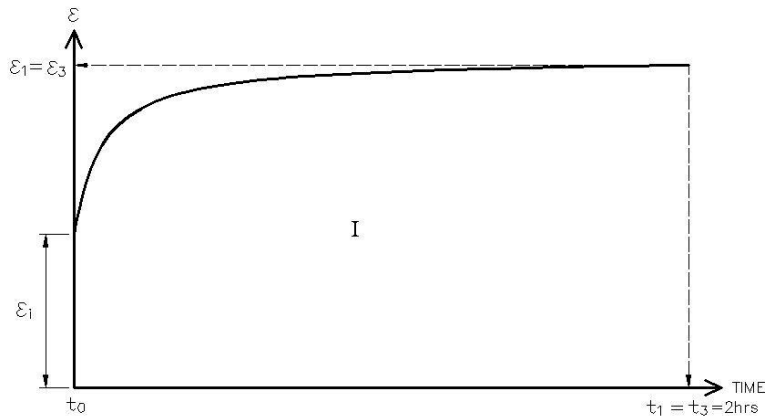
Figure 6.29 Creep pattern governed by primary or secondary creep

Creep curves of the type shown in Figure 6.30 were dominated by secondary or tertiary creep and were modeled as the linear combination of two power laws. The primary creep was often small in comparison to other creep stages.
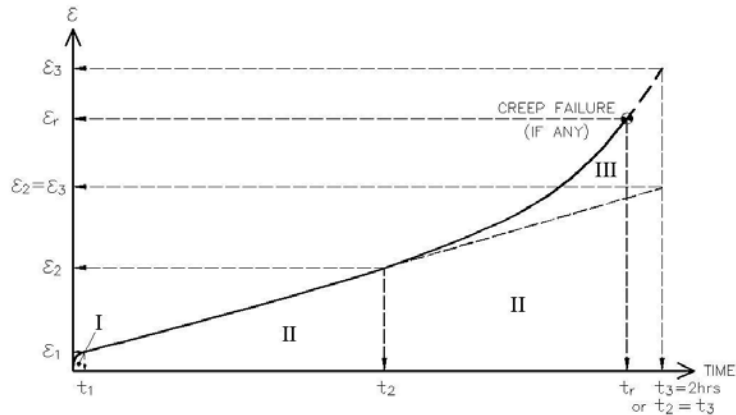
Figure 6.30 Creep pattern governed by secondary or tertiary creep

The first of the two power laws was typically parameterized for primary creep, with the second for secondary/tertiary. As such, the exponent for the first power law was less than one (decreasing strain rate) and the exponent for the second power law was greater than one (increasing strain rate). It should be noted that this pattern of behavior occurred only for tests conducted at least 600°C and/or high stress levels.

201

6.6.2 Suggested Constitutive Creep Model

The suggested creep model combines two power law equations to represent primary and secondary creep or secondary and tertiary creep, and also includes the instantaneous strain. The suggested creep model is summarized in Table 6.11 and Figure 6.31, and is applicable for tests of up to 2-hour length.

Table 6.11 Constitutive creep model

Stage	Time Range	Strain ε (in/in)
Initial	$t = t_0$	$\varepsilon_i = \varepsilon_e + \varepsilon_t$ $= \begin{cases} \dfrac{\sigma}{E} & : \quad \sigma \le F_y \\ \dfrac{F_y}{E} + \dfrac{\sigma - F_y}{E_t} & : F_y < \sigma \le F_u \end{cases}$
Creep	$t_0 < t \le t_{r,} t_3$	$\varepsilon_c = \varepsilon_i + A_1 t^{n_1} + A_2 t^{n_2}$
Parameters & Functions		For $500°C \le T \le 1000°C$ (illustrated in Figure 6.32), $\quad E = 41{,}554 - 37.4\,T, \quad E_t = 3{,}107 - 3.0\,T$ For T = 400°C, $\quad E = 14{,}000$ ksi, $E_t = 900$ ksi

where

σ = Applied stress at steady-state creep test
$\varepsilon_i, \varepsilon_e, \varepsilon_p$ = Instantaneous strain, elastic strain and inelastic strain
F_y, F_u = Yield stress and tensile strength at elevated temperatures (Table 6.12)
E, E_t = Elastic and local secant moduli for given applied stress (Figure 6.32)
A_1, A_2, n_1, n_2 = Power-law parameters, determined empirically (Table 6.13)

Table 6.12 Yield stress and tensile strength (ksi) for creep model

Property	Temperature (°C)						
	400	500	600	700	800	900	1000
F_y	35.4	28.9	16.8	9.0	5.3	4.5	2.9
F_u	60.0	39.2	18.9	9.7	6.1	5.3	3.3
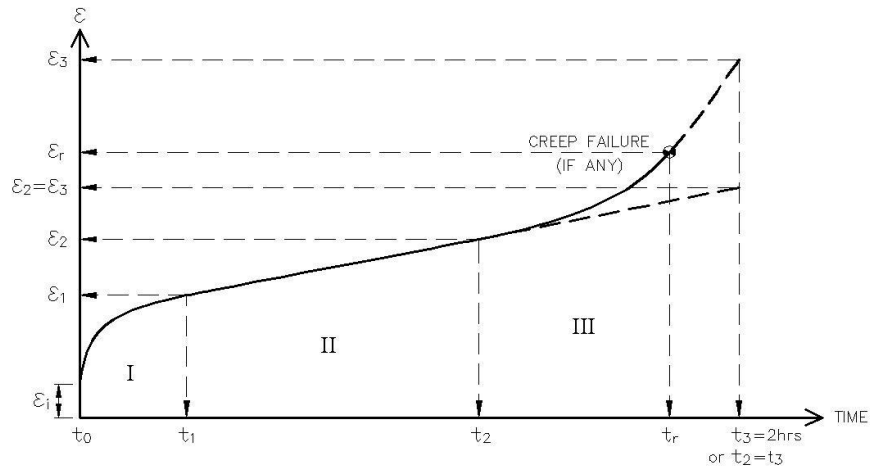
Figure 6.31 Creep strain-time relationships for constitutive model

The elastic modulus and local secant modulus used for the suggested creep model were determined through consideration of the elevated-temperature stress-strain curves. Results from curve-fitting the elastic and initial inelastic region are shown in Figure 6.32.

| *a) Elastic modulus* | *b)Local secant modulus* |
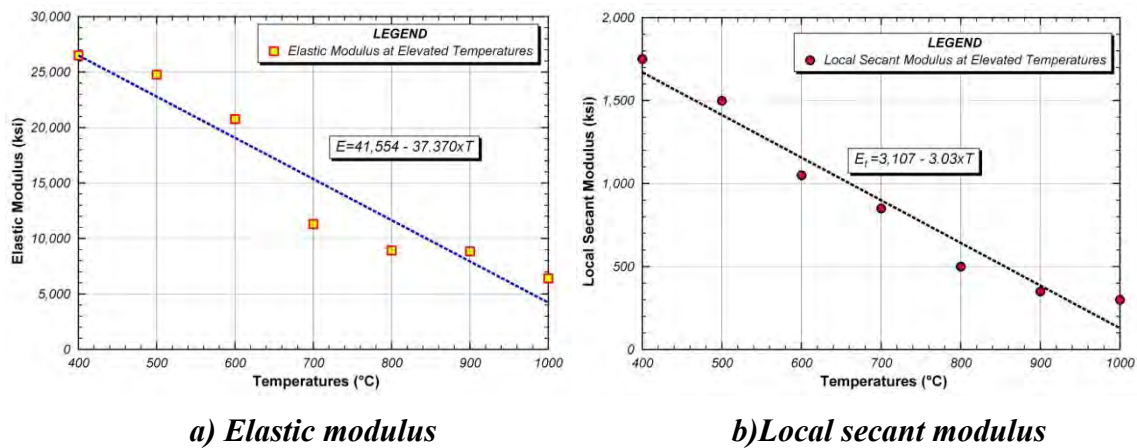
Figure 6.32 Temperature dependence of elastic and local secant moduli

Table 6.13 Parameters for creep model

Temp (°C)	σ (ksi)		t_1, t_r, t_3 (min)	A_1	n_1	A_2	n_2
400	$0.50F_y$	17.7	120	1.00E-04	0.050	-	-
	$0.75F_y$	26.6	120	7.50E-04	0.045	-	-
	$0.90F_y$	31.9	120	1.25E-03	0.040	-	-
	$0.90F_u$	54.0	120	1.25E-02	0.052	-	-
500	$0.50F_y$	14.5	120	5.00E-05	0.310	-	-
	$0.75F_y$	21.7	120	2.50E-04	0.120	-	-
	$0.90F_y$	26.0	120	1.00E-03	0.120	-	-
	$0.90F_u$	35.3	120	2.00E-03	0.300	-	-
600	$0.50F_y$	8.4	120	4.00E-05	0.440	-	-
	$0.75F_y$	12.6	120	3.00E-04	0.230	-	-
	$0.90F_y$	15.1	120	4.00E-04	0.355	-	-
	$0.90F_u$	17.0	120	5.00E-04	0.544	1.00E-07	2.100
700	$0.50F_y$	4.5	120	1.50E-04	0.525	-	-
	$0.75F_y$	6.8	120	2.00E-04	0.665	3.00E-08	2.310
	$0.90F_y$	8.1	120	3.00E-04	0.880	3.00E-08	2.720
	$0.90F_u$	8.7	120	4.00E-04	0.950	3.00E-08	3.000
800	$0.50F_y$	2.7	120	1.50E-04	0.770	2.00E-07	1.980
	$0.75F_y$	4.0	120	6.00E-04	0.800	2.00E-07	2.520
	$0.90F_y$	4.8	120	8.00E-04	1.000	2.00E-11	4.720
	$0.90F_u$	5.5	84	8.00E-04	1.170	2.00E-11	5.200
900	$0.50F_y$	2.3	120	2.00E-04	0.865	2.00E-07	1.770
	$0.75F_y$	3.4	120	5.00E-04	0.890	2.00E-07	2.250
	$0.90F_y$	4.1	118	1.00E-03	0.920	2.00E-18	8.100
	$0.90F_u$	4.8	53	1.50E-03	1.100	2.00E-18	9.630
1000	$0.50F_y$	1.5	120	3.00E-04	0.830	2.00E-07	1.880
	$0.75F_y$	2.2	120	6.00E-04	0.950	2.00E-07	2.280
	$0.90F_y$	2.6	120	2.00E-03	0.860	2.00E-08	3.050
	$0.90F_u$	2.9	120	2.00E-03	0.980	2.00E-08	3.230

The parameters for the suggested creep model (A_1, A_2, n_1 and n_2) were developed as functions of the applied stress, using the creep data for a specific test temperature. To provide a better fit of the data, each parameter is defined piecewise for the two ranges: 0 to $0.50F_y$ (stress of first test), for which linear behavior is assumed, and $0.50F_y$ to $0.90F_u$. The second range included results for the four loading conditions considered, and as such a higher order polynomial fit was required. Table 6.14 to Table 6.17, list the equations for

each parameter. Figure 6.33 to Figure 6.35 provide plots for each parameter as a function of temperature and applied stress.

Table 6.14 A₁ parameter equations

Temp (°C)	Stress Range (ksi)	$A_1 = a\,\sigma^3 + b\,\sigma^2 + c\,\sigma + d$			
		a	b	c	d
400	$0 \leq \sigma < 17$	-	-	3.394E-06	-
	$17 \leq \sigma \leq 55$	4.163E-08	-2.106E-06	3.554E-05	-1.402E-04
500	$0 \leq \sigma < 15$	-	-	8.814E-06	-
	$15 \leq \sigma \leq 35$	-	7.002E-06	-2.293E-04	1.884E-03
600	$0 \leq \sigma < 8$	-	-	7.139E-06	-
	$8 \leq \sigma \leq 17$	2.015E-07	-1.826E-06	7.568E-06	5.751E-06
700	$0 \leq \sigma < 4.5$	-	-	3.329E-05	-
	$4.5 \leq \sigma \leq 9$	8.398E-06	-1.483E-04	8.832E-04	-1.586E-03
800	$0 \leq \sigma < 3$	-	-	5.639E-05	-
	$3 \leq \sigma \leq 5.5$	-4.636E-05	4.890E-04	-1.356E-03	1.169E-03
900	$0 \leq \sigma < 2.5$	-	-	8.932E-05	-
	$2.5 \leq \sigma \leq 5$	-	1.515E-04	-5.295E-04	6.163E-04
1000	$0 \leq \sigma < 1.5$	-	-	2.133E-04	-
	$1.5 \leq \sigma \leq 3$	-	7.725E-04	-2.290E-03	1.992E-03
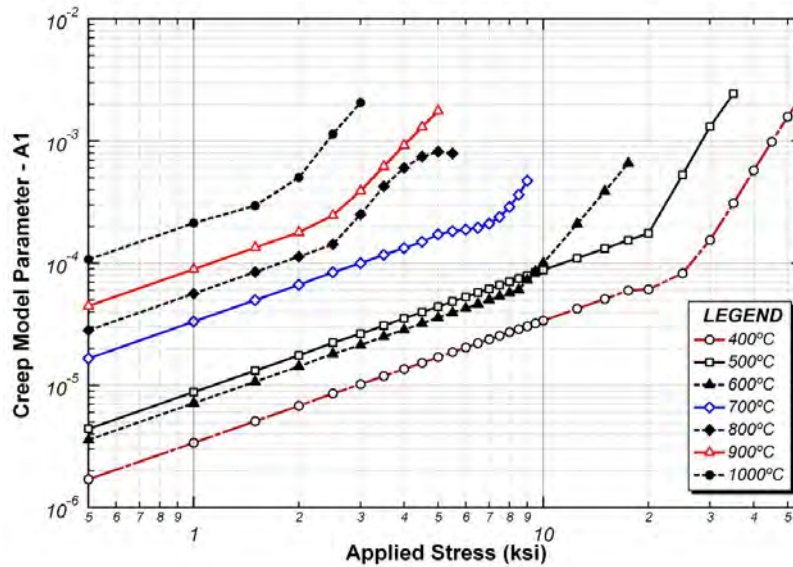
Figure 6.33 Distribution of A₁ parameter

Table 6.15 n_1 parameter equations

Temp (°C)	Stress Range (ksi)	$n_1 = a\,\sigma^3 + b\,\sigma^2 + c\,\sigma + d$			
		a	**b**	**c**	**d**
400	$0 \le \sigma < 17$		-	6.000E-04	-
	$17 \le \sigma \le 55$		-	1.167E-02	-1.963E-01
500	$0 \le \sigma < 15$		-	1.560E-02	-
	$15 \le \sigma \le 35$		9.588E-04	-4.522E-02	6.779E-01
600	$0 \le \sigma < 8$			4.462E-02	-
	$8 \le \sigma \le 17$	8.845E-04	-2.607E-02	2.331E-01	-2.680E-01
700	$0 \le \sigma < 7.0$			1.154E-01	-
	$7.0 \le \sigma \le 9.0$		1.770E-02	-1.281E-01	7.364E-01
800	$0 \le \sigma < 4.0$			2.895E-01	-
	$4.0 \le \sigma \le 5.5$		7.445E-02	-4.564E-01	1.454E+00
900	$0 \le \sigma < 3.5$			3.863E-01	-
	$3.5 \le \sigma \le 5.0$	5.385E-02	-5.060E-01	1.573E+00	-7.235E-01
1000	$0 \le \sigma < 2.0$			5.901E-01	-
	$2.0 \le \sigma \le 3.0$		-8.691E-02	4.762E-01	3.321E-01
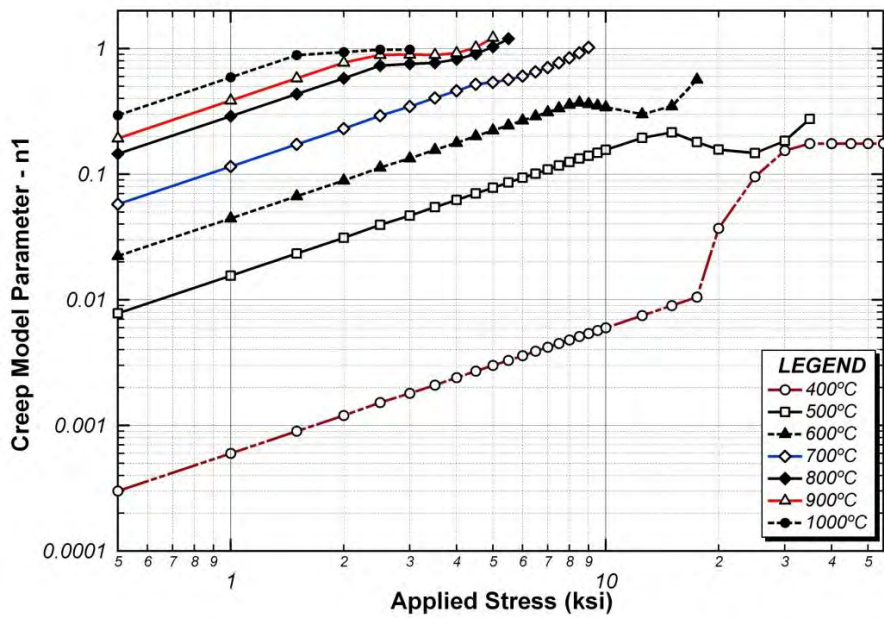
Figure 6.34 Distribution of n_1 parameter

206

Table 6.16 A_2 parameter for different stress ranges

Temp(°C)	Stress Range (ksi)	A_2	Stress Range (ksi)	A_2
600	$0 \leq \sigma < 15$	-	$15 \leq \sigma \leq 17$	1.00E-07
700	$0 \leq \sigma < 6.5$	-	$6.5 \leq \sigma \leq 9.0$	3.00E-08
800	$0 \leq \sigma < 4.0$	2.0E-07	$4.0 \leq \sigma \leq 5.5$	2.00E-11
900	$0 \leq \sigma < 3.5$	2.0E-07	$3.5 \leq \sigma \leq 5.0$	2.00E-18
1000	$0 \leq \sigma < 2.0$	2.0E-07	$2.0 \leq \sigma \leq 3.0$	2.00E-08

Table 6.17 n_2 parameter equations

Temp(°C)	Stress Range (ksi)	$n_2 = a\,\sigma^2 + b\,\sigma + c$		
		a	**b**	**c**
600	$0 \leq \sigma < 15$	-	-	-
	$15 \leq \sigma \leq 17$	-	1.106E+00	-
700	$0 \leq \sigma < 6.5$	-	3.418E-01	-
	$6.5 \leq \sigma \leq 9.0$	8.922E-02	-1.023E+00	5.150E+00
800	$0 \leq \sigma < 4.0$	-8.479E-02	9.699E-01	-
	$4.0 \leq \sigma \leq 5.5$	-1.390E+00	1.496E+01	-3.504E+01
900	$0 \leq \sigma < 3.5$	-1.077E-01	1.032E+00	-
	$3.5 \leq \sigma \leq 5.0$	-4.731E+00	4.367E+01	-9.104E+01
1000	$0 \leq \sigma < 2.0$	-3.640E-01	1.849E+00	-
	$2.0 \leq \sigma \leq 3.0$	-1.646E+00	9.465E+00	-1.036E+01
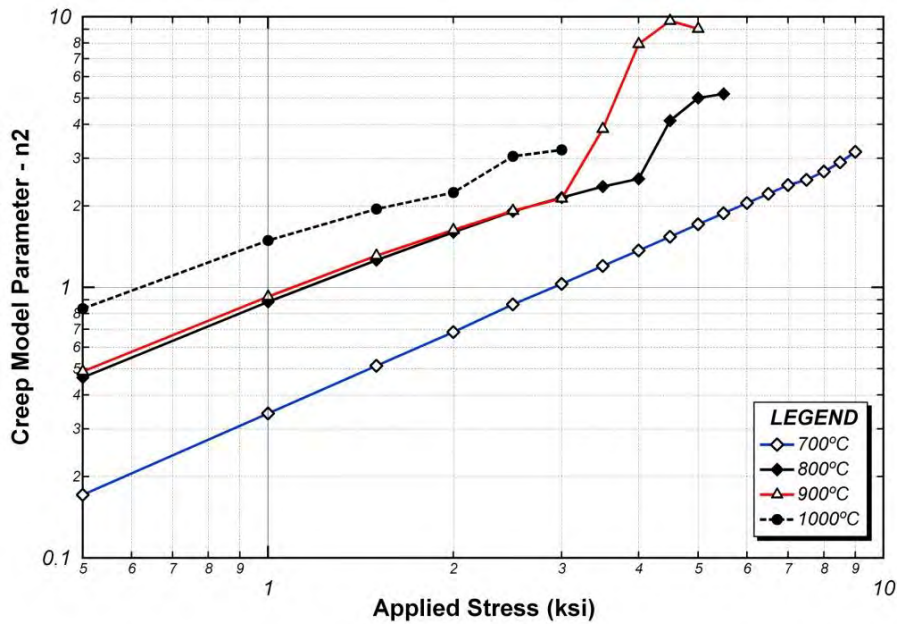
Figure 6.35 Distribution of n2 parameter

6.6.3   Validation of Suggested Creep Model with Test Data

Validation of the suggested creep model was carried out by comparing the results of the creep model and the experimental tests. The suggested creep model was compared with measurements of total strain and creep strain temperatures from 400 to 1000°C, as shown in Figure 6.36 to Figure 6.42. The creep strain did not include the initial strain which was induced by applied loading at beginning of test. As shown in the following figures, the suggested model results matched well with the experimental results of total strain and creep strain for both from 400 to 1000°C. The points of maximum discrepancy were the cases where creep rupture occurred at the end of tertiary creep: at 800 and 900°C for $0.90F_y$ and $0.90F_u$.

208
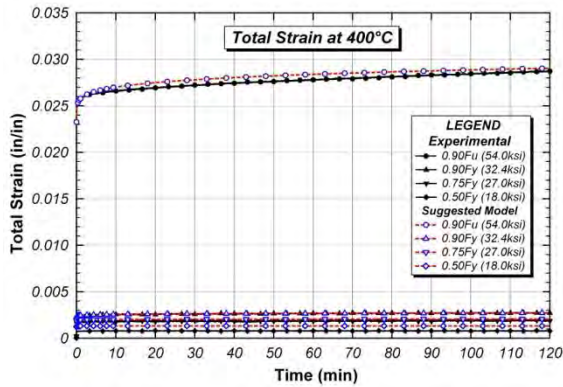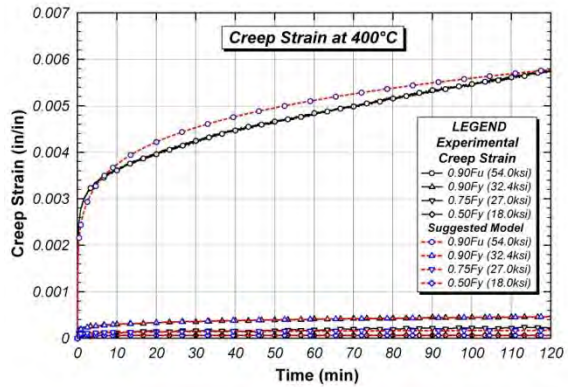
a) Total strain   *b) Creep strain*

Figure 6.36 Creep model compared with tests at 400°C
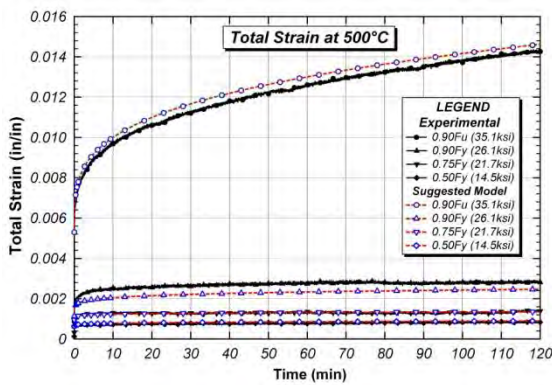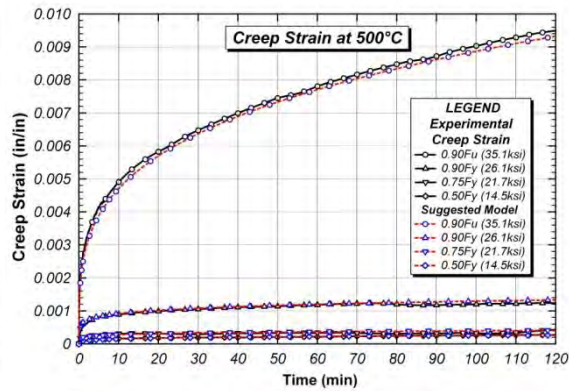
a) Total strain   *b) Creep strain*

Figure 6.37 Creep model compared with tests at 500°C
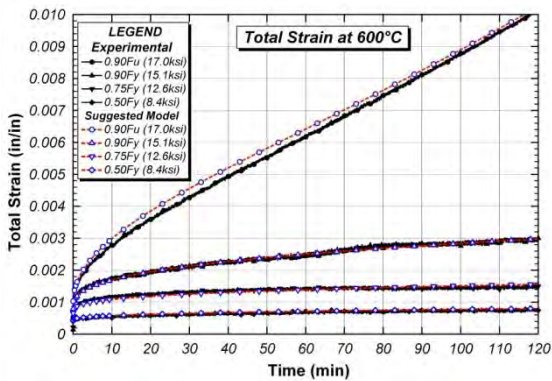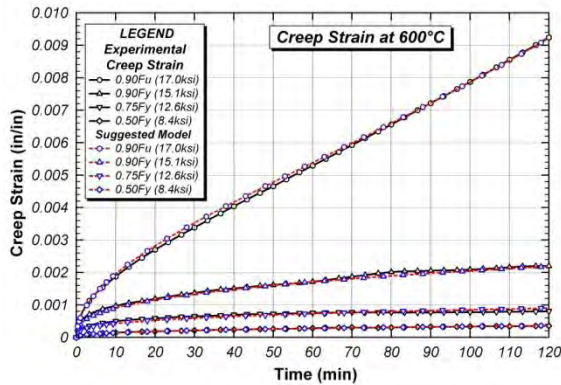
a) Total strain   *b) Creep strain*

Figure 6.38 Creep model compared with tests at 600°C

209
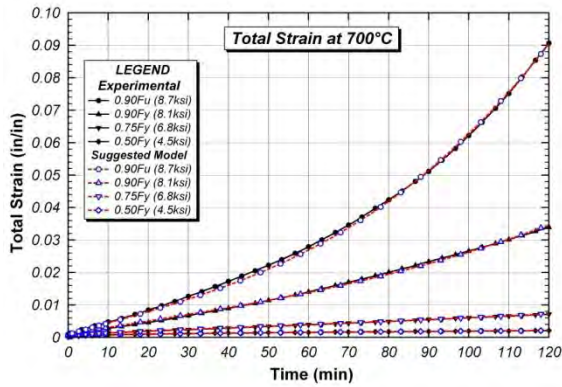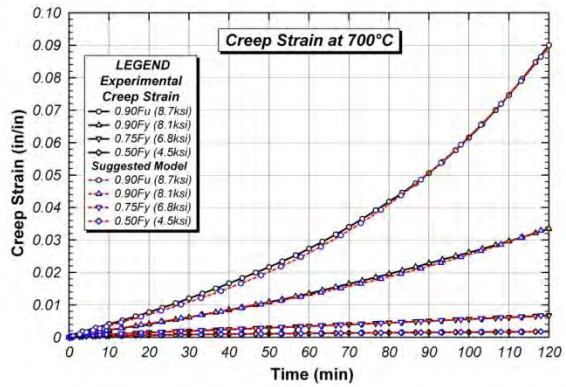
a) Total strain　　　　　　　　　　　　　*b) Creep strain*

Figure 6.39 Creep model compared with tests at 700°C
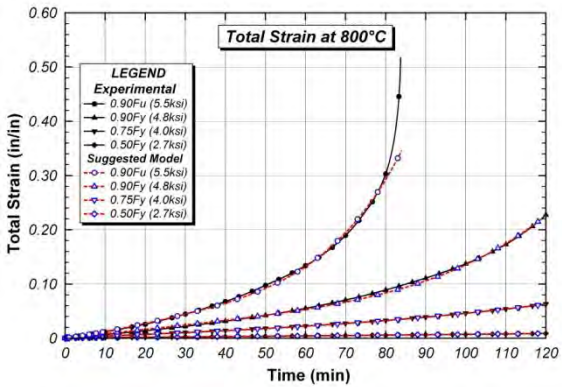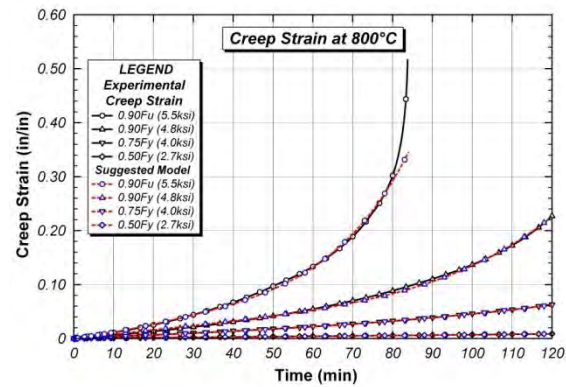
a) Total strain　　　　　　　　　　　　　*b) Creep strain*

Figure 6.40 Creep model compared with tests at 800°C
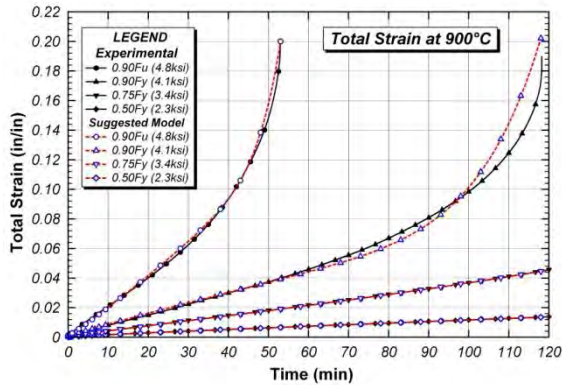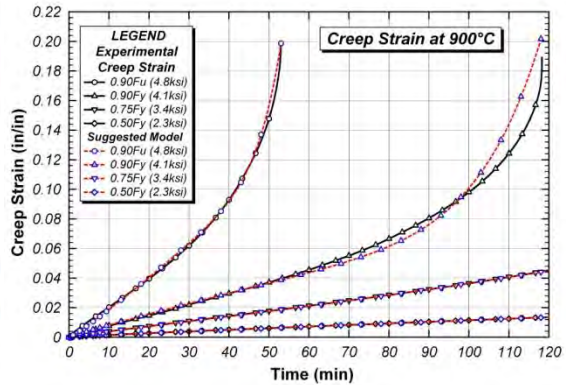
a) Total strain　　　　　　　　　　　　　*b) Creep strain*

Figure 6.41 Creep model compared with tests at 900°C

210

a) Total strain   *b) Creep strain*
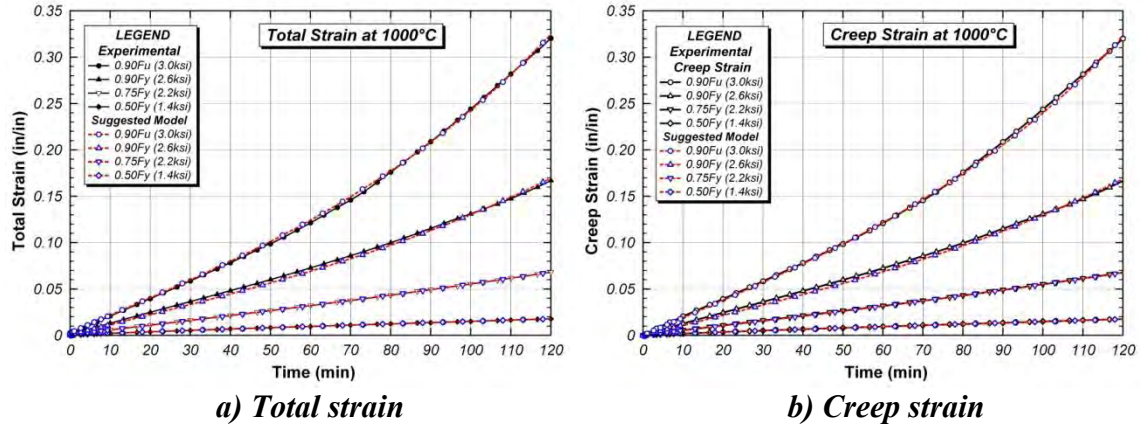
Figure 6.42 Creep model compared with tests at 1000°C

6.6.4 Comparison with Other Creep Models

A variety of creep models has been developed by other researchers (Andrade 1910; Bailey 1929; McVetty 1943; Dorn 1955; Walles and Graham 1955; Harmathy 1967; Ahmadieh and Mukherjee 1975; Fields 1989; Poh 1998; Mukherjee 2002; Batsoulas 2003) . Typically these models approximate the shape of the creep curve using very simple equations, which typically fail to capture all three stages of creep, but can be quite accurate over certain temperature ranges.

$$\varepsilon_c = \left(1 + a_1\, t^{1/3}\right) e^{a_2\, t} - 1 \qquad : \quad \text{Andrade} \qquad (6.5)$$

$$\varepsilon_c = b_1\, t^{b_2} \qquad : \quad \text{Bailey} \qquad (6.6)$$

$$\varepsilon_c = c_1(1 - e^{-c_2 t}) + c_3 t \qquad : \quad \text{McVetty} \qquad (6.7)$$

$$\varepsilon_c = d_1\, t^{1/3} + d_2\, t + d_3\, t^3 \qquad : \quad \text{Graham \& Walles} \qquad (6.8)$$

$$\varepsilon_c = \frac{(\dot{\varepsilon}_1 - \dot{\varepsilon}_2)t}{\left[1 + \left(\frac{t}{\tau_1}\right)^{n_1}\right]^{1/n_1}} + \frac{(\dot{\varepsilon}_2 - \dot{\varepsilon}_3)t}{\left[1 + \left(\frac{t}{\tau_2}\right)^{n_2}\right]^{1/n_2}} + \dot{\varepsilon}_3 t \qquad : \quad \text{Poh} \qquad (6.9)$$

where ε_c = Creep strain, t = time, and a_i, b_i, c_i, d_i, n_i, τ_i = parameters

211

Two creep models from the literature were compared with the suggested creep model developed in this research. These models, Harmathy and Fields and Fields were developed for low-carbon structural steels similar to A992 and were developed specifically for structural-fire engineering analysis

The Harmathy creep model (Harmathy 1967), shown in Equation 6.10, contains two parameters that require additional explanation. The first parameter, θ, is temperature-compensated time, an expression based on the activation energy. According to Dorn's theory (Dorn 1955), under a constant applied stress, creep strain is a function of temperature-compensated time and the applied stress. The other parameter, Z, is the Zenor-Hollomon parameter, which is the first derivative of creep strain with respect to temperature-compensated time during the steady-state creep stage.

Harmathy developed this model for ASTM A36 structural steel for the temperature ranges of 400 to 700°C (750 to 1300°F). The model primarily captures the effects of secondary creep, the temperatures being too low to expect much tertiary creep.

$$\varepsilon_t = (3 \, Z \, \varepsilon_{t0})^{1/3} \, \theta^{1/3} + Z \, \theta \qquad (6.10)$$

where

Z = Zenor-Hollomon parameter

ε_{t0} = Creep parameter of strain

θ = Temperature-compensated time (hours)

$$Z = \begin{cases} 0.026 \, \sigma^{4.7} & : \quad\quad\quad\quad \sigma \leq 15{,}000 \, psi \\ 1.23 \times 10^{16} \, e^{0.0003\sigma} & : 15{,}000 < \sigma \leq 45{,}000 \, psi \end{cases}$$

$\varepsilon_{t0} = 1.7 \times 10^{-10} \, \sigma^{1.75}$

$\theta = \int_0^t e^{-Q_c/RT} \, dt = \left(e^{-Q_c/RT}\right) \times t$

Q_c = activation energy

The other reference creep model is by Fields and Fields (Fields 1989), in which creep was modeled as a power-law equation of applied stress and time, as shown in Equation (6.11). The Fields and Fields creep model was developed for AS A149 steel

212

which is close to ASTM A36 for strains below 6% and temperatures of 350 to 650°C.

Like the Harmathy model, this temperature range is below that maximum temperatures expected in actual fires, and below the range in which tertiary creep was seen in this testing.

$$\varepsilon_T = \varepsilon_e + \varepsilon_p + \varepsilon_c \tag{6.11}$$

where

$\varepsilon_T, \varepsilon_e, \varepsilon_p, \varepsilon_c$ = Total strain, elastic strain, plastic strain, and creep strain

σ = Applied constant stress (ksi)

T = Temperature (°C)

$\varepsilon_e = \dfrac{10^2 \sigma}{(29{,}300 - 12.6\,T)}$

$\varepsilon_p = 10^{-(0.0041\,T^{1.647})}\,\sigma^{T/(147 - 0.016\,T)}$

$\varepsilon_c = 10^\alpha\,t^{(-1.1 + 0.0035\,T)}\,\sigma^{(2.1 + 0.0064\,T)}$

$\alpha = \begin{cases} -(6.10 + 0.0053\,T) & : \quad T < 500°C \\ -(13.25 - 0.00851\,T) & : \quad T \geq 500°C \end{cases}$

The final creep model for comparison is the Batsoulas creep model (2003). The Batsoulas creep model defines the total strain as he sum of an initial elastic strain with a creep strain, as shown in Equation (6.12). This model therefore includes initial plastic strain as part of the creep strain.

$$\varepsilon = \varepsilon_e + \varepsilon_c = \frac{\sigma}{E} + \frac{\sigma e^{\alpha t}}{\alpha \eta + K}\left[1 - e^{-\left(\alpha + \frac{K}{\eta}\right)t}\right] \tag{6.12}$$

where

σ = Applied stress for creep test

E = Elastic modulus of material

α, η, K = Curve fitting parameter from experimental results

Table 6.18 summarizes the conditions for which each of these four creep models was developed. The difference in temperatures is most evident.

213

Table 6.18 Applicable condition of creep model

Creep Model	Material	Temperature Range	Stress Range
Harmathy Model	A36	400–700°C	$\sigma \leq 45$ ksi
Fields and Fields Model	AS A149	350–650°C	$\sigma \leq F_u$
Batsoulas Model	X 8 $C_rN_iM_oN_b$ 16 16	450–700°C	$\sigma \leq 29$ ksi
Suggested Model	A992	400–1000°C	$\sigma \leq F_u$

A realistic comparison between the predicted creep response of a given model and the experimental results can only be made if the stress and temperature conditions are similar to that for which the model was derived. As such, the four stresses and temperature values listed in Table 6.19 were selected. When applying the creep models, the stress value used in the model was scaled according to the yield stress of the steel used to develop the model. For example, the applied stress 27.0 ksi of $0.75F_y$ used in suggested model for A992 ($F_y = 50$ksi) steel was scaled down to 27.0 x 36/50 =19.44 ksi for A36 ($F_y = 36$ksi) steel in the creep models. The applied temperatures slightly exceed the applicable range of temperatures for Fields and Fields model only.

Table 6.19 Selected stress and temperatures for comparison

Applied Stress	Temperatures (°C)			
	400	500	600	700
Stress Level	$0.75F_y$	$0.90F_y$	$0.90F_y$	$0.90F_y$
Value (ksi) for A992	27.0	26.1	15.1	8.1

The comparison of the results of the existing three models to the suggested model is shown in Figure 6.43 to Figure 6.46 by plotting strains up to 30 minutes and up to two hours (the test duration) for 400°C to 700°C. It is noted that the comparison of creep

214

model results was carried out by creep strain only for all three previous creep models and for the suggested model. This means that there is no instantaneous strain included in the models. Although the test data is not plotted in these figures, the test data is very closely represented by the suggested model, as this model was closely fit to the test data.

The most apparent observation is the large deviation between the predictions from the Harmathy, Fields and Fields, Batsoulas and suggested models. One reason for this difference may be that though the creep models had all been developed for low-carbon steel, they were developed for different steels with different creep properties. It is clear that the Harmathy and Fields and Fields models anticipate more secondary creep than was found at these temperatures for A992 steel.

a) Initial 30 min   *b) Entire test*
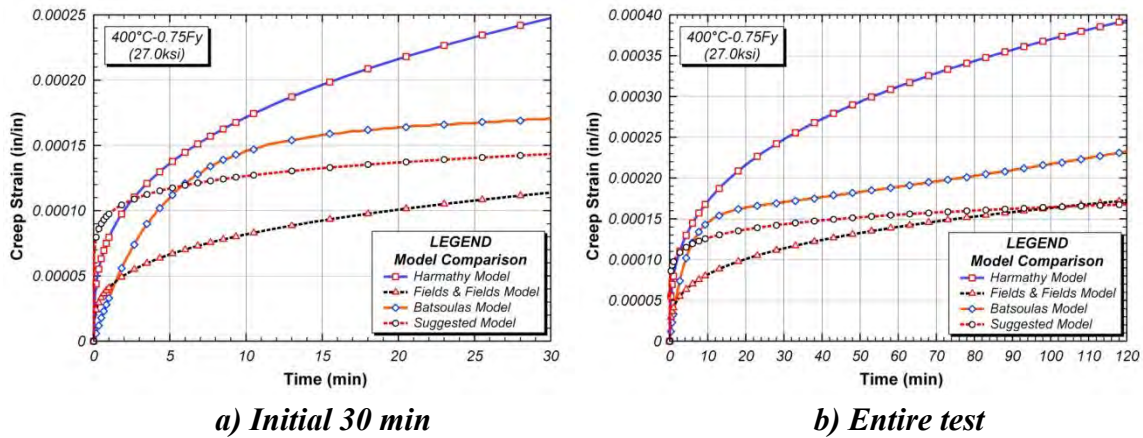
Figure 6.43 Comparison between creep models at 400°C

At 400°C where the measured tensile strength of the material is 27.0 ksi, the general shape of the initial portion of the creep curves by the Harmathy model, by the Fields and Fields, and by the Batsoulas model are similar but then diverge rapidly with increasing time. The Fields and Fields creep model and the suggested model converges around 90 minutes while the Batsoulas model runs parallel with these two models. The Harmathy model deviates significantly from the other models with increasing time. The main gaps between these three models and experimental creep test result on A992 steel were the differences of the secondary creep stage. There is relatively large primary creep

stage strain showing at 400°C and the secondary creep stage is governed by all the previous creep models except for suggested model.

a) Initial 30 min   b) Entire test
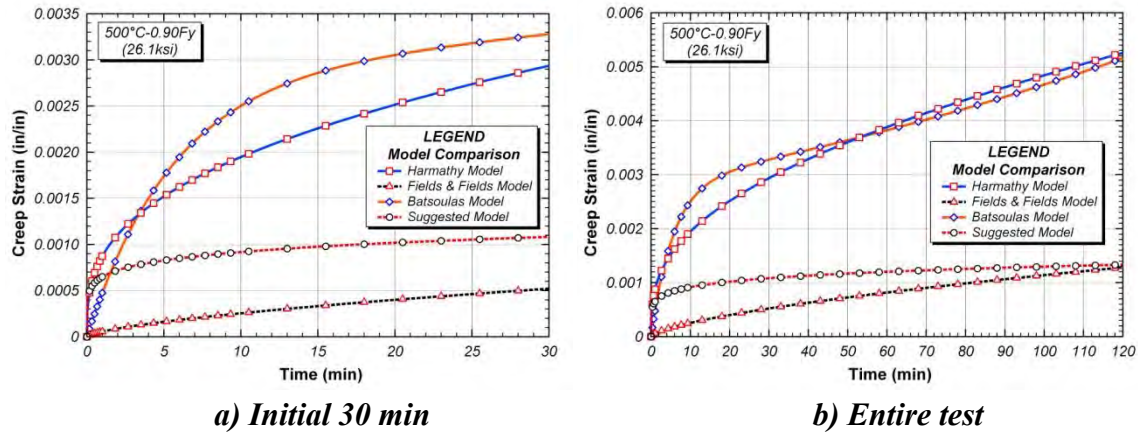
Figure 6.44 Comparison between creep models at 500°C

At 500°C and an applied stress of 26.1 ksi, a major discrepancy in the shape of the creep curves, like that at 400°C, is noted. There are two convergences occurred at 500°C. The Harmathy and Batsoulas models has followed with similar pattern by converging around 50 minutes while the Fields and Fields model and the suggested model has converged around 120 minutes in spite of large differences at the initial stage. The deviation of the Harmathy and the Fields and Fields models is more severe at this temperature: the creep strain provided by Harmathy is five times larger than the Fields and Fields and suggested model. The primary creep of the Fields and Fields model were almost nothing by comparing with other two models and suggested model. However, the Harmathy and Batsoulas model's creep curve are governed by the primary and secondary creep at this temperature.

216
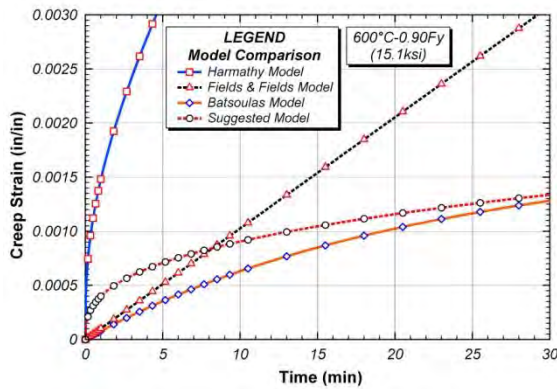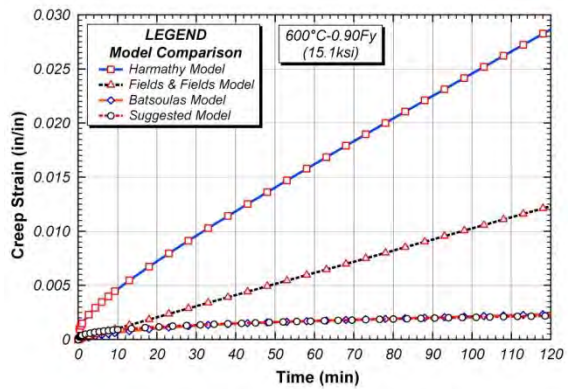
a) Initial 30 min	*b) Entire test*

Figure 6.45 Comparison between creep models at 600°C

At 600°C and the applied stress of 15.1 ksi, the Harmathy and Fields and Fields models are quite inaccurate. The Harmathy model moves beyond primary creep in the first five minutes and the Fields and Fields model engages in the secondary creep stage after the initial stage while the suggested and Batsoulas model's creep curve stayed in the primary stage throughout the two-hour test. There are big gaps between creep models; Harmathy has two times higher strain than Fields and Fields model and eleven times larger than Batsoulas and the suggested models at 120 minutes. The Batsoulas and suggested model's creep curve almost matched together after 30 minutes throughout to two hours.
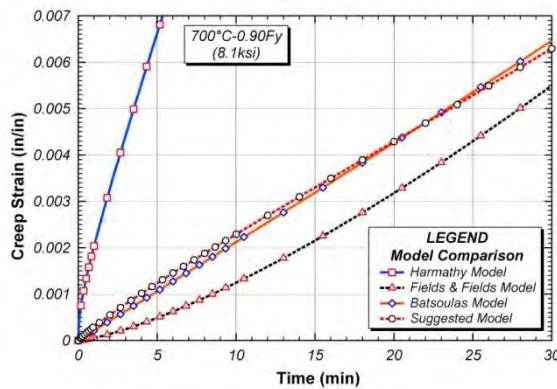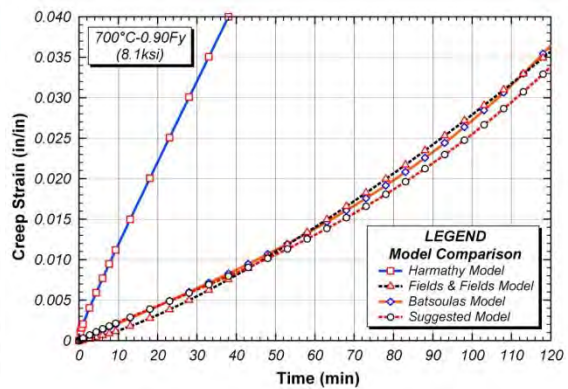
a) Initial 30 min	*b) Entire test*

Figure 6.46 Comparison between creep models at 700°C

217

At 700°C and 8.1 ksi tensile stress, all creep models generally matched well from beginning to end of testing up to two hours except for the Harmathy creep model. . The shape of the creep curve of three models except for Harmathy model are dominated by the tertiary creep.

6.7   SUMMARY

In this chapter, creep testing of A992 structural steel at elevated temperatures has been presented. Creep curves representing behavior at specified stress levels and temperatures have been shown. Based on these tests, a material creep model was suggested. This suggested model was compared with the experimental creep data, alongside other models from the literature.

Several conclusions can be made from this work. First, the test data shows creep strains can be quite significant for temperatures, stress levels, and time durations representative of building structures exposed to fire. This suggests that ignoring creep may lead to highly inaccurate predictions of structural response for some classes of structural fire problems. Secondly, existing creep models may provide poor predictions for A992 steel. Interpretation of creep models is difficult, and it is unclear how far their applicability can be extended beyond the specific steels, temperature ranges and stress levels for which their model parameters were originally developed. Thus, the fundamental conclusion of the author is that the ability to accurately model creep in structural fire-engineering problems, at present, is quite poor. Considering the potential importance of creep in structural fire-engineering analysis, considerable work is needed to develop more robust and accurate creep models for commonly used grades of steel.

CHAPTER 7

Relaxation Testing at Elevated Temperatures

7.1   INTRODUCTION

The behavior of steel at elevated temperatures is time dependent. Though this time dependence can be experimentally studied in different ways, the most common techniques are by creep testing or stress-relaxation testing. In creep testing, steel coupons are held at constant stress, and the increase in strain with time is measured. In stress relaxation testing, the steel coupon is held at a constant strain, and the reduction of stress with time is measured.

The results of an extensive creep testing program were described in Chapter 6. To provide a more comprehensive picture of the time-dependent response of ASTM A992 steel at elevated temperatures, a series of stress-relation tests were conducted. This chapter describes procedures used for the stress relaxation tests, presents the results of the tests and examines models for predicting this response.

7.2   EXPERIMENTAL INVESTIGATION

7.2.1   Test Specimen

The test specimens for relaxation testing were identical to those used for creep testing (Chapter 6). The specimens were 18 inch long coupons (Figure 7.1) taken from the flange of W4x13 sections. Of the ASTM A992 materials used in this research program, the material for the creep and stress-relaxation testing was designated as type MC. The chemical composition, from the Certified Mill Test Report, is given in Table 7.1. More information on the material type, including its room-temperature mechanical properties, is provided in Chapter 3.

Figure 7.1 dimensions: 7 7/16", 3 1/8", 7 7/16", 0.5", 0.5", 2.25", 18", 1", t=0.345"
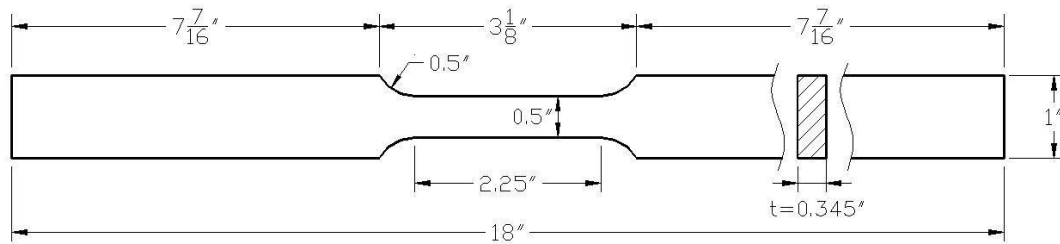
Figure 7.1 Coupon dimensions used in relaxation tests

Table 7.1 Chemical composition of test specimen

Material Type	C	Cr	Mo	V	Ni	Mn	Si	P	S	Cu
MC	0.08	0.10	0.026	0.002	0.09	0.91	0.23	0.011	0.025	0.24

In order to determine the initial strain levels for the relaxation tests, the stress-strain curves at elevated temperatures were required. Tensile coupons were tested at temperatures ranging from room temperature to 1000°C; results of this testing were reported in Chapter 4. In Table 7.2, the values of yield stress found, determined using the 0.2% offset method, are reported.

Table 7.2 Yield stress of Material MC at elevated temperatures

Property	Temperature (°C)									
	20	200	300	400	500	600	700	800	900	1000
F_y (ksi)	51.8	46.7	48.9	35.4	28.9	16.8	9.0	5.3	4.5	2.8

7.2.2 Determining Initial Strain Levels for Relaxation Testing

Four initial strain levels were selected for the relaxation tests. The selected initial strain levels were 50, 75, 90 and 150% of the yield strain of the material at the specified test temperature. These values were selected somewhat arbitrarily, but were intended to provide stress-relaxation data for a fairly wide range of strain values. The initial strain levels are shown qualitatively for a typical elevated temperature stress strain curve in

Figure 7.2. Specific values for the initial strain levels are listed in Table 7.3 and shown graphically in Figure 7.3.
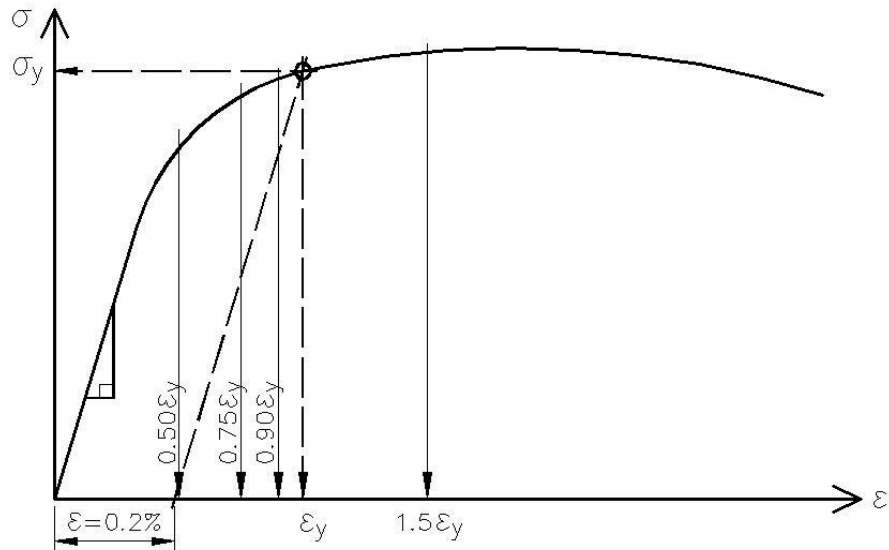
Figure 7.2 Initial strain levels

Table 7.3 Values of initial strain levels used in relaxation tests (in/in)

Temp (°C)	I	II	III	IV
	0.50εy	0.75εy	0.90εy	1.50εy
20	0.001900	0.002850	0.003420	0.005700
400	0.001750	0.002625	0.003150	0.005250
500	0.001600	0.002400	0.002880	0.004800
600	0.001435	0.002153	0.002583	0.004305
700	0.001420	0.002130	0.002556	0.004260
800	0.001235	0.001853	0.002223	0.003705
900	0.001225	0.001838	0.002205	0.003675
1000	0.001210	0.001815	0.002178	0.003630
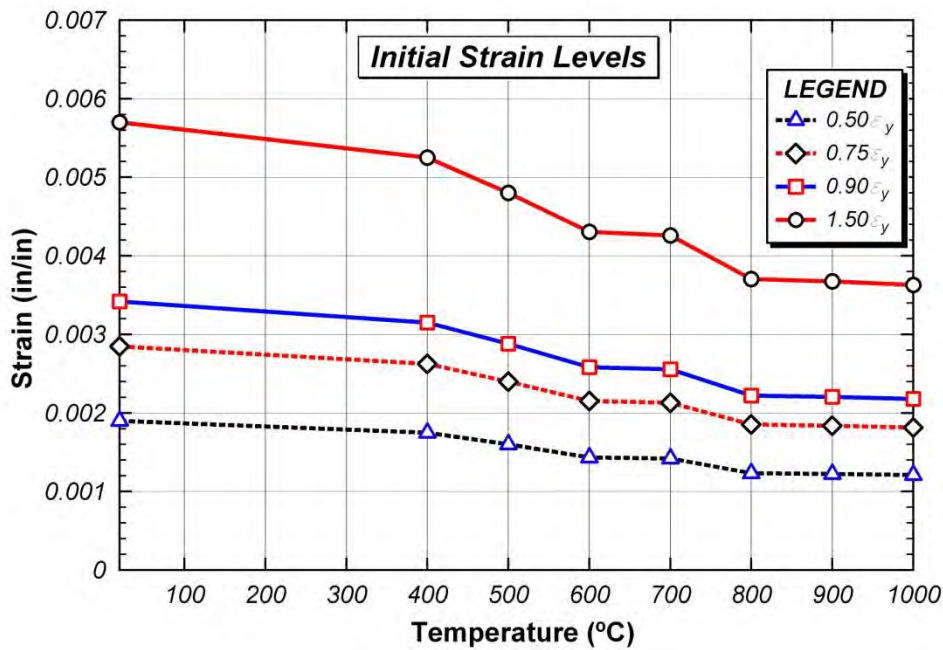
Figure 7.3 Values of initial strain levels for relaxation tests

7.2.3 Test Equipment and Procedures

The equipment used for loading and heating the coupons was the same as that used for the elevated-temperature tension and creep testing described in previous chapters. A description of this equipment is provided in Chapter 3 (Section 3.3). Strains were measured by using a one-inch gage length high temperature extensometer designated as type 1PS, described in Section 3.6. The coupon preparation was also the same as for the high temperature tensile and creep tests described in previous chapters. Coupon preparation included cleaning the coupon surface on the reduced section, grinding the surface on the coupon ends, punching pivots, marking letters on the coupon for identification, measuring dimensions of coupon, and installing thermocouples wrapped in steel foil. Full details of coupon preparation are provided in Section 3.4.2.

The basic test procedure consisted of the following steps. First, the coupon was heated up to the target temperature under zero load. The target test temperatures varied from 400 to 1000°C. Once the coupon was at the target test temperature, load was applied

222

to impose an initial strain on the coupon, where the strain was measured using the 1PS extensometer. Once the initial strain level was achieved, the test machine was controlled to allow no further movement of the crossheads. Load was monitored as a function of time throughout this process, and the test was generally continued for a period of 2 hours. It should be noted that once the initial strain was imposed on the coupon and the machine crossheads held stationary, the strain within the one-inch gauge length of the extensometer was not truly constant. That is, instead of holding the strain constant, the machine crosshead displacement was held constant. This provided more stable control of the test machine. However, this procedure should be kept in mind when interpreting the test data.

7.2.4   Test Repetitions

In order to evaluate the repeatability and consistency of the relaxation test results, relaxation tests were conducted at least three times for every specific initial strain and temperature condition. Figure 7.4 shows an example of the results of repeated tests at 600 and 700°C. As can be seen in this plot, there was some variability in the results of the three test repetitions. In some cases, the cause of anomalies in the test results could be surmised. Anomalies could be caused, for example, by small variations in coupon temperature during a test or variations in pressure of hydraulic fluid entering the test machine. To determine a final representative relaxation curve, the three test results were not averaged, since some of the test results were judged erroneous. Rather, judgment was used in choosing a single test result of the three repetitions as being most the most representative. This judgment was based on observations made during the testing of potential sources of error, and based on evaluations of repeatability.
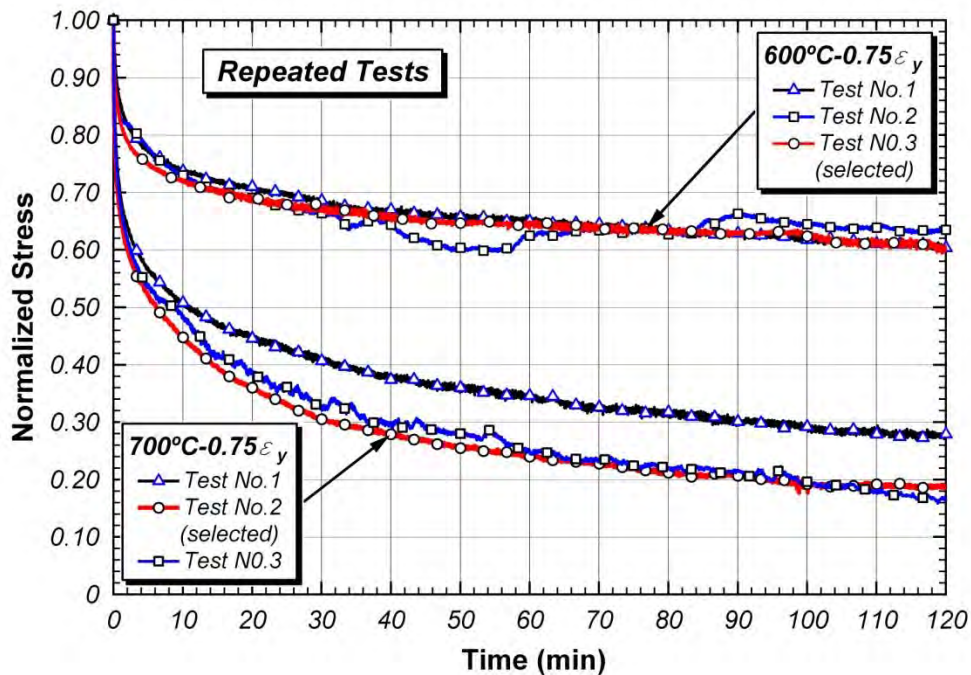
Figure 7.4 Repeated relaxation test results at 600 and 700°C

7.3   TEST RESULTS

The results of the relaxation tests are presented in this section in various formats. Figure 7.5 to Figure 7.12 show results for each test temperature. Results are plotted two ways in this figure. For each temperature, the left plot shows the value of stress as a function of time. Time equal to zero corresponds to the point in the test immediately after the application of the initial strain. The right plot for each temperature shows retention factor as a function of time. The retention factor for a particular time was computed as the stress at that time divided by the stress at time zero. Figure 7.13 to Figure 7.16 show results according to the initial applied strain level. Finally, Figure 7.17 to Figure 7.24 plot the stress rate versus time for each test temperature. The stress rate is the rate of change of stress with time, i.e. the slope of the stress versus time curve. The stress rate is shown two different ways for each temperature. In the left plot, the time is plotted using an arithmetic scale, and in the right plot, the time is plotted using a logarithmic scale.

224

7.3.1 Relaxation Curves by Temperatures

a) Relaxation stress
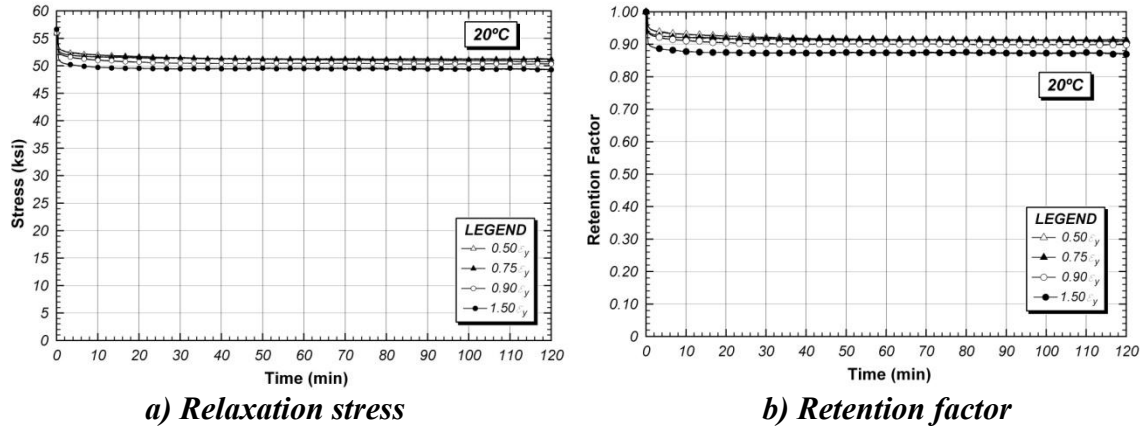
b) Retention factor

Figure 7.5 Relaxation curves at 20°C

a) Relaxation stress
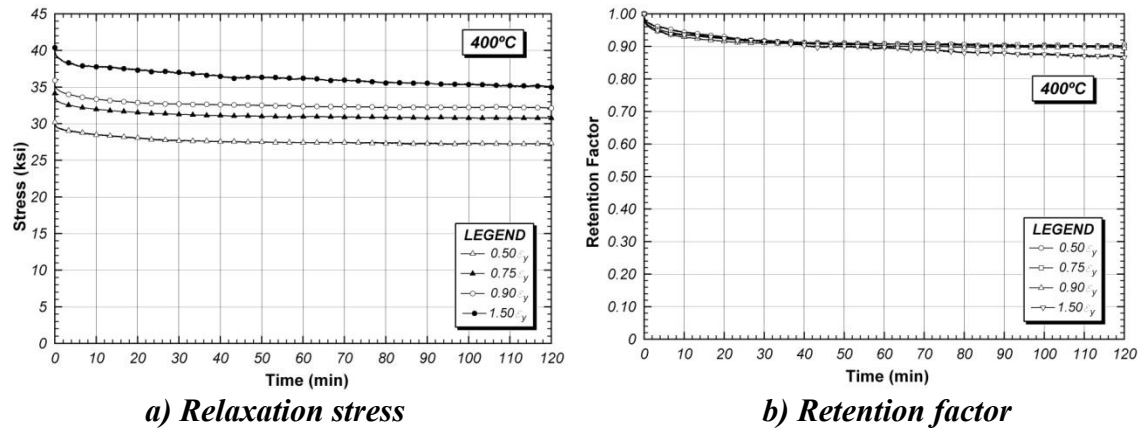
b) Retention factor

Figure 7.6 Relaxation curves at 400°C

a) Relaxation stress
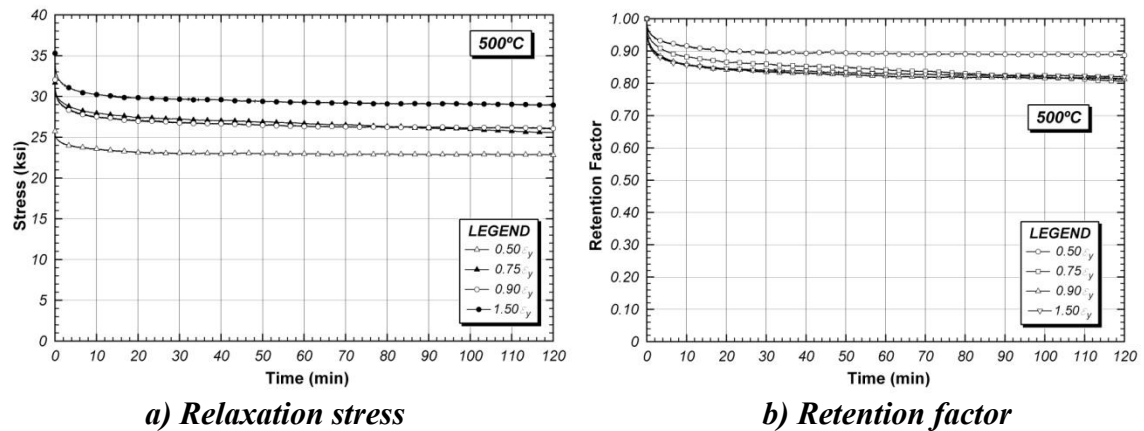
b) Retention factor

Figure 7.7 Relaxation curves at 500°C

225
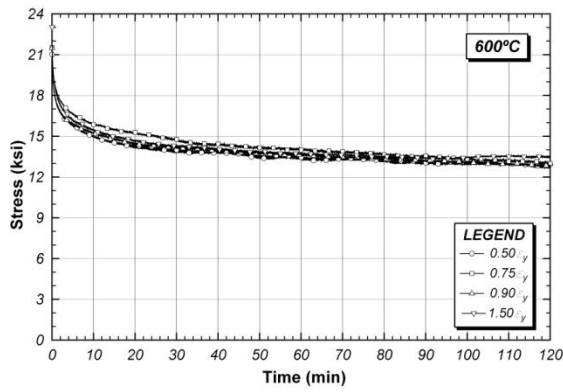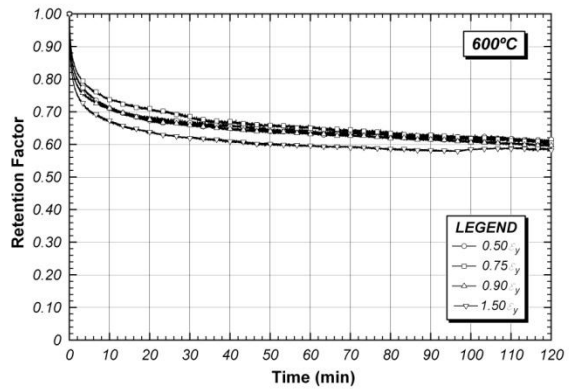
a) Relaxation stress   *b) Retention factor*

Figure 7.8 Relaxation curves at 600°C
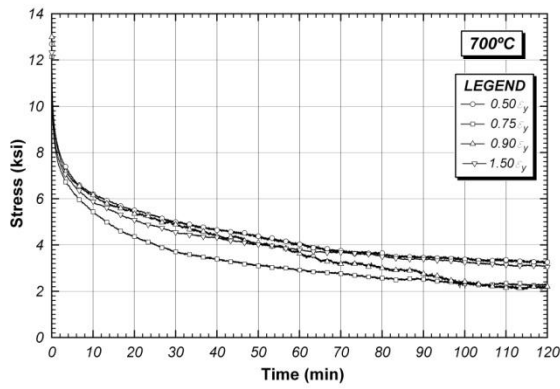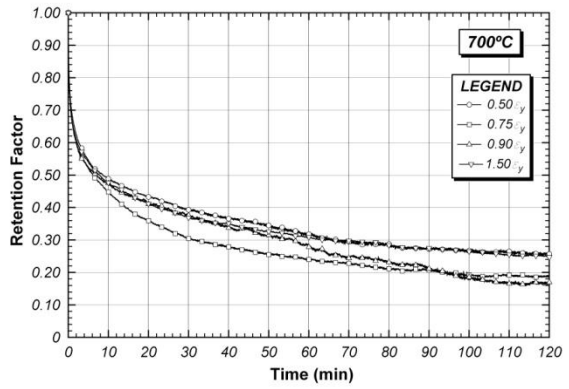
a) Relaxation stress   *b) Retention factor*

Figure 7.9 Relaxation curves at 700°C
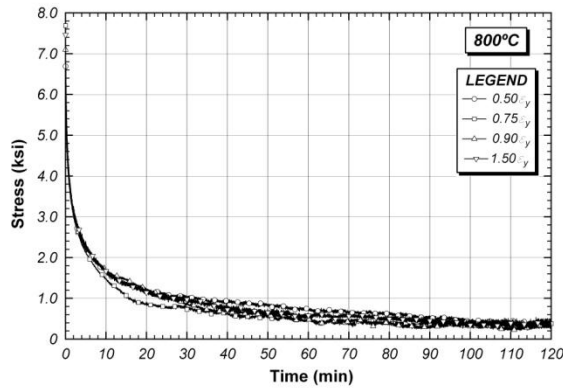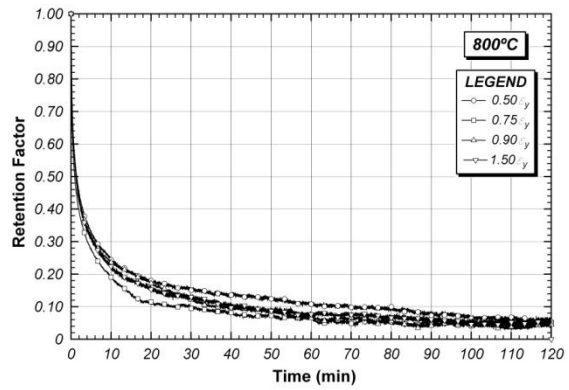
a) Relaxation stress   *b) Retention factor*

Figure 7.10 Relaxation curves at 800°C

226
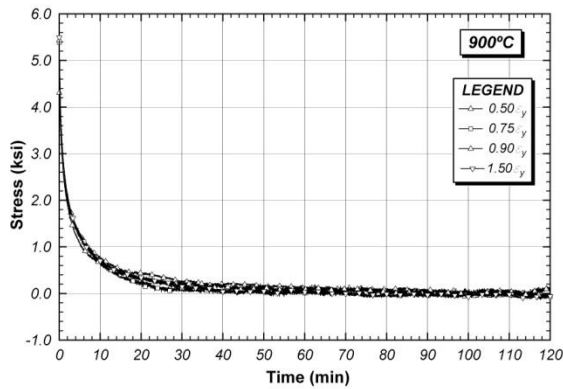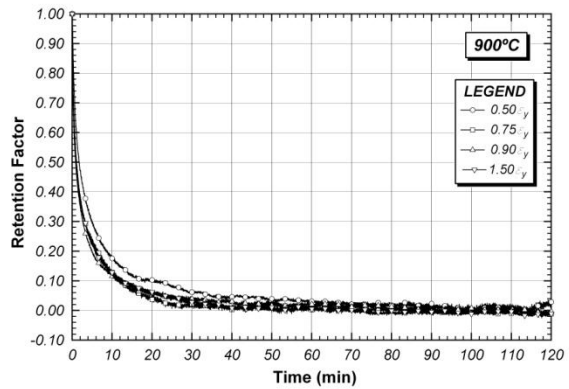
a) Relaxation stress   *b) Retention factor*

Figure 7.11 Relaxation curves at 900°C
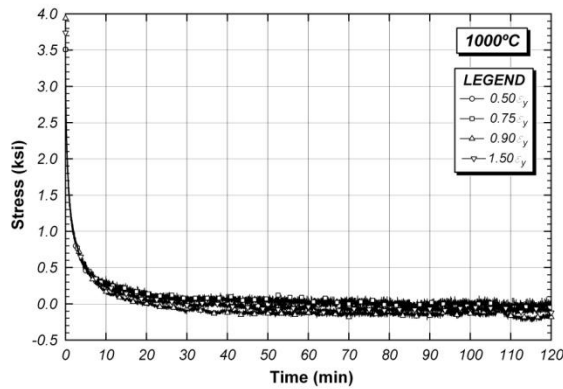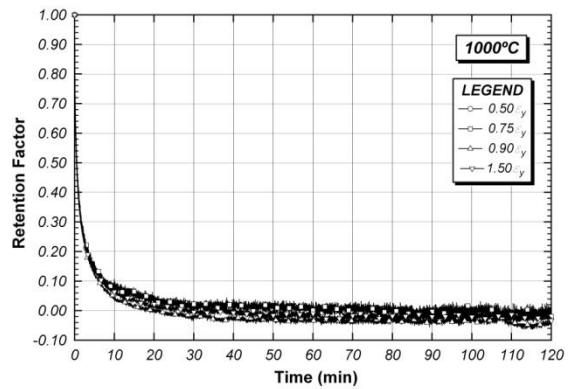
a) Relaxation stress   *b) Retention factor*

Figure 7.12 Relaxation curves at 1000°C
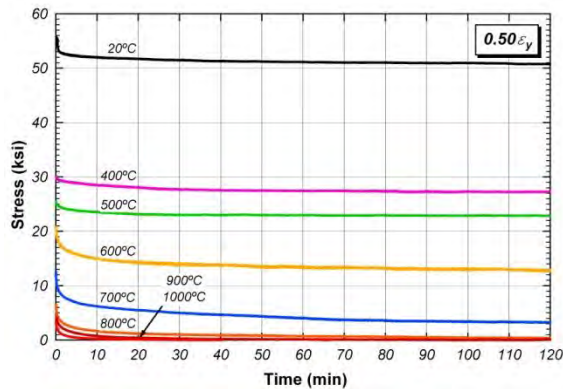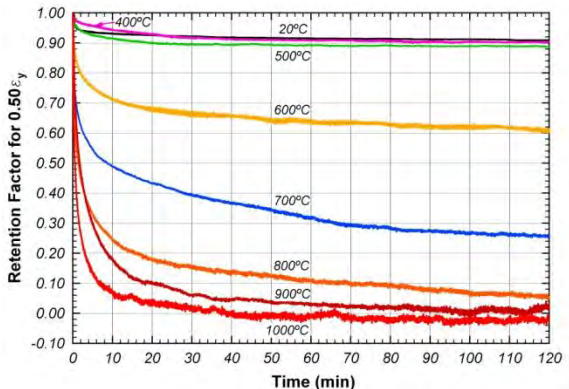
a) Relaxation stress   *b) Retention factor*

Figure 7.13 Relaxation curves at 0.50ε_y

227
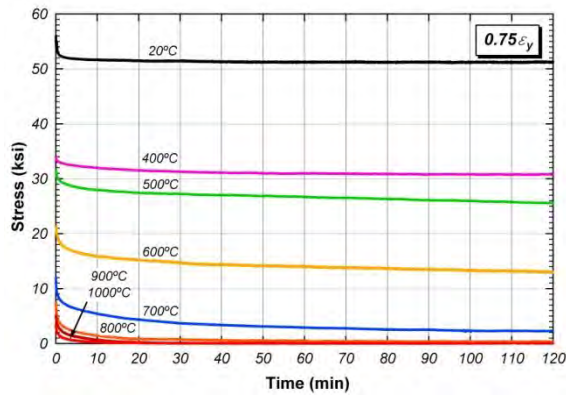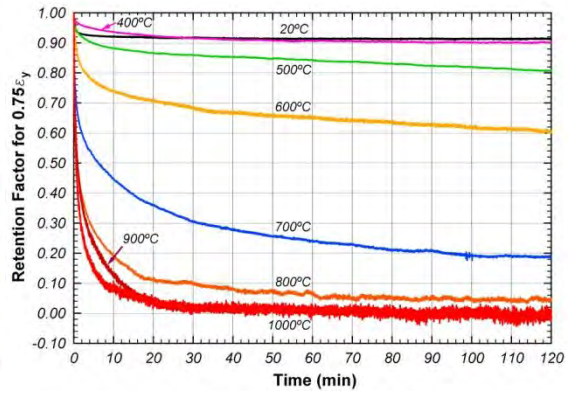
a) Relaxation stress   b) Retention factor

Figure 7.14 Relaxation curves at 0.75ε_y
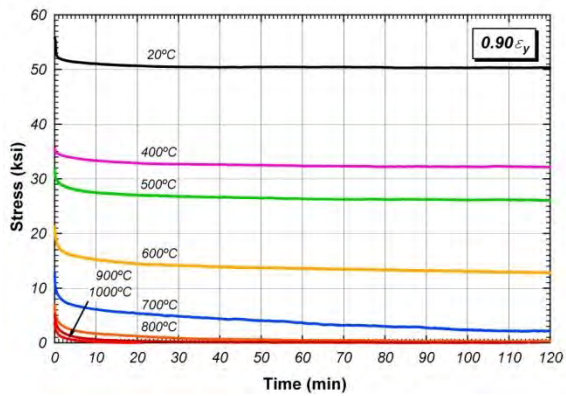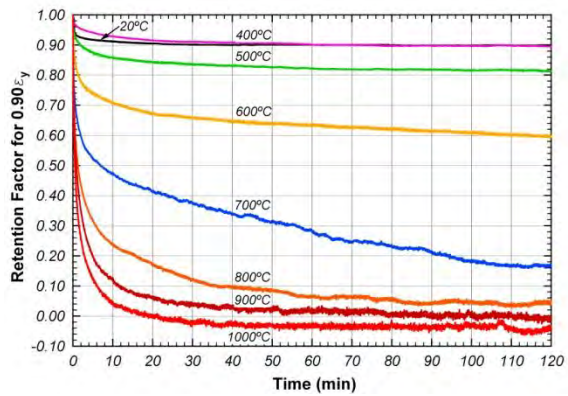
a) Relaxation stress   b) Retention factor

Figure 7.15 Relaxation curves at 0.90ε_y
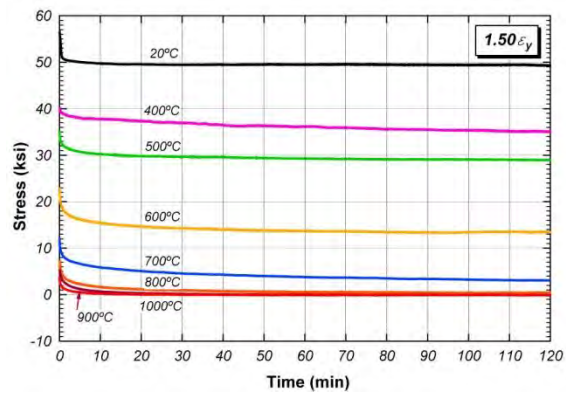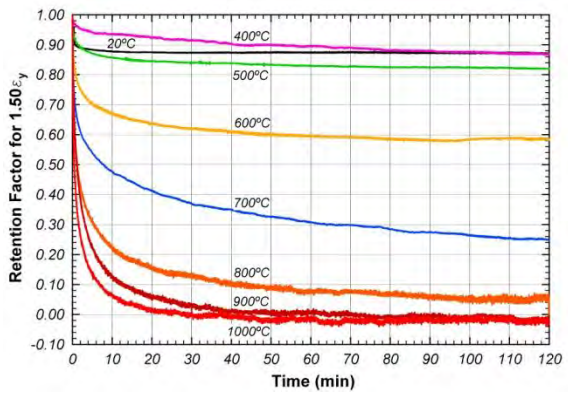
a) Relaxation stress   b) Retention factor

Figure 7.16 Relaxation curves at 1.50ε_y

228
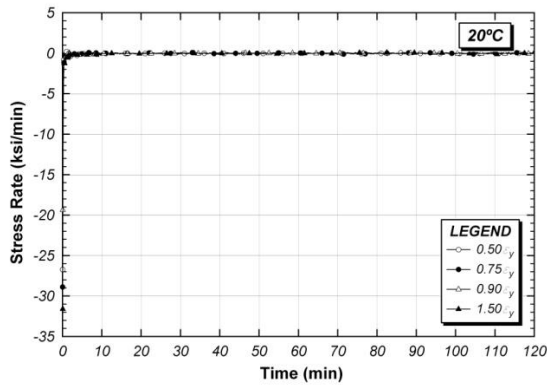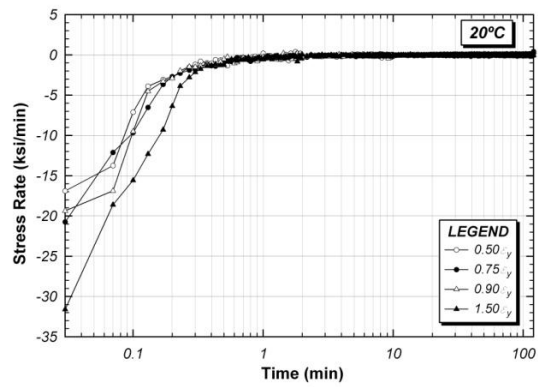
a) With regular scale　　　　　　　　*b) With log scale*

Figure 7.17 Stress rates at 20°C
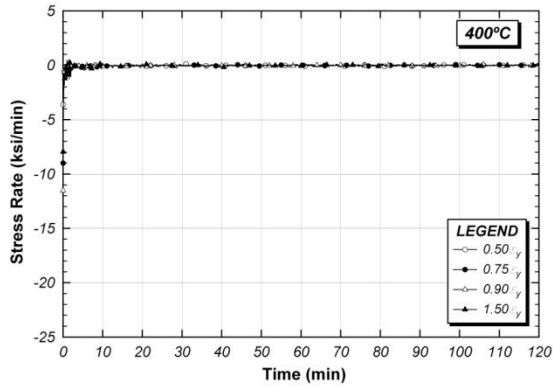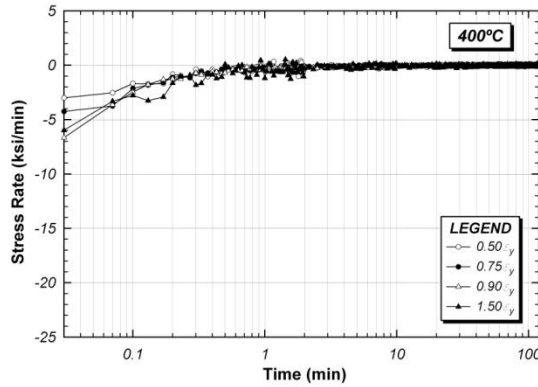
a) With regular scale　　　　　　　　*b) With log scale*

Figure 7.18 Stress rates at 400°C
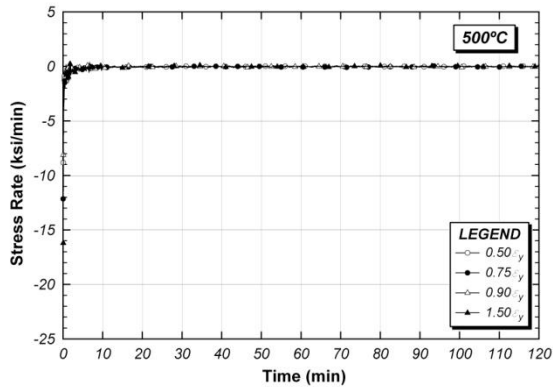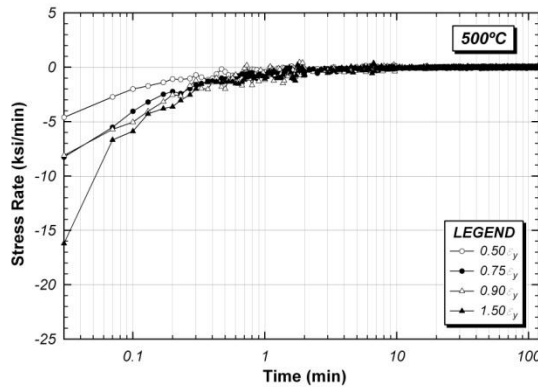
a) With regular scale　　　　　　　　*b) With log scale*

Figure 7.19 Stress rates at 500°C

229
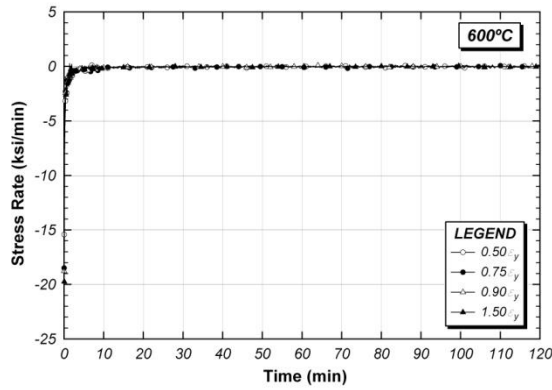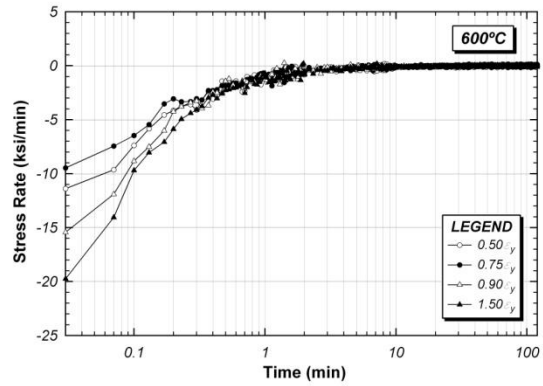
a) With regular scale   b) With log scale

Figure 7.20 Stress rates at 600°C
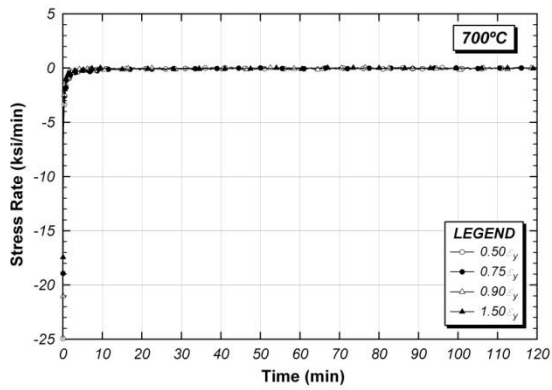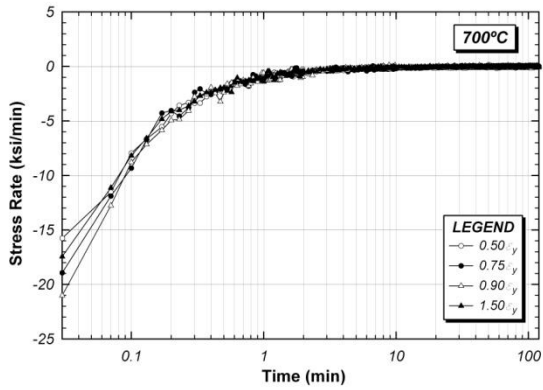
a) With regular scale   b) With log scale

Figure 7.21 Stress rates at 700°C
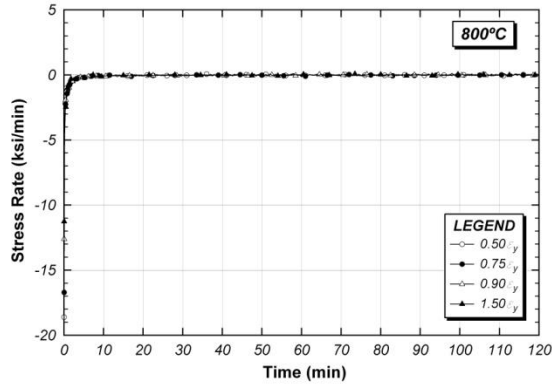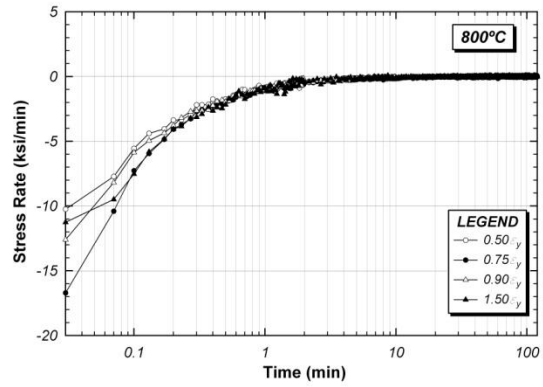
a) With regular scale   b) With log scale

Figure 7.22 Stress rates at 800°C

230
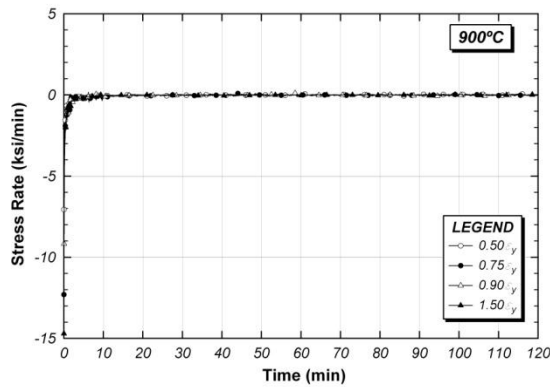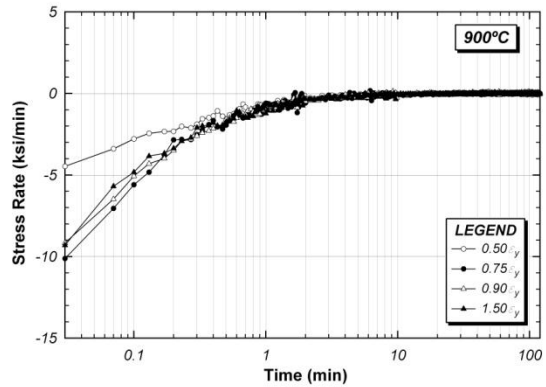
a) With regular scale   *b) With log scale*

Figure 7.23 Stress rates at 900°C
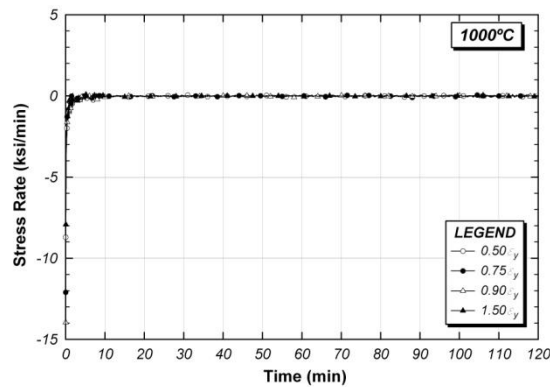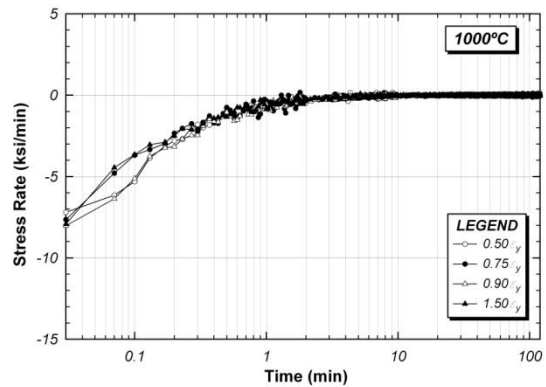
a) With regular scale   *b) With log scale*

Figure 7.24 Stress rates at 1000°C

7.4   OBSERVATIONS ON RELAXATION CURVES

In examining the stress relaxation test results, several observations can be made. First, the magnitude of stress relaxation can be very large for temperatures and times that are representative of fire exposures. At 700°C, for example, the stress reduces to less than 50% of its initial value in only 20 minutes. Like the observations made for the creep test results in Chapter 6, this suggests that time dependent material behavior can be very significant in structure-fire problems. In a structure-fire problem, stress relaxation may be important, for example, when evaluating the forces developed by thermally induced strains. These test results suggest that such forces will change very rapidly with time. At

231

the very high test temperatures of 900 and 1000°C, the stress relaxation is particularly dramatic, with the stress reducing essentially to zero in a period of about 20 to 30 minutes. Such high temperatures can be expected in unprotected steel members subject to a typical compartment fire. Interestingly, at these high temperatures, the coupons actually developed compressive stress after about 30 minutes. Based on information available in the literature, the development of compressive stress in a tensile relaxation test can be related to metallurgical transformations at elevated temperatures.

A typical relaxation curve can be separated into primary, secondary, and tertiary stages similar to creep behavior. General patterns of relaxation behavior are shown in Figure 7.25 to Figure 7.26. The stress rate during the primary stage of relaxation is nonlinear and is decreasing with time. That is, during the primary stage, the initial tensile stress in the coupon deceases rapidly, but then the rate of decrease in stress reduces with time. During the secondary stage of relaxation, the stress rate again changes with time, and the coupon can develop a compressive stress. The tertiary stage of relaxation was only found in tests at 900 and 1000° C.
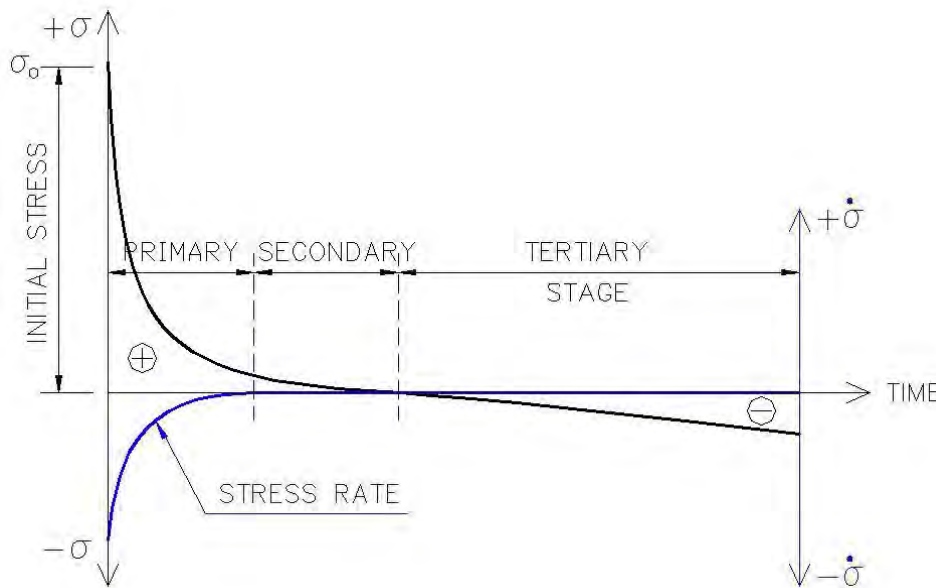
Figure 7.25 Relaxation behavior

232
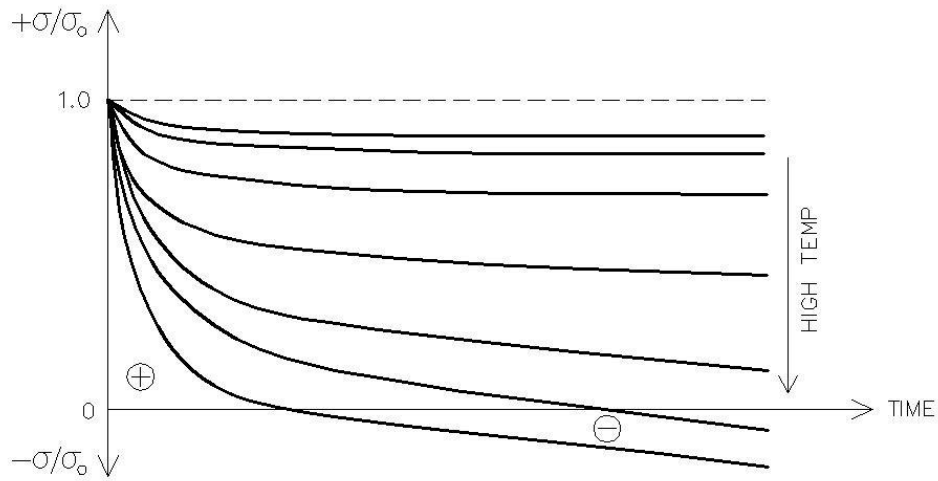
Figure 7.26 Relaxation curve patterns

7.5   SUGGESTED CONSTITUTIVE RELAXATION MODEL

In this section, a model is suggested for predicting stress relaxation of ASTM A992 steel based on the test data. This model is developed essentially through curve fitting to the test data. For this purpose, curve fitting is accomplished using the form of Equation 7.1 that includes a constant term and two exponential terms. In the initial part of the relaxation curve, the stress decreases rapidly. It then gradually decays within the testing period. The first exponential term represents the initial part and the second exponential term represents gradually decreasing part of the relaxation curve. A typical curve fitting example for the relaxation test at 700°C and an initial strain equal to 75% of the yield strain is shown in Figure 7.27. This example suggests that using a single exponential term is not adequate to develop a good fit to the test data, whereas using two exponential terms provides a much better fit over the full time range of the test data.

233

a) Initial part   *b) Up to 2 hours*
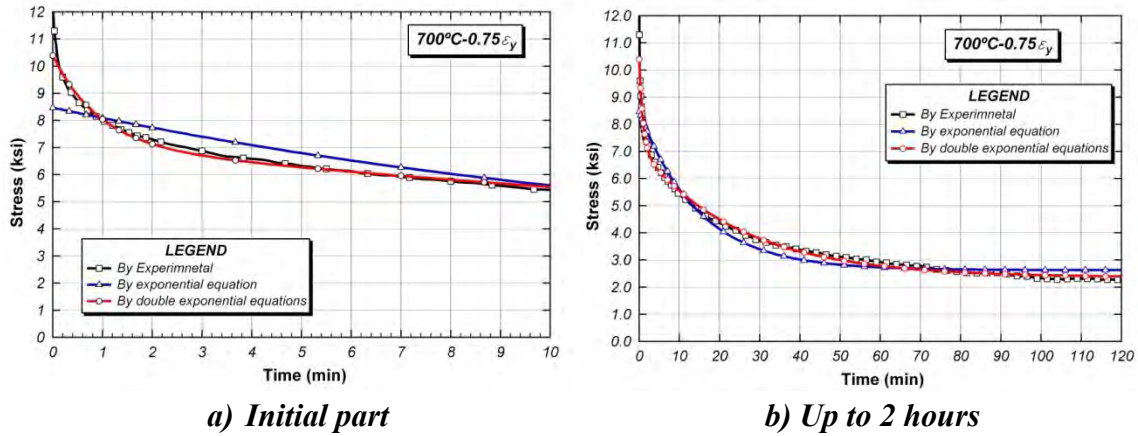
Figure 7.27 Typical example of curve fitting (700°C-0.75εy)

The selected curve fitting model for the relaxation curves is shown in Equation (7.1).

$$\sigma = y_0 + A_1 \exp(-B_1\, t) + A_2 \exp(-B_2\, t) \tag{7.1}$$

where

y_0 = Constant value, where $y_0 = \sigma_0$ at initial time (t = 0)

A_i, B_i = Constants dependent on temperature and initial strain

Table 7.4 lists values of parameters y_o, A_1, A_2, B_1, and B_2.

Table 7.4 Curve fitting parameters

Temp(°C)	σ_o (ksi)		y_o	A_1	B_1	A_2	B_2
400	$0.50\varepsilon_y$	30.21	27.30	2.0641	0.05143	0.6353	1.90560
	$0.75\varepsilon_y$	34.15	30.81	1.9257	0.04655	0.8532	0.90578
	$0.90\varepsilon_y$	35.91	32.22	1.6931	0.04104	1.1670	0.46040
	$1.50\varepsilon_y$	40.39	34.38	3.9062	0.01394	1.4988	0.74844
500	$0.50\varepsilon_y$	25.74	22.92	1.4074	0.08188	0.9627	1.17910
	$0.75\varepsilon_y$	31.69	23.80	4.3537	0.00702	2.3953	0.38887

234

	0.90ε_y	32.05	26.15	2.0994	0.03938	2.3785	0.67039
	1.50ε_y	35.29	29.03	1.8504	0.03507	2.6865	0.72723
600	0.50ε_y	21.02	13.00	3.1284	0.03885	3.5972	0.78645
	0.75ε_y	21.53	13.04	3.6918	0.02509	3.5150	0.67996
	0.90ε_y	21.50	13.01	3.2369	0.03257	3.7483	0.97133
	1.50ε_y	23.00	13.48	3.5112	0.05159	4.1985	1.11450
700	0.50ε_y	12.96	3.06	4.1967	0.02525	3.6058	0.80173
	0.75ε_y	12.14	2.36	4.7663	0.04015	3.2635	1.08610
	0.90ε_y	13.00	0.95	6.0615	0.01385	3.8887	0.82071
	1.50ε_y	12.33	3.14	3.9628	0.03227	3.3765	0.95054
800	0.50ε_y	6.69	0.48	1.8805	0.03991	3.0715	0.74590
	0.75ε_y	7.69	0.42	2.8012	0.09258	2.9733	1.41200
	0.90ε_y	7.10	0.32	2.4097	0.04960	3.0674	0.94800
	1.50ε_y	7.46	0.46	2.2945	0.05769	3.3861	0.98084
900	0.50ε_y	4.31	0.08	1.4993	0.07756	2.2853	0.71759
	0.75ε_y	5.39	0.02	2.5022	0.13358	2.2803	1.81110
	0.90ε_y	5.44	0.06	1.8693	0.11285	2.6290	1.15170
	1.50ε_y	5.50	-0.02	1.8231	0.90928	2.8125	0.89057
1000	0.50ε_y	3.51	-0.04	1.0757	0.12507	1.9755	1.58970
	0.75ε_y	3.51	0.02	1.1950	0.15753	1.7324	1.65150
	0.90ε_y	3.94	-0.13	1.5382	0.16806	1.9643	2.05080
	1.50ε_y	3.74	-0.06	1.3019	0.14974	1.6833	1.69260

7.6 VERIFICATION OF SUGGESTED RELAXATION MODEL WITH TEST DATA

In this section, the proposed relaxation model (Equation (7.1) and Table 7.4) is compared to the test data. These comparisons are shown in Figure 7.28 to Figure 7.34. As shown in these plots, the proposed model matches the test data quite well. This is expected, of course, since the model was based on curve fitting to the test data. In the future, it would be useful to compare this model with test results of other samples of ASTM A992 steel to further evaluate the applicability of this model.

a) Full view   b) Zoomed-in view
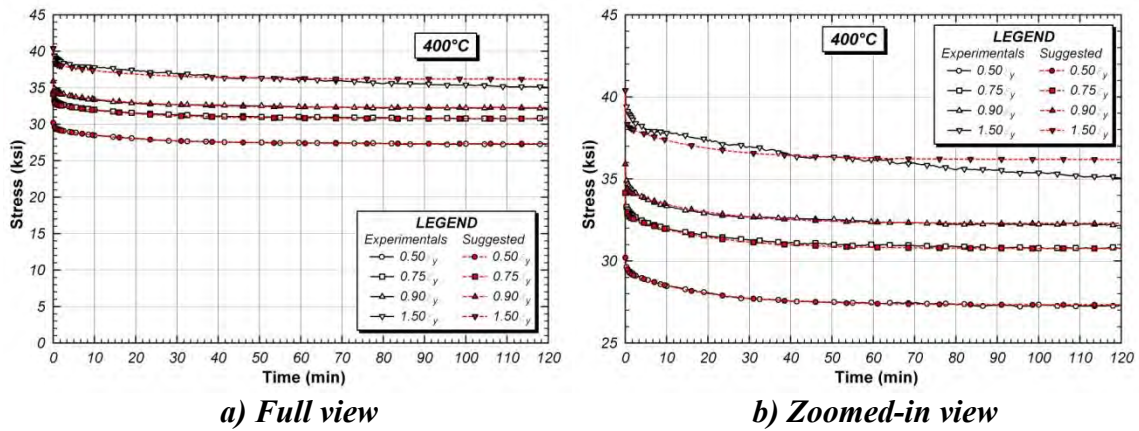
Figure 7.28 Relaxation results at 400°C

a) Full view   b) Zoomed-in view
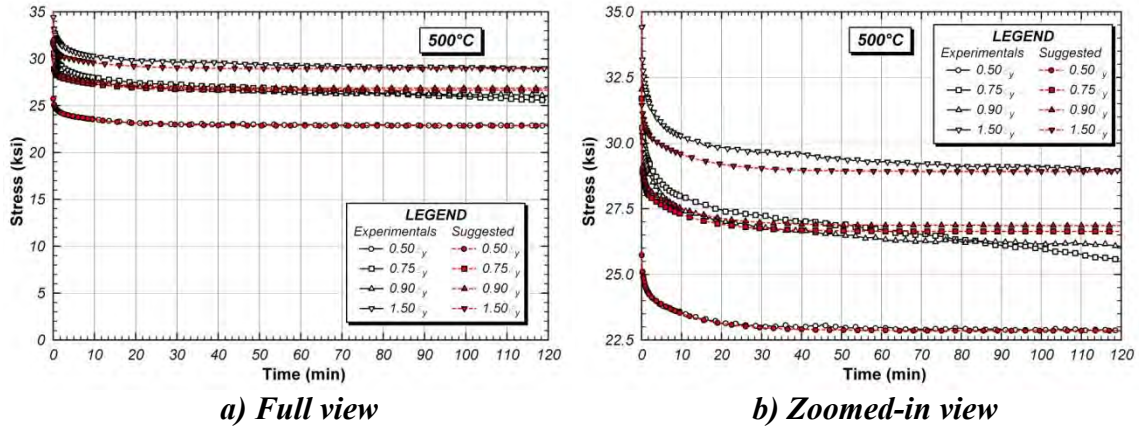
Figure 7.29 Relaxation results at 500°C
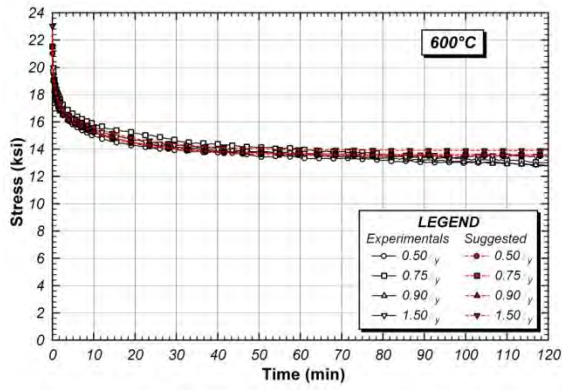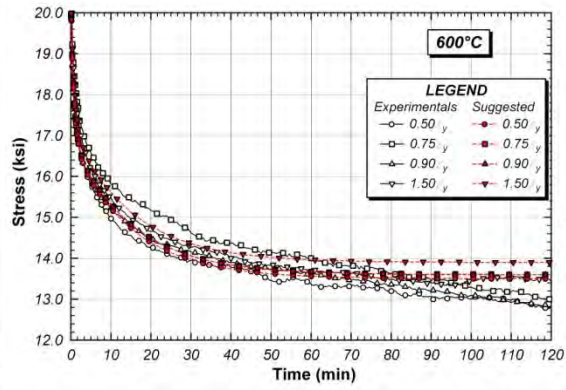
a) Full view   *b) Zoomed-in view*

Figure 7.30 Relaxation results at 600°C
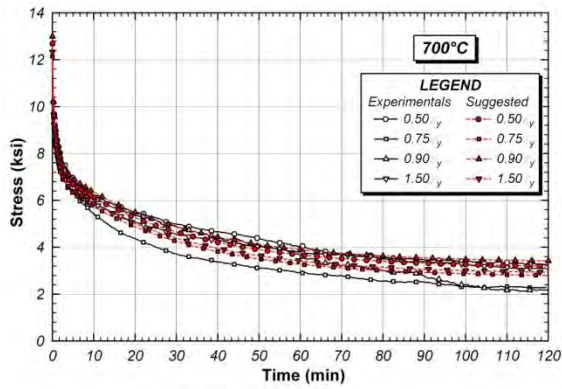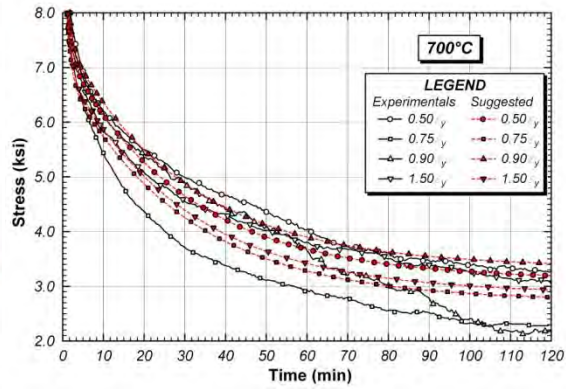
a) Full view   *b) Zoomed-in view*

Figure 7.31 Relaxation results at 700°C
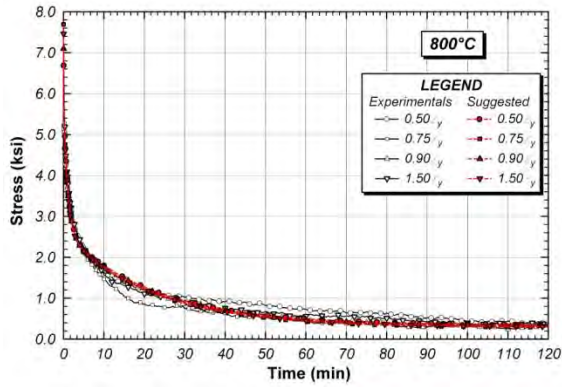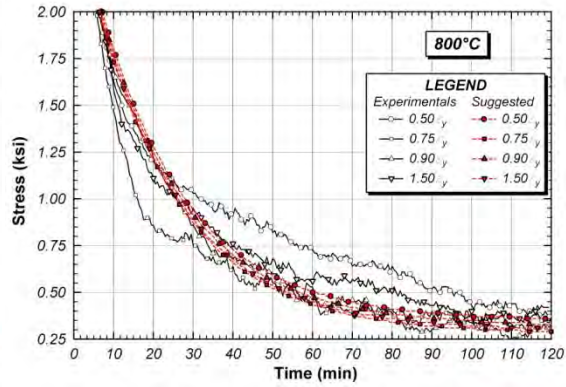
a) Full view   *b) Zoomed-in view*

Figure 7.32 Relaxation results at 800°C

237
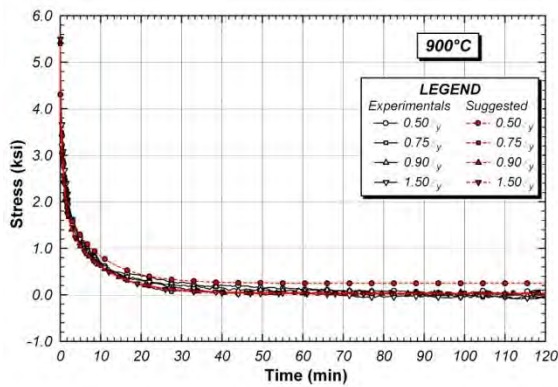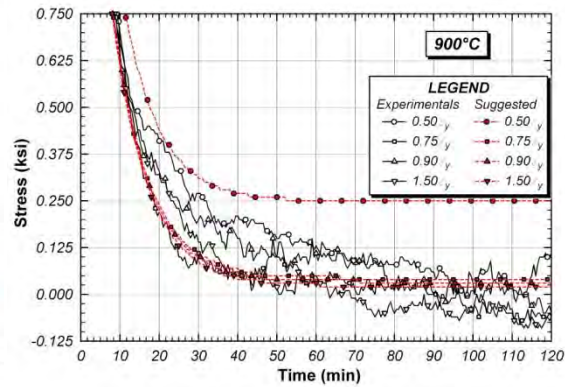
a) Full view   *b) Zoomed-in view*

Figure 7.33 Relaxation results at 900°C
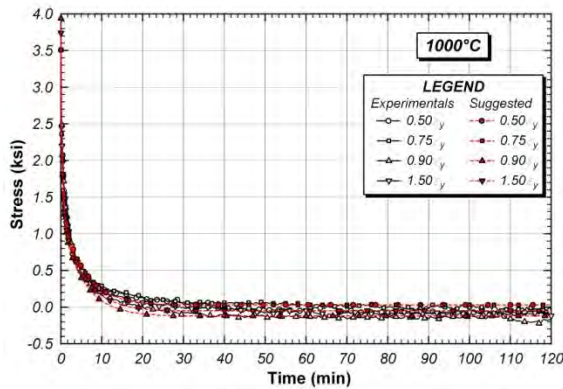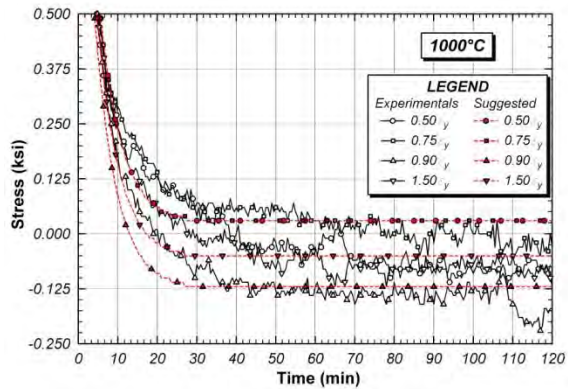
a) Full view   *b) Zoomed-in view*

Figure 7.34 Relaxation results at 1000°C

7.7   STRESS-STRAIN-TIME PLOTS

As is clear from the relaxation data presented in this chapter, as well as the creep data presented in the previous chapter, the stress-strain response of steel is dependent both on temperature and on time. It is therefore instructive to examine the relaxation data in the form of stress-strain-time plots at various temperatures. A qualitative representation of a stress-strain-time plot generated from relaxation data is shown in Figure 7.35. For any given temperature, it is possible to generate a three-dimensional plot of stress vs. strain vs. time using the stress versus time data collected for each of the initial strain values.

238
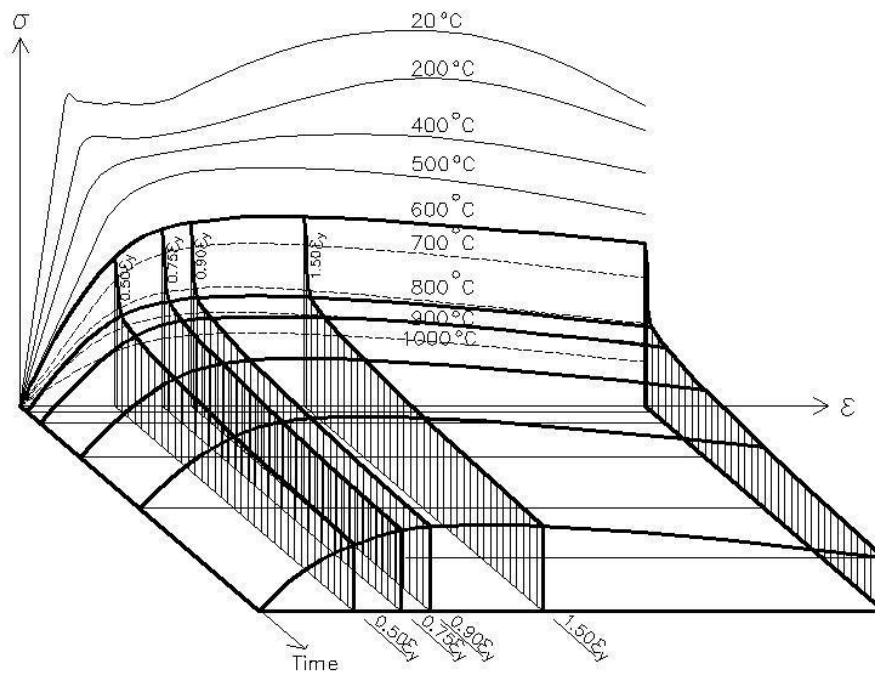
Figure 7.35 Stress-Strain-Time plots based on relaxation data

The resulting three-dimensional stress-strain-time plots based on the relaxation test data are shown in Figure 7.36 for selected temperatures. These plots can be used to help judge the importance of including time-dependent material response in a structure-fire analysis problem. For example, say an analysis of a fire scenario in a building suggests that a structural member will be exposed to high temperatures for a duration of about 30 minutes. These plots show that at 400°C, the stress-strain response is not strongly time-dependent for a 30-minute exposure. However, for higher temperatures, say 600°C, the response is highly time dependent for a 30-minute exposure, and ignoring time dependence in the analysis may lead to significant errors in the structural response predictions.
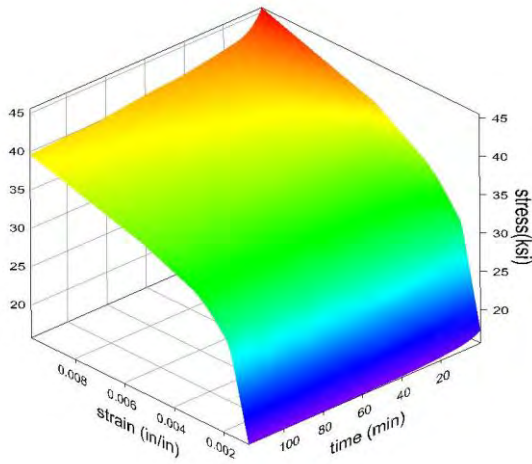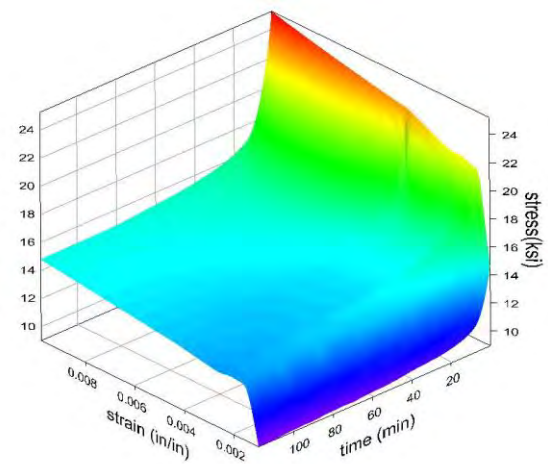
a) 400°C   *b) 600°C*
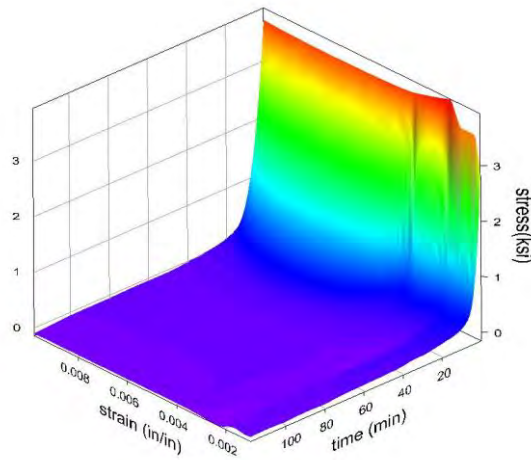
c) 1000°C

Figure 7.36 Examples of stress-strain-time plots

7.8   SUMMARY

This chapter has described an extensive series of elevated-temperature stress-relaxation tests on samples of ASTM A992 steel. The selected material for relaxation testing was the same as for the creep testing, and was taken from a flange of a W4x13 hot-rolled section. Relaxation tests were carried out for temperatures ranging from 400 to 1000°C with a time duration of 2 hours, to collect data pertinent to structure-fire applications.

Results of the tests showed very significant stress relaxation for temperatures and times of interest in structure-fire problems. Like the creep data presented in the previous chapter, this relaxation data provides further evidence of the importance of time-dependent material behavior in structure-fire analysis.

A model was developed to predict stress relaxation of ASTM A992 steel based on temperature, time and initial strain level. This model was developed through a curve fitting process to the test data, and matches the test data quite closely. It is unclear how well this model would predict the behavior of other samples of ASTM A992 steel, and additional relaxation test data would be useful to further evaluate this model. Finally, the relaxation data was presented in the form of three-dimensional stress-strain-time plots, which provide further insights into the importance of time-dependent material response at elevated temperature.

CHAPTER 8
Summary and Conclusions

8.1 SUMMARY

This dissertation has summarized a research program aimed at developing an extensive experimental database on the elevated temperature mechanical properties of ASTM A992 steel, for use in structural-fire engineering analysis. The major focus areas of research included the development of elevated temperature testing techniques, tension testing of A992 steel to obtain elevated temperature stress-strain curves, tension testing of A992 steel after heating and cooling to evaluate post-fire properties, creep testing of A992 steel to obtain data on creep strain versus time for various temperature and stress levels, and stress relaxation testing on A992 steel to obtain data on stress relaxation versus time for various temperature and strain levels. All elevated temperature tests were conducted at temperatures ranging from room temperature up to 1000°C, to encompass temperatures of interest in structural-fire engineering analysis. Creep tests and stress relaxation tests were generally conducted for 2 hours, to encompass time frames of interest in structural-fire engineering analysis.

A strong emphasis was placed in this research on collecting high quality experimental data. Considerable work was done in developing techniques to accurately control and measure temperatures of the steel specimens, as it was found that even small variations in temperature can result in large changes in mechanical response. A great deal of work was also done on strain measurement techniques using high temperature extensometers. In addition, for most types of tests conducted in this program, several replicate specimens were tested to evaluate repeatability of test results and to discern various sources of experimental error. Although the emphasis on this research has been the development of high quality experimental data, efforts were also made to develop constitutive relationships based on the experimental data. Constitutive relationships were

242

suggested for the tensile stress-strain behavior, creep behavior, and stress relaxation behavior of A992 steel at temperatures up to 1000°C. In some cases, these constitutive relationships were based on curve fitting to the experimental data, and so these relationships are strictly only applicable to the specific steels tested in this program. In the case of the tensile stress-strain relationships an attempt was made to develop more general constitutive relationships that are a function of room temperature yield stress and the specific elevated temperature of interest.

Based on this research, a variety of findings have been presented throughout the main chapters of this dissertation. Here, the primary conclusions are repeated for emphasis.

8.2 CONCLUSIONS

8.2.1 Elevated Temperature Testing Techniques

Elevated temperature testing of steel coupons is, in general, far more difficult than testing at room temperature. Testing techniques at elevated temperature are not as well established or standardized as they are for room temperature testing. Specialized equipment is needed to conduct the tests and specialized knowledge is needed to collect high quality data. One of the key difficulties is controlling and measuring the temperature of steel coupons, so that the steel temperature is uniform throughout the coupon, is close to the target test temperature, and remains constant through the duration of the test. To accomplish this goal, techniques were developed to control furnace temperature to achieve a desired specimen temperature, and these techniques are described in detail in Chapter 3. The temperature of steel coupons was measured using thermocouples attached to the coupons. It was found that various methods for attaching the thermocouples to the coupons could result in significantly different temperature measurements. Through an extensive trial and error process, a technique was developed for attaching thermocouples

243

to the steel coupons that is believed to provide accurate measurements of steel temperature. This technique is described in Chapter 3.

An additional challenge in elevated temperature testing is the measurement of strain on the steel coupons. For this research, strain was measured by using high temperature contact type extensometers that attach to the specimen by pressure mounted ceramic rods. Considerable experience was needed to develop the appropriate tip profile for the ceramic rods, appropriate pressure levels between the rods and the steel coupon, and appropriate extensometer cooling techniques, in order to be able to collect accurate strain data. One of the objectives of this testing program was to collect very accurate strain data at low levels of strain, to be able to estimate elastic modulus, proportional limit, and yield stress. This required accurate measurements at strains less than 1%   An additional objective was to be able to characterize the full stress-strain curve of steel at elevated temperatures, which required measurements in excess of 100% strain. Commercially available high temperature extensometers are not able to do both. Extensometers that can measure small strains accurately have maximum strain capacities on the order of 10%. On the other hand, extensometers that can measures very large strains, on the order of 50%, cannot accurately measure small strains. To solve this problem, a high accuracy – small strain limit high temperature extensometer was used in this research. To then measure large strains, a technique was developed to reset the extensometer several times during a test. A methodology was then developed to reassemble the strain data into a continuous stress-strain curve.

8.2.2   Tension Testing at Elevated Temperatures

A series of tests were conducted to measure the uniaxial tensile stress-strain curves of A992 steel at temperatures from 20°C up to 1000°C. The objectives of these tests were to examine the fundamental changes in the stress-strain curves as temperature increases, and to measure changes in important mechanical properties with temperature, including yield stress, tensile strength, elastic modulus, proportional limit, and elongation

244

at fracture. For each of these properties, retention factors were developed that provide the ratio of the elevated temperature property to the same property measured at room temperature. An additional objective of these tests was to provide data to support the development of mathematical models of stress-strain response at elevated temperatures.

One of the unique features of these tests is that the entire stress-strain curve, up through fracture, was measured and reported. Although a number of previous investigators measured elevated temperature properties of various steels, a review of the literature found few cases in which the entire stress-strain curve is reported.

The test results showed the stress-strain behavior undergoes significant changes as temperature increases. In general terms, the steel loses strength and stiffness with increase in temperature. More specifically, at elevated temperatures, both the yield stress and the modulus of elasticity are reduced from their room-temperature values. Except for low temperatures, the tensile strength also reduces with temperature. In addition to the reduction in yield stress, tensile strength and modulus of elasticity, the shape of the stress-strain curve at elevated temperatures is fundamentally different from that at room temperature. At temperatures above 300° to 400°C, the stress-strain curve does not exhibit a well-defined yield plateau and becomes highly nonlinear at low levels of stress. That is, the proportional limit occurs at a stress significantly less than the yield stress. The greater nonlinearity exhibited by the stress-strain curves at high temperatures can have a significant influence on member behaviors governed by stability modes of failure, where tangent modulus is a critical material property.

Elongation, i.e., the strain at fracture, increased gradually for elevated temperature up to 800°C, and subsequently decreased for higher temperatures. Another property that was examined was the strain at the development of the tensile strength. This is the strain that occurs at the peak of the engineering stress-strain curve. The strain at the tensile strength showed a dramatic decrease with increasing temperature from 400 to 800 °C. The lowest values of strain at the development of the tensile strength occurred at

245

temperatures of 700 to 800 °C. At these temperatures, the strains at the development of the tensile strength were on the order of 1 to 2%, representing a very large reduction from the ambient temperature values, which were on the order of 16 to 18%. Note also that the peak of the engineering stress-strain curve corresponds to the start of necking. These test results indicates that necking can begin at very low levels of strain at elevated temperatures. Thus, while the strain at fracture may be very large, the strain at the start of necking can be very small. For example, at 800°C the strain at fracture exceeds 100%, whereas the strain at the start of necking is about 1%. This trend further reinforces the observation that the basic shape of the stress-strain curve for steel at elevated temperature can be dramatically different than at room temperature.

Using the test data, retention factors were computed for elastic modulus, proportional limit, yield stress, tensile strength, strain at the development of tensile strength, and strain at fracture. Eurocode 3 and the AISC Specification provide recommended retention factors for structural steel at elevated temperatures, for elastic modulus, proportional limit, yield stress, and tensile strength. Note that the retention factors in the AISC Specification were adopted directly from Eurcode 3, so the retention factors in these two design standards are identical.

For elastic modulus, proportional limit, and tensile strength, the retention factors computed from the test data compared reasonably well with those recommended in Eurocode 3, although some differences were noted. For yield stress, on the other hand, large differences were seen between the computed retention factors for the A992 test data with those reported in Eurocode 3, especially for temperatures below 600°C. However, in examining the basis for the Eurocode 3 yield stress retention factors, it was found that the major differences with the test data was the result of the definition used for yield stress. For the A992 test data, the yield stress was first computed using the conventional ASTM definition for materials that do not exhibit a well-defined yield plateau, which was the case for these elevated temperature stress-strain curves. For such materials, ASTM defines the yield stress as the stress that occurs at 0.2% offset strain. Using the 0.2%

246

offset strain definition to establish the yield stress from the A992 test data, the computed retention factors were significantly smaller than recommended by Eurocode 3, for temperatures less than 600°C. For example, at 400°C, the measured yield stress retention factor for the tested A992 steel was 0.7 using the 0.2% offset definition. This indicates that at 400°C, the yield stress is 70% of its room temperature value. On the other hand, Eurocode 3 recommends a yield stress retention factor of 1.0 at 400°C, indicating the yield stress is the same at 400°C as it is at room temperature.

In examining the literature, it appears that Eurocode 3 does not define yield stress using the conventional 0.2% offset definition. Rather, the literature suggests that Eurocode 3 defines yield stress at elevated temperature as the stress at a total strain (not offset strain) of 2% (not 0.2%). In examining typical elevated temperature stress-strain curves from this test program, it was found that defining the yield stress using 0.2% offset strain versus 2% total strain resulted in dramatically different values of yield stress. Consequently, the yield stress retention factors for the A992 test data were recomputed using the 2% total strain definition of yield stress. In this case, the yield stress retention factors computed for the A992 test data compared quite closely with those recommended in Eurocode 3. That is, as long as the same definition of yield stress is used, the yield stress retention factors from the test data compared very well with Eurocode 3.

The comparison of yield stress retention factors raised an interesting question: what is the most appropriate definition of yield stress of structural steel at elevated temperature, for use in structural-fire engineering analysis and design? This question was beyond the scope of this research. It is noted, however, that a review of the literature found no clear rationale or justification for the definition of yield stress adopted by Eurocode 3. Consequently, further work appears justified in developing a rational basis for defining elevated temperature yield stress of structural steel for structure-fire applications.

Lastly, using the test data, suggested models were developed for computing the elevated temperature stress-strain response of A992 steel. Two different models were

developed: a detailed model and a simplified model. The detailed model provides a fairly comprehensive set of equations to predict the full non-linear stress strain response at temperatures up to 1000°C. The detailed model is intended primarily for use in finite element analysis of steel structures subject to fire. A simplified model was also developed, using a tri-linear representation of the A992 stress-strain curves up to 1000°C. The predictions of the detailed model matched the test data closely. The simplified model did not match the data as well, but still captured the overall response in a reasonable manner. Since these models were based on curve-fitting this test data, it is unclear how representative these models would be for other samples of A992 steel or similar structural steels at elevated temperature. Additional test data would be desirable to further evaluate the applicability of the proposed models.

8.2.3   Mechanical Properties after Heating and Cooling

A series of tests were conducted wherein samples of ASTM A992 steel were heated to temperatures ranging from 200 to 1000°C, and then subsequently cooled. Three different cooling techniques were used, referred to herein as cooled-in-blanket (CIB), cooled-in-air (CIA), and cooled-in-water (CIW). These three different cooling techniques were intended to provide a wide range of cooling rates. After cooling, tensile tests, Charpy V-notch tests, and hardness tests were conducted on the steel samples. The purpose of this test series was to gain insights into the post-fire mechanical properties of steel.

The test results showed that the process of heating and cooling caused no significant reduction in yield stress until the temperature exceeded 700°C. However, even up to 1000°C, the reduction in yield stress was only about 20%. For tensile strength, there was essentially no reduction, even for coupons heated to 1000°C. For coupons cooled-in-water (CIW), there was an increase in tensile strength for heating temperatures greater than 500°C.

248

The most significant effect seen in this test series was a reduction in Charpy V-notch (CVN) values for steel samples that were heated above 600°C and then cooled rapidly in water (CIW). These samples showed a large drop in CVN values. For example, for the sample heated to 1000°C and then cooled-in-water, the CVN value was only about 20% of that for an unheated virgin sample. CVN values are indicative of fracture toughness, and the loss of fracture toughness due to heating and then rapid cooling in water may be of concern in some applications, for example in a steel bridge girder subjected to fire and then cooled rapidly by water from fire-fighting operations. It may be possible to detect hardening and loss of fracture toughness of steel in a structure that was subjected to fire and then cooled rapidly by the use of field hardness measurements.

8.2.4 Creep Testing at Elevated Temperatures

A series of creep tests were conducted on coupons of ASTM A992 steel, at temperatures ranging from 400 to 1000°C. For each test, the coupon was first heated to the target temperature under no load; that is, the coupon was free to expand. Once the coupon reached the target temperature, load was applied to the coupon and held constant for a period up to 2-hours. During the loading process and while holding the load constant, strain was measured as a function of time. For each target temperature, coupons were tested at four different load levels. The load levels were selected to provide engineering stress levels within the coupons equal to $0.5F_y$, $0.75F_y$, $0.9F_y$, and $0.9F_u$, where F_y and F_u were the measured yield stress and tensile strength of the material at the target temperature. For this test series, temperatures, stress levels, and time durations were selected to be representative of structure-fire problems.

Test results were presented in the form of plots of strain versus time for each temperature and stress level. A creep model was developed by examining the experimentally observed patterns of creep behavior and then by curve fitting to the

experimental data. The experimental data was compared to this model, as well as to creep models for structural steel developed by other researchers.

The results of this test series show that creep strains can be quite significant for temperatures, stress levels, and time durations representative of building structures exposed to fire. This suggests that ignoring creep may lead to inaccurate predictions of structural response for some classes of structure-fire problems. Existing models may provide poor predictions of creep when compared to experimental data for A992 steel.

8.2.5   Relaxation Testing at Elevated Temperatures

A series of stress relaxation tests were conducted on coupons of ASTM A992 steel, at temperatures ranging from 400 to 1000°C. For each test, the coupon was first heated to the target temperature under no load. Once the coupon reached the target temperature, displacement was applied to the coupon and held constant for a period of up to 2 hours. While the displacement was held constant, the reduction in stress was measured as a function of time. For each target temperature, coupons were tested at four different displacement levels. The displacement levels were selected to provide engineering strain levels within the coupons equal to $0.5\varepsilon_y$, $0.75\varepsilon_y$, $0.9\varepsilon_y$, and $1.5\varepsilon_y$, where ε_y is the measured value of yield strain at the target temperature based on the 0.2% offset strain definition of yield. Temperatures, strain levels, and time durations were selected to be representative of structure-fire problems.

Test results were presented in the form of plots of stress versus time for each temperature and strain level. A model was developed to predict stress relaxation of ASTM A992 steel based on temperature, time, and initial strain level. This model was developed through a curve fitting process to the test data. Results of the tests showed very significant stress relaxation for temperatures and times of interest in structure-fire

problems. Like the creep data, this relaxation data provides further evidence of the importance of time-dependent material behavior in structure-fire analysis.

8.3   RESEARCH NEEDS

To further advance capabilities to predict the response of steel structures to fire, additional research is needed to better characterize steel material response at elevated temperatures. Following is a list of suggested research needs in this area.

- Additional work is needed on the development of improved equipment and techniques for conducting elevated temperature tests on steel materials. Of particular value would be the development of better techniques for measuring strain at elevated temperatures. Improved strain measuring devices are needed that can measure very small levels of strain accurately to permit characterization of elastic modulus, proportional limit, and yield stress, all of which occur generally at strain values of less than 1 to 2%. At the same time, these devices should be capable of measuring very large strains, on the order of 120%, to allow characterization of the full stress-strain curves and full creep strain-time curves without the need for resetting. It would also be desirable to measure strains on opposite sides of a steel coupon simultaneously, to minimize measurement errors due to bending of steel coupons during testing. Of further value would be the capability to measure the change in cross-sectional dimensions along the length of a coupon during testing at elevated temperatures. As seen in this test program, necking can initiate at very low levels of strain, say on the order of 1 to 2% at elevated temperatures, compared to 15 to 20% at room temperature. Being able to measure the reduction in coupon cross-section dimensions would allow better characterization of material response at elevated temperature, especially for better characterization and control of true stress during testing. In addition, well developed, validated and standardized methods for measuring the temperature of steel coupons are needed. As seen in this research, inadequate temperature measurement and control can be the source of significant

251

experimental error, and better temperature measurement techniques are needed to reduce such errors.

- The experimental database on the elevated temperature stress-strain response of structural steels is still very limited. Additional testing on various heats of common grades of structural steel is needed to better characterize elevated temperature mechanical properties and variability in these properties.

- A number of different definitions for yield stress at elevated temperature have been used by past researchers and by building standards such as Eurocode 3 and the AISC Specification. As shown in this research, the choice of definition of yield stress can have a very large effect on the reported value of yield stress, particularly for temperatures below 600°C. Further work is needed to examine the implications of using various definitions of yield stress in structural-fire engineering analysis and to support the adoption of a standardized definition of yield stress.

- As shown in the creep and relaxation testing conducted in this research, time-dependent effects can be very significant for steel material behavior at elevated temperatures, particularly for temperatures greater than about 500°C. Further, the amount of experimental data on time-dependent effects is very small. In general, the characterization and understanding of time-dependent material response for structural-fire engineering analysis is quite limited. For example, Eurocode 3 and the AISC Specification provide significant guidance on the analysis and design of steel structures subjected to fire. However, both of these building standards are completely silent on time-dependent effects. More experimental work is needed to characterize time-dependent response of steel materials at elevated temperatures. In addition, more comprehensive and robust models are needed to analytically predict time-dependent response.

APPENDIX A

Curve-Connection Process

A.1 OVERVIEW

As discussed in Chapter 3, the primary extensometer used for elevated-temperature testing, the 1PS extensometer had a limited measurement range (10% strain). As a result, this extensometer had to be reset multiple times during testing. In the most extreme circumstances (tension test at 800°C), the extensometer was reset over 10 times.

A direct result of resetting the extensometer was discontinuous strain data. In Section 3.7, the procedure by which this raw data was fashioned into a continuous stress-strain curve was discussed. The purpose of this appendix is to extend the general discussion contained in Chapter 3 with more particulars.

This appendix contains a detailed step-by-step procedure for curve connection. The steps were engineered for three attributes: making the stress-strain curve continuous (Steps A.2 to A.5), smooth (Step A.6) and accurate (Step A.7).

A.2 CREATE THE INITIAL STRESS-STRAIN CURVE FROM RAW DATA

In Microsoft Excel, open the raw data file saved by the MTS program (a ".dat" file). From the recorded load and the measured coupon sectional area, calculate the stress. Graph the stress vs. strain as is shown in Figure A.1.
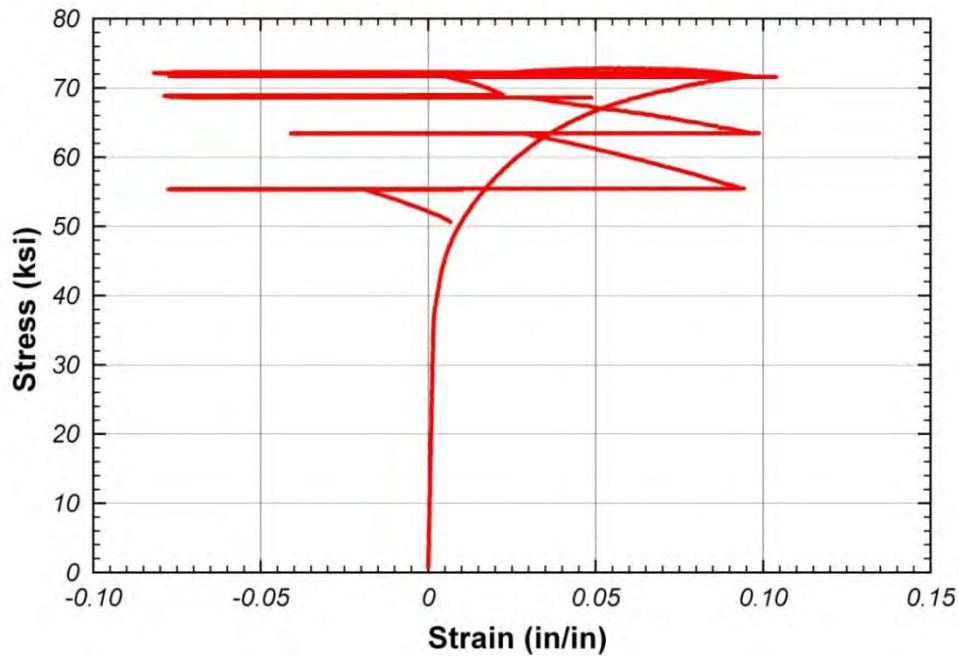
Figure A.1 Initial stress-strain curve from raw data

A.3 DELETE THE STRAIN DATA RECORDED DURING THE RESETTING PROCESS

Find the data that was collected during the process of resetting the extensometer and delete it as shown in Table A.1. The resetting process typically lasted 15–30 seconds.

a. Find a region in which there appears to be a discontinuity in stress values. Hold the mouse near a data point in that region until a tooltip appears with the coordinates (strain, stress). Creating an alternate graph with only a portion of the data and altered axes may help if you are having trouble finding a single point.

b. Find that point in the tabulated data.

c. Select all nearby strain values which do not agree with a near-constant strain rate and delete them.

d. Repeat process until all strains recorded during resetting have been deleted as in Figure A.2.

254

Table A.1 Invalid strain data: found and deleted

	A	B	C		A	B	C
7	Time	Axial Force	Axial Strain	7	Time	Axial Force	Axial Strain
8	Sec	lbf	in/in	8	Sec	lbf	in/in
1075	2134	19349.15	0.09751901000	1075	2134	19349.15	0.09751901000
1076	2136	19356.47	0.09763457600	1076	2136	19356.47	0.09763457600
1077	2138	19353.41	0.09772581600	1077	2138	19353.41	0.09772581600
1078	2140	19354.39	0.08857630200	1078	2140	19354.39	
1079	2142	19360.93	-0.04300875200	1079	2142	19360.93	
1080	2144	19363.90	-0.04521387100	1080	2144	19363.90	
1081	2146	19365.08	-0.04543512300	1081	2146	19365.08	
1082	2148	19370.69	-0.04533080400	1082	2148	19370.69	
1083	2150	19375.96	-0.07283123600	1083	2150	19375.96	
1084	2152	19374.89	-0.07268630000	1084	2152	19374.89	
1085	2154	19373.42	-0.07265976800	1085	2154	19373.42	
1086	2156	19373.35	-0.07265575200	1086	2156	19373.35	
1087	2158	19378.26	-0.07253864400	1087	2158	19378.26	
1088	2160	19378.37	-0.05830344600	1088	2160	19378.37	
1089	2162	19380.80	-0.06753408900	1089	2162	19380.80	
1090	2164	19386.15	-0.07318593600	1090	2164	19386.15	
1091	2166	19390.47	-0.07226370300	1091	2166	19390.47	
1092	2168	19397.13	-0.00151302200	1092	2168	19397.13	
1093	2170	19396.66	-0.02736748900	1093	2170	19396.66	-0.02736748900
1094	2172	19398.50	-0.02728376700	1094	2172	19398.50	-0.02728376700
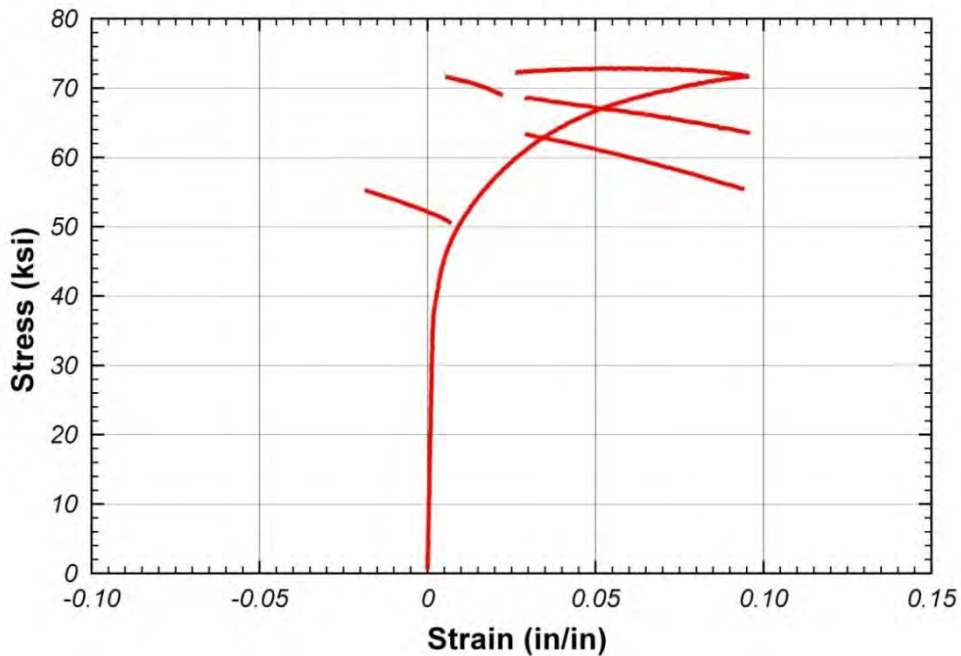
Figure A.2 Stress-strain curve after deleting strains recorded during resetting periods

255

A.4   REPLACE THE DELETED STRAIN DATA

In order to create a curve more representative of the material response during the extensometer-reset period, extrapolate the strains from nearby data. This process is completed through use of the average increment of strain increase over the adjacent data.

As a note, since the time interval between data points was constant (2 seconds for tension testing), generating strain data using the average strain increment is functionally equivalent to assuming that a constant strain rate (calculated from the adjacent data) was acting on the coupon during resetting.

a. Calculate the strain increment.

    i. First, find the strain immediately adjacent to the deleted region.

    ii. Calculate the difference between this strain and a strain a specified number of intervals away (e.g. 100, 200, 300).

    iii. Divide this difference by the number of increments separating the two strains.

Data collected after resetting the extensometer to capture the necking region will generally be more representative of the actual strain, and should therefore be used by default. Notes for choosing a proper strain increment are given in Section A.5.

b. In a separate column, create substitute strain data.

    i. Add/subtract the strain increment from the first strain after the deleted region to get the last missing strain values.

    ii. Repeat this process, adding/subtracting the strain increment from the strain listed below, until reaching the first strain in the deleted region.

c. Copy and paste the values of the generated strain data to the deleted region, using the "Paste Special: Values" function.

Table A.2 Copying generated strain to deleted region

	A	B	C	D	E	F	G	H
7	Time	Axial Force	Axial Strain					
8	Sec	lbf	in/in					
1077	2138	19353.41	0.09772581600					
1078	2140	19354.39	-0.02892453160	-0.02892453160				
1079	2142	19360.93	-0.02882072876	-0.02882072876				
1080	2144	19363.90	-0.02871692592	-0.02871692592				
1081	2146	19365.08	-0.02861312308	-0.02861312308				
1082	2148	19370.69	-0.02850932024	-0.02850932024				
1083	2150	19375.96	-0.02840551740	-0.02840551740				
1084	2152	19374.89	-0.02830171456	-0.02830171456				
1085	2154	19373.42	-0.02819791172	-0.02819791172				
1086	2156	19373.35	-0.02809410888	-0.02809410888				
1087	2158	19378.26	-0.02799030604	-0.02799030604				
1088	2160	19378.37	-0.02788650320	-0.02788650320				
1089	2162	19380.80	-0.02778270036	-0.02778270036 ...				
1090	2164	19386.15	-0.02767889752	-0.02767889752	=D1091+D$1093			
1091	2166	19390.47	-0.02757509468	-0.02757509468	=D1092+D$1093			
1092	2168	19397.13	-0.02747129184	-0.02747129184	=C1093+D1093			
1093	2170	19396.66	-0.02736748900	-0.000103803	= Strain Increment =(C1093-C1193)/100			
1094	2172	19398.50	-0.02728376700					

A.5   MOVE CURVE SEGMENTS, ONE BY ONE, TO THE END OF THE EXISTING CURVE

To make the stress-strain curve continuous, the individual curve segments must be shifted so that they appear in order of increasing strain. This process is shown in Figure A.3 and Figure A.4.

a. Calculate the amount of shift necessary to make the curve continuous.

    i. Find the difference between the first strain in the curve segment being shifted and the end of the portion of the currently continuous stress-strain data.

    ii. Add to this difference one strain increment (equal to the difference between the second and first strain in segment being shifted).

b. Add the resulting strain value (labeled as "Constant" in Table A.3) to each of the data points in the segment.

257

c. Copy and paste the generated strain values over the previous strain values for the segment, again using "Paste Special: Values."

Table A.3 Strain data points before shift

	A	B	C	D	E	F	G	H
7	Time	Axial Force	Axial Strain					
8	Sec	lbf	in/in					
1076	2136	19356.47	0.09763457600					
1077	2138	19353.41	0.09772581600	0.12675415044	= Constant = C1077+C1079-2*C1078			
1078	2140	19354.39	-0.02892453160	0.09782961884	=C1078+D$1077			
1079	2142	19360.93	-0.02882072876	0.09793342168	=C1079+D$1077			
1080	2144	19363.90	-0.02871692592	0.09803722452	...			
1081	2146	19365.08	-0.02861312308	0.09814102736				
1082	2148	19370.69	-0.02850932024	0.09824483020				
1083	2150	19375.96	-0.02840551740	0.09834863304				
1084	2152	19374.89	-0.02830171456	0.09845243588				
1085	2154	19373.42	-0.02819791172	0.09855623872				
1086	2156	19373.35	-0.02809410888	0.09866004156				
1087	2158	19378.26	-0.02799030604	0.09876384440				
1088	2160	19378.37	-0.02788650320	0.09886764724				
1089	2162	19380.80	-0.02778270036	0.09897145008				
1090	2164	19386.15	-0.02767889752	0.09907525292				
1091	2166	19390.47	-0.02757509468	0.09917905576				
1092	2168	19397.13	-0.02747129184	0.09928285860				
1093	2170	19396.66	-0.02736748900	0.09938666144				
1094	2172	19398.50	-0.02726376700	0.09947038344				

Table A.4 Strain data after pasting

	A	B	C	D	E	F	G	H
7	Time	Axial Force	Axial Strain					
8	Sec	lbf	in/in					
1076	2136	19356.47	0.09763457600					
1077	2138	19353.41	0.09772581600	0.00000000000	= Constant = C1077+C1079-2*C1078			
1078	2140	19354.39	0.09782961884	0.09782961884	=C1078+D$1077			
1079	2142	19360.93	0.09793342168	0.09793342168	=C1079+D$1077			
1080	2144	19363.90	0.09803722452	0.09803722452	...			
1081	2146	19365.08	0.09814102736	0.09814102736				
1082	2148	19370.69	0.09824483020	0.09824483020				
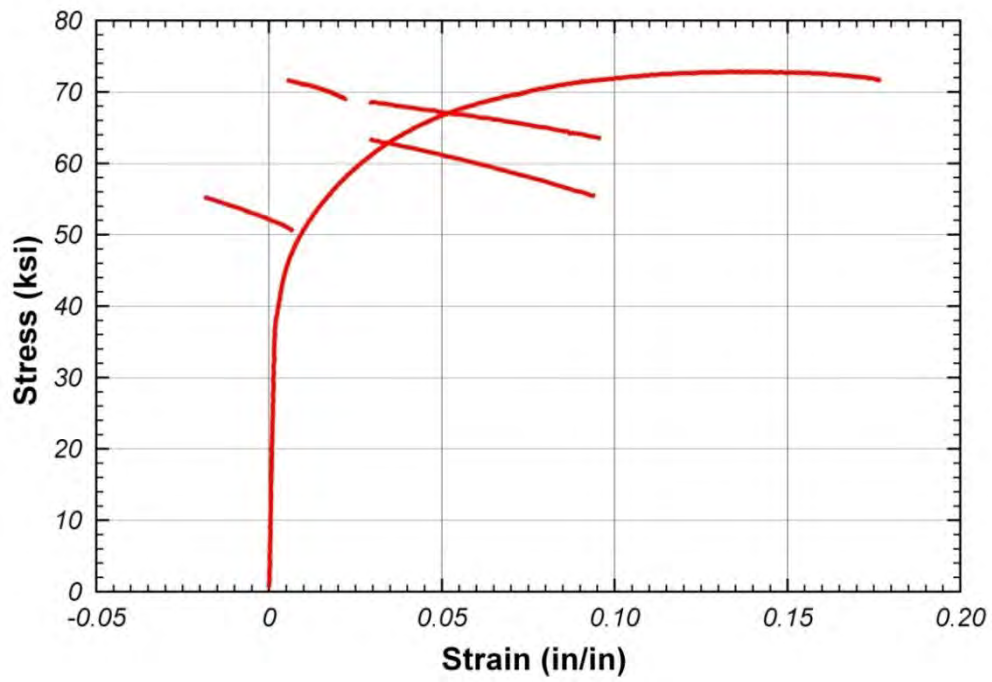
Figure A.3 Curve after moving first segment to the end of the graph
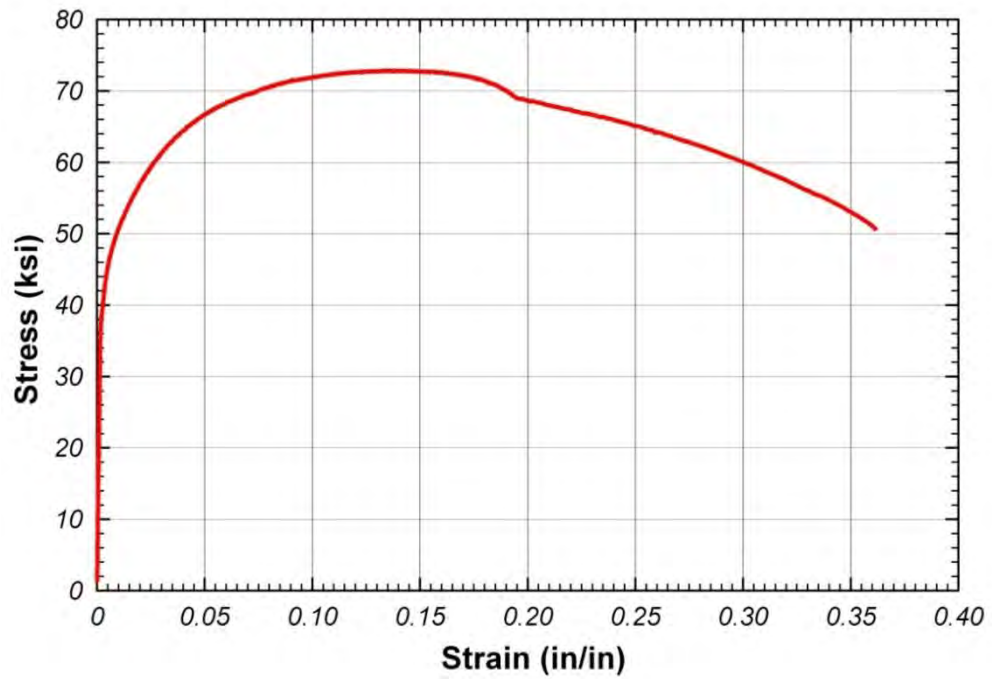
Figure A.4 Stress-strain curve after shifting all segments

259

A.6   SMOOTH OUT STRESS-STRAIN CURVE

At this point, all discontinuities in stress values have been eliminated from the stress values of the entire curve. However, there may still be discontinuities in the slope, like that shown in Figure A.5. These slope discontinuities can arise if the extensometer is placed such that it only partially captures necking.
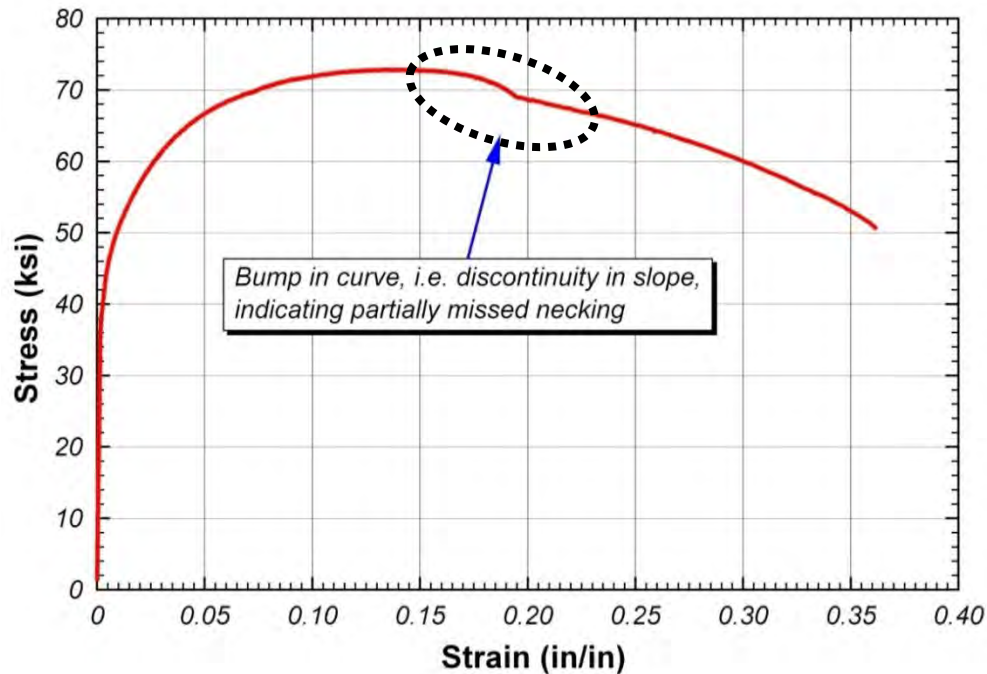
Figure A.5 Bump in stress-strain curve due to necking

The smoothing of the curve can be accomplished by the following steps:

a. Find the point in the data where the slope discontinuity exists.

b. Determine an average strain increment from the data immediately after reset of the extensometer as per Section A.4. Use of the strain rate after resetting will generally yield better results because each time, to the best of the experimenter's ability, the extensometer would be reset to a position so that it would be capturing the necking behavior.

c. Apply that strain increment to the data preceding the slope discontinuity up to the point where the slope appears is more continuous. This step is shown in Figure A.6 and Figure A.*7*.

d. Shift the newly generated discontinuous curve segment (Figure A.8) as done in Section A.5.
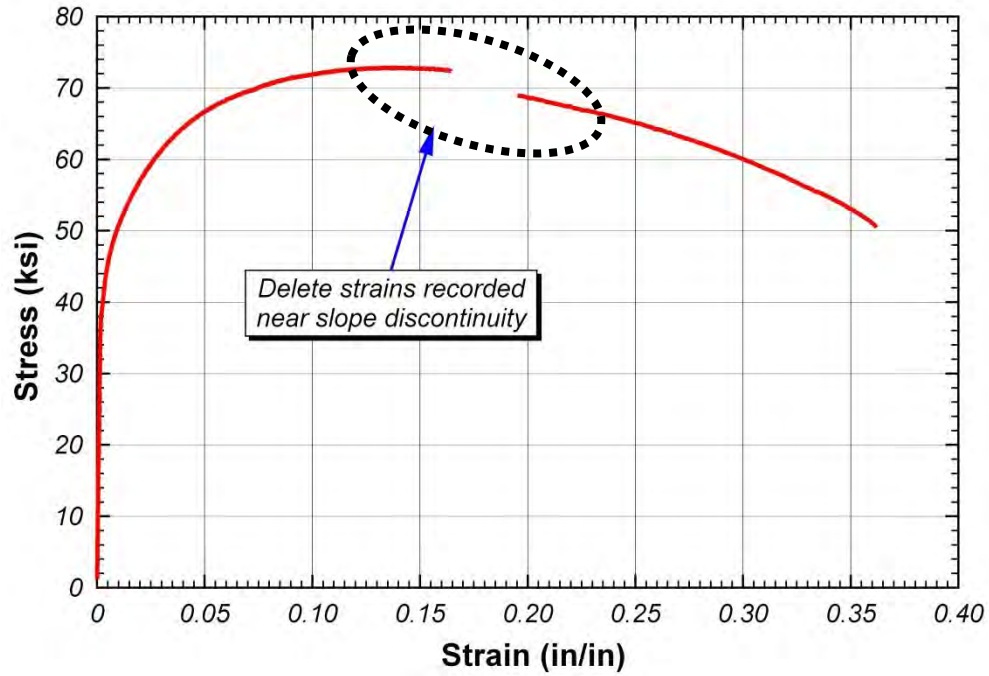
Figure A.6 Delete the data during missed necking part
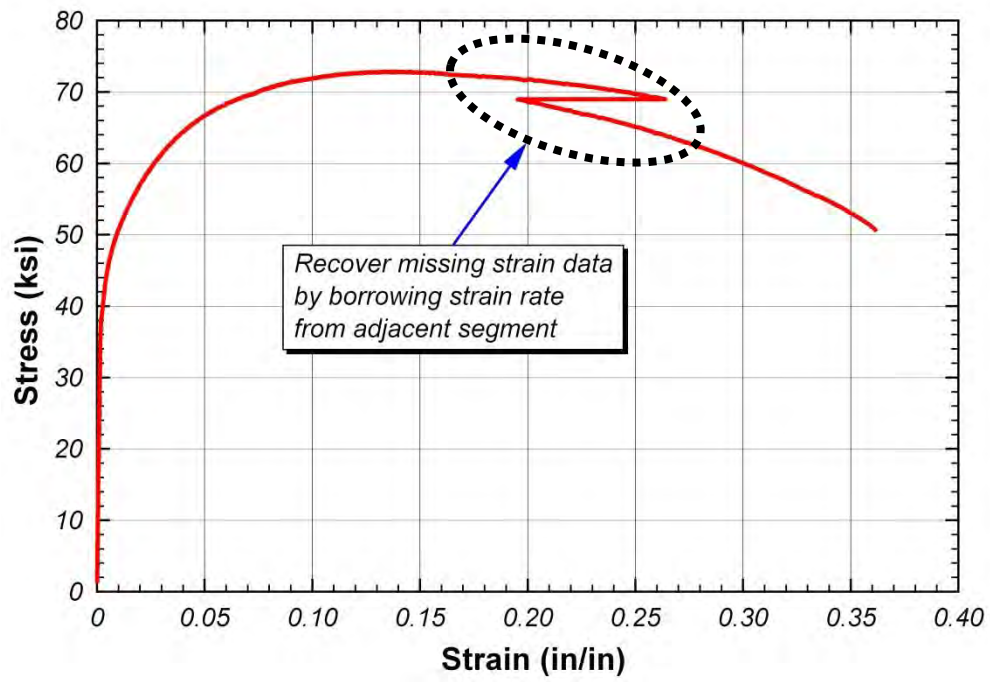
Figure A.7 Recover the strain around missed necking part
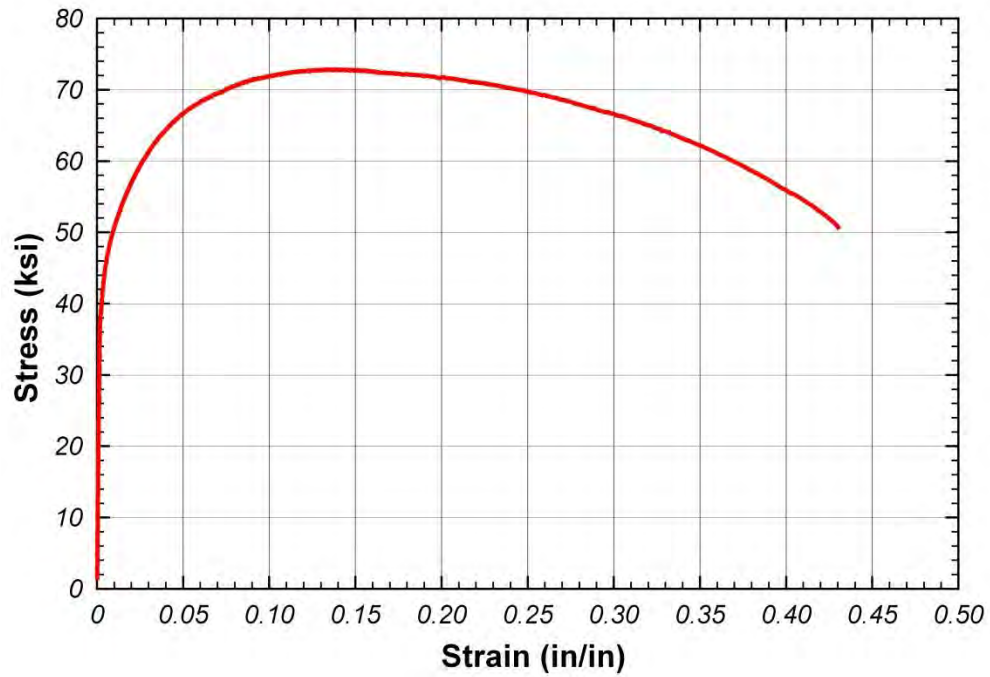
Figure A.8 Completed stress-strain curve after data recovery

262

In tests where the extensometer must be reset multiple times, the strain data from some portions may be inaccurate due to problems setting the extensometer into place. In such cases, the strain rate from data collected immediately before or after the affected portions may more accurately reflect the strain rate, and can be used in a similar procedure to replace the data in question.

However, data collected during different periods of the test will have different rates of strain increase due to necking and other factors, so discretion should be used when altering data. In the following steps for data deleting, recovering and shifting process shown in Figure A.6 to Figure A.8.

A.7 IMPROVE ACCURACY BY CONSIDERING MEASUREMENTS OF FAILURE COUPONS

With the stress data and its derivative (slope) both made continuous, the last step in the process is to improve the accuracy of the strain data. Due to the possibility of partially missed necking and assumptions made during data post-processing (also the stretching of previously instrumented lengths of the coupon, discussed in Section 3.7.2), some error is inherent in the final strain generated through this curve-connection process. As discussed in Section 3.6, direct measurement of the failure strain was performed for every coupon. This was done using calipers and punch marks on the coupon surface.

In order to improve the accuracy of the completed stress-strain curve, then, the strains should be adjusted by the caliper-measured failure strains. This was done through use of an adjustment factor, as shown below.

a. Calculate the strain from the caliper measurements as is shown in Table A.5.

Table A.5 Measured strain using calipers

Temp (°C)	Measurement between Punch Marks		
	Initial (in)	Final (in)	Strain (in/in)
400	0.975	1.452	0.4892

263

b. Multiply all strain data greater than 0.10 in/in by the correction factor given by Equation (A.1). Strains before the first resetting at 10% need not be changed since they were not altered by the resetting process and are assumed to be correct.

$$\varepsilon = 0.10 + (\varepsilon_i - 0.10)\left(\frac{\varepsilon_f - 1}{\varepsilon_l - 1}\right) \tag{A.1}$$

where

ε_i = Arbitrary strain greater than 0.10 in/in (that is, 10%)

ε_f = Final strain measured after failure with calipers

ε_l = Last strain from raw data, after completing curve connecting

In this case, the last strain after completing the curve-connecting process is 0.4308 in/in and the final strain from the measurement of the fractured coupon is 0.4892 in/in. The adjustment factor was applied to the data as shown in Table A.6.

With adjustment of strain to the measured value from the fractured coupons, the curve-connection process is complete. The resulting stress-strain curve is as shown in Figure A.9.

Table A.6 Correction factor after 10 % strain

	A	B	C	J	K	L	M
7	Time	Axial Force	Axial Strain 1	Corrected Strain			
8	Sec	lbf	in/in				
903	1790.01	17955.62	0.0992980515				
904	1792.01	17952.67	0.0993881735				
905	1794.01	17956.48	0.0993722815	Corrected strain			
906	1796.01	17964.50	0.0995797205	el=	0.43083480	= Last strain after curve connecting	
907	1798.01	17965.74	0.0997881355	ef=	0.48923077	= Final measured strain after failure	
908	1800.01	17971.71	0.0999622035	Scale Factor=	1.17651095	=(L907-0.1)/(L906-0.1)	
909	1802.01	17976.55	0.1000933815	0.100109864327	=0.1+(C909-0.1)*K908		
910	1804.01	17977.78	0.1003139608	0.100369378328			
911	1806.01	17985.67	0.1003919058	0.100461081506			
912	1808.01	17983.46	0.1006782192	0.100797932301			
913	1810.01	17986.02	0.1007629750	0.100897648485			
914	1812.01	17993.40	0.1008535511	0.101004212199			
915	1814.01	17990.30	0.1009802237	0.101153243878			
916	1816.01	17996.32	0.1012149341	0.101429383240			
917	1818.01	18000.08	0.1014475138	0.101703015857			
918	1820.01	18003.48	0.1016503078	0.101941605238			
919	1822.01	17991.15	0.1016656837	0.101959695061			
920	1824.01	17982.01	0.1019064507	0.102242960172			
921	1826.01	17983.51	0.1021195357	0.102493656958			
922	1828.01	17982.10	0.1023222156	0.102732112074			
923	1830.01	17979.62	0.1024534213	0.102886476991			
924	1832.01	17991.88	0.1025805939	0.103036096946			
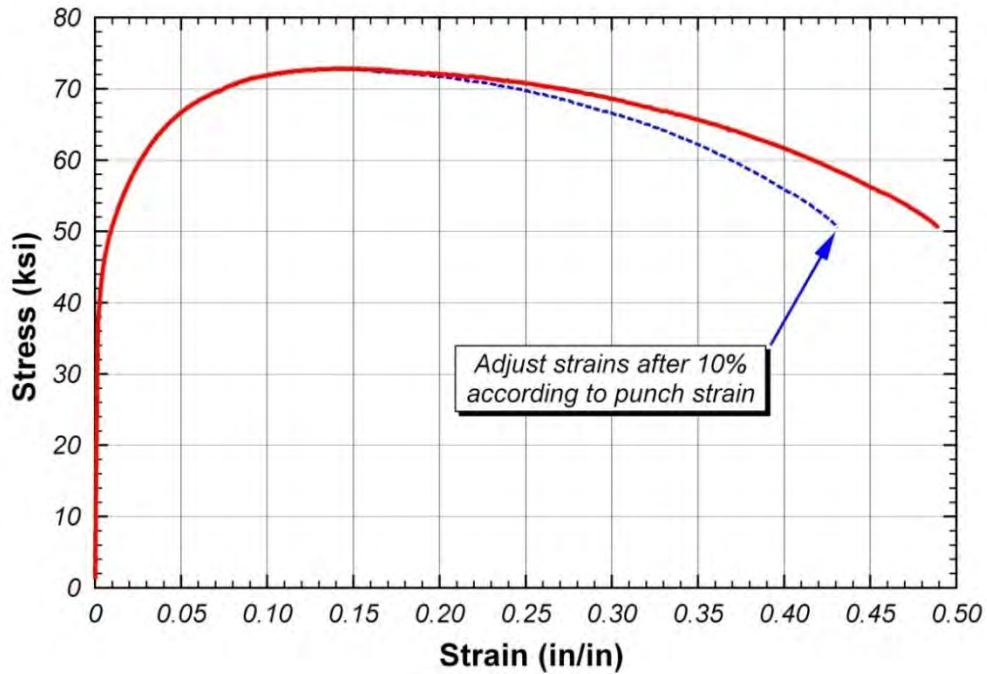
Figure A.9 Completed full stress-strain curve after correcting

265

APPENDIX B

Tension Test Results at Elevated Temperatures

This appendix presents representative tension test results of ASTM A992 steel at elevated temperatures which were discussed in Chapter 4.

B.1 HEATING CURVES
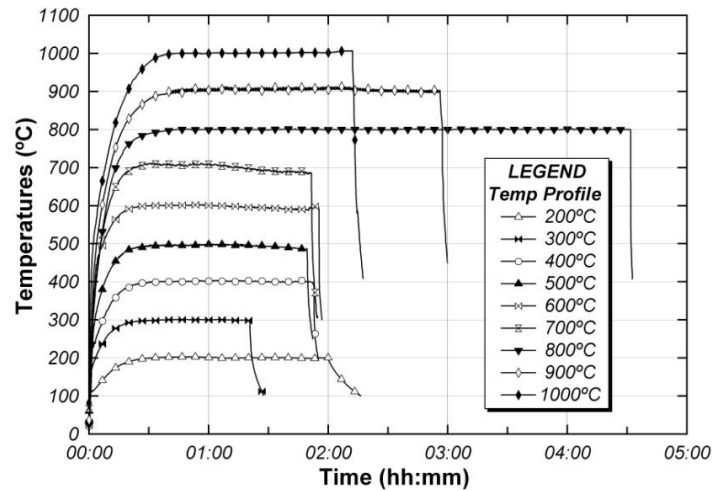
Figure B.1 Temperature profile

Figure B.2 Heating rate

266
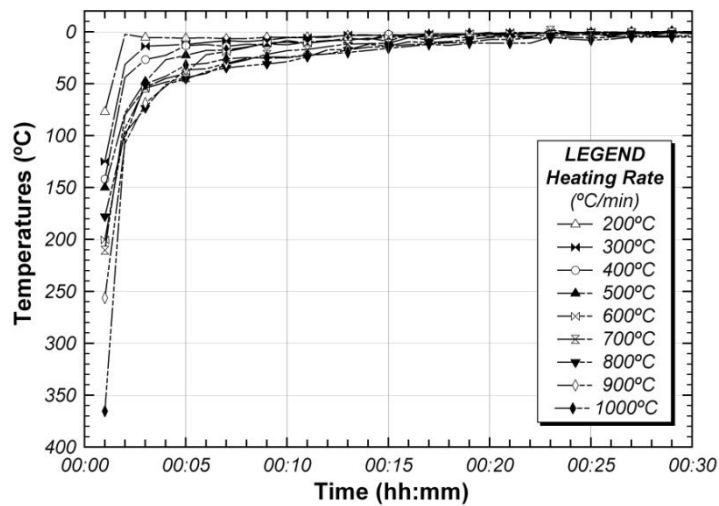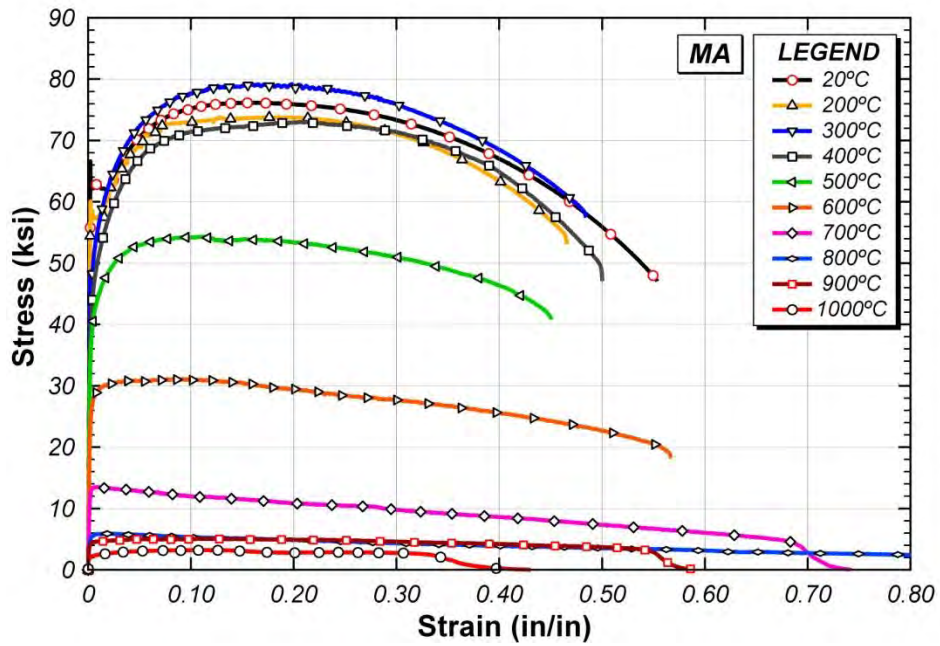
Figure B.3 Full stress-strain curves for MA material
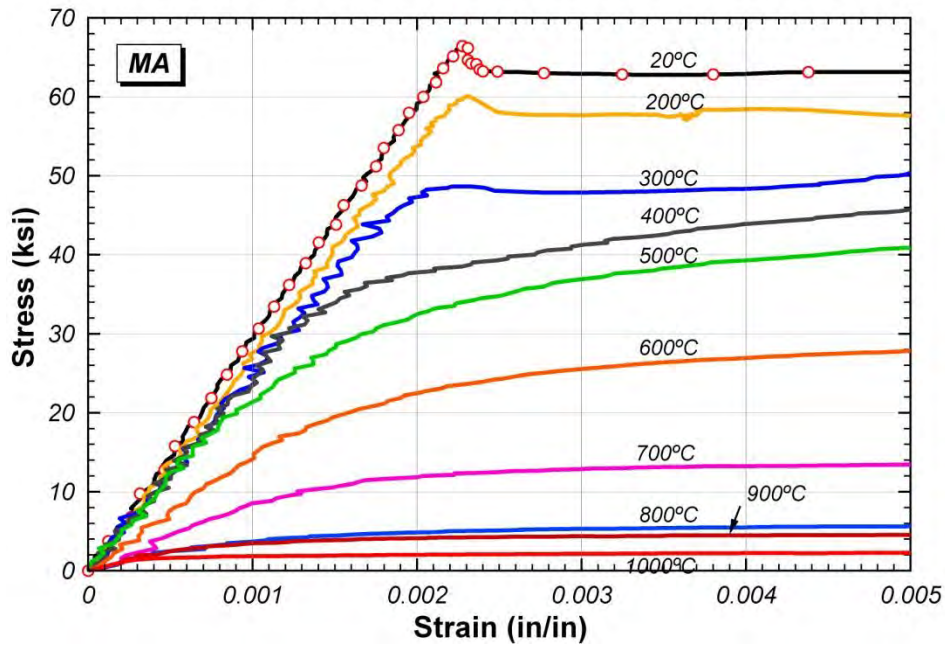
Figure B.4 Initial stress-strain curves for MA material

267
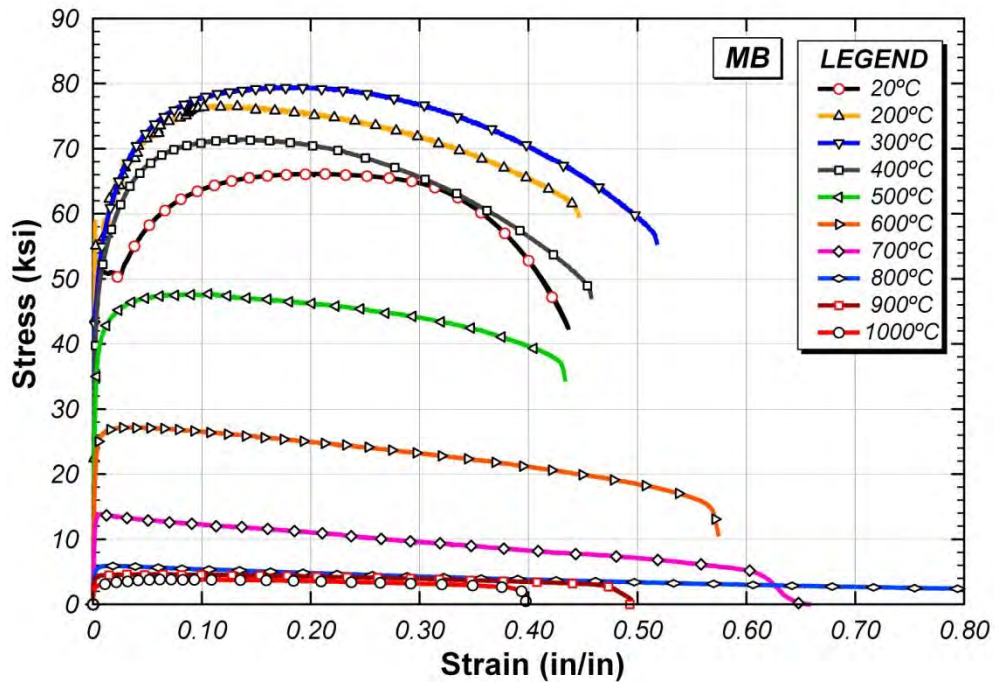
Figure B.5 Full stress-strain curves for MB material
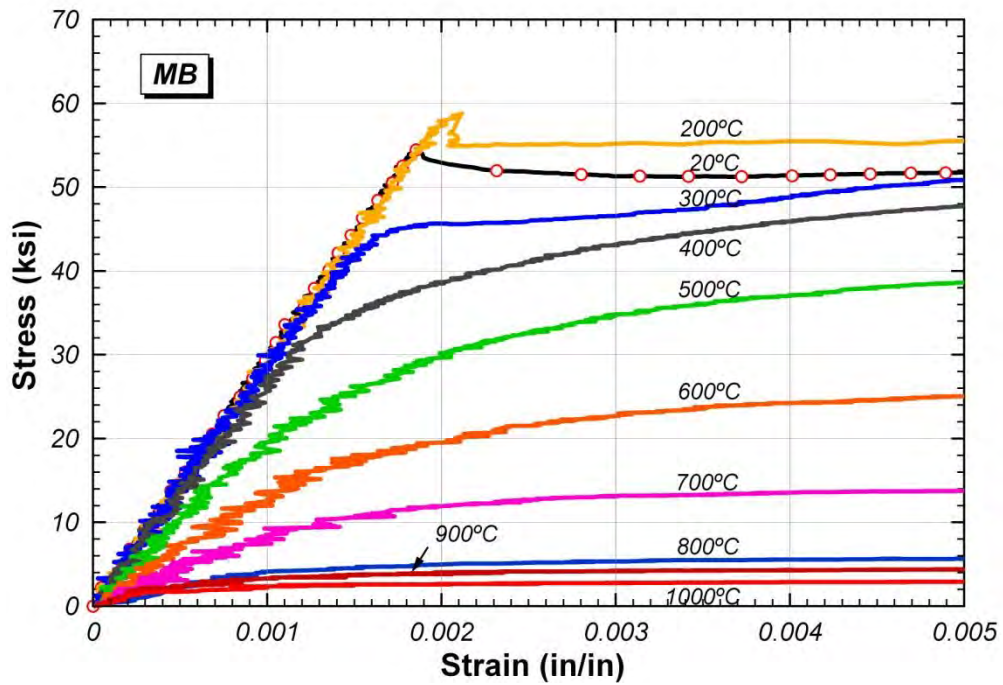
Figure B.6 Initial stress-strain curves for MB material

268
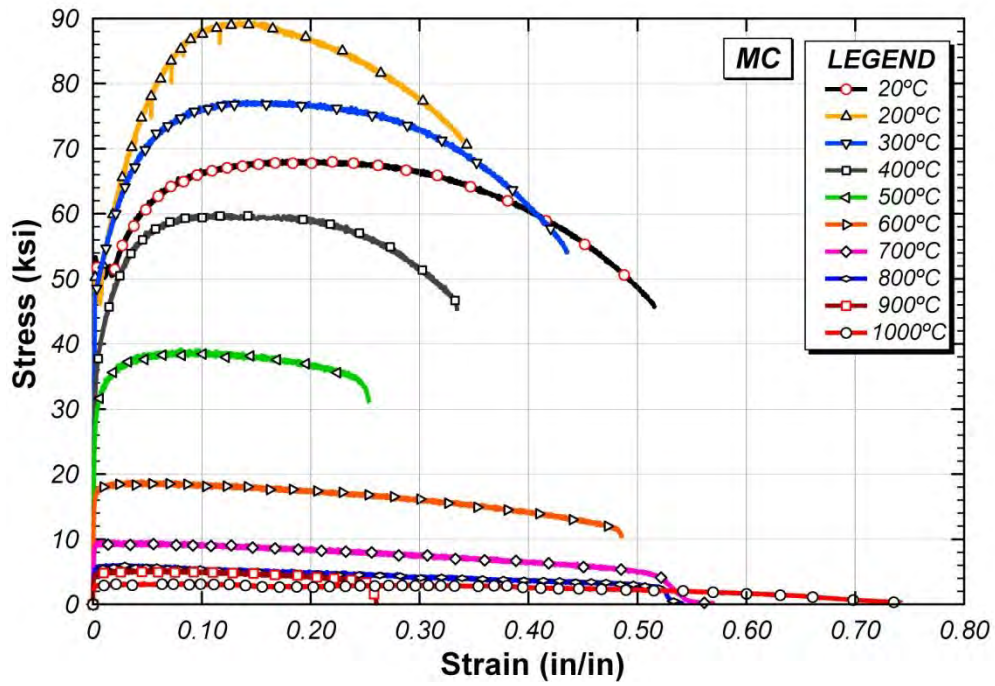
Figure B.7 Full stress-strain curves for MC material
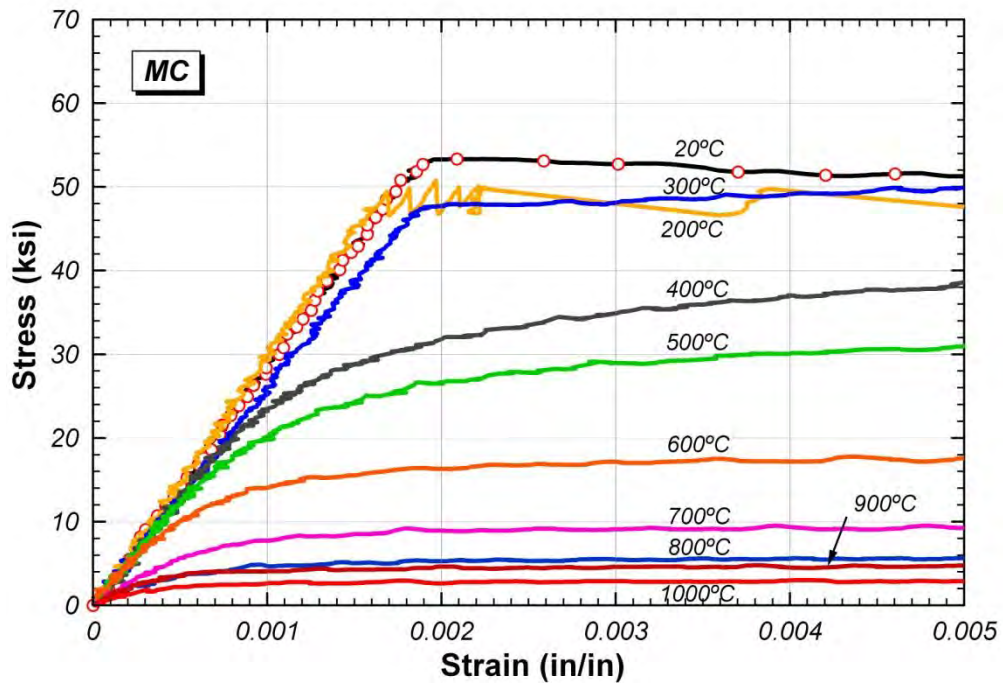
Figure B.8 Initial stress-strain curves for MC material

269
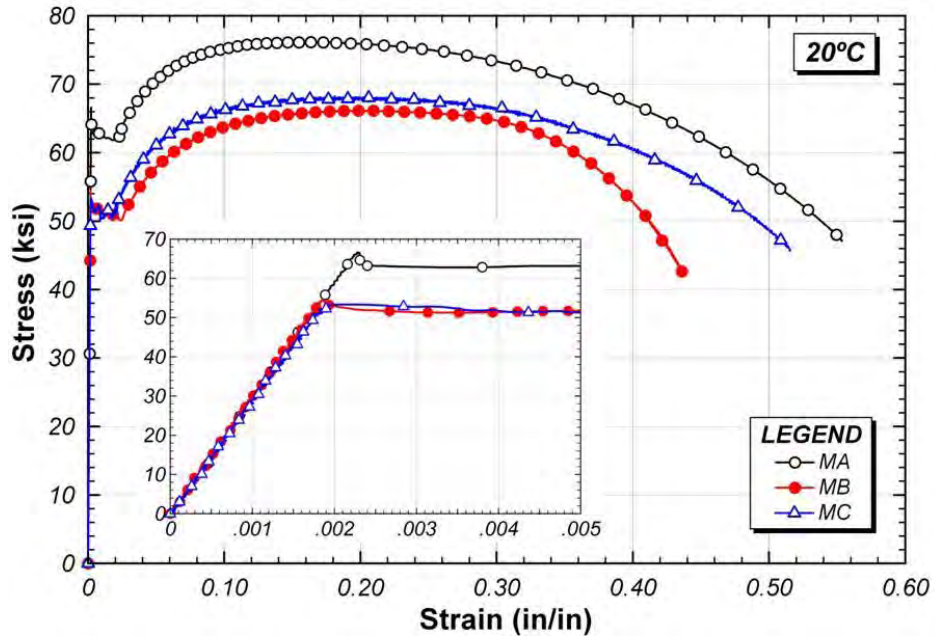
Figure B.9 Combined stress-strain curves at 20°C
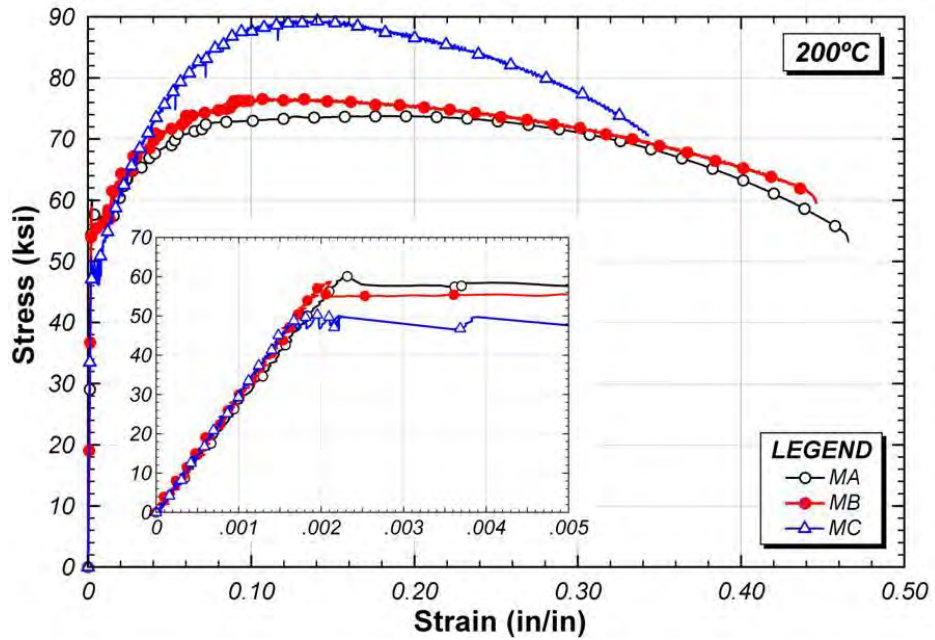
Figure B.10 Combined stress-strain curves at 200°C

270
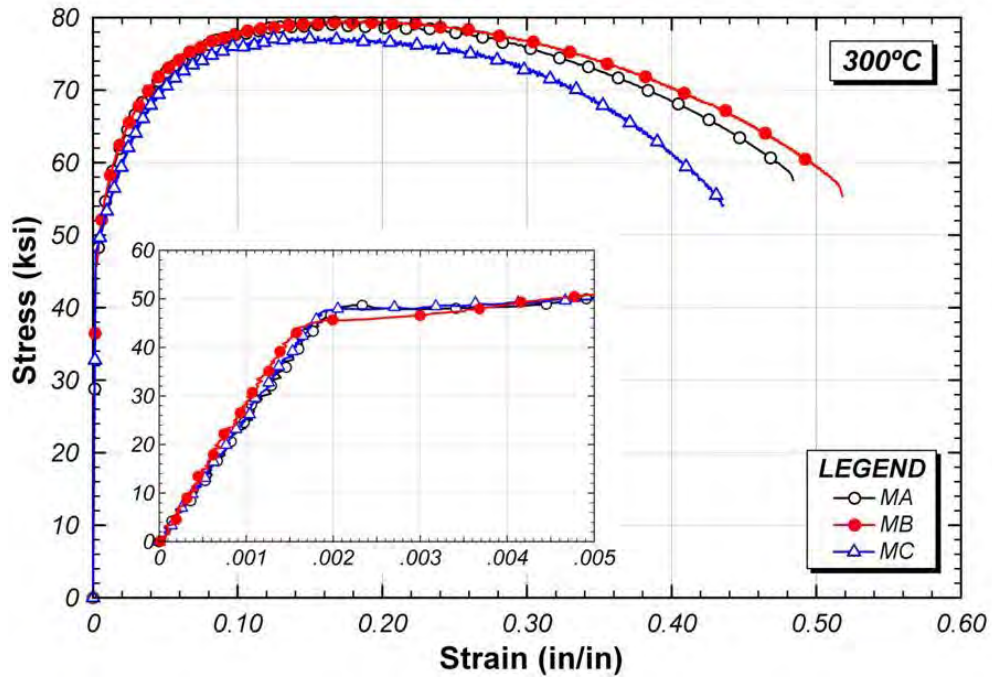
Figure B.11 Combined stress-strain curves at 300°C
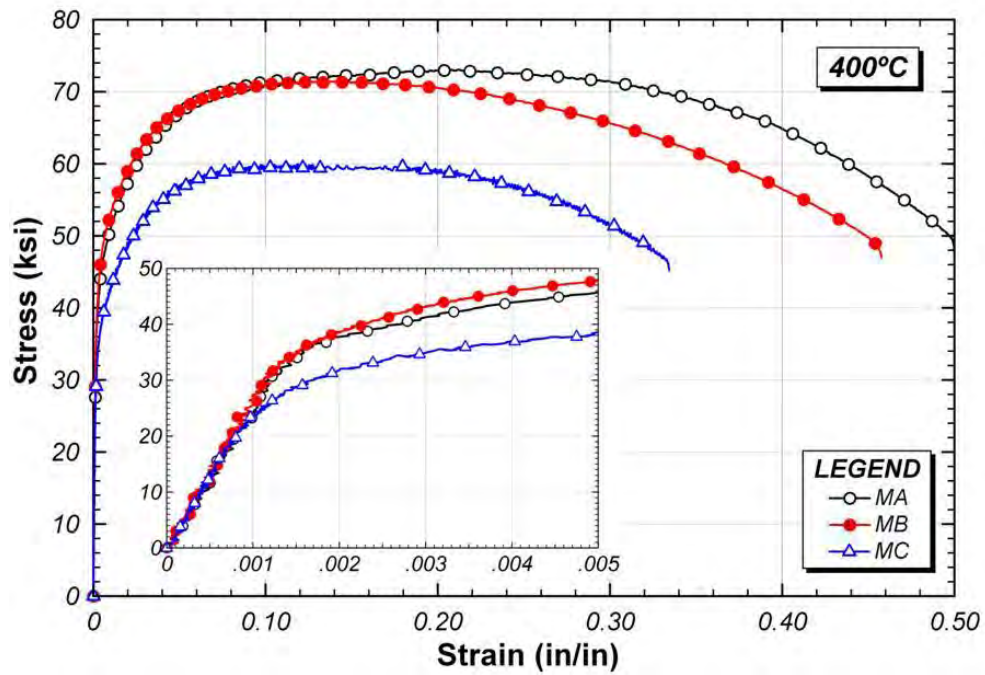
Figure B.12 Combined stress-strain curves at 400°C

271
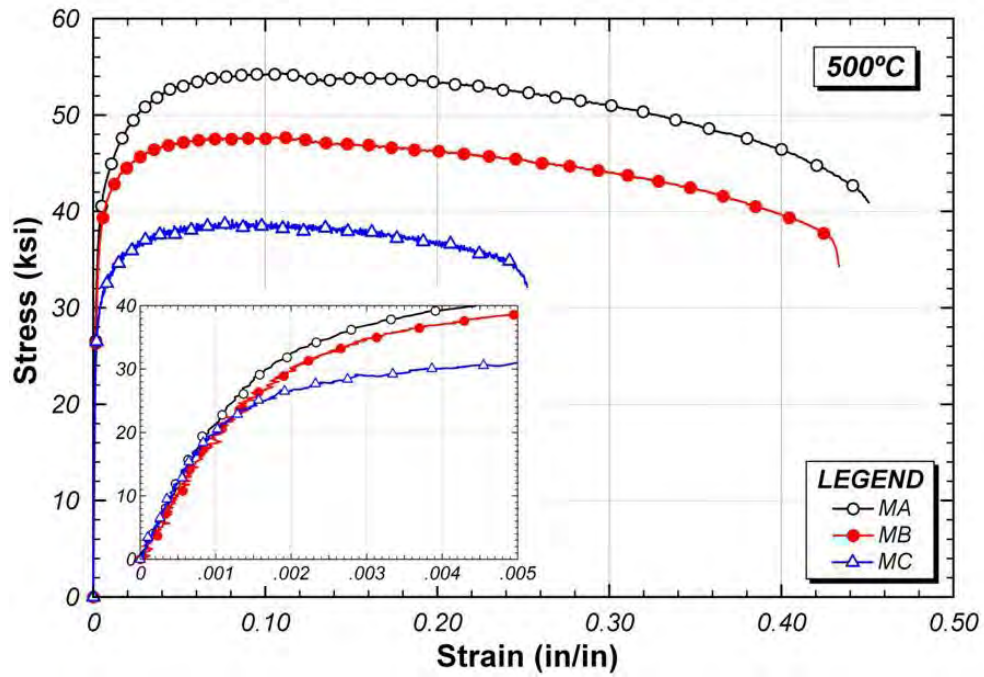
Figure B.13 Combined stress-strain curves at 500°C
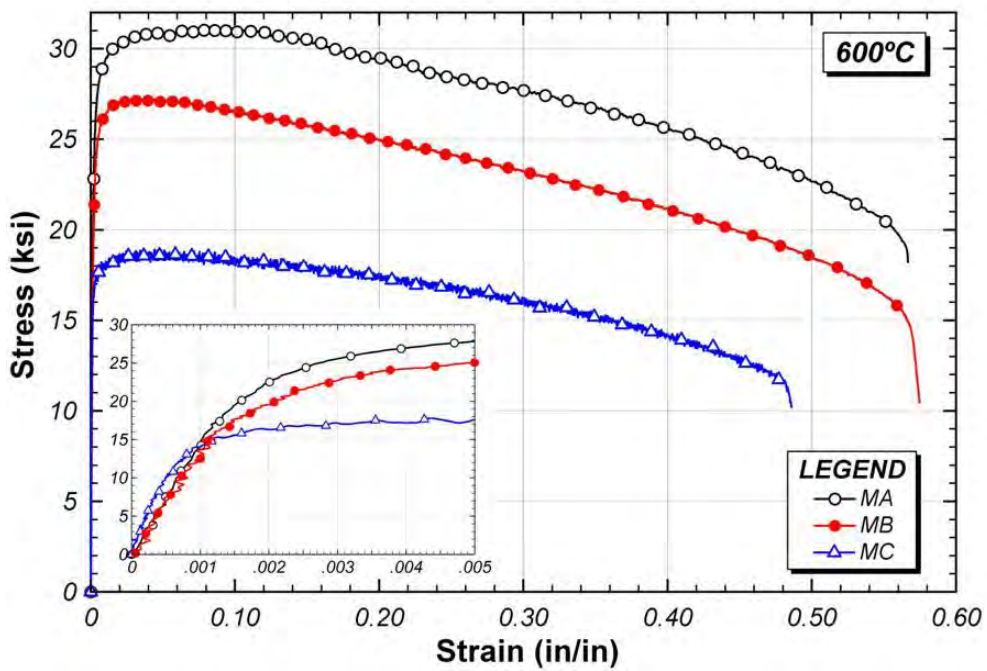
Figure B.14 Combined stress-strain curves at 600°C

272
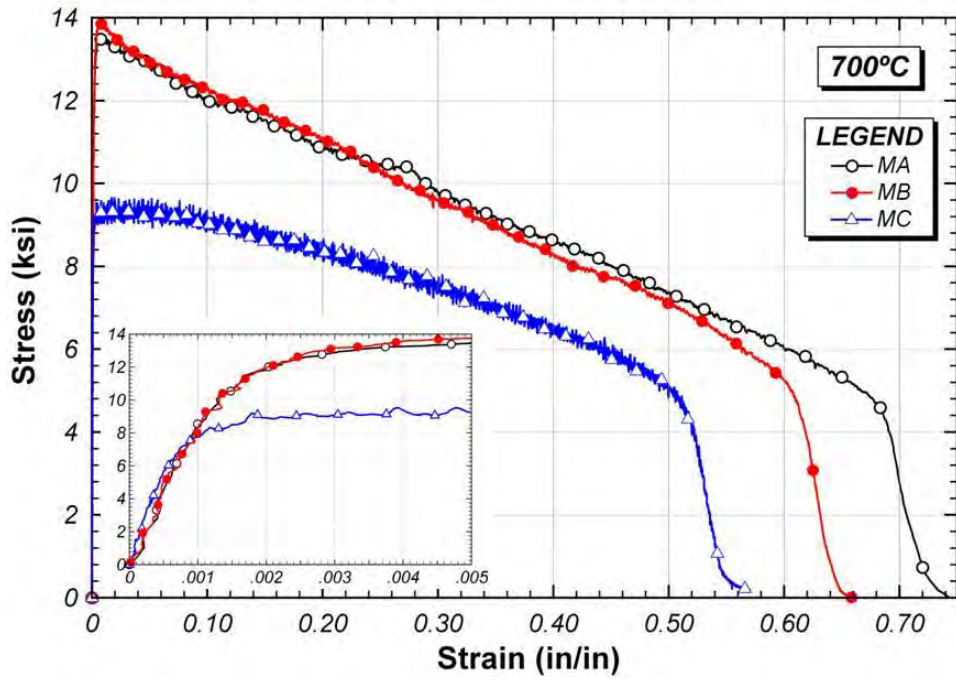
Figure B.15 Combined stress-strain curves at 700°C
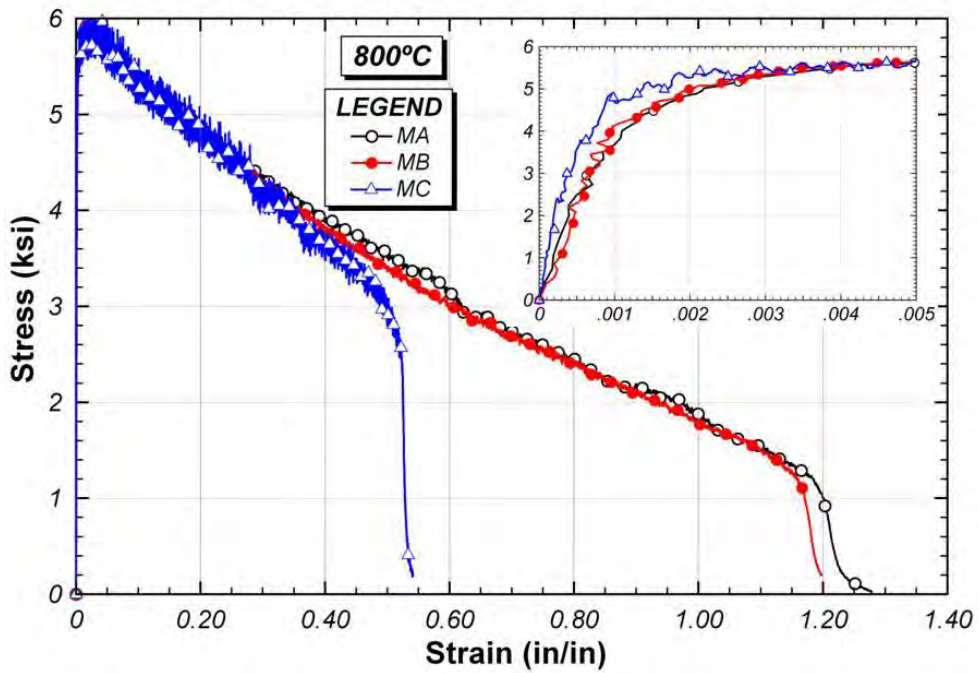
Figure B.16 Combined stress-strain curves at 800°C

273
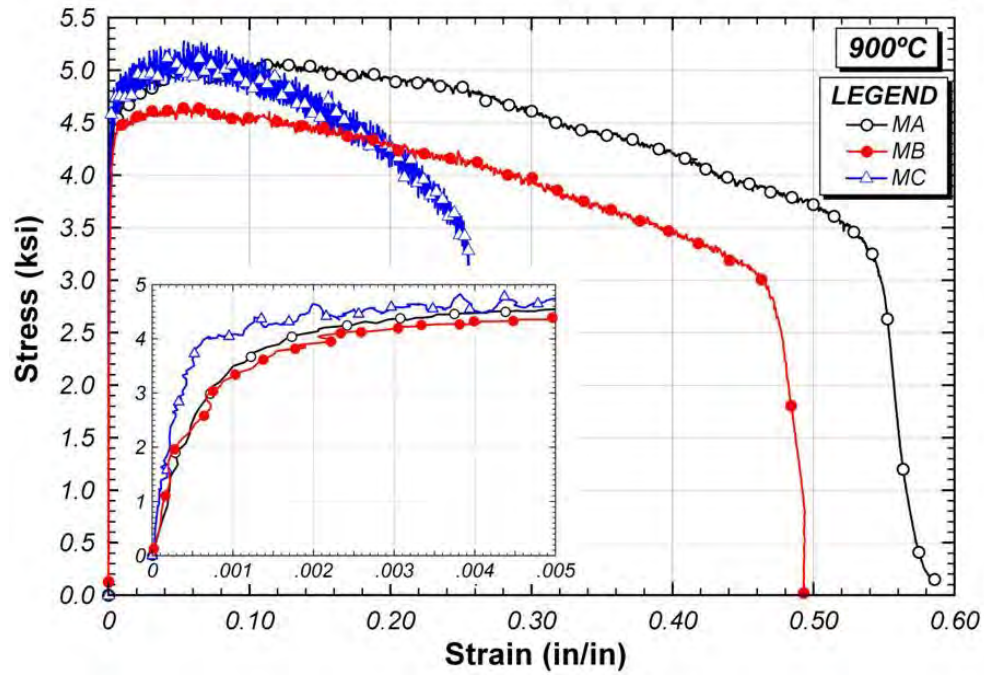
Figure B.17 Combined stress-strain curves at 900°C
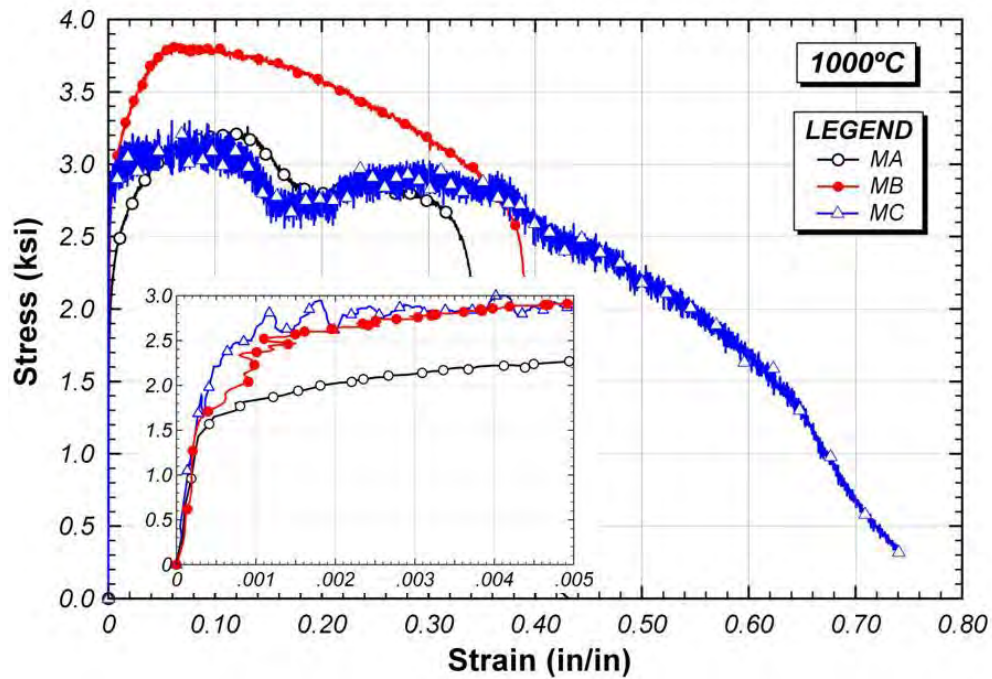
Figure B.18 Combined stress-strain curves at 1000°C

274

B.4 CONSTITUTIVE MODEL
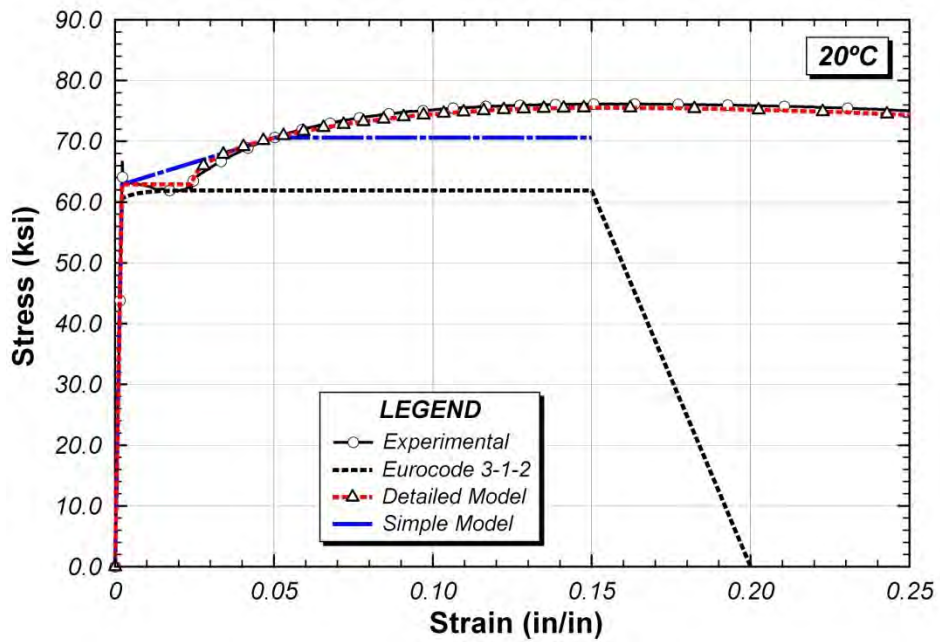
Figure B.19 Initial stress-strain curve of constitutive model at 20°C
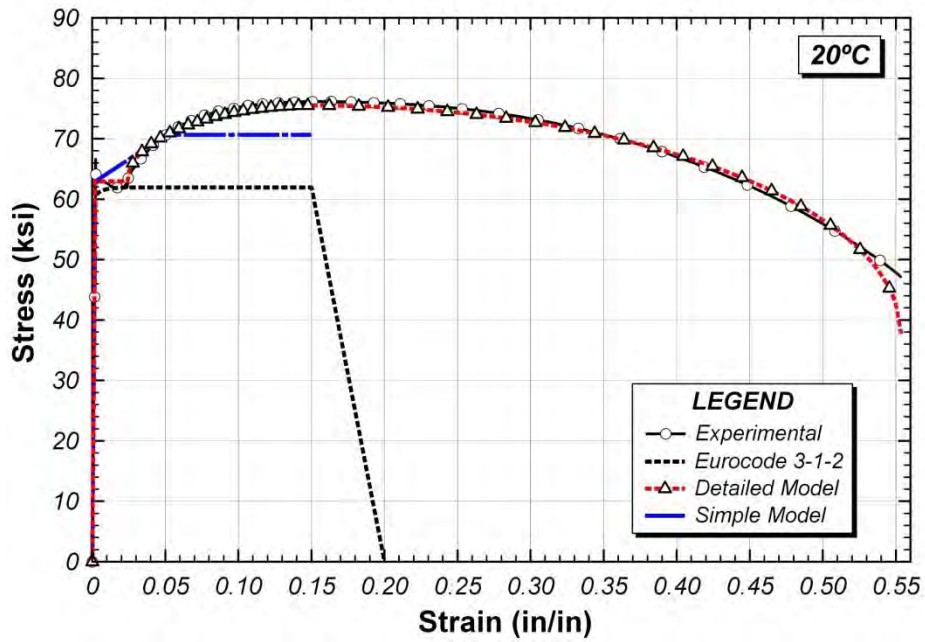
Figure B.20 Full stress-strain curve of constitutive model at 20°C
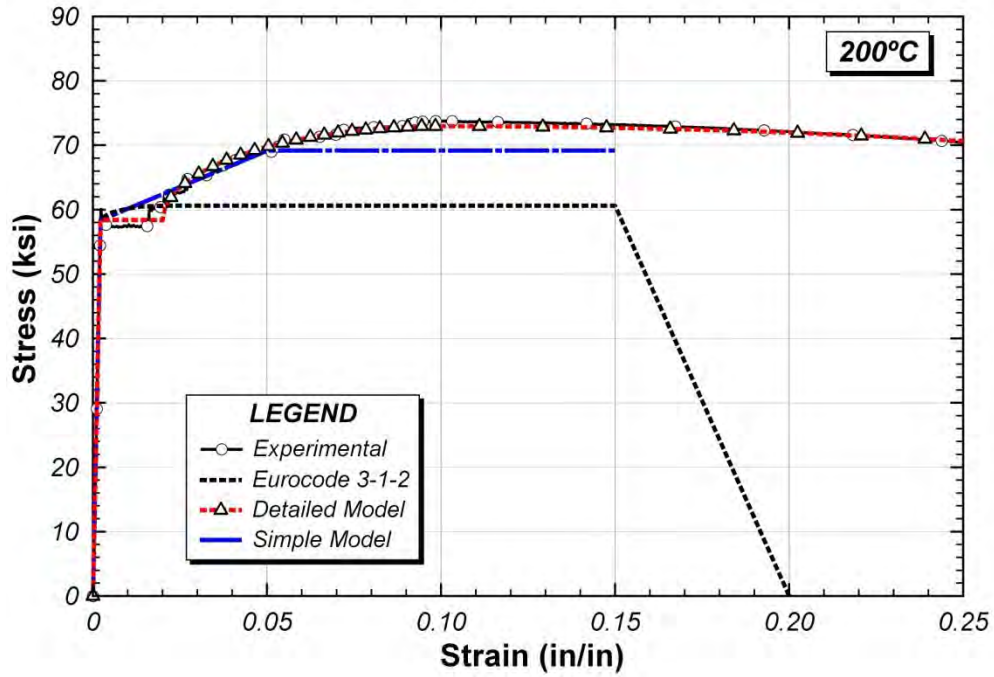
Figure B.21 Initial stress-strain curve of constitutive model at 200°C
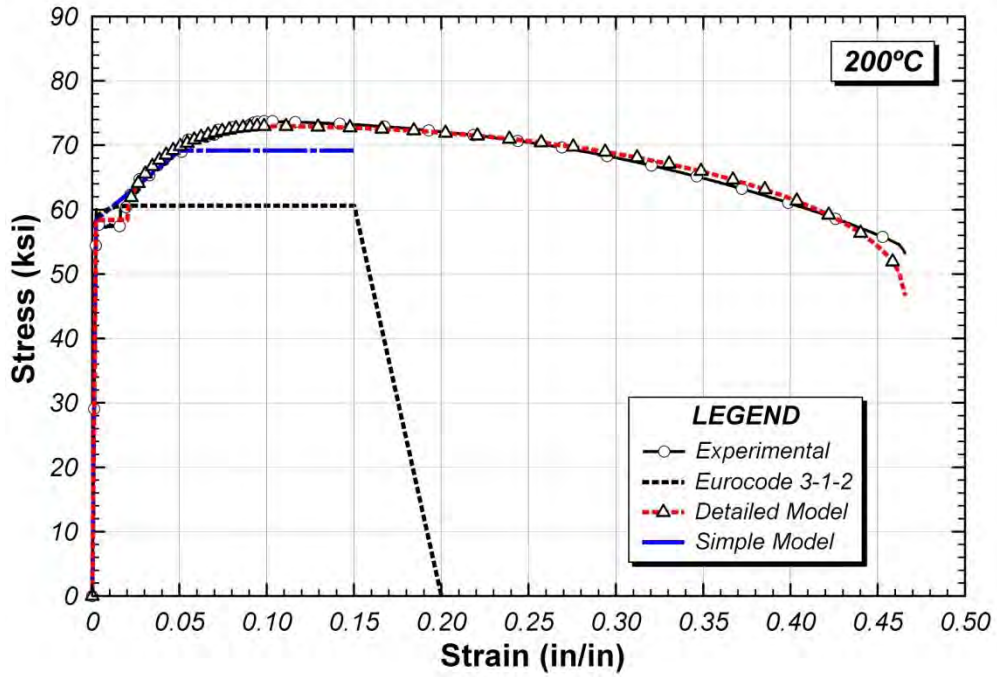
Figure B.22 Full stress-strain curve of constitutive model at 200°C

276
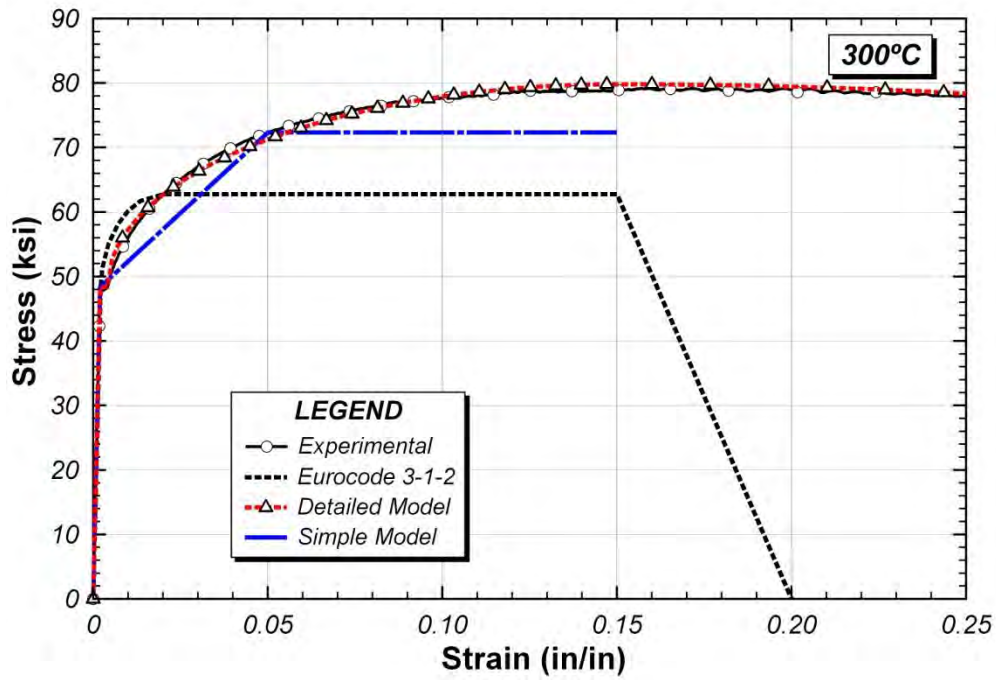
Figure B.23 Initial stress-strain curve of constitutive model at 300°C
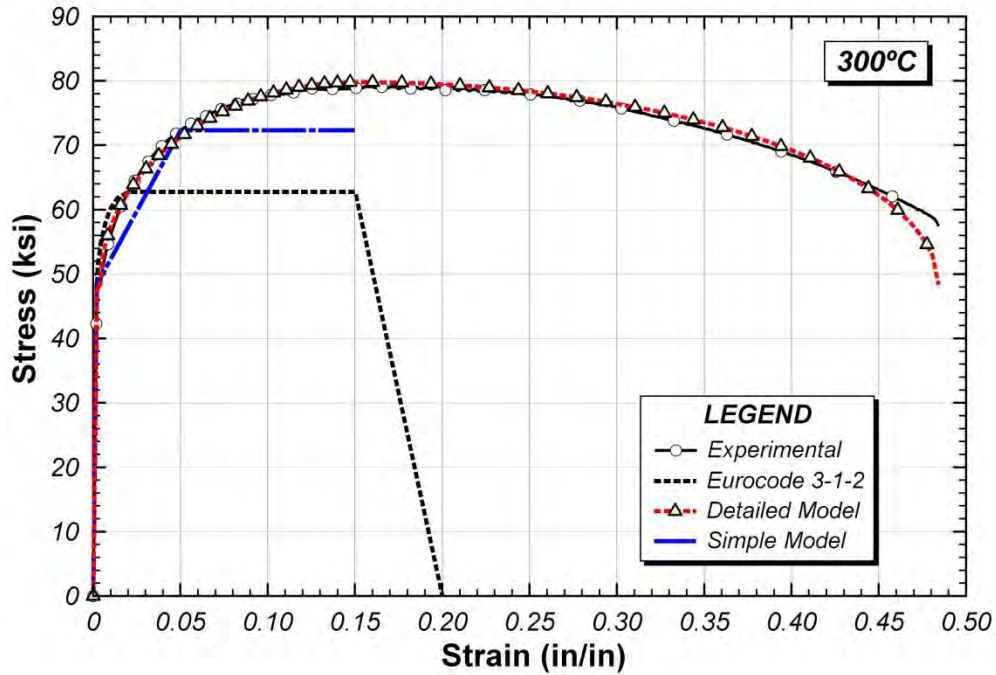
Figure B.24 Full stress-strain curve of constitutive model at 300°C

277
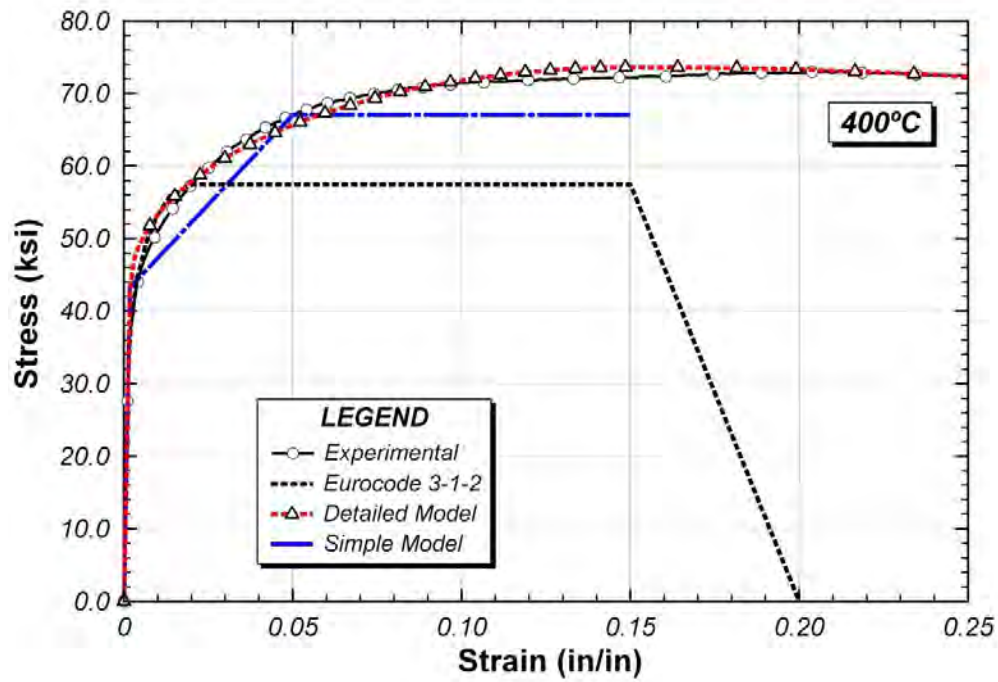
Figure B.25 Initial stress-strain curve of constitutive model at 400°C
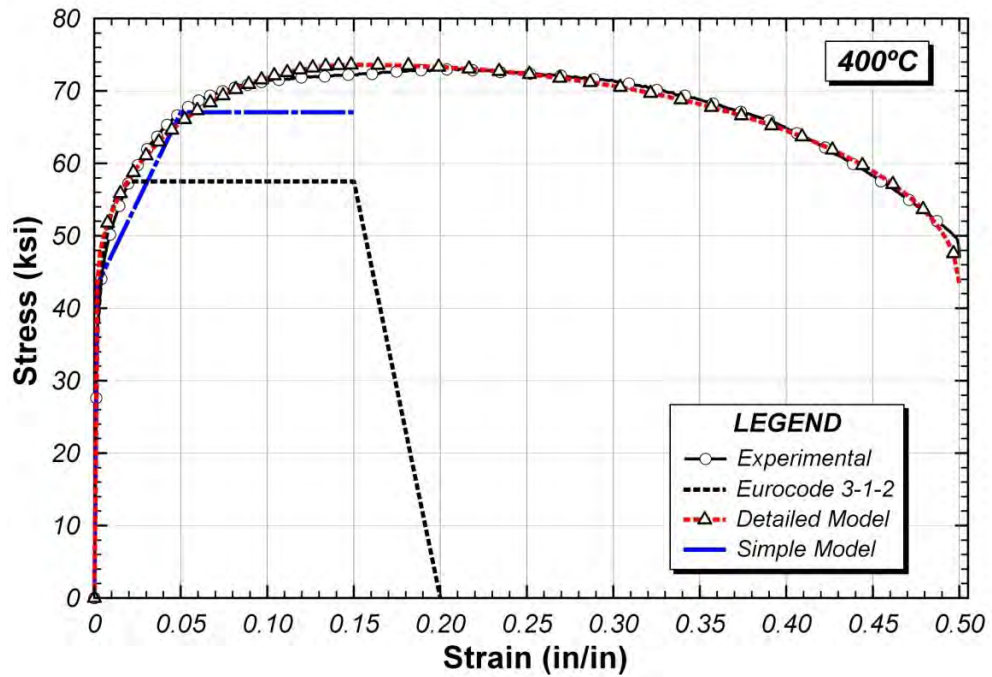
Figure B.26 Full stress-strain curve of constitutive model at 400°C

278
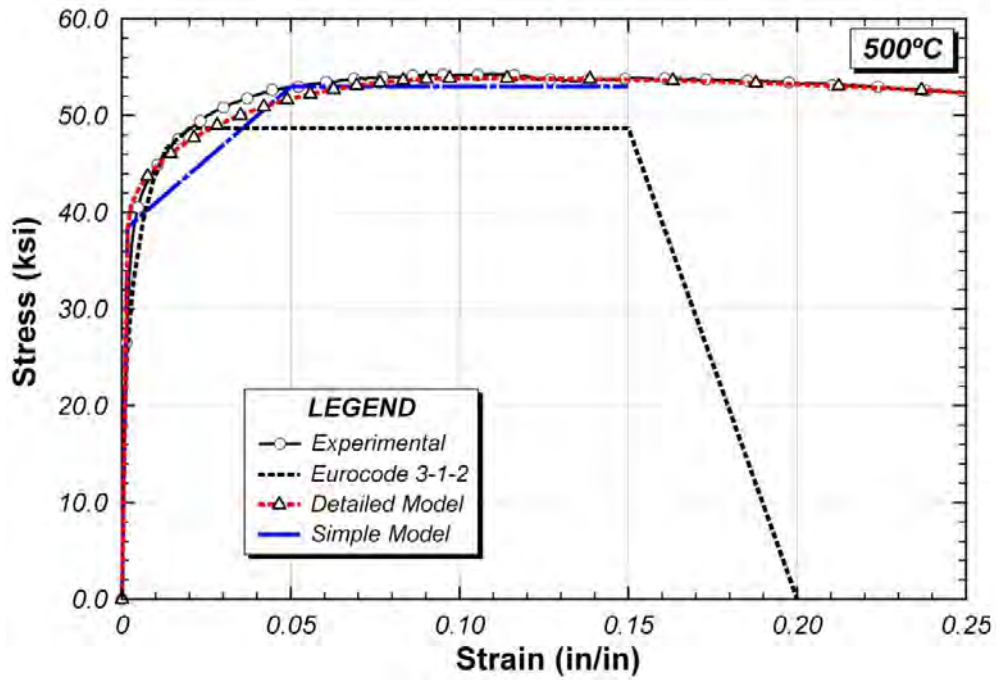
Figure B.27 Initial stress-strain curve of constitutive model at 500°C
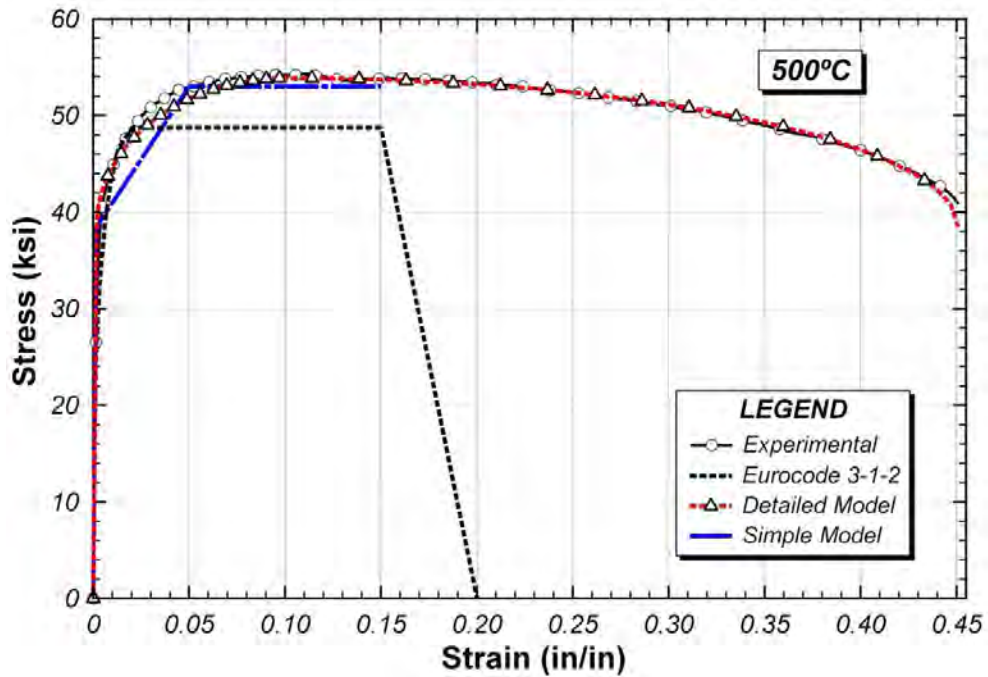
Figure B.28 Full stress-strain curve of constitutive model at 500°C

279
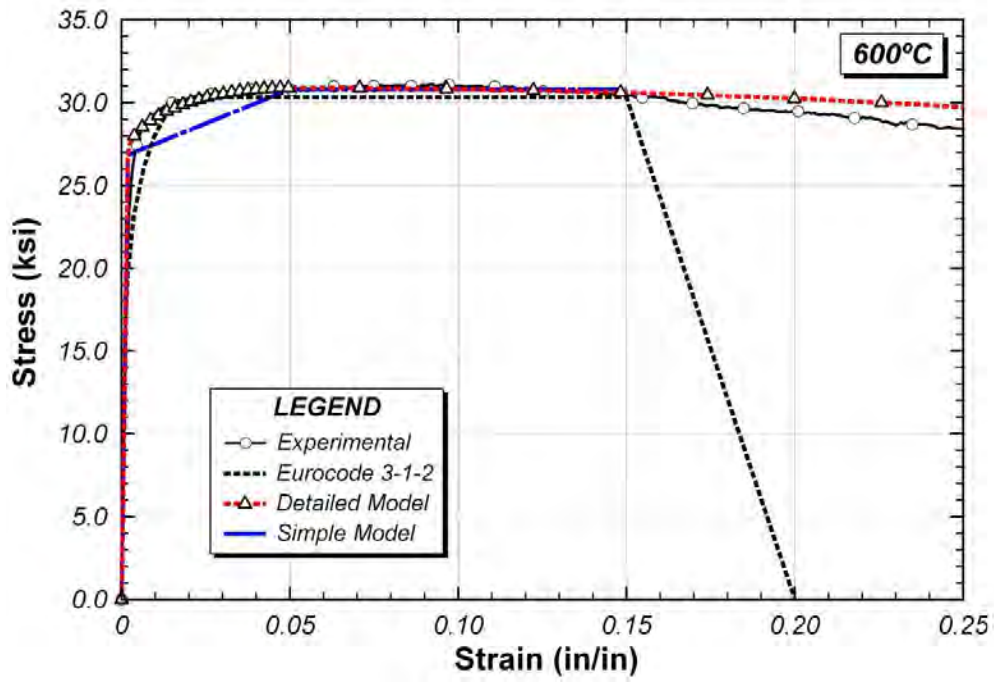
Figure B.29 Initial stress-strain curve of constitutive model at 600°C
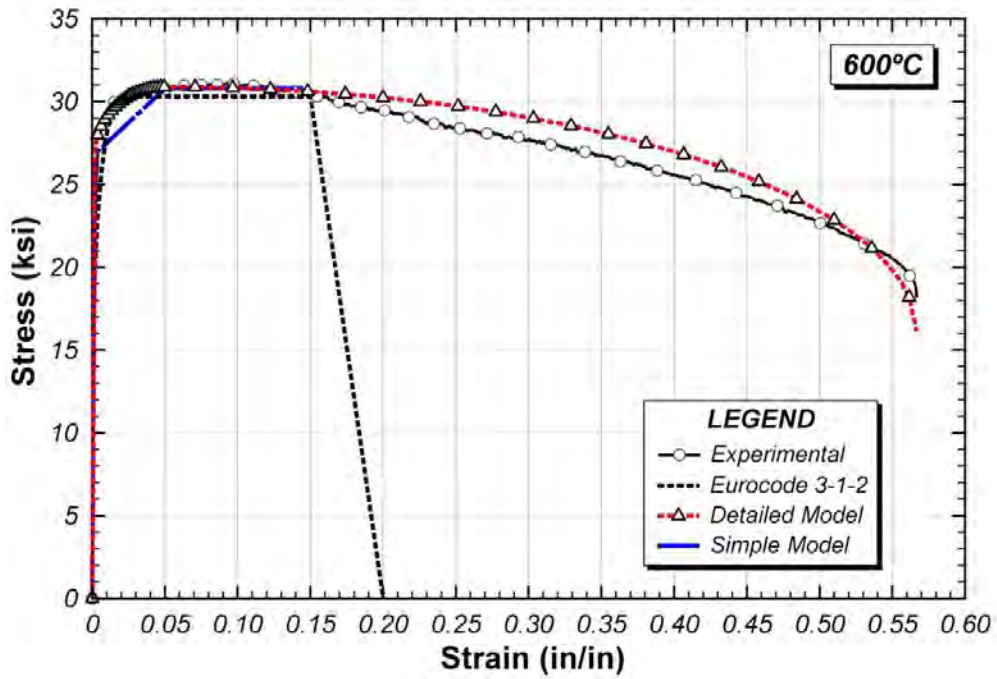
Figure B.30 Full stress-strain curve of constitutive model at 600°C

280
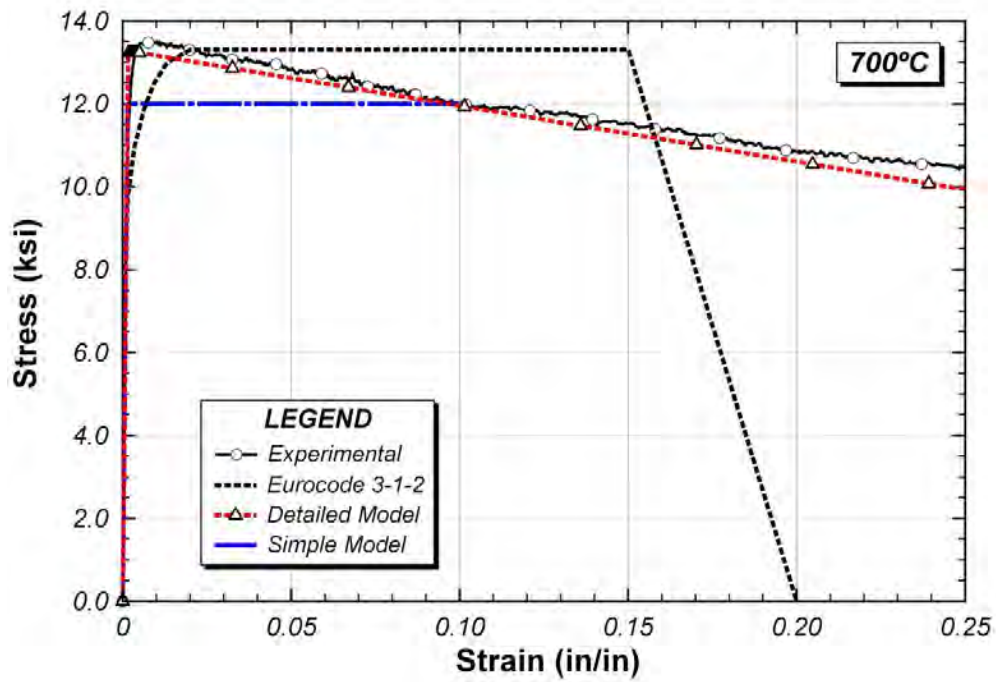
Figure B.31 Initial stress-strain curve of constitutive model at 700°C
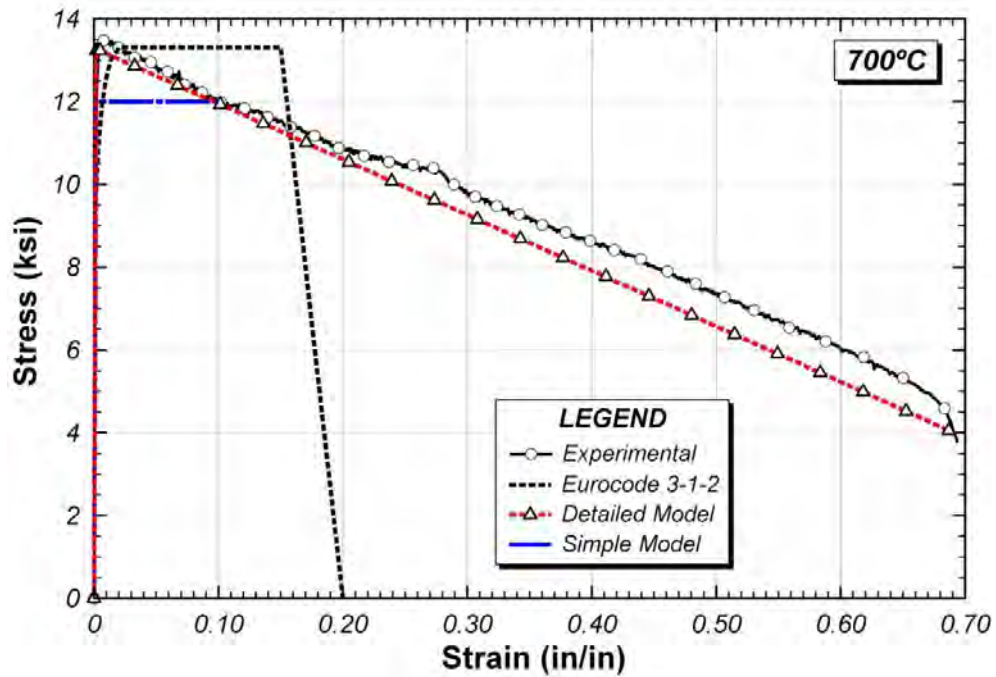
Figure B.32 Full stress-strain curve of constitutive model at 700°C

281
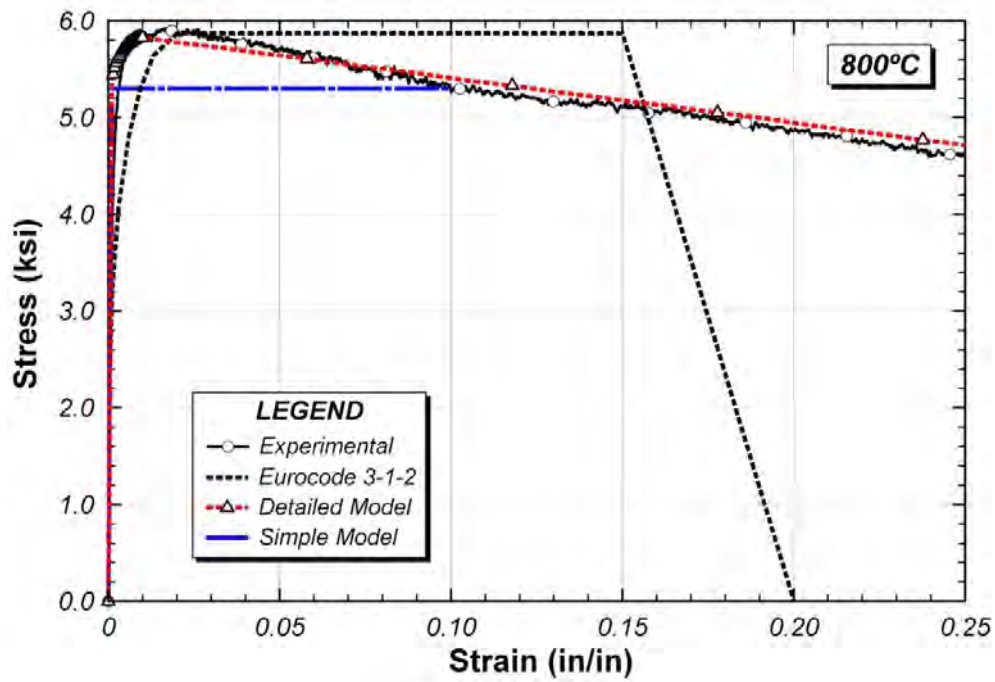
Figure B.33 Initial stress-strain curve of constitutive model at 800°C
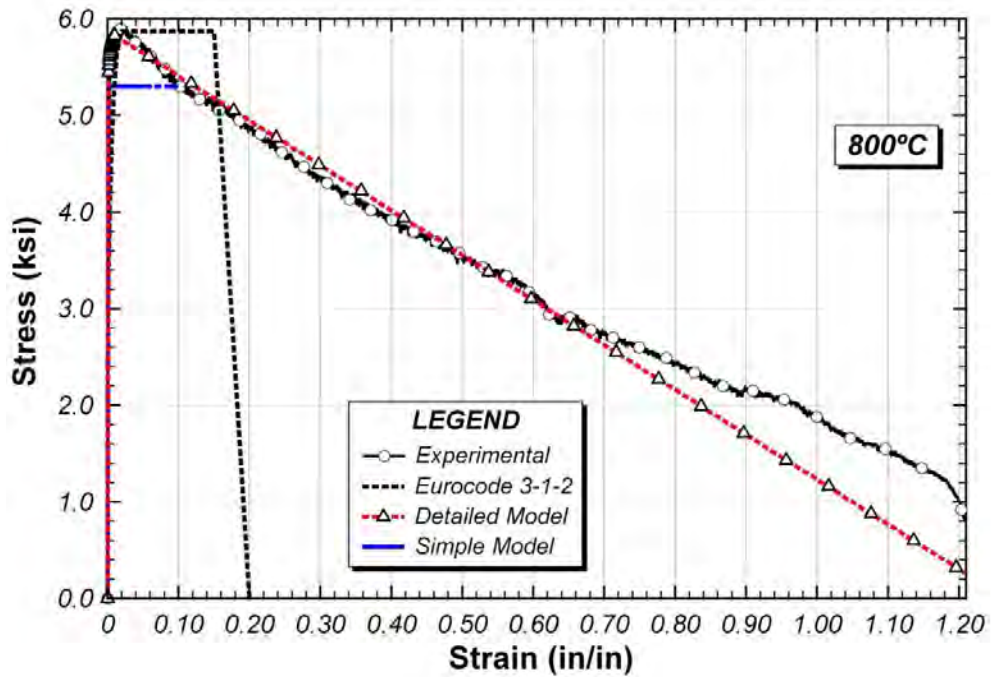
Figure B.34 Full stress-strain curve of constitutive model at 800°C

282
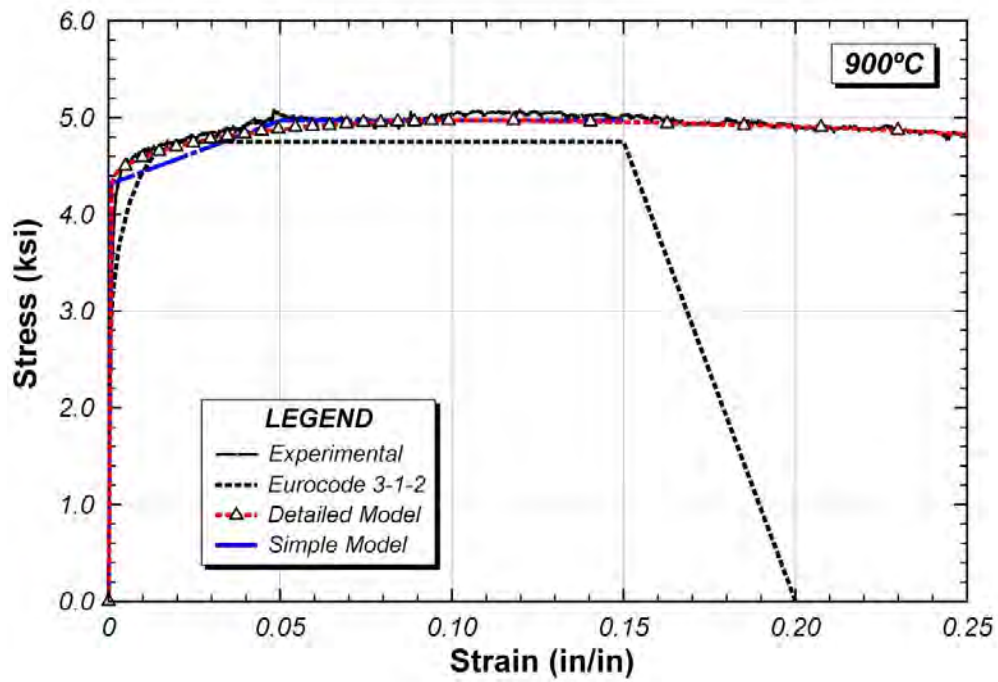
Figure B.35 Initial stress-strain curve of constitutive model at 900°C
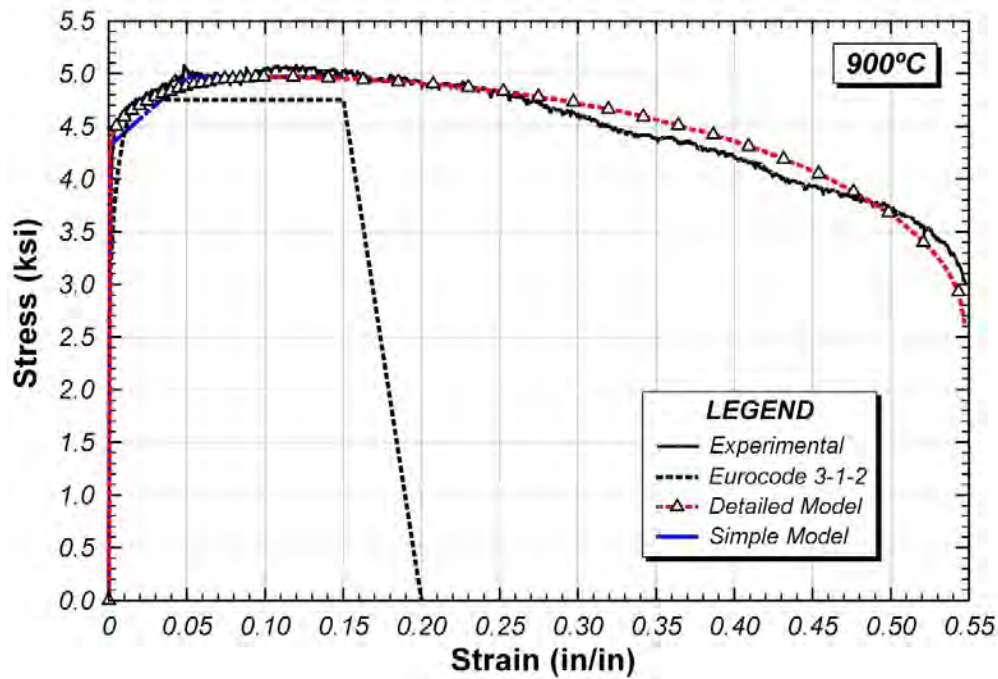
Figure B.36 Full stress-strain curve of constitutive model at 900°C

283
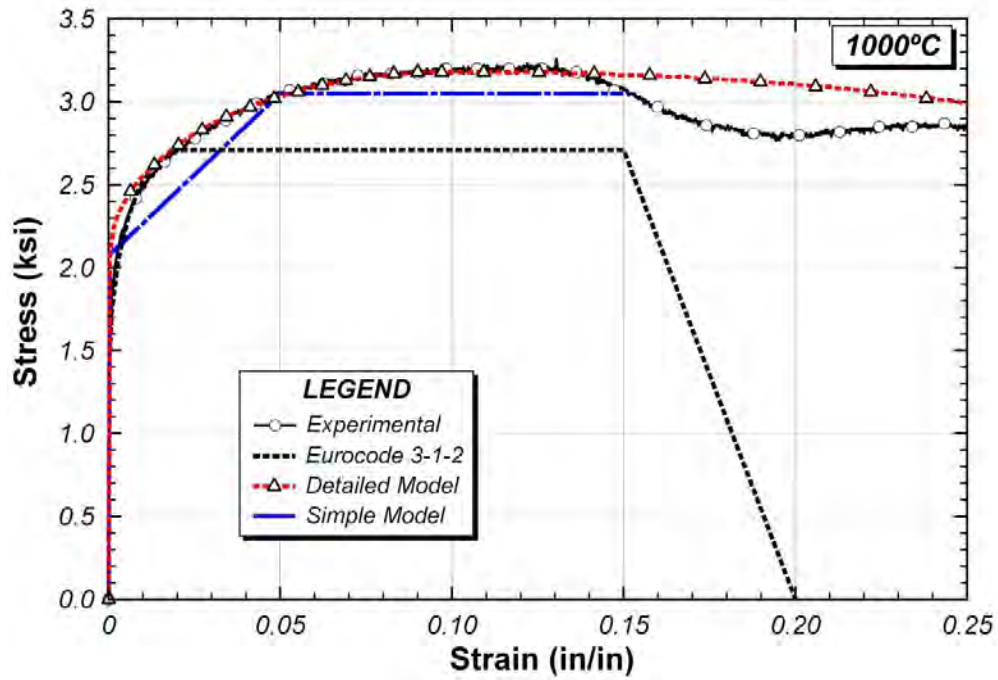
Figure B.37 Initial stress-strain curve of constitutive model at 1000°C
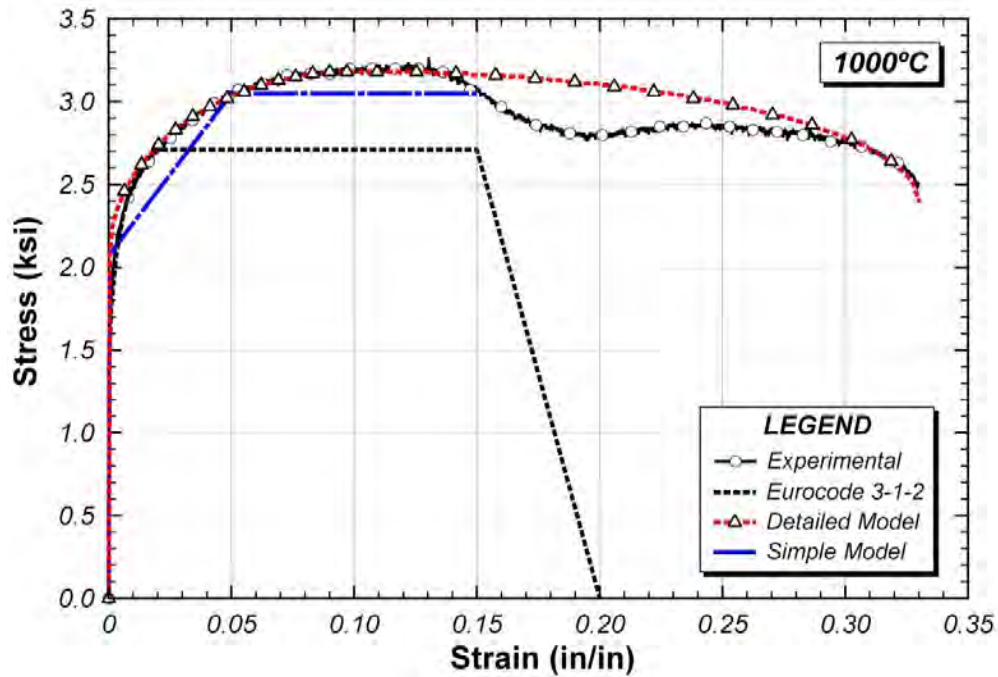
Figure B.38 Full stress-strain curve of constitutive model at 1000°C

APPENDIX C

Tension Test Results after Heating and Cooling

This appendix presented representative tension test results after heating up to specific target temperature and cooling down to room temperature and discussed in Chapter 5.

C.1   STRESS-STRAIN CURVES BY TEMPERATURE
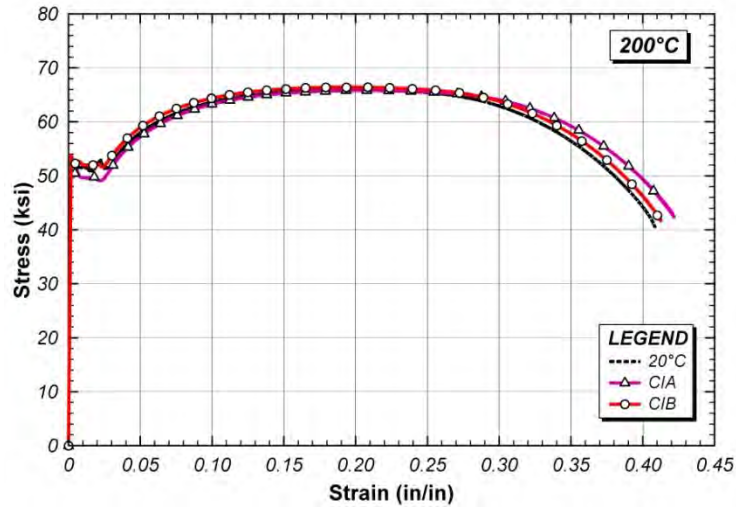
Figure C.1 Combined full stress-strain curve at 200°C
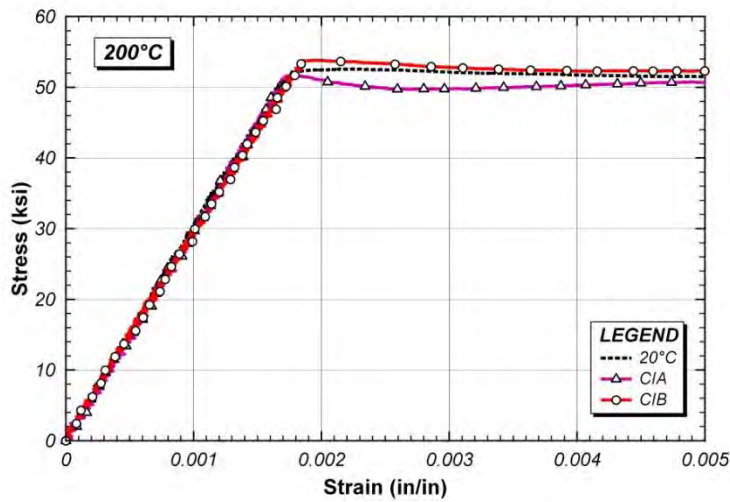
Figure C.2 Combined initial stress-strain curve at 200°C

285
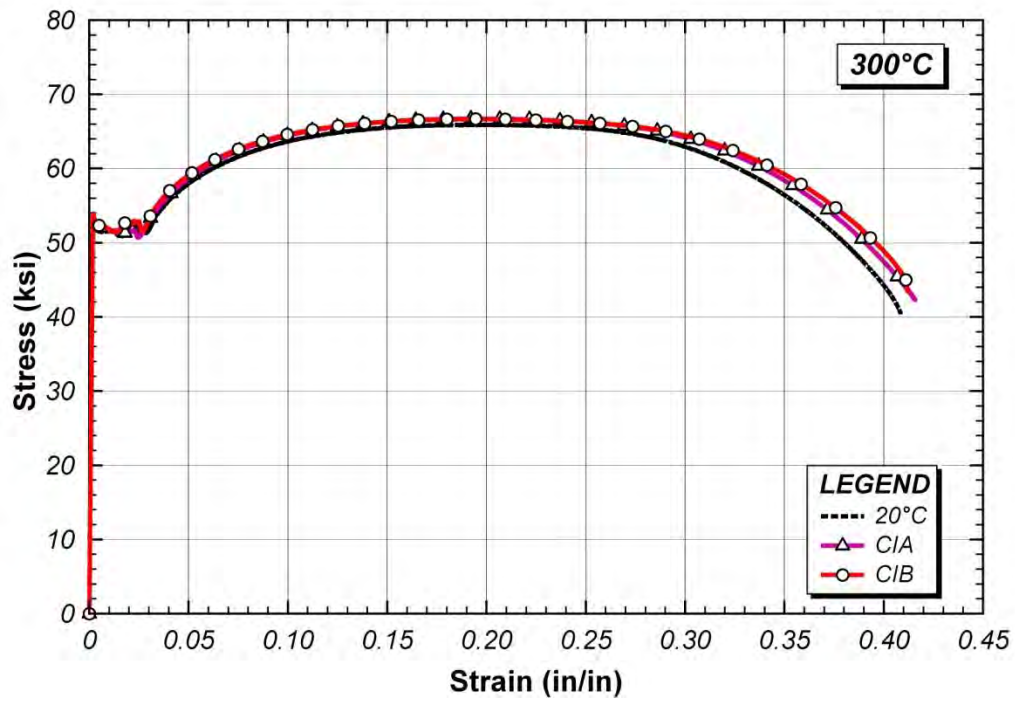
Figure C.3 Combined full stress-strain curve at 300°C
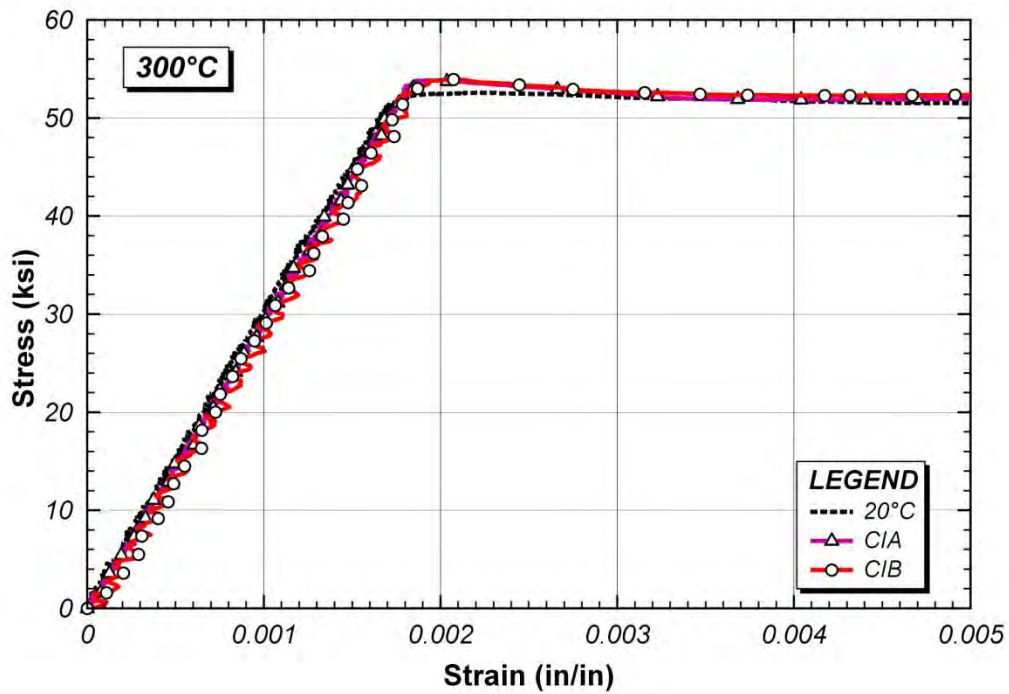
Figure C.4 Combined initial stress-strain curve at 300°C

286
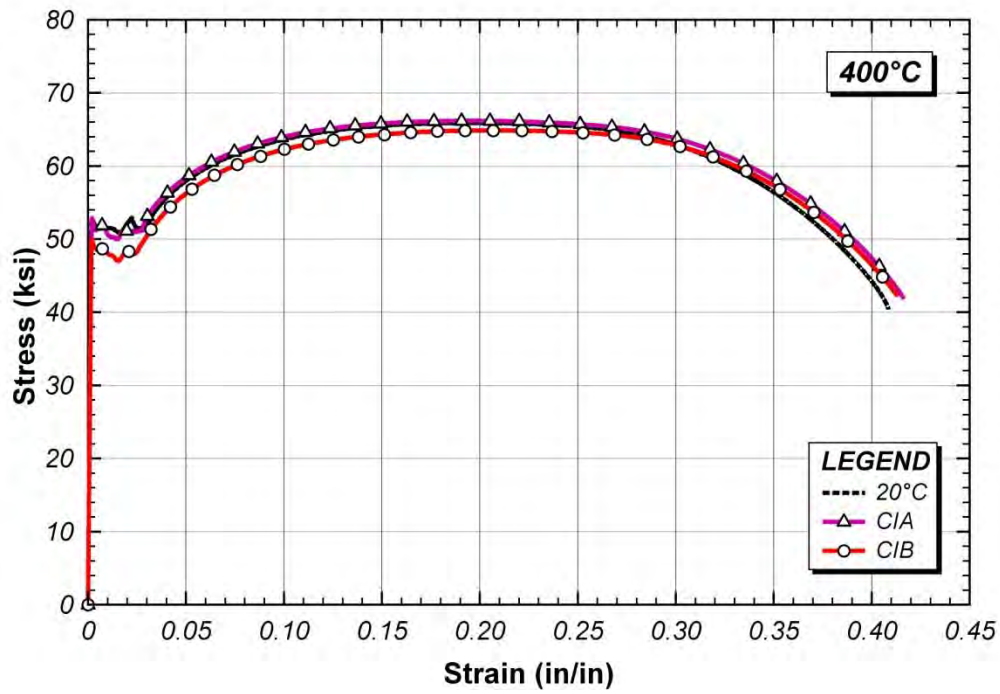
Figure C.5 Combined full stress-strain curve at 400°C
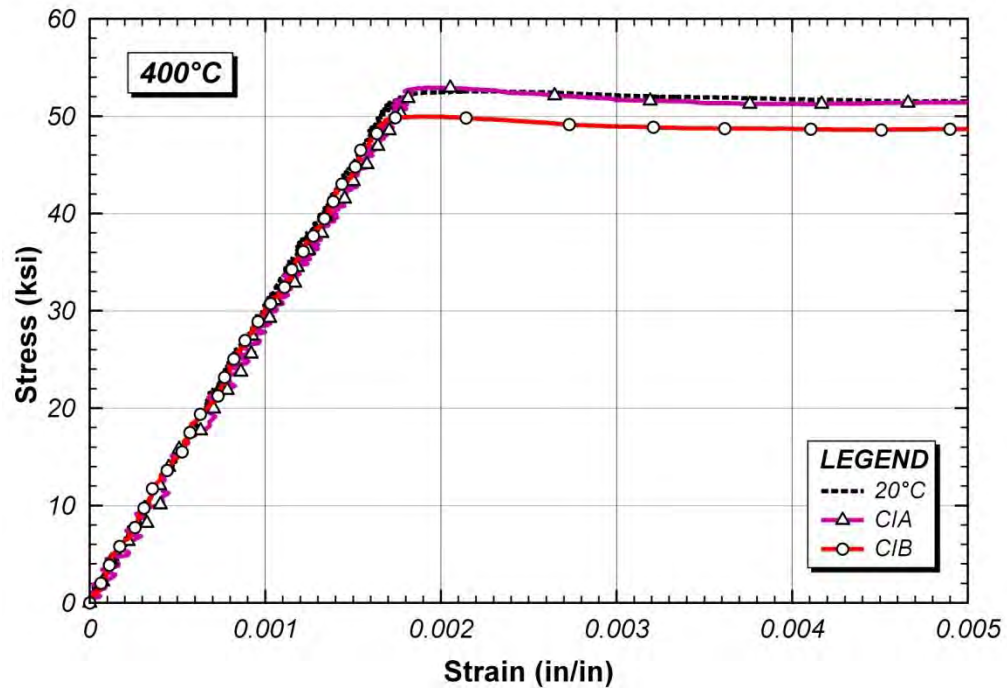
Figure C.6 Combined initial stress-strain curve at 400°C

287
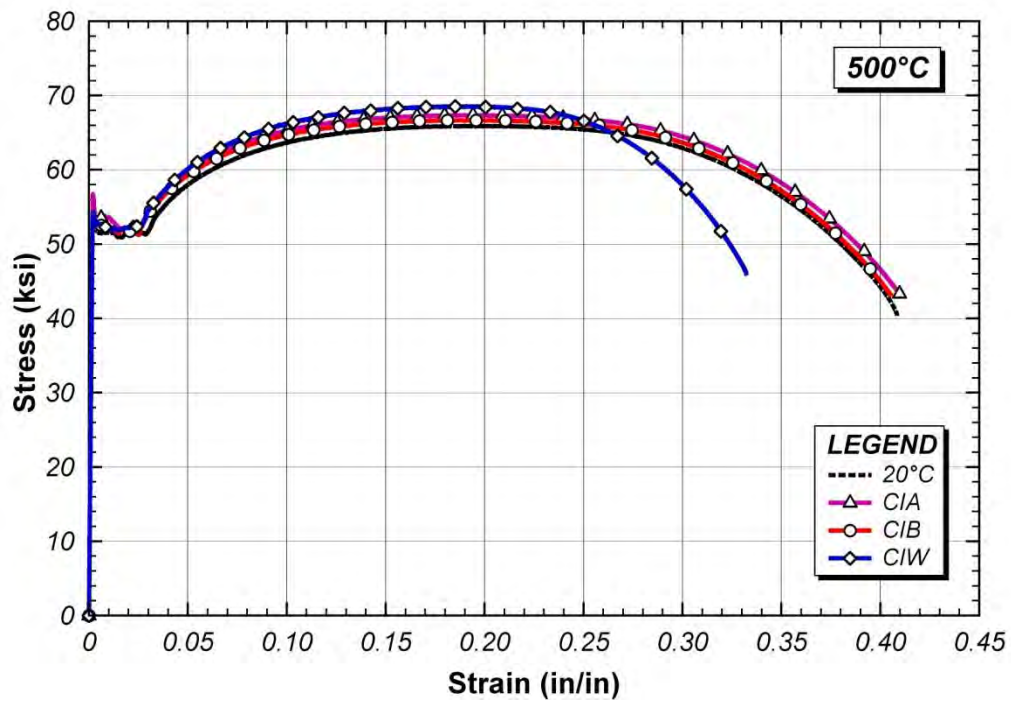
Figure C.7 Combined full stress-strain curve at 500°C
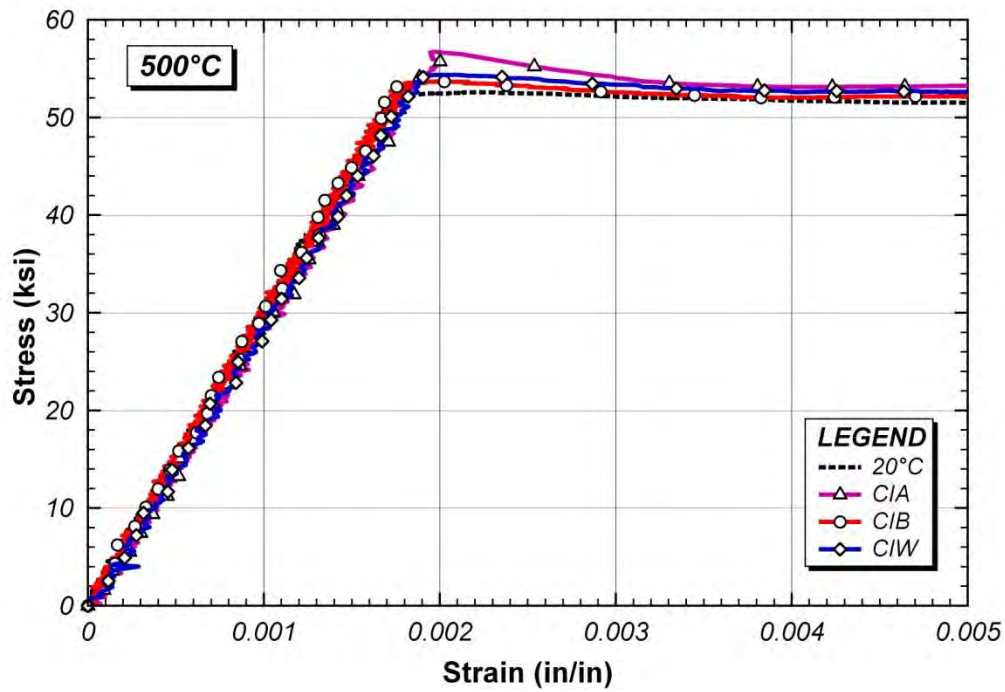
Figure C.8 Combined initial stress-strain curve at 500°C

288
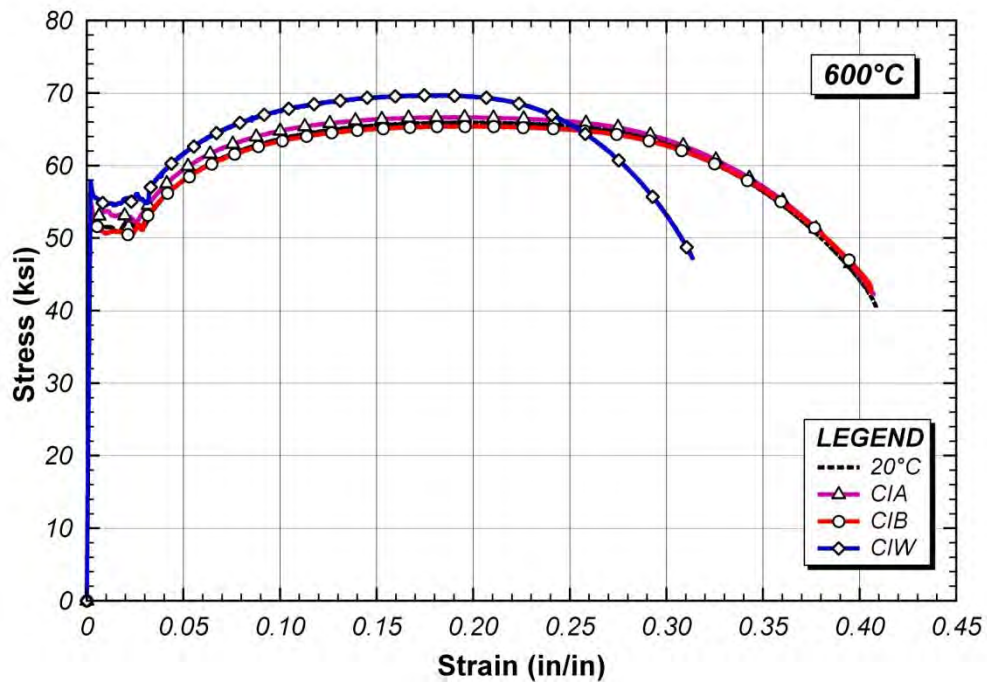
Figure C.9 Combined full stress-strain curve at 600°C
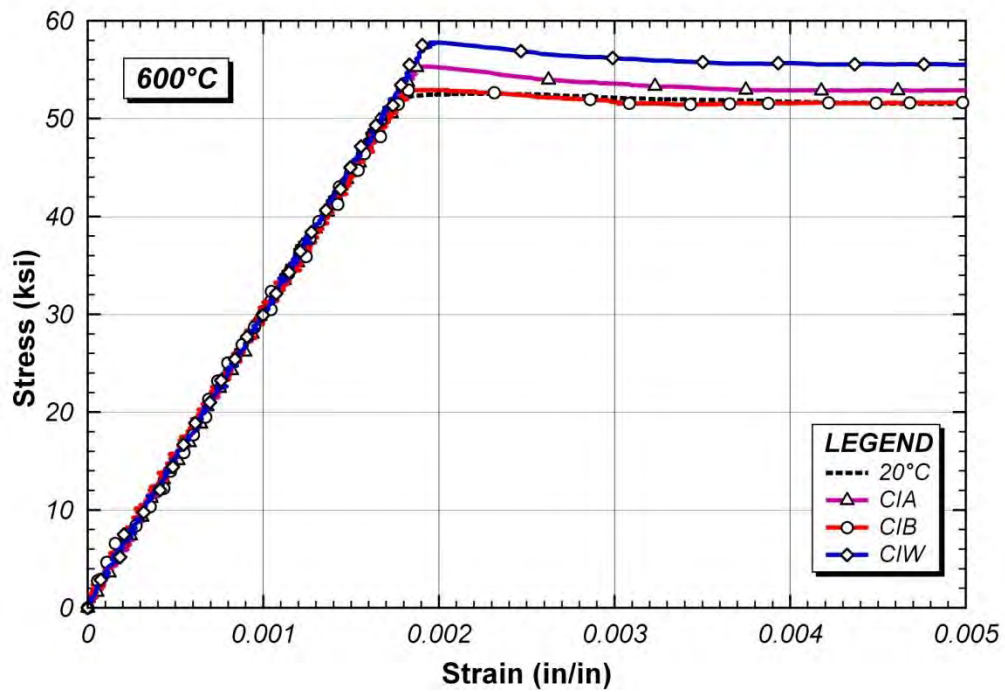
Figure C.10 Combined initial stress-strain curve at 600°C

289
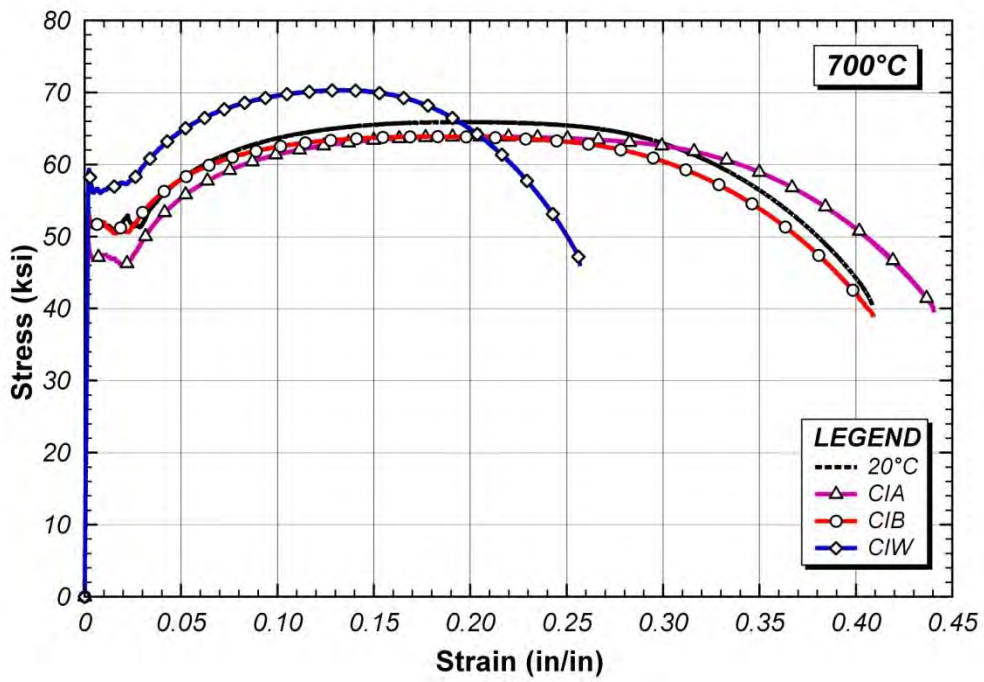
Figure C.11 Combined full stress-strain curve at 700°C
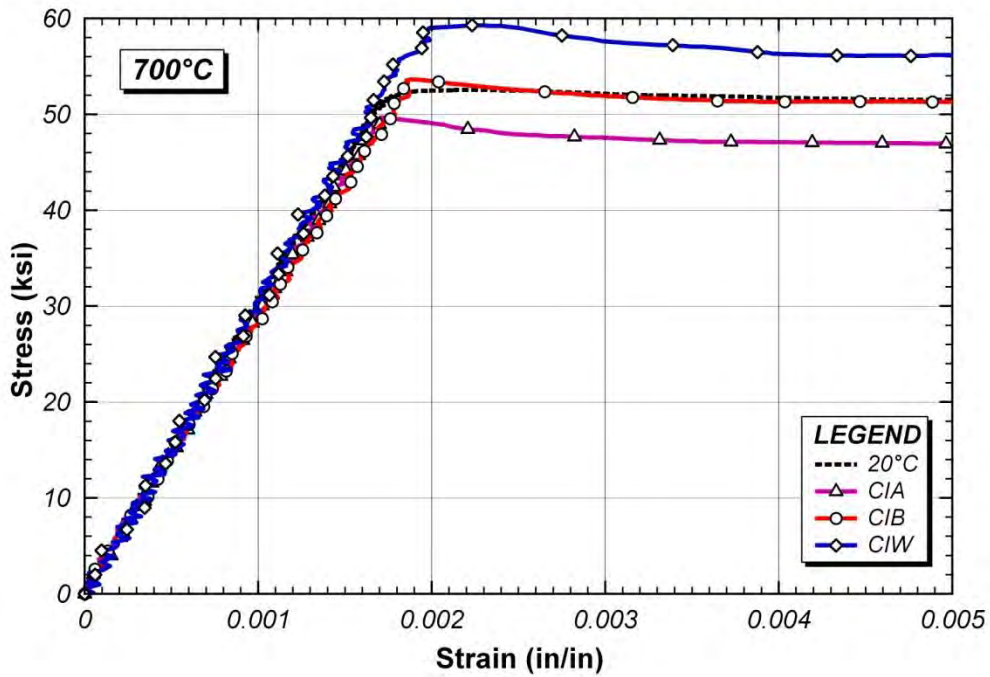
Figure C.12 Combined initial stress-strain curve at 700°C

290
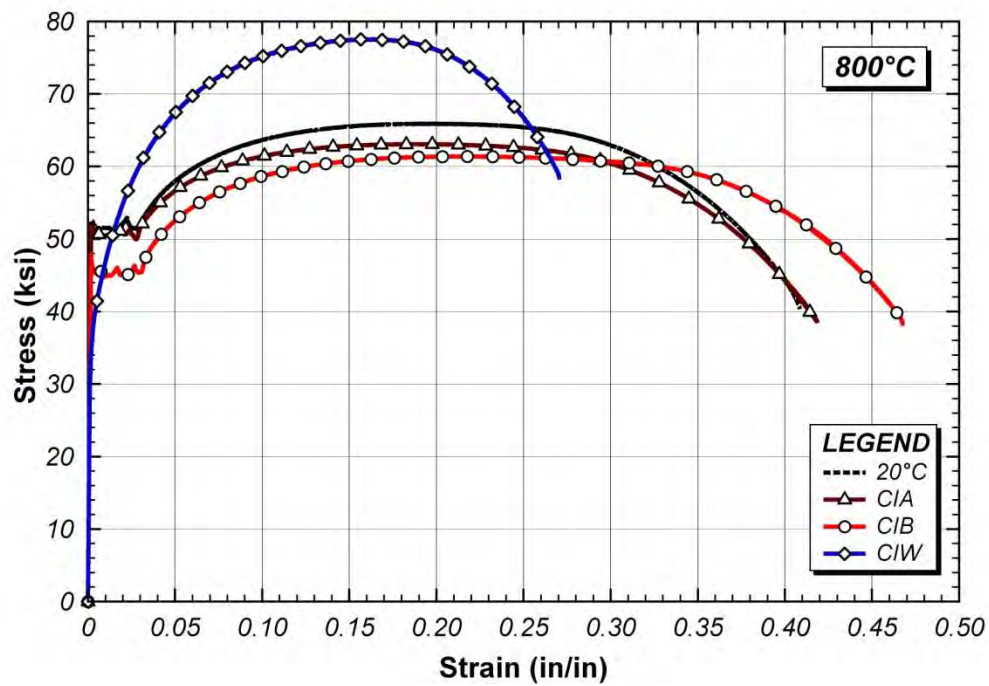
Figure C.13 Combined full stress-strain curve at 800°C
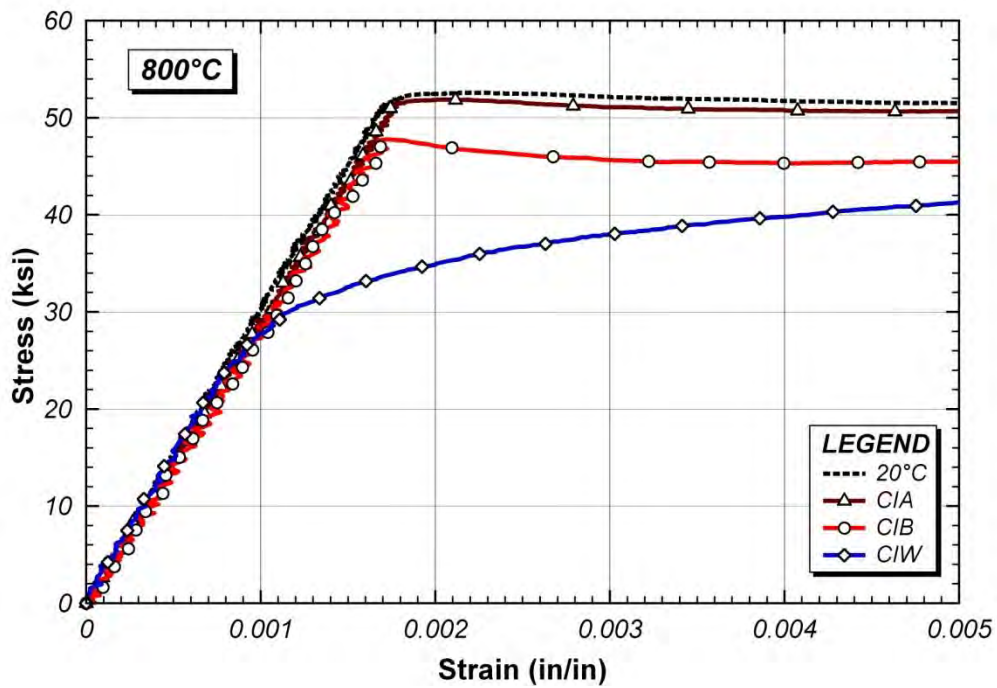
Figure C.14 Combined initial stress-strain curve at 800°C

291
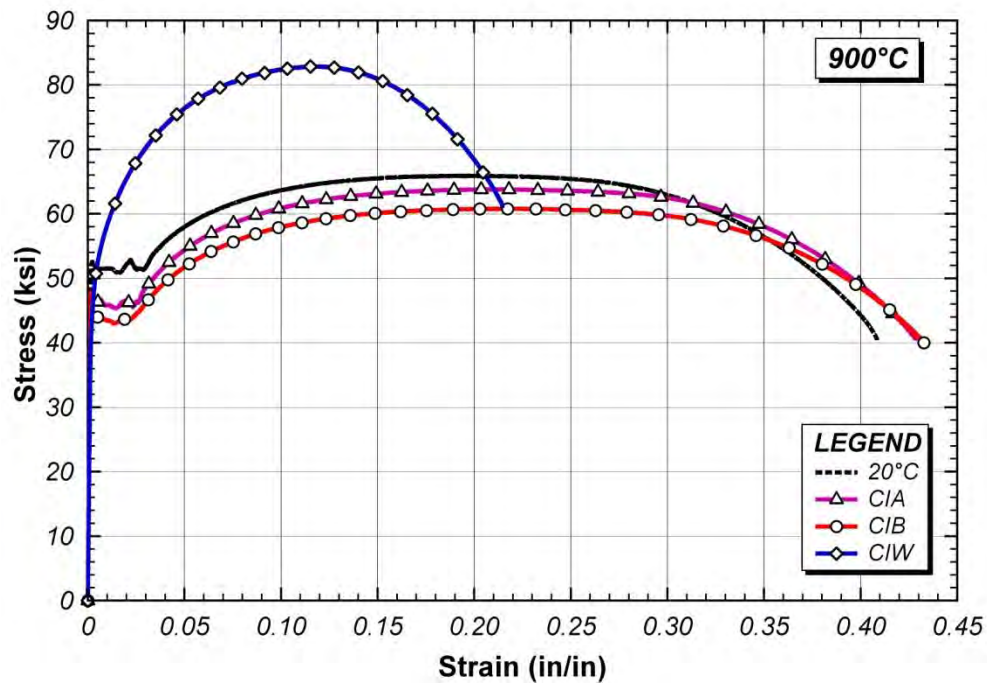
Figure C.15 Combined full stress-strain curve at 900°C
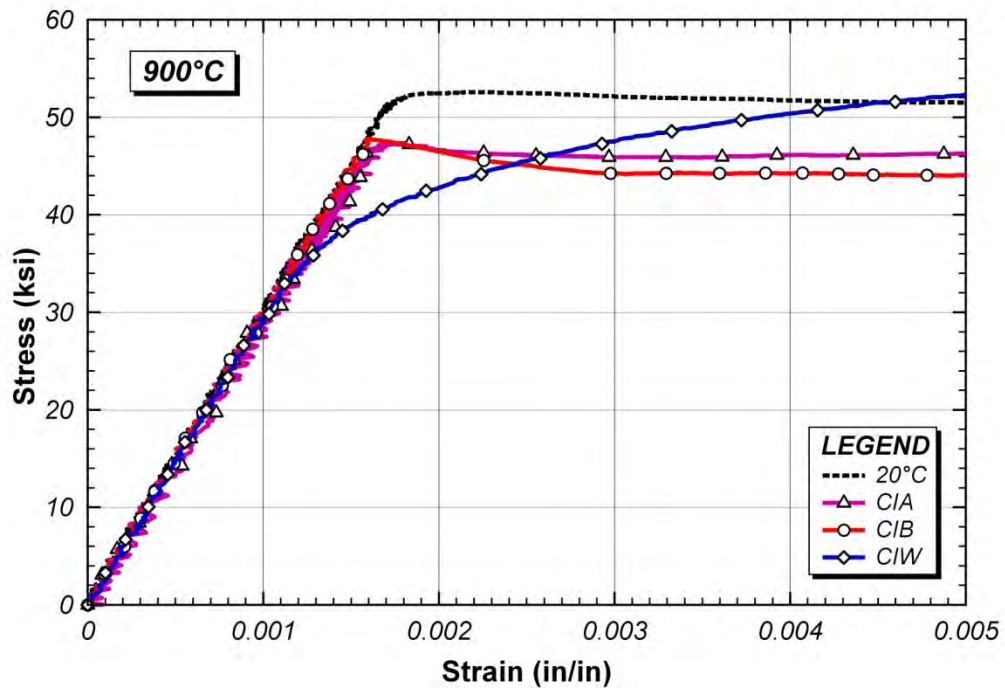
Figure C.16 Combined initial stress-strain curve at 900°C

292
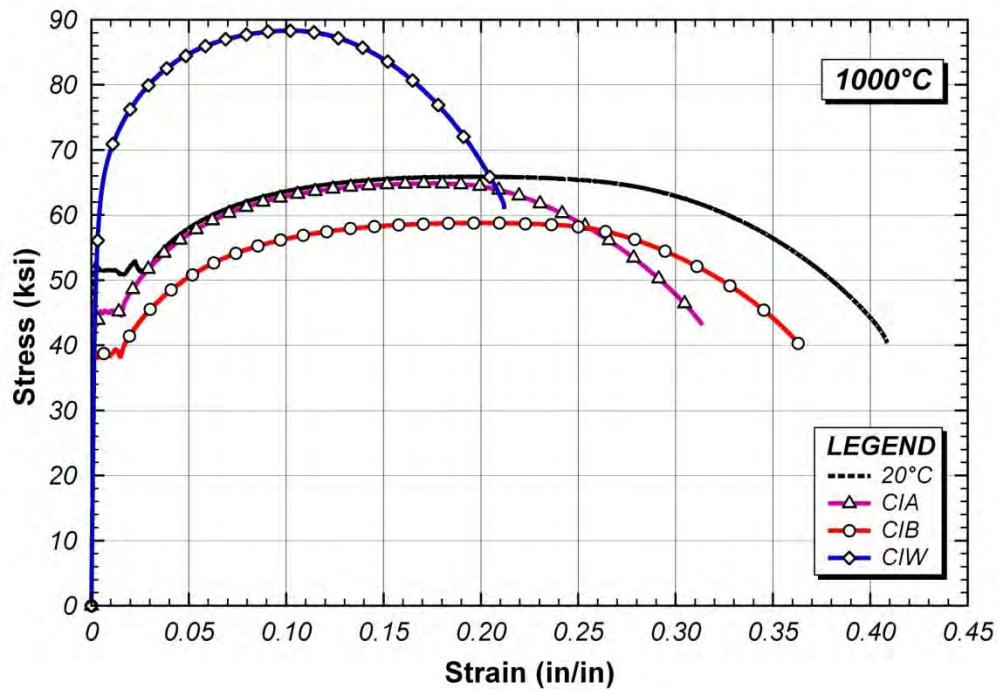
Figure C.17 Combined full stress-strain curve at 1,000°C
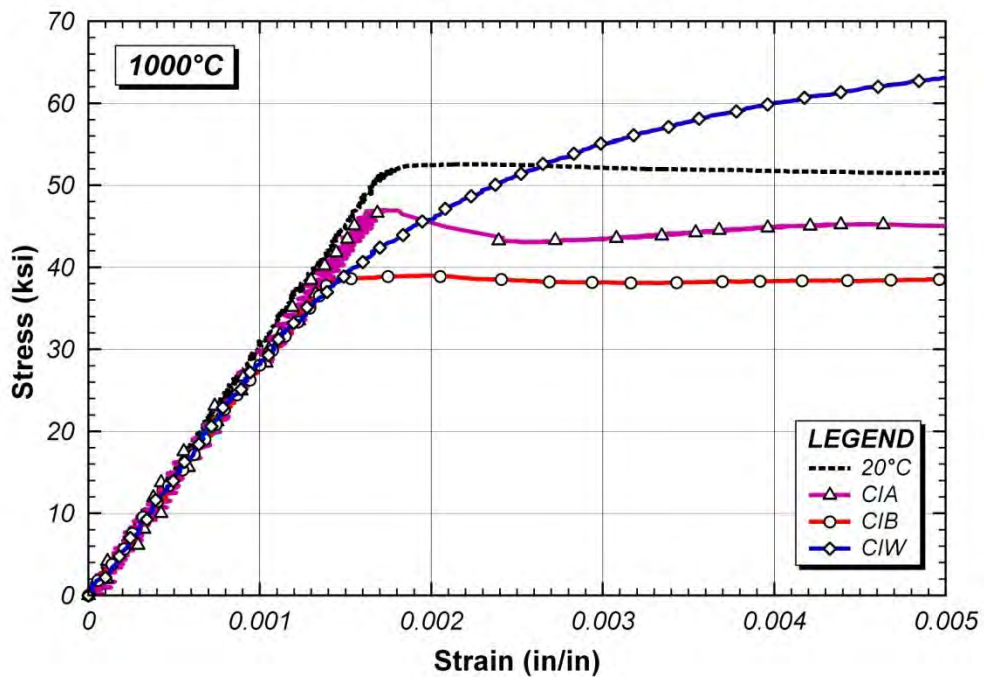
Figure C.18 Combined initial stress-strain curve at 1,000°C

293

APPENDIX D

Creep Test Results at Elevated Temperatures

This appendix was presented representative creep test results at elevated temperatures as well as the figures of used in Chapter 6.

D.1   TOTAL- AND CREEP-STRAIN CURVES BY TEMPERATURE
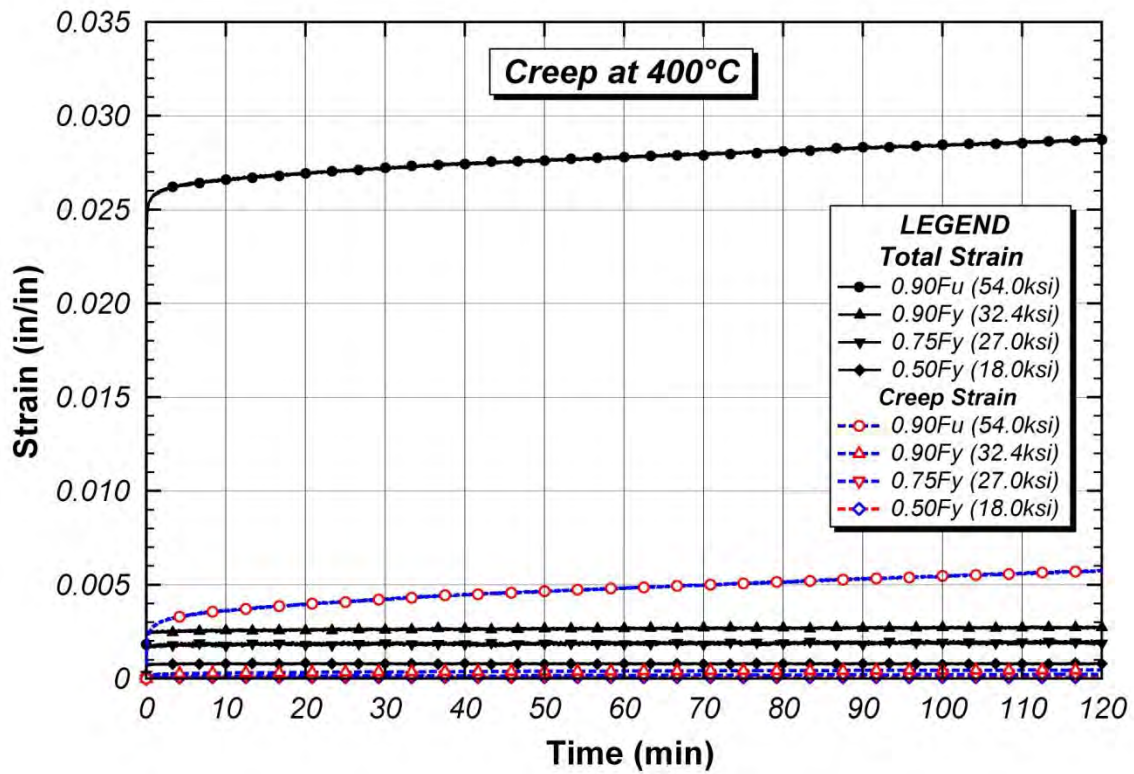
Figure D.1 Creep curves at 400°C
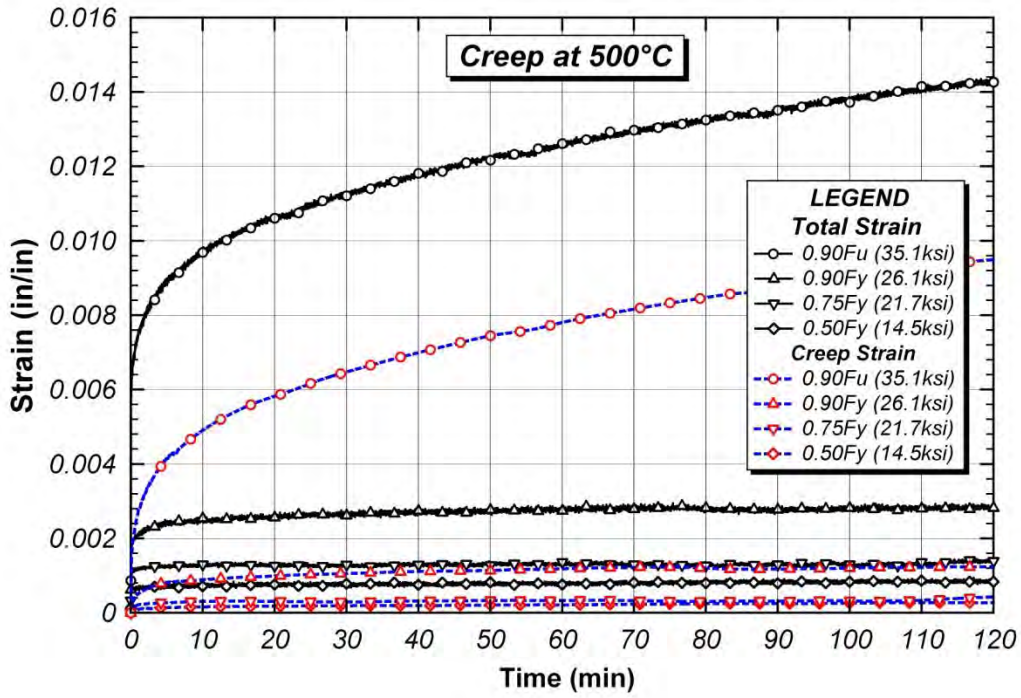
Figure D.2 Creep curves at 500°C
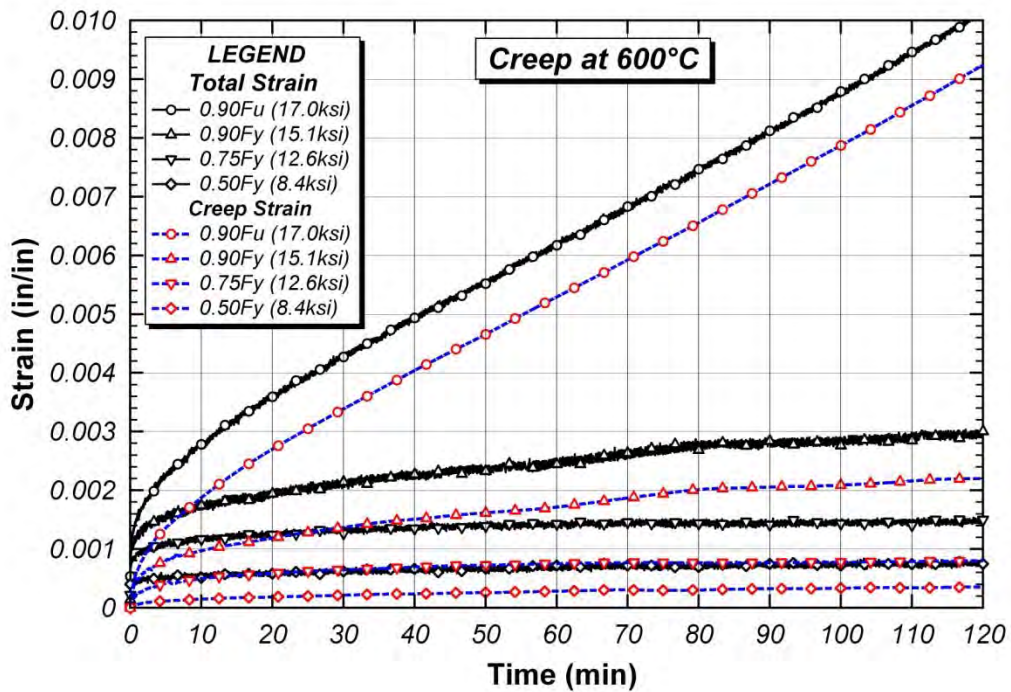
Figure D.3 Creep curves at 600°C

295
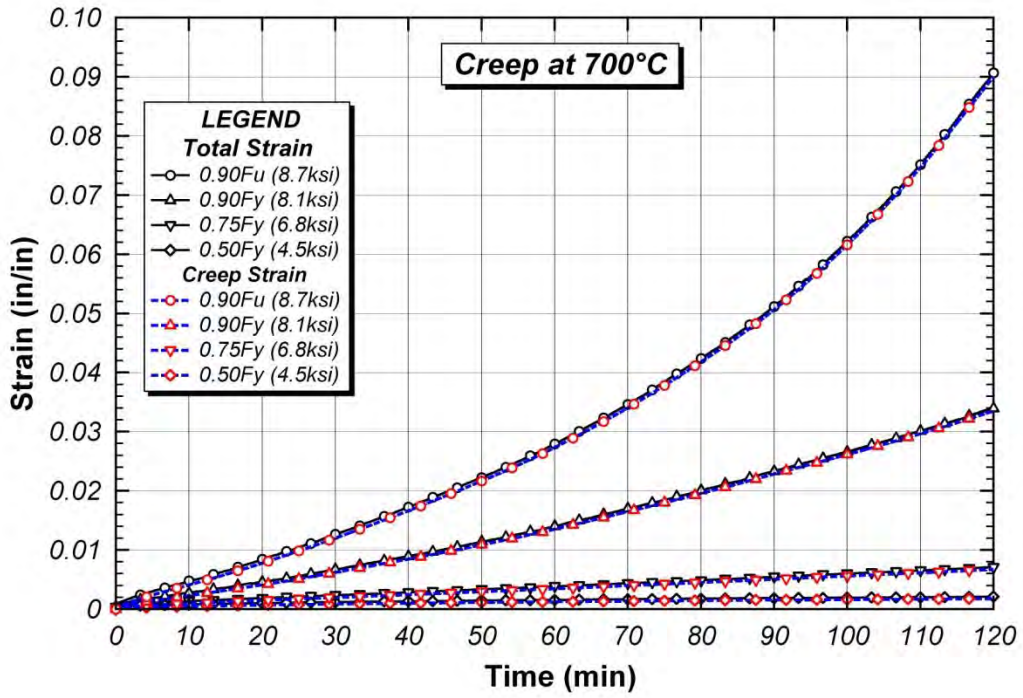
Figure D.4 Creep curves at 700°C
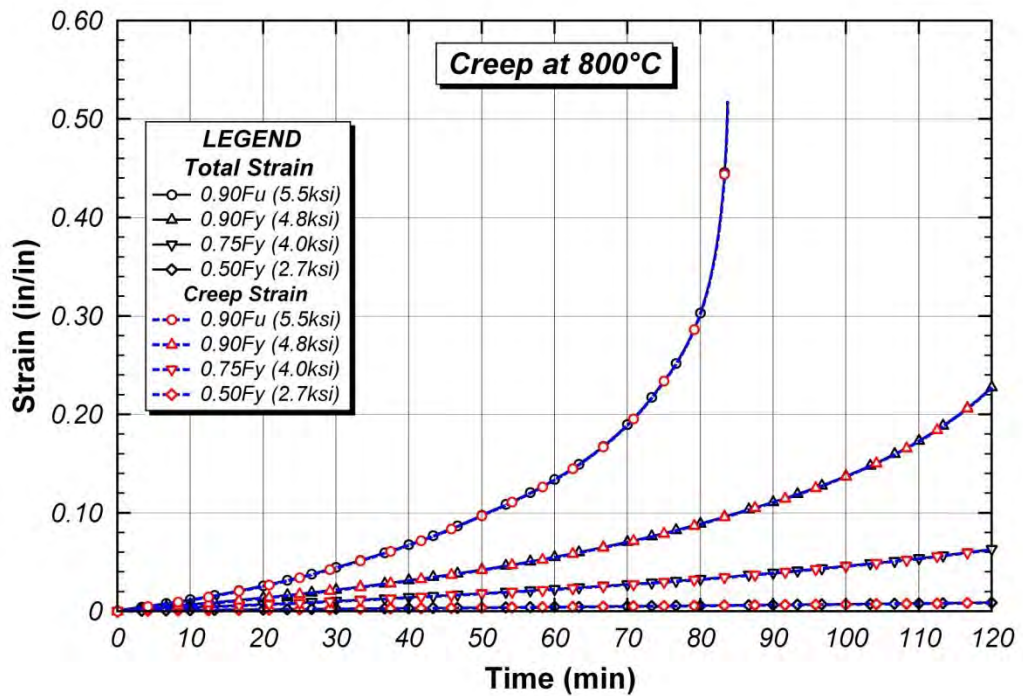
Figure D.5 Creep curves at 800°C

296
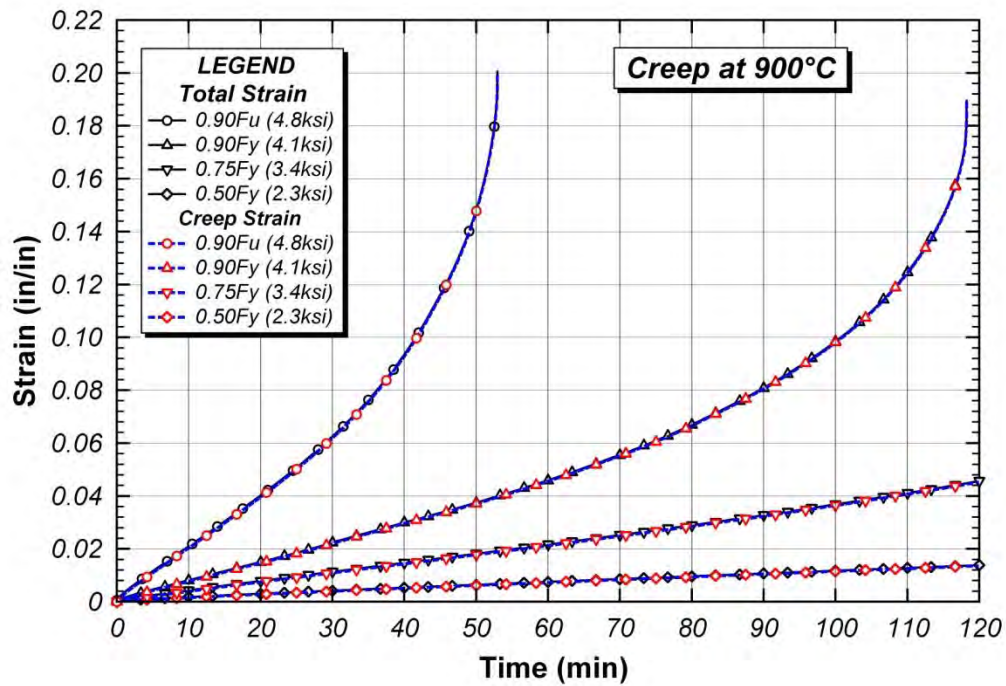
Figure D.6 Creep curves at 900°C
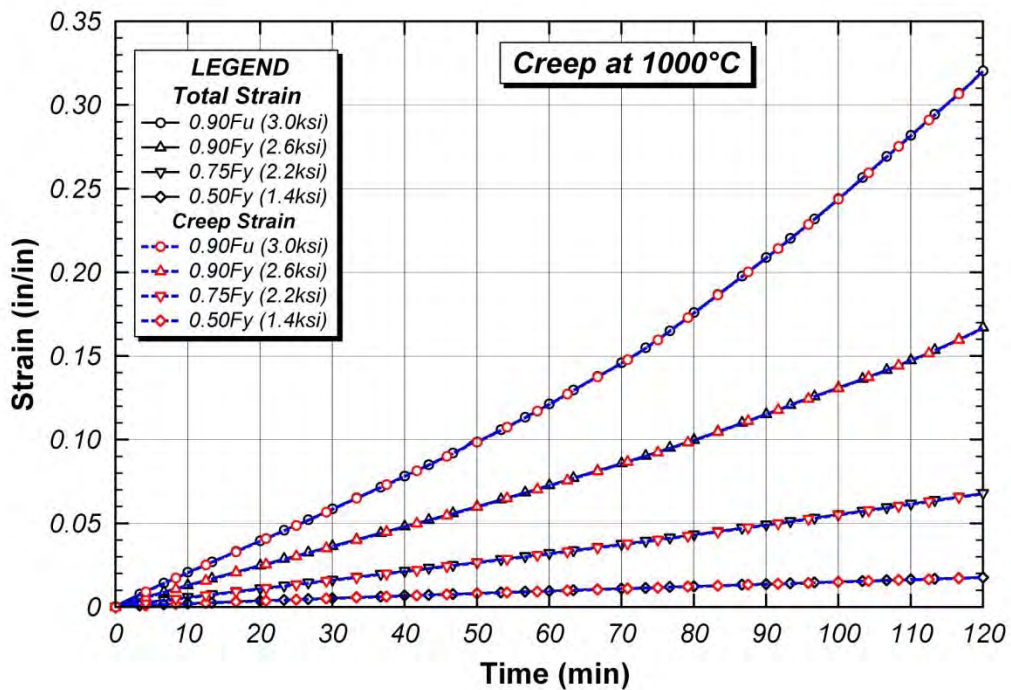
Figure D.7 Creep curves at 1000°C

297

D.2 CREEP CURVES BY STRESS LEVEL
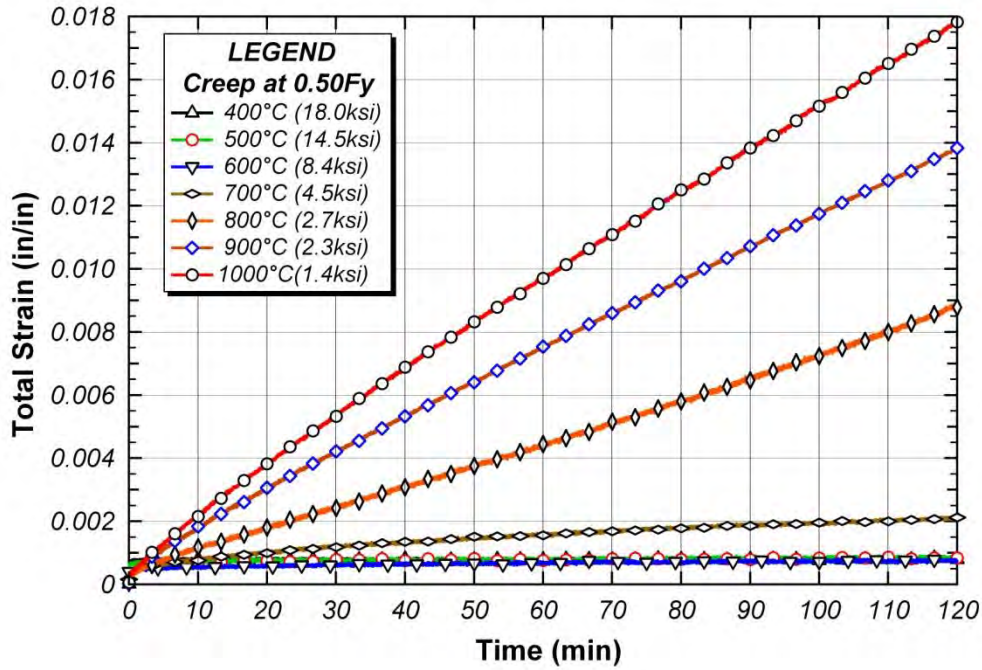
Figure D.8 Creep curves by 0.50F$_y$ stress level
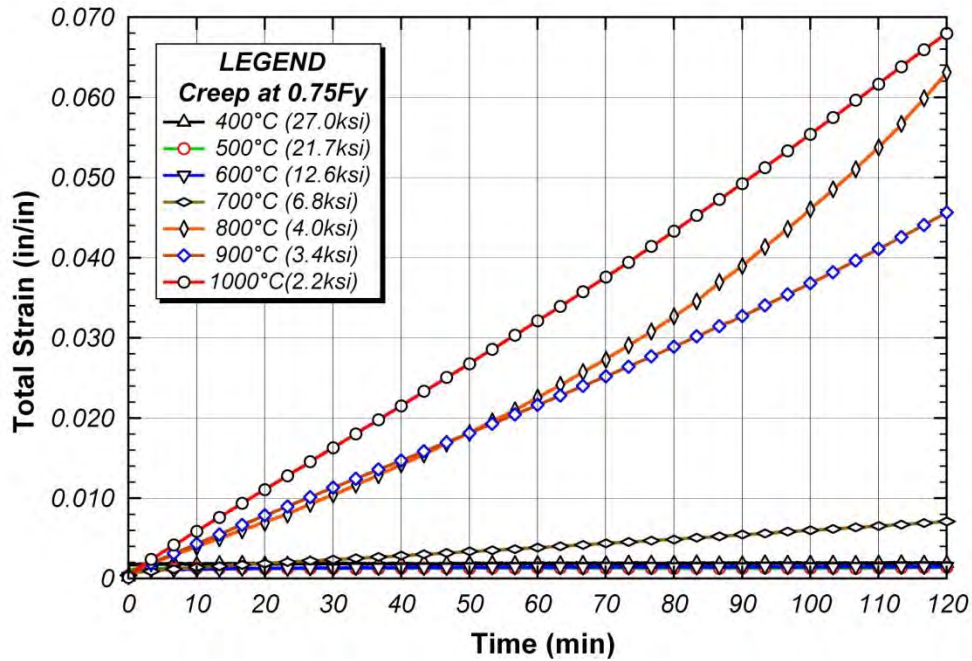
Figure D.9 Creep curves by 0.75F$_y$ stress level

298
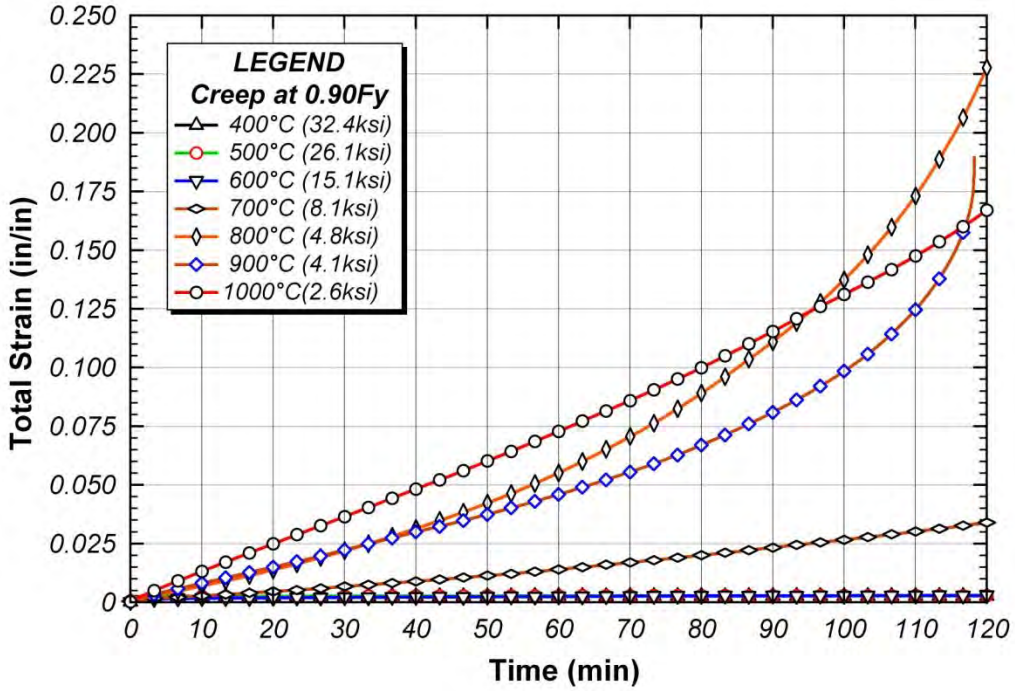
Figure D.10 Creep curves by 0.90F$_y$ stress level
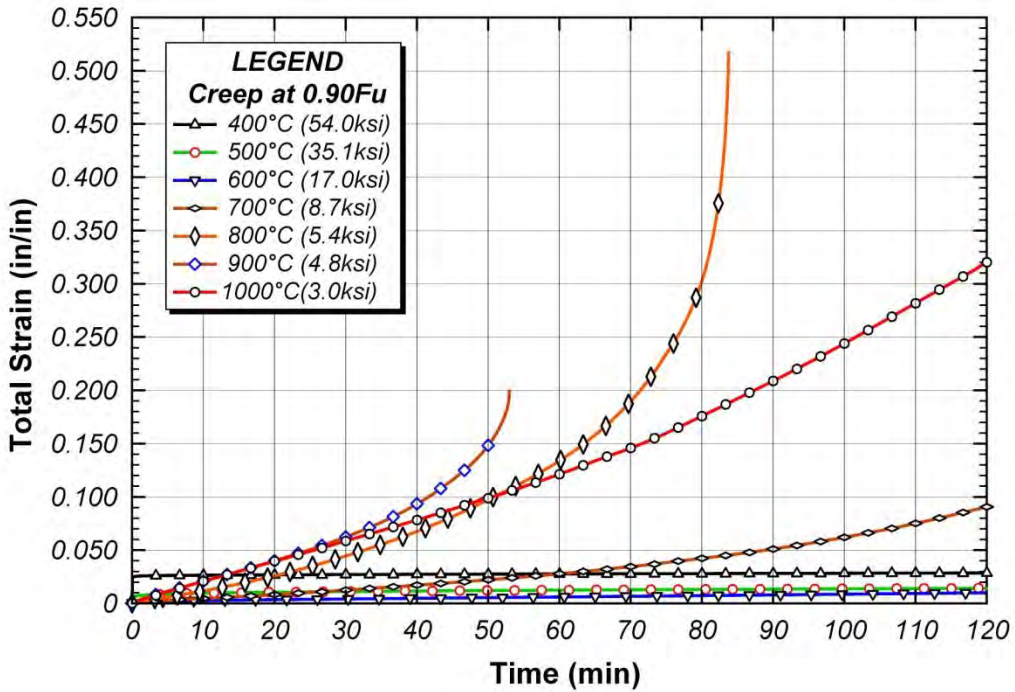
Figure D.11 Creep curves by 0.90F$_u$ stress level

299

D.3 Verification of Suggested Creep Model by Creep Strain
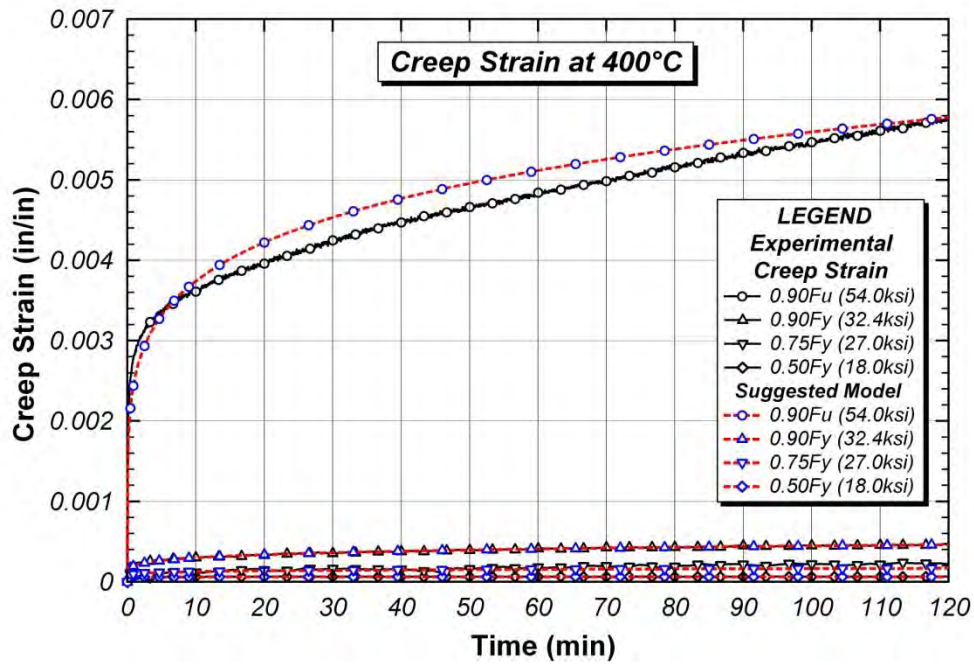
Figure D.12 Creep model verification at 400°C
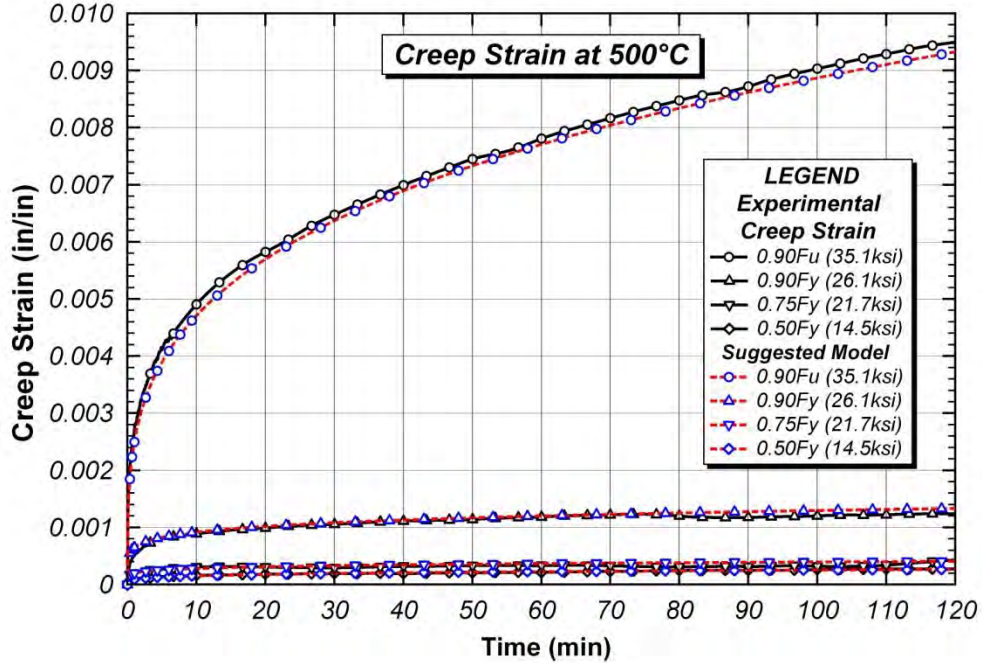
Figure D.13 Creep model verification at 500°C

300
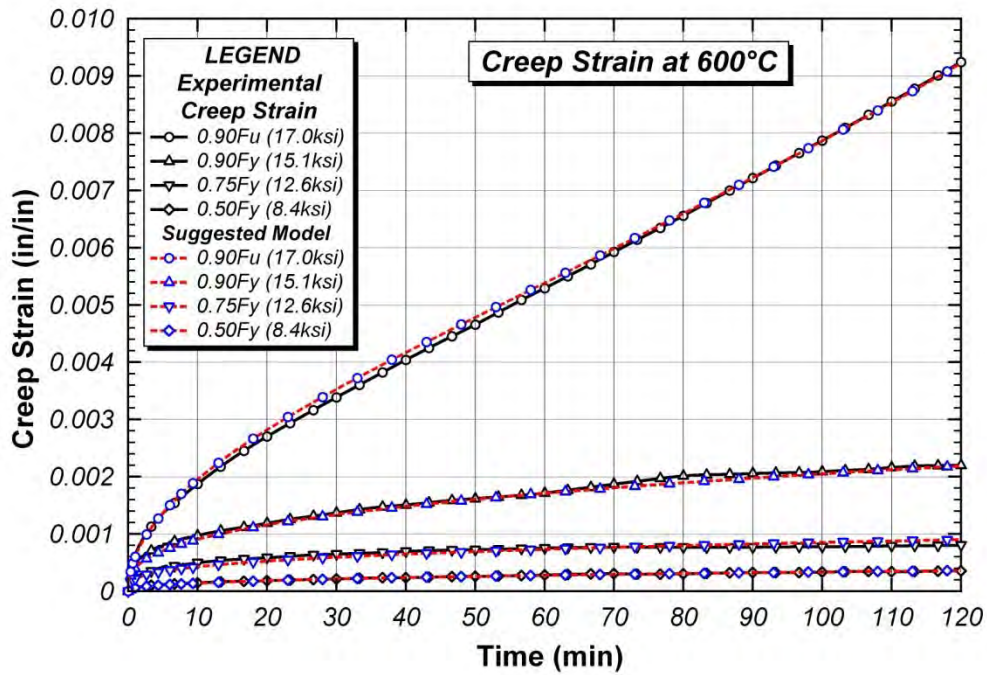
Figure D.14 Creep model verification at 600°C
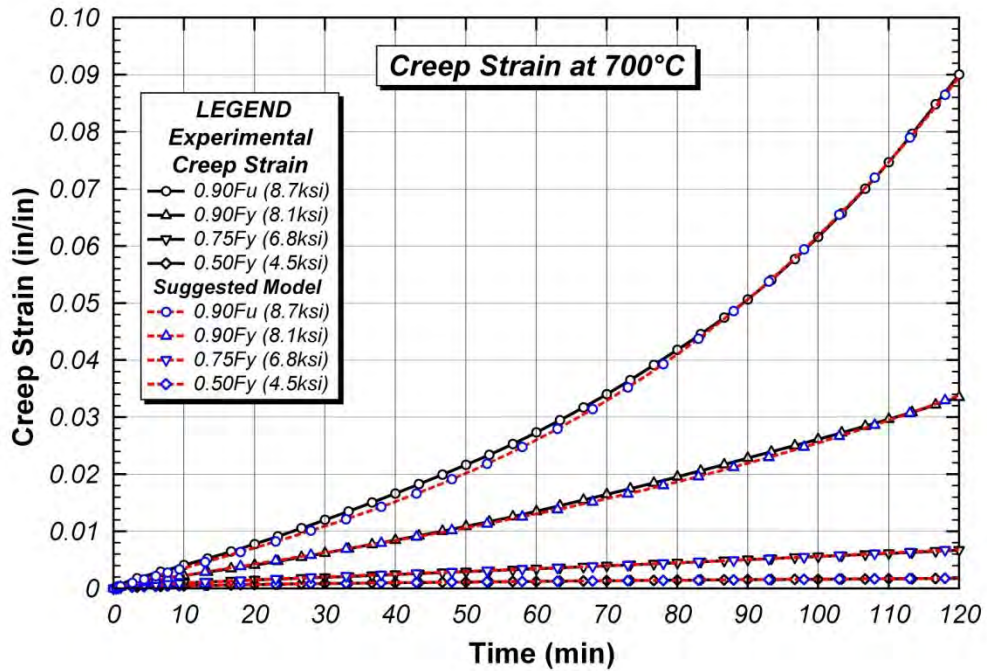
Figure D.15 Creep model verification at 700°C

301
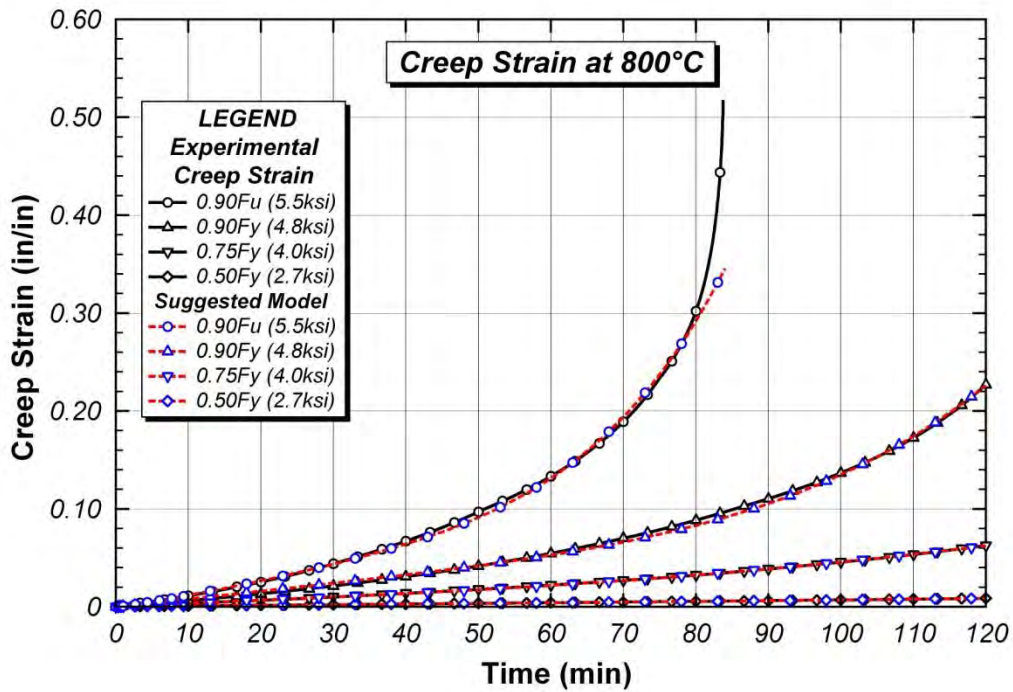
Figure D.16 Creep model verification at 800°C
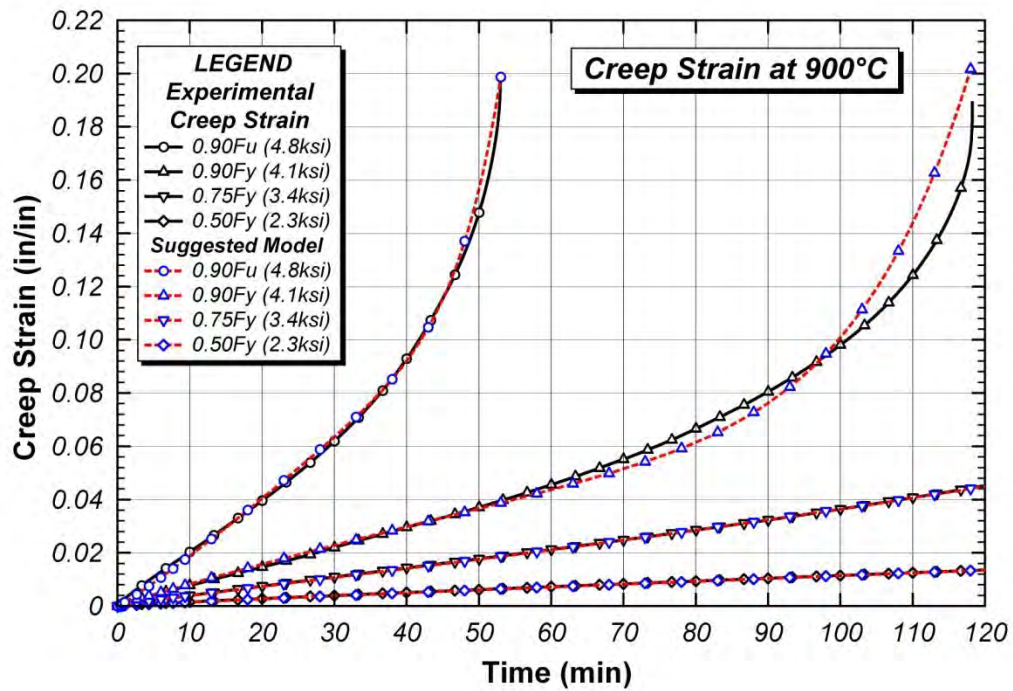
Figure D.17 Creep model verification at 900°C

302
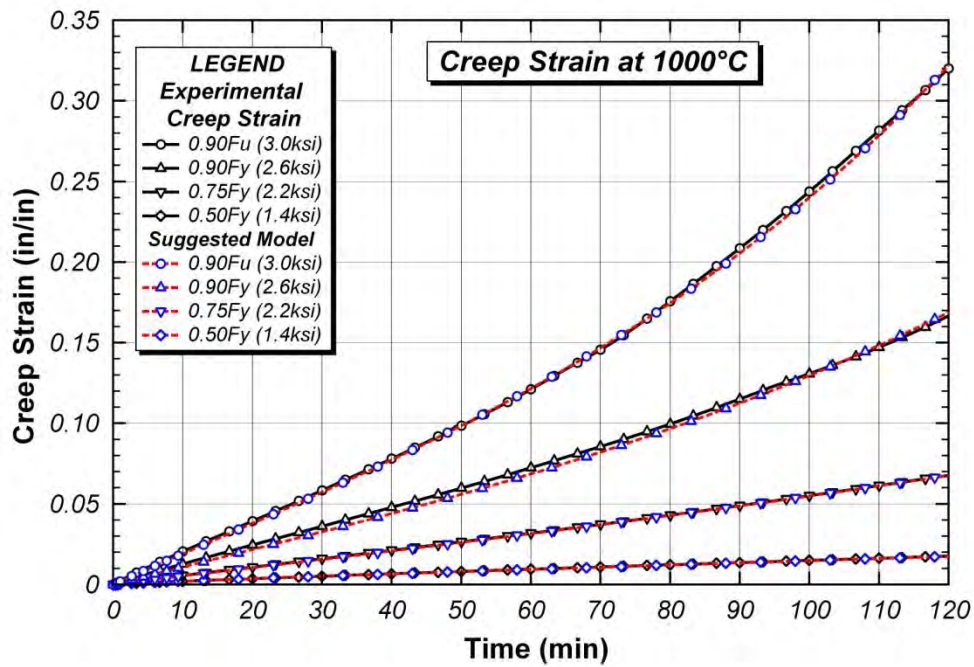
Figure D.18 Creep model verification at 1000°C

D.4 CREEP MODEL COMPARISON
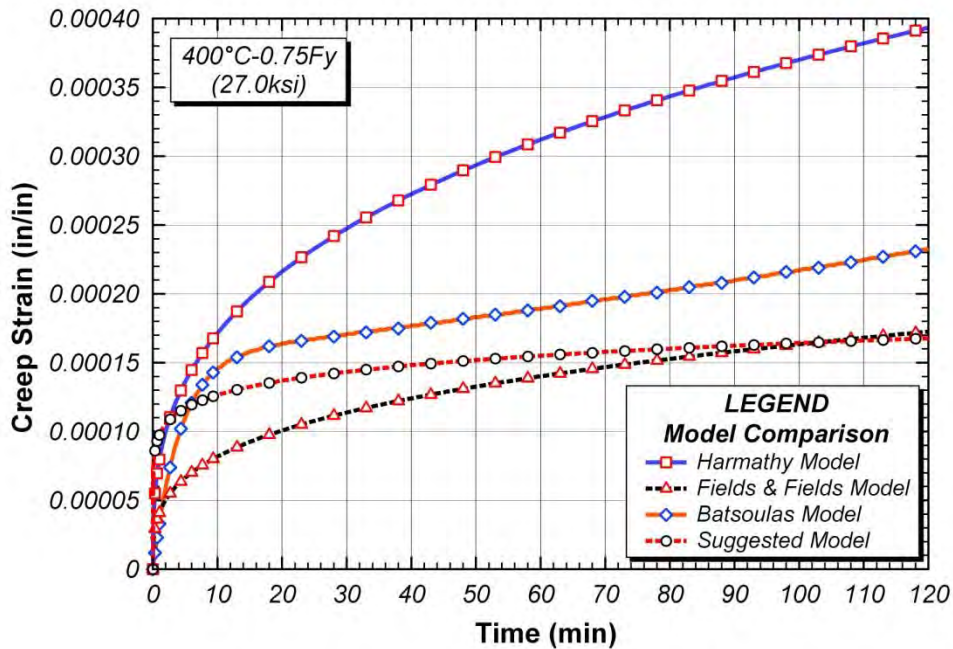
Figure D.19 Creep model comparison at 400°C-0.75F$_y$

303
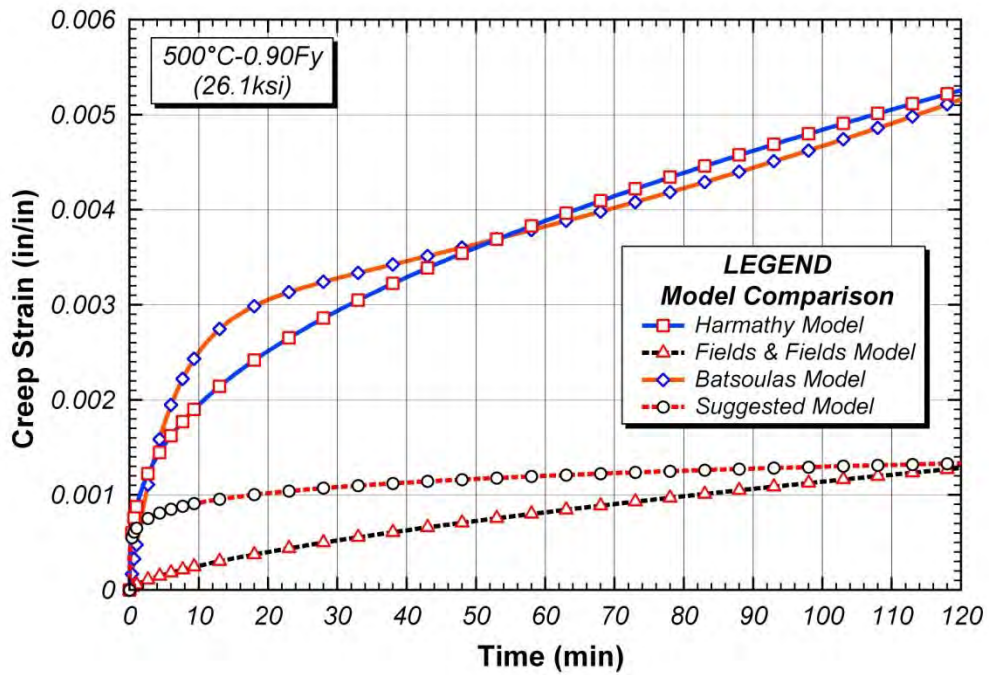
Figure D.20 Creep model comparison at 500°C-0.90F$_y$
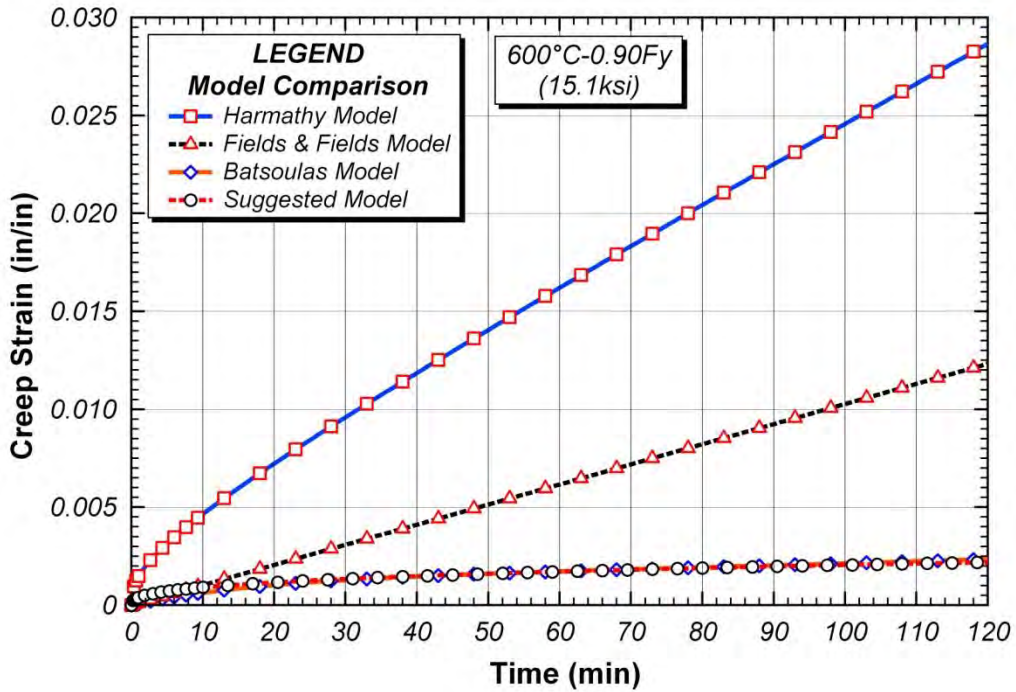
Figure D.21 Creep model comparison at 600°C-0.90F$_y$

304
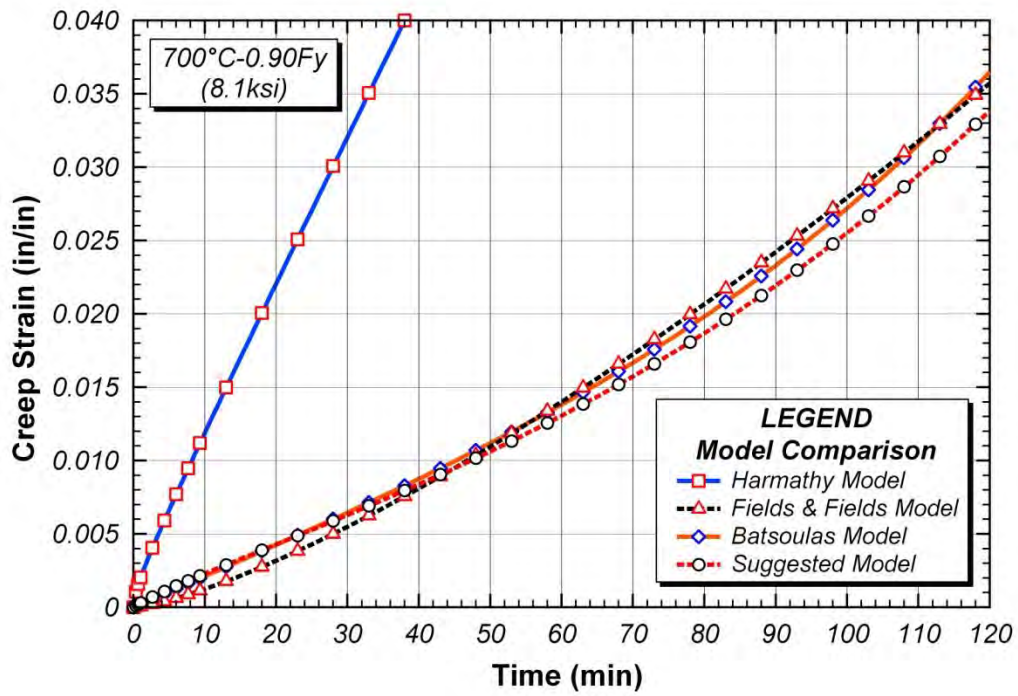
Figure D.22 Creep model comparison at 700°C-0.90F$_y$

APPENDIX E

Relaxation Test Results at Elevated Temperatures

This appendix was presented representative graphs of relaxation test conducted at elevated temperatures which were discussed in Chapter 7.

E.1 RELAXATION CURVES BY TEMPERATURE
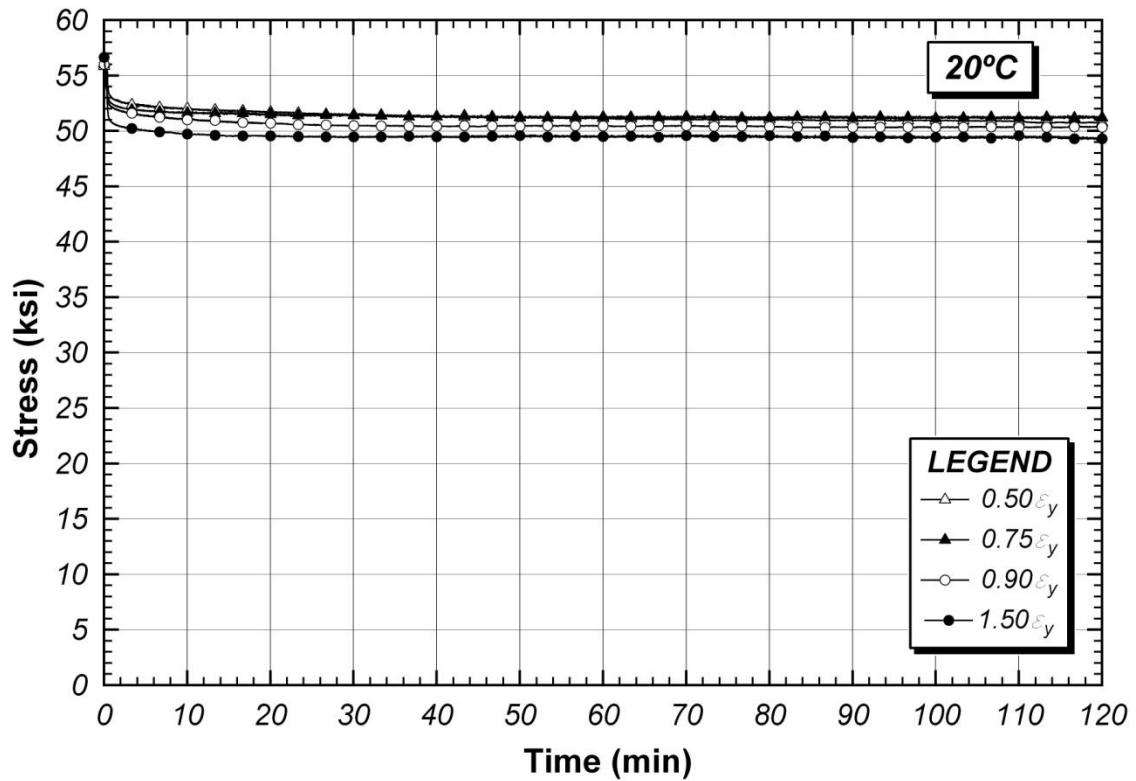
Figure E.1 Relaxation curves at 20°C
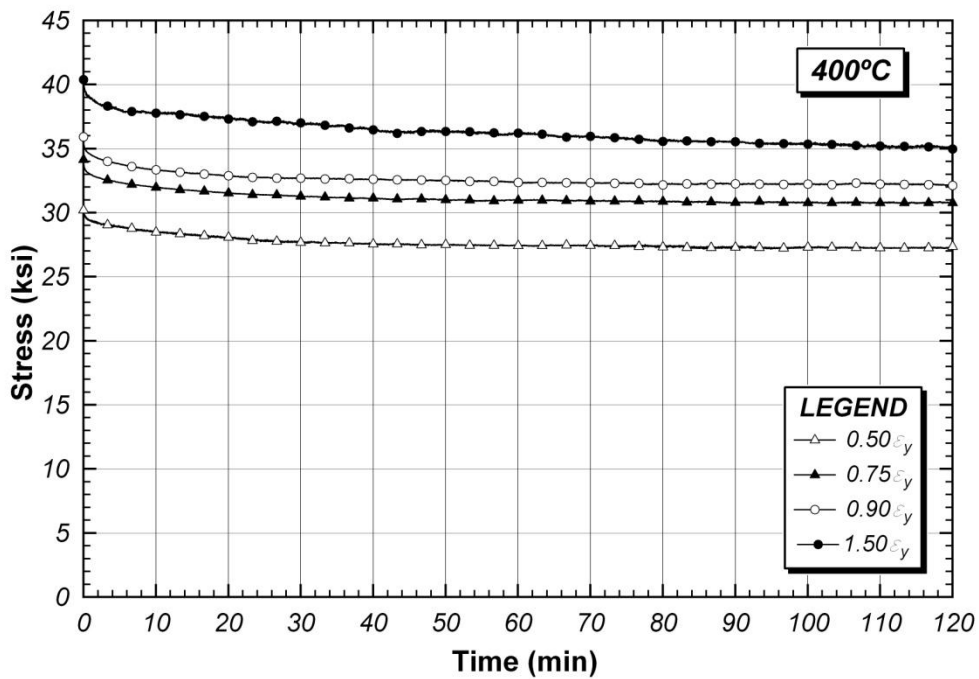
Figure E.2 Relaxation curves at 400°C
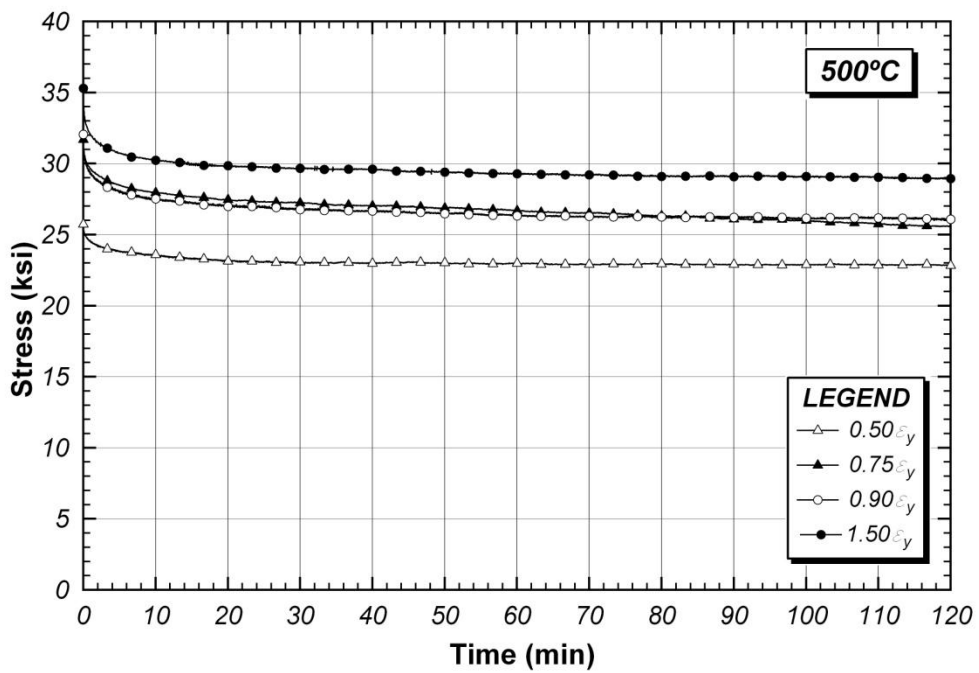
Figure E.3 Relaxation curves at 500°C

307
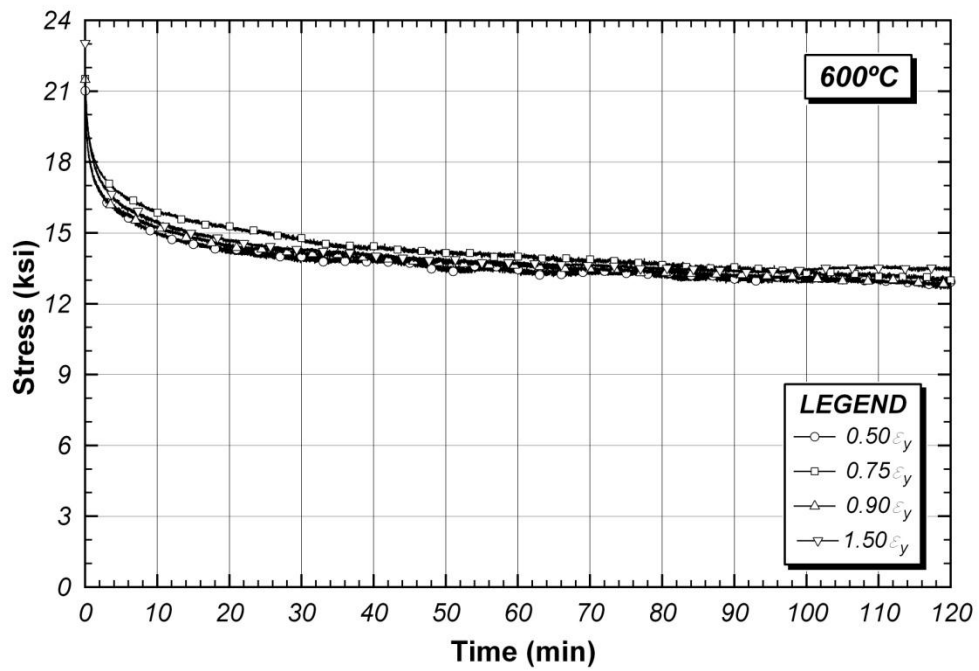
Figure E.4 Relaxation curves at 600°C
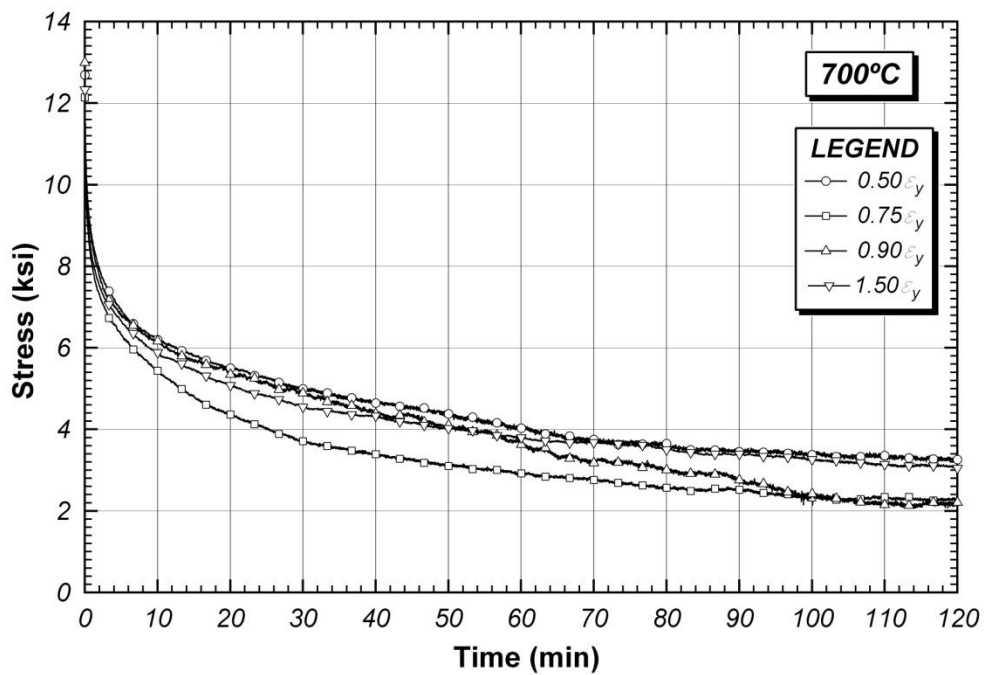
Figure E.5 Relaxation curves at 700°C

308
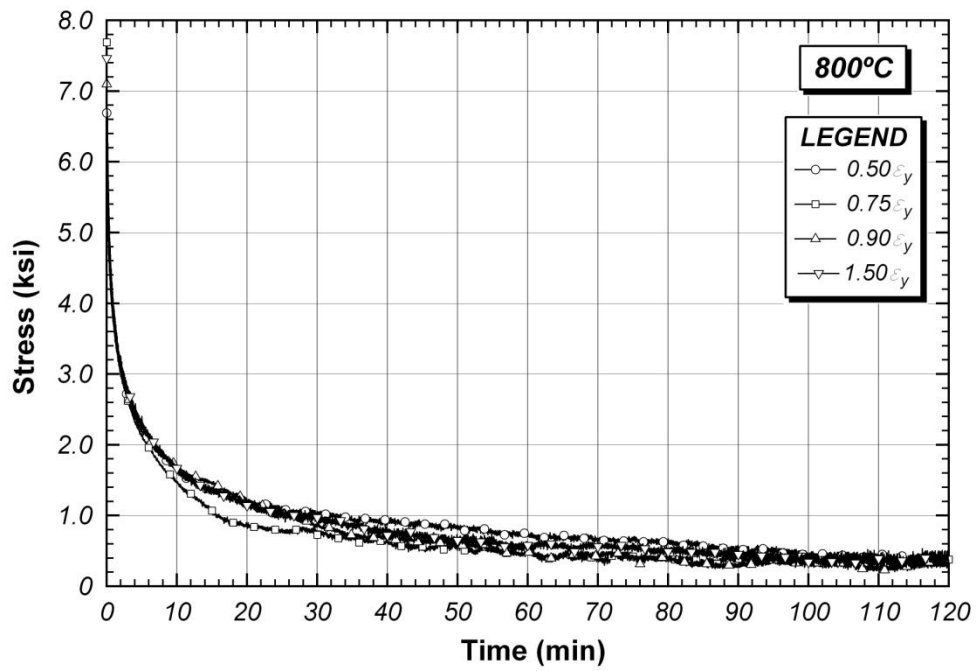
Figure E.6 Relaxation curves at 800°C
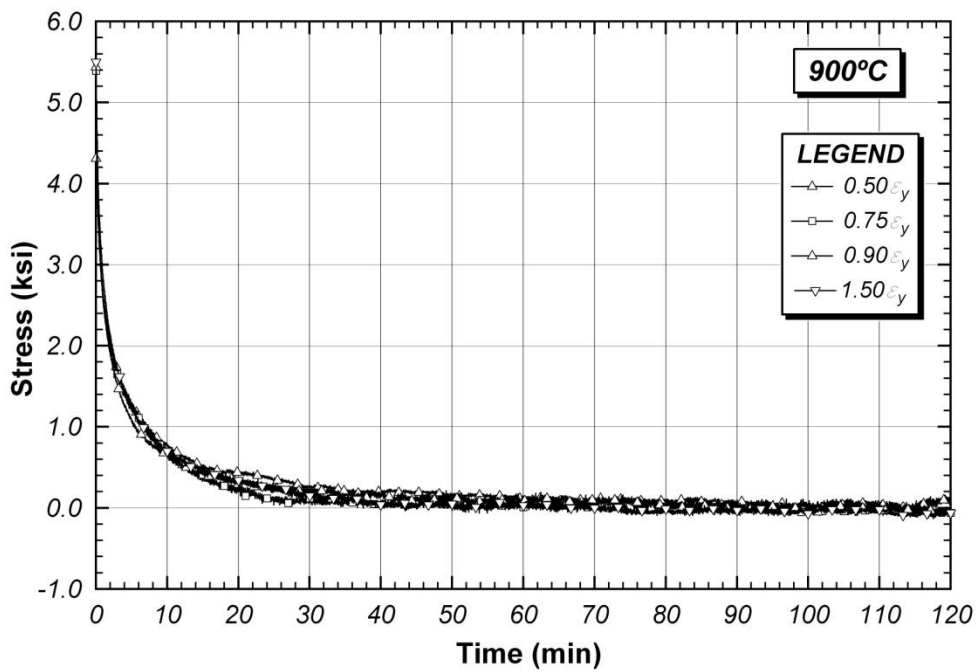
Figure E.7 Relaxation curves at 900°C

309
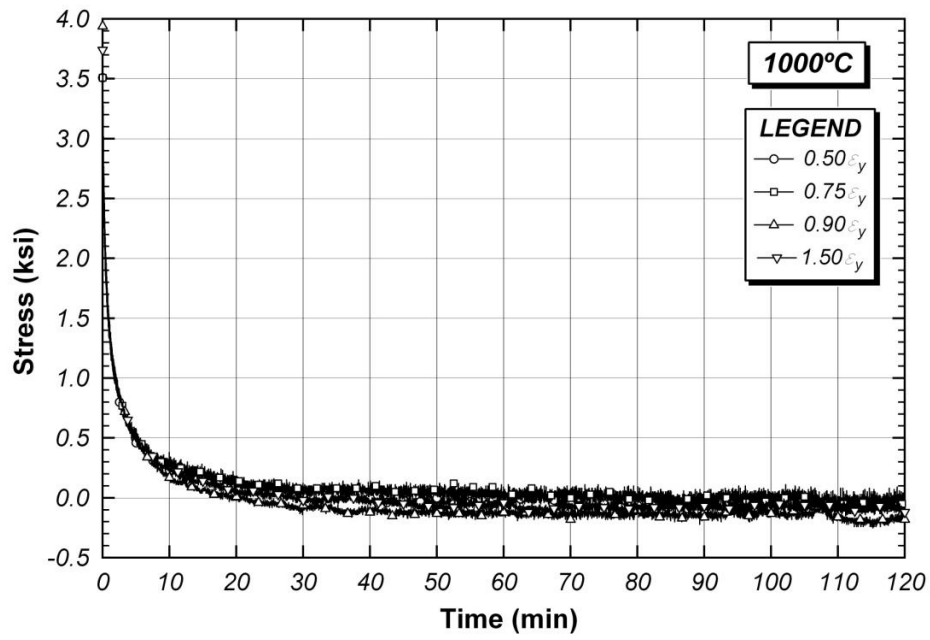
Figure E.8 Relaxation curves at 1000°C

E.2 **RETENTION FACTOR BY TEMPERATURE**
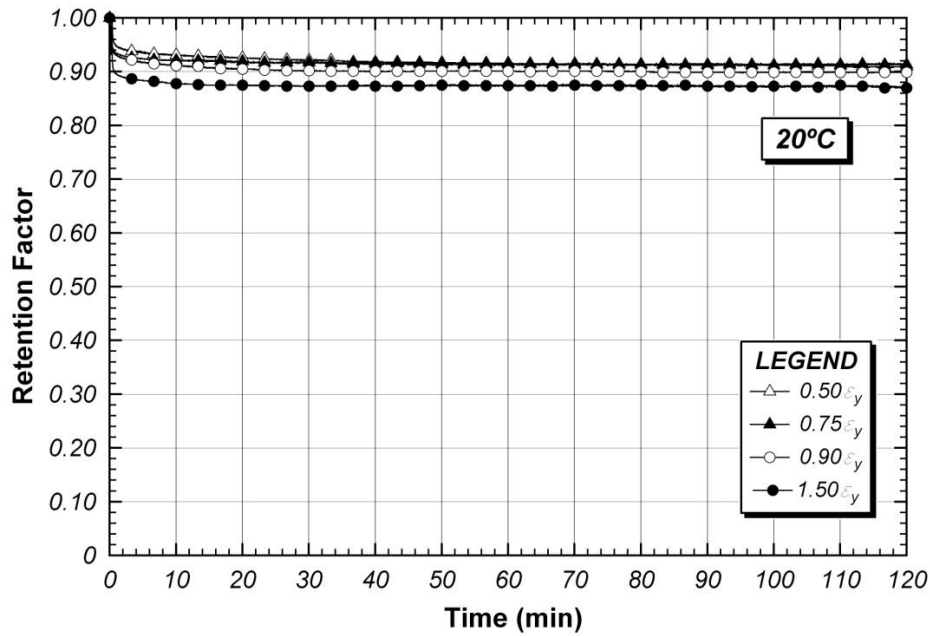
Figure E.9 Retention factor at 20°C

310
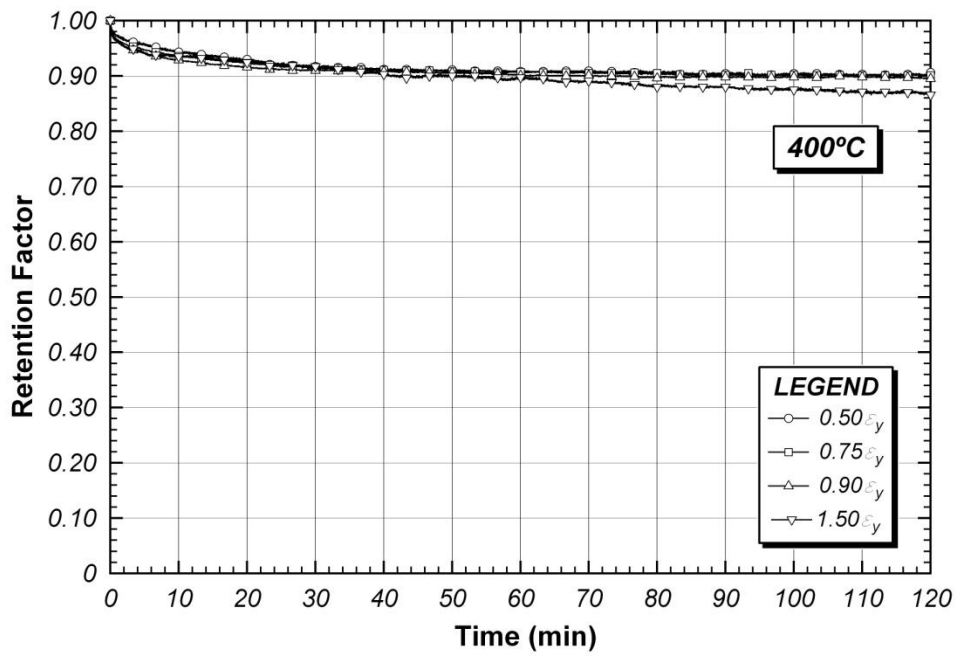
Figure E.10 Retention factor at 400°C
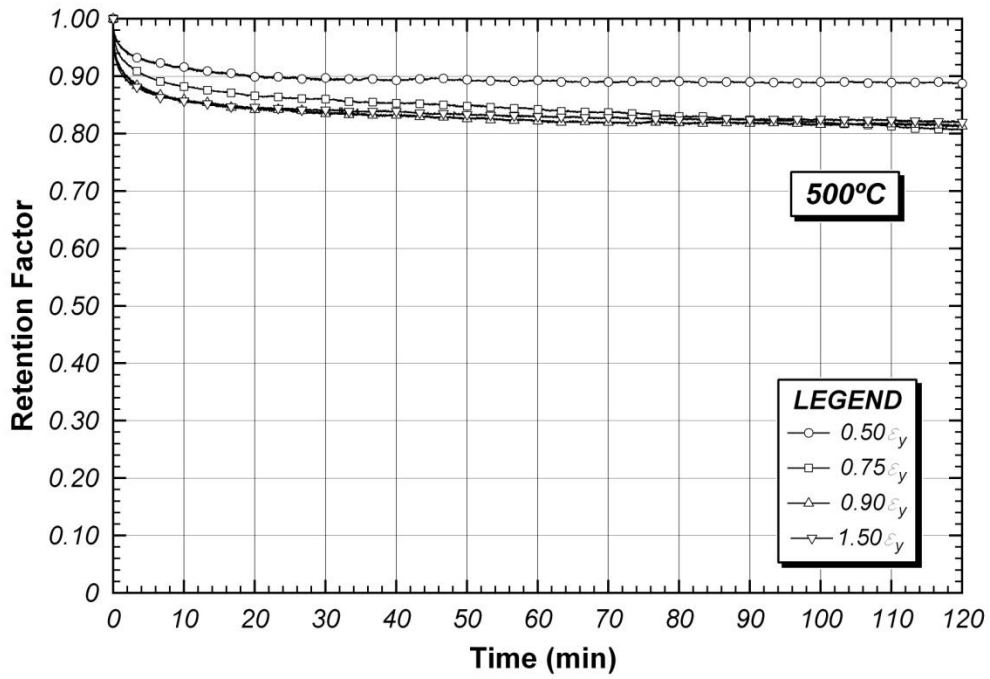
Figure E.11 Retention factor at 500°C

311
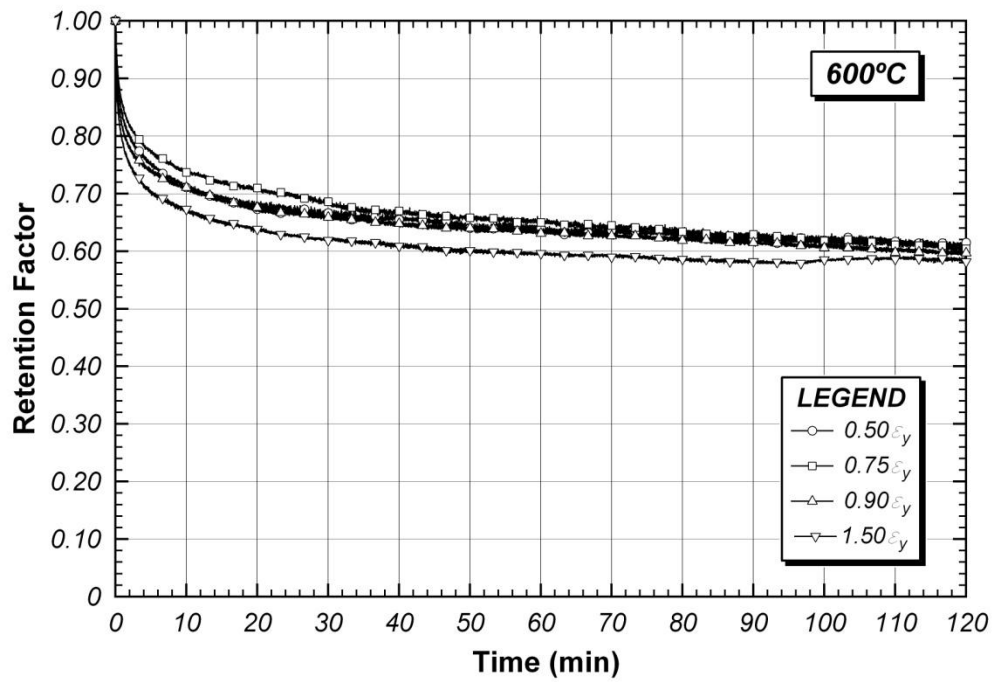
Figure E.12 Retention factor at 600°C
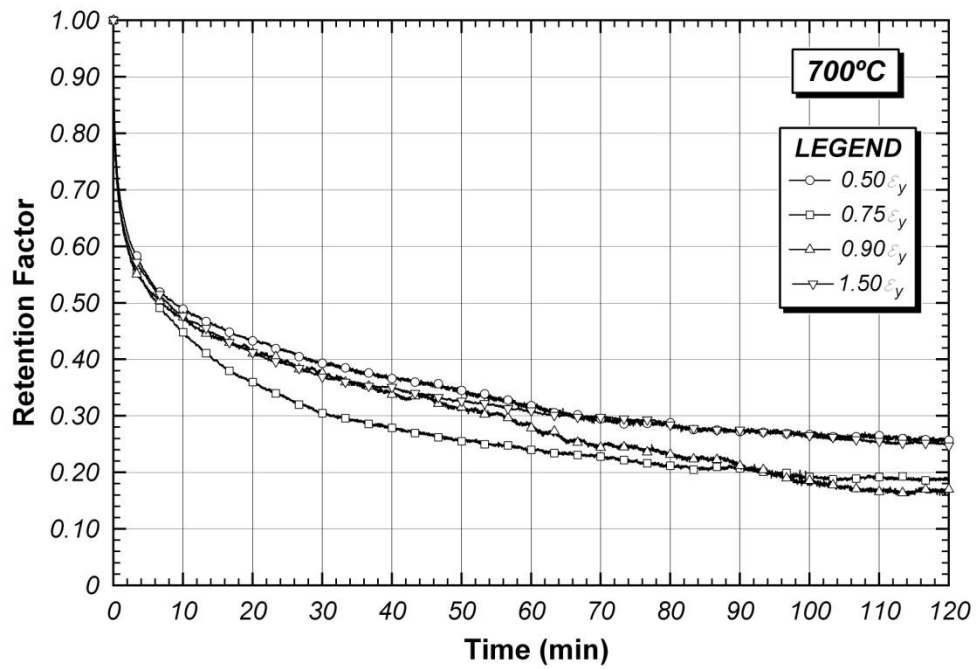
Figure E.13 Retention factor at 700°C
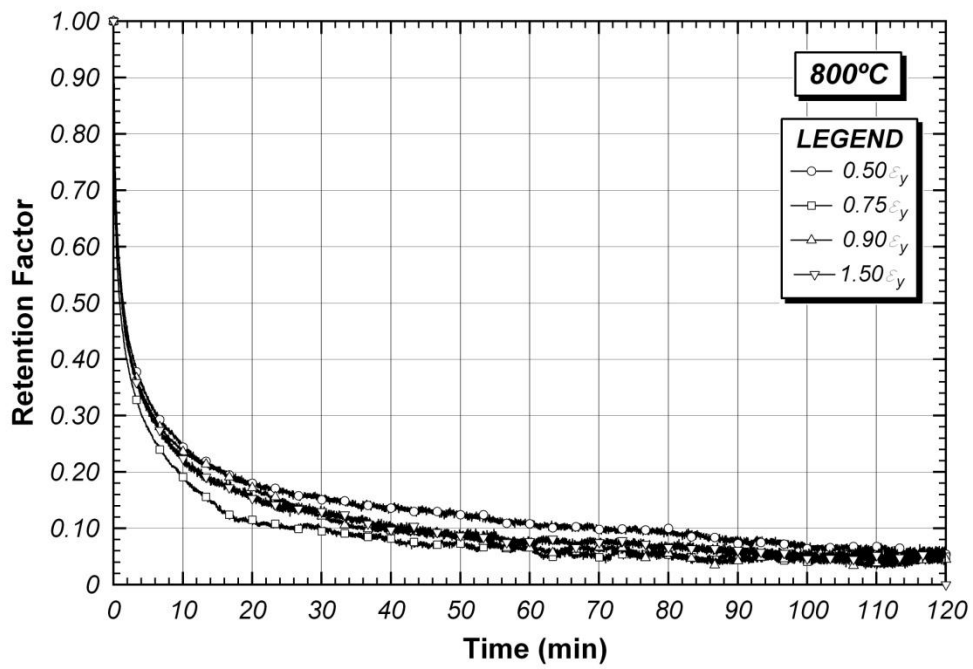
Figure E.14 Retention factor at 800°C
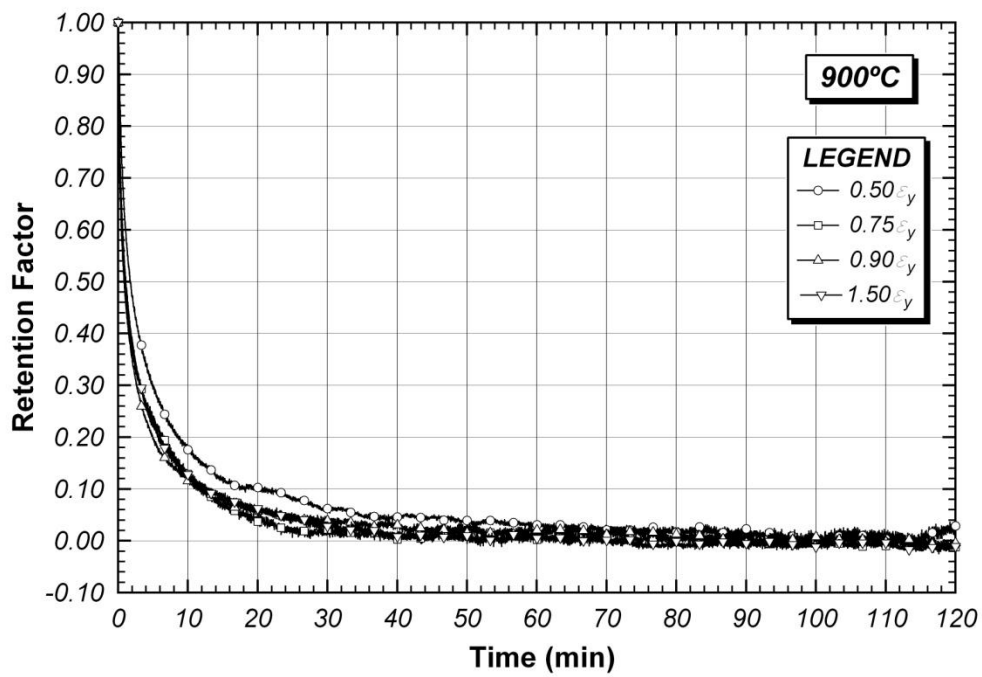
Figure E.15 Retention factor at 900°C

313
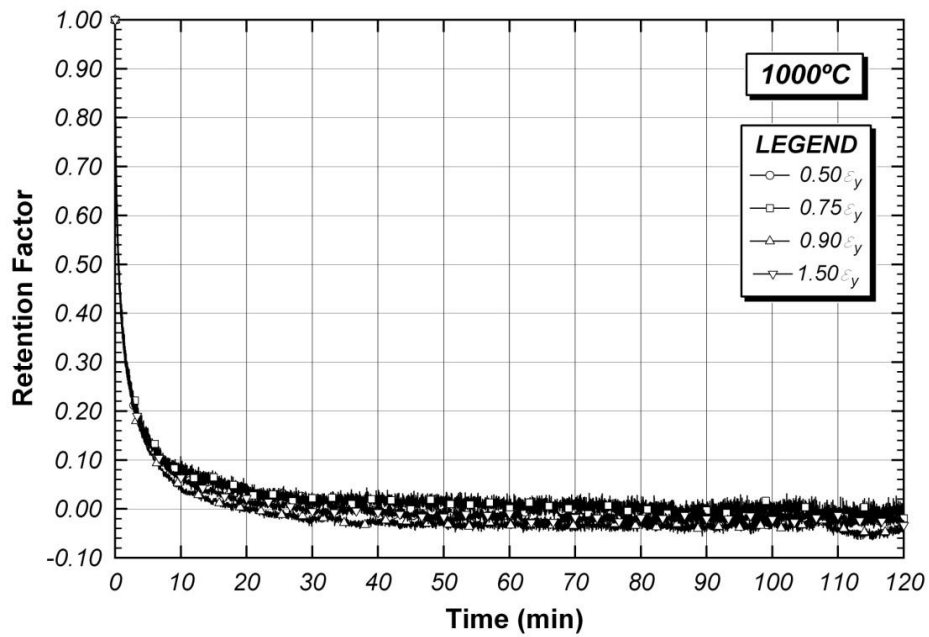
Figure E.16 Retention factor at 1000°C

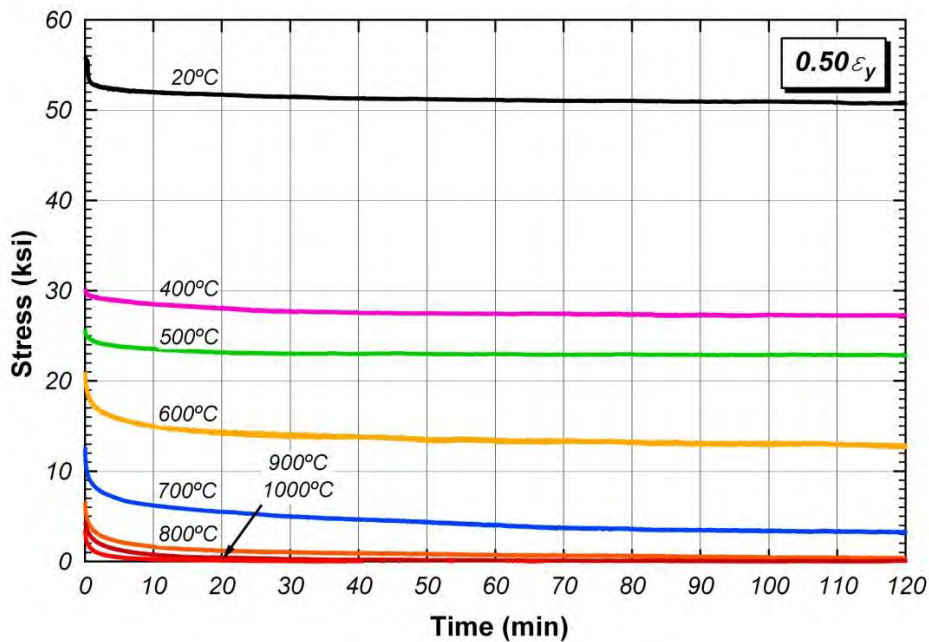**E.3 RELAXATION CURVES AND RETENTION FACTOR BY LOADING STRAIN**
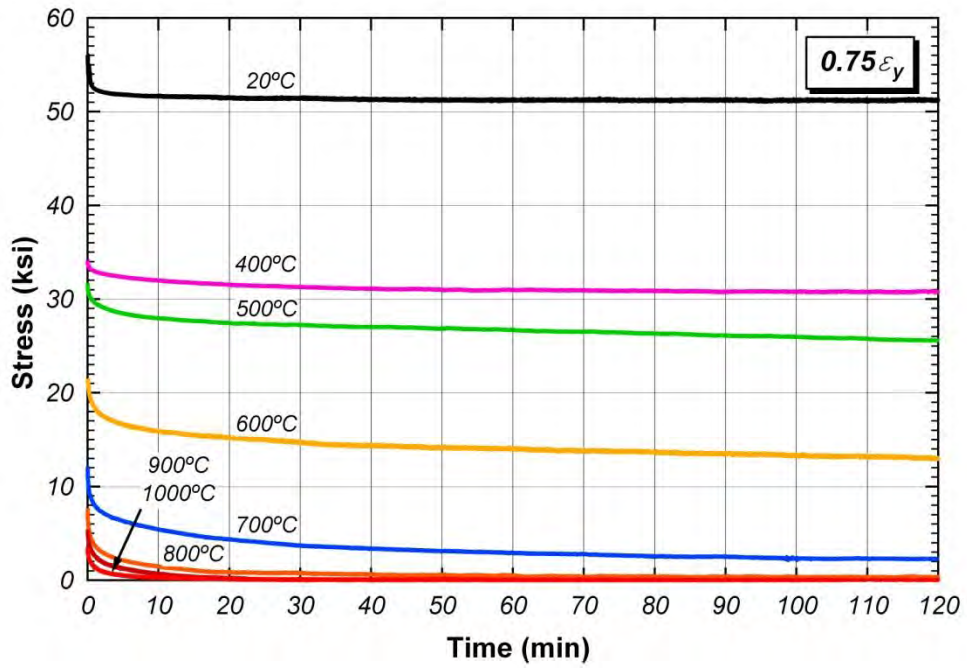

Figure E.17 Relaxation curves at 0.50εy
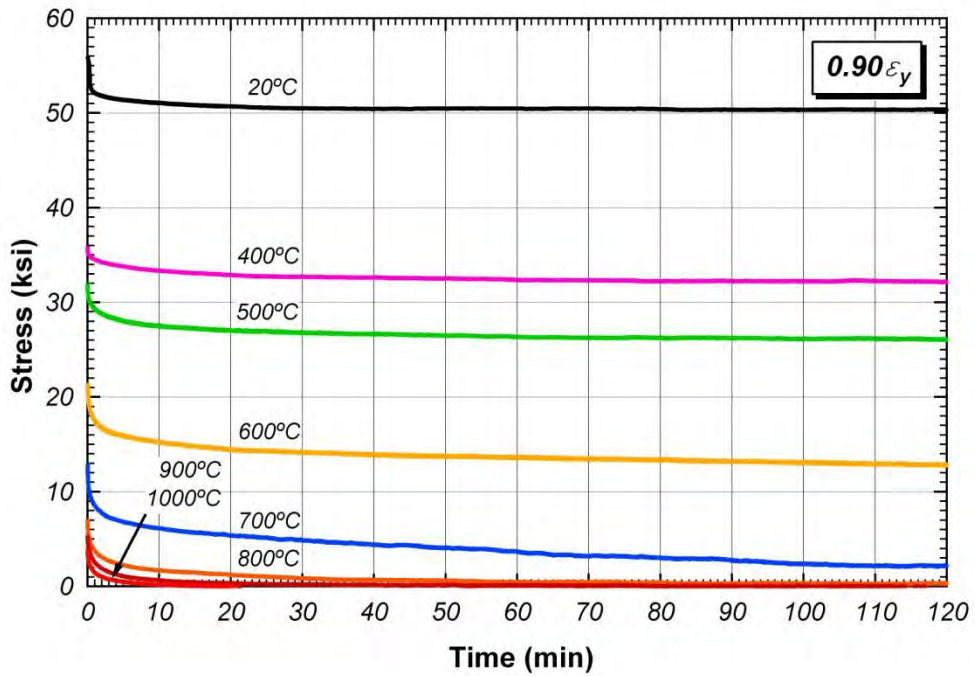
314

Figure E.18 Relaxation curves at 0.75εy

Figure E.19 Relaxation curves at 0.90εy

315
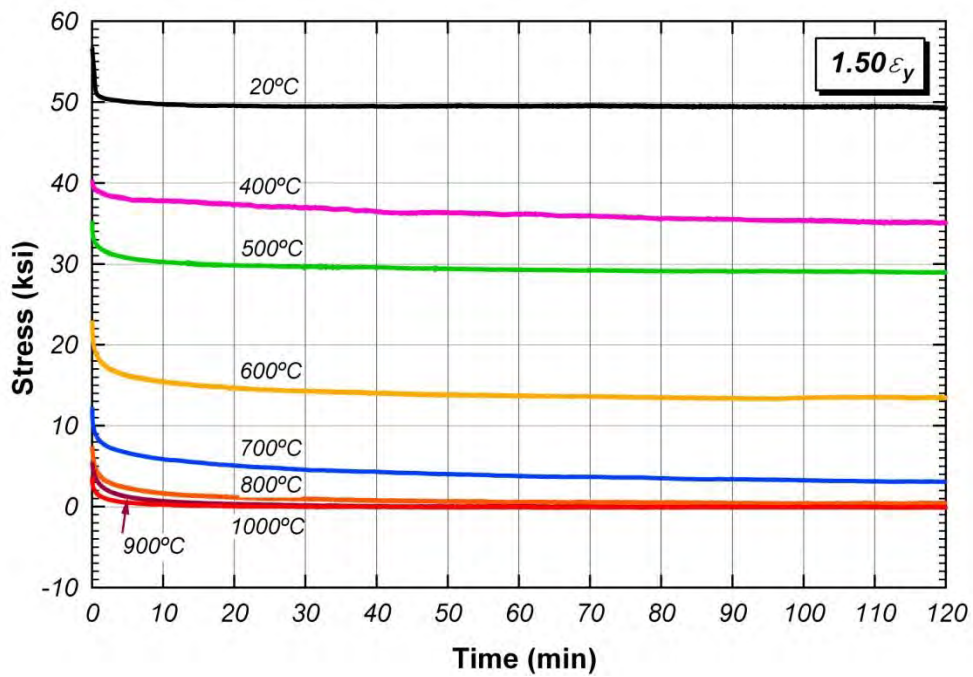
Figure E.20 Relaxation curves at 1.50εy
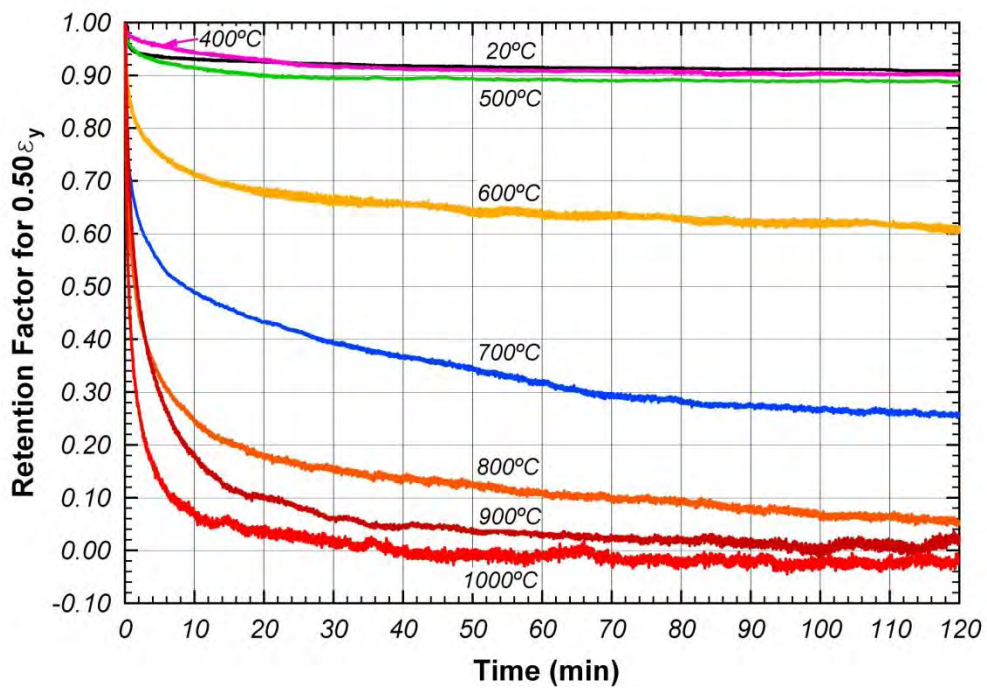
Figure E.21 Retention factor at 0.50εy
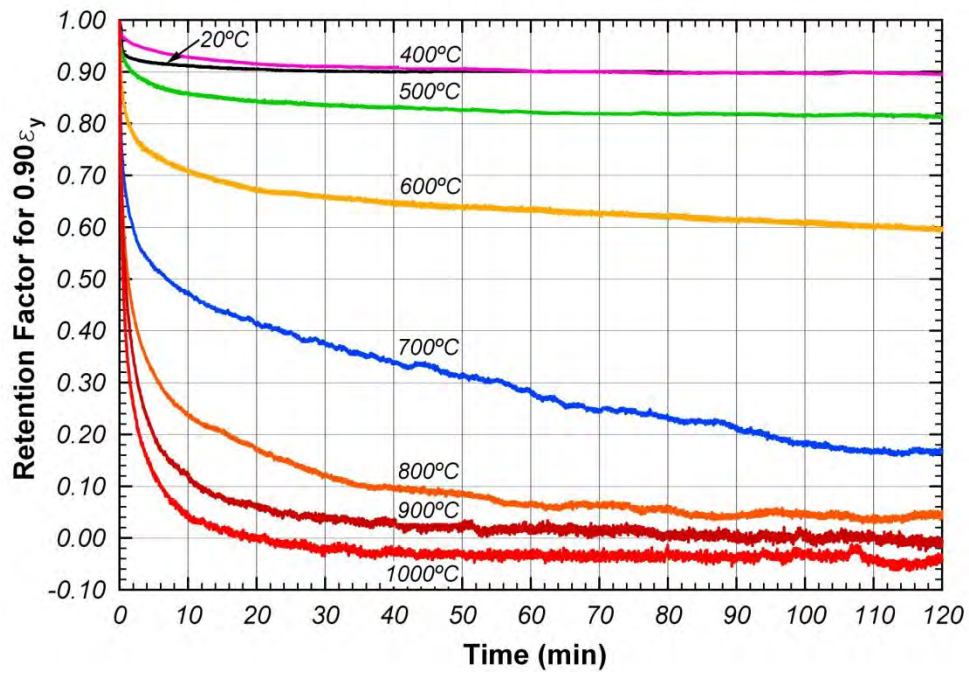
316
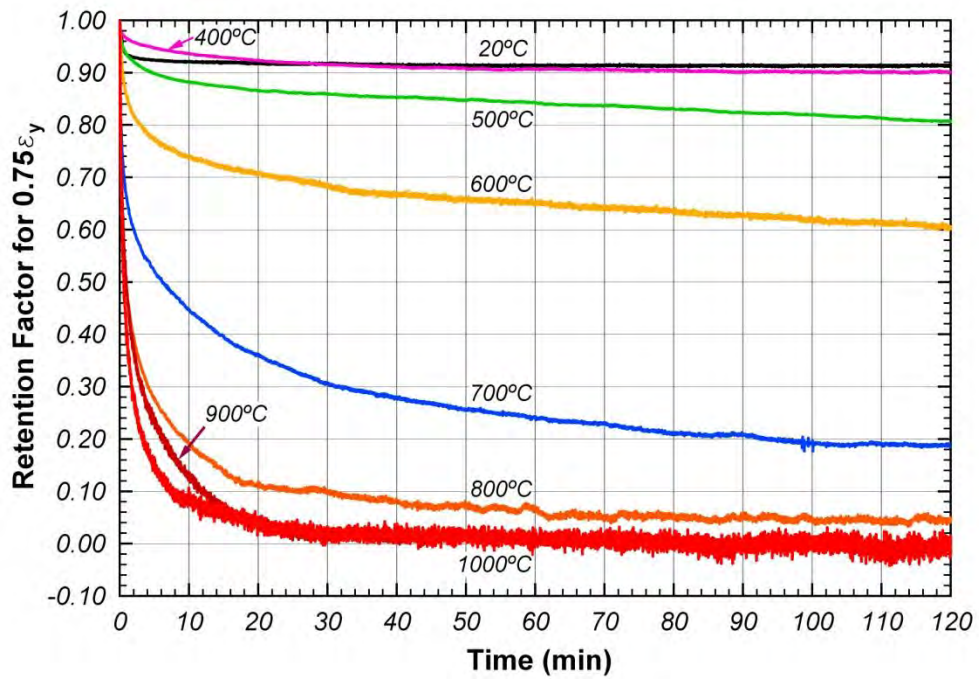
Figure E.22 Retention factor at 0.75εy

Figure E.23 Retention factor at 0.90εy

317
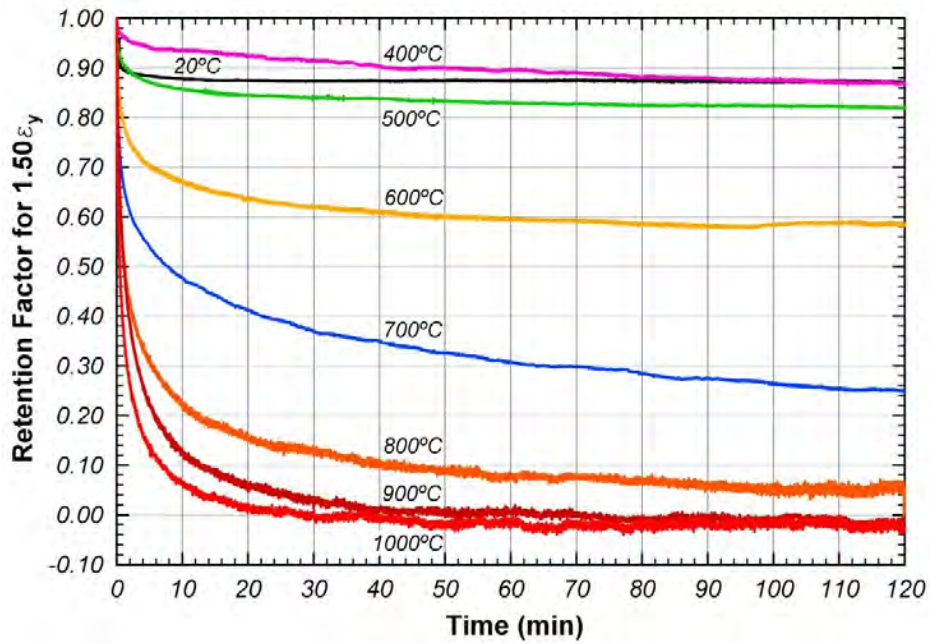
Figure E.24 Retention factor at 1.50ɛy

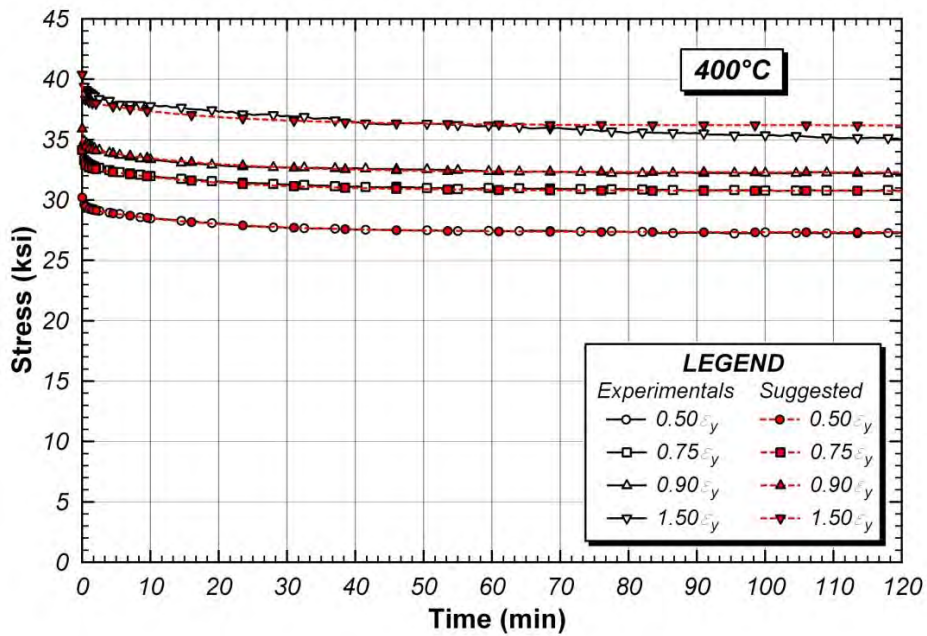### E.4 RELAXATION MODEL COMPARISONS

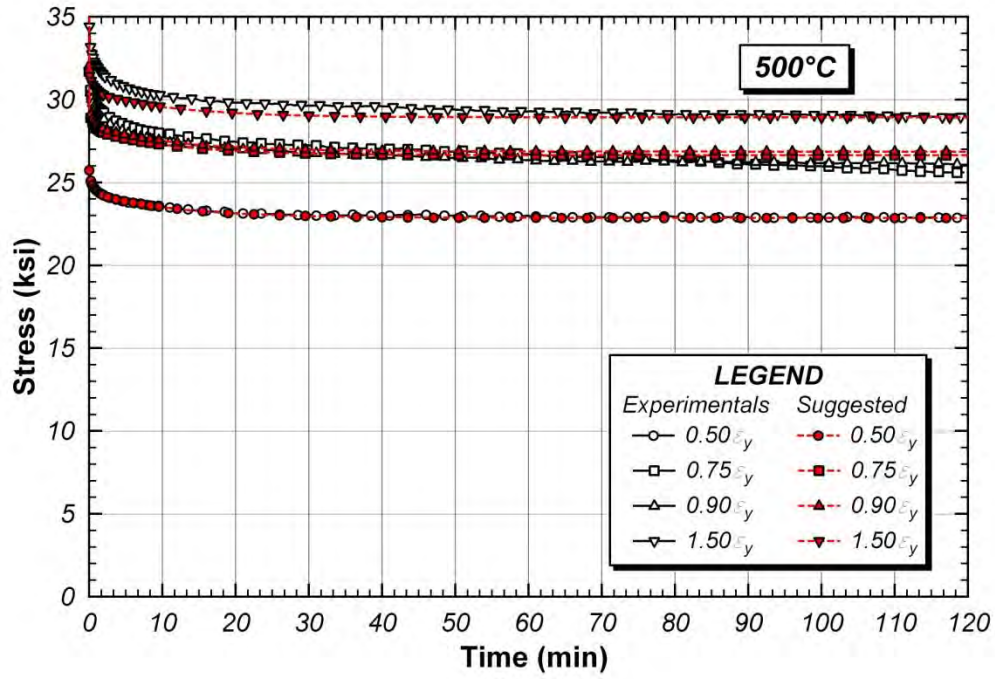*Figure E.25 Comparison curves at 400°C*

318

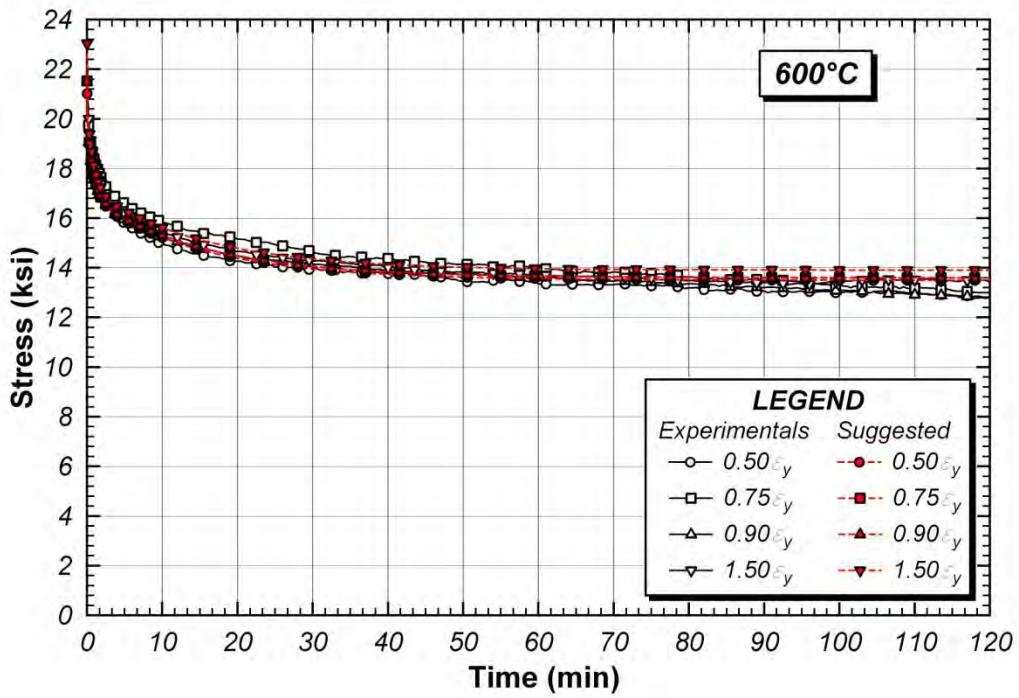*Figure E.26 Comparison curves at 500°C*

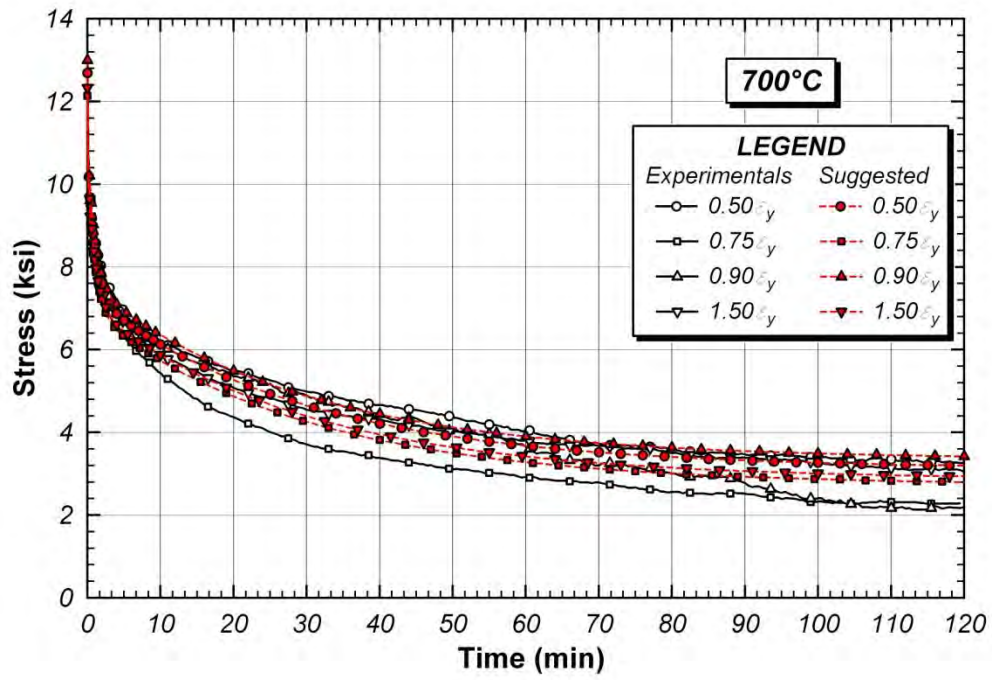*Figure E.27 Comparison curves at 600°C*

319

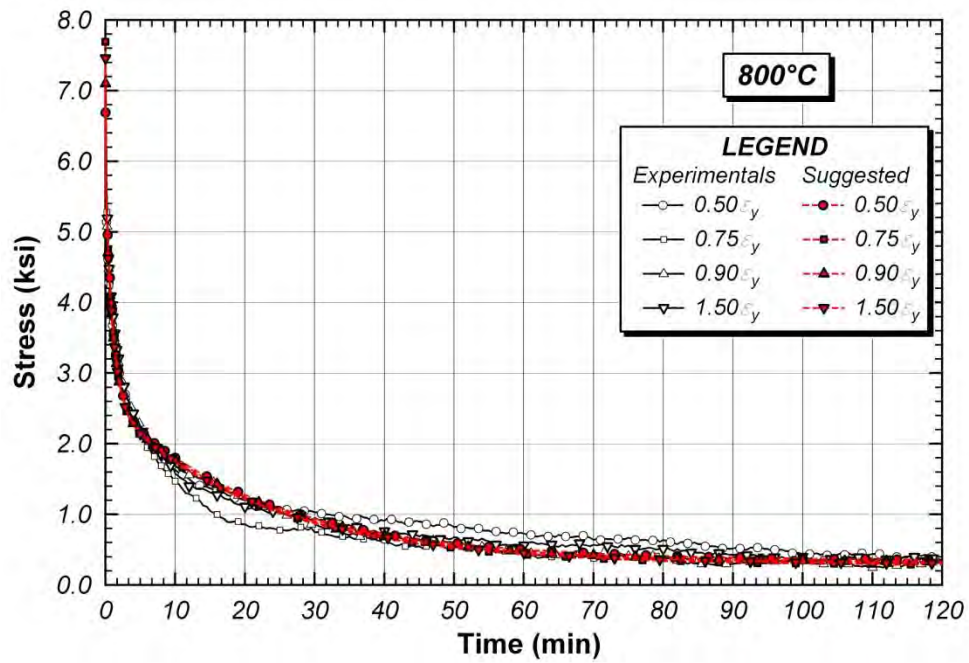*Figure E.28 Comparison curves at 700°C*

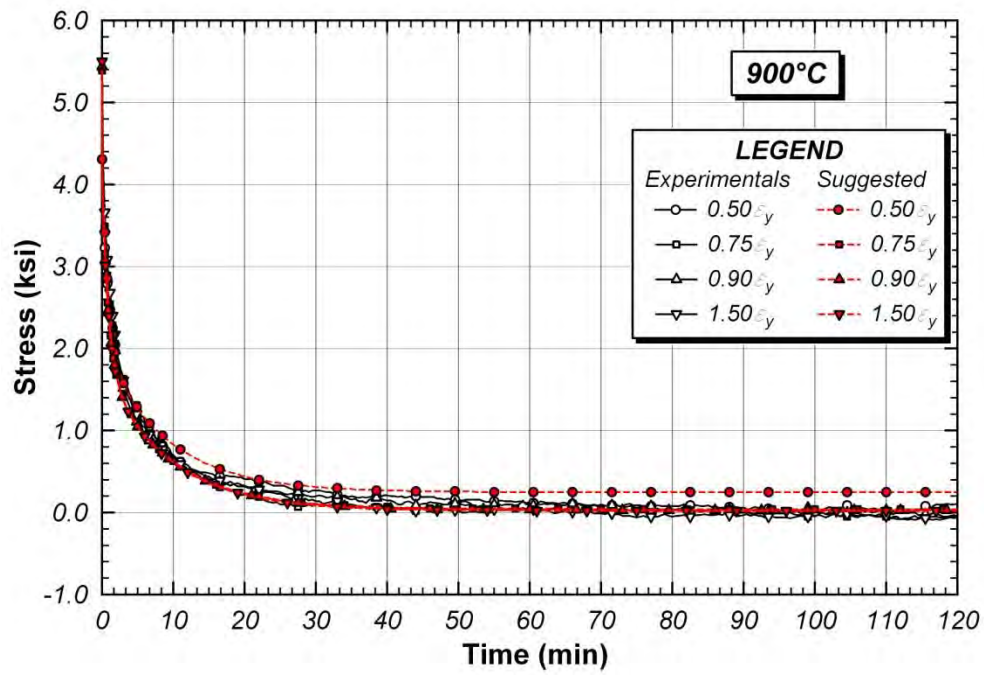*Figure E.29 Comparison curves at 800°C*
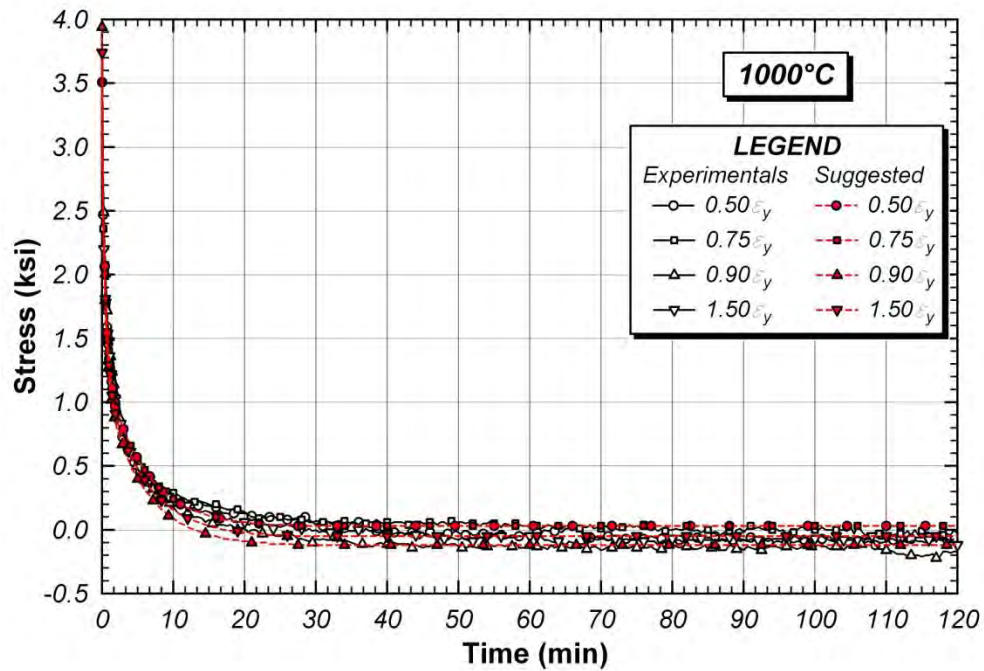
320

Figure E.30 Comparison curves at 900°C

Figure E.31 Comparison curves at 1000°C

REFERENCES

ASTMA370, A. (2008). Standard Test Methods and Definitions for Mechanical Testing of Steel Product. A370, ASTM: 47.

A370, A. (2012). Standard Test Methods and Definitions for Mechanical Testing of Steel Product. A370, ASTM: 47.

A992, A. (2011). "Standard Specification for Structural Steel Shapes." American Society of Testing and Materials.

Ahmadieh, A. and A. K. Mukherjee (1975). "Stress-temperature-time correlation for high temperature creep curves." Materials Science and Engineering 21(0): 115-124.

AISC (2005). Specification for structural steel buildings. Chicago, IL, American Institute of Steel Construction.

Andrade, E. N. (1910). "On the Viscous Flow in Metals, and Allied Phenomena." Proceedings of the Royal Society, Mathematical, Physical and Engineering Sciences 84(567): 1-12.

Bailey, R. W. (1929). "Creep of steel under simple and compound stresses." Engineer 148(3853): 528-529.

Banovic, S. W. a. F., T. (2005). Federal Building and Fire Safety Investigation of the World Trade Center Disaster: Damage and Failure Modes of Structural Steel Components. Gaithersburg, Maryland, National Institute of Standards and Technology.

Batsoulas, N. D. (2003). "Prediction of metallic materials relaxation at elevated temperature." Steel Research International 74(3): 176-+.

Callister (2007). Materials science and engineering an introduction, p.262, John Wiley & Sons, Inc.

Chen, B. Y. (2006). "Behavior of High Strength Structural Steel at Elevated Temperatures." Journal of Structural Engineering - ASCE 1: 1948-1954.

Davis, C. L. and J. E. King (1993). "Effect of cooling rate on intercritically reheated microstructure and toughness in high-strength low-alloy steel." Materials Science and Technology 9(1): 8-15.

Dhua, S. K., D. Mukerjee, et al. (2003). "Effect of cooling rate on the As-quenched microstructure and mechanical properties of HSLA-100 steel plates." Metallurgical and Materials Transactions a-Physical Metallurgy and Materials Science 34A(11): 2493-2504.

Dorn, J. E. (1955). "Some fundamental experiments on high temperature creep." Journal of the Mechanics and Physics of Solids 3(2): 85-116.

Elghazouli, A. Y., K. A. Cashell, et al. (2009). "Experimental evaluation of the mechanical properties of steel reinforcement at elevated temperature." Fire Safety Journal 44(6): 909-919.

Eurocode (1993). Eurocode 3 - Design of Steel Structures Part 1-2: General rules - Structural Fire Design, CEN: 74.

Fields, B. A., Fields, R.J. (1989). Elevated temperature deformation of structural steel (NISTIR 88-3899). Gaitherburg, MD, National Institute of Standards Technology. 1.

Gardner, L., A. Insausti, et al. (2010). "Elevated temperature material properties of stainless steel alloys." Journal of Constructional Steel Research 66(5): 634-647.

Guo-Qiang Li, S.-C. J., Ying-Zhi Yin, Kai Chen, Ming-Fei Li (2003). "Experimental studies on the properties of constructional steel at elevated temperatures." Journal of Structural Engineering - ASCE 1(1): 1717-1721.

Harmathy (1970). "Elevated temperature tensile and creep properties of some structural and prestressing steels." American Society for Testing and Materials, ASTM STP 464 1: 23.

Harmathy, T. Z. (1967). "A Comprehensive Creep Model." Journal of Basic Engineering 89(3): 496-&.

Ju Chen, B. Y. (2006). "Behavior of High Strength Structural Steel at Elevated Temperatures." Journal of Structural Engineering - ASCE 1: 1948-1954.

Kankanamge, N. D. and M. Mahendran (2011). "Mechanical properties of cold-formed steels at elevated temperatures." Thin-Walled Structures 49(1): 26-44.

Kirby, B. R. and R. R. Preston (1988). "High temperature properties of hot-rolled, structural steels for use in fire engineering design studies." Fire Safety Journal 13(1): 27-37.

Latella, B. A. and S. R. Humphries (2004). "Young's modulus of a 2.25Cr-1Mo steel at elevated temperature." Scripta Materialia 51(7): 635-639.

Lee, J. H., M. Mahendran, et al. (2003). "Prediction of mechanical properties of light gauge steels at elevated temperatures." Journal of Constructional Steel Research 59(12): 1517-1532.

McVetty, P. G. (1943). "Creep of metals at elevated temperatures -- Hyperbolic-sine relation between stress and creep rate." American Society of Mechanical Engineers -- Transactions 65(7): 761-767.

Mukherjee, A. K. (2002). "An examination of the constitutive equation for elevated temperature plasticity." Materials Science and Engineering: A 322(1-2): 1-22.

NIST (2005). Federal Building and Fire Safety Investigation of the World Trade Center Disaster. Gaithersburg, MD, NIST.

Norton, F. H., Ed. (1929). The creep of steel at high temperatures. New York, McGraw-Hill Book Company Inc.

Outinen, J. (2001). High-Tempeature Testing of Structural Steel and Modelling of Structures at Fire Temperatures. 1: 120.

Outinen, J. and P. Makelainen (2004). "Mechanical properties of structural steel at elevated temperatures and after cooling down." Fire and Materials 28(2-4): 237-251.

Poh, K. W. (1998). "General creep-time equation." Journal of Materials in Civil Engineering 10(2): 118-120.

Pyshmintsev, I., A. Boryakova, et al. (2008). "Effect of cooling rate on the structure and properties of low-carbon tube steel." Metallurgist 52(7-8): 464-469.

Ranawaka, T. and M. Mahendran (2009). "Experimental study of the mechanical properties of light gauge cold-formed steels at elevated temperatures." Fire Safety Journal 44(2): 219-229.

Schneider, R. and J. Lange (2010). Constitutive Equations and Empirical Creep Law of Structural Steel S460 at High Temperatures.

Sherby, O. D. and P. M. Burke (1967). "Mechanical behavior of crystalline solids at elevated temperature." Progress in Materials Science 13(7): 325-390.

Sherby, O. D. and P. M. Burke (1968). Mechanical behavior of crystalline solids at elevated temperature, Pergamon Press.

Smith, C. I., B. R. Kirby, et al. (1981). "The reinstatement of fire damaged steel framed structures." Fire Safety Journal 4(1): 21-62.

Walles, K. F. A. and A. Graham (1955). "Relationships between long- and short-time creep and tensile properties of commercial alloy." Iron and Steel Institute -- Journal 179(Part 2): 105-120.

Yu, L. A. and K. H. Frank (2009). "Shear Behavior of A325 and A490 High-Strength Bolts in Fire and Post-Fire." Engineering Journal-American Institute of Steel Construction Inc 46(2): 99-106.

Vita

Jinwoo Lee was born in Jinju, South Korea on 1963 and attended Jinju High School. In 1983 he entered the Civil Engineering Department at Pusan National University in South Korea to pursue a Bachelor of Science. In order to deeper his understanding in structural engineering, he subsequently studied for a Master's Degree of Science in Civil Engineering at the same university from 1987 to 1989.

In 1990 he joined the Civil Structural Department of Korea Power Engineering Company (KOPEC), which designed new nuclear and fossil power plants and renovated existing ones in Korea and globally. He was placed in charge of analysis and design work of steel structures in new nuclear power plants and served for the renovating and maintenance work of existing power plants up to 2005. He achieved the structural professional engineering license (S.E.) of South Korea in 1997 as well as the professional engineering (P.E.) of civil engineering in the state of Oregon in 2000. He has served as engineering group leader of the Turbine Building Design Group from 2003 to 2007 prior to his beginning the PhD program at The University of Texas at Austin.

He believes in the love of God and enjoys traveling the world with family for finding insights of the human being.

Permanent address: Hyundai Apt. 408-206, 92 Seohyun-dong, Bundang-gu, Sungnam-si, Kyunggi-do, South Korea, Zip 463-777, jinwoo@utexas.edu

This dissertation was typed by the author.